REPORT DOCUMENTATION PAGE

Form Approved OMB No. 0704-0188

1. REPORT DATE *(DD-MM-YYYY)*	2. REPORT TYPE	3. DATES COVERED *(From – To)*
30-01-2006	Final Report	01-Oct-02 - 01-Jan-06

4. TITLE AND SUBTITLE

Electric Discharge/ Afterglow Kinetics for Laser Mixtures with Carbon Monoxide, Oxygen and Iodine

5a. CONTRACT NUMBER
ISTC Registration No: 2415

5b. GRANT NUMBER

5c. PROGRAM ELEMENT NUMBER

6. AUTHOR(S)

Professor Andrey Ionin

5d. PROJECT NUMBER

5d. TASK NUMBER

5e. WORK UNIT NUMBER

7. PERFORMING ORGANIZATION NAME(S) AND ADDRESS(ES)

Lebedev Physics Institute
53 Leninsky Prospect
Moscow 119991
Russia

8. PERFORMING ORGANIZATION REPORT NUMBER

N/A

9. SPONSORING/MONITORING AGENCY NAME(S) AND ADDRESS(ES)

EOARD
PSC 802 BOX 14
FPO 09499-0014

10. SPONSOR/MONITOR'S ACRONYM(S)

11. SPONSOR/MONITOR'S REPORT NUMBER(S)
ISTC 02-7001

12. DISTRIBUTION/AVAILABILITY STATEMENT

Approved for public release; distribution is unlimited.

13. SUPPLEMENTARY NOTES

14. ABSTRACT

This report results from a contract tasking Lebedev Physics Institute as follows: Previous research carried out under the ISTC partner contracts has demonstrated that an electric discharge could be a powerful means for producing highly excited CO molecules needed for overtone CO lasers, for producing electrically excited oxygen and for obtaining iodine atoms via iodine dissociation, which can be extremely useful for the development of the electrically assisted oxygen-iodine laser. Therefore, the Project will be aimed at improving understanding of three main problems tightly related to each other:

· the experimental and theoretical study of the kinetics of highly excited CO molecules in an E-beam and RF discharge, which is extremely important for development of efficient overtone CO laser (including the supersonic CO laser);

· the experimental and theoretical study of singlet-delta oxygen (SDO) kinetics in E-beam and DC discharges, which is important for efficient SDO production and development of an electrically-assisted oxygen-iodine laser;

· the experimental and theoretical study of the kinetics of atomic iodine production in vortex flow DC discharges, which is important for the improvement of chemical oxygen-iodine lasers.

The research team proposed for this project consists of experts from the Gas Laser Lab and Chemical Lasers Lab of the Quantum Radiophysics Institute of the Lebedev Physics Institute in Moscow and the Samara Branch of the Lebedev Institute. The research team has extensive experience in the field of experimental and theoretical fundamental research on kinetic processes taking place in the active media of different electric discharge and chemical lasers.

15. SUBJECT TERMS

EOARD, Physics, Optics

16. SECURITY CLASSIFICATION OF:			17. LIMITATION OF ABSTRACT	18, NUMBER OF PAGES	19a. NAME OF RESPONSIBLE PERSON
a. REPORT	b. ABSTRACT	c. THIS PAGE			DONALD J SMITH
UNCLAS	UNCLAS	UNCLAS	UL	250	19b. TELEPHONE NUMBER *(Include area code)* +44 (0)20 7514 4953

RUSSIAN ACADEMY OF SCIENCES
P.N. LEBEDEV PHYSICS INSTITUTE

Физический институт имени П.Н.Лебедева
Ф И А Н

53 Leninsky prospect, 119991
Moscow, Russia

Approved by Dr. A.N.Starodub

Deputy Director of
N.G. Basov Quantum Radiophysics Institute
of P.N. Lebedev Physics Institute
of Russian Academy of Sciences

ISTC 2415 **EOARD Project 027001**

Final Project Technical Report of ISTC 2415

Electric discharge and afterglow kinetics for laser mixtures with carbon monoxide, oxygen and iodine

(From 01 October 2002 to 31 December 2005 for 39 months)

Andrei Alekseevich Ionin
(Project Manager)
P.N. Lebedev Physics Institute
Phone: (095) 132-0425; Fax: (095) 132-0425; e-mail: aion@sci.lebedev.ru

January 2006

This work was supported financially by EOARD and performed under the contract to the International Science and Technology Center (ISTC), Moscow.

LIST OF PARTICIPANTS:

1. Prof. A.A. Ionin
2. Prof. A.P. Napartovich
3. Prof. Yu.B. Konev
4. Dr. N.N. Yuryshev
5. Dr. I.V. Kochetov
6. Dr. A.K. Kurnosov
7. Dr. S.L. Shnyrev
8. Dr. A.A. Kotkov
9. Dr. D.V. Sinitsyn
10. Dr. L.V. Seleznev
11. Dr. S.V. Ivanov
12. Dr. N.P. Vagin
13. Dr. M.P. Frolov
14. Dr. P.A. Mikheev
15. Dr. A.A. Shelepenko
16. Dr. S.Yu.Savinov
17. Yu.M. Klimachev
18. N.A. Ionina
19. S.A. Vetoshkin
20. A.Yu. Kozlov
21. O.A.Rulev
22. Yu.V. Terekhov
23. Yu.V. Lobarev
24. Yu.P. Podmar'kov
25. A.I. Voronov
26. O.S. Kartamysheva
27. N.V. Kupryayev

LIST OF CONTENTS

INTRODUCTION

The activity on the Project 2415P was being developed on three main directions, which were being solved in parallel:

- the experimental and theoretical study of the kinetics of highly excited CO molecules in e-beam sustained discharge (EBSD) and RF discharge, which is extremely important for development of efficient overtone CO laser including supersonic CO laser;
- the experimental and theoretical study of singlet delta oxygen (SDO) kinetics in EBSD, DC, RF and MW discharges, which is important for efficient SDO production and development of electrically-assisted oxygen-iodine laser;
- the experimental and theoretical study of the kinetics of atomic iodine production in vortex flow DC discharge, which is important for the improvement of chemical oxygen-iodine laser.

During the Project the research was being carried out according to the work plan and was aimed at the fulfillment of the following tasks.

YEAR I.

Task 1A

Subtask 1A.1. Inclusion of the latest values of V-V exchange rates calculated by the Billing's group into the existing kinetic model. The design of probe CO laser including overtone CO laser.
Subtask 1A.2. Experiments on influence of gas dynamics on overtone CO laser characteristics. EBSD laser at experimental conditions (gas pressure, temperature) of supersonic CO laser.
Subtask 1A.3. Verification of the kinetic and RF discharge models by comparison with the experimental data, obtained experimentally at room temperature. Modification of the existing RF discharge facility for lasing experiments at room temperature.
Subtask 1A.4. Modification of the RF discharge pumped laser model for output power calculations. RF discharge fundamental band CO laser. Experiments on small signal gain (SSG) measurements with a probe overtone/fundamental CO laser.

Task 1B

Subtask 1B.1. Study of EBSD in oxygen containing mixtures. Adaptation of the existing numerical model of e-beam sustained discharge to experiment conditions. Experiments on electric breakdown in SDO obtained from a chemical SDO generator. Evaluation of ionization cross section of SDO.
Subtask 1B.2. Formulation of equation system for description of transition region in glow discharge. Determination of limits for EBSD (breakdown; maximum specific input energy, etc.). Calibration of SDO detecting schemes: high-sensitive photodetector, titration techniques, intracavity spectroscopy. SDO concentration is to be measured, varying flow velocity and interelectrode distance for vortex discharge.
Subtask 1B.3. Simulation of structure of transition region for condition of experiment. Verification of the model by comparison with the experimental data. Parametric study of DC discharge plasma characteristics vs. SDO concentration (probe and volt-ampere characteristics).
Subtask 1B.4. Comparison with measured electric probe characteristics and extraction of information about kinetic processes. Application of different detector for SDO measurement including intracavity spectroscopy.

Task 1C

Subtask 1C.1. Development of an existing discharge chamber design for atomic iodine production with the help of DC glow discharge at high pressures, considering the results of previous

experiments. Application of the discharge electrode configuration found for achieving stable DC discharge at higher pressure of Ar or other gases.
Subtask 1C.2. Development of the equipment and technique for production of NO_2 (needed to measure atomic iodine concentration) using thermal decomposition of $Pb(NO_3)_2$.
Subtask 1C.3. Manufacturing and assembling of an improved discharge chamber for atomic iodine production. The apparatus for determination of I_2 concentration by measuring absorption in the visible region will be developed and equipped with light source, photo receiver and data acquisition system.
Subtask 1C.4. The design of the equipment necessary for HI production will be chosen taking into account the known experimental methods of HI production. Development of the method of atomic iodine concentration measurement.

YEAR II.

Task 2A
Subtask 2A.1. Analysis of data on EBSD laser characteristics in nitrogen containing mixtures using the latest version of the kinetic model. Experiments on gas temperature and density temporal behavior, including experimental conditions for supersonic CO laser. Technical proposal on new RF discharge facility with cryogenic gas cooling.
Subtask 2A.2. Modifications of RF discharge model by inclusion coupling between electron and vibrational kinetics. Design of the new cryogenically cooled RF discharge facility.
Subtask 2A.3. Experimental study of RF discharge cryogenically cooled fundamental band CO laser. Comparison of SSG experiments with theory.
Subtask 2A.4. Comparison of modified RF discharge theory with RF discharge CO laser operating at low temperatures

Task 2B
Subtask 2B.1. Experimental measurement of temperature of EBSD in oxygen containing mixture. Analysis of gas heating processes in e-beam sustained discharge and extension of the model for variable gas temperature. Formulation of the numerical model for the positive column of glow discharge attached to chemical SDO generator.
Subtask 2B.2. Parametric study of effects influencing upon SDO production.
Subtask 2B.3. Comparison with experimental data on SDO yield. Comparison with experimental results on positive column of glow discharge at SDO content.
Subtask 2B.4. Determination of positive factors influencing upon maximum SDO yield. Modifications of the model, if necessary, and preliminary predictions of optimum conditions for SDO generation. Conclusion about quality of the model developed. Determination of the best kinetic package for dynamic model. Experimental varying of mean electron energy in discharge and removing quenchers in the downstream afterglow of vortex discharge to study SDO yield. The SDO concentration is to be measured using discharge with different mean electron energies. Electron energy will be varied changing gas mixture and combining two discharges. Also, the experiments with removal of quenchers increased by recombination in the downstream afterglow are planned.

Task 2C
Subtask 2C.1. Measurements of atomic iodine concentration by measuring the concentration of molecular iodine. These measurements are to be performed if the tunable semiconductor laser is not available. In the presence of NO_2 rapid recombination of iodine atoms takes place. Concentration of iodine molecules I_2 will be measured using absorption in the visible region.

Subtask 2C.2. Study on iodine atoms production, using HI as precursor. Measurements of atomic iodine concentration produced when HI is added into discharge region. The use of HI should prevent discharge chamber contamination observed in experiments with methyl iodide.
Subtask 2C.3. Measurements of excited iodine atoms concentration in the discharge products. Excited iodine atoms are produced when iodides are admixed in the discharge region or in the downstream afterglow. Determination of exited atoms concentration by measuring absolute intensity of iodine emission at 1.315 μm. Technique calibration against black body radiation.
Subtask 2C.4. Study on iodine atoms production decomposing iodides by discharge products. The measurements of iodine atoms concentration produced in the downstream afterglow by chemically active particles that exist in glow discharge in oxygen and oxygen mixtures.

YEAR III.

TASKS a, b, c, d, e, f, g

a). Repairing the hot cathode of the e-beam gun inside e-beam sustained discharge facility.
b). Cleaning the inner surfaces of the laser chamber and e-beam chamber of the facility.
c). Full disassembling of probe CO laser and cleaning quartz and metallic parts of its gas duct.
d). Modification of RF CO laser resonator system.
e). Calibration of measuring electronic equipment.
f). Repairing the central heating system in lab rooms.
g). Preparing publications.

TASK 3

Subtask 3.1. Study of slab RF discharge in oxygen mixtures. Inclusion the ion current effect into the theoretical model of an electric discharge in oxygen. Small signal gain measurements on different carbon monoxide ro-vibrational transitions for oxygen gas mixtures with carbon monoxide additives. Usage of intracavity laser spectroscopy (ICLS) facility to measure the concentration of SDO produced in different type of MW and RF discharge generators. Development of new type of an electric SDO generator based on the non-self sustained slab discharge initiated by high-voltage pulses. Incorporation this generator into the ICLS facility.
Subtask 3.2. Extension of theoretical model for SDO generation by incorporating vibrational kinetics of O_2 (X) and CO molecules. Collection of available rate coefficients and development of a relevant subroutine. Revision of predicted data on E/N in positive column of a glow discharge at the output of SDO chemical generator. Development of SDO luminescence detection scheme with reduced noise using multi- pulse summing and averaging technique for RF slab discharge in oxygen. Measurement of gas temperature time behavior in oxygen gas mixtures with carbon monoxide additives using SSG data. Study of electrical parameters of non-self sustained slab discharge initiated by high-voltage pulses under different experimental conditions.
Subtask 3.3. Theoretical evaluation of electric discharge oxygen-iodine laser feasibility. Parametric study of influence of experimental conditions on SDO luminescence intensity in RF discharge oxygen-containing plasma afterglow. Numerical simulations of gas temperature time behavior with improved theoretical model for oxygen gas mixtures with carbon monoxide additives. Parametric study of SDO production in electrical generators driven by MW and /or RF discharge. Designing and manufacturing of an experimental facility based on the most promising SDO electrical generator for obtaining the laser effect.
Subtask 3.4. Parametric study of SDO production in a generator based on the non-self sustained slab discharge initiated by high-voltage pulses by ICLS method for SDO measuring. Application of theoretical model to interpretation of experimental data on SDO in slab RF discharge and estimation of perspectives to realize discharge pumped OIL.

PART I. CO LASER KINETICS
(Tasks 1A and 2A)

Part I.1. KINETICS OF A CO LASER OPERATING ON HIGHLY EXCITED VIBRATIONAL LEVELS
(Subtasks 1A.1, 1A.2, 1A.4, 2A.1 and 2A.3)

Introduction

Small-signal gain (SSG) time behavior is a very important characteristic for a CO laser especially when the laser operates as a first-overtone (FO) CO laser with supersonic flow of active medium through a laser resonator (McCord, 2003). SSG time behavior for a pulsed e-beam sustained discharge (EBSD) CO laser amplifier (LA) operating on fundamental band vibrational transitions V→V-1 from 5→4 up to 14→13 was studied for the first time in (Bones, 1975) by using a master oscillator (MO) - LA system. Experiments on measuring SSG time behavior for the same sort of a CO LA running on about the same vibrational transitions between 7→6 and 15→14, were also described in (Basov, 1983). There was no any comparison between experimental and theoretical results on SSG time behavior at all. It should be noticed that the SSG time behavior was just measured for vibrational transitions V→V-1 with vibrational numbers lower than V~15 typical for a pulsed EBSD fundamental band CO laser. However, an efficient FO CO laser emitting radiation within 3.0÷4.0 μm spectral band (Hager, 2000) coinciding with the atmospheric "transparency window" operates on higher vibrational transitions V→V-2 with V being in the range of 15÷38. Just the opportunity for a FO CO laser to run within the "transparency window" stimulates a great interest in this sort of a CO laser (Hager, 2000; Zeyfang, 2001; Bohn, 2002; McCord, 2003; www.afrl.af.mil/successstories/2001/emerg.tech…). In order to measure SSG time behavior inside pulsed EBSD CO laser active medium and to compare experimental data with results of theoretical simulation we developed MO - LA system operated on vibrational transitions with V=6÷32.

One of the purposes of our work was to extend the kinetic model of CO laser. Our earlier studies on characteristics of cryogenic FO CO laser demonstrated a necessity to modify the kinetic model improving description of VV-exchange processes taking place for molecules on high vibrational levels (Ionin, 2001a, b). In our papers (Ionin, 2000; Ionin, 2001a; Basov, 2002), analyzing experimentally and theoretically kinetic processes taking place in active medium of a pulsed CO laser, we demonstrated that the multi-quantum theoretical model of vibrational exchange instead of a single-quantum one should be applied for a correct theoretical description of a CO laser operating on vibrational transitions V→V-1 and V→V-2 with V>15 (so-called "high" vibrational transitions). The commonly used single quantum exchange (SQE) model could be applied to simulate a vibrational distribution function (VDF) only for low vibrational levels (V<15). For high vibrational levels one should take into account the multiquantum vibrational exchange (MQE) and especially an asymmetric cross-exchange of two vibrational quanta for CO molecules on the highest levels with one quantum for CO and/or N_2 molecules in the ground state. Besides the cross-exchange processes, in electric discharge an interaction of electrons with molecules is much stronger than with rare gas atoms and sensitive to vibrational excitation degree of molecular gases. The kinetic model including numerical calculation of required rate coefficients using the latest methods and molecular interaction potential forms was developed.

The developed model was applied to simulate SSG time behavior for both first-overtone and fundamental vibrational transitions. Our analysis revealed that the results of SSG simulation are very sensitive to the local values of specific input energy (SIE). This feature makes the comparison of the theoretically calculated and experimentally measured SSG characteristics rather difficult, because experimentally measured value of SIE Q_{in} is an averaged one over the gas discharge

chamber (GDC) volume (it is not a local SIE value). In order to find more accurately the local value of SIE, the dependence of calculated SSG upon SIE values was studied. The comparison of SSG measurements with a corrected numerical simulation demonstrated that our developed theoretical model adequately describes the SSG time behavior. The agreement with experiment takes place for the wide range of vibrational transitions and gas densities, and this agreement can be considered as an experimental verification of the derived set of VV and VV' rate constants. A strong dependence of the SSG characteristics upon the rotational quantum number of rotational vibrational transition gives the chance to measure gas temperature variations caused by Joule heating in discharge and energy release in collisions of neutrals. In this work the method of gas temperature reconstruction by using gain/absorption time behavior measurement on several ro-vibrational transitions of CO molecule was developed in order to study gas temperature time behavior inside the CO laser medium.

Inclusion of the latest values of V-V exchange rates calculated by the Billing's group into the existing kinetic model.
(*Subtask 1A.1.*)

The purpose of our work was to extend the kinetic model of CO laser. Our earlier studies (Ionin, 2001a, b) demonstrated a necessity to modify the kinetic model improving description of VV-exchange processes taking place on high vibrational levels. Arranging direct contacts with the group of Prof. G. Billing (the University of Copenhagen, Denmark), we used a rather complete set of most reliable to these days VV-exchange rate constants for CO molecules. Data published earlier in (Coletti & Billing, 2000) provide incomplete and fragmentary information about VV-exchange processes. A full matrix of rate constants was constructed in (Ionin, 2001b) using interpolation and extrapolation procedures. Therefore, the MQE model formulated in (Ionin, 2001b) can be viewed as an intermediate one. More complete new data (Billing, 2003) make it possible not to do extrapolations and provide a solid basis for arranging the full matrix of rate coefficients.

Calculations of the rate constants for these processes have been carried out with the interaction potential described in (Coletti & Billing, 2000) using the time-dependent coupled state semi-classical method. The calculation procedure involved 18 classical equations of motion coupled to a set of time-dependent equations for the vibrational motions (usually less than 100).

The rate coefficients have been found by computing cross sections at the following energies: 100, 200, 350, 500, 650, 800, 1000, 1500, 3000, 5000, 7500, 10000 cm^{-1} and running 500÷1000 trajectories for each energy value, thus ensuring an accuracy of about 15-20% for the rate constants. So, the rate constants were computed for 114 exothermic VV-exchange processes for T=100, 200, 300, 500, 700, 1000 K. Furthermore the procedure of data preparation included calculation of rate constants for endothermic processes and logarithmic interpolation throughout T values.

The corresponding novel kinetic data were combined with the data from (Coletti & Billing, 2000) forming a complete matrix of rate constants for single-, double-, three-, and four- quantum exchanges, and for asymmetric one-to-two quanta exchange, too. The latest data for three- and four-quantum processes make it possible to clear up the role of these processes in vibrational kinetics.

In particular, looking at **Fig.I.1.1** where the rate constants for the processes $CO(36-\Delta v)+CO(v) \rightarrow CO(36)+CO(v-\Delta v)$ versus quantum number V are presented for $\Delta v=1\div4$, Δv is the number of exchanged quanta at T=100 K, the conclusion can be made that the rate coefficients for the processes with different numbers of the exchanged quanta are of the same order, so the four-quantum exchange processes cannot be neglected in this range of vibrational levels numbers.

The rate constants for exact resonance are not shown in **Fig.I.1.1** because these processes do not change the vibrational state of a pair of molecules. It is worth to note that the width of the resonance diminishes with the number of exchanged quanta. This effect is more evident in **Fig.I.1.2**,

where the tuning function Φ(36, Δu) is presented describing the relative variations of rate constants versus energy mismatch proportional to Δu.

This tuning function is defined as the ratio of rate coefficients for the processes with energy mismatch depending on Δu to the rate coefficient for the nearest to resonance exothermic process with Δu=1:

$$\Phi(36,\ \Delta u)=\frac{k(36-\Delta v,36+\Delta v-\Delta u\rightarrow 36,36-\Delta u)}{k(36-\Delta v,35+\Delta v\rightarrow 36,35)}.$$

The width of this function is indeed smaller for larger Δv=3, 4.

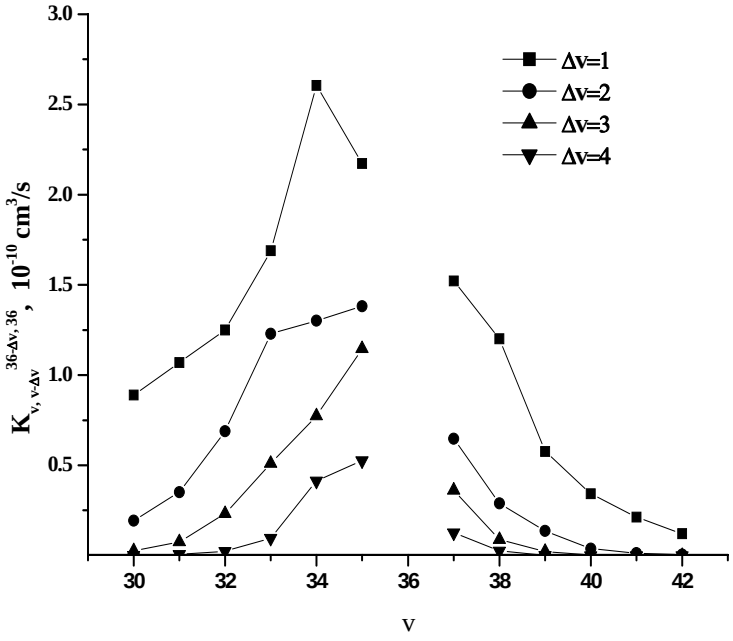

Fig.I.1.1. Rate constants for the processes CO(36-Δv)+CO(v)→CO(36)+CO(v-Δv) as functions of V for different numbers of exchanged quanta Δv, gas temperature T=100 K.

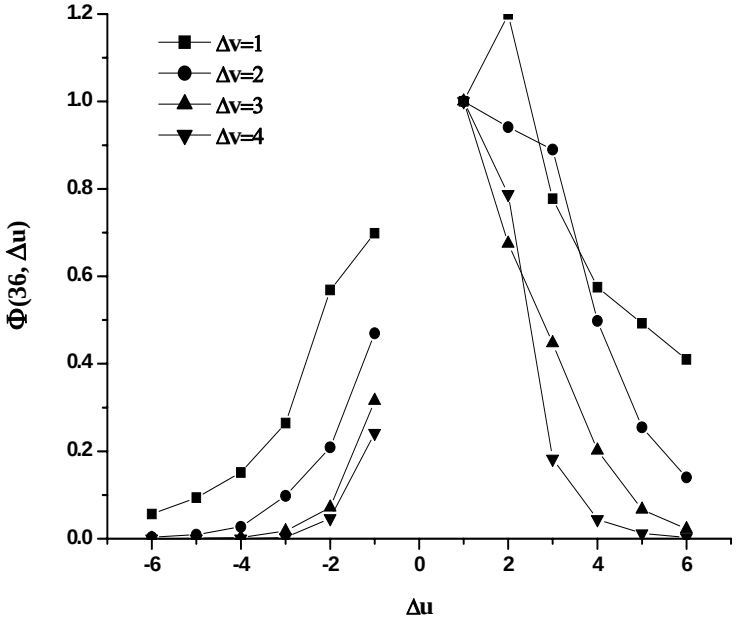

Fig.I.1.2. The tuning function Φ(36, Δu) defined above for different numbers of exchanged quanta Δu.

Thus the full and complete set of MQE rate coefficients is prepared for further exploiting in the FO CO laser kinetic model.

It is of great interest to find out the degree of influence of the MQE model modifications on results of simulations of the FO CO laser. We compared the results of numerical simulations performed using three theoretical models. Model I is essentially the single quantum exchange (SQE) model as described in (Belykh, 1994; Ionin, 1998). Model II is described in detail in (Ionin, 2001a), and based on MQE vibrational kinetics, with the energy exchange rate constant (EERC) values interpolated from the data of (Cacciatore & Billing, 1981; Billing & Cacciatore, 1983). Finally, model III includes a complete set of the EERCs reported in (Billing, 2003).

The conditions of numerical simulations were selected close to those obtained experimentally in (Basov, 2002) for the FO CO laser, but not exactly the same. A CO:He = 1:4 laser mixture at temperature 100 K and density 0.2 Amagat was assumed to be excited by EBSD with duration 30 μs and specific input energy 200 J/(l Amagat). In numerical simulations, gas expansion induced by energy release into heating was ignored, for simplicity. Therefore, we do not try to make a direct comparison with existing experimental data for similar conditions (Basov, 2002). To make the interpretation of comparison results easier, vibrational–translational (V–T) relaxation rate constants and spontaneous emission rates were taken as identical in all three models, and are described in (Ionin, 2001a; Reid, 1995; Cacciatore, 1983; Langhof, 1995). The evolution of VDF and the characteristics of the FO CO laser was numerically calculated using the three models in turn. **Fig.I.1.3** shows a comparison of the VDFs at the times 50, 100, 200 and 300 μs after discharge started. It is interesting that the shapes of the VDFs found in SQE (I) and in the latest model (III) are very similar, while the early MQE model (II) predicts faster appearance of population on high levels and lowers the plateau at later times. However, it is very important to note that model III predicts slower evolution of the VDF than model I.

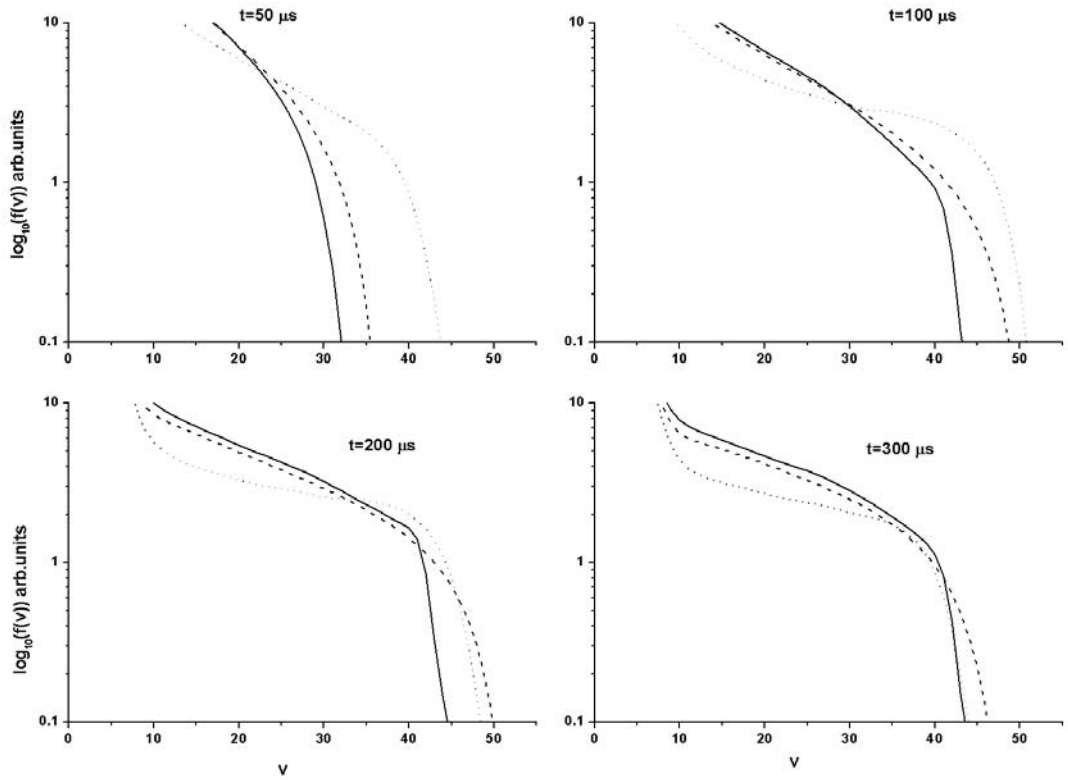

Fig.I.1.3. VDF time evolution calculated with different models: dashed curve - model I, dotted curve - model II, solid curve - model III.

Generally, VV exchange processes within the whole manifold of vibrational levels govern the VDF shape dynamics. Laser parameters, in particular when the laser operates in a frequency selective mode, are controlled by VV exchange processes within a local region of vibrational levels where the VDF is disturbed by laser action.

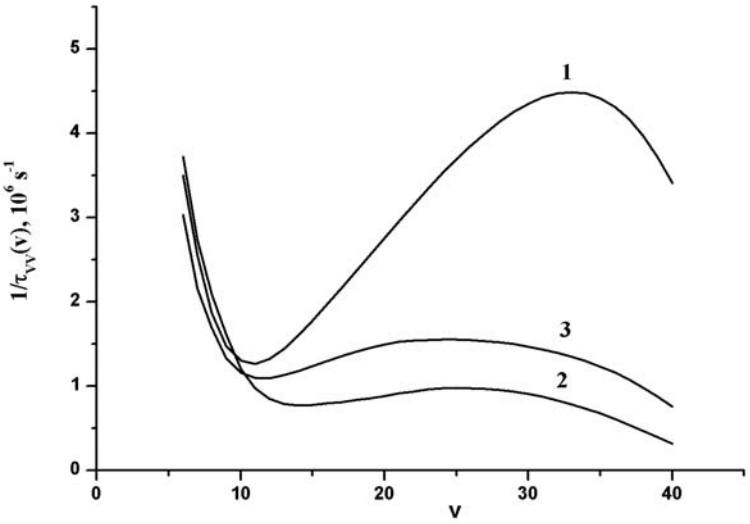

Fig.I.1.4. VV exchange frequency $1/\tau_{VV}$ at 300 μs after discharge as a function of the vibrational quantum number V calculated with different models: 1 - model I, 2 - model II, 3 - model III.

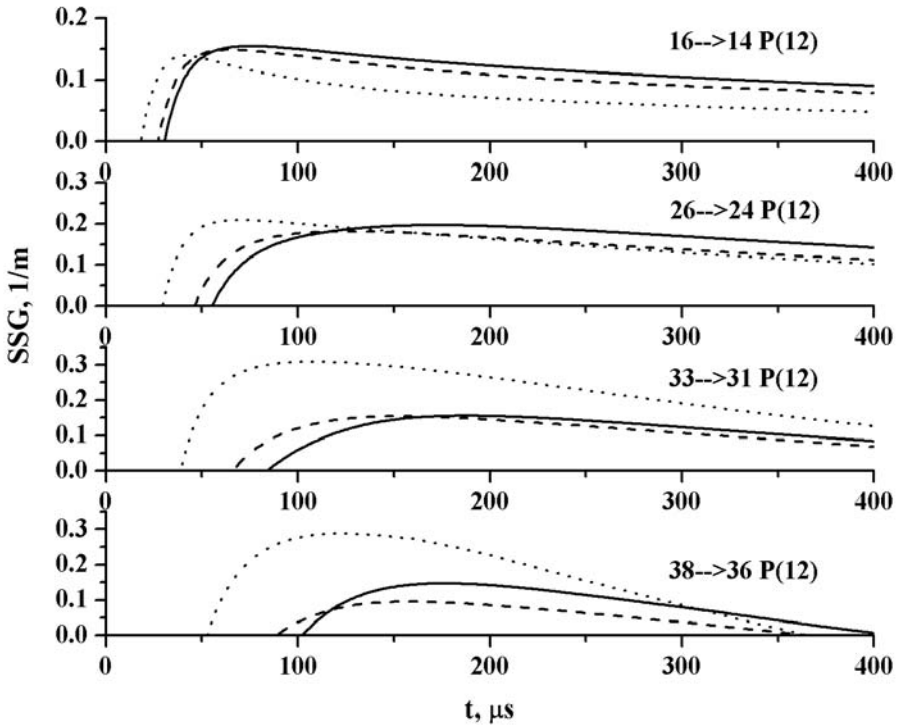

Fig.I.1.5. SSG dynamics on high overtone transitions calculated using different models: dashed curve - model I, dotted curve - model II, solid curve - model III.

It was shown in (Ionin, 2001a) that dynamics of local disturbances of the VDF can be characterized by a local frequency of VV exchange collisions, resulting in the removal of a CO molecule from the selected level, V. This frequency can be expressed in the form

$\frac{1}{\tau_{VV}} = \sum_{m\geq 1}\left(\sum_{i\geq 0} n_i \cdot Q_{vv-m}^{i,i+m} + \sum_{i\geq m} n_i \cdot Q_{v,v+m}^{i,i-m}\right)$. Here n_i is the vibrational population on level *i*, and $Q_{v,v-m}^{i,i+m}$, $Q_{v,v+m}^{i,i-m}$ are the rate constants of the VV exchange processes depopulating the level V. It is seen from this equation that the magnitude of $1/\tau_{VV}$ is sensitive not only to the values of EERCs but to the shape of the VDF as well. **Fig.I.1.4** shows that the introduced local VV exchange frequency is strongly different for different models. In particular, while the VDF shapes in models I and III were close enough, the magnitude of $1/\tau_{VV}$ for V > 10 is quite different. It is interesting that the two versions of the MQE model have similar V-dependence of VV exchange frequency. It has been previously shown (Ionin, 2001a) that model II describes high levels population dynamics in a more realistic way than model I. The same conclusion holds for model III.

The FO CO laser gain is a characteristic, which is sensitive to the local magnitude of the VDF and to its local slope. A comparison of the SSG evolution for four high transitions calculated by the different models is shown in **Fig.I.1.5**.

Note that the updated and more complete version III predicts the longest delay of gain appearance. It was reported earlier (Basov, 2002) that the theoretical analysis predicted remarkably faster laser pulse appearance than observed experimentally. A similar conclusion was made in (Porshnev, 1996) when comparing experimental and theoretical data on dynamics of populations on high selected levels at optical pumping by resonance IR radiation. The slower evolution of the VDF predicted by model III in comparison with other models thus provides the correct description. To simulate laser pulses, a selective resonator was assumed with the following parameters: gain length 1 m; round trip loss 10% and independent of laser wavelength.

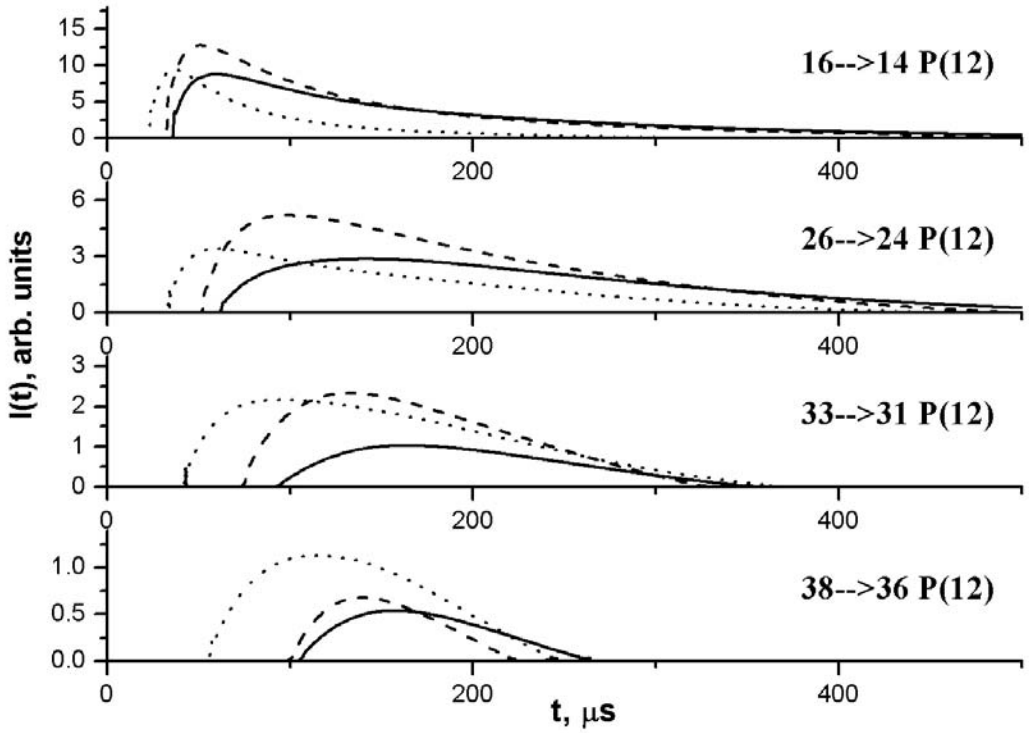

Fig.I.1.6. Output laser intensity dynamics for the frequency selective FO CO laser calculated with different models: dashed curve - model I, dotted curve - model II, solid curve - model III.

Fig.I.1.6 shows that model III predicts a later start and lower peak for the laser pulse at high transitions than models I and II. The dependence of laser efficiency operated in a selective mode on vibrational level number is compared for the three models in **Fig.I.1.7**. The laser efficiency EFF is

defined as a ratio of the laser pulse energy and the input electric energy. The difference between the three curves is quite significant and clearly demonstrates a high sensitivity of laser characteristics to the 'quality' of the vibrational kinetics model.

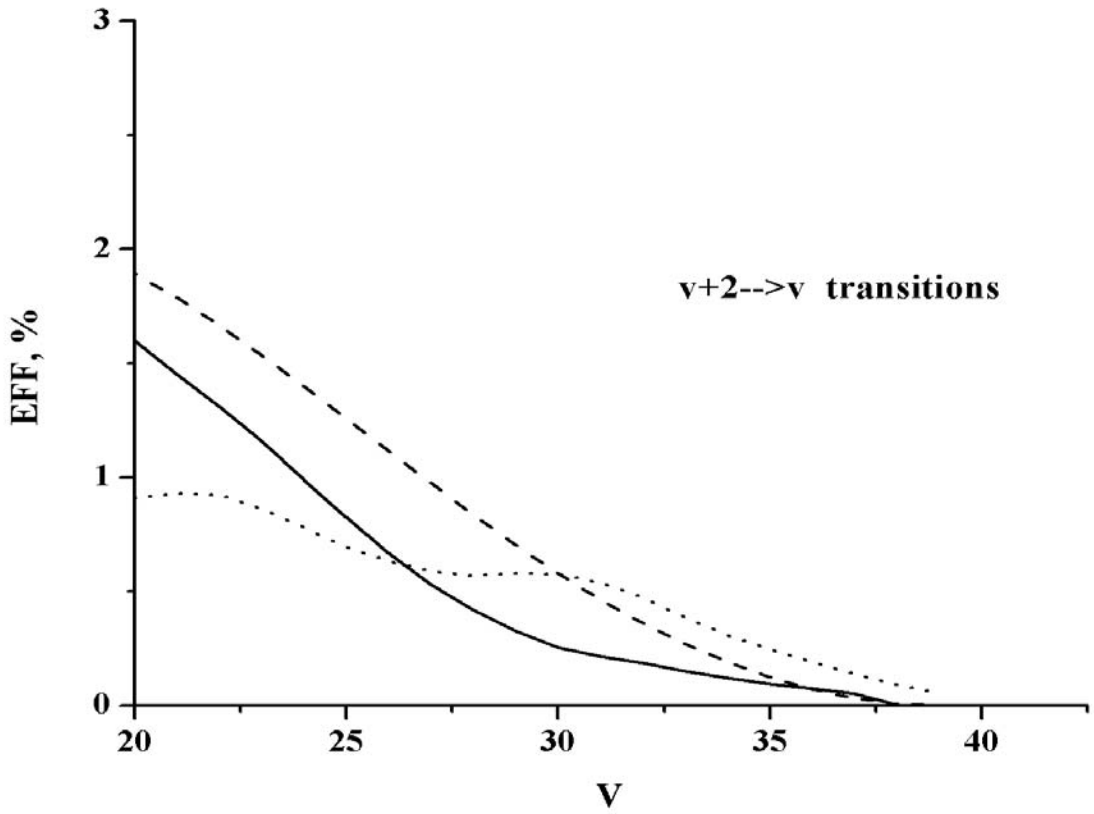

Fig.I.1.7. Laser efficiency (EFF) for the frequency selective FO CO laser as a function of the vibrational level number, V, calculated with different models: dashed curve - model I, dotted curve - model II, solid curve - model III.

Analysis of data on EBSD laser characteristics in nitrogen containing mixtures using the latest version of the kinetic model
(*Subtask 2A.1)*

Energy exchange processes in laser mixtures containing two sorts of molecular gas (CO and N_2) are much more rich than in mixtures CO:X (X is rare gas). Besides cross-exchange processes between vibrationally excited CO and N_2 molecules, interaction of electrons with N_2 molecules is much stronger than with rare gas atoms and more sensitive to vibrational excitation degree of both molecular gases. Second kind collisions of electrons with CO(v) result in redistribution of energy input between CO and N_2 (Islamov, 1984). This redistribution essentially depends on gas temperature (Treanor, 1968).

As it was noted earlier (Basov, 2002), dynamics of CO molecules on upper levels is rather sensitive to asymmetric VV' exchange processes:

$$CO(v) + N_2(u) \rightarrow CO(v\text{-}2) + N_2(u+1). \qquad (I.1.1)$$

Even at low N_2 content (≤10%) these processes play an important role, which was evidenced by results of the experiments (Basov, 2000). For the mixtures with a high percentage of N_2 commonly used in CO lasers the role of asymmetric exchange processes (I.1.1) should be even more important. Rate constants for u≤2 were calculated by (Kurnosov, 2003), (Cacciatore, 2004) in

frames of semi-classical theory of VV' exchange. Besides inter-molecular processes (I.1.1), there exist similar intra-molecular asymmetric exchange processes

$$CO(v) + CO(0) \rightarrow CO(v-2) + CO(1)\,, \qquad \text{(I.1.2)}$$

competing with (I.1.1). Rate constants for these processes are shown in **Fig. I.1.8.** as functions of high-levels vibrational numbers for two values of gas temperature.

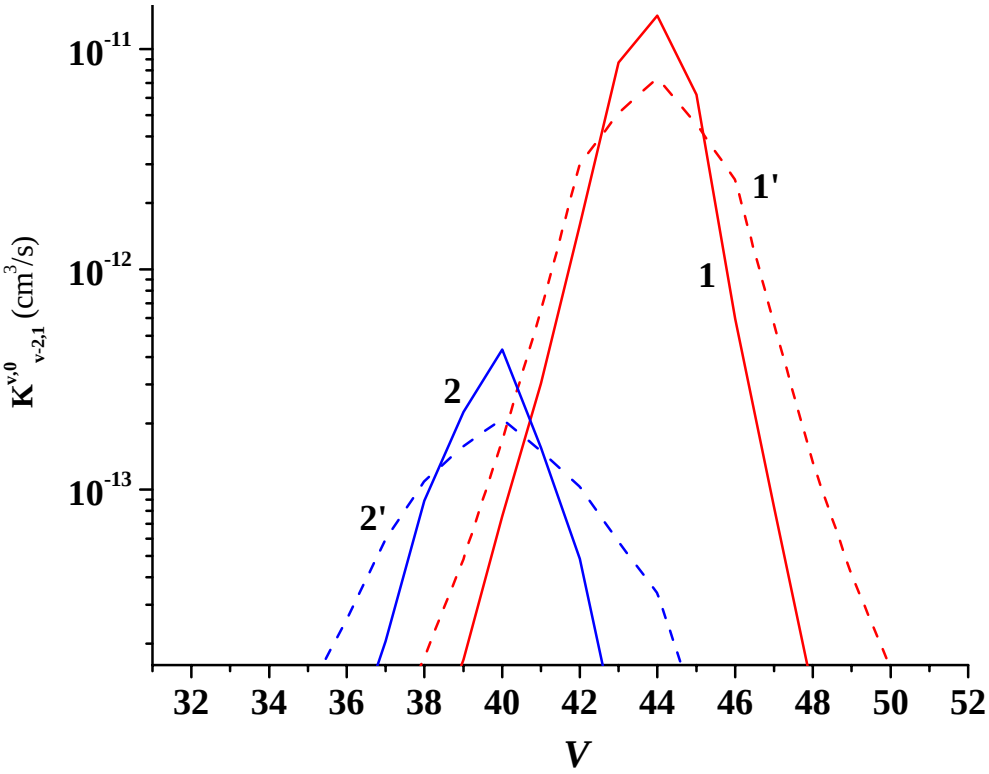

Fig. I.1.8. Rate constants of the processes CO(v)+CO(0)→CO(v-2)+CO(1) (1,1') and CO(v)+N_2(0)→CO(v-2)+N_2(1) (2, 2') vs. number **v** of vibrational level. T=100 K (1, 2) and T=300 K (1', 2') (Cacciatore, 2004).

The maximum rate of intra-molecular exchange is much faster but the resonance peak for the inter-molecular exchange processes is located at lower vibrational levels. Therefore, at [N_2]>>[CO] anharmonicity-induced vibrational quanta upward flux is, in a large degree, intercepted by energy transfer to lowest levels of N_2. Appearing in the result of such exchange N_2(v), v=1, 2 molecules share their energy with CO molecules on lower levels. However, the rate constants for such exchange at low levels are significantly smaller.

Besides, the energy defect released into gas heating is of much greater magnitude than typical anharmonicity energy. Dilution of CO:N_2 mixture by He makes dynamics of CO populations on high levels still more complicated. The point is that He atoms are much more effective in relaxation of vibrational energy than CO or N_2 molecules. It means that at some level number, v**, the rate of relaxation by He atoms is becoming comparable with the rate of VV exchange, which depends on the vibrational levels populations. At levels with v>v**, the relaxation processes are dominant resulting in abrupt fall of populations.

Then competition of these three processes (VV and VV' asymmetric exchange and VT relaxation) is rather sensitive to many parameters like gas mixture composition, pumping power, gas temperature. Let us note that near-resonance VV' exchanges between CO and N_2 at high levels is

negligible because of a very low vibrational population of N_2 molecules. This, in turn, is caused by an effective energy transfer from $N_2(v)$, v=1, 2, 3,…, 8 to CO molecules.

The kinetic model developed by us takes into account all these peculiarities appearing in three-component mixtures. In a whole, our model includes description of multi-quantum VV exchange processes with the number of quanta exchanged up to 4, asymmetric exchange between both CO and N_2 molecules, VV' exchange processes in single-quantum approximation (the last is for the lower vibrational levels), and of VT processes practically important for highly excited molecules.

Electron – molecule interactions are specified in dependence on vibrational level numbers including resonant and potential scattering processes. The respective rate coefficients are found from iterative solving electron Boltzmann equation taking into account variation of plasma parameters, vibrational levels populations, gas density (Basov, 2002), and so on.

The progress in development of the kinetic model gave us a chance to study the specific features of the vibrational kinetics in CO:He/Ar:N_2 gas mixtures for a wide range of nitrogen content (Cacciatore, 2004). In this investigation, particular emphasis was also given on the different role played by the N_2 molecules in the CO laser dynamics with respect to the vibration-translation relaxation of CO in high v levels in collisions with He or Ar atoms. This was achieved by varying the gas composition of the considered lasing mixtures.

Finally, an attention was paid to the calculations of the experimentally measurable characteristics, such as the small signal gain (SSG) and the tuning curves of CO selective laser operated in the fundamental or overtone band, particularly at high vibrational transitions.

Table I.1.1.

Parameters of the laser mixtures, laser cavity and excitation pulse, selected in the kinetic modelling.

Gas density (Amagat)	0.2
Gas temperature (K)	100
E/N (10^{-16} V cm^2)	1
Discharge pulse duration (μs)	30
Specific input energy (J/l Amagat)	200
Gain length (cm)	100
Total losses of selective laser cavity (%)	10
Output coupling (%)	5
The gas mixture CO:R:N_2 (R is inert gas)	1:4:N (N=0-20)

The parameters of the laser mixtures, laser cavity and excitation pulse, selected in the kinetic modelling are reported in **Table I.1.1**. The electric current and discharge voltage pulses were taken both as step-wise functions, while the gas density was taken constant in time. The gas mixture CO:R:N_2 was changed by varying the N_2 concentration in the range from 0% up to 80% by step of 10%.

To avoid discussions of some effects that are specific for the experiments but not necessarily appearing in a general case, we select laser parameters similar but not exactly the same as in the experiments performed and discussed in (Basov, 2002). In particular, we ignore gas dynamic expansion effects, which influence the vibrational dynamics in the late phase of the expansion equally for any gas composition under consideration. As a result of the nitrogen addition into the laser mixture, the energy loaded in the molecular vibrations is distributed among the vibrational levels of CO and N_2. This effect is illustrated in **Fig. I.1.9**, where the input energy branching ratios over the vibrational energy content of CO and N_2 achieved at the end of the discharge pulse are reported for different N_2 concentrations.

The main part of the energy deposited into the N_2 vibrations returns to the CO molecules, with some delay. Hence, one may expect that the dynamics of the CO vibrational distribution function (VDF) as whole does not strongly suffer from the changes caused by the N_2 addition.

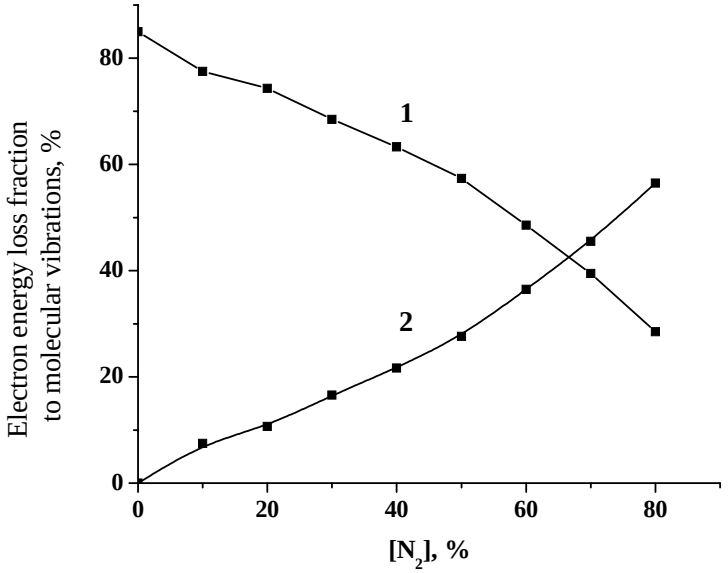

Fig. I.1.9. The calculated dependences of discharge energy branching over vibrations of CO (solid line) and N_2 (dash-dot line) versus nitrogen concentration in the mixtures CO:He:N_2=1:4:X.. The points (■) correspond to results of calculations, curves 1, 2 interpolate these results.

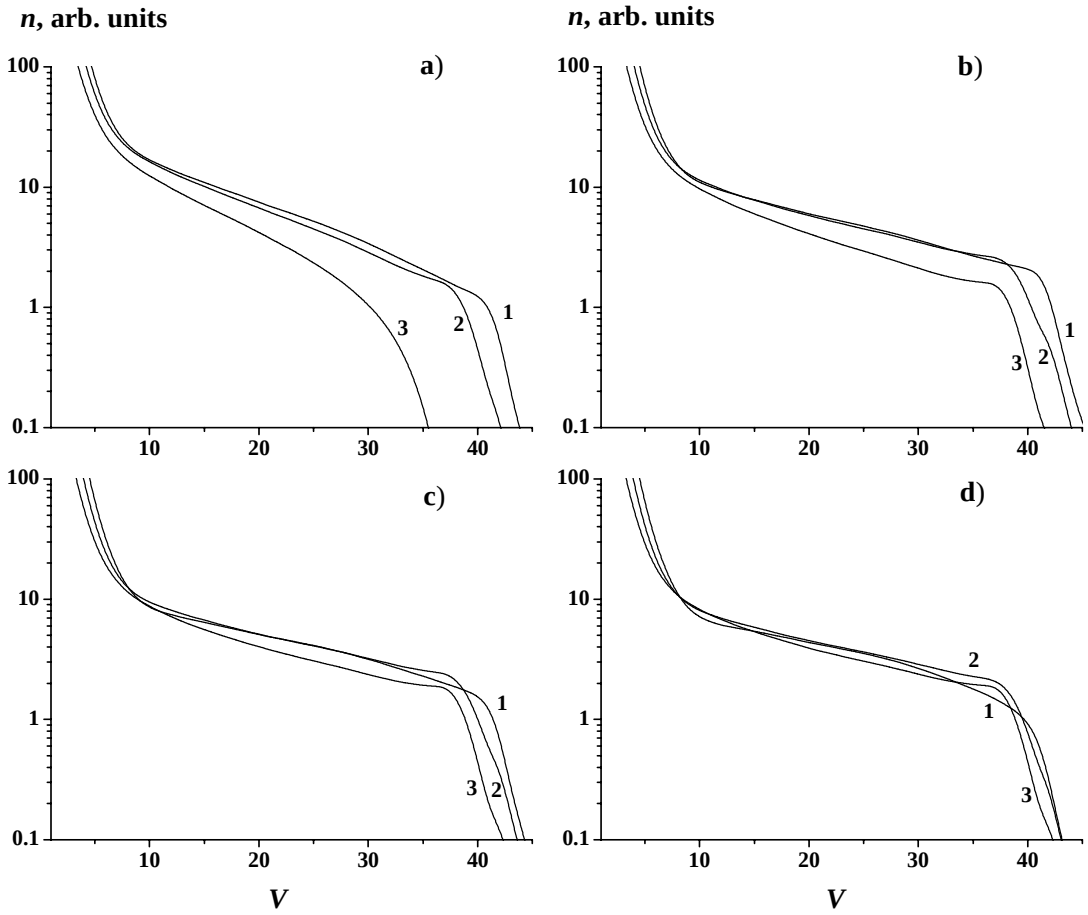

Fig. I.1.10. Computed vibrational distribution functions, VDFs vs vibrational quantum number v at different times: 100 (a), 200 (b), 300 (c) and 400 (d) μs after onset of discharge and at different N_2 concentrations 0% (1), 50% (2), 80% (3) (Cacciatore, 2004).

Indeed, this is confirmed in **Fig. I.1.10** where the time evolution of the VDF of the CO molecules in CO:He:N_2 mixtures with nitrogen concentrations equal to 0, 50 and 80% are reported at the times 100, 200, 300 and 400 μs after the discharge onset.

From the reported data, we note that for N_2 concentration lower than 80% the VDF does not change significantly with respect to the distributions obtained for pure CO. For long-term conditions (t=400 μs), the variations in the VDF's shape are not so strong at N_2 concentration 80%, too.

The most remarkable difference in the population dynamics is seen for the highest levels (v >37). Such a behaviour is explained by looking at the resonant dependences of the asymmetric V-V and V-V' exchange rate constants. Some delay in VDF evolution, particularly pronounced at 80% of N_2, is a result of the above mentioned energy redistribution between N_2 and CO vibrations followed by a relatively slow energy transfer from N_2 to CO.

The features of the VDF cause the time behavior of the SSG on high transitions of the fundamental and first overtone bands shown in **Fig. I.1.11**. In particular, the high sensitivity of the SSG dynamics to nitrogen content on extremely high transitions seems quite evident, as well as the very weak dependence of the SSG dynamics upon the N_2 concentration for transitions lower than 37→35 and 37→36. The data in **Fig. I.1.11** also show a significant slowing down of the SSG dynamics at N_2 concentration equal to 80%.

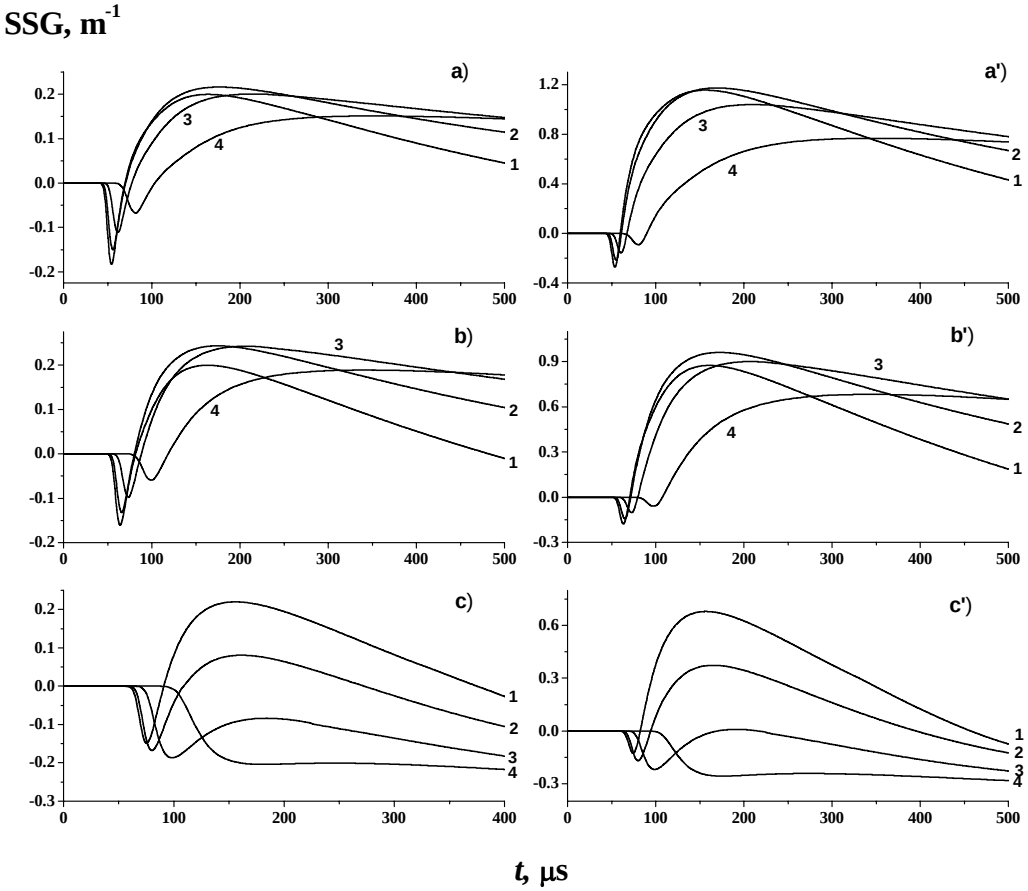

Fig. I.1.11. The SSG dynamics for the vibrational transitions 30-28 P(12) (a), 34-32 P(12) (b), 38-36 P(12) (c) and 30-29 P(12) (a'), 34-33 P(12) (b'), 38-37 P(12) (c') in the laser mixture CO:He:N_2=1:4:X, calculated at different N_2 concentration 0% (1), 30% (2), 60% (3) and 80% (4).

In **Figs.I.1.12a, I.1.12b** the tuning curves for the frequency-selective CO laser on the ro-vibrational transitions of the overtone and fundamental bands are shown. These curves exhibit some common features. Namely, with the increase of N_2 content up to 60% the laser energy for transitions

starting from 37→35, 37→36 and lower rises; for higher transitions the lasing terminates or becomes much weaker. The energy growth for transitions lower than 37→35, 37→36 is partially due to the positive role played by the asymmetric VV' exchanges which, in fact, drive part of the vibrational energy back into the lower N_2 vibrational levels. A similar effect was found for the asymmetric V-V' exchange in pure CO (Dem'yanov, 1980).

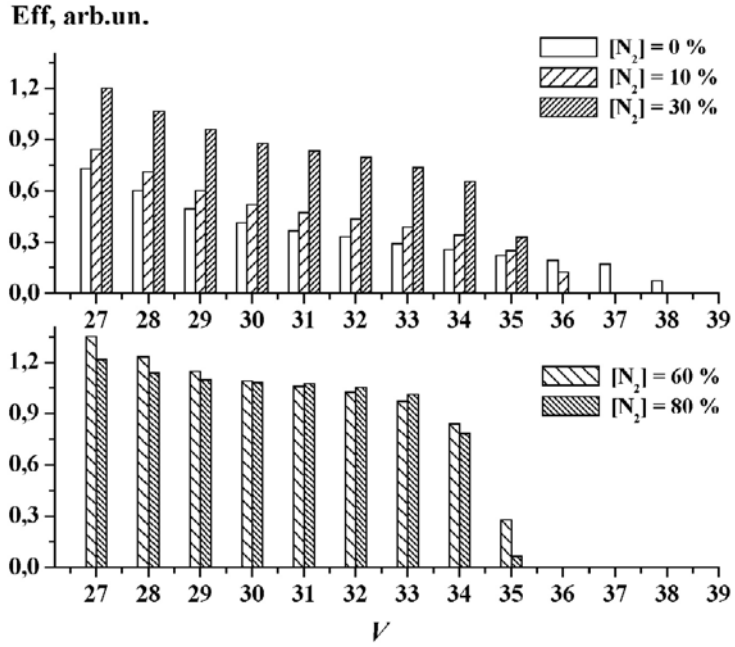

Fig. I.1.12a. Tuning curves of frequency-selective CO overtone laser vs vibrational quantum number V (V+2→V) for laser mixture

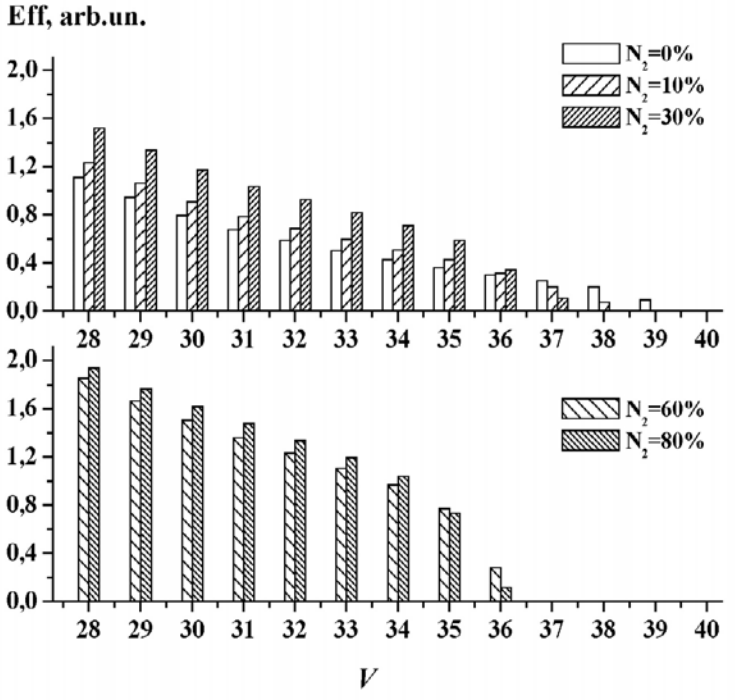

Fig. I.1.12b. Tuning curves of frequency-selective fundamental-band CO laser vs vibrational quantum number V (V+1→V) for laser mixture CO:He:N_2=1:4:X.

On the other hand, an increase of the nitrogen fraction in the CO:He:N_2 mixture results in diminishing the rate of the V-T relaxation in total, since the rate constants of the V-T relaxation in N_2-N_2 and N_2-CO collisions are much smaller than the constants for He-CO collisions. This effect also leads to the laser output energy growth. When the N_2 concentration achieves 80%, the laser energy reduction is observed. **Fig. I.1.9** shows that at N_2 concentrations higher than about 67% more than a half of the power consumed by molecular vibrations goes to excitation of N_2 vibrations. Then the energy defects lost in the V-V' exchanges between N_2 and CO are of a remarkable value. Besides, the energy stored in the N_2 vibrations becomes comparable to that transferred to CO molecules. Both these effects result in reduction of laser power seen in **Figs.I.1.12a, b**.

The influence of the V-T relaxation processes on the selective laser spectrum at the highest transitions can be illustrated by considering CO:Ar:N_2 mixture. The calculated tuning curves of the CO laser frequencies for the last mixture are shown in **Figs. I.1.13a, b**. From these figures we see that an addition of nitrogen into the mixture results in the decrease of laser energy, which is mostly pronounced at high transitions corresponding to the long-wavelength spectral range. When the N_2 concentration reaches 80% the laser energy reduction is more remarkable and takes place more uniformly on all transitions.

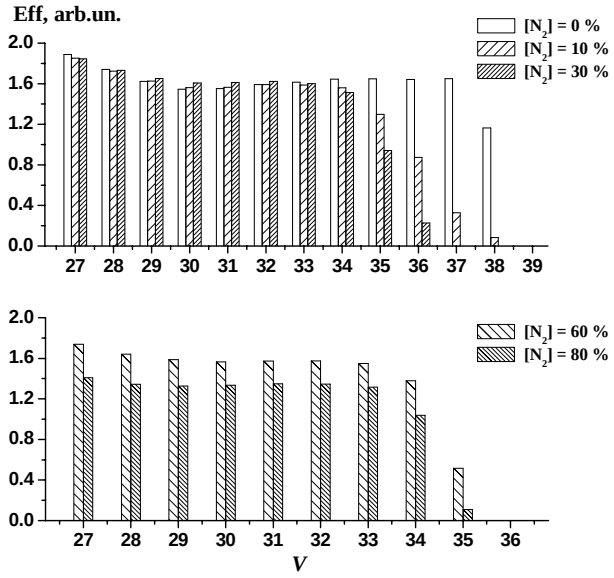

Fig. I.1.13a. Tuning curves of frequency-selective CO overtone laser vs vibrational quantum number V (V+2→V) for laser mixture CO:Ar:N_2=1:4:X.

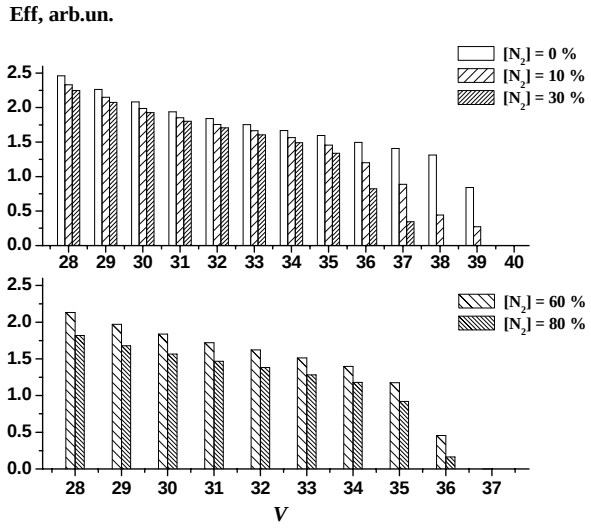

Fig. I.1.13b. Tuning curves of frequency-selective fundamental-band CO laser vs vibrational quantum number V (V+1→V) for laser mixture CO:Ar:N_2=1:4:X.

Because of the extremely slow V-T relaxation in Ar-CO/N_2 collisions we can neglect this process completely. Then the populations on highest vibrational CO levels are controlled by competitive asymmetric VV and VV' exchange processes. In the binary mixture CO:Ar as a consequence of the collisional processes (I.1.2), half of the vibrational quanta is pumped down into the lowest vibrational levels of CO. The addition of N_2 leads to appearance of the processes (I.1.1), according to which part of the vibrational quanta is gained by the CO molecules, with some energy loss due to the energy defect in single-quantum VV' exchanges between CO and N_2. This explains some not very essential reduction of laser efficiency with N_2 concentration growth. For N_2 concentrations higher than about 67% the mechanism of laser efficiency reduction is the same as for the He-based mixtures.

The SSG dynamics in mixtures CO:Ar:N_2 (**Fig. I.1.14**) is similar to the one calculated for CO:He:N_2 (**Fig. I.1.11**). It is noteworthy that the level of SSG values for v-numbers around 30 is higher for Ar-based mixtures. Besides, their variation with addition of N_2 is weaker. These facts are explained by appearance of higher vibrational populations in absence of V-T relaxation and, as a consequence, faster intra-molecular VV exchanges. Higher N_2 concentrations are required that V-V' exchanges CO-N_2 can compete with VV exchange processes.

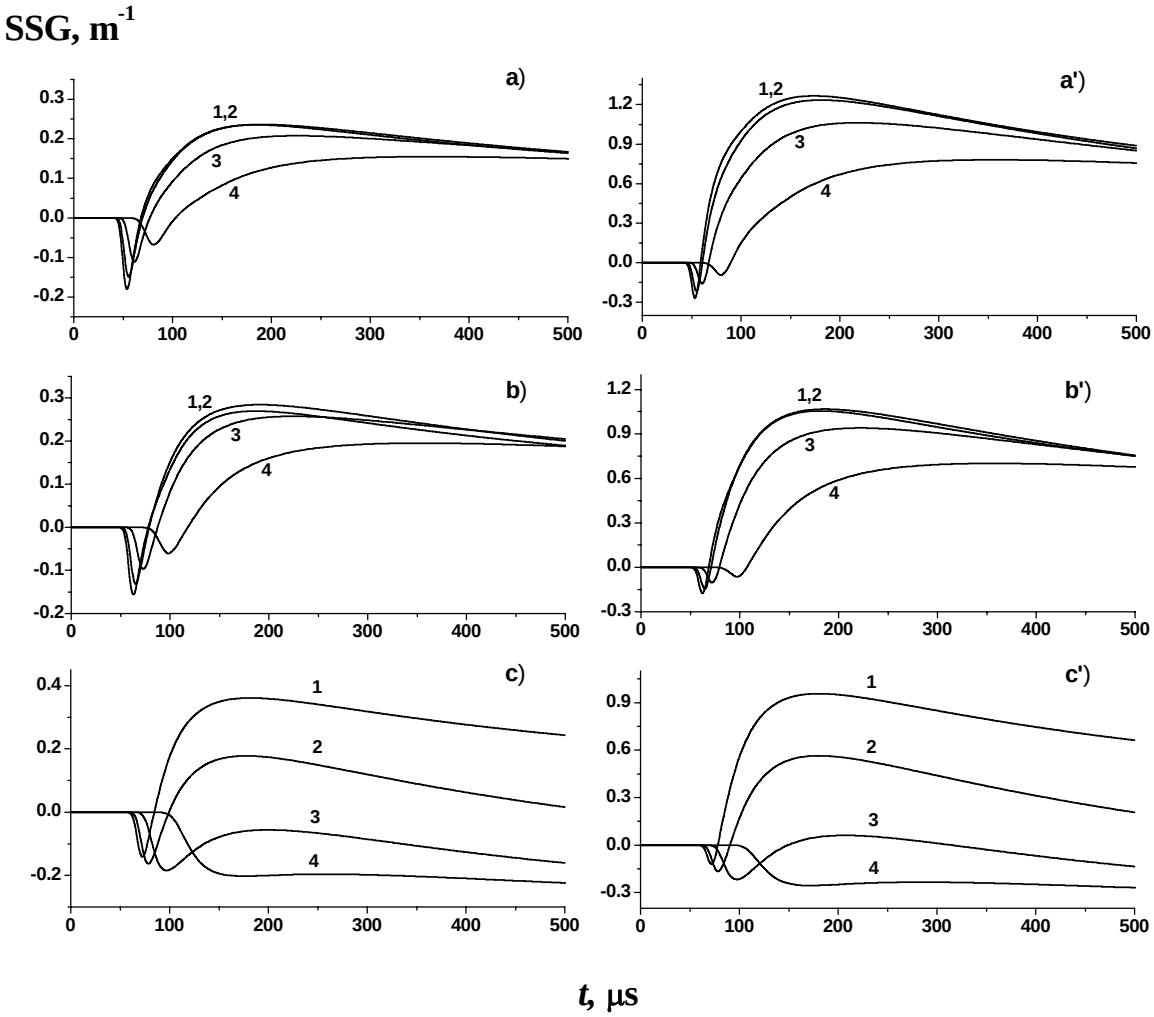

Fig. I.1.14. The SSG dynamics for the vibrational transitions 30-28 P(12) (a), 34-32 P(12) (b), 38-36 P(12) (c) and 30-29 P(12) (a'), 34-33 P(12) (b'), 38-37 P(12) (c') in the laser mixture CO:Ar:N_2=1:4:X, calculated at different N_2 concentration 0% (1), 30% (2), 60% (3) and 80% (4).

The design of a probe CO laser including overtone CO laser
(*Subtask 1A.1.*)

The design of a low-pressure DC discharge CW CO laser with slow gas flow and cryogenic cooling of the active medium was developed (**Fig.I.1.15**). Quartz tube 2 of 1 m length and 18 mm inner diameter (wall thickness 1.5 mm) is placed in polyurethane bath 1 with liquid nitrogen. The cooled part length of quartz tube is 90 cm. The ends of the tube are covered with optical-mechanical units used for arrangement of optical elements (Brewster's windows 3 made of CaF_2), discharge electrodes 4 (Tungsten) and 5 (Aluminum), and gas inlet/outlet. Electric discharge driver system is consisted of stabilized DC power supply with variable output voltage (U_{max}=25 kV, I_{max}=50 mA), ballast resistor 10 (R=800 kOhm) and discharge current and voltage meters (11 and 12 respectively). The gas system for preparing, supplying and pumping laser active medium allows us to mix up to 4 gas components (He, CO, N_2 and Air) with continuous monitoring mixture composition, flow rate and pressures. The system consists of inlet manually operating dosing valves 9, gas mixture reservoir 7, liquid nitrogen trap 6 and pressure meters 8. Gases He, CO, N_2 are put into the gas system from soft reservoirs (are not shown in **Fig.I.1.15**). Therefore pressures of these gases are equalized (~1 atm) before inlet dosing valves 9. It allows us to monitor partial pressure of the gas mixture components. Typical gas mixtures in our experiments were He:CO:N_2:Air=7.0:0.5÷1.0:0.5:0.1 at total pressure at the inlet 8-9 Torr.

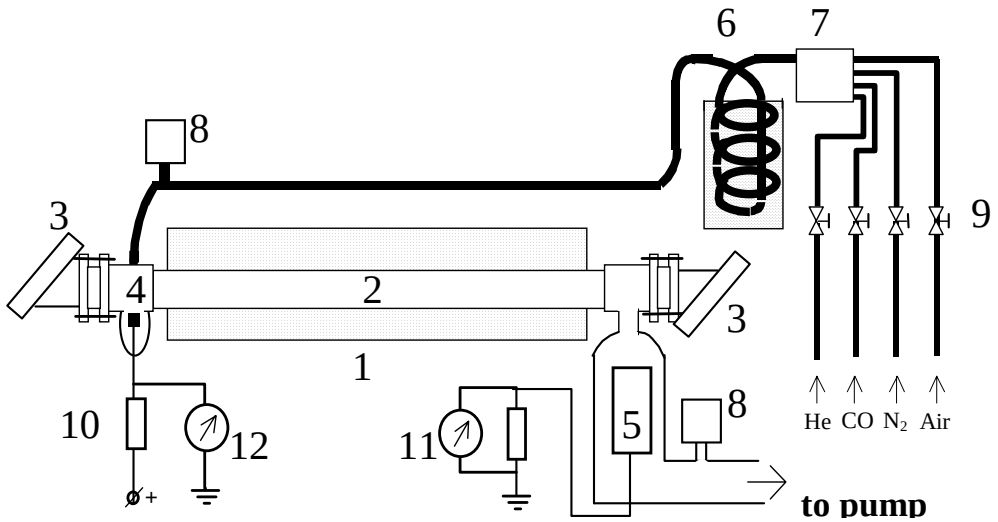

Fig.I.1.15. Design of low-pressure DC discharge CW CO laser with slow gas flow and cryogenic cooling of the active medium. 1 - Polyurethane bath with liquid nitrogen, 2 - Quartz tube, 3 - Brewster's windows made of CaF_2, 4 – Anode, 5 – Cathode, 6 - Liquid nitrogen trap, 7 - Gas mixture reservoir, 8 - Pressure meter, 9 - Inlet dosing valves, 10 - Ballast resistor, 11 - Current meter, 12 - Voltage meter.

Test experiments on measuring gas mixture temperature in the discharge tube at the characteristic pump rate were carried out in conditions of tube cooling without discharge. A thermopile sensor was introduced in the center of quartz tube cross-section located 5 cm downstream the beginning of quartz tube cooled part. This temperature was ~80 K in these experiments.

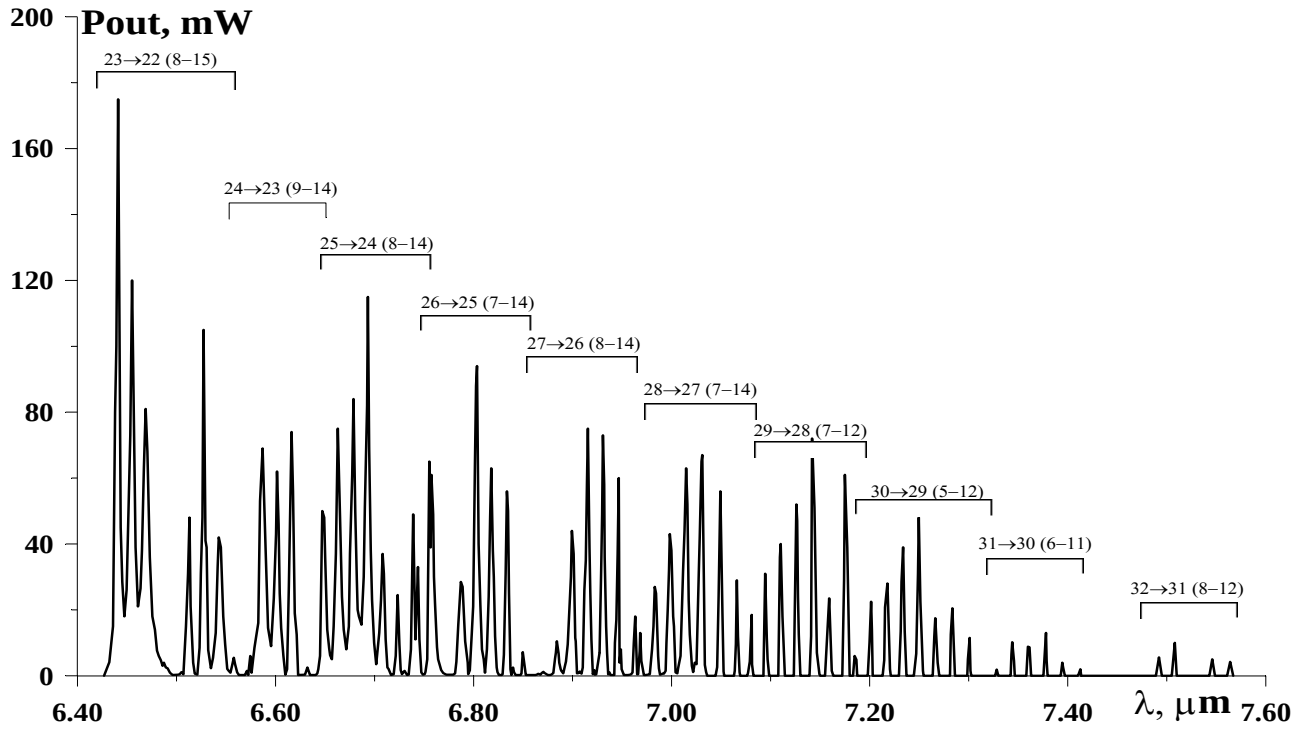

Fig.I.1.16. CW CO laser output power P_{out} as a function of a wavelength λ. Rotational number ranges are shown in brackets.

Optical elements of the laser cavity are placed on hard metallic optical rail, which is mechanically isolated from discharge tube and all possible sources of vibrations. Output power of ~30 W with efficiency of ~21% was obtained for the CO laser operating in free running multiline mode on fundamental band rotational-vibrational transitions.

The laser cavity consisted of flat output mirror (reflection coefficient R~75%) and concave total reflecting mirror (r = 5 m). The laser action on more than 200 laser lines from vibrational band 6→5 (λ~5.0 μm) to vibrational band 32→31 (λ~7.5 μm) was observed in frequency selective mode of CO laser operation with single line output power up to 1.5 W. The laser cavity in this case consisted of concave (r = 5 m) total reflecting mirror and diffraction grating (Richardson Grating Laboratory Catalog number 35-53-*-880, 150 grooves/mm, λ_{max}~6.0 μm). Laser output went out through the zero order of the diffraction grating. Output power P_{out} of CW CO laser as a function of a wavelength λ in the range of λ~6.4-7.6 μm is shown in **Fig.I.1.16**.

Another diffraction grating (Richardson Grating Laboratory Catalog number 35-53-*-820) was used to obtain frequency selective mode of CO laser operation on overtone (V→V-2) rotational-vibrational transitions.

CO lasing on three overtone vibrational bands 32→30, 33→31 and 34→32 (λ~3.68÷3.84 μm) was observed in frequency selective mode. The FO CO laser operated at single line output power up to 1 mW (**Fig.I.1.17**). The output power of ~450 mW (efficiency ~1%) for the CO laser operating on overtone band in free running multiline mode was obtained.

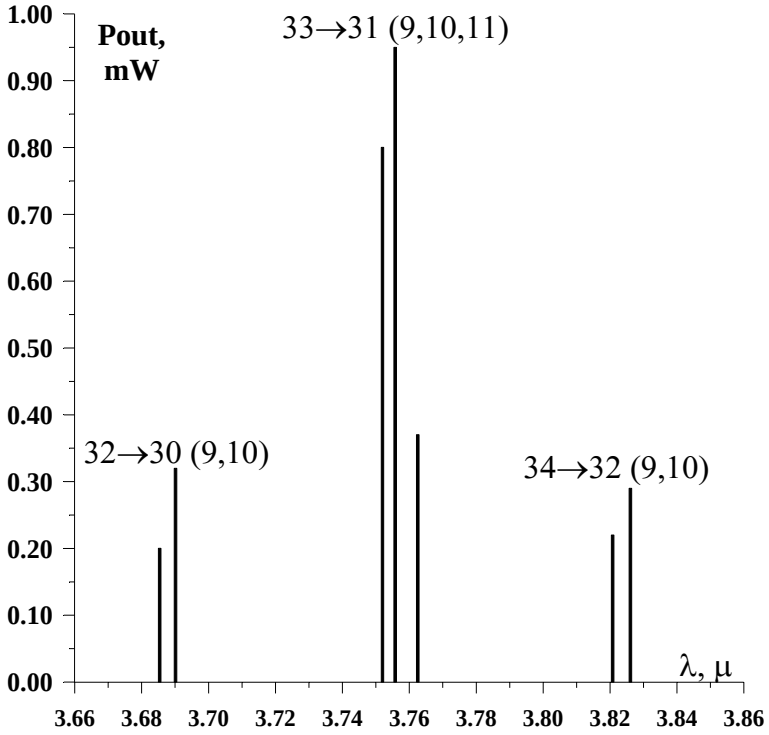

Fig.I.1.17. Single line output power of FO CO laser operating in frequency selective mode.

Experiments on SSG measurements with a probe overtone/fundamental band CO laser (*Subtask 1A.4.*)

The optical scheme developed for SSG time behavior measurements is presented in **Fig.I.1.18**.

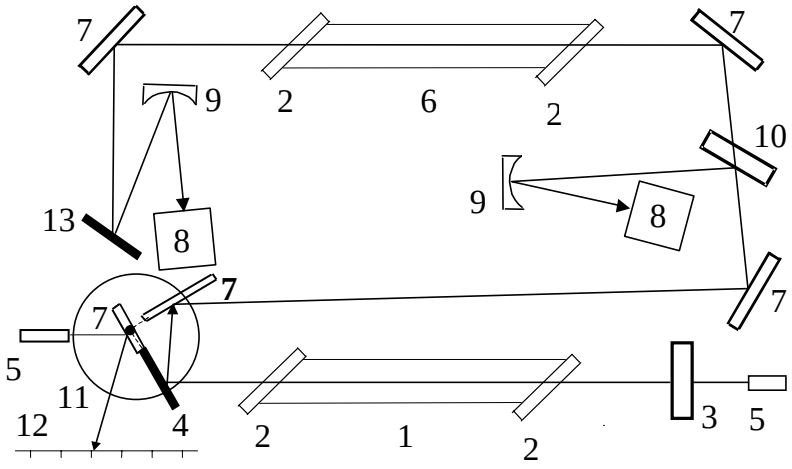

Fig.I.1.18. Optical scheme used for measuring SSG time behavior.
1 - active medium of CW CO laser,
2 - CaF_2 Brewster window,
3 - concave total reflecting mirror,
4 and 13 - diffraction grating,
5 - semiconductor laser,
6 - active medium of pulsed CO LA,
7 - flat mirror, 8 - photodetector,
9 - concave mirror,
10 - flat mirror (R=30%),
11 - rotatable mount, 12 - screen.

The radiation of the MO CO laser was splitted into two beams by flat mirror 10 (reflection coefficient R=30%). Reflected part of the laser radiation was used for controlling the constancy of the MO radiation intensity at the input of the pulsed CO LA during the time interval of SSG measurements (~2200 μs). Another part of the MO radiation was directed into the active medium (AM) of pulsed CO LA 6 by reflection from flat mirrors 7. Both laser beams were focused on photodetectors 8 (response time ~10^{-9}s) by concave mirrors 9. Two semiconductor lasers 5

(λ=650 nm) were used for alignment the optical scheme and controlling the working angle of diffraction grating 4 and CW CO laser wavelength corresponding to it. The another diffraction grating 13 was used in the experiments at high Q_{in} (more than 100 J/l Amagat) in AM of the pulsed CO LA in order to select probe beam radiation from the pretty strong spontaneous radiation taking place in the pulsed CO LA under the experimental conditions.

A typical oscillogram of the signals from the photodetectors is shown in **Fig.I.1.19**. Curves 1* and 2* correspond to radiation intensity at the input and output of the pulsed CO LA, respectively. Curves 1 and 2 correspond to absence of radiation at the photodetectors (zero level). The moment which is marked at the oscillogram as t=0 (in **Fig.I.1.19**) corresponds to the beginning of the EBSD pump pulse.

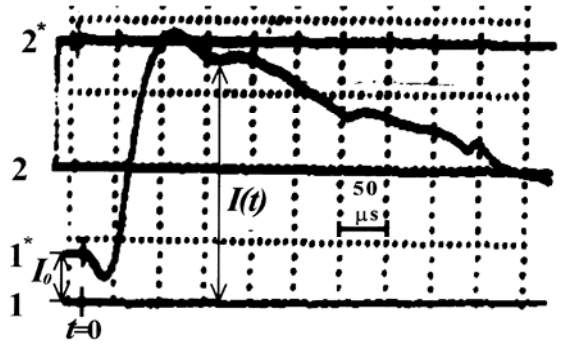

Fig.I.1.19. Typical oscillogram. Transition 8→7 P(9), Q_{in}=105 J/l Amagat.

It could be assumed that the output power of CW CO laser is constant during measuring time because signals 2 and 2* are represented as parallel lines. The intensity of MO radiation going through the AM of the LA was far less than the saturation intensity and experimental SSG time behavior can be calculated from the oscillogram by the formula:

$$G(t)=(1/l)*ln\ (I(t)/I_0),$$

where I_0 is the initial signal before the EBSD pump pulse, $I(t)$ is a signal at any next moment of time, l is the active length of the pulsed CO LA (l =1.2 m).

The SSG time behavior was measured with the optical scheme and calculated by the procedure described above for many vibrational-rotational transitions in vibrational bands from 6→5 up to 32→31 for different rotational numbers at the values of Q_{in} in the range of 70÷250 J/l Amagat. The examples of the SSG time behavior for some high vibrational-rotational transitions are shown in **Fig.I.1.20** together with experimental errors.

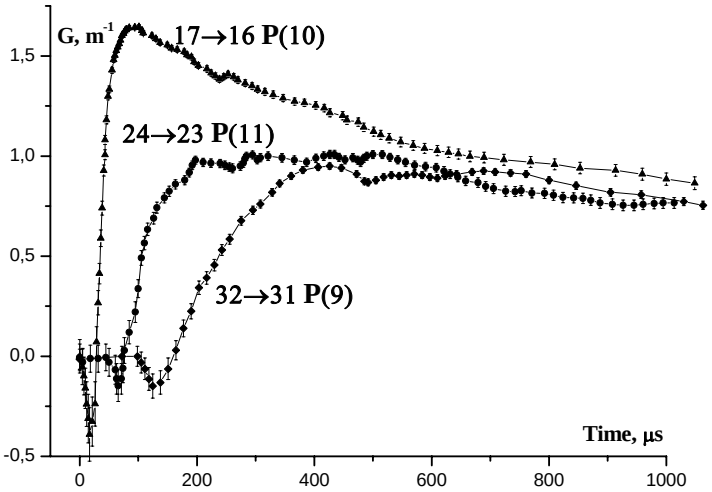

Fig.I.1.20. SSG time behavior for high vibrational-rotational transitions,
Q_{in} =250 J/(l Amagat).

In the experiments the SSG maximum value decreases with increase of vibrational number V (under the same experimental conditions including the same rotational number). One can see from **Fig.I.1.20** some subsequent moments in the SSG time behavior for each transition: a moment of the beginning of negative SSG (absorption) (τ_1), a moment corresponding to maximum of absorption (τ_2), a moment of the beginning of positive SSG (amplification) (τ_3), a moment corresponding to SSG maximum (τ_4). It should be noted that the moment t=0 corresponds to the beginning of EBSD pumping pulse of the CO LA.

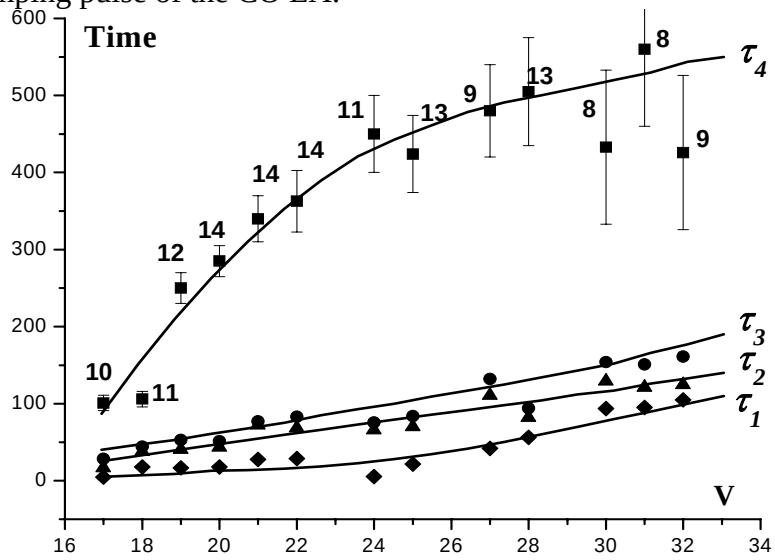

Fig.I.1.21. The dependence of characteristic moments of time (τ_1, τ_2, τ_3 and τ_4) on vibrational number V. Q_{in}=250 J/(l Amagat). Experimental errors for three low curves are within markers.

The moment τ_1 is associated with the appearance of population on the lower level of the transition. The moment τ_2 is associated with maximum of negative difference between population of the upper and lower levels of the transition. The moment τ_3 is associated with appearance of inversion population on the transition. The moment τ_4 is associated with maximum of inversion population on transition. The dependence of all these moments of time (τ_1, τ_2, τ_3 and τ_4), described above on vibrational number V is shown in **Fig. I.1.21**. The rotational numbers of the vibrational-rotational transitions are shown nearby the upper curve in **Fig.I.1.21**. All these moments of time increase with increasing vibrational number V.

Such behavior of the dependencies (**Fig.I.1.21**) is related to the process of the vibrational excitation wave propagation through vibrational levels of CO molecule due to VV-exchange. All the characteristic moments of time increase with the Q_{in} decrease for the selected vibrational-rotational transition under the same experimental conditions. The SSG maximum decreases with the Q_{in} decrease.

The examples of the SSG time behavior for vibrational-rotational transition 16→15 P(11) at different Q_{in} are shown in **Fig.I.1.22**. An analysis of the temporal behavior of SSG for high transitions of CO molecule enables us to get information about time characterizing absorption and amplification in the AM of the CO LA. Time τ_4 being from 100 up to 500 μs (gas density 0.12 Amagat) is needed for the SSG to get its maximum value. This information is very important for designing fast-flow CO lasers including a first-overtone CO laser operating on high (V>15) vibrational levels.

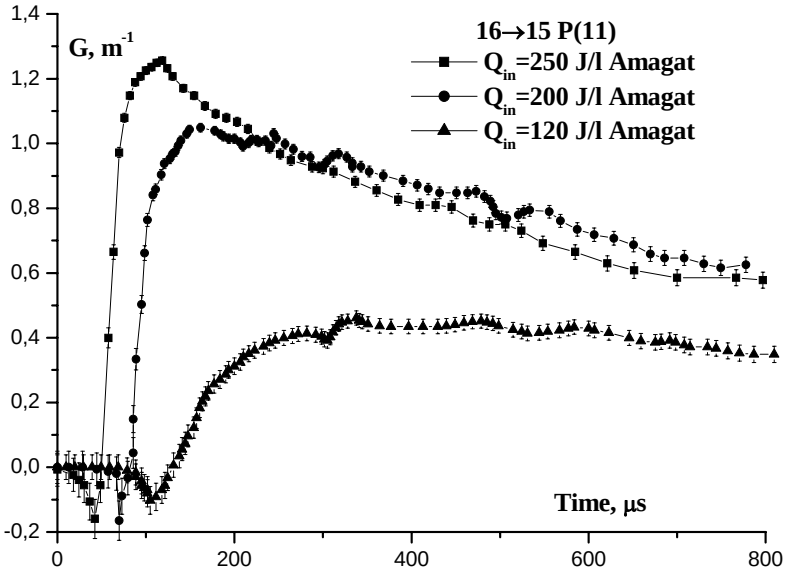

Fig.I.1.22. SSG time behavior for vibrational-rotational transition 16→15 P(11) at different Q_{in}.

The highest value of SSG obtained in our experiments came up 3.3 m^{-1} (transition 8→7 P(10), Q_{in}=250 J/l Amagat). The SSG maximum observed in the experiments for the highest and lowest transitions was 1.5 m^{-1} (transition 6→5 P(14), Q_{in}=250 J/l Amagat) and 1.2 m^{-1} (transition 32→31 P(9), Q_{in}=250 J/l Amagat), accordingly.

Experiments on influence of gas dynamics on overtone CO laser characteristics (*Subtask 1A.2.*)

Special measurements of the experimental conditions were carried out to make more exact master data for theoretical calculation of the SSG time behavior inside the FO CO laser active medium. The initial gas temperature was measured in the previous experiments (Ionin, 2001) as the gas temperature averaged on the cryogenically cooled EBSD chamber large volume (~0.2 m^3). A matrix of thermocouples was used to measure the gas temperature distribution inside the discharge region (~0.02 m^3). The matrix consisted of 24 copper-constantan thermocouples spaced 20 mm and located in one vertical plane. The thermocouple matrix can be relocated along the axis of symmetry of the discharge region (**Fig.I.1.23**).

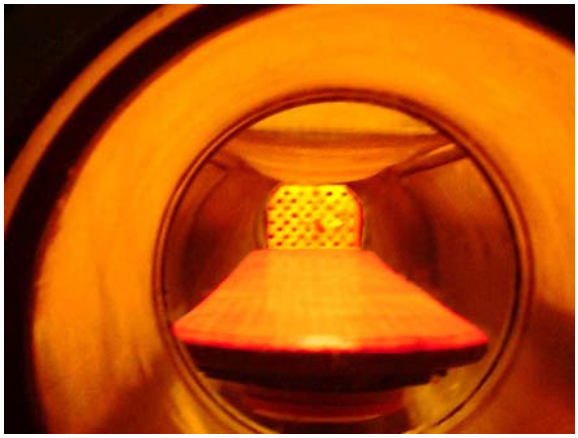

Fig.I.1.23. The picture of the EBSD chamber with the thermocouple matrix (11x9 cm^2) located near the rear edge of the discharge region. One can see the bottom copper electrode (anode) and the upper mesh electrode (cathode).

The gas temperature was measured relatively the temperature of liquid nitrogen (77 K). The results of the measurements are presented in **Fig.I.1.24**. The measured temperature increased with altitude (**Fig.I.1.24a**) from ~100 K near the bottom electrode up to ~135 K near the upper "hot" electrode. The temperature near the "cold" bottom electrode appeared to be equal to the mean value of the gas temperature inside the EBSD chamber. The gas density decreased correspondingly from 0.12 down to ~0.09 Amagat. The gas temperature was much more uniform on horizontal plane (**Fig.I.1.24b**).

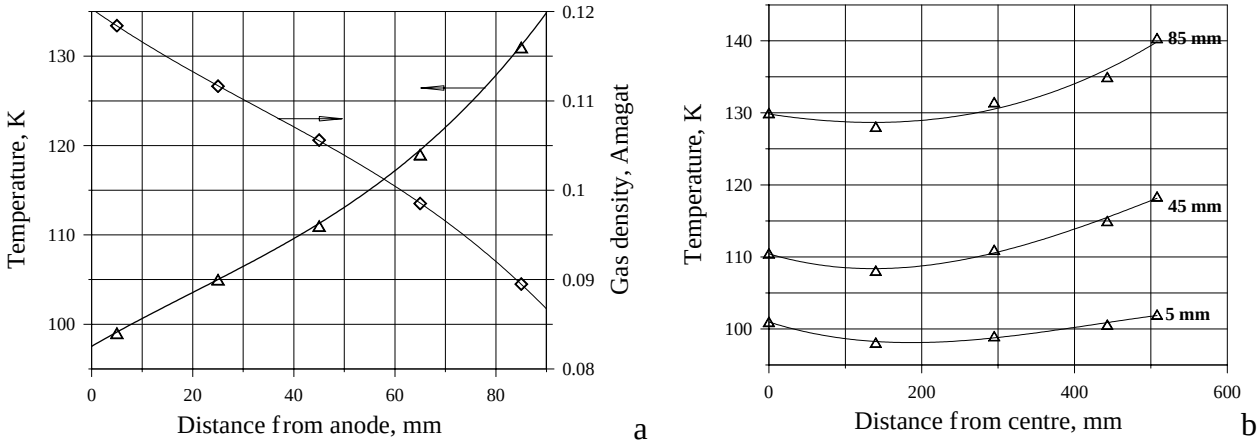

Fig.I.1.24. The temperature of the gas mixture CO:He=1:4; (a) - versus the distance from the bottom electrode at the center of the EBSD region (the local gas density is indicated at the right axis); (b) - versus the distance from the center of the EBSD region at the altitudes 5, 45 and 85 mm. The mean values of the gas temperature and gas density were 100 K and 0.12 Amagat.

The acoustic detector with sensitivity 1.3 mV/Pa was used to measure acoustic pressure after the EBSD discharge. The detector was located inside the EBSD chamber near the output optical window. The measured acoustic pressure increased linearly with the increase of specific input energy Q_{in} from 40 up to 300 J/l/Amagat (**Fig.I.1.25**).

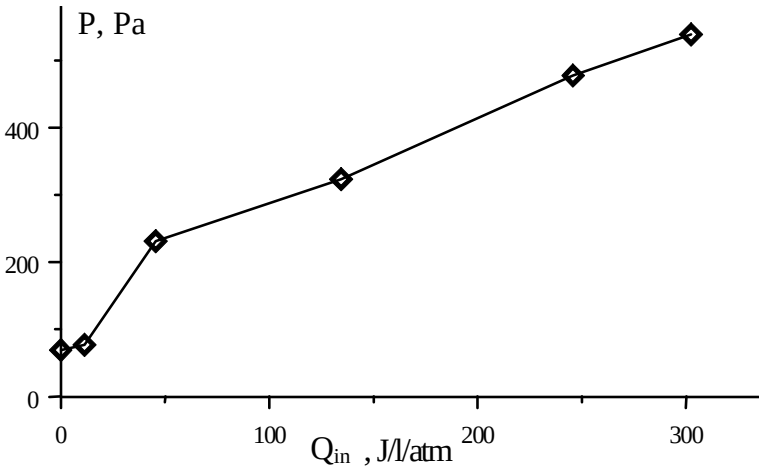

Fig.I.1.25. Acoustic pressure P after discharge versus specific input energy (Q_{in}).

The characteristics of the EBSD: current pulse duration ~0.1 ms; gas – N_2 at the initial pressure 0.2 atm; initial gas temperature ~300 K. It should be noted that the point in which Q_{in} equals to zero corresponds to the electron beam excitation only.

To make the model more adequate to the experimental conditions, the gas density variation induced by the gas-dynamic expansion caused by heating in discharge and also in VV exchange and

VT relaxation processes was taken into account. The estimates showed that in the experiments gas density is approximately uniform for several tens of microseconds after the onset of pumping. The gas expansion at later stage proceeds at constant pressure due to the large buffer volume (~0.2 m^3). The density variation of the active medium in this case is approximately taken into account within the framework of the uniform model, because the laser beam aperture in experiments amounted to only a small fraction of the discharge cross section area. The density variations of the active medium affect the vibrational dynamics and hence the SSG time behavior. We described the time dependence of the active-medium density *N(t)* by the approximate expression:

$$N(t) = N_0 \exp\left(\frac{t}{\tau}\right) + N_0 \frac{T_0}{T}\left[1 - \exp\left(-\frac{t}{\tau}\right)\right],$$

which simulates a transition to the isobaric regime. Here N_0 and T_0 are the initial density and temperature of the active medium; $\tau = \Delta r / v_s$; Δr is the characteristic transverse dimension of the active medium; v_s is the sound velocity. A similar approach was earlier employed in (Akishev, 1982). The translational temperature of the active medium in this case was calculated from the equation $\frac{dT}{dt} = \frac{W}{N \cdot C_v} + \frac{kT}{N \cdot C_v} \cdot \frac{dN}{dt}$, where W is the power density of heat release due to direct heating and vibrational relaxation; C_v is the heat capacity of the active medium and the k is the Boltzmann constant. The density variation of the active medium was accordingly taken into account in the solution of kinetic equations for vibrational populations, as well. The SSG time behavior on overtone transition 26→24P(12) calculated both in framework of constant density approximation and with approximation described above is illustrated in **Fig.I.1.26**.

It can be seen, that the more realistic model taking into account the gas-dynamic expansion leads to the sizeable effect, namely to slower decrease of SSG with time, only at the later stage of energy exchange. The role of this factor is greater if the specific input energy is enlarged.

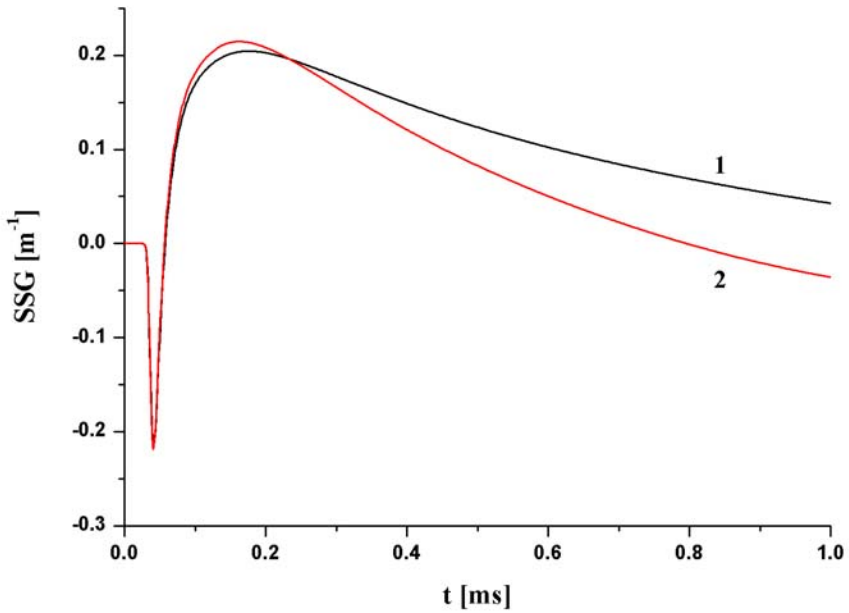

Fig.I.1.26. The SSG time behavior calculated for the transition 26→24P(12). 1 - gas expansion is taken into account; 2 - the calculations are made with constant density approximation; T_0=110 K, N_0=0.18 Amagat, Q_{in}=200 J/l Amagat

EBSD laser at experimental conditions (gas pressure, temperature) of supersonic CO laser (*Subtask 1A.2.*)

Experimental study of the EBSD CO laser at the experimental conditions (gas pressure and temperature) of the supersonic CO laser was carried out. Frequency selective laser resonator consisted of a rear spherical mirror and the diffraction grating (200 groves/mm, λ_{max}=3.2 μm) installed in the Littrow scheme. Laser output was detected through the zero-order of the diffraction grating by cryogenically cooled Ge-Au photodetector. Two gas mixtures CO:He=1:4 (regular mixture for the EBSD CO laser) and CO:He=1:7 (regular mixture for the supersonic CO laser) at gas temperature of ~100 K were tested.

In the supersonic CO laser the regular gas pressure is about 5-10 Torr at gas temperature ~100 K that corresponds to rather low gas density of 0.02-0.04 Amagat. One of the most important characteristics of the active medium is the time interval needed for the SSG to reach a lasing threshold value. In the pulsed EBSD CO laser the interval was named a time delay (time interval between the beginnings of pump and lasing pulse). Experimentally obtained dependencies of the time delay on gas density for three laser transitions (27→25, 31→29 and 35→33) are presented in **Fig.I.1.27**.

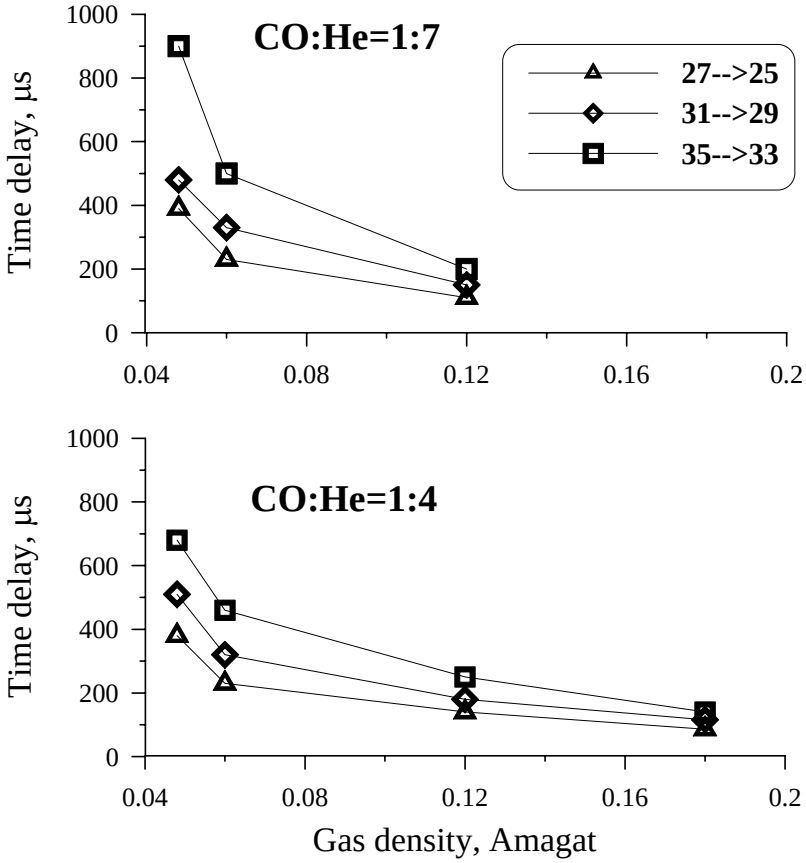

Fig.I.1.27. Dependencies of laser pulse time delay on gas density for the different laser transitions (27→25, 31→29 and 35→33) at the different gas ratio CO:He of 1:7 and 1:4. Q_{in} was ~250 J/(l Amagat).

Depending on the grating reflection, the lasing threshold values of the SSG were about 0.06, 0.07 and 0.08 m^{-1} for the laser transitions 27→25, 31→29 and 35→33, correspondingly. The time delay slowly increased with gas density decreasing down to ~0.06 Amagat. There was fast growing time delay with further density decreasing. It should be noted that there is no lasing at gas density lower than 0.048 Amagat (~13 Torr at 100 K) at all. The fact seems to be related to changing a mechanism of spectral line broadening from pressure broadening to Doppler one and corresponding

to the SSG decrease with gas density decreasing. The time delay of lasing on high vibrational transition 35→33 reached up to ~900 μs at gas density of 0.048 Amagat for gas mixture CO:He=1:7.

To study main specific features of the cryogenic FO CO laser with low density of active medium (typical for the supersonic laser with RF discharge excitation) we simulated numerically the SSG time behavior of the pulsed FO CO laser at low gas density. The calculations were carried out for the gas mixtures CO:He=1:4 and CO:He=1:7. The gas density was varied in the interval 0.024÷0.18 Amagat; the specific input energy values of 100, 150, 200, and 250 J/(l Amagat) were used in calculations. Typical overtone SSG time behavior calculated for the transitions 26→24P(12), 29→27P(12), 33→31P(12), 36→34P(12) at the 'intermediate' specific input energy 150 J/(l Amagat) is presented in **Fig.I.1.28**.

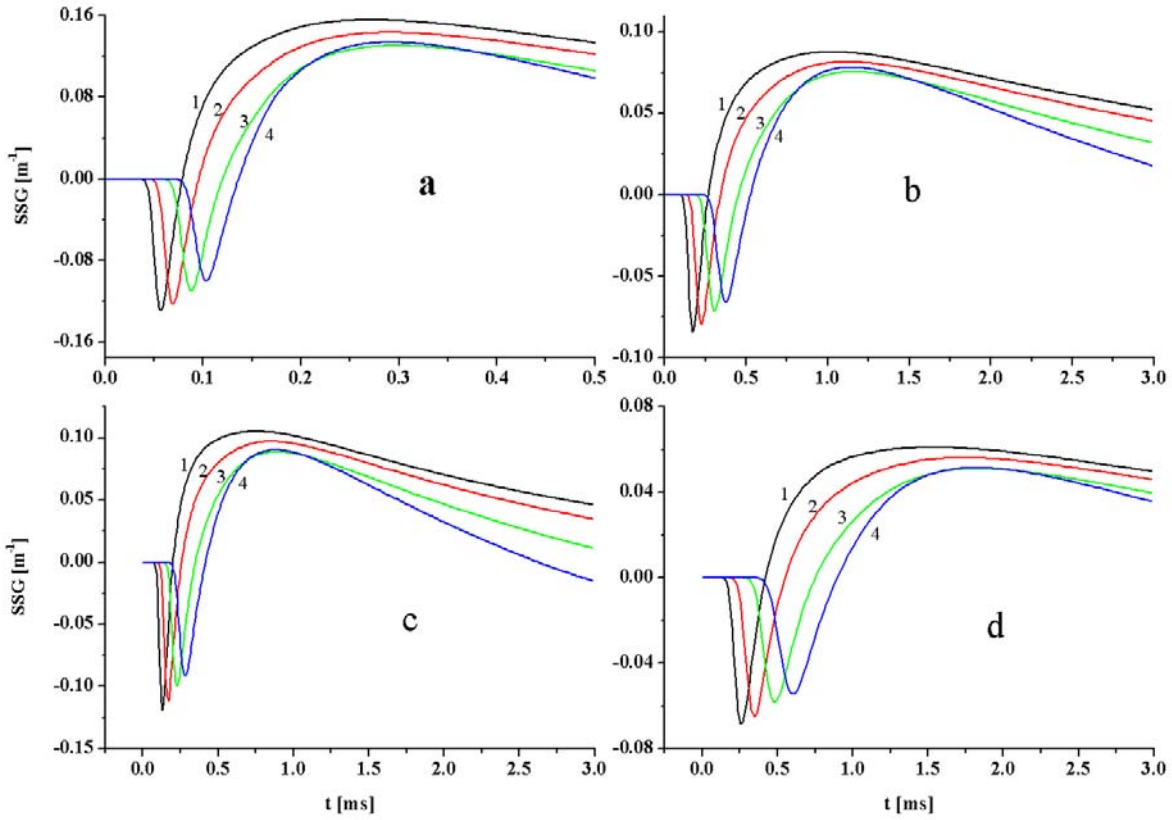

Fig.I.1.28. The SSG time behavior on high overtone transitions calculated for different gas densities and mixtures. **a** - CO:He=1:4, N=0.18 Amagat; **b** - CO:He=1:4, N=0.048 Amagat; **c** - CO:He=1:7, N=0.048 Amagat; d - CO:He=1:7, N=0.024 Amagat. T_0=110 K, Q_{in} = 150 J/(l Amagat). Curves 1, 2, 3, 4 – correspond to transitions 26→24P(12), 29→27P(12), 33→31P(12), 36→34P(12).

These results demonstrate two main particular features of the SSG time behavior typical for gas mixture of low density: relatively low gain coefficients and their slow evolution. The drop of the gain coefficients is explained by the change of the line broadening mechanism. For active media density 0.18 Amagat the collisional line broadening is dominant. In this case, the gain coefficient really does not depend on the gas density for fixed specific input energy, gas temperature and active medium composition. For the gas density ≤0.024 Amagat the Doppler broadening plays the dominant role, and the gain is approximately proportional to the gas density. For the density 0.048

Amagat both mechanisms of line broadening are comparable. In the conditions corresponding to **Fig.I.1.28b**, the ratio of collisional and Doppler widths for the transition 26→24P(12) (λ=3.341 μm) at the time moment 1 ms is ≈1:2. Slow evolution of SSG at low gas densities (see **Fig.I.1.28b, c, d**) is explained evidently by proportionality of VV pumping rate to squared gas density.

Experiments on gas temperature and density temporal behaviour including experimental conditions for supersonic CO laser
(Subtasks 2A.1)

Gas temperature, pressure and density are molecular parameters controlling the kinetics of electric discharge inside molecular gases because collision rates are strongly dependent on the values of the parameters. It is known that the gas temperature in electric discharge is difficult to measure *in situ*. Nevertheless, the time behavior of gas temperature, density and pressure in electron beam sustained discharge (EBSD) CO laser medium was measured in our experiments under different experimental conditions including condition typical for supersonic CO laser.

In order to measure gas temperature in electric discharge we used the fact that the gas temperature is equal to rotational temperature of molecular excited states. Therefore, special attention was paid to the analysis of the rotational distribution of the excited states of CO molecule. The time behavior of SSG was measured with low-pressure CW CO laser, which was used as a frequency selective probe laser. Optical scheme and procedure of SSG measurement were described above. As a first stage of our experiments we selected those spectral lines, which correspond to the same vibrational band of CO molecule and lie separately at a long distance in spectrum from adjacent spectral lines. One can see the measured time behavior of SSG in **Fig.I.1.29a** for spectral lines P(11), P(14), P(13) and P(18) corresponding to highly excited vibrational transition 19→18 under experimental condition modeling supersonic CO laser: gas mixture CO:He=1:4 at low gas density 0.04 Amagat. These experimental data were processed to reconstruct the time history of gas temperature and density presented in **Fig.I.1.29b**. The applied procedure (Basov, 1983) is the solution of a system of equations for SSG as a function of gas temperature (Patel, 1966).

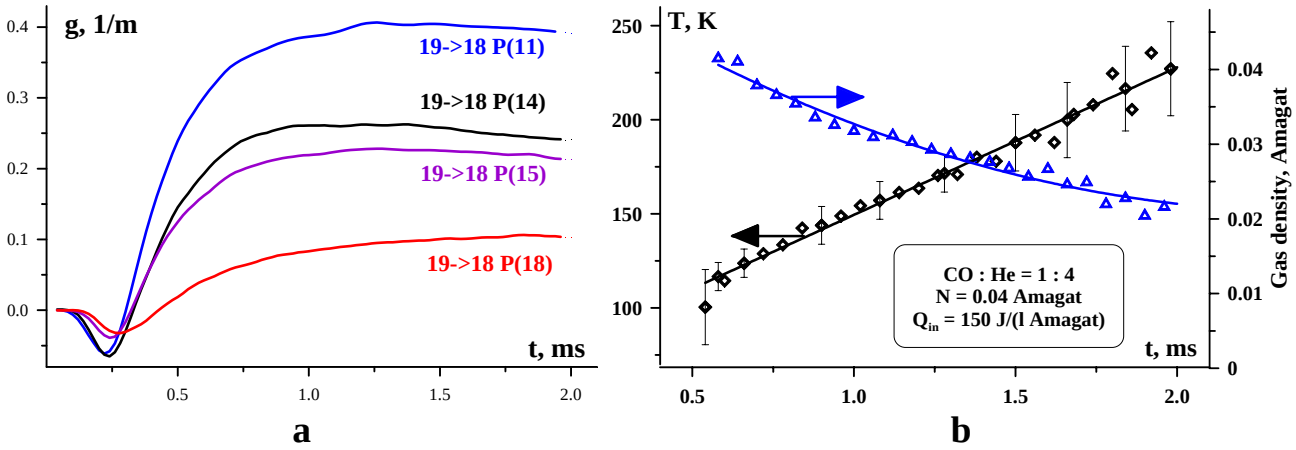

Fig. I.1.29. Time behavior of small signal gain g (a) and gas temperature T (b) in EBSD CO laser medium at the specific input energy Q_{in}=150 J/(l Amagat), gas density 0.04 Amagat, initial gas temperature 110 K.

The same procedure was used to reconstruct gas temperature in nitrogen containing gas mixture CO:N_2=1:9 at gas density 0.12 Amagat for the Q_{in} = 430 J/l·Amagat. In **Fig.I.1.30a** one can see time behavior of SSG for ro-vibrational transitions 14→13 P(8), P(10) and P(13). The reconstructed time history of the gas temperature is presented in **Fig.I.1.30b**.

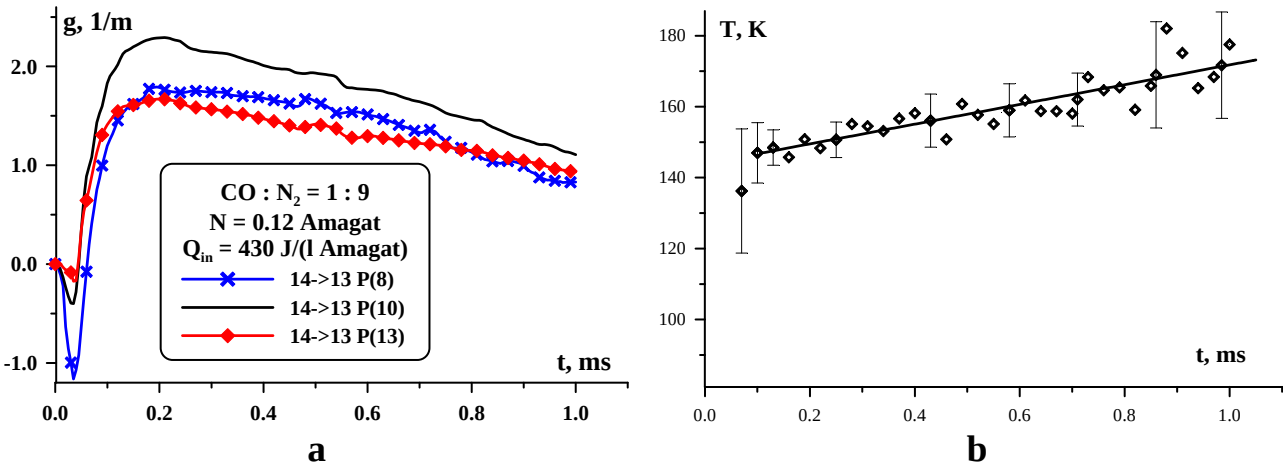

Fig. I.1.30. Time behavior of small signal gain g (a) and gas temperature T (b) in EBSD CO laser medium at the specific input energy Q_{in}= 430 J/(l·Amagat). Gas density 0.12 Amagat, initial gas temperature 120 K.

Gas pressure was measured with magnetic induction detector at the voltage sensitivity 4.1 Pa/mV and frequency band 0-5 kHz. The time behavior of gas pressure in EBSD pumped (specific input energy Q_{in}=260 J/l·Amagat, pulse duration 30 μs) CO laser gas mixture CO:He=1:4 at the gas density N = 0.12 Amagat with initial gas temperature T_0 = 165 K is presented in **Fig. I.1.31**. The rise time of gas pressure inside EBSD chamber was 13 ± 2 ms, ΔP = 0.81 kPa = 0.11 P_0, $\Delta T = T_0 \Delta P/P_0 \approx 18$ K. Taking into account the relationship between volume of gas pumped in EBSD and total volume of the EBSD chamber being of 0.11 the increase of gas temperature in EBSD could be about 160 K without gas-dynamic expansion.

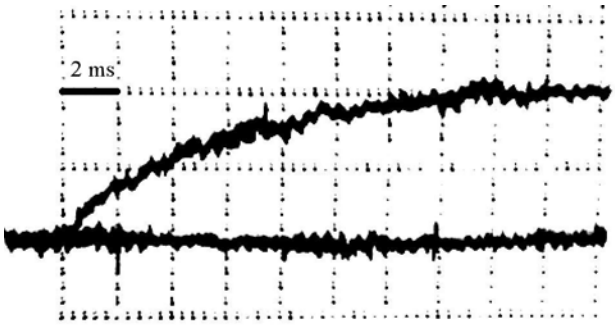

Fig.I.1.31. Time behavior of gas pressure in EBSD pumped CO laser gas mixture CO:He=1:4. N = 0.12 Amagat, T_0 = 165 K, specific input energy Q_{in}=260 J/l·Amagat.

Gas temperature is a very important thermodynamic parameter for CO laser because collision rates and, hence, kinetics in such laser medium strongly depend on this parameter. The approach of gas temperature reconstruction through measurement of SSG for three rotational transitions belonging to one vibrational band (Basov, 1983) was used for our preliminary study. However, accuracy of 10% typical for SSG measurement results in high (~200 K) error of gas temperature definition at this reconstruction approach (Vjazovetski, 1988; Didukov, 1989). The error could be diminished with an increase of the number of involved ro-vibrational transitions because reconstruction of gas temperature is a search of theoretical (bell-shaped) curve, which is the best-fit curve for measured values of SSG. This method requires careful selection of ro-vibrational transitions: 1) each transition must be exactly identified because an overlapping with other transition results in an error increase; 2) SSG value should be measured with as high as possible accuracy for each transition. Our analysis showed up that the number of ro-vibrational transitions met these requirements seldom exceeds three per each vibrational band for the available probe CO laser. Therefore, we selected ten transitions from three adjacent vibrational bands for our study on gas

temperature temporal behavior inside active medium of pulsed EBSD CO laser. Gas temperature was reconstructed due to minimization of the following residual function:

$$F(T,\mathbf{N}) = \sum_{V,J}\left(\frac{\alpha_{V,J}^{Theory}(T,N_V,N_{V+1}) - \alpha_{V,J}^{Exp}(t)}{\sigma_{V,J}^{Exp}(t)}\right)^2, \qquad \text{(I.1.3)}$$

where **N** is a matrix of populations of lower N_V and upper N_{V+1} vibrational levels, α^{Theory} – theoretically calculated SSG, $\alpha^{Exp}(t)$ – value of measured SSG for time moment t, $\sigma^{Exp}(t)$ - standard deviation of experimental data (this factor is absent in (Vjazovetski, 1988; Didukov, 1989)).

For our study on gas temperature temporal behavior we analyzed a location of ~5000 spectral lines corresponding to ro-vibrational transitions (P- and R-branches) for natural mixture of isotopes: $^{12}C^{16}O$ (most abundant isotope $y_1 \approx 0.987$) and $^{13}C^{16}O$ ($y_2 \approx 0.011$) (Guelachvili, 1983), in order to avoid any overlapping of selected spectral lines. From 700 $^{12}C^{16}O$ laser P-branch transitions $V+1 \rightarrow V$ ($J-1 \rightarrow J$), where $V=2\div36$ and $J=4\div23$, we revealed 250 transitions (7±3 per each vibrational band). Chosen spectral lines were spaced from adjacent spectral lines by more than 0.2 y_n cm^{-1} taking into account abundance y_n (n=1 or 2) of isotope which transition corresponds to the adjacent spectral line. (The number of selected lines falls to 130 when increasing criterion of selection to 0.3 y_n cm^{-1}.) The full width at half maximum of CO laser spectral lines is about 0.1 cm^{-1} Amagat^{-1} depending on gas mixture, density, temperature and rotational number that was taken into account for calculation of α^{Theory}. Then we compared the set of revealed lines with the spectral characteristics of our probe CO laser (~200 spectral lines, $V=5\div31$). This comparison showed that the number of CO laser spectral lines suitable for reconstruction of gas temperature seldom exceeds three per each vibrational band. Nevertheless, an error of temperature reconstruction could be diminished when involving ro-vibrational spectral lines belonging to different vibrational bands (Vjazovetski, 1988; Didukov, 1989). An increase of the number m of unknown populations N_V for chosen vibrational bands should be taken into account in this case (for one vibrational band $m=2$). The number of unknown quantities increases by two (m+2) per one added vibrational band and only for adjacent vibrational band the number increases by one (m+1) due to the fact that upper vibrational level of one ro-vibrational transition coincides with lower level of another transition. Our analysis showed that 13 spectral lines belonging to adjacent vibrational bands with $V=12\div14$ are suitable for our experiments. But three of them with high rotational numbers ($J=17$ and 18) were rejected during the experiment because CO lasing on these lines in probe laser was accompanied by simultaneous non-removable lasing on other stronger lines from higher vibrational bands. Finally, we selected ten spectral lines from three sequential vibrational bands: **13→12** P(9), P(13), P(15); **14→13** P(8), P(10), P(13), P(14); **15→14** P(10), P(14), P(16). For each selected spectral line the value $\alpha^{Exp}(t)$ of SSG was measured several (9-12) times in order to remove random errors and to evaluate standard deviation $\sigma^{Exp}(t)$. For CO:N_2 and CO:He laser mixtures the mean value $<\sigma^{Exp}(t)>$ was from 0.02 to 0.06 m^{-1} (as a rule lower value of deviation corresponds to higher SSG value). The measurement of $\alpha^{Exp}(t)$ and the evaluation of $\sigma^{Exp}(t)$ were carried out for two temporal intervals 0-200 μs and 0-1000 μs (t = 0 corresponded to a beginning of EBSD pulse).

Gas temperature $T(t)$ and vibrational populations $\mathbf{N}(t)$ were reconstructed through minimization of residual function (I.1.3) with two different procedures. One of them was an application of steepest descent method for the multidimensional function $F(T, \mathbf{N})$. Another procedure being an iterative technique searched a minimum for single parametric function $F(T, \mathbf{N}(T))$, where populations $\mathbf{N}(T)$ reducing to a minimum of residual function were calculated analytically due to linear dependence of α^{Theory} (Patel, 1966) on vibrational populations N_V and N_{V+1}. It should be noted that minimization procedure described in (Vjazovetski, 1988; Didukov, 1989) could be applied only for CW mode of laser medium excitation. Both applied procedures were

calibrated by reconstruction of gas temperature from modeling SSG data, which were simulated with kinetic model, and gave close results for real experimental data. A decision of some problems connected with data processing at the temperature reconstruction (absence or excess of solutions, occurrence of negative values for temperature and populations) was discussed in (Vjazovetski, 1988; Didukov, 1989).

The reconstructed time behavior of gas temperature is presented in **Fig.I.1.32** for nitrogen (**a**) and helium (**b**) based gas mixtures. In order to evaluate an error of such reconstruction we calculated a set of temperatures (25 values) for random SSG values $\alpha_{V,J}$ having the normal distribution with mean $\alpha^{Exp}_{V,J}$ and standard deviation $\sigma^{Exp}_{V,J}$. The mean value of temperature and the square root of the unbiased sample variance (~5 K average value for pulse duration) of this temperature are presented in **Fig. I.1.32** in the form of the dots and error bars respectively. During the first ~100 μs after beginning of EBSD the gas temperature grew up to (155±6) K (**a**) and (150±4) K (**b**). Then it was staying near this value for a long time (up to 1 ms). Taking into account the specific heat capacity at constant volume for these gas mixtures being ~0.94 J/(l·Amagat·K) for CO:N_2=1:9 and ~0.64 J/(l·Amagat·K) for CO:He=1:4, one can conclude that the Joule heating fraction of input energy was ~17% for nitrogen and ~10% for helium based gas mixtures. The temperature rise time (from 0.1 to 0.9 levels) being ~10 μs for nitrogen and ~20 μs for helium based mixtures should be measured more carefully because of high errors near the temperature pulse edge.

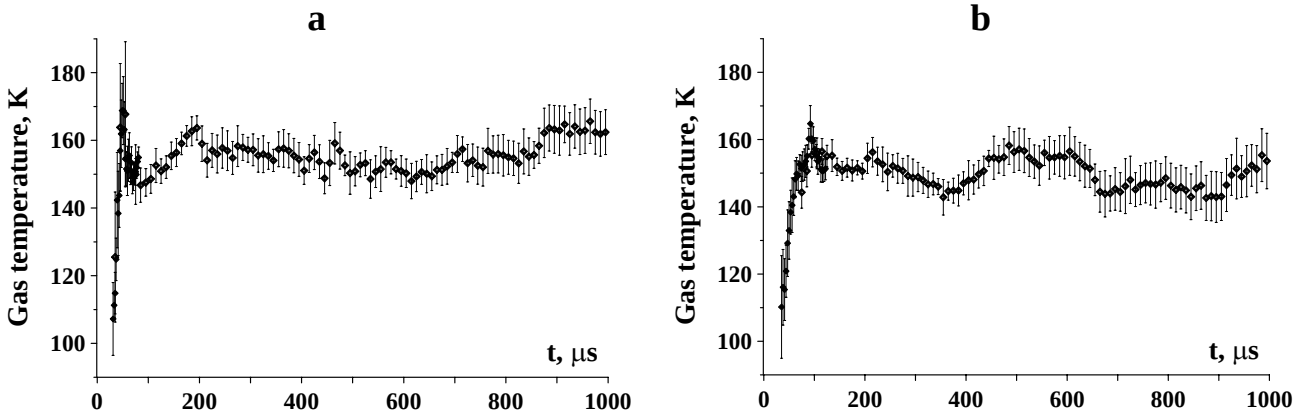

Fig. I.1.32. Time behavior of gas temperature in EBSD CO laser active medium for CO:N_2=1:9 (**a**) and CO:He=1:4 (**b**) gas mixtures at the specific input energy Q= 250 J/(l·Amagat), gas density 0.12 Amagat, initial gas temperature 110 K.

The method of gas temperature reconstruction by using gain/absorption time behavior on several ro-vibrational transitions of CO molecule was applied for studying the temperature time behavior inside active medium of pulsed EBSD CO laser. Our analysis showed that an application of semiconductor, solid state or any condensed matter lasers as a probe laser for measurement of SSG time behavior in CO laser active medium is problematic because of narrow line (less than 0.1 cm^{-1}) lasing requirement in order to avoid an overlapping of CO spectral lines. In our experiments the probe low-pressure CW CO laser was applied due to its narrow line lasing. Gas temperature time behavior was reconstructed with high accuracy due to the improvement of the applied method for CO laser mixtures CO:He=1:4 and CO:N_2=1:9. Gas temperature grew from 110 K (initial temperature) to quasi steady-state value of ~150 K for the first hundred microseconds after beginning of EBSD and was staying at this value for a time up to 1 ms.

Comparison of SSG experiments with theory
(Subtask 2A.3)

SSG measurements in the active medium of the EBSD CO laser provide us the gain amplitude and its temporal behavior, giving thus the information concerning the processes of vibrational dynamics in discharge and the excitation wave spreading through the "plateau" region of the VDF. As well known, time resolved gas temperature measurements during and after discharge pulse are the serious experimental problem. A strong dependence of the SSG characteristics upon the number of rotational component gives the chance to measure with a rather high accuracy the temperature variations caused by Joule heating in discharge and energy release in collisions of neutrals. The SSG measurements can be realized in selected regions of the gain medium, which are characterized by a volume much smaller than that of GDC. Thus, the discussed measurements are really the instrument for the local diagnostics of the gain medium.

The developed theoretical model was employed to simulate first-overtone SSG time behavior for high vibrational levels. Firstly, we analyzed the experimental data obtained earlier in (Basov, 2002) by the calibrated loss method. The following experimental parameters were taken into account for numerical simulation: gas mixture $CO:N_2=1:9$ at initial gas temperature 110 K and initial gas density 0.18 Amagat, EBSD pulse duration 30 μs.

In our preliminary analysis it was revealed that the results of SSG dynamics simulation are very sensitive to the used value of SIE. This feature makes the comparison of the theoretically calculated SSG characteristics with experimentally measured ones rather difficult, because experimentally measured value of SIE Q_{in} is a value of SIE averaged over the estimated electric discharge volume (thus, it is not a local value of SIE). As a result of spatial inhomogeneity of gas ionization by high-energy electron beam, the local values of SIE might be markedly different from average value Q_{in}. In order to find more accurately the local value of SIE in a prescribed region of GDC, the dependence of calculated SSG upon SIE value was studied. The local SIE value was varied from 200 to 380 (J/l·Amagat). The average SIE evaluated in (Basov, 2002) was Q_{in}= 380 (J/l·Amagat).

In **Fig. I.1.33** we compare the experimental data on the SSG dynamics for first-overtone transitions 26→24P(12), 29→27P(12), 33→31P(12), 36→34P(12) with results of numerical simulation. In the experiment the temporal characteristics was defined through measurement of CO lasing time delay because a varied value of threshold SSG in laser resonator (using calibrated intracavity losses) controls a lasing time delay. The results of numerical simulation for local SIE 200 and 300 (J/l·Amagat) are presented in **Fig. I.1.33**. It was found that the best agreement for SSG time behavior (at the same local SIE for all transitions) takes place at local SIE = 200 (J/l·Amagat) though the agreement is not so good for high transitions 33→31 and 36→34. Besides, one can see that the magnitude of the measured SSG for most transitions at long time ($t \geq 250$ μs) was notably higher than that of calculated ones. At local SIE=300 (J/l·Amagat) the level of the SSG values is closer to the experimental values at long time ($t \geq 250$ μs) in contrast with short-time behavior of SSG ($t < 250$ μs). The variation of local SIE value allows us to find the best fit for experimental data. This analysis demonstrated that SSG dynamics is a very sensitive to the value of local SIE.

In order to avoid some inherent drawbacks of the method of calibrated losses we carried out direct measurement of SSG time behavior in CO laser mixtures using the probe frequency selective CO laser. Further, experimental data of such measurements will be compared with the results theoretical calculations.

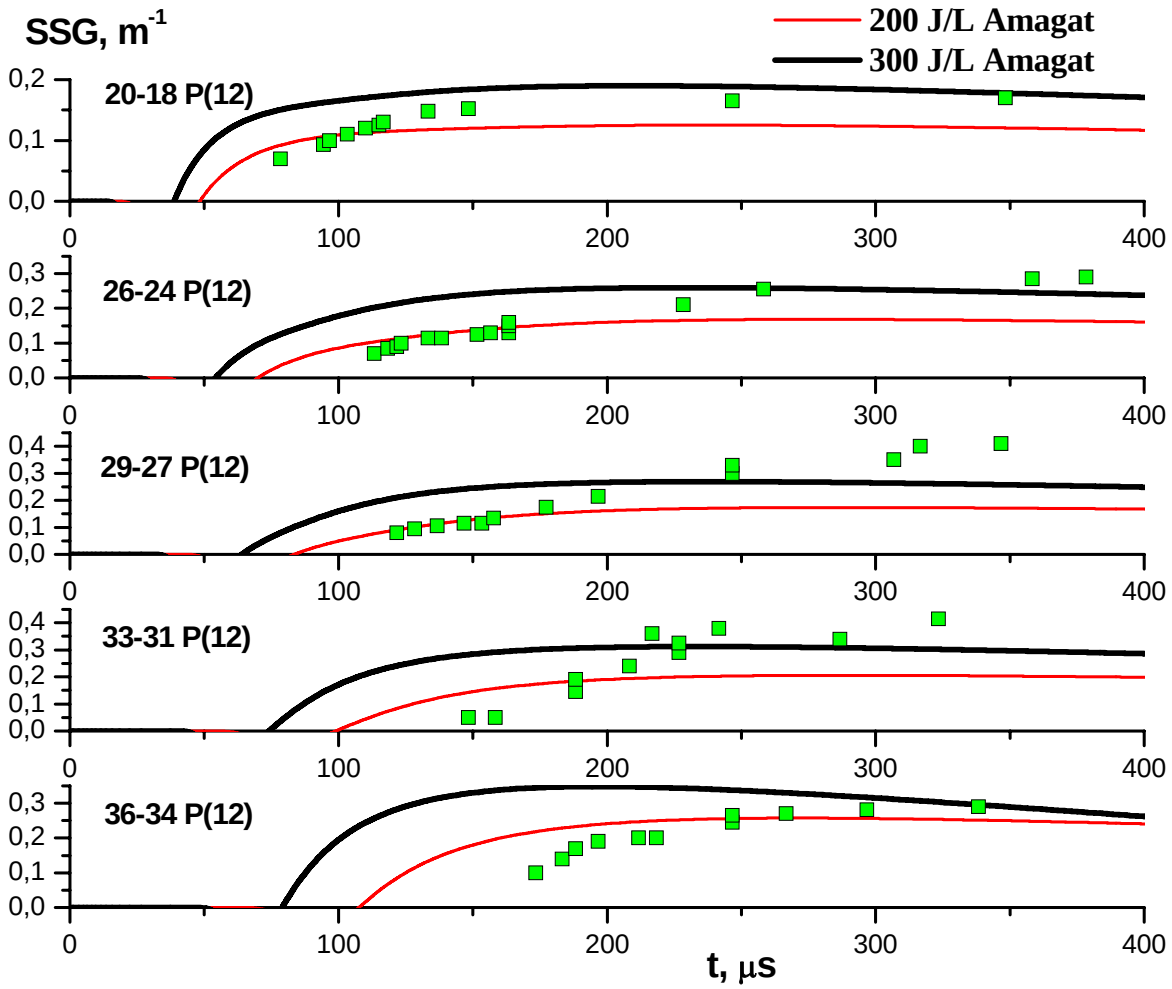

Fig. I.1.33. SSG time behavior for transitions 20→18P(12), 26→24P(12), 29→27P(12), 33→31P(12), 36→34P(12). Markers - experimental data (Basov, 2002) obtained by the calibrated optical loss method ($CO:N_2$=1:9, T=110 K, N=0.18 Amagat, pump pulse duration 30 μs, Q_{in}=380 J/l Amagat). Curves - results of numerical simulations for different values of local SIE.

The time behavior of SSG calculated for three different values of local SIE are presented in **Fig.I.1.34**. The ro-vibtational transition is 21→20(P14), gas mixture - CO:He=1:4 at initial gas density 0.12 Amagat. These curves are compared with the experimentally measured SSG for average SIE value equal to 150 (J/l·Amagat). Apparently, a satisfactory agreement of the theory with experiment takes place in the case, when the local SIE value taken in calculations was equal to 94 (J/l·Amagat), which is less than the average SIE value approximately by 37%. Such correction of the local SIE leads to satisfactory theoretical description of SSG dynamics in the mixture CO:He=1:4 for a wide range of vibration transitions and for various gas densities. Therefore, most theoretical calculations for gas mixture CO:He=1:4 were carried out for local SIE values reduced on 37% relative to average SIE Q_{in}. The experimental data on SSG time behavior for six ro-vibrational transitions are compared with results of numerical simulation in **Fig. I.1.35**.

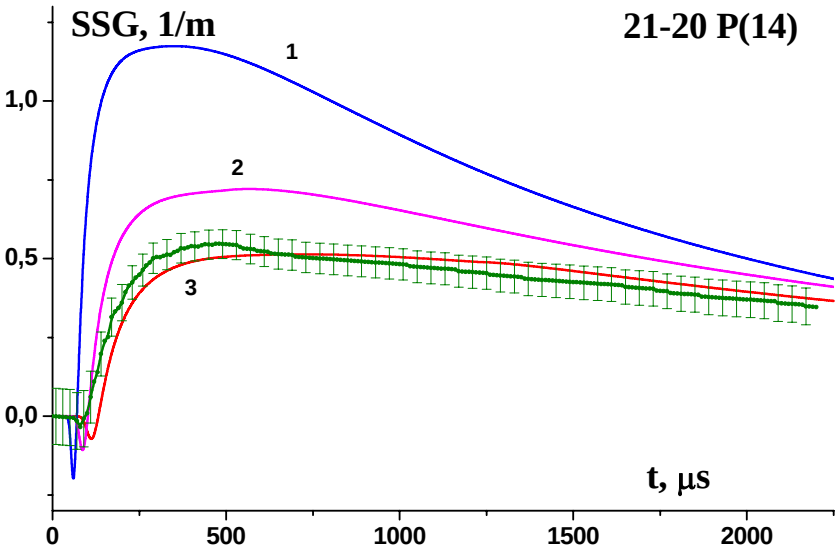

Fig.I.1.34. SSG time behavior for the transition 21→20(P14) in the mixture CO:He=1:4. The initial gas density 0.12 Amagat, temperature 120 K. 1 - SIE=150 J/l·Amagat, 2 – 110 J/l·Amagat, 3 - 94 J/l·Amagat, respectively. The experimental data for average Q_{in}= 150 J/l·Amagat are plotted by line with bars showing the experimental error.

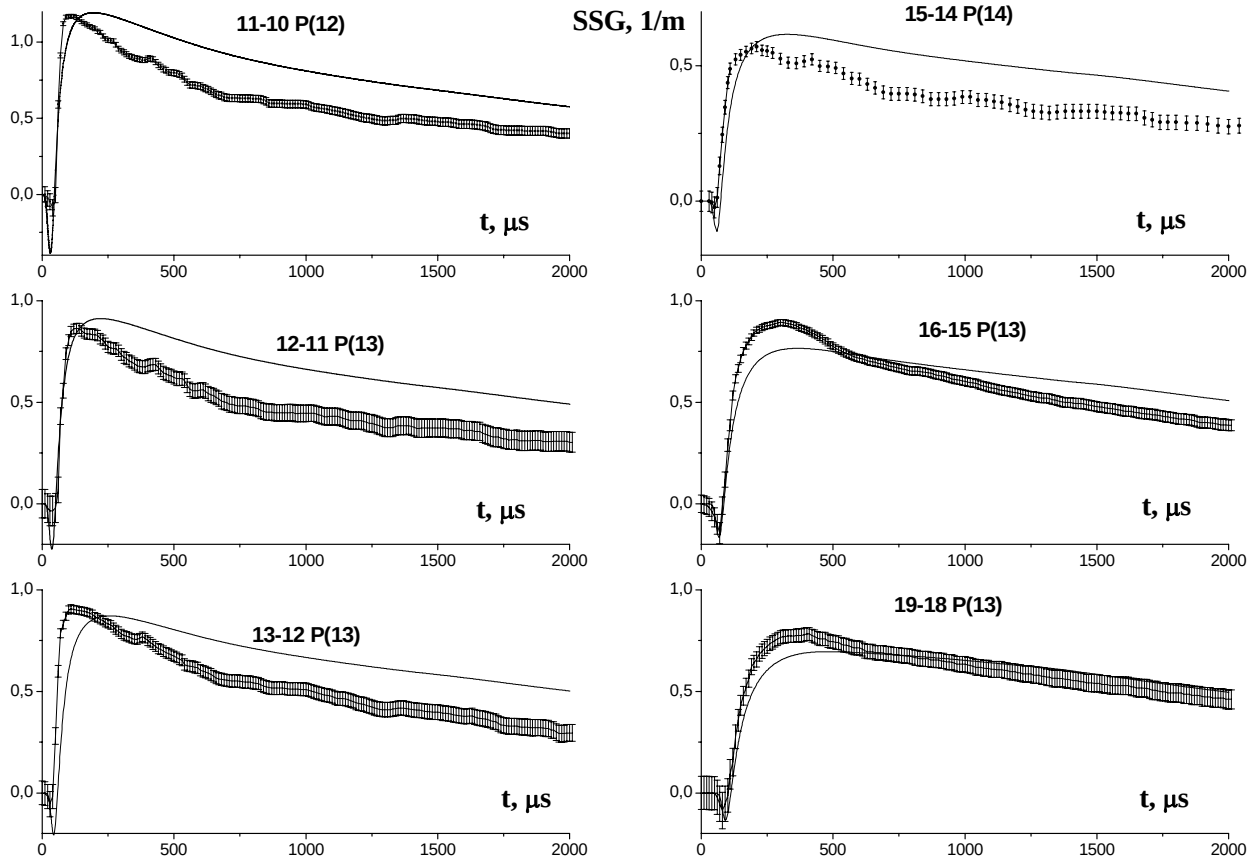

Fig. I.1.35. SSG time behavior for six vibrational transitions, CO:He=1:4, gas density 0.12 Amagat, initial temperature 120 K. Solid lines show theoretical results for local SIE = 94 J/l·Amagat. The experimental data are shown with experimental errors, average Q_{in}= 150 J/l·Amagat.

The theoretical model satisfactorily describes the experimental data, in particular delay time for appearance of positive gain, the maximum value of SSG, and SSG temporal characteristics in a whole. The specific features of the experimentally measured SSG dynamics for halved density of the gas mixture CO:He=1:4 are satisfactorily modeled by our kinetic model, too. This is demonstrated in **Fig. I.1.36**, where the experimental and theoretical SSG time behavior are presented for the initial gas density equal to 0.06 Amagat.

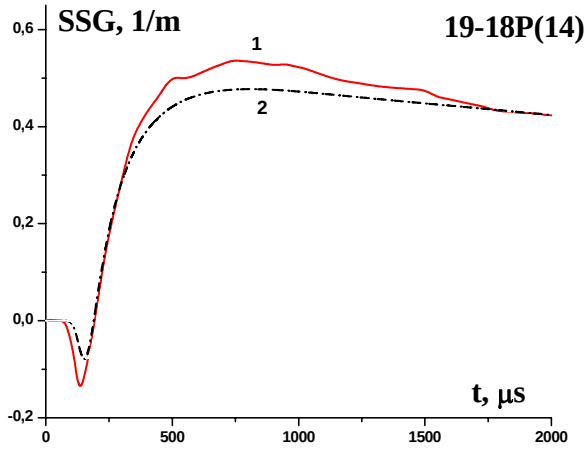

Fig.I.1.36. SSG time behavior for transition 19→18(P14) at gas density 0.06 Amagat.
Gas mixture CO:He=1:4,
initial gas temperature 120 K.
1 – experiment. Q_{in}= 150 J/l·Amagat,
2 – theory. Calculation for local SIE 94 J/l Amagat.

Comparison of the calculated and measured SSG time behavior for the nitrogen containing mixture CO:N_2=1:9 was carried out. The local SIE value used for calculations in CO:N_2=1:9 mixture was chosen as a fitting parameter providing the best agreement between the theory and experiment. As well as for the gas mixture CO:He=1:4, the local SIE value for CO:N_2=1:9 mixture is less than the average value Q_{in}. In **Fig. I.1.37** the experimental SSG time behavior in CO:N_2=1:9 at average SIE value Q_{in}= 250 (J/l·Amagat) is compared with theoretical one. The local SIE value found in calculations was 180 (J/l·Amagat), i.e. less than the average value by 28%. The comparison is performed for five ro-vibrational transitions: 13→12 P(9), 13→12 P(15), 16→15 P(10), 16→15 P(14), 16→15 P(16). One can see that for CO:N_2 gas mixture the satisfactory agreement between theoretical results and experimental data is reached with notably smaller correction of local SIE value than for CO:He mixture. Much slower gas heating in the former mixture than in the last one can explain this effect.

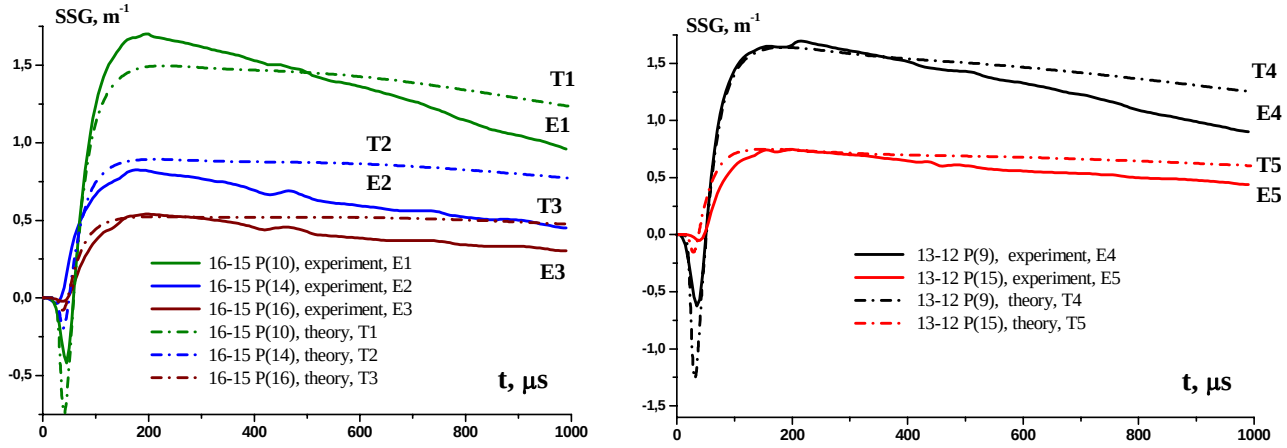

Fig. I.1.37. SSG time behavior for different ro-vibrational transitions in the mixture CO:N_2=1:9; density 0.12 Amagat, temperature 120 K. Curves **T1 - T5** are the theoretical dependences for transitions 13→12 P(9), 13→12 P(15), 16→15 P(10), 16→15 P(14), 16→15 P(16) at local SIE=180 (J/l·Amagat). Experimental dependences **E1 - E5** for the same transitions correspond to average Q_{in}=250 (J/l·Amagat).

Thus the developed theoretical model gives the adequate description of the SSG dynamics. The agreement with experiment takes place for the wide range of vibrational transitions and gas densities, and this agreement can be considered as an experimental verification of the derived set of VV rate constants.

The difference between the experimentally determined average SIE and the local SIE values, used in calculations, was explained partially by discussed above physical phenomena. There is one more factor, which could cause some discrepancy. The point is that the content of isotope-modified molecules $C^{13}O^{16}$in the natural carbon monoxide is about 1%. Due to smaller vibration frequency, energy exchange between regular and isotope-modified molecules results in preferable energy transfer to the isotope molecules. This leads to accumulation of about 10% of the whole vibrational energy (Konev, 1983). Thus, we may conclude, that the inevitable admixture of $C^{13}O^{16}$ in gain medium is equivalent to some reduction of vibration excitation degree of CO molecules in discharge. It means that the real influence of discharge plasma inhomogeneity on measured laser gain is probably somewhat lower.

Conclusions

A SSG time behavior for a pulsed CO LA on fundamental band vibrational-rotational transitions in vibrational bands from $6\rightarrow5$ ($\lambda\sim5.0$ μm) up to $32\rightarrow31$ ($\lambda\sim7.5$ μm) was studied both experimentally and theoretically. A MO - LA system was used in the experiments for SSG time behavior measuring. The highest value of SSG observed in the experiments reached up to 3.3 m^{-1} (transition $8\rightarrow7$ P(10), Q_{in}=250 J/l Amagat). Special attention was paid to the SSG time behavior on high vibrational transitions $V\rightarrow V\text{-}1$ (V>15). The obtained information is very important for designing fast-flow CO lasers including a first-overtone CO laser operating on high (V>15) vibrational levels.

The method of gas temperature reconstruction by using gain/absorption time behavior on several ro-vibrational transitions of CO molecule was applied for studying the temperature time behavior inside active medium of pulsed EBSD CO laser. Our analysis showed that an application of semiconductor, solid state or any condensed matter lasers as a probe laser for measurement of SSG time behavior in CO laser active medium is problematic because of narrow line (less than 0.1 cm^{-1}) lasing requirement in order to avoid an overlapping of CO spectral lines. In our experiments the probe low-pressure CW CO laser was applied due to its narrow line lasing. Gas temperature time behavior was reconstructed with high accuracy due to the improvement of the applied method for CO laser mixtures CO:He=1:4 and CO:N_2=1:9.

A rather complete set of VV-exchange rate constants for CO molecules includes a full matrix of rate constants for single-, double-, three-, four-quantum exchanges, and for asymmetric one-to-two quanta exchange for gas temperatures 100, 200, 300, 500, 700, 1000 K. From the qualitative point of view it enables us to evaluate which processes are mostly significant for vibrational kinetic modelling. In particular, it was found that rate constants of processes involving different numbers of exchanged vibrational quanta have different resonant behavior. Furthermore, on the quantitative side, the number of computed rate constants is sufficient to construct the full matrix of VV rate constants without resorting to heuristic suggestions based on extrapolation and/or interpolation. Inclusion of the asymmetric one-to-two quanta exchange processes allows us to explain naturally the abrupt reduction of vibrational populations at these levels observed experimentally in (Deleon, 1986), where it is explained by the introduction of a V–E non-adiabatic collisional process. As to FO CO lasing characteristics, a significant sensitivity of these to the choice of the rate constant set is rather strong, and thus only an accurate and complete set (like the one reported here) should be recommended.

The most full set of rate coefficients for asymmetric one-to-two quanta in VV' and VV energy exchanges was used in the kinetic modeling for the CO:He:N_2 lasing mixtures at different N_2 concentrations. The results of the complex kinetic study (Cacciatore, 2004) may serve as a reliable basis for understanding the role of nitrogen in CO laser operated in the fundamental and overtone bands. In particular, it was found that nitrogen admixture with low and moderate concentrations (30-60%) leads to a considerable rise of the CO laser energy efficiency on transitions lower than v=(37→35), v=(37→36). This effect is caused mainly by the asymmetric V-V' exchange processes, which are in competition with the V-T relaxation for molecules in vibrational levels in the range v=36÷40. The V-T relaxation frequencies in gas mixtures containing N_2 are also lowered with respect to the V-T relaxation involving only CO and Ar/He.

The VDF of CO in high levels in mixtures with low V-T relaxation rates (characteristic for Ar containing mixtures) is controlled by VV exchange processes between CO molecules. In such mixtures, the asymmetric VV' exchange processes between CO and N_2 molecules, when intercepting the vibrational quanta flowing upward through the vibrational ladder, change only slightly the populations of the lower levels, but diminish effectively the populations of levels with v >37. As a result, a dilution of such mixtures with N_2 suppresses the lasing action on the transitions higher than v=(37→35), v=(37→36). However, the laser action on these transitions terminates at N_2 concentrations notably greater than in the mixtures with higher V-T relaxation rates (CO:He:N_2 mixtures).

The research (Part I.1) was carried out for two years. The third year of the project for Part I.1 was not financed by the decision of the project manager due to the diminished budget partially cut by the Partner.

References for Part I.1.

Akishev Yu.S., Dem'yanov A.V., Kochetov I.V. et al. (1982). *High Temp.,* **20**, 815.

Basov N.G., Kazakevich V.S., Kovsh I.B., Mikryukov A.N. (1983). *Sov.J.Quant. Electron.*, **13**, 667.

Basov N.G., Hager G.D. et al, (2000). *IEEE Journal of QE,* **36,** 810.

Basov N.G., Ionin A.A., Klimachev Yu. M. et al. (2002). *Quantum Electronics*, **32** (5), 404.

Belykh A. D., Gurashvili V. A., Kochetov I. V. et al. (1994). *SPIE Proc.*, **2117**, 12.

Billing G. D. and Cacciatore M. (1983). *Chem. Phys. Lett.*, **94**, 218.

Billing G. D., Coletti C., Kurnosov A. K., Napartovich A. P. (2003). *J. Physics B: At. Mol. Opt. Phys.* **36**, 1175.

Bohn W.L., Eckel H.-A., Riede W., Walther S. (2002). *Proc. SPIE.* **4760**, 230.

Bones M.J.W., Center R.E. (1975). *Appl. Phys. Lett*., **26** (9), 511.

Cacciatore M. and Billing G. D. (1981). *Chem. Phys.*, **58**, 395.

Cacciatore M., Capitelli M. and Billing G. D. (1983). *Chem. Phys.* **82**, 1.

Cacciatore M., Kurnosov, A. Napartovich A. and Shnyrev S. (2004). *Journal of Physics B: Atomic, Molecular and Optical Physics*, **37,** 3379.

Coletti C. and Billing G. D. (2000). *Journal of Chem. Phys.*, **113**, 4896.

Dem'yanov A. V., Kochetov I. V., Napartovich A. P. et al. (1980). *High Temp*., **18**, 695.

Deleon R. L. and Rich J. W. (1986). *Chem. Phys.,* **107**, 283.

Didukov A.I., Kirko V.Yu., Kulagin Yu.A., Shelepin L.A. (1989). *Preprint FIAN (LPI)* #109 (in Russian).

Guelachvili G., de Villienuve D., Farrenq R., Urban W., Verges J. (1983). *J. Molecular Spectroscopy*, **98**, 64.

Hager G. D., Ionin A. A., Kotkov A.A. et al. (2000). *IEEE J.Quant. Electron.*, **36** (7), 810.

Ionin A. A., Kotkov A. A., Kurnosov A. K. et al. (1998). *Opt. Commun.*, **155**, 197.

Ionin A. A., Klimachev Yu. M., Konev Yu.B. et al. (2000). *Quantum Electronics*, **30** (7), 573.

Ionin A. A., Klimachev Yu. M., Konev Yu. B. et al. (2001a). *J. Phys. D: Appl. Phys.*, **34**, 2230.

Ionin A et al. (2001b). Final report on the ISTC Project 1865 P " First-overtone CO laser: gain kinetics, RF discharge and atmospheric spectroscopy".

Islamov R.Sh., Konev Yu.B. et al. (1984). *Kvantovaya Electronika*, **11**, 142.

Konev Y.B., Kochetov I.V., Kurnosov A.K. (1983). *Preprint of I.V. Kurchatov Atomic Energy Institute*, № **3829/11**, Moscow.

Kurnosov A., Cacciatore M. and Billing G. D. (2003). *J. Phys. Chem.*, **A107**, 2403.

Langhoff S. R. and Bauschlicher C. W. (1995). *J. Chem. Phys.* **102**, 5220.

McCord J. E., Hager G. D., Dass S., Ionin A. A. (2003). *Preprint AIAA* **2003-3475**, 34th AIAA plasmadynamics and Lasers Conference, 23-26 June 2003, Orlando, Florida, USA.

Patel C.K.N. (1964). *Phys. Rev*., **136A,** 1187.

Patel C.K.N. (1966). *Phys. Rev*., **141**, 71.

Porshnev P. I. et al. (1996). *Chem. Phys.*, **213**, 111.

Reid J. P., Simpson C. J. S. M. et al. (1995). *J. Chem. Phys.*, **103** 2528.

Treanor C.A., Rich J.W., Rehm R.G., (1968). *J. Chem. Phys.*, **48**, 1798.

Vjazovetski N.M., Didukov A.I., Kirko V.Yu., Kulagin Yu.A., Shelepin L.A. (1988). *Preprint FIAN (LPI)* #**221** (in Russian).

http:\\www.afrl.af.mil/successstories/2001/emerg.tech. “Supersonic carbon monoxide overtone laser” AFRL.

Zeyfang E., Mayerhofer W., Walther S. (2001). *Proc. SPIE*, **4184**, 230.

Part I.2. RF DISCHARGE CO LASER
(Subtasks 1A.3, 1A.4, 2A.1, 2A.2, 2A.3, and 2A.4))

Introduction

A significant progress is achieved now in the development of slab and capillary CO_2 and CO lasers with excitation of its active media by transverse capacitive radio-frequency (RF) discharge (frequency range 1-200 MHz). Heat removing from the active gas mixture is realized in these lasers through the cooled electrodes to which RF voltage is applied (Colley, 1995; Udalov, 1995; Xin Jianguo, 1999). RF discharge has some advantages as compared to DC discharge. Mainly, these are: lower voltage of power supply, higher electrical efficiency, the simplicity of output laser power modulation and driving. RF discharge gives the possibility to excite large volume of the active gas (in planar geometry) without using external source of ionization. In comparison with DC discharge, RF discharge appeared to be more stable because there is no need to form cathode layer which connects discharge current with electrode and supports the current through the discharge gap. Anode and cathode in RF discharge changes each other depending on the phase of the fast-alternative electric field and connection of electric current to the temporary cathode is realized by displacement current.

Experimental researches on properties of RF discharge used for pumping slab CO lasers are actually absent. We know only two references (Kunn, 1995; Ionin, 2001) where RF discharge properties are investigated using discharge chambers developed for CO lasers. The usage of "laser installations" (not developed specially for studying discharge properties) strongly complicates the study of RF discharge. Usually in such kind of the experimental facilities one can observe significant discrepancy between experimental results and theoretically calculated data because of edge effects and other non-uniformities along the discharge electrodes. In (Vitruk, 1992; Baker, 1996), the studies of RF discharge properties in gas mixtures containing CO_2 molecules were carried out at the discharge installation specially designed for this purpose.

On the other hand, one of promising methods to design CO laser (including an overtone one) is the excitation of its active gas medium in RF discharge in subsonic region with following gas-dynamic expansion and cooling or in diffusion cooled slab channel. The key problem in modeling RF pumped overtone CO laser is the development of the RF discharge model. Two-dimensional model is most adequate for the description of the RF discharge in a fast flow. This model can hardly be developed in a near future due to complicated vibrational kinetics. A one-dimensional model for typical mixture of the overtone CO laser was developed earlier. This model provides spatial profiles for discharge power density and excitation rates for a number of lower vibrational levels. This information can be exploited in one- or two-dimensional models of vibrational kinetics of flowing gas. At the moment, we have developed a simple version of one-dimensional model of RF discharge with diffusion cooling, and introduced the system of vibrational kinetic equations in single-quantum exchange approximation in this model. The further step was to include a subroutine for calculations of laser power based on usage waveguide optical modes, both for a constant refractive index profile and for index gradient produced by electrodes cooling. This completes the model of RF discharge CO laser operating in the fundamental band.

Comparison with the experiments will allow us to evaluate applicability of the RF discharge CO laser model. Further modifications of the theoretical model are necessary for RF discharge laser operating in the overtone band. In particular, the influence of vibrationally excited molecules on ionization balance should be taken into account properly for a correct description of the plasma. Besides, the correct description of the RF discharge model requires non-local effects to be included. This will be done by introduction of additional gradient terms into continuity equation for electrons.

In this report we present results on experimental study of RF discharge properties in gas mixtures containing CO molecules. The experiments were carried out using discharge chamber of special design at different content of CO in gas mixtures of different working pressure. Also, using 1D theoretical model (Baker, 1996; Ionin, 2001; Starostin, 2001; Vitruk, 1992), numerical calculations were performed for the experimental conditions. The measured RF discharge characteristics were compared with theoretical data. Existing RF discharge facility operating at room temperature was used as a prototype for design a new RF discharge facility with cryogenically cooled gas mixture. This facility was developed and used for comparison of experiment and theory for fundamental band CO lasing.

Verification of the kinetic and RF discharge models by comparison with the experimental data obtained experimentally at room temperature.
(*Subtask 1A.3.*)

One-dimensional model was employed to calculate power-dependence of root mean square (RMS) discharge voltage. A similar model was developed earlier to simulate RF discharges in gas mixtures containing CO_2 and CO molecules (Ionin, 2001; Starostin, 2002). The numerical code for RF discharge includes electron and positive ion kinetics. Fluid equations for both these components were solved in space-time in parallel with Poisson equation. It was assumed that the electron attachment is completely compensated by detachment processes in collisions of negative ions with CO molecules. Electrical drift and diffusion of electrons were taken into account.

It was found earlier (Starostin, 2002) that under conditions typical for an RF CO_2 laser, particularly at low pressure, it is important to take into account the deviations of electron transport and rate coefficients from their values calculated as functions of a local E/N-parameter. Here E is the electric field strength and N is the gas density. The simplest way to do this is to introduce a time-dependent balance equation for mean electron energy including electron thermal conductivity.

All the transport and kinetic rate coefficients were calculated separately from solution of the steady-state electron Boltzmann equation at a fixed magnitude of E/N-parameter and tabulated as functions of the mean electron energy corresponding to the same value of E/N. The set of indicated equations was completed by respective boundary and initial conditions. The discharge voltage was a parameter fit to get a prescribed discharge power.

Gas temperature spatial profile was calculated from a steady state thermal balance equation. We used the method of calculations of thermal conductivity coefficients for gas mixtures exploited in the active medium, which was proposed in (Syed Wahid, 2000). In this method, the thermal conductivity coefficient for the laser mixture has been calculated using known molecular weights and thermal conductivity coefficients for individual gas components of the mixture, which were taken from (Grigor'ev, 1991).

Non-uniform numerical mesh over space was employed in calculations with a mesh step reducing to electrodes. Typically, the number of spatial steps was 100. Regular oscillations were established after calculating a couple of thousands of RF field cycles.

The experimental RF discharge facility of special design was developed for detailed studying slab RF discharge properties in gas mixtures containing carbon monoxide molecules. The experimental setup (**Fig.I.2.1**) consisted of RF generator, power reflectometer, matching circuit, RF voltmeter, and discharge chamber 1. The chamber consisted of two diffusively cooled cylindrical copper discharge electrodes 2 (d=10 mm, L=150 mm) aligned at the same axis with the 1.9 mm gap between the electrodes (the RF discharge volume ~ 0.15 cm^3). Such a cylindrical geometry of the discharge region has far less inhomogeneities and edge effects comparing to typical laser devices. RF power was supplied from an RF generator to the electrodes through the power reflectometer and matching circuit using two connectors 3.

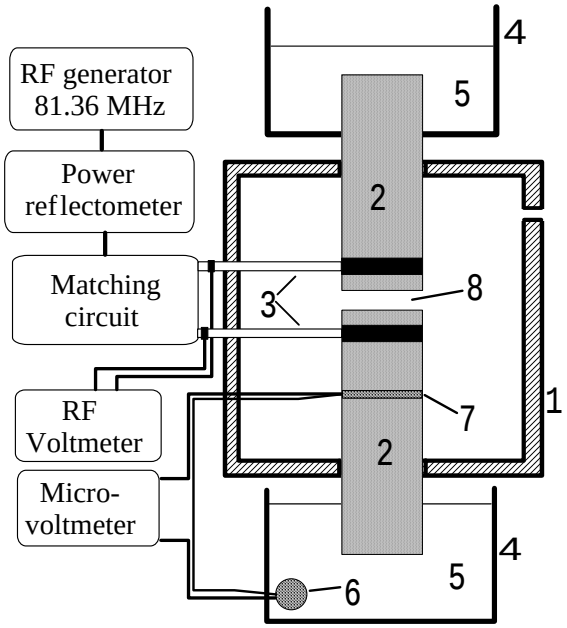

Fig.I.2.1. Experimental setup for studying RF discharge properties.

An air cooled RF generator (working frequency 81.36 MHz) with changeable output power (maximal value ~200 Watts) was used in the experiments as a source of RF voltage. The matching circuit was placed near the discharge chamber to match the output RF generator impedance (50 Ohm) with the impedance of the discharge chamber. Two reservoirs 4 with water 5 were attached to the electrodes for cooling down the discharge region 8. Calibrated thermopile system 6, 7 was used to measure the power loaded into the discharge region. One of two thermo-junctions 7 was attached to one of the electrodes 2 (6 cm away from the discharge region). Another thermo-junction 6 was maintained in reservoir 4 with water 5. The experiments were carried out at room temperature of cooling water. Calibration of such thermo-metrical system was made by heating the electrodes at the DC discharge conditions with controlled parameters. The DC discharge was switched on for fixed time. Two series of the calibration experiments were carried out at the same conditions when the electrode with thermojunction 7 was as a cathode and as an anode. The RF discharge power input measurements were carried out during the same time as it was in a process of the calibrating by DC discharge.

The temperature of discharge vessel walls and electrodes was assumed to be independent of discharge power and equal to 293 K (actually, the maximum temperature increment in the experiments was about (5-10) K).

Fig.I.2.2 shows correlation between measured and calculated dependence of discharge RMS-voltage on input power density for gas mixtures CO:He at pressure 100 Torr. Data agree reasonably well. Numerical simulations made for the experimental conditions show the discharge voltage growth with an increase of molecular component percentage in the mixture at low input power densities. At higher power, an agreement of the theory with the experiment is not so good.

How the gas pressure affects discharge voltage is shown in **Fig.I.2.3** for the gas mixture CO:He=1:10. Experimentally, the discharge voltage is observed to be almost independent of gas pressure, while the theory predicts more than twice growth of the discharge voltage for power density 35 W/cm^2 with gas pressure diminishing from 100 to 30 Torr. Reasons for such a different behavior are not clear at the moment. One of possible explanations could be electric breakdown of gas mixture surrounding the discharge gap at low values of a product pd, p is the gas pressure, d is discharge gap length. It is worth to note that in (Zhao, 1991) the maximum CO laser power was achieved at gas pressure 80-100 Torr.

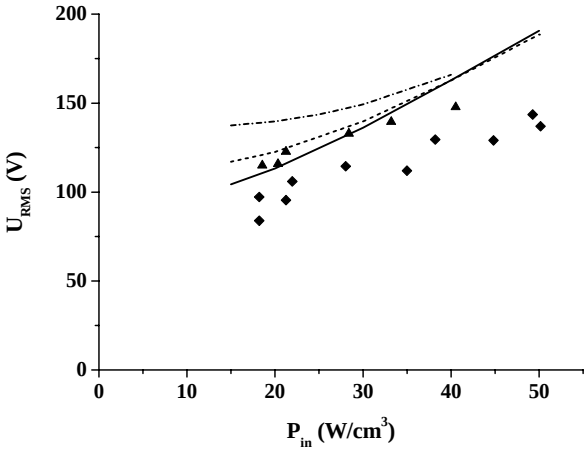

Fig.I.2.2. RMS discharge voltage vs. input power density. Curves are calculation results, and markers are experimental data. Dot line, ♦ - CO:He=1:10; dash-dot line, ▲ - CO:He=1:5; solid line, ● - CO:He=1:20. P=100 Torr, f=81.3 MHz, d=1.9 mm.

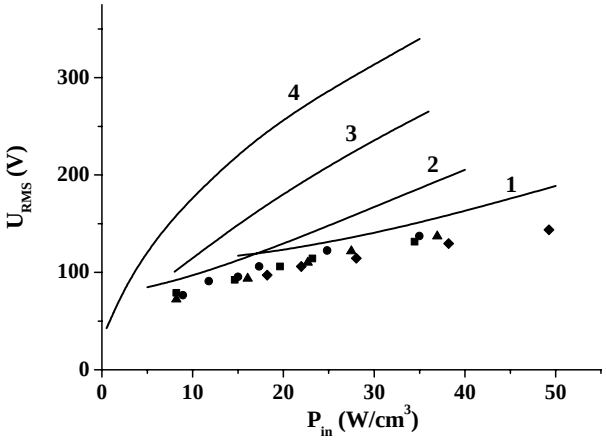

Fig.I.2.3. RMS discharge voltage vs. input power density. Curves show calculation results, and markers are experimental data. 1, ♦ - P=100 Torr; 2, ▲ - P=60 Torr; 3, ● - P=30 Torr; 4, ■ - P=10 Torr. f=81.3 MHz, d=1.9 mm, CO:He=1:10.

For evaluation of laser efficiency it is important to know what a fraction of the discharge power is ion Joule heating. This fraction is shown in **Fig.I.2.4** as a function of the total input power density. Numerical simulations demonstrated that ion Joule heating is localized in the small vicinity of electrodes. Positive ion-heating fraction grows with the total discharge power. At gas pressure 30 Torr and total power density 40 W/cm^3 ion-heating fraction amounts 40%.

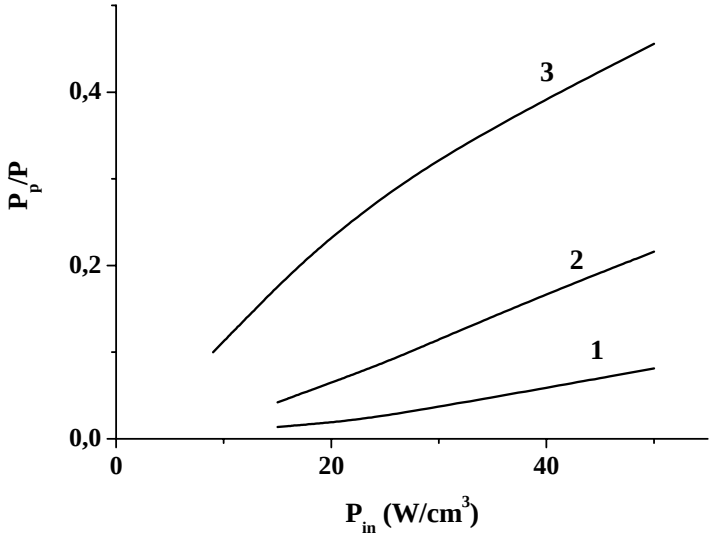

Fig.I.2.4. Ratio of ion-heating rate, P_p, to total discharge power density vs. discharge power density.
1 - P=100 Torr;
2 - P=60 Torr;
3 - P=30 Torr.
f=81.3 MHz, d=1.9 mm,
CO:He:Xe:O_2=50:500:15:2.

Another important characteristic of the discharge is maximum gas temperature achieved in the gap center. If the laser does not operate (there is no radiation output), the discharge power is completely converted into the gas heating. Calculations showed that the spatial profile of gas temperature is close to the parabolic one. The maximum temperature and $(E/N)_{RMS}$-parameter at the discharge axis are listed in **Table I.2.1** for different mixtures and gas pressures. Dilution of CO by He (at P_{in}=Const) leads to reduction of $(E/N)_{RMS}$ and the decrease of the gas temperature. Gas pressure growth for a fixed mixture composition results in a weak diminishing $(E/N)_{RMS}$ and gas

temperature rise. The latter is explained by distortion of discharge power density spatial profile caused by reduction of ion-heating fraction with gas pressure (see **Fig.I.2.4**).

Table I.2.1.

Plasma characteristics at the center of the discharge region.

Gas mixture	P , Torr	P_{in} , W/cm^3	$(E/N)_{RMS}$, 10^{-16} V·cm^2	T , K
CO:He=1:5	100	40	2.15	473
CO:He=1:10	100	40	1.59	438
CO:He=1:20	100	40	1.30	420
CO:He:Xe:O_2==50:500:15:2	30	50	1.69	429
	60	50	1.50	450
	100	50	1.39	467

The experimental RF discharge facility of special design developed for measuring Voltage-Power characteristics let us make more accurate measurements of the root-mean-square voltage on the discharge gap as a function of RF input power for different mixtures containing CO molecules at different gas pressures. Voltage-Power characteristics and spatial profiles for relevant quantities were calculated using the one-dimensional model. A satisfactory agreement with the experiment is achieved for gas mixtures at gas pressure 100 Torr, which is optimum for laser operation. With pressure diminishing down to 30 Torr the calculated RMS-voltage is notably higher than the measured one. Explanation of this discrepancy requires additional studies to be performed.

Modification of the existing RF discharge facility for lasing experiments at room temperature. (*Subtask 1A.3.*)

A slab RF excited CW CO_2 laser setup was available before our experiments. It was quasi-sealed, i.e. both mirrors of the laser resonator were placed inside the laser chamber and could be aligned along the laser axis only when the top cover of the chamber was opened. Stationary CO_2 laser radiation was extracted from the chamber through the optical NaCl-window that was glued to the chamber wall. This laser setup was very inconvenient for CO lasing experiments with different pairs of resonator mirrors. The laser setup was modified to have a possibility of flexible changing and aligning the laser resonator mirrors (see **Fig.I.2.5**). The output mirror holder 1 compatible with different diameters of output mirror was attached to the laser chamber wall instead of NaCl window. The rear mirror holder 2 was attached to the opposite chamber wall in such a way, that the mirror was placed at minimal distance from the discharge region. Both outer holders (1 and 2) are flexibly adjustable and changeable.

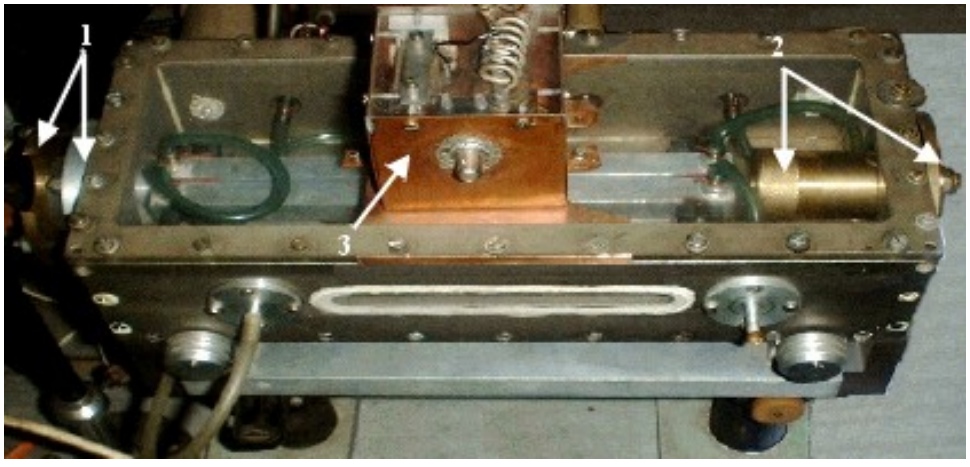

Fig.I.2.5. CW slab RF CO_2 laser setup modified for CO lasing experiments.

A more convenient manually tuned wide range matching circuit 3 (see **Fig.I.2.5**) was developed to match the chamber impedance with output impedance of the RF generator (50 Ohm) over a wide range of the experimental conditions (active gas mixture content and gas pressure). This modification was needed because the existed (in slab CO_2 laser configuration) matching circuit was suitable for fixed conditions of CO_2 lasing.

Modification of the RF discharge pumped laser model for output power calculations. (*Subtask 1A.4.*)

It was achieved experimentally (Xin, 1999) 1 kW output power for a CO slab laser with RF pumping at cryogenic temperature. The maximum efficiency was 25%. It was earlier reported about development of the one-dimensional (1D) model of the RF discharge allowing us to calculate Voltage-Power Characteristic (VPC) of RF discharge in CO containing gas mixtures (Ionin, 2001). A comparison of theoretically predicted VPC with experimentally measured (Kunn, 1995; Ionin, 2002) demonstrated rather good agreement. In (Ionin, 2001) the kinetic subroutine calculating dynamics of vibrational levels populations was incorporated into the model of the RF discharge. This allows us to simulate small signal gain evolution for a manifold of CO vibrational levels in the RF excited laser. The next step in development of 1D model of RF slab CO laser was made by incorporation of stimulated emission processes. The resulting model is capable to calculate laser power for the different laser transitions.

1D model of the RF discharge including calculation of the vibrational distribution function (VDF) of CO molecules is described in detail in (Ionin, 2001). Calculations of stimulated emission requires spatial profile of intensities to be defined. A specific intensity profile depends on laser cavity and an amount of oscillating spatial modes. In our model the spatial intensity profiles were taken the same for all transitions. The specific choice will be presented below. The terms in the vibrational kinetic equations responsible for the stimulated emission have the form $\frac{I_V}{h\nu_V} I_0(x) g_{V,J}(x)$, where $\frac{I_V}{h\nu_V}$ is the total intensity at the given transition with frequency ν_V, $g_{V,J}(x)$ is the gain coefficient at this transition, $I_0(x)$ is the normalized spatial profile. The magnitude of the intensity $\frac{I_V}{h\nu_V}$ was determined from equality of the intensity weighted average value of gain coefficient to cavity loss coefficient Γ:

$$G_{V,J} = \int_0^d I^0(x) g_{V,J}(x) dx \Big/ \int_0^d I^0(x) dx = \Gamma, \qquad \text{(I.2.1)}$$

where d is the inter-electrode distance. For slab geometry it is typical to employ 1D unstable resonator for which the loss coefficient is equal to $\Gamma = \frac{\ln M}{2L}$, where M is the resonator magnification, L is the length of the gain region. Calculations of free-running laser spectrum defined by magnitudes of intensities $\frac{I_V}{h\nu_V}$ first started from the lowest transition from V, where the averaged SSG coefficient $G^0_{V.J}$ overcomes the cavity losses. The rotational quantum number was taken from the condition for the gain coefficient to be maximum. The laser intensity at the transition considered was found when equation (I.2.1) was satisfied. Higher-transitions exert a weak influence on intensities for the lower transitions. Nevertheless, an opportunity is reserved in the program to

perform iterations in the whole spectrum of lines calculations to increase an accuracy of result. Typically, the maximum deviation from lasing condition (I.2.1) amounts 12% at the first iteration and 2.5% at the second iteration. The laser efficiency was defined as a ratio of total laser power to the discharge power. Then characteristics of the RF discharge were re-calculated taking into account that the laser radiation removes a part of power out of plasma. Iterations were continued until the laser power was found with a prescribed accuracy.

For numerical simulations conditions of the experiment (Xin, 1999) were chosen. Gas mixture CO:He:Xe:O_2 = 24:71:4:1 at gas pressure P = 60 Torr was excited by RF electric field with frequency f = 90 MHz, inter-electrode distance was 0.2 cm, the discharge power density amounts 23 W/cm^3. The facility walls were cooled by liquid nitrogen. There is no information about the real temperature of the walls. Therefore, simulations were performed for walls temperature T_w varied in the interval 80-130 K.

In modeling two spatial mode intensity profiles were considered: $I_0(x) = 1/d$ correspondent approximately to multi-mode oscillations, and $I_0(x) = (2/d)\sin^2(\pi x/d)$, related to the fundamental waveguide mode. Actually, there exists thermally induced refraction index profile leading to de-focusing of wave field and resulting in deformation of optical modes. The problem of calculation of optical modes in a waveguide with graded index was considered in (Blok, 1999) for IR Xe slab laser. Calculation of realistic patterns of optical modes was not a purpose of this work. Therefore, two typical mode patterns were considered.

In the vicinity of electrodes the electric power is dissipated by ion current, and its density is low (**Fig.I.2.6**, curve 1). Inside discharge gap the power density consumed for CO vibration excitation grows, curve 2 in **Fig.I.2.6**. Laser power density grows inside the gap due to the increase of pumping power density (curves 3, 3'). However, gas temperature rise causes formation of a shallow dip in the laser power profile in the center. Please note a clear difference between laser power profiles for multi-mode (3) and single-mode (3') lasing. Because of low intensity of the fundamental mode nearby electrodes, the emitted power density is lower than for the multi-mode operation. The VT rate increases fast with gas temperature and becomes a notable one in the center (curve 4). Power dissipation in processes of VV-exchange (effect of anharmonicity) and spontaneous emission is slow. Respective fractions of power dissipated in the center are equal to 6% (VV-exchange) and 1.6% (spontaneous emission).

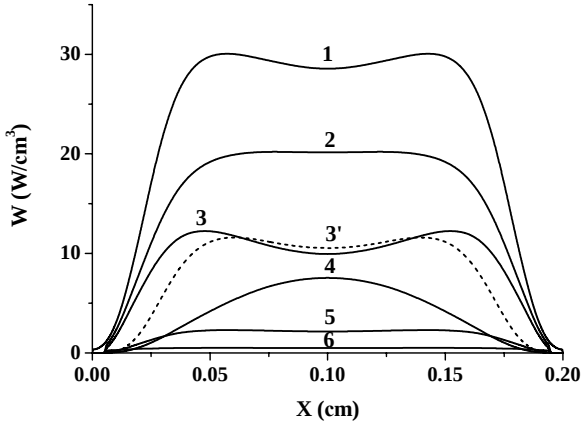

Fig.I.2.6. Local discharge power balance profile:
1 - discharge power density;
2 - power fraction going to CO vibration excitation;
3, 3' - laser power emitted by unit volume;
4 - gas heating rate due to VT relaxation;
5 - gas heating rate due to VV exchange;
6 - spontaneous emission power density.
1, 2, 3, 4, 5, 6 are for multi-mode regime;
3' fundamental-mode lasing.
T_w = 100 K.

Calculated temperature profile within discharge is close to the parabolic one. Gas temperature in the center calculated for different wall temperatures in the absence of lasing, for multi-mode and single-mode lasing are listed in **Table I.2.2**. It is seen that gas temperature for the laser with a high

efficiency is remarkably lower than that of the discharge without lasing. The CO VDFs calculated for different locations are compared in **Fig.I.2.7** for the cases of multi-mode lasing (solid lines) and absence of lasing (dashed lines). The relative vibrational temperatures for low levels near the electrodes are lower than in the center. This is explained by growth of gas temperature and pumping power along the direction from the wall to the center of the gap. In agreement with the theory (Napartovich, 1977), laser oscillations onset influences only on populations of levels higher than the last level involved into lasing.

Table I.2.2.
Gas temperature in the center of discharge gap at various wall temperatures

T_w, K	T, K (No lasing)	T, K (Multi-mode lasing)	T, K (Fundamental-mode lasing)
80	311	224	240
100	322	255	264
120	333	299	325
130	338	322	-

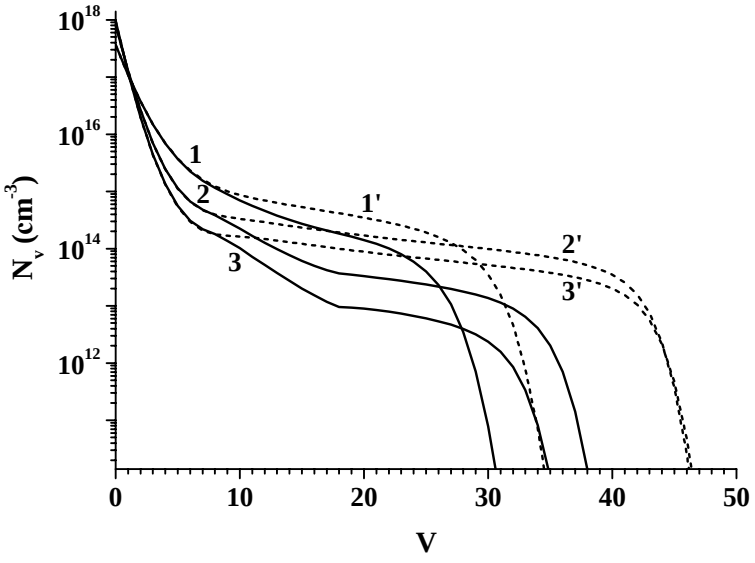

Fig.I.2.7. VDF of CO molecules calculated in different locations:
1, 1' – x = 0.1 cm;
2, 2' –0.013 cm;
3, 3' – 0.008 cm.
1, 2, 3 – multi-mode lasing;
1', 2', 3' – no lasing.
T_w = 100 K.

Spatial variation of SSG coefficients at a number of transitions is illustrated in **Fig.I.2.8**. VP(J) means the transition V, J-1→V-1, J. Transitions selected for illustration were defined by a condition that the spatially averaged SSG is higher than the threshold. The rotational number corresponds to the maximum SSG at the given vibrational band (V→V-1). Onset of lasing leads to gain saturation. **Fig.I.2.9** illustrates gain saturation effect in the case of multi-mode lasing for the same transitions as in **Fig.I.2.8.** The threshold gain is shown by dash-dot line. Traditionally the gain coefficient as a function of laser intensity is approximated by an expression:

$$g = \frac{g_0}{1 + \frac{I}{I_S}}$$

where g_0 is the SSG, and I_s saturation intensity.

Taking g, g_0 and I calculated for the center, saturation intensity can be determined for conditions of **Fig.I.2.9**. Values of I_S found by this way are equal to 1030, 660, 430, 280, and 84 W/cm^2 for transitions 9P(15), 10P(13), 11P(12), 12P(11), 13P(11), respectively. It is seen that the saturation intensity defined in such a manner is not simply proportional to inverse of stimulated emission cross section (it grows linearly with V) but depends essentially on effective VV relaxation frequency proportional to vibrational populations (Napartovich, 1977).

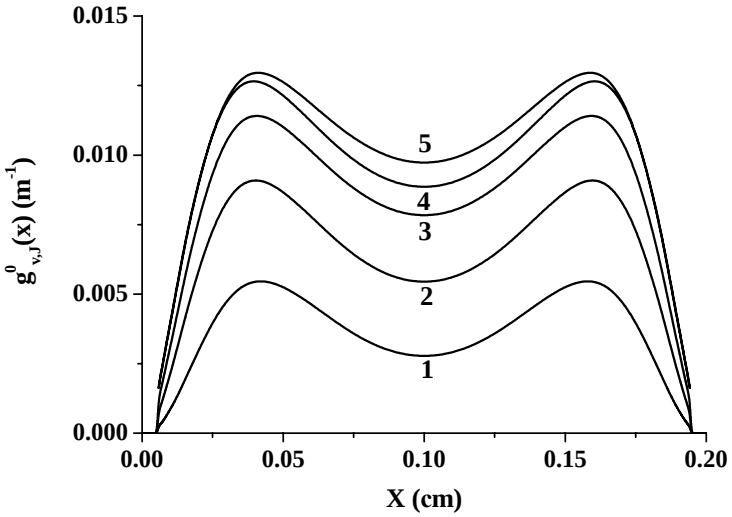

Fig.I.2.8. Spatial profiles of SSG for a number of rotational-vibrational transitions:
1 - 9P(15);
2 - 10P(13);
3 - 11P(12);
4 - 12P(11);
5 - 13P(11).
T_w = 100 K.

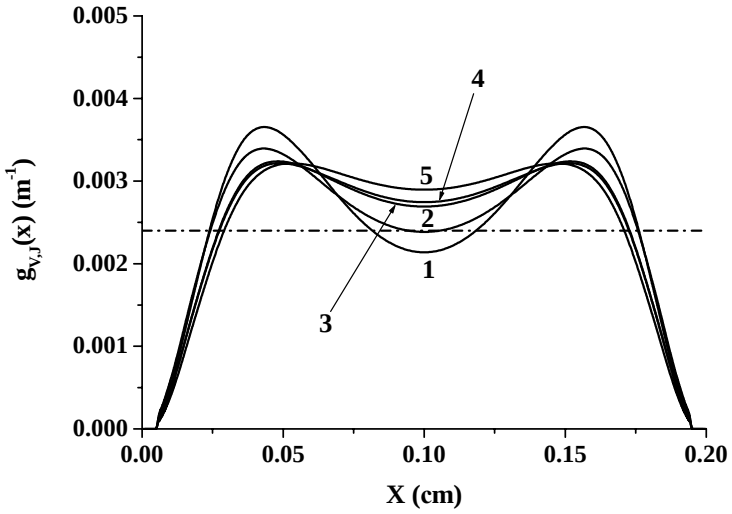

Fig.I.2.9. Spatial profiles of saturated gain coefficient for conditions of multi-mode lasing:
1 - 9P(15);
2 - 10P(13);
3 - 11P(12);
4 - 12P(11);
5 - 13P(11),
T_w = 100 K.

Generally, CO laser emits radiation on many ro-vibrational lines. In our model many vibrational transitions are included, but in each vibrational band only one rotational line is assumed to be a lasing one. This line is defined as one having maximum gain spatially averaged over the discharge gap. **Fig.I.2.10** demonstrates such a gain coefficient being maximum over each vibrational band as a function of vibrational band number, V. Both, SSG and saturated gain coefficients are plotted, the numbers near the curves indicate the rotational quantum number, *J*. It is interesting that the SSG and saturated gain have maxima at different rotational numbers. Calculations of the

saturated gain were made for multi-mode intensity profile. Saturated gain has a maximum at higher *J* than the SSG because the VDF falls down faster under lasing than without lasing (**Fig.I.2.7**).

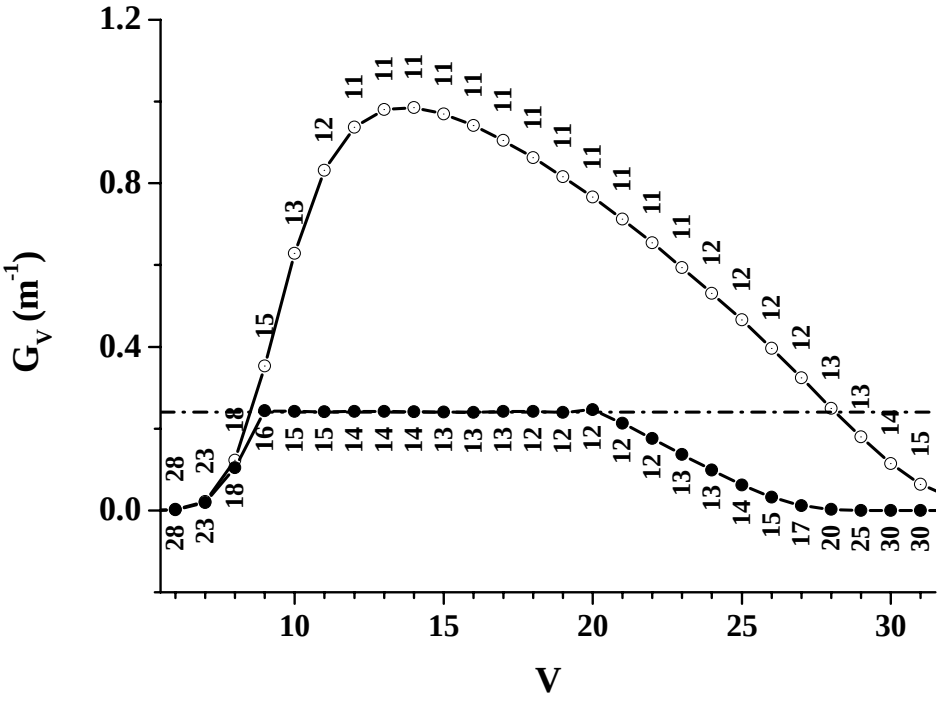

Fig.I.2.10. Spatially averaged maximum SSG coefficient (open circles) and saturated gain coefficient for conditions of multi-mode lasing, T_w = 100 K.

RF discharge fundamental band CO laser.
(*Subtask 1A.4.*)

Fig.I.2.11 a, b, c for multi-mode lasing illustrate variation of the laser spectrum caused by the change of wall temperature from 80 to 120 K. **Fig.I.2.11 d** shows the laser spectrum for fundamental mode lasing at the wall temperature 100 K. At the top of histograms rotational numbers are indicated. At the wall temperature 120 K a red shift of the spectrum is observed correspondent to disappearance of lowest transition V=9→8. Rotational numbers of oscillating transitions increased with temperature rise. When the fundamental mode is oscillating, the laser intensity is higher in the center of the gap where the gas temperature is higher. As a result, in the single-mode regime rotational numbers of laser transitions are higher than in the multi-mode regime (compare **Fig.I.2.11 b** and **d**).

Fig.I.2.12 demonstrates how the wall temperature influences on laser efficiency. As expected, the laser efficiency falls down with the wall temperature rise (curves 2 and 3). This behavior agrees with available experimental facts (Zhao, 1991; Colley, 1994). Curve 1 in **Fig.I.2.12** is the result of numerical calculations when extraction of energy by radiation was ignored. It is seen that gas cooling by laser radiation is a very important factor.

For single-mode operation the laser efficiency is lower because the mode intensity is concentrated near the gap center where the gas temperature is higher, and overlap of gain and intensity profiles is worse. Similar reduction of the laser efficiency was observed in the experiments (Colley, 1994) for the single-mode operation. In the experimental work (Xin, 1999) the laser

efficiency 25% was achieved for conditions of cryogenic cooling of walls. Our simulations for the multi-mode regime predict such value of laser efficiency at the wall temperature 115 K. The wall temperature was not measured in (Xin, 1999), but this value of temperature seems to be quite reasonable.

The laser efficiency is governed by a product of two factors: fraction of discharge power going to CO vibrations, η_V, and efficiency of transformation of vibrational energy into laser power, η_{PR}. Dependence of these factors on wall temperature is presented in **Fig.I.2.13**.

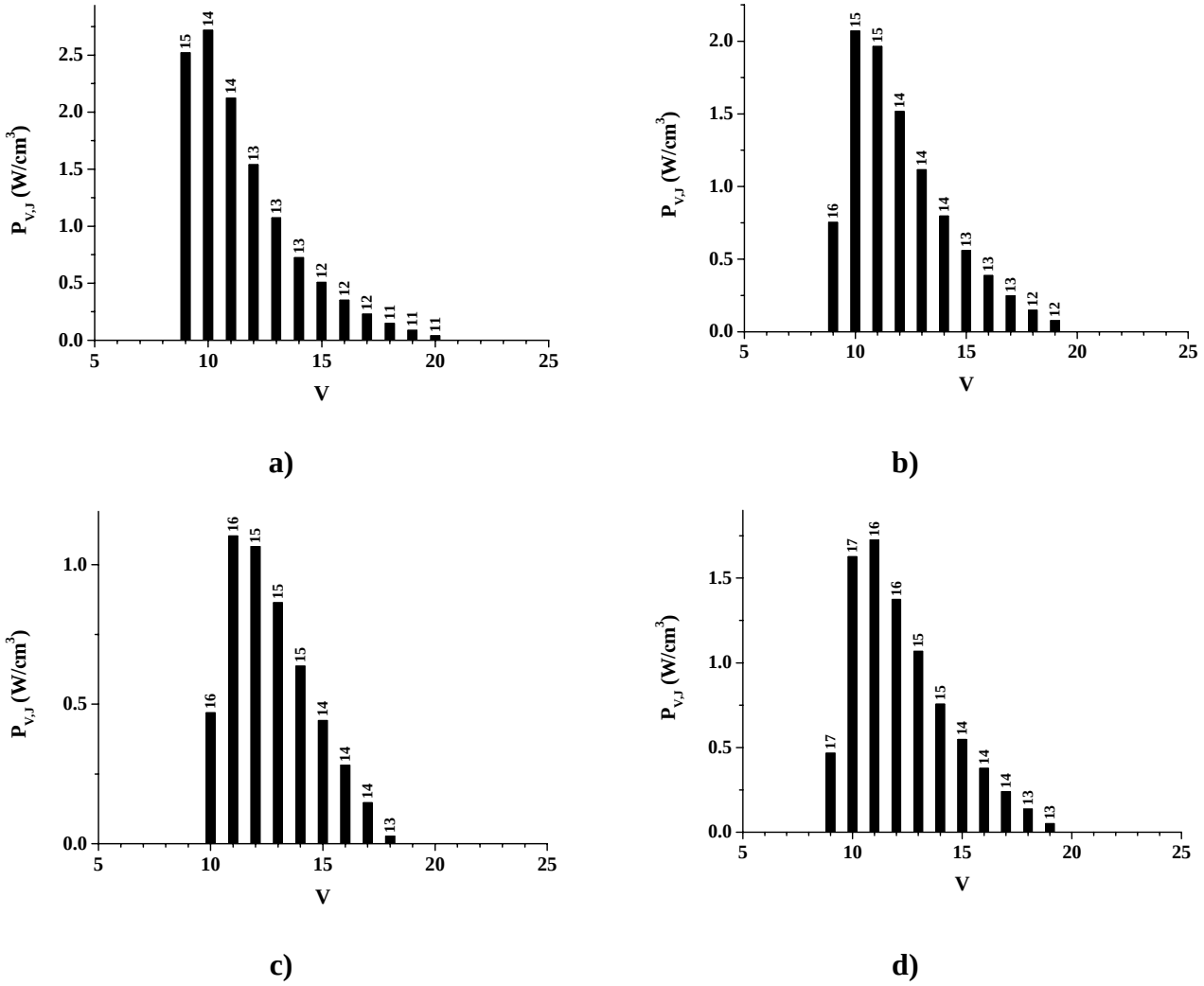

Fig.I.2.11. Laser spectrum: a) T_w = 80 K, multi-mode lasing; b) T_w = 100 K, multi-mode lasing; c) T_w = 120 K, multi-mode lasing; d) T_w = 100 K, fundamental-mode lasing.

Vibrational excitation fraction is almost independent of the wall temperature. The efficiency of vibrational energy transformation into coherent radiation strongly diminishes with temperature rise. This can be explained by reduction of gain coefficient with gas temperature rise. Effect of gain reduction is more remarkable for single-mode regime (compare curves 2 and 2'in **Fig.I.2.13**).

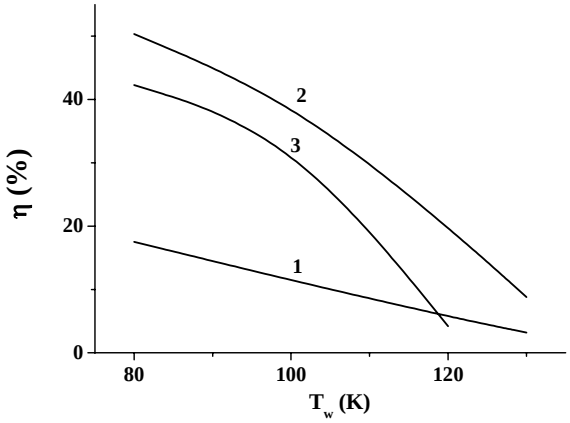

Fig.I.2.12. Laser efficiency as a function of T_w. 1 cooling by laser radiation is ignored; 2 – multi-mode lasing; 3 – fundamental-mode lasing.

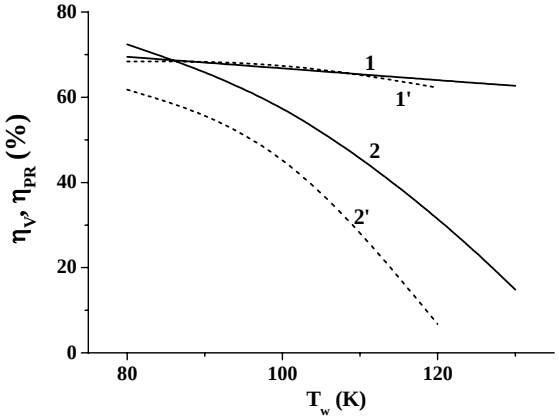

Fig.I.2.13. Fraction of discharge power going to CO vibrations, η_V, (1, 1') and efficiency of transformation of vibrational energy into laser power, η_{PR} (2, 2') vs wall temperature T_w. 1, 2 – multi-mode lasing; 1', 2' - fundamental-mode lasing.

Modifications of RF discharge model by inclusion coupling between electron and vibrational kinetics.
(Subtask 2A.2).

It is known that the distribution of CO molecules over vibrational levels in CO laser gain medium is characterized by vibrational temperature at lower levels about ~3000 K, and has an extended so-called plateau located above Treanor's number (Gordiets, 1986). For this reason collisions of electrons with vibrationally excited molecules result in excess heating of electrons. Besides, new ionization channels associated with high-excited CO molecules come into the play. Earlier some ionization channels were considered in analyses of glow discharge positive column in CO-containing gas mixtures (Grigor'yan, 1992).

Our model of RF discharge in CO-containing mixtures was modified to include the above-mentioned phenomena and make more reliable predictions of the RF discharge characteristics for conditions typical for CO laser operation. Special numerical tests proved that under typical conditions of RF pumped CO laser the electron mean energy and transport coefficients (electron drift velocity, diffusion coefficient) are weakly influenced by a degree of vibrational excitation, and this effect may be neglected.

In contrast, the electron impact ionization rate is rather sensitive to vibrational excitation degree through appearance of high-energy electrons gaining additional energy in collisions with vibrationally excited molecules. It was shown (Alexandrov, 1987) that rate enhancement caused by this additional electron heating for any process with a high threshold could be approximated with the following expression:

$$\lg\left[\frac{K(z)}{K(0)}\right] = \frac{Cz}{\left(E/N\right)^2} \qquad \text{(I.2.2)}$$

where K is the rate coefficient for the respective process, E electric field strength, N gas density, $z = \exp(-\hbar\omega/T_v)$, $\hbar\omega$ vibrational energy quantum, and T_v vibrational temperature for lowest vibrational levels. The factor C is to be found from solution of electron Boltzmann equation taking

into account electron collisions with vibrationally excited molecules. For mixtures of CO with atomic gases it was shown (Alexandrov, 1978) that *C* is the same for ionization and excitation of electronic levels, as well. In our approach, the rate coefficient for unexcited gas *K*(0) is computed as a function of the mean electron energy, while its correction associated with vibrational excitation degree is the function of local value of *E/N*.

The low-levels vibrational temperature T_v has been calculated in a cell of spatial numerical grid using a procedure described in (Gordiets, 1986). This procedure is reduced to fitting two forms of the vibrational distribution function (VDF); one of them is valid for lower levels (so-called Treanor function (Treanor, 1968)) and another for the plateau, where an expression for the VDF is following: $f_V = \frac{c}{\mathbf{V}+1}$, **V** is the vibrational level number; the factor $c = (w/\nu)^{0.5}$, $\boldsymbol{w}$ is the rate of vibrational levels excitation, $\boldsymbol{\nu}$ is an effective VV exchange frequency dependent on gas temperature and density. The rate of vibrational excitation is defined as $w = \frac{W_V}{N_{CO}\hbar\omega}$, where W_V is the reduced power density going to molecular vibrations averaged over RF cycle. An expression for the effective VV-exchange frequency was taken from Ref. (Demyanov, 1984). The resulting analytical shape of the VDF is illustrated in **Fig. I.2.14** for typical conditions of CO laser.

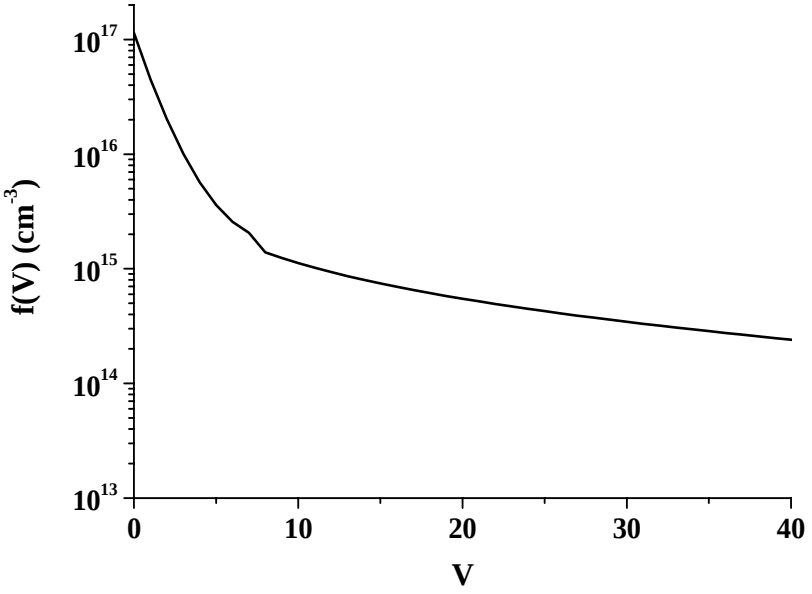

Fig. I.2.14. Typical vibrational distribution function calculated analytically.

A new mechanism of ionization was proposed in (Grigor'yan, 1992), which can produce additional ionization in typical for CO laser conditions (see **Fig. I.2.15** illustrating CO energy levels involved in this mechanism). A key process is an associative ionization:

$$CO(V>15) + CO(I^1\Sigma^-) \rightarrow C_2O_2^+. \qquad (I.2.3)$$

To account properly this mechanism, the following processes were introduced additionally in our model: electron-impact excitation of metastable state $CO(I^1\Sigma^-)$, collisional quenching of this metastable by CO molecules and the process (I.2.3). Rate constants and cross sections for respective processes were taken from (Grigor'yan, 1992). Direct electron excitation and collisional quenching by CO molecules in ground state control the balance of molecules in the state $I^1\Sigma^-$. Therefore, the ionization rate in the process (I.2.3) is proportional to the ratio of rate constants for process (I.2.3) and for ordinary collisional quenching. This ratio was determined in (Grigor'yan, 1992). The

$CO(I^1\Sigma^-)$ quenching rate value falls into microsecond range, while the RF half-cycle is shorter than 0.01 of μs. Hence, the $CO(I^1\Sigma^-)$ excitation rate strongly modulated in time can be averaged over the RF cycle while calculating dynamics of $CO(I^1\Sigma^-)$ population. Populations of CO(V) molecules for V>15 were calculated by above-mentioned analytical formulas.

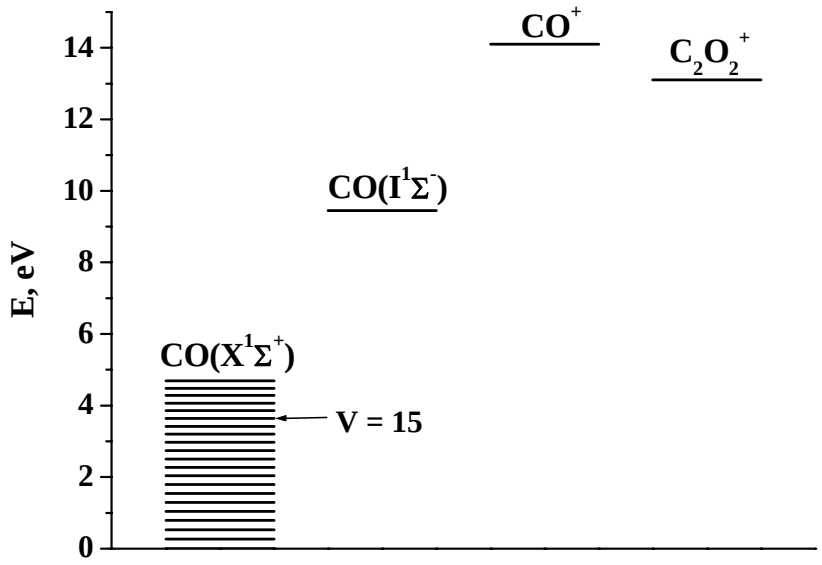

Fig. I.2.15. Schematic of levels of CO molecule involved into new ionization mechanisms.

In numerical calculations we used the non-uniform spatial grid with the cell size diminishing to electrodes. Typically, the number of cells was 100. Space-time dynamics has established usually after a couple of thousands of cycles.

The above-described model allows us to evaluate a role played by vibrational excitation in balances of particles and energy in the RF discharge for typical for CO laser conditions. **Fig. I.2.16** shows spatial profiles of RMS-value of electric field calculated by modified and by old models, respectively. Introduction into the model of new ionization mechanisms associated with CO vibrational excitation results in reduction of E/N_{RMS} value in the discharge center on 10-20%. An additional study reveals that growth of electron-impact ionization rate according (I.2.2) plays minor role in comparison with the associative ionization (I.2.3).

At fixed discharge power, the reduction of E/N_{RMS} in plasma is followed by its rise in the vicinity of electrodes. Such transformation is a consequence of electric current amplitude increase. In the near-electrode regions the dominant component of the current is the displacement current, which can be increased by virtue of electric-field amplitude rise. As a result, the Voltage-Power Characteristic (VPC) of the RF discharge is insensitive to modifications of our model described in this report. **Fig. I.2.17** illustrates the degree to which vibrational excitation influences on the VPC.

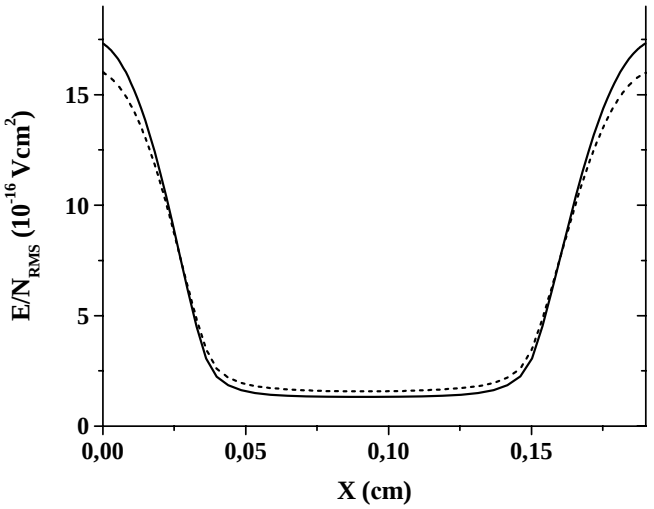

Fig. I.2.16. Predicted E/N_{RMS} spatial profiles. Solid line – present model, dotted line – our old model ignoring vibrational excitation of CO.
f = 81.3 MHz;
d = 0.19 cm;
CO:He=1:10;
P = 100 Torr;
W= 50 W/cm^3.

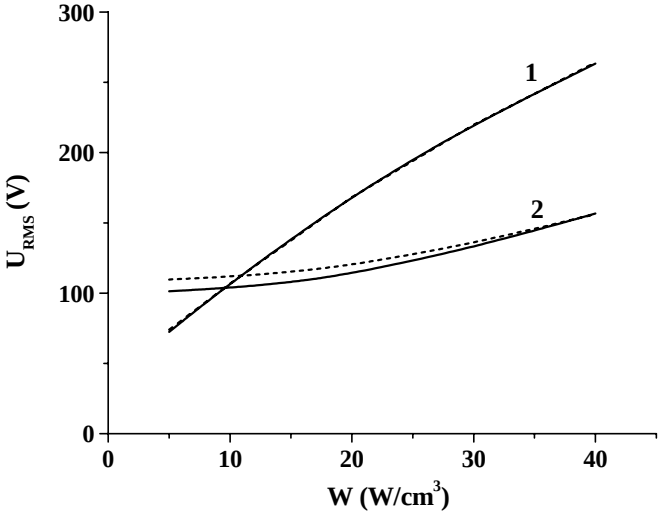

Fig. I.2.17. Predicted dependences of RMS discharge voltage on space-averaged discharge power density.
Solid line – present model,
dotted line – our old model ignoring vibrational excitation of CO.
f = 81.3 MHz;
d = 0.19 cm;
CO:He = 1:10;
1 - P=30 Torr;
2 - P=100 Torr.

The modified model predicts lower voltage at higher pressures and lower power. At gas pressure of 30 Torr the effect is negligible. In plasma, the value of E/N_{RMS} for typical conditions falls into the range where vibration excitation efficiency is a declining function. Since the additional ionization at high vibrational excitation degree leads to lowering E/N_{RMS}, the vibration excitation efficiency grows (**Fig. I.2.18**). As a result, the laser efficiency rises, too.

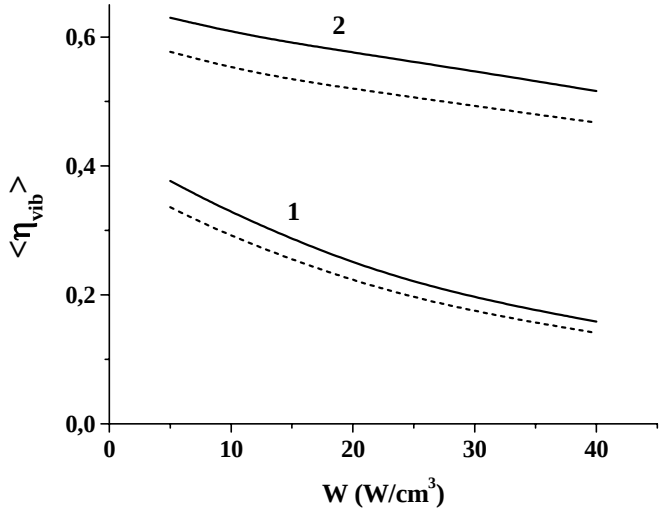

Fig. I.2.18. Predicted dependence of vibration excitation efficiency on space-averaged discharge power density.
Solid line – present model,
dotted line – our old model ignoring vibrational excitation of CO.
f = 81.3 MHz;
d = 0.19 cm;
CO:He = 1:10;
1 - P=30 Torr;
2 - P=100 Torr.

Extension of the model to cover additional molecular vibrations-induced ionization mechanisms gives also some redistribution of discharge power density in the discharge gap. Estimations of energy transfer with vibrationally excited molecules give the result that the local gas-heating rate can be approximated by discharge power density with a good accuracy. Then the gas temperature in the center of spacing at the fixed total power varies within some limits with variations of power density profile. Addition of ionization processes associated with vibrational excitation degree leads to E/N_{RMS} and power density reduction in plasma, but growth of them in near-electrode layers. As a result, the gas temperature in the gap center diminishes.

Technical proposal on new RF discharge facility with cryogenic gas cooling.
(*Subtasks 2A.1)*

The temperature of the active medium is an important parameter which influences strongly upon the operation efficiency of CO lasers and, in particular, CO lasers with RF excitation of active gas medium. Besides that, new experimental data on RF discharge properties and RF excited CO laser characteristics at cryogenic temperatures of the active gas mixture are needed for further verification of the RF discharge slab CO laser theoretical model which, as was shown earlier, satisfactory described RF discharge and lasing parameters for slab CO laser operating at room temperature of the active gas mixture. Experimental laser facility was designed and manufactured to obtain the data in conditions of diffusive cryogenic cooling of active gas mixture RF excited in planar slab electrode system. The laser facility (**Fig.I.2.19**) was equipped with vacuum pump system, gas mixture components supply system, RF discharge monitoring system and system for laser parameters measurements. The main features of proposed laser facility are shown in **Table I.2.3.**

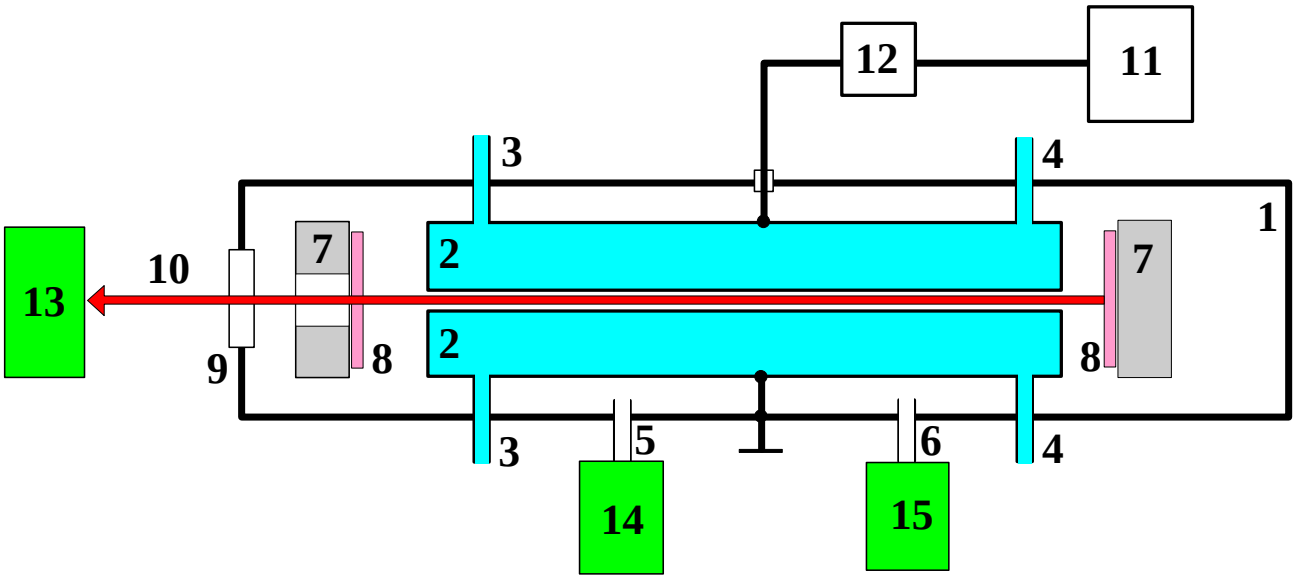

Fig. I.2.19. Schematic of RF discharge CO slab laser facility. 1 - laser chamber; 2 - electrodes; 3,4 - liquid nitrogen inlet/outlet; 5 - gas mixture inlet; 6 - vacuum pumping; 7 - optical holders, 8 - mirrors; 9 - output optical window; 10 - laser output; 11 - RF generator; 12 - reflected RF power meter; 13 - laser radiation parameters measuring system; 14 - gas mixture preparing system; 15 - pump system.

Table I.2.3.
Parameters of RF CO slab laser facility.

Parameter	Value
Working RF frequency	81.36 (±5%) MHz
RF generator output power	500 W (max)
Electrode system:	
gap	1.5÷3 mm
width	15÷20 mm
length	250÷300 mm
Discharge volume	5÷15 cm^3
Laser chamber inner volume	~5 liters
Working gas mixture pressure	up to 150 Torr
Gas mixture components	CO, He, N_2, Ar, O_2
Cooling substance	liquid nitrogen
Laser resonator	internal, manual driven

Design of the new cryogenically cooled RF discharge facility.
(Subtask 2A.2)

According to proposed concept (see above), experimental laser facility was designed and manufactured to obtain the data in conditions of diffusive cryogenic cooling of active gas mixture RF excited in planar slab electrode system. The facility consists of two main parts: a) laser chamber, b) RF power supply. Also, there are additional systems needed for: vacuum pumping and gas mixture preparing, supplying discharge electrodes with liquid nitrogen, vacuum and laser gas mixture pressure control, laser resonator elements alignment and laser output power measurements, equalization of the discharge chamber input impedance with output impedance of RF power supply.

Laser chamber.

The laser chamber (**Fig. I.2.20**) made of organic glass consists of main body, lower and upper covers. The main body is equipped with optical CaF_2 windows for laser radiation output and four rotation inlets for manually alignment of the laser resonator mirrors.

The lower cover have two outside holders that are used for adjusting the position of the laser chamber with respect to the optical table. At the inner side of the lower cover, the massive metallic plate supported electrode system and laser resonator optics is located.

The upper cover is equipped with four identical (in/out)lets for liquid nitrogen supplying and removing (separately for each electrode), and with two RF power inlets of the same design. All six inlets have teflon thermo-isolation preventing the material of the cover (organic glass) from cryogenic temperatures of the inlets.

RF discharge electrode system (**Fig. I.2.21**) is located inside the laser chamber. The system consists of two prismatic hollow brass electrodes of hexagonal crossection. The length of the electrode along the laser resonator axis is 250 mm, the slab width - 16 mm. Working surfaces of both electrodes was polished and gold-coated to exclude some chemical processes in the discharge and avoid the oxygenation of brass. The RF discharge gap of ~2 mm is formed between two electrodes which are fixed at the massive metallic base by three dielectric holders with tuning screws. Each electrode has two flanges connected by soft polyethylene tubes with liquid nitrogen (in/out)lets in upper cover of the laser chamber. Also, there are two cooper conductors connecting the electrodes with RF power inlets.

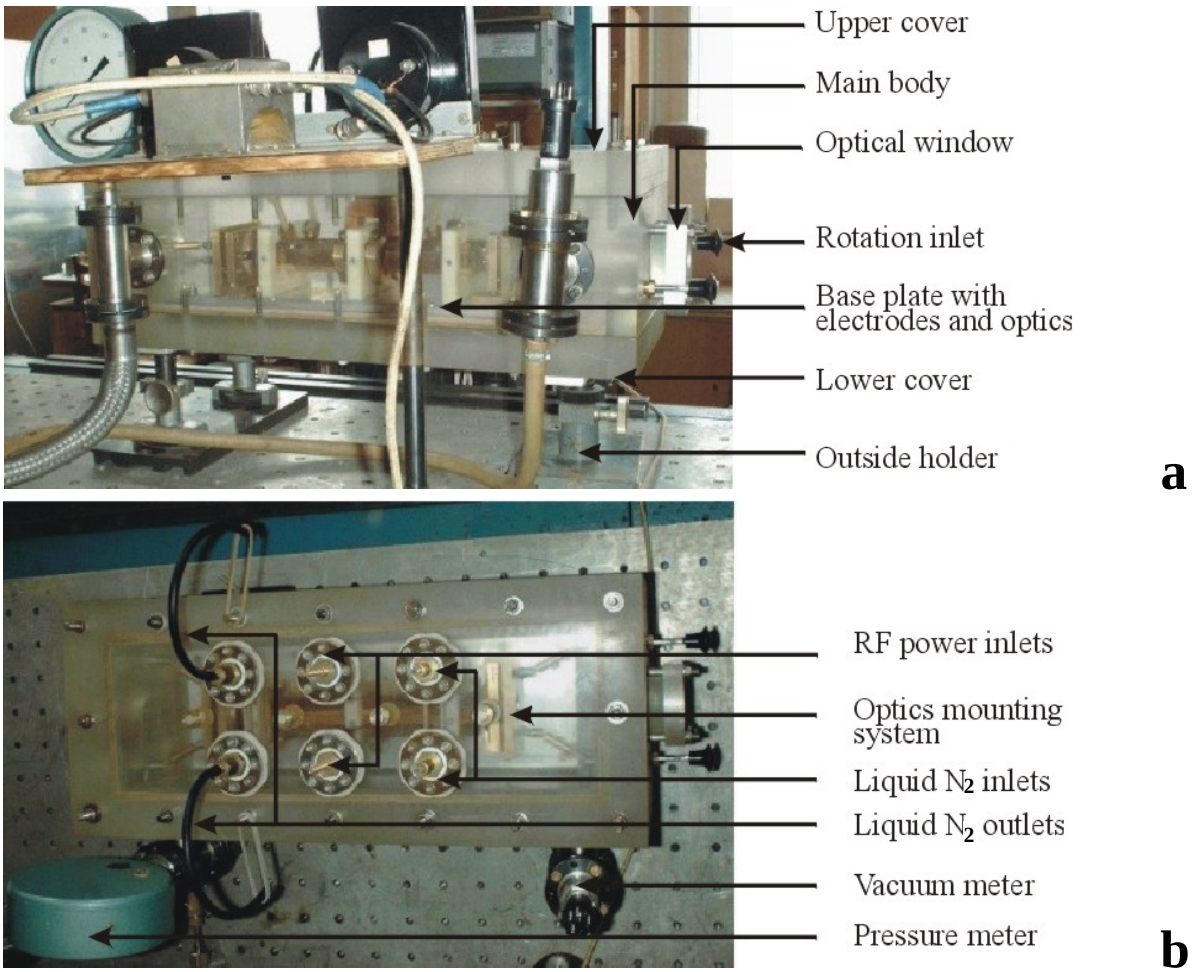

Fig.I.2.20. RF CO laser discharge chamber. **a** - rear view, **b** - top view

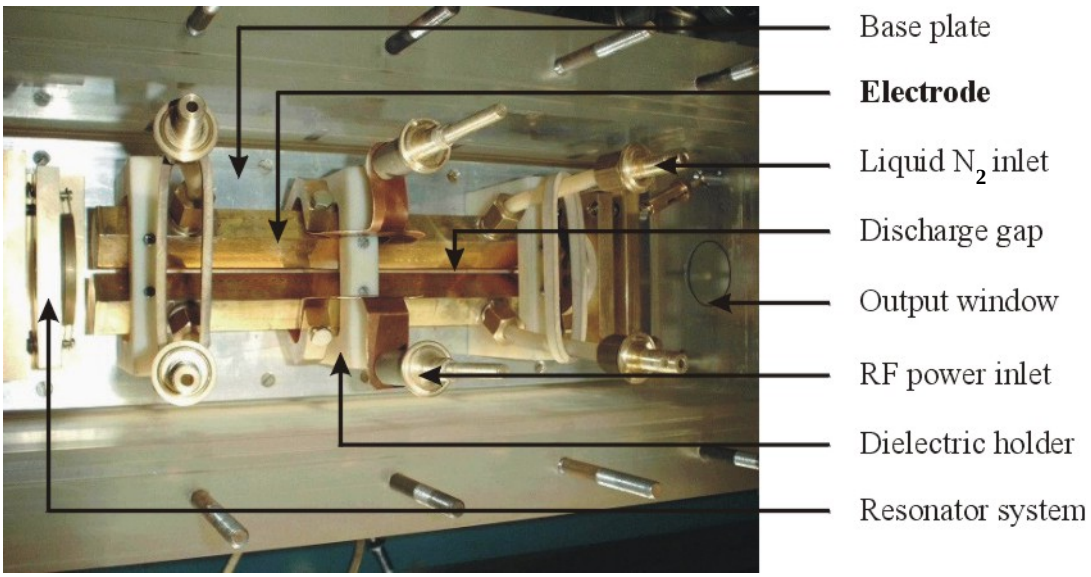

Fig.I.2.21. RF discharge electrode system (top view).

Laser resonator optics mounting system (**Fig. I.2.22**) consists of two identical mirror's holders. Each holder has a possibility of precise turning the mirror in two orthogonal degrees of freedom.

The heads of holder's tuning screws are connected with the rotation inlets in the main body of the laser chamber by means of flexible removable Cardan shafts. The mirror's holders are located at the same massive metallic base which is used as electrode system base in such a way that the distance between the laser resonator mirrors is equal to 260-280 mm (depending on the thickness of the mirrors used).

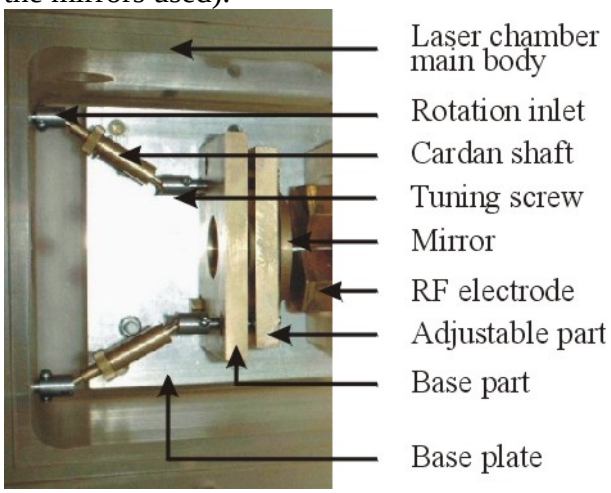

Fig. I.2.22. Laser resonator optical system (top view)

Fig. I.2.23. RF power supply

RF power supply.

RF power supply (model RFPS 500AM) (**Fig. I.2.23**) was ordered and manufactured in Russian company "Polygon" (http://www.polygon.vrn.ru) through the ISTC. This model has following characteristics (**Table I.2.4**).

Table I.2.4.
RFPS 500AM characteristics.

Parameter	Value
Working frequency band	81.36 MHz ± 1%
Nominal output impedance	50 Ohm
Maximal output power	500 W
Output power regulation range by voltage amplitude by pulse width/length modulation *(modulation frequency 0.1-25 KHz)*	 25-100% of P_{max} 10-100% of P_{max}
Cooling	Internal, by air
Electric power consumption	220 VAC, 50 Hz, 1200 W

This model of the RF power supply has special mode of operation with pulse width/length modulation: there is the possibility of using "super pre-pulse" (short pulse of increased amplitude at the front of each modulating pulse) to simplify the process of RF discharge ignition. Also RF power supply has an automatic defense system against overheating and load mismatch.

Additional systems

RF discharge CO laser facility is equipped with different additional systems needed for its operation (some of them are presented in **Fig.I.2.24**).

Laser chamber may be evacuated down to the pressure level ~10^{-3} Torr. Gas mixture preparing system (**Fig.I.2.24a**) allow to prepare gas mixtures containing up to five gas components with total pressure up to 200 Torr.

Direction sensitive RF power splitter (**Fig.I.2.24b**) is introduced in coaxial cable between RF power supply and laser chamber. The splitter monitors respective levels of inputted and reflected RF electric power. Minimal reflection corresponds to equalization the RF discharge impedance with the output impedance of RF power supply (50 Ohm). This equalization is carried out manually by usual T-like matching LC-circuit with variable parameters.

a **b** **c**

Fig.I.2.24. Additional systems. **a** - vacuum pumping and gas mixture preparing system, **b** - impedance equalization control, **c** - liquid nitrogen supplying system.

Cryogenic cooling system consists of single reservoir with two symmetric LN_2 outputs (**Fig.I.2.24c**). The outputs are connected to laser chamber LN_2 inlets by soft polyethylene tubes. Nitrogen evaporated inside the hollow electrodes is removed from the laser chamber through the LN_2 outlets.

The first preliminary test experiments with the RF CO laser facility demonstrated the lasing effect (near the gain threshold) at following conditions: stable waveguide resonator (effective transparency of ~10%), laser gas mixture CO:He:Xe:N_2=1:12:2:3, initial pressure ~30 Torr, electrode temperature ~150 K.

Experimental study of RF discharge cryogenically cooled fundamental band CO laser. *(Subtask 2A.3)*

Electrode system cooling

It is very important to know the translational temperature of a laser mixture because this parameter influences strongly on efficient CO lasing (the lower the working temperature, the higher the laser efficiency). This information is also necessary for adequate modeling of CO laser output characteristics. For these reasons, experiments were carried out to measure the time behavior of the RF discharge electrode system temperature during its cooling by liquid nitrogen (LN_2) without applying RF discharge. Simultaneously, the temperature gradient along the RF discharge electrodes was measured. The temperature measurements were performed with thermopiles coupled with the body of one of the electrodes in two points - near the LN_2 inlet (T1) and near LN_2 outlet (T2) (see **Fig.I.2.25**).

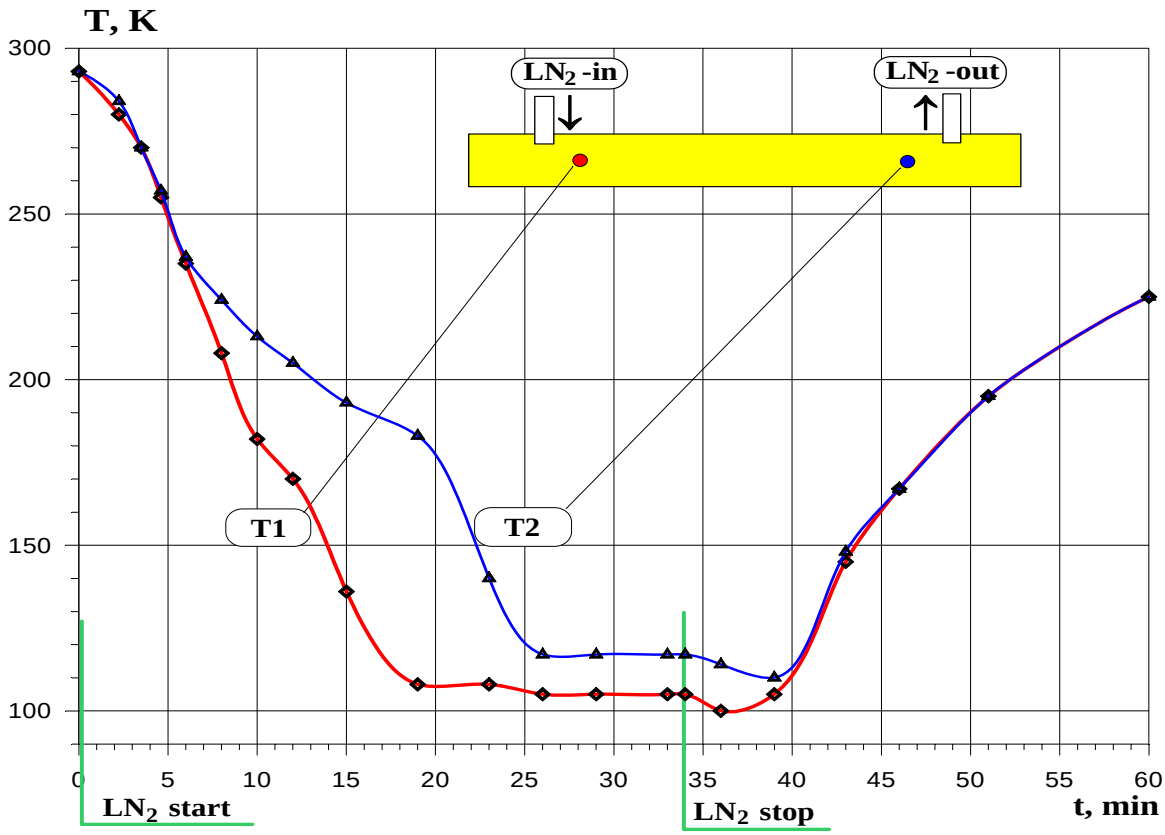

Fig.I.2.25. Time dependency of RF electrode temperature on cooling time. Cooling without RF discharge. T1 (T2) – the temperature near the LN_2 inlet (outlet). Zero point at the time axis corresponds to the beginning of LN_2 supplying. The temperature measurement accuracy ±2K.

Significant temperature gradient was observed in the experiments during the cooling of the electrode system. Its maximum value reached 60-80K (see **Fig.I.2.25**) along the total RF electrode length (250 mm) at the middle stage of cooling (t=15-25 minutes after the beginning of the cooling process). It was shown that about 30-35 minutes was needed for thermalization of the RF discharge electrode system cooled by the LN_2 flow of constant velocity. After this period, the temperature of the electrodes was stabilized at ~110K with maximal T1-T2 difference of ~10-15K.

Elimination of LN_2 supply resulted in symmetrization of thermal loss processes and, as a consequence, in fast (3-4 min) diminishing T1-T2 difference down to ~3-5K (see time period t>35 min in **Fig.I.2.25**). About the same diminishing T1-T2 difference was observed during further cooling of the electrodes after the time period t~45-50 min (**Fig.I.2.26a**). It should be noted that the experiments were carried out without RF discharge between the electrodes.

Test measurements were performed to show how the temperature of pre-cooled electrodes changes when the RF pumping of the gas in the discharge gap was turned on during fixed time interval (**Fig.I.2.26b-d**).

After the cooling time period t~45 min (T1, T2 ~ 105K), about 100W RF discharge average power <Pin> (F_{RF}=81.36 MHz) was supplied to the electrodes during Δt=1 min (gas - pure He at initial pressure 40 Torr, discharge gap ~2.8 mm) (**Fig.I.2.26b**). The electrode temperature increased (T1 and T2 synchronously) of about 4 K. The same experiments with RF discharge average power of ~100W and ~200W turned on during Δt=2 min gave the increase of T1 and T2 of about 5-6K and 10-12K, respectively (**Fig.I.2.26c, d**).

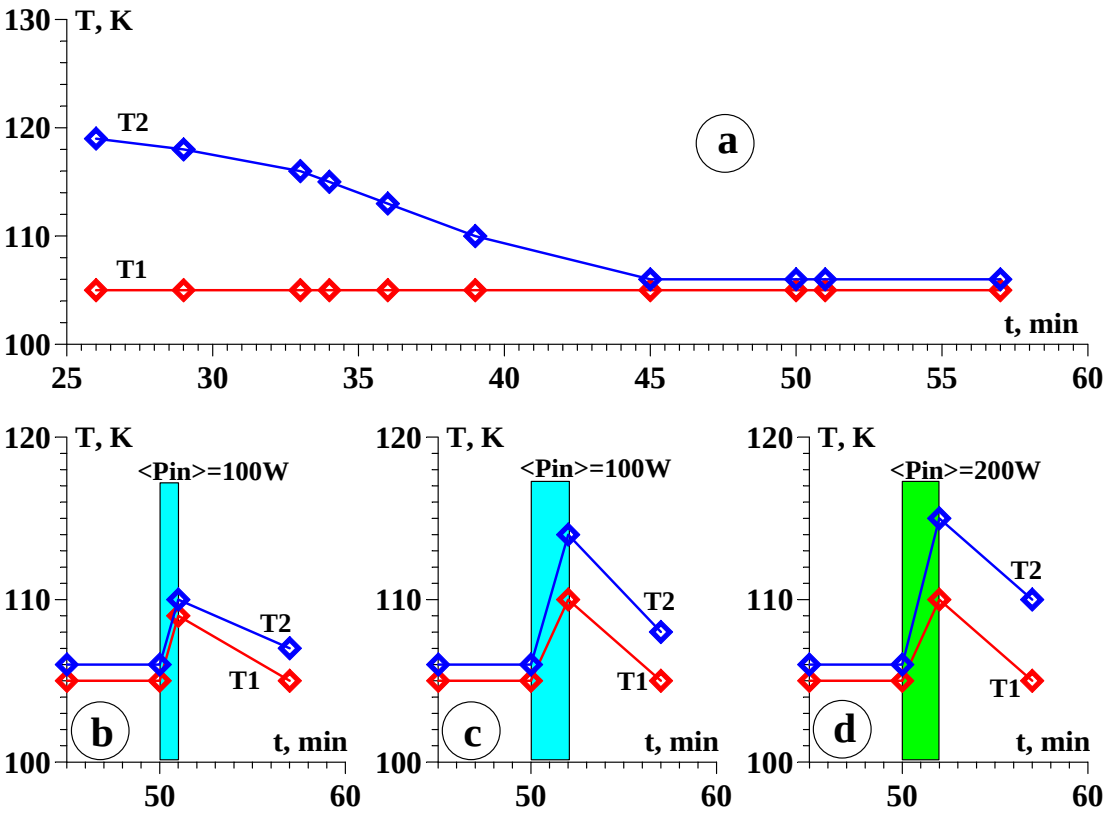

Fig.I.2.26. Temporal behavior of electrode temperatures T1 and T2 (designations as in **Fig.I.2.12**) without RF pumping of a gas mixture (a) and with RF discharge turned on during a fixed time interval Δt (b-d). <Pin>=100W (b, c) and 200W (d); Δt=1 min (b) and 2 min (c, d);

As a conclusion, it was shown that respectively long time period (~1 hour) is needed to cool the electrode system down to the temperature ~105-110K and to equalize the temperature along the electrode length with the accuracy better than ±3-5K. It was also demonstrated that RF power up to ~200 W loaded into the gas in the discharge gap did not lead to dramatic increase of the electrodes temperature.

RF discharge slab CO laser characteristics

Before lasing experiments, thermopile equipment was removed from the facility to avoid additional electrical contacts between the RF electrodes, ground points and other elements of the RF discharge laser installation.

Optical scheme of the RF discharge CO laser experiments is presented in **Fig.I.2.27**. The laser resonator of 280 mm length consisted of concave (R_{curv}=5 m) totally reflecting Au-coated copper mirror 1 and dielectric coated CaF_2 plane mirror 2 with total reflectivity of 90-95% in spectral range of 1800-1950 cm^{-1}. Output laser radiation was splitted into different calibrated parts and directed successively to the laser power meter, photo-detector and IR spectrograph.

The procedure of RF discharge electrodes cooling was performed as described above during the time period of about 1 hour. Gas mixture He : CO : Air = 10 : 1 : 1 at initial pressure of 42 Torr was used in the experiments. The initial pressure was measured as a mean pressure inside the discharge chamber having room temperature walls. Taking into account that the gas temperature inside discharge gap was about 110K, the active particles density in the gap was assumed about

three times higher than one corresponding to the initial pressure inside the discharge chamber being at ~300K. The results of measuring CO laser mean output power $<P_{out}>$ versus the mean RF power loaded into the discharge gap are presented in **Fig.I.2.28a**.

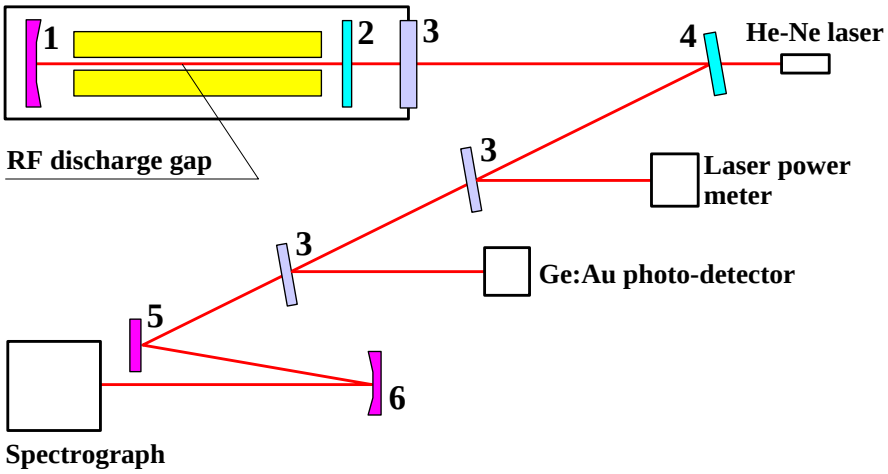

Fig.I.2.27. Optical scheme of RF discharge CO laser experiments. 1, 2 - laser resonator mirrors, 3 - CaF_2 plane plate, 4 - dielectric coated CaF_2 plane beam splitter (reflectivity of 83 % for λ^{-1}=1850-2000 cm^{-1}), 5 - plane Al-coated quartz mirror, 6 - concave Al-coated quartz mirror.

Variation of the input RF power was performed by changing the ratio of T_P/T_0 ($<P_{in}>$= 500·(T_P/T_0) [W], see **Fig.I.2.28a**) at constant frequency $1/T_0$=F=500 Hz of amplitude modulation. (Pulsed RF power input was fixed and equaled to the maximal value of 500 W.)

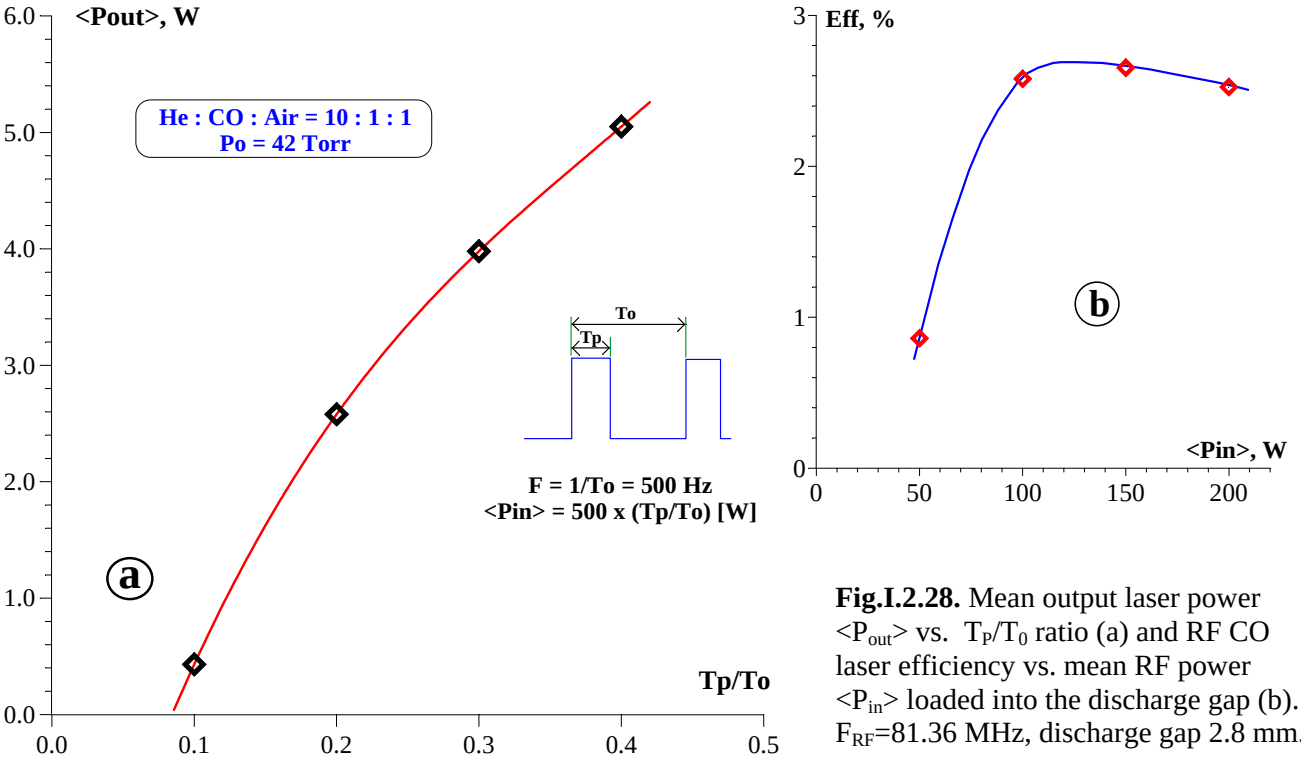

Fig.I.2.28. Mean output laser power $<P_{out}>$ vs. T_P/T_0 ratio (a) and RF CO laser efficiency vs. mean RF power $<P_{in}>$ loaded into the discharge gap (b). F_{RF}=81.36 MHz, discharge gap 2.8 mm.

Dependency of RF CO laser efficiency on mean RF power loaded into the discharge gap is presented in **Fig.I.2.28b**. The lowest value of lasing efficiency (~1 %) at $<P_{in}>$ ~ 50 W corresponded

to the unstable mode of RF discharge when the discharge plasma did not fill the total volume of the discharge gap.

Stable mode of RF discharge (when all the gap volume was filled with the discharge plasma) is characterized by the CO lasing efficiency ~2.5 %.

Typical time behavior of RF CO laser output power obtained with the photo-detector (see **Fig.I.2.27)** is presented in **Fig.I.2.29**. Here one can see the first peak with following decrease of the radiation intensity during each RF pumping pulse and the second peak corresponding to the end of the RF pumping pulse.

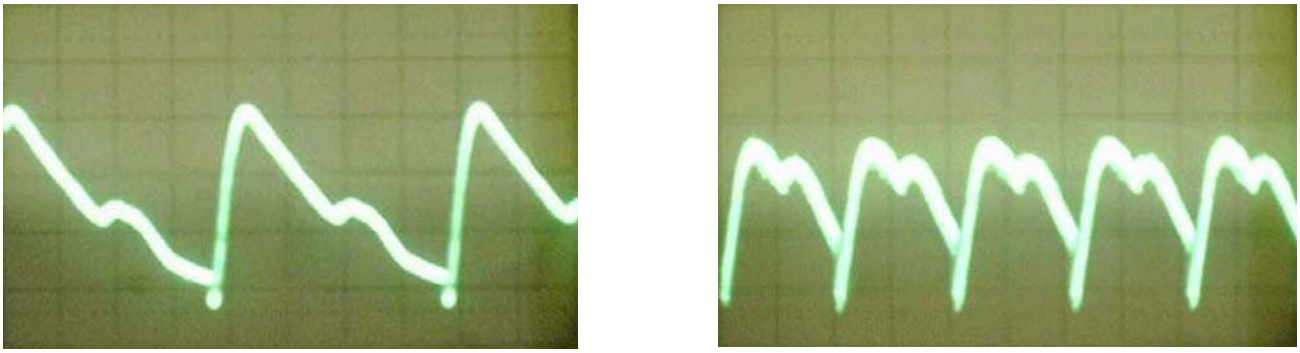

a **b**

Fig.I.2.29. Time resolved behavior of RF CO laser output power. He:CO:Air = 10:1:1, initial pressure 42 Torr, discharge gap 2.8 mm, F_{RF}=81.36 MHz, F=500 Hz (a) and 1000 Hz (b), T_P/T_0=0.4. Time scale 0.5 ms / div.

During the experiments it was found that the output laser power decreased rapidly in time under the constant RF pumping conditions. Typical time period of stable output laser power was not longer than 25-30 s at lower pump power and 10-15 s at $<P_{in}>$ ~ 200 W.

Having a look into the laser chamber after the experiments described above, one could see that the elements of the RF discharge electrode system were coated with dark powder-like substance which probably is carbon. The density of this coating appeared to be maximal at the working surfaces of the discharge gap. This low-reflecting coating appeared at the RF discharge electrode surfaces resulted in suppressing effective wave-guide mode of CO laser operation, and it is apparently one of the main reasons of the very low RF CO laser efficiency at cryogenic temperatures of active gas mixture.

For these reasons the experiments were performed at T_P/T_0 ratio <0.4 corresponding to ($<P_{in}>$) <200 W. The same reason did not give the possibility to measure precisely RF CO laser output spectrum. It was observed in the experiments but it may be described only as "6÷8 lasing lines within 1860-1960 cm^{-1} spectral range".

Further RF discharge CO laser facility development.

Taking into account the results of the experiments described above we decided to modify the laser installation, namely, a closed circle transverse gas flow system (**Fig.I.2.30**) was introduced in the discharge chamber to remove products of chemical reactions from RF discharge gap volume during the operation of RF excited CO laser with cryogenic cooling of the electrodes.

Also, for higher thermal stability of the laser resonator, mirrors mounting system was mechanically separated from the cooled elements of the RF discharge electrode system, and two invar rods was used for stabilization of the laser resonator length and alignment. New design of the optics mounting system is presented in **Fig. I.2.31**.

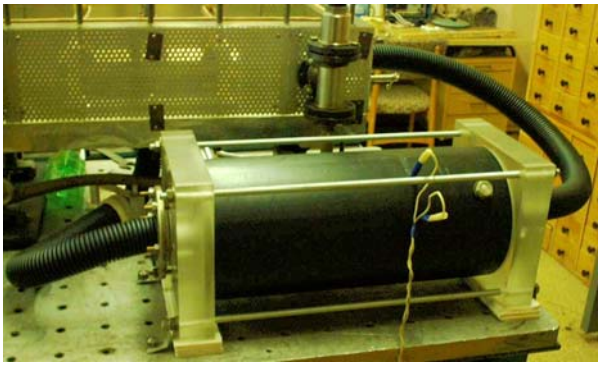

Fig.I.2.30. Fan unit of closed circle transverse gas flow system.

Fig. I.2.31. New design of the optics mounting system.

Comparison of modified RF discharge theory with RF discharge CO laser operating at low temperatures
(Subtask 2A.4)

Earlier developed 1D model of the RF discharge including calculation of the vibrational distribution function (VDF) of CO molecules was described in detail in (Ionin, 2001). Actually, this model was applied only to N_2 free laser mixtures. In our experiments (see ***Subtask 2A.3***) the mixture He:CO:Air=10:1:1 was used. **Fig. I.2.32** shows the electron energy balance components responding for vibrational excitations of molecules as a function of E/N for this mixture. As usually, the balance was computed by solving electron Boltzmann equation. Numerical simulations of discharge characteristics for conditions of the experiment (**Fig. I.2.33)** gave $(E/N)_{RMS}$ values in discharge gap vary between $2.0 \cdot 10^{-16}$ V cm^2 in the middle and $2.8 \cdot 10^{-16}$ V cm^2 near the electrodes, where molecular vibrations are excited less effectively (see **Fig.I.2.34**). It is seen in **Fig. I.2.32** that in the working range of $(E/N)_{RMS}$ excitation of O_2 vibrations can be neglected. It is known from vibrational kinetics that the vibrational energy from N_2 vibrations is effectively transferred to CO molecules resulting in a low population of N_2 vibrational levels. Therefore, we did not include equations for molecular vibrations of N_2 and assumed that all energy consumed by vibrations of N_2 molecules is transferred to CO vibrational levels.

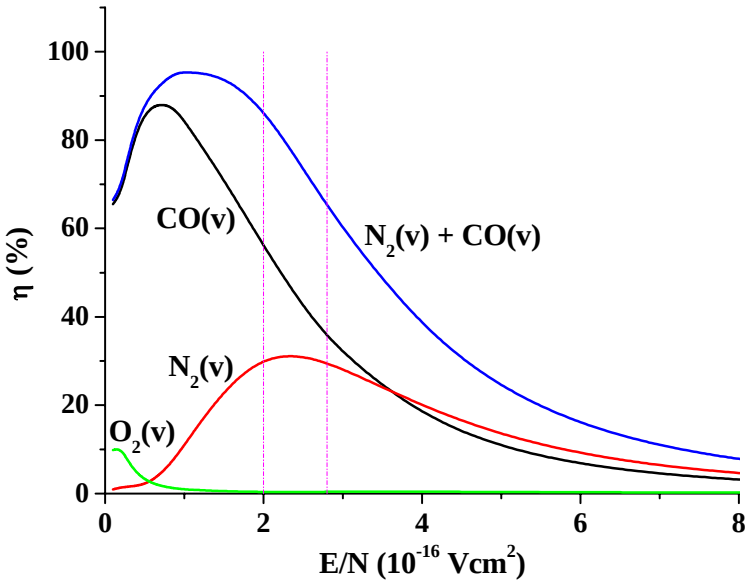

Fig.I.2.32. Fractions of electron energy in plasma spent to excitation of molecular vibrations in mixture He:CO:Air=10:1:1.

Earlier developed model of RF pumped CO laser is applicable to description of steady state discharge and laser. In the above described experiments RF field was step-wise 100% modulated by intensity. Processes of switching on and off RF field induce variations of gas temperature and vibrational distribution function (VDF) of CO molecules. The rigorous approach requires that time-dependent kinetic equations be solved in parallel with plasma equations (including the electron Boltzmann equation) and gas thermal balance equation. There is no available information about existence of numerical codes appropriate to solution of above problem. Therefore, to make upper and lower estimations of laser operation we consider two limiting cases. Assuming the relaxation time of gas temperature and the CO VDF is less than duration of one pulse composed of about 10^5 RF cycles, calculations were made for the *maximum* pump power. The wall temperature was assumed 110 K. **Fig. I.2.33** shows spatial profiles of $(E/N)_{RMS}$, the total power density, W_{Total}, and power density going into molecular vibrations, W_{vib}. The reduced rms electric field strength in the middle of gap $(E/N)_{RMS} = 2.0 \cdot 10^{-16}$ V cm^2 and grows to electrodes. In the middle of the gap vibration excitation efficiency is 72%, while averaged over gap it is about 40%. In the second limiting case, when gas temperature and CO VDF vary slowly so that they feel only *average* pump power, results of calculations are shown in **Fig. I.2.34** for the duty factor 0.4. The vibration excitation efficiency in the middle of discharge has not changed, while the space-averaged efficiency increased up to 58%.

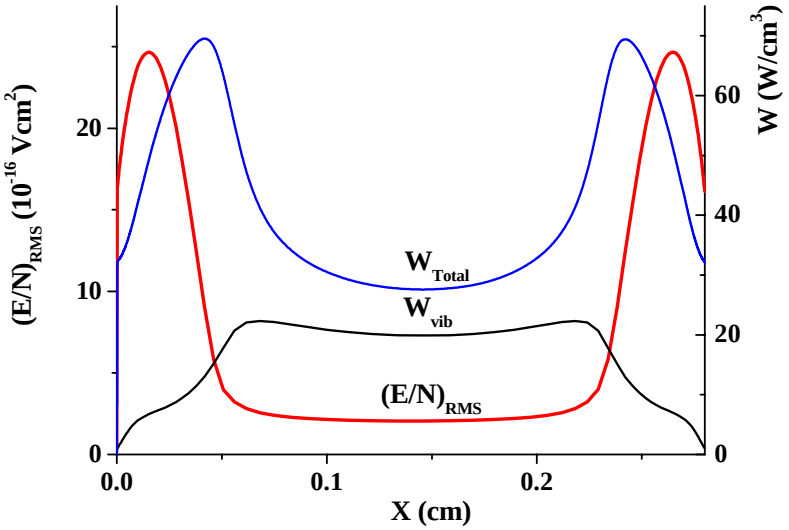

Fig.I.2.33. Spatial profiles of $(E/N)_{RMS}$, the total power density, W_{Total}, and power density going into molecular vibrations, W_{vib}. He:CO:Air=10:1:1, P = 42 Torr, W = 42 W/cm^3, f = 81.36 MHz.

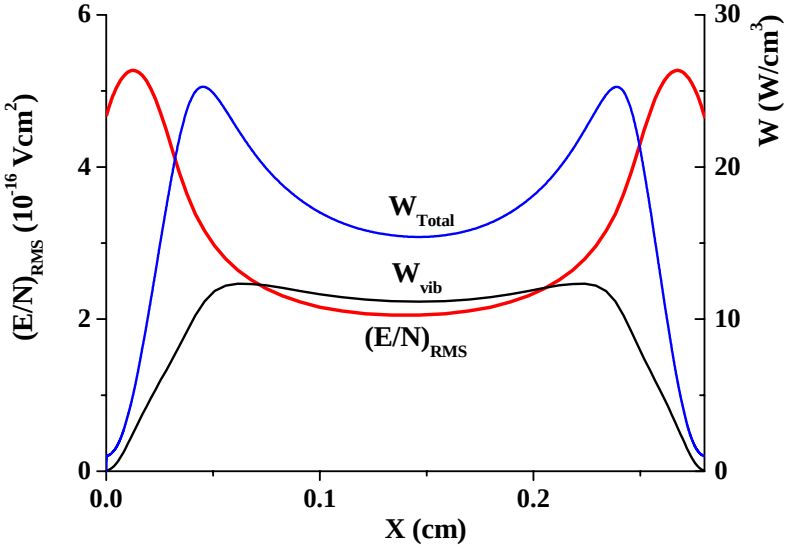

Fig. I.2.34. Spatial profiles of $(E/N)_{RMS}$, the total power density, W_{Total}, and power density going into molecular vibrations, W_{vib}. He:CO:Air=10:1:1, P = 42 Torr, W=16.8W/cm^3, f = 81.36 MHz.

Computed gas temperature distributions over discharge gap are shown for pump powers 42 and 16.8 W/cm^3 in **Fig. I.2.35**. Gas temperature in the middle of the discharge gap is equal to 433 and 299 K, respectively. Calculated for these two limiting cases dependences of small signal gain (SSG) on vibrational transition number are shown in **Fig. I.2.36.** For every vibrational transition the SSG corresponds to the maximum value over rotational lines. In the same figure, the threshold gains are shown for the reflection of outcoupling mirror R = 0.9 and 0.95, which correspond to maximum and minimum values estimated for the experiments. It is seen that at high pump power all SSGs are lower than the threshold value. This is explained by overheating of gas.

At the average pump power the computed laser efficiency is equal to 36.3% and 27.2% for mirror reflectance R = 0.95 and R = 0.90, respectively. The measured experimentally laser efficiency is equal to 2.5 %.

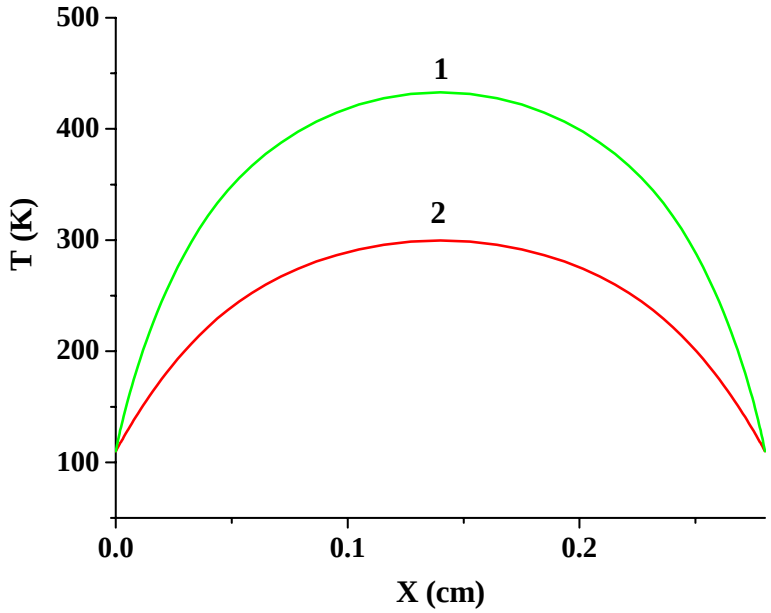

Fig. I.2.35. Spatial profile of gas temperature.
He:CO:Air=10:1:1,
P = 42 Torr,
f = 81.36 MHz.
1 - W = 42 W/cm^3;
2 - W = 16.8 W/cm^3.

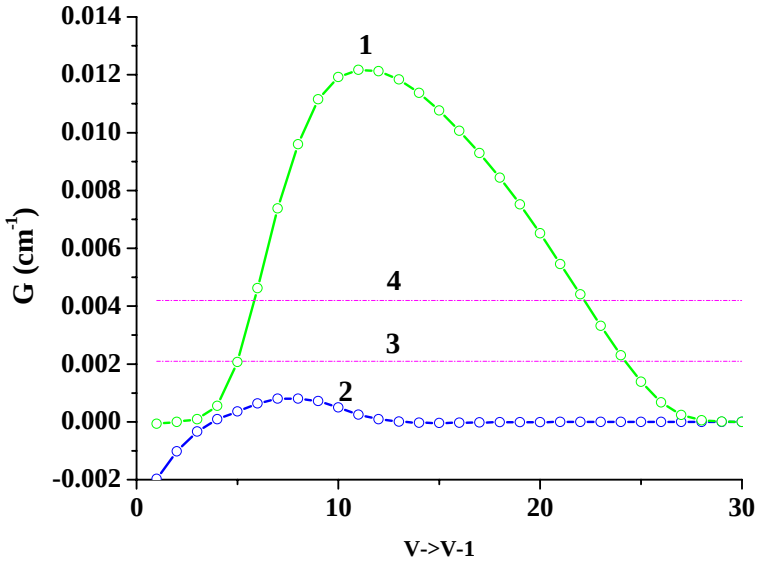

Fig.I.2.36. Dependence of SSG on vibrational transition number. He:CO:Air=10:1:1,
P = 42 Torr,
f = 81.36 MHz.
1 - W = 16.8 W/cm^3,
2 - W = 42 W/cm^3,
3 and 4 show threshold gain coefficient for output mirror reflectance R = 0.95 and 0.9, respectively.

To evaluate what a limiting case is closer to the experimental conditions, calculations were made of dynamics of establishing gas temperature and maximum over all ro-vibrational transitions SSG. In these calculations the dynamic 0-dimensional kinetic model was used. It was found that a

typical relaxation time is about 1 ms. **Fig**. **I.2.37** shows dynamics of gas temperature variation computed in assumption that all the discharge power is dissipated into gas heating. **Fig**. **I.2.38** demonstrates variations of the maximum SSG for the *maximum* pump power at constant gas temperature for a few values of this temperature.

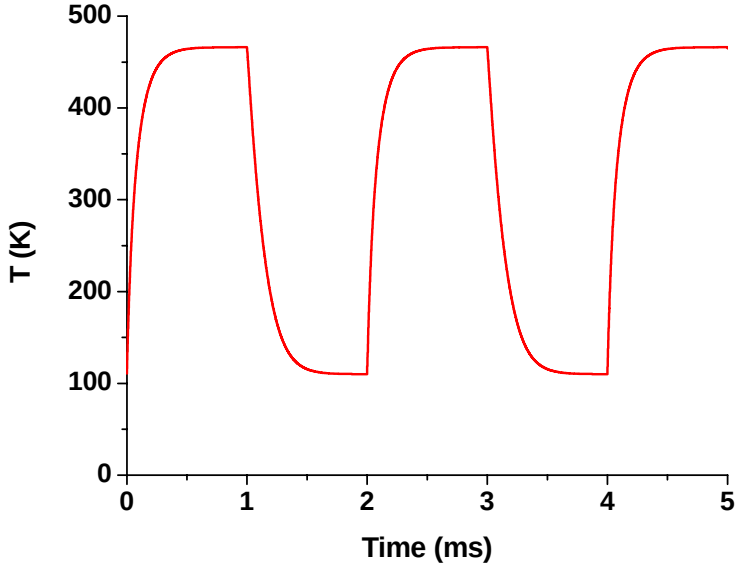

Fig. I.2.37. Gas temperature dynamics**.**
He:CO:Air=10:1:1,
P = 42 Torr,
maximum power density
W = 42 W/cm^3,
duty factor 0.5.

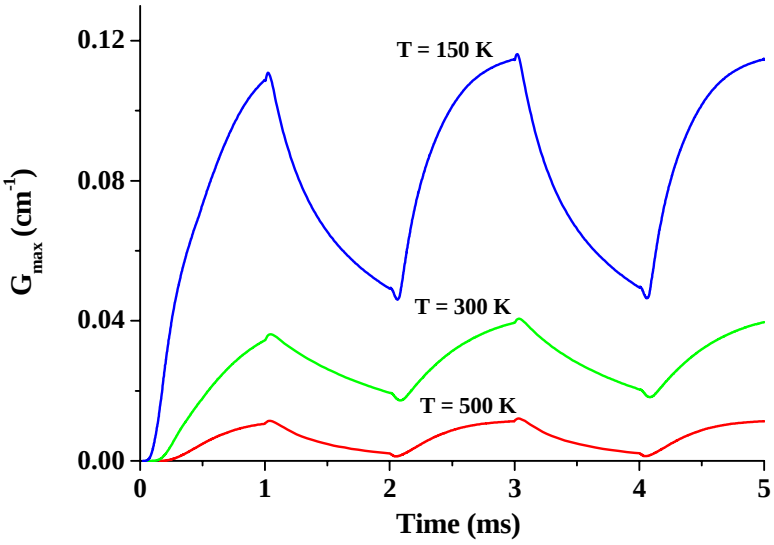

Fig. I.2.38. Time history of maximum SSG at various gas temperatures.
He:CO:Air=10:1:1,
P = 42 Torr,
maximum power density
W = 42 W/cm^3,
duty factor 0.5.

It is seen that characteristic time for establishing gain is on the order of 1 ms. Amplitude of variations of gain is rather big. Maximum of gain is remarkably lower at higher gas temperatures. In such situation, it is clear that time variations of gas temperature and SSG cannot be neglected for experimental conditions. Hence, more correct description of studied experimentally CO laser excited by RF discharge with modulated pump power within range of a few milliseconds requires much more sophisticated model not existing at present.

Conclusions

Development of the discharge chamber of special design for studying RF discharge properties such as Volt-Power characteristic gave us the possibility to measure dependency of RMS voltage across discharge gap vs. RF input power at different gas mixtures and pressures more exactly with respect to the experiments performed at using "laser" chamber (Ionin, 2001). Calculations of Volt-Power and other characteristics of the RF discharge were carried out for the experimental conditions using 1D theoretical model. A good agreement between experimentally measured and numerically calculated Volt-Power characteristics was obtained for the gas mixture pressure ~100 Torr optimal for slab CO lasers operation. Decreasing gas pressure down to ~30 Torr leaded to the result that the calculated RMS voltage across discharge gap became significantly higher than measured one. The observed discrepancy needs some additional study.

Further, 1D model of CO slab laser excited by the RF discharge was developed. For this purpose, the kinetic subroutine calculating dynamics of vibrational levels populations was incorporated into the model of the RF discharge. This model allows us to calculate self-consistently spatial patterns of capacitive RF discharge taking into account for gas heating in discharge and cooling by laser radiation in processes of stimulated emission. Laser power and spectrum in free-running regime are computed for the prescribed laser intensity profile. Influence of wall temperature and intensity profile on the laser power and spectrum were studied. An important role of gas cooling by laser radiation is revealed. Comparison of the predicted CO laser characteristics with available experimental data (Xin, 1999) demonstrated reasonably good agreement between them. The next step was modification of our model of RF discharge to include heating of electrons in collisions with vibrationally excited molecules and new ionization channels associated with high-excited CO molecules. This allows us to make more reliable predictions of the RF discharge characteristics for conditions typical for CO laser operation. Comparison of the developed theory with the experiments was complicated by the fact that in the experiments the RF discharge operated in pulse periodic regime, while the theory is applicable to simulations of steady-state regimes. The conclusion was made that more correct description of studied experimentally CO laser excited by RF discharge with modulated pump power within range of a few milliseconds requires much more sophisticated model than existing at present.

The research (Part I.2) was carried out for two years. The third year of the project for Part I.2 was not financed by the decision of the project manager due to the diminished budget partially cut by the Partner.

References for Part I.2.

Alexandrov N.L., Kochetov I.V. (1987). *TVT*, **25**, 1062.

Alexandrov N.L., Son E.N. (1978). in a book: "Plasma Chemistry", #7, Ed. Smirnov B.M., Atomizdat.

Baker H.J. (1996). *Meas. Sci. Technol*., **7**, 1631.

Blok F.J., Elkin N.N., Kochetov I.V., Napartovich A.P., Peters P.J.M., Starostin S.A., Troschieva V.N., Udalov Y.B., Witteman W.J. (1999). *IEEE J. of Quantum Electron.,* **35**, 1786.

Colley A.D., Villarreal F., Baker H.J., Hall D.R. (1994). *Appl. Phys. Lett.*, **64**, 2914.

Colley A.D., Villarreal F., Cameron A.A., Vitruk P.P., Baker H.J., Hall D.R. (1995). High power CW molecular gas laser using narrow gap slab waveguides. Gas Laser – Recent Developments and Future Prospects. Edited by W. J. Witteman and V. N. Ochkin. *NATO ASI Series 3: High Technology*, **10**, 89.

Demyanov A.V., Kochetov I.V., Napartovich A.P. et al, (1984). *TVT*, **22**, 216.

Gordiets B.F., Zhdanok S.A. (1986). in a book: "Nonequilibrium vibrational kinetics", Ed. M. Capitelli, Springer Verlag.

Grigor'yan G.M., Ionikh Y.Z., Kochetov I.V., Pevgov V.G. (1992). *J. Phys. D: Appl. Phys.* **25**, 1064.

Grigor'ev I.S., and Meilikhov E.Z. (1991). *Handbook of Physical Quantities*, Energoizdat, Moscow; (CRC, Boca Raton, (1997)).

Ionin A.A., Klimachev Yu.M., Kochetov I.V., Napartovich A.P., Sinitsyn D.V., Starostin S.A., and Terekhov Yu.V. (2001). Theoretical and experimental study of RF discharge in gas mixtures containing CO molecules, *Preprint FIAN* #53.

Ionin A.A., Kochetov I.V., Napartovich A.P., Sinitsyn D.V., Starostin S.A., Terekhov Yu.V. (2002). "Slab RF discharge modeling for gas mixtures typical for carbon monoxide lasers", *Preprint FIAN* #34.

Kunn V.V., Leont'ev V.G., Novgorodov M.Z., Ochkin V.N., Shishkanov E.P., Stepanov V.A., (1995). "Compact gap single-mode radio-frequency excited laser with a hybrid unstable and waveguide cavity", ICPIG XXII Haboken, **3**, 67.

Napartovich A.P., Novobrantsev A.N., Starostin S.A. (1977). *Sov. J. Quantum Electronics*, **7**, 1216.

Starostin S.A., Peters P.J.M., Van-der Pull G., et al. (2001). *Plasma Physics*, **27**, 458 (in Russian).

Starostin S.A., Boller K.J., Peters P.J.M., Udalov Yu.B., Kochetov I.V., and Napartovich A.P., (2002). *Plasma Physics Reports*, **28**, 63.

Syed Wahid M.S., Madhusudana C.V., (2000). *Int. J. of Heat and Mass Transfer*, **43**, 4483.

Treanor C.E., Rich J.W., Rehm R.G., (1968). *J. Chem. Phys.*, **48**, 1798.

Udalov Y.B., Tskhai S.N., Peters P.J.M., Witteman W.J., Kochetov I.V., Ochkin V.N. (1995). RF excited gas lasers – recent progress. Gas Laser – Recent Developments and Future Prospects. Edited by W. J. Witteman and V. N. Ochkin. *NATO ASI Series 3: High Technology*. **10**, 73.

Vitruk P.P., Baker H.J., Hall D.R. (1992). *J. Phys. D: Appl. Phys.*, **25**, 1767.

Xin Jianguo, Zhang Wang, Jiao Wentao (1999). *Appl. Phys. Lett.*, **75**, 1369.

Zhao H., Baker H.J., Hall D.R. (1991). *Appl. Phys. Lett.*, **59**, 1281.

r

PART II. SINGLET DELTA OXYGEN PRODUCTION IN ELECTRIC DISCHARGE (Tasks 1B, 2B and 3)

Part II.1. ELECTRIC DISCHARGE IN SINGLET DELTA OXYGEN GOING FROM A CHEMICAL GENERATOR

(Subtasks 1B.1, 1B2, 1B.3, 1B.4, 2B.1, 2B.3 and 3.2)

Introduction

The solution of a problem of SDO generation in electric discharge needs the adequate numerical models to predict the expected SDO yield. The development of a model, which describes correctly the SDO generation processes, can be possible, if correct kinetic information is available. Electron-excited molecules can play an important role in plasma kinetics, especially if we consider long-lived states. One of the most long-lived electron states is the $a^1\Delta_g$ oxygen state with energy of 0.98 eV. It is well known that, when a SDO molecule collides with O^- and O_2^- negative ions, it causes their disintegration. However, the interaction of SDO molecules with electrons is still poorly investigated.

Unfortunately, so far, there is no experimental information about a plasma balance for gas mixtures with high content of SDO. One can suppose that such information can be obtained by studying characteristics of a glow discharge ignited in oxygen with high concentration of SDO. Such gas mixture can be obtained by using chemical SDO generator (SOG) successfully operating to drive chemical oxygen-iodine laser. The new approach to get necessary information was developed in the Project (*Subtasks 1B.1, 1B2, 1B.3, 1B.4*). The clue of the method is to place the self-sustained electric discharge chamber at the exit of a traditional chemical SDO generator. Such an approach makes it possible to vary the concentration of the SDO within a very wide range and, thus, to study its influence on the electric discharge characteristics.

In the project execution (see also Ref. Vagin, 2000a) electric breakdown in an oxygen flow with a high SDO content was investigated at the output of a chemical SOG. It is shown that, the breakdown parameters of oxygen with a high SDO content can be adequately described under the assumption that the dependence of the cross section for ionization of $O_2(^1\Delta_g)$ molecules on the reduced electric field in a discharge has the same shape as the cross section for ionization of oxygen in the ground state, but is shifted as a whole toward the lower energies by an energy equal to the excitation threshold energy 0.98 eV.

The high SDO concentration in the gas flow strongly affects the electron balance in discharge plasma. In the project (see also Ref. Vagin, 2000b) the parameters of the longitudinal discharge plasma in an oxygen flow from a chemical SOG were studied. It was shown that the plasma parameters changed substantially in the presence of SDO. However, a reliable interpretation of the experimental data and the acquisition of data on elementary processes were hindered because, at the pressures used, the discharge gap was too short to produce sufficiently homogeneous plasma. SDO was shown to affect plasma parameters very strongly. However, a strong plasma nonuniformity taking place for a so-called Faraday dark space of the relatively short distance electric discharge at given gas pressures, made it difficult to get reliable interpretation of the experimental results obtained and to extract information on elementary processes. In particular, an increased rate constant for electron attachment to excited molecules in comparison with ground state molecules is compensated completely by quite fast detachment reactions resulting in effective destruction of negative ions and elimination of influence of electron attachment on discharge parameters. Therefore, at high $O_2(^1\Delta_g)$ content one may expect the operating reduced electric field strength $(E/N)_c$ to be considerably lower than for unexcited gas. This effect may be very essential for SDO

generation in electric discharge. The measurement of the positive column characteristics of a glow discharge in effluent of traditional chemical SDO generator with following comparison with predicted data allows for making a conclusion about adequacy of the theory. This approach was realized in the project (*2B.1, 2B.3 and 3.2*).

Experiments on electric breakdown in SDO obtained from a chemical SDO generator. (*Subtask 1B.1*.)

We studied the breakdown characteristics of low-pressure oxygen with 50% content of SDO and compared them with the breakdown characteristics of unexcited oxygen. A high concentration of SDO was obtained in a bubbling chemical SOG with a discharge unit attached to the generator output.

In order to obtain oxygen fluxes with a high concentration of excited $O_2(a^1\Delta_g)$ molecules, we used the reaction of chlorinating the alkaline solution of hydrogen peroxide. This reaction is the most efficient source of SDO (McDermott, 1978). The reaction proceeded in a simple and reliable bubbling SOG consisting of a quartz cylinder 150 mm in diameter and 270 mm in height, which was filled with a working solution (a mixture of 750 ml of 50% H_2O_2 and 400 ml of 50% KOH aqueous solutions). Chlorine was supplied through the punched bottom. SDO was produced as a result of the reaction of chlorine with the surface film of the solution. For the 100 l/s fixed pumping rate, the SOG provided an oxygen flux with a pressure up to 3 Torr and a SDO content up to 50% with respect to the total oxygen pressure. Since the generator used the hydrogen peroxide and alkaline aqueous solutions, the gas flux at the generator output contained water vapor. The water-vapor content depends on the solution temperature. Since the reaction of the SDO production is exothermic, the temperature does not stay constant in the course of experiment; consequently, the water content also changes.

The breakdown voltage as a function of the composition, temperature, and pressure of the gas mixture was measured in the discharge chamber connected to the gas channel at a 25-cm distance from the SOG. The electric field was directed perpendicularly to the gas flow (**Fig.II.1.1**). The sphere-plane electrode system made of stainless steel consisted of a plane electrode 54.8 mm in diameter and 10 mm thick, with rounded edges (curvature radius 5 mm) and a sphere 20.2 mm in diameter. The gap *d* between the electrodes was 6.6 mm. The DC voltage (which can be smoothly varied in the range 100÷2500 V) was applied to the discharge chamber by a VMS-2500 stabilized source through a 100 kΩ limiting resistor. The spherical electrode was at the negative potential.

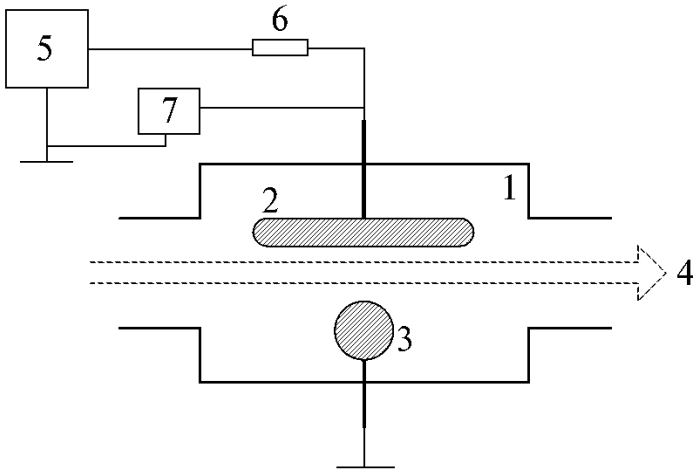

Fig.II.1.1. Schematic of experiments on the measurement of the breakdown voltage for a glow discharge: (*1*) discharge chamber, (*2*) plane electrode, (*3*) spherical electrode, (*4*) gas-mixture flow, (*5*) VMS-2500 DC high-voltage source, (*6*) limiting ballast resistor, and (*7*) digital voltmeter.

The voltage *U* at the discharge-chamber electrodes was monitored by a highly resistive (R > 10 MΩ) B7-22 digital voltmeter. The breakdown instant was determined by a sharp decrease in the voltage at the discharge chamber as the output voltage of the source was smoothly increased. The accuracy of determining the breakdown voltage was ~0.5%. To decrease the experimental error, each measurement was carried out four times in approximately one minute; during this time, the basic parameters of the gas mixture flowing through the discharge chamber remained almost unchanged.

Before the working solution was poured into the SOG, we measured the breakdown voltage as a function of the dry-oxygen pressure. The results were used to test the method and determine the extent to which the water pressure affects the measurements. With the same purpose, we carried out measurements at different temperatures of the working gas. The measurements showed that, as the temperature of the solution increases (which is equivalent to an increase in the water-vapor pressure), the breakdown voltage increases, which is opposite to the effect produced by SDO. Since the water-vapor pressure in the SDO generation regime can exceed the water-vapor pressure in the unexcited-oxygen bubbling regime, the observed difference in the values of the measured breakdown voltage can be attributed to the presence of SDO molecules in the gas flow. In the first five columns of the **Table II.1.1**, we present experimental data for different pressures of the mixture and different water-vapor contents. The value of the electric field is defined as *U/d.* The last column presents the calculated (for the given *E/N)* values of αd, where α is the first Townsend coefficient. We studied both the mixtures that do not contain SDO and those with 50% SDO.

Table II.1.1.

#	$[O_2 + O_2(^1\Delta)]$ (torr)	$O_2(^1\Delta)$	$[H_2O]$ (torr)	*U* (V)	*Nd* (10^{18} cm^{-2})	*E/N* (10^{-16} Vcm^2)	αd
1	1.4	-	0.1	543	0.0327	166.2	11.31
2	1.4	+	0.1	520	0.0327	159.2	11.32
3	2.1	-	0.15	604	0.0490	123.3	13.86
4	2.0	+	0.15	565	0.0468	120.7	13.52
5	2.1	-	0.09	606	0.0477	127.1	13.82
6	2.0	+	0.09	552	0.0455	121.3	13.22
7	1.4	-	0.2	541	0.0348	155.2	11.56
8	1.4	+	0.2	533	0.0348	152.9	11.83
9	2.1	-	0.03	600	0.0464	129.3	13.62
10	2.1	-	0.27	611	0.0516	118.4	14.12
11	2.0	+	0.7	603	0.0588	102.5	14.66
12	0.88	-	0.01	495.6	0.0194	255.7	8.23
13	0.9	+	0.01	478	0.0198	241.2	8.37
14	0.9	+	0.03	479	0.0203	236.5	8.46
15	0.9	+	0.06	482	0.0209	230.5	8.59
16	0.9	+	0.07	490	0.0211	231.9	8.68
17	0.97	-	-	535.8	0.0211	253.6	12.27
18	1.66	-	-	579.6	0.0362	160.3	8.96

Evaluation of ionization cross section of SDO.
(*Subtask 1B.1.*)

The data from the **Table II.1.1** are plotted in **Fig.II.1.2** in the form of the dependence of the breakdown voltage on the parameter *Nd* (the so-called Paschen curve for the breakdown of a uniform gap (Raizer, 1991)). The same figure presents the data (Thomas-Betts & Davies, 1969) for pure oxygen taken from (Eliasson, 1986). Our data for dry oxygen and those cited are connected by polygonal lines. It is seen that the behavior of the breakdown voltage with increasing *Nd* is similar in both cases. The difference in the values of the breakdown voltage measured in (Thomas-Betts, 1969) and in our experiments may be ascribed to the difference in the cathode substance (steel in our experiments, gold and platinum in (Thomas-Betts, 1969)).

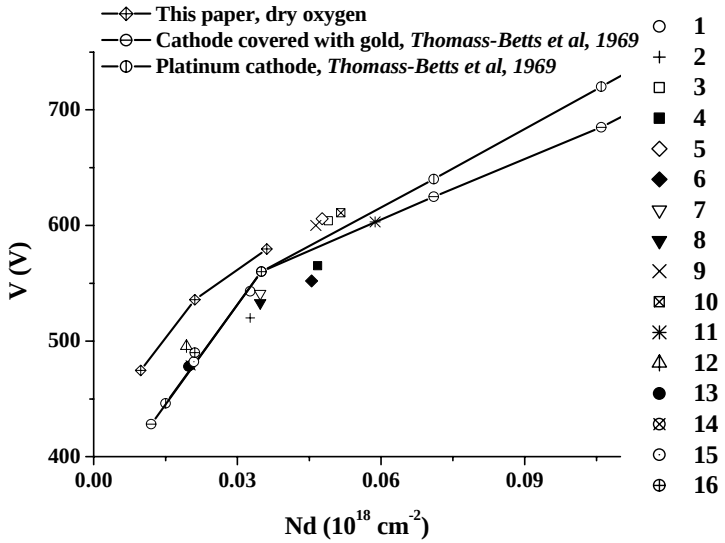

Fig.II.1.2. Breakdown voltage as a function of *Nd*. Closed symbols and symbols with numbers *2*, *11*, *14*, *15*, and *16* relate to the mixture containing 50% SDO. The symbol numbers correspond to the row numbers in the **Table II.1.1**.

The experimental points related to humid oxygen and the mixture containing SDO are not connected by curves, because at first glance the scatter in these points is on the same order as the distance between the sets of points. Note that the breakdown voltage for dry oxygen substantially exceeds that for humid oxygen. To understand the reason for this difference, we calculated the first Townsend coefficient α for the oxygen - water vapor mixtures and the mixtures of a gas containing SDO with water vapor at the constant total gas density. This coefficient for the typical value of the reduced field $E/N = 120 \cdot 10^{-16}$ V cm^2 is presented in **Fig.II.1.3**.

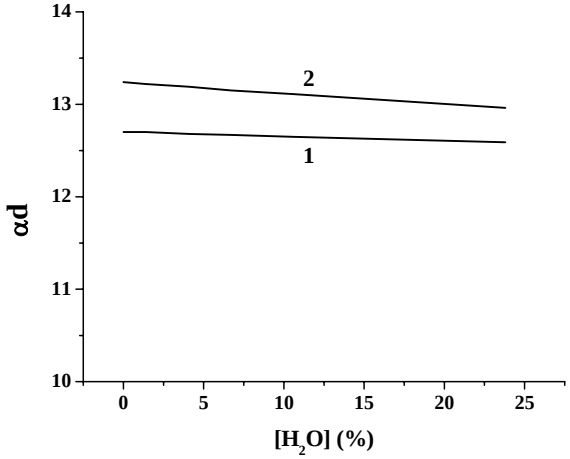

Fig.II.1.3. Parameter αd as a function of the water-vapor concentration at P = 2.1 Torr and $E/N = 120 \cdot 10^{-16}$ Vcm^2 for unexcited oxygen (1) and mixture containing 50% SDO (2).

In calculating the Townsend coefficient, we solved the Boltzmann equation for the electron energy distribution function (EEDF) taking into account certain processes of electron excitation of oxygen molecules, ionization, and attachment. We used the two-term approximation and found the EEDF under non-steady Townsend conditions. Such a formulation of the problem does not completely correspond to the experiment, but is rather close to it if the influence of the ionization on the EEDF is included correctly. The most of the necessary cross sections are taken from (Eliasson, 1986). Because of the high values of *E/N* (see **Table II.1.1**), the calculated quantity αd is almost insensitive to uncertainties in the cross-section data. The ionization cross sections appear to be of the most importance (for example, the dissociative attachment rate for SDO and oxygen in the ground state is two orders of magnitude less than the ionization rate). The direct data on the ionization cross sections for SDO are absent. However, the position of the molecular terms for $O_2(a^1\Delta_g)$ and $O_2(X^3\Sigma_g)$ states allows us to say that a simple downward shift along the energy axis gives satisfactory ionization cross section for SDO. The cross section for the collisions of the second kind was found from the principle of detailed balance. It was verified that, for typical values of *E/N*, collisions of the second kind have little or no effect on the EEDF shape. The other cross sections for inelastic collisions with SDO molecules were also taken to be equal to the corresponding cross sections for the ground state with a 0.98-eV shift. The transport cross section for SDO was assumed to be the same as that for the ground state of oxygen. The set of cross sections for scattering by water molecules was chosen according to (Yousfi, 1968). For mixtures containing SDO, the dimensionless quantity αd characterizing the amplification in the electron avalanche is somewhat more sensitive to the water-vapor content. However, on the whole, the water vapor insignificantly influences on the ionization rate; estimates show that this influence can be neglected. Estimates also show that, for values of *E/N* typical of the breakdown, the attachment processes can be neglected. Thus, the observed difference in the breakdown voltage for dry and humid oxygen can only be explained by the change in the secondary-emission properties of the cathode surface in the presence of water vapor. Further, we will neglect the possible dependence of the effective secondary-emission coefficient on the water-vapor concentration at a constant gas density. The reason for ignoring both this dependence and the role of SDO in the secondary-emission processes is seen in **Fig**.**II.1.4**, in which the quantity αd calculated for the experimental values of the breakdown voltage (see also the last column of the **Table II.1.1**) is plotted as a function of *Nd*. It is seen that almost all of the points lie on the same smooth curve. The dry-oxygen data are somewhat apart (points 17 and 18), which can be explained by the difference in the effective secondary-emission coefficients, as was mentioned above. Note that, according to the elementary breakdown theory, the almost twofold change in αd corresponds to the change in the secondary-emission coefficient γ from $10^{-6.5}$ to $10^{-3.5}$. The exact reason for such a change in γ is not clear. However, it is noted in (Loeb, 1965) that, in the general case, the quantity αd varies within the range $9 < \alpha d < 18$. The possible reasons for the change in the breakdown value of αd are also discussed in (Loeb, 1965).

Thus, if we assume that αd is independent of the concentration of SDO and water vapor (**Fig**.**II.1.3**), which is confirmed by the set of points in **Fig. II.1.4**, we can calculate the breakdown voltage and compare it with the experimental values. The calculation procedure is clarified in **Fig**.**II.1.5**. The first two items in the **Table II.1.1** are obtained for humid oxygen and the mixture containing SDO at the same gas density. In this case, by calculating αd for humid oxygen for the experimentally determined value of *E/N* corresponding to the breakdown and equating this value to αd for the mixture containing SDO, we find *E/N* for the breakdown in the mixture containing SDO. In the particular case corresponding to **Fig**. **II.1.5**, the calculated values of *E/N* and *U* in the mixture containing 50% SDO are in good agreement with the experiment.

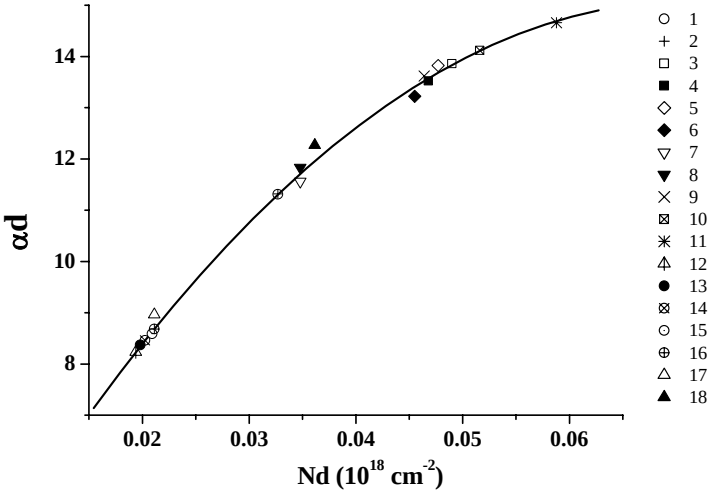

Fig. II.1.4. Parameter αd as a function of *Nd*. The curve is plotted using the data from the **Table II.1.1**. The symbol numbers correspond to the row numbers in the **Table II.1.1**. The solid curve is the polynomial interpolation.

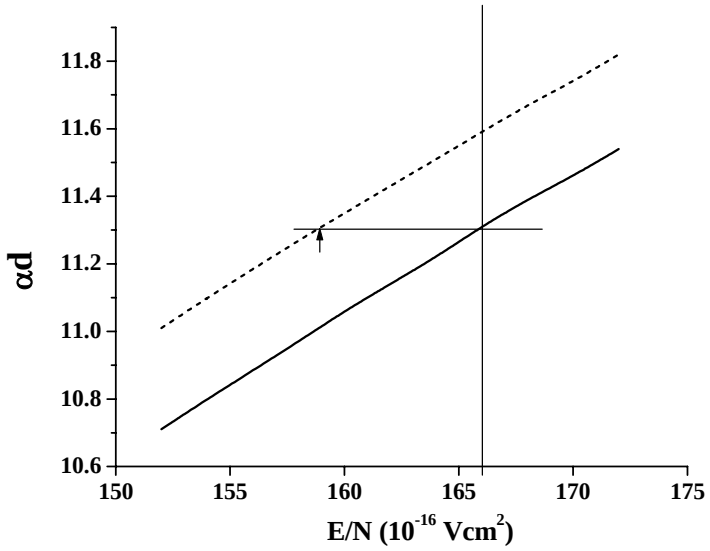

Fig.II.1.5. Explanation for the calculation of the breakdown fields. The dashed and solid lines correspond to humid oxygen (1.4 Torr O_2 + 0.1 Torr H_2O) and the mixture containing SDO. The arrow shows the experimental value of *E/N*.

The remaining points do not contain data referring to the constant value of *Nd;* consequently, the direct calculation of the difference between the breakdown voltages is impossible. Therefore, we use the following procedure.

The dependence of *N/E* on *Nd* was approximated by the second-power polynomial and drawn through the experimental points for the humid-oxygen breakdown (solid line in **Fig**.**II.1.6**). Note that the points on the solid and dashed curves at the same value of *E/N* correspond to the same calculated values of αd. Assuming that αd is independent of the concentrations of water and SDO, we derived the dependence of *N/E* on *Nd* for the 50% SDO mixture (dashed curve in **Fig.II.1.6**).

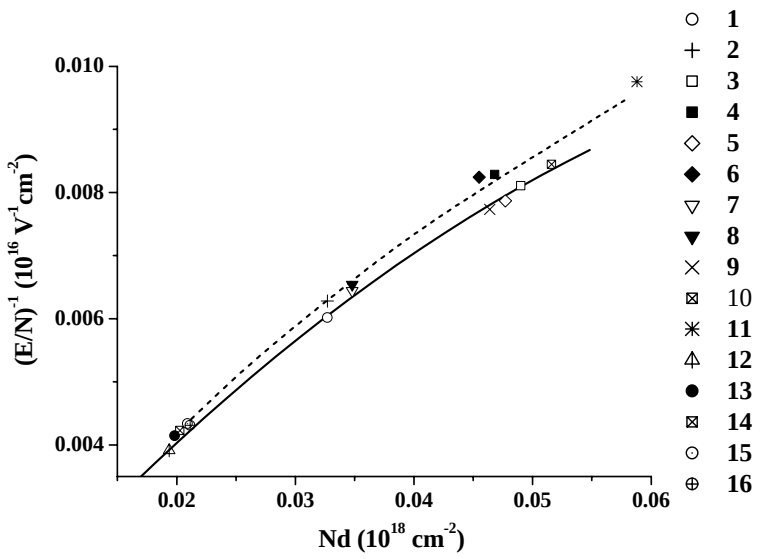

Fig.II.1.6. Comparison of the calculated breakdown values of E/N with the experimental data. The solid line is the polynomial interpolation of the experimental data for unexcited oxygen, and the dashed line is calculated for the mixtures containing SDO. The symbol number corresponds to the row numbers in the **Table II.1.1**.

As is seen, the theoretical curve agrees well with the experimental data. The size of the markers in the figure is approximately equal to the experimental error. The use of a large number of the experimental points allows us to conclude that the threshold breakdown voltage decreases when oxygen is excited on the singlet level. Good agreement between the theoretical and experimental data also justifies the procedure of calculating the SDO ionization cross section that is based on the assumption that this cross section is equal to the oxygen ionization cross section in the ground state shifted 0.98 eV toward the lower energies.

Formulation of equation system for description of transition region in glow discharge. (*Subtask 1B.2.*)

To describe a transition region between cathode sheath and positive column of glow discharge in a gas flow, a system of fluid equations for charged particles number densities can be applied. A specific feature of the transition region is an existence of a beam of electrons with energy approximately equal to the cathode voltage drop (300-400 V). These electrons ionize very efficiently the gas resulting in a local high electron number density and low electric field strength. In the positive column, which is formed at about 1 cm distance from the cathode, the electric field approaches a value, at which ionization by plasma electrons compensate recombination/diffusion losses. In the transition region including negative glow and dark Faraday space the electric field grows from a very low value to that of positive column. In this region, electron flux, Γ_e, consists of drift, diffusion and "thermo-diffusion" induced by the electric field gradient (Aleksandrov, 1980). Respectively, the electron transport equation has a form:

$$\frac{d\Gamma_e}{dx} = \nu_i n_e + q - \alpha n_e n_+ - \nu_a n_e + \nu_d n_- ,$$

where

$$\Gamma_e = \mu n_e - n_e V + D_L \frac{dn_e}{dx} + D_E \frac{n_e}{E}\frac{dE}{dx} ,$$

q is the cathode electron-beam ionization source, ν_i, ν_a, ν_d are ionization, attachment and detachment frequencies, correspondingly, D_L, D_E are diffusion-type coefficients, defined in (Aleksandrov, 1980), μ_e is electron mobility, V gas flow velocity. The positive and negative ion transport equations have a form:

$$\frac{d(n_+ v_+ + n_+ V)}{dx} = \nu_i n_e + q - \alpha n_e n_+ - \beta n_- n_+ ,$$

$$-\frac{d(n_- v_- - n_- V)}{dx} = \nu_a n_e - \nu_d n_- - \beta n_- n_+ ,$$

where v_+, v_- are drift velocities of positive and negative ions, α and β are electron-ion and ion-ion recombination coefficients. Plasma quasi-neutrality condition is

$$n_+ = n_e + n_- .$$

For the anode-side, the boundary condition on plasma component densities can be formulated asymptotically. There is a problem of formulation correct boundary conditions on a cathode-side border of plasma. Analysis of this problem demonstrates necessity to perform a series of additional calculations with variable unknown parameters to fit the results to experimental data. Such a study is labor- and time-consuming one, and cannot exclude uncertainties in boundary conditions.

Simulation of structure of transition region for the condition of experiment on electric discharge in SDO.
(*Subtask 1B.3.*)

It was observed in our experiments a strong longitudinal non-uniformity of discharge luminosity. A negative glow region (NGR) is characterized by a bright emission. Farther away from the cathode the NGR transforms into so-called Faraday dark space extending almost to the anode. In the very vicinity of the anode a glowing anode layer is observed. In the dark space, electric discharge plasma and electric field change self-consistently from a state, in which charged particle balance is governed by ionization by a cathode electron beam and plasma diffusion, to the state of a positive column, in which ionization produced by plasma electrons is balanced by charge losses such as ambipolar diffusion, attachment/detachment and recombination. As a border between the NGR and the dark space is unknown in advance and depends on plasma parameters such as a discharge current and gas pressure, it is reasonable to formulate a theoretical model that could also describe a region of the NGR. As was mentioned above, the process of ionization by electrons produced in a cathode layer is a very important factor for the NGR description. The process can adequately be described only by direct modeling of electron distribution by Monte-Carlo method taking into account a self-consistent change of the electric field and a real cathode design. Because of complexity of such calculations that were previously made only for a flat cathode and pure He and Ne, we included an ionization source imitating cathode electrons into our theoretical model.

Therefore, the plasma region, which we have to describe, includes two regions, namely, the NGR and Faraday dark space. The NGR border is geometrically close to a cathode structure. Strictly speaking, one should step out of it by a distance corresponding to a typical size of the structure element. At anode side similar distance is determined by a period of anode grid. Taking into account these limitations, plasma characteristics change primarily along discharge current.

It enables us to formulate one-dimensional theoretical model on the basis of equations formulated above. These equations were derived earlier in (Alexandrov, 1980). The required

transport and kinetic coefficients were calculated by solving an appropriate electron Boltzmann equation following the procedure described in (Alexandrov, 1980).

In the experiments, it was difficult to avoid appearance of water vapor coming from a chemical SDO generator. Therefore, kinetic coefficients were calculated for humid oxygen, too. **Fig.II.1.7** shows dependence of diffusion coefficients entered into equation system on *E/N*-parameter for both oxygen mixtures: with ground state oxygen and 50% of oxygen in singlet delta state. It is seen that addition of water vapor influences strongly on values of diffusion coefficients. In contrast, kinetic coefficients shown in **Fig.II.1.8** are more sensitive to SDO percentage than to water content.

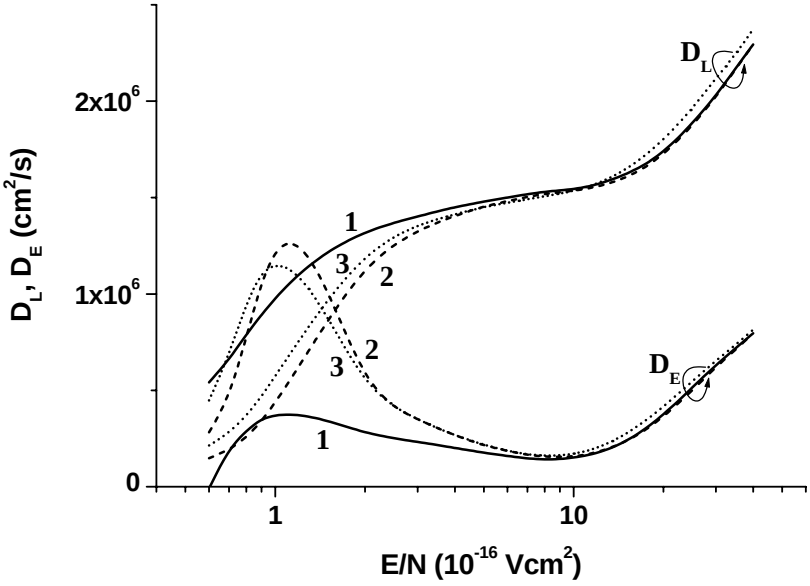

Fig.II.1.7. Theoretical dependencies of diffusion coefficients D_L and D_E on parameter E/N for pure oxygen (1), humid oxygen O_2:H_2O=90:10 (2) and gas mixture with SDO - O_2:SDO:H_2O=45:45:10 (3). T=300 K

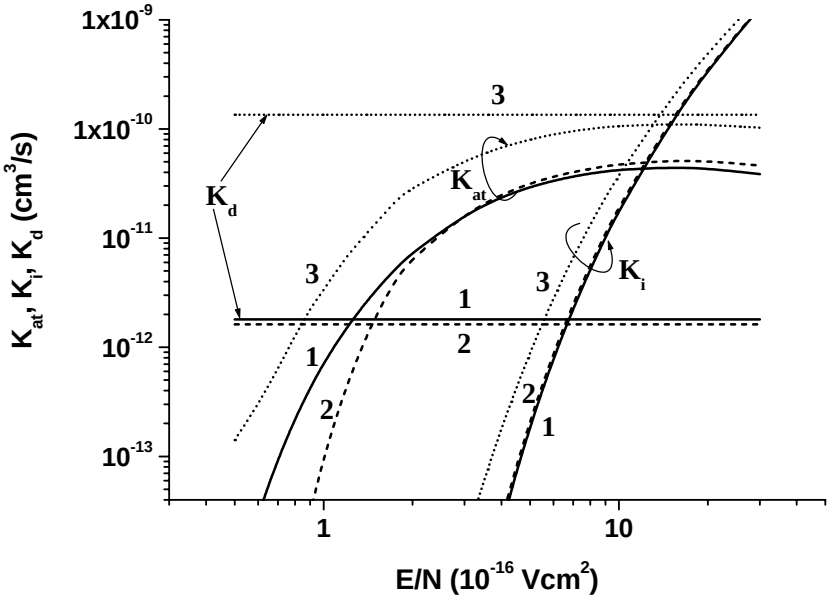

Fig. II.1.8. Dependence of effective constants of ionization, attachment and detachment on parameter E/N for pure oxygen (1); humid oxygen O_2:H_2O=90:10 (2) and gas mixture with SDO O_2:SDO:H_2O=45:45:10 (3); T=300 K.

Verification of the model by comparison with the experimental data.

(*Subtask 1B.3.*)

Figs II.1.7 and **II.1.8** demonstrate that generally changes of transport and kinetic coefficients induced by the SDO are sufficiently large to lead to observable effects. However, it is a problem to propose reasonable boundary conditions on both ends of the region under consideration. Appearance of transverse non-uniformity of plasma near cathode and anode makes it practically impossible to derive well-grounded relations between quantities subject to calculation. Therefore, a conclusion can be made that any progress in this direction is highly questionable. The uncertainties introduced by poor knowledge of plasma behavior near electrodes turned out to prevent from comparison of theoretical predictions with accumulated experimental data. Our efforts in following were focused to studies of characteristics of glow discharge positive column in SDO containing gases.

Parametric study of DC discharge plasma characteristics vs. SDO concentration (probe and volt-ampere characteristics).
(*Subtask 1B.3.*)

Experimental facility for studying DC discharge properties in gas mixtures containing SDO consisted of a chemical sparger type SDO generator (SDOG), a gas duct and an electric discharge chamber (**Fig**.**II.1.9**). The sparger type chemical SDOG is described in detail elsewhere (Vagin, 1985). Investigation of a performance of a pulsed COIL based on this chemical SDOG makes it possible to estimate the yield of SDO is about 50 % at operation pressure of 1 Torr and pump capacity of 80 l / s.

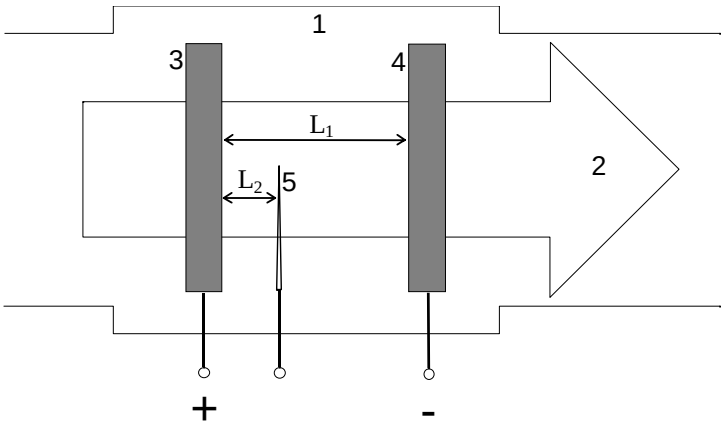

Fig.II.1.9. Schematic of the experiment: 1 - electric discharge chamber, 2 - gas flow, 3 - anode, 4 -cathode, 5 - needle probe, L_1 - intra-electrode distance, L_2 - distance between anode and probe.

A water vapor trap was incorporated into the gas duct between the SDOG and the discharge chamber. An electric field being longitudinal relative to gas flow 2 was produced with electrode system consisted of upstream anode 3 and downstream cathode 4 with spacing L_1. The cathode was cooled by water. Electric potentials of plasma column in different points situated at the distance L_2 from the anode were measured with a metallic needle probe 5.

Experiments were carried out with pure oxygen going directly to the discharge chamber from a cylinder (dry oxygen “D”), pure oxygen from the cylinder going through the not operating SDOG and a water vapor trap (humid oxygen “H”) and gas mixture of oxygen containing 50% SDO going from SDOG through a water vapor trap to the discharge chamber. An initial SDOG temperature was ~-20^{o}C, water vapor trap temperature being –65^{o}C. The distance L_1 was 19 mm, the distance L_2=7 mm. Probe and total volt-ampere characteristics of the electric discharge for pure oxygen "D", humid oxygen "H" and gas mixture O_2: SDO=1:1 at gas pressure of ~1 Torr are presented in **Fig**.**II.1.10**. As one can see in the figure, there is a big difference between the characteristics for

pure oxygen and SDO, which indicates the fact that the two substances have different electrical features. Water vapor does not much influence upon the characteristics.

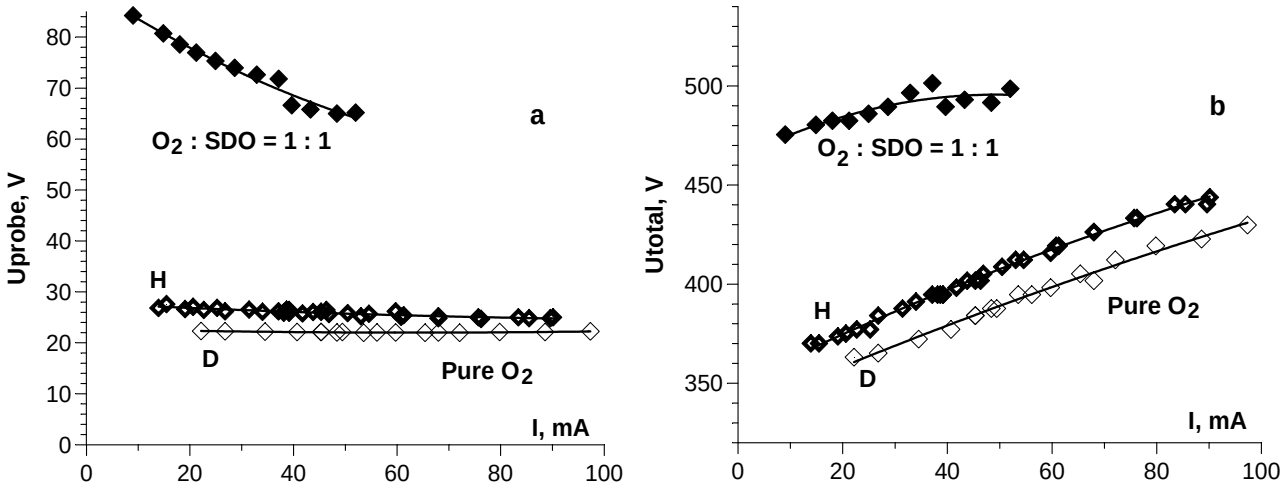

Fig.II.1.10. Probe (a) and total (b) volt-ampere characteristics of electric discharge in pure humid (H) and dry (D) oxygen and gas mixture O_2 : SDO=1:1; P=1.2 Torr, V=80 l/s.

It should be noted that the experimental results were obtained for relatively short electric discharge chamber, which did not permit to have a positive column of the electric discharge plasma. Although we observed the marked difference between the volt-ampere characteristics for pure oxygen and SDO, experiments should be done for longer discharge tube with a positive column, which makes it easy to analyze electric discharge characteristics.

Comparison with measured electric probe characteristics and extraction of information about kinetic processes.
(*Subtask 1B.4.*)

At the beginning of Part II.1 the electric breakdown in oxygen containing the rather high concentration (up to 50 %) of molecules in $O_2(^1\Delta_g)$ state was studied. It was shown that in this case the breakdown parameters can be adequately described, if one supposes the dependence of $O_2(^1\Delta_g)$ ionization cross-section on reduced electric field strength is the same as that for the ground state being shifted to lower energies by the state excitation value, i.e. by 0.98 eV. The high concentration of SDO strongly modifies the electrons balance in electric discharge plasma. SDO was shown to affect plasma parameters very strongly. However, a strong plasma nonuniformity taking place for a so-called Faraday dark space of the relatively short distance electric discharge at given gas pressures, made it difficult to get reliable interpretation of the experimental results obtained and to extract information on elementary processes. In particular, an increased rate constant for electron attachment to excited molecules in comparison with ground state molecules is compensated completely by quite fast detachment reactions resulting in effective destruction of negative ions and elimination of influence of electron attachment on discharge parameters. Therefore, at high $O_2(^1\Delta_g)$ content one may expect the operating reduced electric field strength $(E/N)_c$ to be considerably lower than for unexcited gas. The preliminary results on measuring the positive column characteristics of a glow discharge in effluent of traditional chemical SDO generator are presented below.

In the experiments a discharge chamber (**Fig.II.1.11**) for measuring the characteristics of a longitudinal glow discharge in SDO was mounted in one arm of a discharge tube early used as an

element of a pulsed COIL initiated by a longitudinal electric discharge (Vagin, 1995). The gas flow in the electric discharge chamber was formed with a gas mixing system feeding the chemical SDO generator installed upstream of the electric discharge chamber. As soon as the water solutions are used for chemical production of SDO, the effluents of chemical SOG contain the water vapor which partial pressure is governed by the temperature of working solution. The low temperature trap cooled down to -65^{o} C made it possible to minimize the water vapor pressure to the level allowing one to ignore its influence on the experimental results.

The gas exhaust system consisting of four mechanical pumps provided the pump capacity of 80 l/s. The gas flow linear velocity in the electric discharge chamber was about 30 m/s, which corresponded to a residence time of 20 ms. Gas temperature at the chamber inlet was close to the room temperature. Both the principle of operation and design of chemical SDO generator are described in detail elsewhere (Vagin, 1985).

The electric discharge chamber of 40 mm inner diameter and 60 cm length (**Fig.II.1.12**) was made of fused silica tube. The electrode sections of a pulsed flash lamp IFP – 20,000 were used as its cathode and anode. Four needle-tip probes 10 cm apart to measure plasma parameters for different areas were located in such a way that their ends were placed at the chamber axis. The body of each probe except its end was insulated with a Teflon tube. Electric signals from resistive voltage dividers (R_1/R_2~220 MOhm/22 kOhm) and current shunt (R_4=100 Ohm) were monitored with a multichannel digital acquisition board connected to a PC.

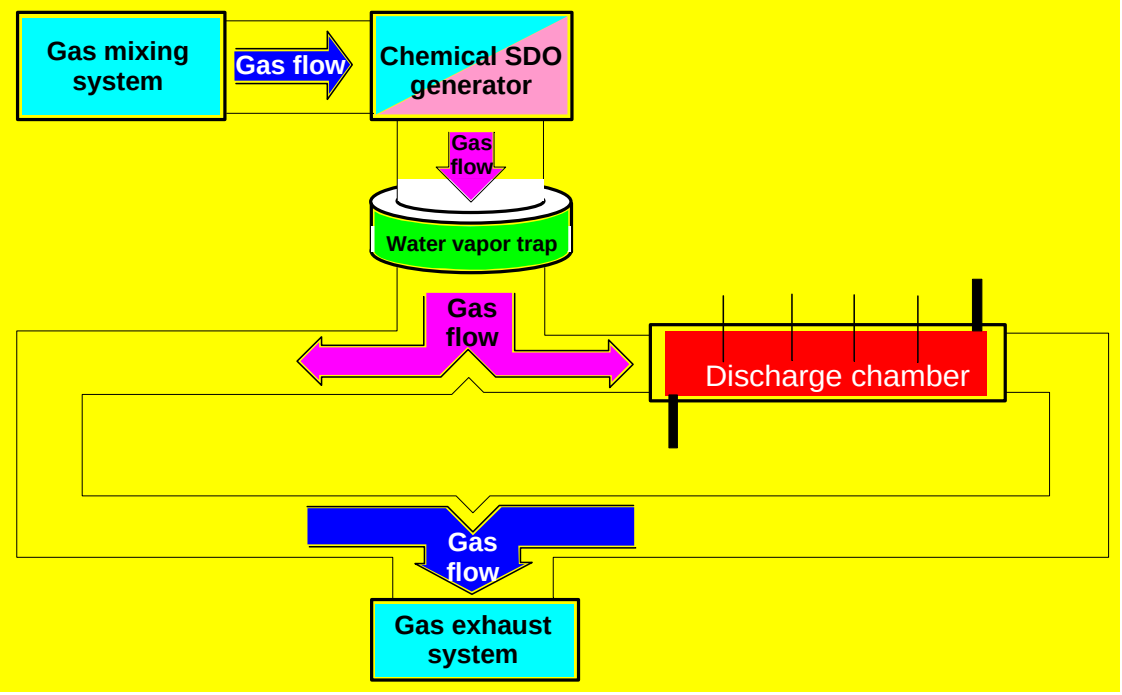

Fig.II.1.11. Schematic of the experimental setup.

Before studying plasma parameters in singlet delta oxygen, a calibration of the detecting circuit was made by measuring characteristics of electric discharge in helium and pure oxygen. Stationary electric potential distributions in DC discharge along the discharge chamber length for helium and oxygen at different gas pressures and discharge currents were experimentally measured (**Fig.II.1.13**).

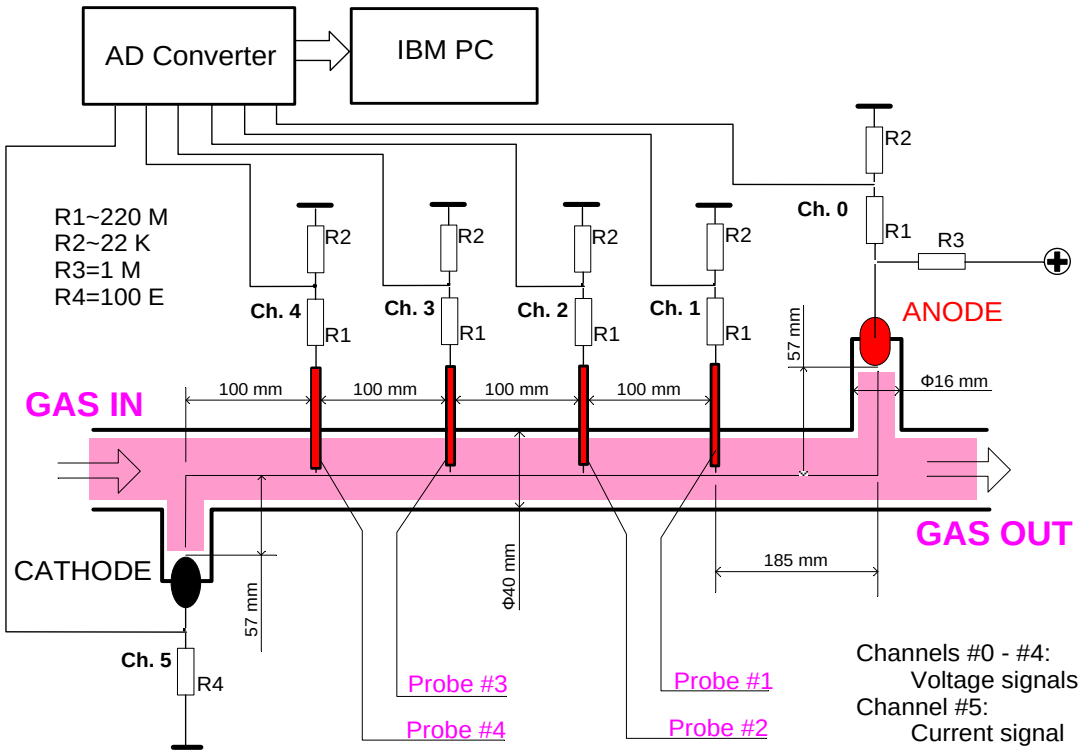

Fig.II.1.12. Schematic of the discharge chamber and diagnostic setup.

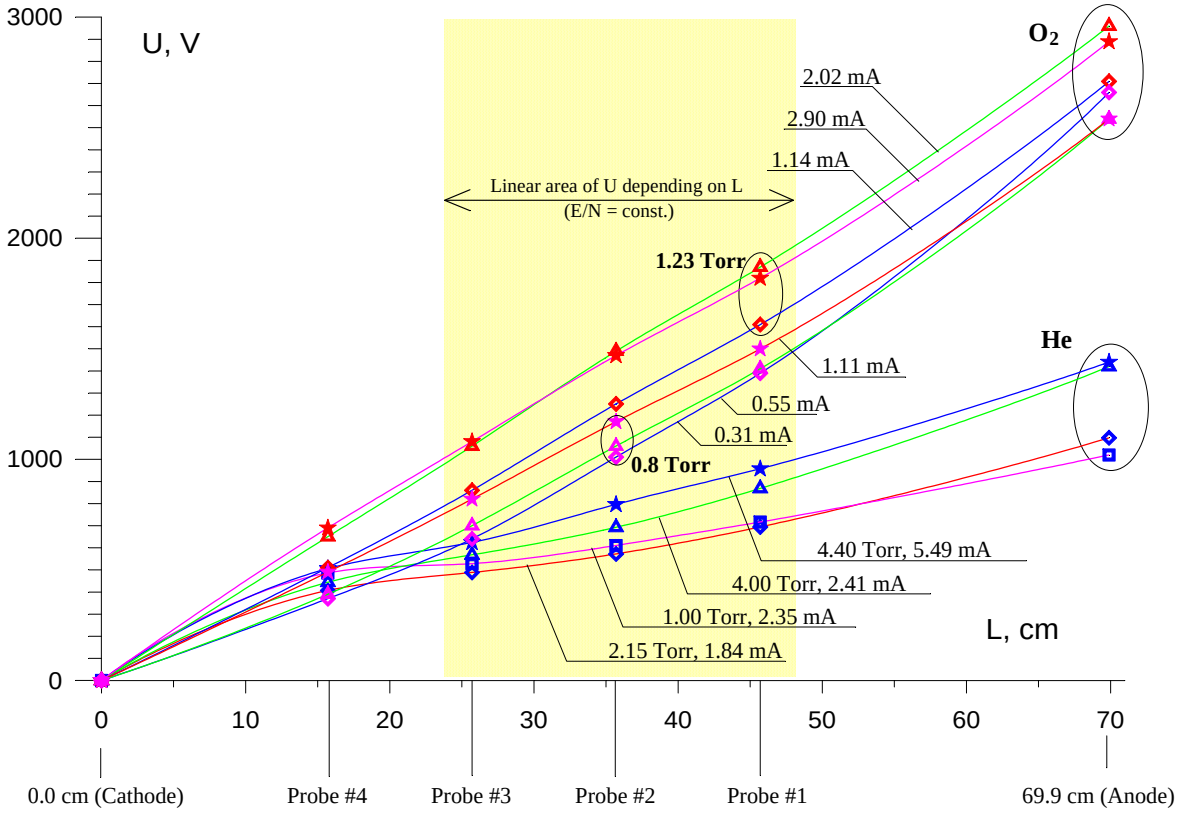

Fig.II.1.13. Stationary electric potential distributions in DC discharge along the discharge chamber length for different gases, gas pressures and discharge currents.

Probes calibration procedure showed the potential distribution between probes #1 - 3 to be a linear one with a good accuracy, while the potential measured by the probe #4 deviates from the straight line plotted over remaining locations. We believe that a dark Faraday space located near the cathode region may disturb registration of the probe #4. Therefore, only data measured by probes ##1-3 were further treated to calculate the electric field strength.

When measuring the electric discharge probe characteristics, a detection of voltage and current signals was carried out with a sampling rate of 2 kHz and total registration time ~5.5 s. The following procedure of voltage applying to the discharge gap was chosen for optimization of a ratio between the total registration time and the sampling rate. Before switching on an electric power source it was tuned in such a way that its output voltage was higher than igniting one. At given gas flow pressure, the power source was switched on, that resulted in ignition of electric discharge, which current was governed by the ballast resistor (R3=1 MOhm) and electric discharge resistance. After that, the power source output voltage was increased by hand up to values corresponding to the maximal discharge current (~15 mA). After this procedure the voltage was decreased by hand and the power source was switched off. Typical temporal behavior of probe and anode voltage, and discharge current during one measuring cycle is presented in **Fig.II.1.14**.

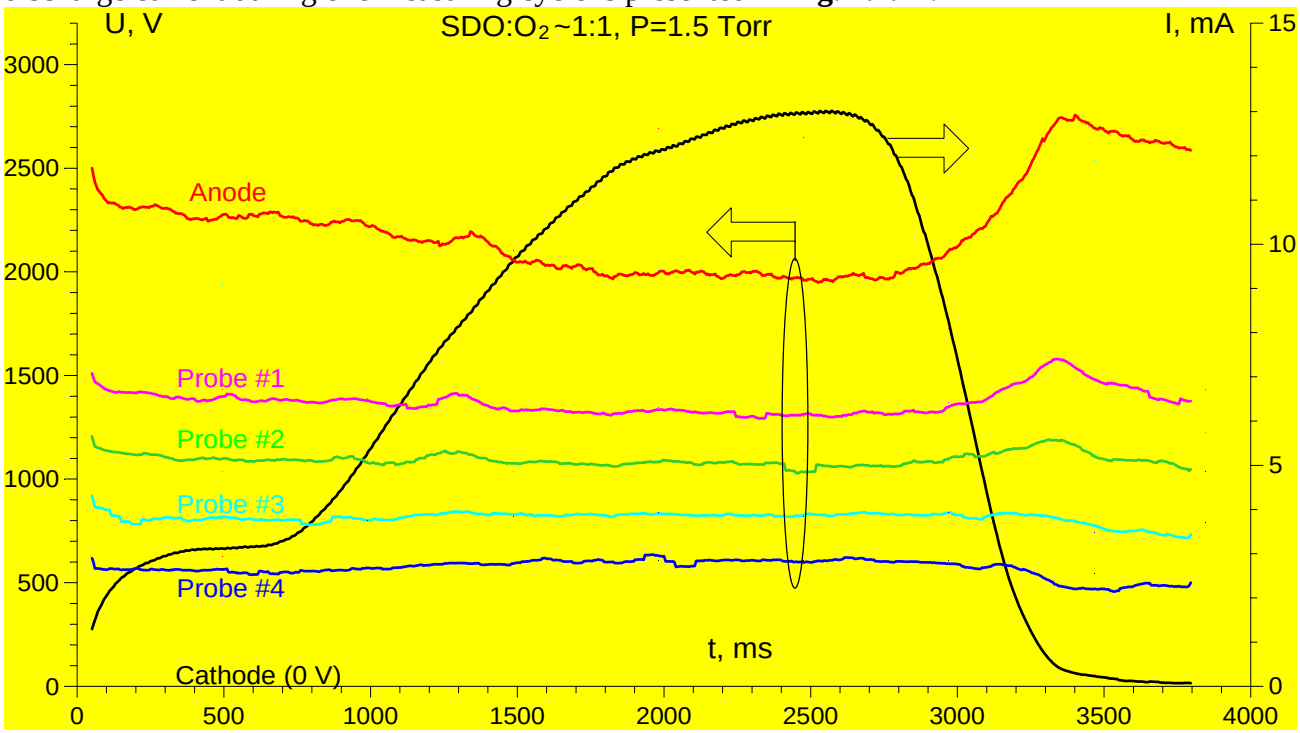

Fig.II.1.14. Typical temporal behavior of probe and anode voltages and discharge current during one measuring circle.

The procedure developed will be used to measure the positive column characteristics of a glow discharge in singlet delta oxygen.

Formulation of the numerical model for the positive column of glow discharge attached to chemical SDO generator.
(*Subtask 2B.1*)

A detailed kinetic model was developed to describe the evolution of the plasma parameters in the gas outflowing from the chemical singlet oxygen generator. The preliminary estimates of the plasma parameters showed that, under our experimental conditions, the radial electron density profile in the discharge chamber was to a large extent governed by ambipolar diffusion. The electron and ion transport along the glow-discharge positive column could be ignored. The gas flow was also of minor importance.

The elementary processes incorporated in the kinetic scheme are listed in the **Table II.1.2**.

Table II.1.2.

No.	Reaction	k_f , cm^3/s, cm^6/s	k_r , cm^3/s, cm_6/s
1	$O_2 + e \leftrightarrow O_2(v) + e$	EEDF	EEDF
2	$O_2 + e \leftrightarrow O_2(0.98) + e$	EEDF	EEDF
3	$O_2 + e \leftrightarrow O_2(1.63) + e$	EEDF	EEDF
4	$O_2(0.98) + e \leftrightarrow O_2(1.63) + e$	EEDF	EEDF
5	$O_2 + e \rightarrow O^- + O$	EEDF	
6	$O_2(v) + e \rightarrow O^- + O$	EEDF	
7	$O_2(0.98) + e \rightarrow O^- + O$	EEDF	
8	$O_2(1.63) + e \rightarrow O^- + O$	EEDF	
9	$O_2 + e \leftrightarrow O_2(4.5) + e$	EEDF	EEDF
10	$O_2(v) + e \leftrightarrow O_2(4.5) + e$	EEDF	EEDF
11	$O_2(0.98) + e \leftrightarrow O_2(4.5) + e$	EEDF	EEDF
12	$O_2(1.63) + e \leftrightarrow O_2(4.5) + e$	EEDF	EEDF
13	$O_2 + e \rightarrow O + O + e$	EEDF	
14	$O_2(v) + e \rightarrow O + O + e$	EEDF	
15	$O_2(0.98) + e \rightarrow O + O + e$	EEDF	
16	$O_2(1.63) + e \rightarrow O + O + e$	EEDF	
17	$O_2 + e \rightarrow O(^1D) + O + e$	EEDF	
18	$O_2(v) + e \rightarrow O(^1D) + O + e$	EEDF	
19	$O_2(0.98) + e \rightarrow O(^1D) + O + e$	EEDF	
20	$O_2(1.63) + e \rightarrow O(^1D) + O + e$	EEDF	
21	$O_2 + e \rightarrow O_2^+ + e + e$	EEDF	
22	$O_2(v) + e \rightarrow O_2^+ + e + e$	EEDF	
23	$O_2(0.98) + e \rightarrow O_2^+ + e + e$	EEDF	
24	$O_2(1.63) + e \rightarrow O_2^+ + e + e$	EEDF	
25	$O_2 + e \rightarrow O^+ + O + e + e$	EEDF	
26	$O_2(v) + e \rightarrow O^+ + O + e + e$	EEDF	
27	$O_2(0.98) + e \rightarrow O^+ + O + e + e$	EEDF	
28	$O_2(1.63) + e \rightarrow O^+ + O + e + e$	EEDF	
29	$O_2^+ + e \rightarrow O + O$	EEDF	
30	$O + e \rightarrow O^+ + e + e$	EEDF	
31	$O(^1D) + e \rightarrow O^+ + e + e$	EEDF	
32	$O_2(v) + M \rightarrow O_2 + M$	$1.0 \cdot 10^{-13}$	
33	$O_2(4.5) + M \rightarrow O_2(0.98) + M$	$1.0 \cdot 10^{-13}$	

34	$O_2(4.5) + M \rightarrow O_2(1.63) + M$	$9.0\cdot10^{-13}$	
35	$O + O + M \rightarrow O_2 + M$	$4.8\cdot10^{-33}$	
36	$O + O + M \rightarrow O_2(0.98) + M$	$2.4\cdot10^{-33}$	
37	$O + O + M \rightarrow O_2(1.63) + M$	$1.2\cdot10^{-33}$	
38	$O + O_2 + M \rightarrow O_3 + M$	$6.9\cdot10^{-34}$	
39	$O + O_3 \rightarrow O_2 + O_2$	$4.2\cdot10^{-15}$	
40	$O + O_3 \rightarrow O_2(0.98) + O_2$	$2.8\cdot10^{-15}$	
41	$O + O_3 \rightarrow O_2(1.63) + O_2$	$1.4\cdot10^{-15}$	
42	$O + O(^1D) \rightarrow O + O$	$7.5\cdot10^{-11}$	
43	$O(^1D) + O_2 \rightarrow O + O_2(1.63)$	$3.08\cdot10^{-11}$	
44	$O(^1D) + O_2 \rightarrow O + O_2$	$7.2\cdot10^{-12}$	
45	$O(^1D) + O_3 \rightarrow O_2 + O + O$	$1.2\cdot10^{-10}$	
46	$O(^1D) + O_3 \rightarrow O_2 + O_2$	$1.2\cdot10^{-10}$	
47	$O(^1D) + O_3 \rightarrow O_2(0.98) + O_2$	$1.5\cdot10^{-11}$	
48	$O(^1D) + O_3 \rightarrow O_2(1.63) + O_2$	$7.7\cdot10^{-12}$	
49	$O_2(0.98) + O \rightarrow O_2 + O$	$1.6\cdot10^{-16}$	
50	$O_2(0.98) + O_2 \rightarrow O_2 + O_2$	$2.2\cdot10^{-18}$	
51	$O_2(0.98) + O_3 \rightarrow O_2 + O_2 + O$	$3.8\cdot10^{-15}$	
52	$O_2(0.98) + O_2(0.98) \rightarrow O_2(1.63) + O_2$	$2.2\cdot10^{-18}$	
53	$O_2(1.63) + O \rightarrow O_2 + O$	$4.0\cdot10^{-14}$	
54	$O_2(1.63) + O \rightarrow O_2(0.98) + O$	$4.0\cdot10^{-14}$	
55	$O_2(1.63) + O_2 \rightarrow O_2 + O_2$	$8.0\cdot10^{-18}$	
56	$O_2(1.63) + O_2 \rightarrow O_2(0.98) + O_2$	$3.2\cdot10^{-17}$	
57	$O_2(1.63) + O_3 \rightarrow O_2 + O_2 + O$	$1.54\cdot10^{-11}$	
58	$O_2(1.63) + O_3 \rightarrow O_2(0.98) + O_2 + O$	$7.0\cdot10^{-12}$	
59	$O_3 + e \rightarrow O_2 + O + e$	$8.8\cdot10^{-10}$	
60	$O_3 + e \rightarrow O_2(0.98) + O + e$	$1.2\cdot10^{-10}$	
61	$O_2 + e + O \leftrightarrow O_2 + O^-$	$1.0\cdot10^{-31}$	f(E/N)
62	$O_2 + e + O_2 \leftrightarrow O_2^- + O_2$	f(E/N)	f(E/N)
63	$O_3 + e + O_2 \leftrightarrow O_3^- + O_2$	$4.6\cdot10^{-29}$	$1.0\cdot10^{-14}$
64	$O_3 + e \leftrightarrow O^- + O_2$	$9.0\cdot10^{-12}$	$5.0\cdot10^{-15}$
65	$O^- + O \rightarrow e + O_2$	$1.9\cdot10^{-10}$	
66	$O^- + O_2(0.98) \rightarrow e + O_3$	$3.0\cdot10^{-10}$	
67	$O^- + O_2(1.63) \rightarrow O + e + O_2$	$7.0\cdot10^{-10}$	
68	$O^- + e \rightarrow O + e + e$	$4.0\cdot10^{-8}$	
69	$O^- + O_2 \leftrightarrow O + O_2^-$	f(E/N)	$3.3\cdot10^{-10}$
70	$O^- + O_3 \leftrightarrow O + O_3^-$	$5.3\cdot10^{-10}$	$1.0\cdot10^{-13}$
71	$O^- + O_3 \rightarrow O_2 + O_2 + e$	$3.0\cdot10^{-10}$	
72	$O^- + O_2 + O_2 \rightarrow O_3^- + O_2$	f(E/N)	
73	$O_2^- + O_2(0.98) \rightarrow O_2 + O_2 + e$	$2.0\cdot10^{-10}$	
74	$O_2^- + O_2(1.63) \rightarrow O_2 + O_2 + e$	$3.6\cdot10^{-10}$	
75	$O_2^- + O \leftrightarrow O_3 + e$	$3.0\cdot10^{-10}$	
76	$O_2^- + O_3 \rightarrow O_3^- + O_2$	$4.0\cdot10^{-10}$	
77	$O_3^- + O \rightarrow O_2 + O_2 + e$	$1.0\cdot10^{-13}$	
78	$O_3^- + O \rightarrow O_2^- + O_2$	$3.2\cdot10^{-10}$	
79	$O_3^- + O_3 \rightarrow O_2 + O_2 + O_2 + e$	$1.0\cdot10^{-12}$	
80	$O^+ + O_2 \rightarrow O_2^+ + O_2$	$1.9\cdot10^{-11}$	

81	$O_2^+ + O_2 + O_2 \leftrightarrow O_4^+ + O_2$	$2.4\cdot10^{-30}$	$1.73\cdot10^{-13}$
82	$O_4^+ + O_2(0.98) \rightarrow O_2^+ + O_2 + O_2$	$1.0\cdot10^{-10}$	
83	$O_4^+ + O_2(1.63) \rightarrow O_2^+ + O_2 + O_2$	$1.0\cdot10^{-10}$	
84	$O_4^+ + O \rightarrow O_2^+ + O_3$	$3.0\cdot10^{-10}$	
85	$O^- + O_4^+ \rightarrow O_2 + O_3$	f(E/N)	
86	$O^- + O_2^+ \rightarrow O + O_2$	f(E/N)	
87	$O_2^- + O_4^+ \rightarrow O_2 + O_2 + O + O$	f(E/N)	
88	$O_2^- + O_2^+ \rightarrow O_2 + O_2$	f(E/N)	
89	$O_3^- + O_4^+ \rightarrow O_2 + O_2 + O_3$	f(E/N)	
90	$O_3^- + O_2^+ \rightarrow O_3 + O_2$	f(E/N)	
91	$e + O^+ + O_2 \rightarrow O + O_2$	$1.0\cdot10^{-26}$	
92	$e + O_4^+ \rightarrow O_2 + O_2$	$2.2\cdot10^{-7}$	

Note: - k_f and k_r are the rate constants of the forward and reverse processes, respectively;
- EEDF means that the rate constant is calculated by the Boltzmann equation;
- *f*(*E*/*N*) means that the rate constant is assumed to be a function of *E*/*N*;
- the asterisks denote the cross sections for stepwise processes obtained by shifting the cross sections for the corresponding transitions from the ground state toward the lower energies by the particle excitation energy.

The rate constants for the processes with the participation of electrons were calculated by solving the time-independent Boltzmann equation for the electron energy distribution function (EEDF). The time-independent Boltzmann equation was solved numerically in the two-term approximation. For the sake of simplicity, the vibrational levels of an oxygen molecule were combined into one "reservoir," $O_2(\mathbf{v})$. The rate constant for the excitation of the reservoir of vibrational energy, $O_2(\mathbf{v})$, was calculated using the effective excitation cross section $\sigma_{eff}^{V} = \sum V\sigma_V$, where **V** is the number of the vibrational level and σ_V is the cross section for the electron-impact excitation of a molecule to the vibrational level **V**. When calculating the EEDF, in addition to inelastic processes listed in Table, the elastic scattering of electrons by oxygen molecules in different excited states and oxygen atoms was taken into account. In this model, the excitation of the rotational levels of an oxygen molecule was ignored. Special test calculations showed the applicability of this approximation under the conditions of a self-sustained discharge in oxygen.

The majority of the cross sections incorporated in the model were taken from (Eliasson and Kogelschatz, 1986). The set of the cross sections for the dissociation of an oxygen molecule and its excitation to the electronic states was somewhat modified. In particular, the cross sections for the excitation of an oxygen molecule to the $O_2(A^3\Sigma, c^1\Sigma, C^3\Delta)$ state with a threshold energy of 4.5 eV and the dissociation of an oxygen molecule were taken from (Klopovskii and Rakhimova, 1994). Since the energies of the $A^3\Sigma$, $c^1\Sigma$ and $C^3\Delta$ electronic states of an oxygen molecule are fairly close to each other, they were combined into one effective level, which is below referred to as $O_2(4.5)$. The modified set of cross sections allowed us to achieve better agreement when modeling the experiments on the excitation to the $O_2(b^1\Sigma^+_g)$ (Lawton and Phelps, 1978) and $O_2(a^1\Delta_g)$ states in oxygen-argon mixtures (Tachibana and Phelps, 1981). In the presented table, these two lower states are denoted as $O_2(1.63)$ and $O_2(0.98)$, respectively. The electronically excited states with energies higher than 8.4 eV can result in the dissociation of O_2 molecules with the production of excited $O(^1D)$ atoms. The model incorporates two channels for the ionization of an oxygen molecule from the ground state: the ionization with the production of O_2^+ ions and the dissociative ionization with the production of O^+ ions (process no. 25). Obviously, the higher the mean electron energy (i.e., the higher the reduced electric field *E*/*N*), the larger the role of the latter process.

A distinctive feature of the model is that it allows one to take into account the change in the gas mixture composition as the concentrations of oxygen atoms, ozone molecules, and $O_2(a^1\Delta_g)$ and $O_2(b^1\Sigma^+_g)$ oxygen metastable molecules in the plasma increase, which is necessary to self-consistently calculate the EEDF. Indeed, under the given conditions, the relative concentrations of the particles produced in the discharge can be as high as ten and even several tens percent. In this situation, the electron-impact excitation and dissociation of the produced particles begin to play an important role in the total kinetic balance. Apparently, in this case, the set of cross sections should be supplemented with the cross sections for the interaction between electrons and excited particles; i.e., it is necessary to take into account stepwise processes, in our model, the cross sections for stepwise processes were constructed by using the cross sections for the interactions with particles in the ground states. These cross sections were shifted as a whole along the energy axis toward the lower energies by the excitation energy; the shape and the absolute values of the original cross sections were not changed. The validity of this procedure of finding the cross section for ionization from the $O_2(a^1\Delta_g)$ state was proved in (Vagin, 2000a).

The processes listed in the table are an integral part of the air plasma model described in detail in (Akishev, 1994). The rate constants of some processes with the participation of ions were tabulated as functions of the reduced electric field E/N (see (Akishev, 1994) for details). These data were used to solve a set of time-dependent balance equations for the plasma components, including electrons, positive ions, negative ions, and chemical components (such as O_2, O, O_3, $O_2(\mathbf{v})$, $O_2(0.98)$, $O_2(1.63)$, $O_2(4.5)$, $O(^3P)$, $O(^1D)$, O^+, O_2^+, O_4^+, O^-, O_2^-, and O_3^-). Note that the numbers in parentheses show the energy of the corresponding molecular (atomic) states in eV.

The heating of the gas during its motion was neglected. The discharge was fed from a power supply through a ballast resistance such that the voltage drops across the discharge and the ballast resistor were approximately equal to each other.

Two stages could usually be distinguished in the calculated plasma evolution. In the first stage, the plasma parameters changed rapidly (with a characteristic time of ~100 μs), and, in the second stage, they slowly evolved with a characteristic time of about tens of milliseconds. Taking into account that, under our experimental conditions, the gas stayed in the discharge zone for ~20 ms, the time at which the calculated electric current and the discharge voltage became equal their measured values was, for definiteness, set at 16 ms for pure oxygen in the ground state and 2 ms for oxygen with a 50% SDO content. Thus, the time during which the discharge current in mixtures with a high SDO content is established is significantly shorter than that in pure oxygen. This is because the $O_2(a^1\Delta_g)$ and O components (which are responsible for detachment in pure oxygen) are produced more slowly in the latter case.

Let us briefly discuss the role of ambipolar diffusion in the plasma balance in the positive column of a glow discharge. To adequately describe the radial density distribution of the plasma components in an oxygen glow discharge, at least three plasma components should be taken into consideration, namely, electrons, positive ions, and negative ions (several positive and negative ion species were usually taken into account). Generally, the diffusion equations for the plasma components cannot be reduced to one equation for ambipolar diffusion; hence, it is impossible to obtain a simple expression for the diffusive losses of charged particles by averaging over the discharge chamber volume. However, under our experimental conditions, attachment and detachment are the most rapid processes in the balance equation for negative ions. Among the attachment processes, dissociative attachment is dominant, which is characteristic of a low-pressure self-sustained discharge. By setting the attachment rate equal to the decay rate of negative ions, one can find that the electron density and the negative ion density are related to each other by the expression $n\ n = n_e\ \nu_a/\nu_d$, where ν_a and ν_d are the attachment and detachment rates, respectively. Assuming that the plasma is quasineutral, the rest of the balance equations for electrons and positive

ions can be reduced to the equation of ambipolar diffusion. The next step is to average this equation over the volume and to approximate the diffusion flux toward the wall by the well-known expression corresponding to the Shottky approximation. When there are several positive ion species in the plasma, we also assume that the diffusion fluxes of the different ion species are proportional to each other under different conditions. In this case, by equating the diffusive loss of electrons to the loss of all the positive ion species, one can obtain explicit expressions for the diffusive loss of each ion species. The set of equations obtained was solved numerically together with the equations for the plasma chemical components and the electric-circuit equation.

The effect of electron collisions with $O_2(a^1\Delta_g)$ molecules is illustrated in **Fig. II.1.15,** which shows the fractions of the electron energy lost in different plasma processes as functions of the reduced electric field. (Note that the energy fractions are normalized to the energy acquired by the electrons from the electric field; the energy fractions are plotted on a logarithmic scale; and, for negative energy fractions, their absolute values are shown.) The calculated results for pure oxygen in the ground state are shown in **Fig. II.1.15a**.

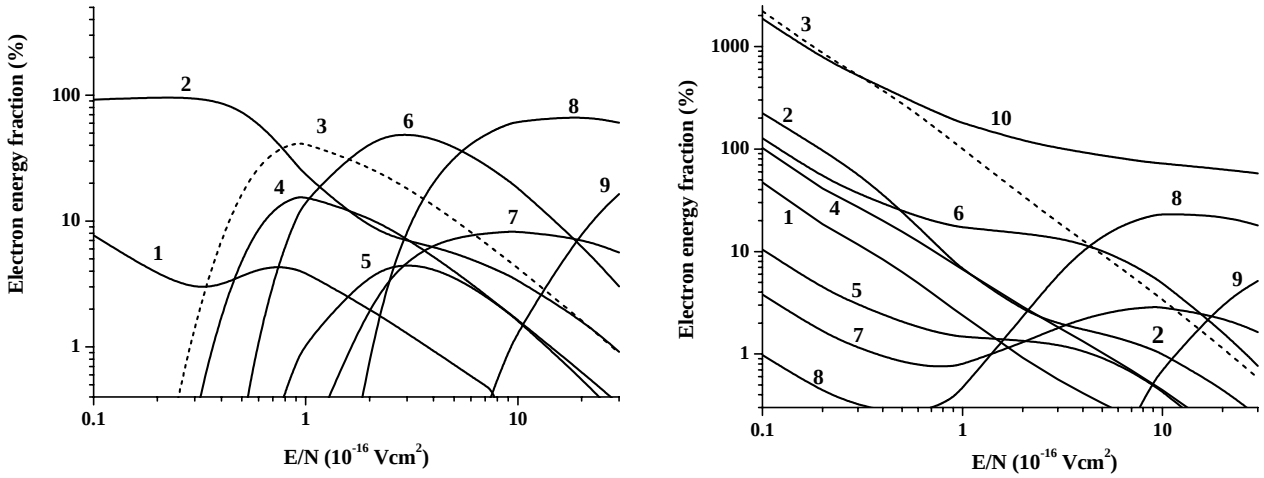

Fig. II.1.15. Fractions of the electron energy lost in different plasma processes in pure O_2 (**a**) and a mixture with a 50% $O_2(a^1\Delta_g)$ content (**b**): (1) - elastic losses and the excitation of molecule rotations, (2) - excitation of molecule vibrations, (3) - excitation of $O_2(a^1\Delta_g)$ (in **Fig. 15b**, the absolute value of this fraction is shown), (4) - excitation of $O_2(b^1\Sigma^+_g)$, (5) - attachment, (6) - excitation of the effective electronic level of O_2* with a threshold energy of 4.5 eV, (7) - dissociation into $O(^3P)$ atoms, (8) - dissociation to $O(^3P)$ and $O(^1D)$ atoms, (9) - ionization, and (10) - total excitation from the $O_2(a^1\Delta_g)$ state to the higher lying states.

It can be seen that the fraction of the electron energy spent on the direct excitation of the $O_2(a^1\Delta_g)$ state has a pronounced maximum (0.43 at E/N= $0.87\cdot10^{-16}$ Vcm^2). **Fig. II.1.15b** presents the calculated fractions of the electron energy lost in different plasma processes in a mixture with an ~50% $O_2(a^1\Delta_g)$ content, the other excited states being neglected. It is seen that, at low electric fields, the rate of energy transfer from $O_2(a^1\Delta_g)$ molecules to electrons is ten times higher (1000%) than the rate at which the electrons acquire energy from the electric field (Napartovich, 2001). In addition to the processes presented in **Fig. II.1.15a**, the following processes with the participation of $O_2(a^1\Delta_g)$ molecules were taken into account: electron de-excitation, electron attachment, transitions to the higher electronic states, dissociation, and ionization. At low electric fields, the electron energy balance is maintained by the approximate equality between the energy delivered from $O_2(a^1\Delta_g)$ molecules and the energy spent on the excitation of $O_2(a^1\Delta_g)$ molecules to the higher energy levels, dissociation, and ionization (curve 10). Since the potential curves of the ground and singlet

electronic states are similar in shape, the cross sections for the transitions from the $O_2(a^1\Delta_g)$ state were obtained from the cross sections for the corresponding transitions from the ground state by shifting them toward the lower energies by an energy of 0.98 eV. A comparison between **Figs. II.1.15a** and **b** shows a drastic change in the electron energy balance. However, at electric fields typical for a self-sustained glow discharge, the energy flux from $O_2(a^1\Delta_g)$ molecules to electrons amounts to only about 10% of the power acquired by the electrons from the electric field. For this reason, at reduced electric fields of higher than $6\cdot10^{-16}$ Vcm^2, the electron transport coefficients (the drift velocity and the diffusion coefficient) change only slightly (Vagin, 2000a).

Comparison with experimental results on positive column of glow discharge at SDO content. (*Subtask 2B.3*)

Experiment.

The experimental facility and procedure of measuring the plasma parameters are described in detail elsewhere (see above). The probe measurements in the positive column of a dc glow discharge were carried out for both pure oxygen and oxygen with an SDO admixture at total gas pressures of 1.5 and 2.0 Torr. For this purpose, the SOG filled with a working solution was blown through with either oxygen (in this case, there was no chemical reaction and the discharge chamber was supplied with pure oxygen) or chlorine (in this case, the chemical reaction proceeded in the SOG and the discharge chamber was supplied with oxygen containing ~50% O_2 ($a^1\Delta_g$). For the discharge currents taken from the graph for time evolution of the probe voltages the potential drops between probes were calculated.

Results and discussion.

The experiments show that there is a region in the discharge where the electric field is nearly constant. The reduced electric field *E*/*N* in this region was measured as a function of the discharge current for two gas mixture pressures (1.5 and 2 Torr). The results of these measurements are presented in **Fig. II.1.16.** The average gas temperature in the discharge chamber increases with increasing discharge current. Taking this effect into account, we made a correction for the averaged gas heating (and, consequently, for the reduction in the gas density) and found that the *E*/*N* value remains essentially unchanged as the current increases from 3 to 11 mA (**Fig. II.1.17.**).

Fig. II.1.17a shows the measured and calculated *E*/*N* values for oxygen at a pressure of 1.5 Torr. It can be seen that, in pure oxygen, the calculated and measured reduced electric fields are in good agreement. Here, the reduced electric field is determined by the balance between the production of plasma particles due to ionization and their loss via both attachment (detachment) and ambipolar diffusion. Note that, within a large part of the discharge (along the gas flow), the electron attachment is, to some extent, balanced by detachment in collisions with SDO molecules and oxygen atoms produced in the discharge. However, the densities of these components are not high enough to significantly change the plasma balance. The decrease in the reduced electric field in discharges in an oxygen gas mixture with a 50% O_2 ($a^1\Delta_g$) content is due to the much higher detachment rate in collisions with SDO molecules. This effect turns out to be much greater than the increase in the attachment rate in collisions with SDO molecules. In this case, the total loss of the charged particles is, to a great extent, controlled by the diffusion losses. For an O_2 ($a^1\Delta_g$) concentration of ~50%, the calculated decrease in the reduced electric field is remarkably deeper than the measured one. It is not surprising if one takes into account that the available data on the processes with the participation of O_2 ($a^1\Delta_g$) molecules are far from complete. A possible reason for this discrepancy could be an enhanced by vibrational excitation electron attachment, the process ignored in this study. It is planned to explore this issue more carefully in the future. A similar situation is observed for gas mixtures at the pressure of 2 Torr. It can be seen in **Fig. II.1.17b** that,

for a discharge in pure oxygen at the pressure of 2 Torr, the reduced electric field is lower than that at the pressure of 1.5 Torr. A similar reduction in *E*/*N* with increasing pressure is observed at SDO concentration of ~50%, although in this case, the scatter in the experimental data is larger than for pure oxygen.

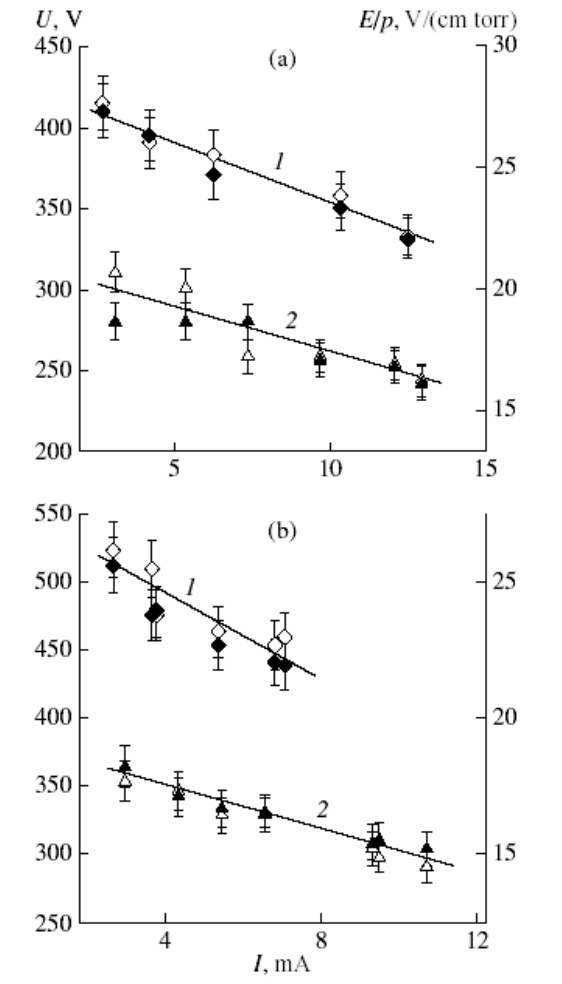

Fig. II.1.16. Current–voltage characteristics of the positive column of a DC discharge in pure oxygen (*1*, ◆, ◇) and the $O_2 : O_2(a^1\Delta_g)$ ~ 1 : 1 mixture (*2*, ▲, △) for *P* = 1.5 Torr (a) and 2.0 Torr (b).

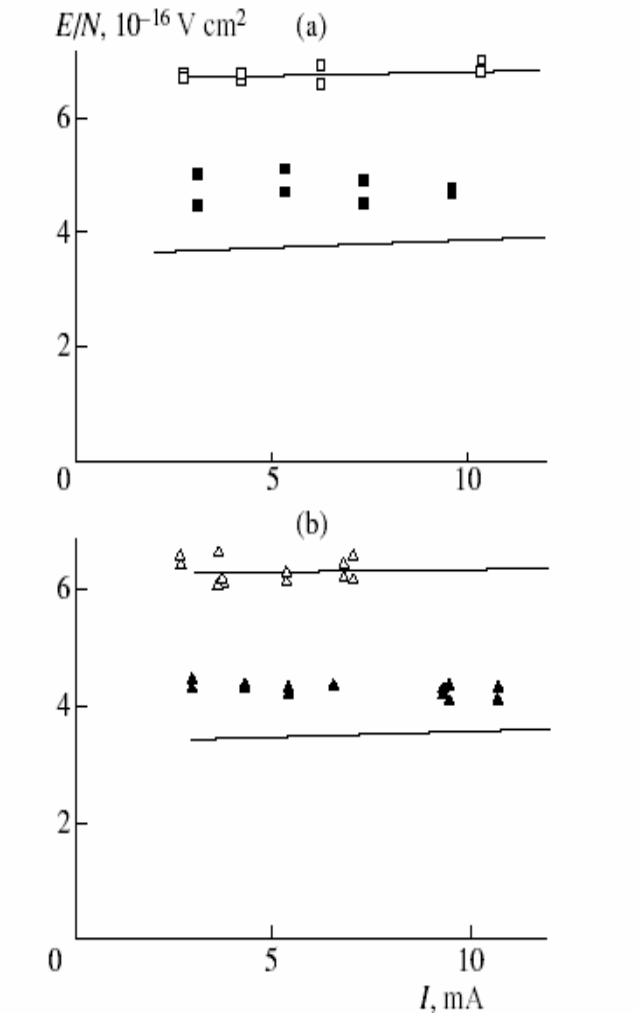

Fig. II.1.17. Measured (symbols) and calculated (solid lines) reduced electric field in an oxygen discharge at pressures of 1.5 Torr (a) and 2 Torr (b) for an SDO content of 0 % (□, △) and 50 % (■, ▲).

Revision of predicted data on E/N in positive column of a glow discharge at the output of SDO chemical generator
(*Subtask 3.2*)

Earlier (Vagin, 2003) we have made a comparison between experimentally measured and theoretically predicted values of the reduced electric field strength in the positive column of glow discharge maintained in the gas mixture from the chemical singlet oxygen generator (SOG). As a reference point, similar measurements and calculations were made for the oxygen flow coming through not active SOG (no Cl_2 was supplied). The comparison demonstrated that the theory describes satisfactorily the experimental data but the predicted E/N value was about 16% lower than

the experimental value for the oxygen with 50% singlet oxygen yield. It is our purpose to find out possible sources of this discrepancy.

Since in the experimental measurements (Vagin, 2003) there were problems with an accurate determination of the gas pressure in the discharge tube, we compared actually the relative magnitude of E/N in the singlet oxygen flow with respect to pure oxygen flow. One of the factors influencing on operated point (E/N vs electric current) could be dependence of dissociative attachment rate to $O_2(v)$ molecules on vibrational level number. It is known (O'Malley, 1967; Akhmanov, 1983) that the dissociative attachment rate grows with the vibrational level number. After our model extension for inclusion of vibrational kinetics was made, we return to this analysis.

Besides, some additional improvements of our mode were made associated with a refinement of description of ambipolar diffusion losses in 0-D model. It was found in (Vagin, 2003) that an important channel in electrons' losses is the ambipolar diffusion to the tube walls. In oxygen containing mixtures there are at least two sorts of ions: positive and negative (actually, plasma consists of a few types of positive and a few types of negative ions). Appearance of negative ions notably modifies ambipolar diffusion. The simplified description of the ambipolar diffusion adopted in (Vagin, 2003) can be improved with respect to more accurate account for negative ion kinetics. This correction is becoming important when the ratio of the negative ion to electron number density is high. Such situation is realized in glow discharge in pure oxygen. More accurate description of the ambipolar diffusion was made following the work (Bogdanov, 2003). In the mixture with 50% of oxygen in $a^1\Delta_g$ state the strong detachment of electrons from negative ions leads to essential reduction of negative ion concentration (it becomes lower than that of electrons).

Modeling of the experiments of (Vagin, 2003) using the updated model results in remarkably better agreement between the experiment and the theory, as shown in **Fig. II.1.18**. Fitting calculated E/N values to the experimentally measured values for the pure oxygen, the same model was applied to simulations of the glow discharge in the mixture with 50% of oxygen in the state $a^1\Delta_g$. The predicted E/N values turned out to be only 9% lower than the experimentally measured. This difference is completely within the error of the measurements.

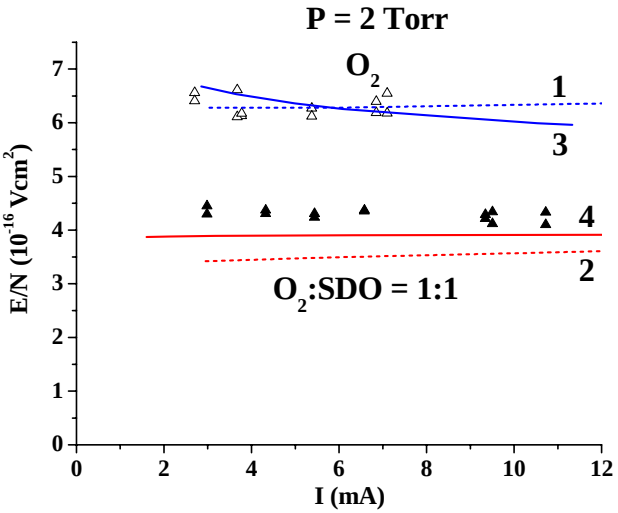

Fig. II.1.18. Measured (symbols) and calculated (solid lines) reduced electric field in an oxygen discharge at pressure of 2 Torr for SDO content 0% (Δ) and 50% (▲) 1, 2 - from (Vagin, 2003); 3,4 – present simulation.

Conclusions

We have experimentally observed a decrease of the breakdown voltage at the presence of 50% $O_2(a^1\Delta_g)$ in the mixture of oxygen with water vapor as compared to an unexcited gas. The results of

calculations agree well with the experimental data. The analysis of a large number of the experimental points allows us to conclude that the threshold breakdown voltage decreases when oxygen is excited on the singlet level. Good agreement between the theoretical and experimental data also justifies the procedure of calculating the singlet-oxygen ionization cross section that is based on the assumption that this cross section is equal to the oxygen ionization cross section in the ground state shifted 0.98 eV toward the lower energies.

On the basis of a system of fluid equations for charged particles number densities, one-dimensional theoretical model describing a transition region between cathode sheath and positive column of glow discharge in a gas flow was formulated. The required transport and kinetic coefficients were calculated by solving an appropriate electron Boltzmann equation. It was shown that addition of water vapor to the oxygen containing gas mixtures influence strongly on diffusion coefficients entered into equation system. In contrast, effective constants of ionization, attachment and detachment appeared to be more sensitive to SDO percentage than to water vapor content.

A strong plasma nonuniformity taking place for a so-called Faraday dark space of the relative short distance electric discharge at given gas pressures, made it difficult to get reliable interpretation of the experimental results obtained and to extract information on elementary processes. For this reason, a new, relatively long DC discharge tube was developed to study volt-ampere and probe characteristics of glow discharge in gas mixtures containing SDO molecules.

The parameters of the positive column of a glow discharge in an oxygen flow at the output of a chemical SOG have been studied both experimentally and theoretically. It has been found that the reduced electric field in a discharge in an oxygen mixture with a 50% SDO content is lower than that in unexcited oxygen. A detailed kinetic model describing the parameters of plasma containing significant amounts of different excited oxygen species has been developed. It is shown that, at low electric fields, the 50% SDO admixture to oxygen strongly affects the electron energy balance. However, for electric fields characteristic of a self-sustained glow discharge, the power transferred to electrons from the SDO molecules amounts to only 10% of the deposited electric power. With the discharge chamber dimensions and gas pressures used in this study, the electric field in the positive column of a glow discharge is determined by the balance between the production of charged particles due to ionization and their loss via both attachment (detachment) in collisions with oxygen molecules and diffusion toward the wall. At high SDO concentrations, the destruction of negative ions in collisions with SDO molecules is of major importance. The theoretical calculations have somewhat overestimated the effect of the electric field reduction in an oxygen mixture with a 50% SDO content.

Additional analysis of electron number balance showed an effect associated with enhanced electron attachment to vibrationally excited oxygen plays a minor role in conditions of the experiments (Vagin, 2003). The reason why these processes are insignificant is too low vibrational excitation of oxygen molecules in the discharge due to small excitation cross sections. This conclusion is in agreement with predictions of the theoretical simulations of glow discharge in the mixture of O_2 and Ar (Rybkin, 2005). The improvement of description of the ambipolar diffusion in presence of negative ions plays more important role. Modeling of the experiments of (Vagin, 2003) using the updated model results in remarkably better agreement between the experiment and the theory.

References for Part II.1.

Akhmanov S.L., Klopovskiy K.S., Osipov A.P. (1983). *VINITI*, Moscow, №5472-83, (in Russian).

Akishev Yu.S., Deryugin A.A. et al. (1994). *Plasma Phys. Rep.,* **20**, 511.

Alexandrov N.L., Napartovich A.P., Starostin A.N., 1980, *Sov. J. Plasma Phys.* **6**, 618.

Alexandrov N.L. (1988). *Sov. Physics - Uspekhi,* **31**, 101.

Azarov A.V., Mit'ko S.V., Ochkin V.N., Savinov S.Yu. (2003). *Quantum Electronics*, **33**(5) 419.

Baev V.M., Latz T., Toschek P.E. (1999). *Appl. Phys. B.,* **B 69**, 171.

Basov N.G., Babaev I.K., et al. (1979). *Quantum Electronics*, **6**, 772.

Basov N.G., Ionin A.A., et al. (2002). *Quantum Electronics*, **32**(5), 404.

Billing G.D., Coletti C., et al. (2003). *J. Phys. B.: At. Mol. Opt. Phys.*, **36**, 1175.

Bogdanov E.A., Kudryvtsev A.A., Tsendin L.D., et al. (2003). *Technical Physics*, **48**, 1151.

Cacciatore M., Kurnosov A., et al. (2004). *J.Phys. B: At. Mol. Opt. Phys*., **37**, 3379.

Capitelli M., Ferreira C. et al. (2000). "Plasma Kinetics in Atmospheric Gases", Springer.

Carroll D., et al. (2005a). *IEEE Journal of Quantum Electronics,* **41**, 213.

Carroll D. L., et al. (2005b). *IEEE Journal of Quantum Electronics*, **41**, 1309.

Carroll D.L., et al. (2005c). *Appl. Phys. Letters*, **86**, 111104-1.

Coletti C., Billing G.D. (2002). *Chem. Phys. Letters*, **356**, 14.

Eliasson B., Kogelschatz U., 1986, *Report #CH-5405* (Brown Boveri Forschungszentrum, Baden).

Frolov M.P., et al. (2005). *Proc.SPIE*, **5777,** 70.

Gilles M.K., et al. (1996). *J Phys. Chem*. **100**, 14005.

Hill A., 1998, *Proc. SPIE,* **3343**, 1069.

Hoag E., Pease H., Staal J., Zar J. (1973). *Quantum Electronics*, **QE-9**, 652.

Itami S., et al. (1999). *Proc. SPIE*, **3889**, 503.

Kaufman F. (1961). *Prog. React. Kinet*. **1**, 1.

Kitaeva V.F., Osipov Yu.I. (1968). *J. Tech. Phys.*, **38**(2), 384.

Klopovskii K.S. and Rakhimova T.V. (1994). private communication.

Kolobyanin Yu.V., et al. (2005). *AIAA Paper 2005-4920***,** 36th AIAA Plasmadynamics and Laser Conference, 6-9 June 2005, Toronto, Canada.

Kuznetsov A.A., Novgorodov M.Z., Ochkin V.N., et al. (2000). *Quantum Electronics*, **30**, 399.

Lawton S.A. and Phelps A.V. (1978). *J. Chem. Phys.*, **69**, 1055.

Loeb L.B., 1965, Electrical Coronas, University of California Press, Berkeley, p. 29.

McDaniel E.W., Mason E.A. (1973). "The mobility and diffusion of ions in gases", "J.Wiley an Sons".

McDermott W. E., Pchelkin N. R., et al., 1978, *Appl. Phys. Lett.*, **32**, 469.

McEwan M.J. & Phillips L.F. (1975). "Chemistry of the atmosphere", Chemistry Department, University of Canterbery Christchurch, New Zealand.

Napartovich A.P., Deryugin A.A., Kochetov I.V. (2001). *J. Phys. D*, **34**, 1827.

O'Malley T.F. (1967). *Phys. Rev*., **155**, 59.

Pazyuk V.S., Podmar'kov Yu.P., Raspopov N.A, Frolov M.P. (2001). *Quantum Electron*., **31**, 363.

Raizer Yu. P., 1991, Gas Discharge Physics, Nauka, Moscow, 1987; Springer-Verlag, Berlin, 1991.

Reilly J.P. (1972). *J. Appl. Phys.*, **43**, 3411.

Rybkin V.V., Smirnov S.A., Ivanov A.N. (2005). Proceeding of the IV International Symposium on Theoretical and Applied Plasma Chemistry, Ivanovo, Russia, Published by Ivanovo State University of Chemistry and Technology, **1**, 247 (in Russian).

Tachibana K. and Phelps A.V. (1981). *J. Chem. Phys.*, **75**, 3315.

Thomas-Betts A., Davies D.E., 1969, *Br. J. Appl. Phys.*, Ser. **22**, 213.

Vagin N.P., Kryukov P.G., Yuryshev N.N., 1985, *Sov. J. Quantum Eelectronics*, **15**, 1268.

Vagin N.P., Pazyuk V.S., Yuryshev N.N., 1995, *Quantum Eelectronics*, **25**, 746.

Vagin N.P., Deryugin A.A. et al. (2000a). *Plasma Phys. Rep*. **26**, 278.

Vagin N.P., Ionin A.A., Klimachev Yu.M., et al. (2000b). "Glow discharge plasma in gas mixtures with high content of single delta oxygen", Preprint No.57 of the Lebedev Physical Institute, Moscow (in Russian).

Vagin N.P., Ionin A.A. et al. (2003). *Plasma Physics Reports*, **29**, 211.

Vasilijeva A.N., Klopvskiy K.S., Kovalev A.S. et al. (2004). *J. Phys.D: Appl. Phys.*, **37,** 2455.

Wang B., Gu Y. (1998). *J. Phys. Chem. A.*, **102**, 9367.

Webster H., Bair E. J. (1972). *J. of Chemical Physics*, **56**, 6104.

Yousfi M., Azzi N., Gallimberti I., Stangherlin S., 1988, Electron-Molecule Collision Cross Section and Electron Swarm Parameters in Some Atmospheric Gases (N_2, 0_2, CO_2 and H_2O), *Data Base Collection*, (Toulouse-Padova).

Yuryshev N.N., et al. (2004). *Proc. SPIE*, **5448,** 790.

Part II.2. EXPERIMENTAL METHODS OF SINGLET DELTA OXYGEN DETECTION *(Subtasks 1B.2, 1B.4, 3.1 and 3.2)*

Introduction

Great efforts in research of electrically generated singlet delta oxygen (SDO) resulted in achievement of SDO yield exceeding the room temperature threshold level. Observation of positive gain (Carroll, 2005a) and oscillation of oxygen-iodine laser with electrical generator of SDO (Carroll, 2005c) validated the feasibility of electrically driven oxygen iodine laser. Thus, the problem of efficiency and usability of electrical SDO generator becomes of great importance now. This fact makes scientists to research the different types of electrical discharges looking for the best of them as a source of SDO for oxygen iodine laser. So far, the different types of electrical discharges such as radio frequency (RF) discharge, microwave (MW) discharge, non-self sustained discharge were used to generate SDO. Some of them demonstrated their ability to provide the SDO yield adequate for getting oxygen-iodine lasing at relatively low gas temperatures. Today the RF discharge demonstrates the most promising results (Carroll, 2005a,c), but MW one is now developed up to the level also providing positive gain in the oxygen-iodine mixture (Kolobyanin, 2005). However, in spite of positive results obtained, the information on processes governing SDO formation in low-temperature plasma is, so far, rather poor. It makes scientists to intensify their investigations into this field.

The high sensitivity of oxygen iodine laser performance to SDO yield makes it possible to consider the task of correct measurement of this parameter as a critical factor in a problem of development of electrically driven singlet delta oxygen generator. In spite of a lot approaches used at present to measure SDO yield the accuracy of such measurements does not meet the requirements of Discharge Oxygen Iodine Laser. Quite recently some of scientists engaged in this activity estimated the accuracy of measurements was good to within a factor of 2÷3 (Solomon, 2002). The difficulties which one meets in the way to improve the accuracy are the result of both very week signal of SDO and absence of reference source with well known parameters.

We believe that chemically produced SDO that typically used in COIL can be successfully used as a reference source. Indeed, it may be argued the COIL having ~25 % of chemical efficiency utilizes the oxygen with SDO yield of over ~50% (~20% - is a value of threshold yield, ~25 % - is a fraction emitted as laser energy, ~10 % - is a value of SDO spent for dissociation of I_2 and other losses). Thus, this value of SDO yield is a low limit of estimation. The upper limit is 100%. Thus, the average value of SDO yield is about 75% ± 25%. Really the upper limit is lower than 100% and, thus the accuracy is higher. Therefore, chemically produced SDO feeding COIL with parameters mentioned above can be used as a reference source in which the SDO yield value is known with accuracy of better than 30 %.

The purpose of the present research is to develop methods of measuring SDO yield and concentration of components, which can be responsible for SDO formation and its relaxation at the post-discharge stage. The different approaches based on application of different instruments are considered. The latter makes it possible the researcher to choose the approach meeting the opportunities of instruments available.

Absolute calibration of SDO detector using He-Ne laser

(*Subtasks 1B.2 and 1B.4*)

He–Ne laser (λ = 633 nm) was used for absolute calibration of a system monitoring the dimole radiation (λ = 634 nm) of SDO. The presence of this radiation in luminescence of effluents of SDO generator is an evidence of a high concentration of SDO in a flow. The chemical SDO generator was used as a source of oxygen flow with known SDO yield.

Fig. II.2.1 presents the layout of experiments on monitoring the luminescence of chemically produced SDO (upper) and absolute calibration using the He-Ne laser (lower).

The dimole emission of chemically produced SDO emitted from D_d = 4.5 cm i.d. and L_d =120 cm length glass cell (emitting volume is V_d =1900 cm^3) was focused with the Al coated mirrors M_2 (plane) and M_3 (spherical f = 50 cm) to the slit of the prism spectrograph ISP-51. The measured reflectance R_{2-3} of the mirror pair M_2, M_3 was as high as 0.75. The plane Al coated mirror M_1 being perpendicular to the optical axis makes it possible to increase 1.74 times the light flow to the spectrograph. The total pathway from the cell output window to the spectrograph slit was as long as 700 cm. The spectra were recorded with a CCD array having 2776 pixels. The element size was 11x11μm.

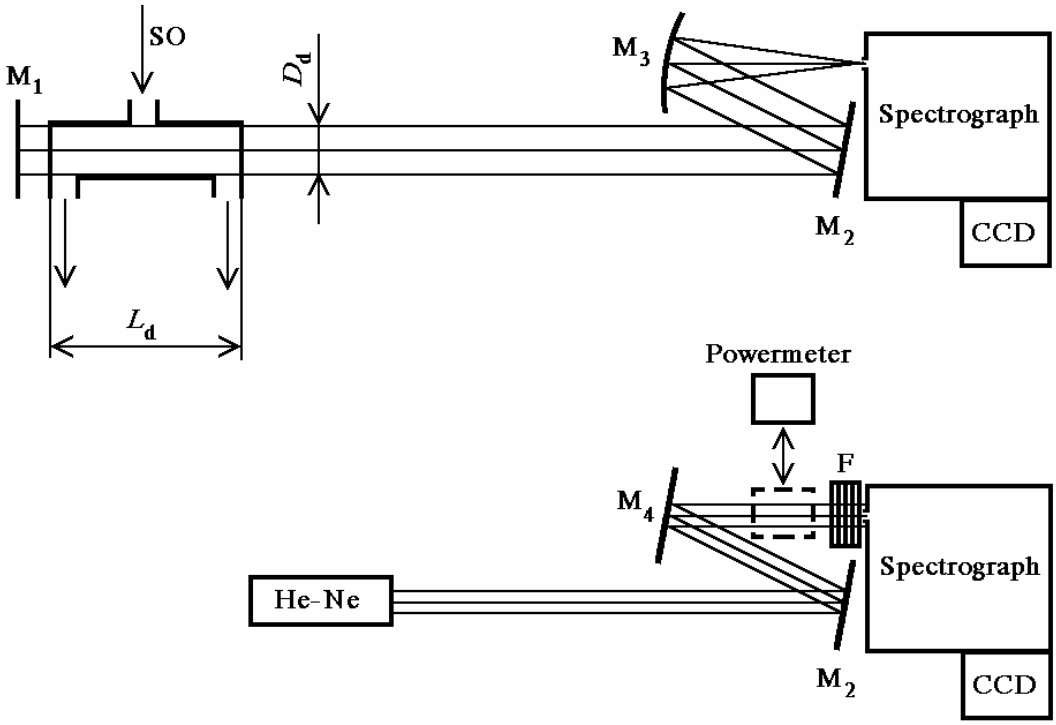

Fig.II.2.1. The layout of experiment on dimole emission detection (upper) and absolute calibration (lower).

The unfocused He-Ne radiation laser located 550 cm apart of spectrograph slit was used for absolute calibration. In this case the spherical mirror M_3 was substituted for plane one M_4. The laser operated on the fundamental transverse mode. The laser beam was centered with the spectrograph slit and its diameter in the slit plane was 7 mm (FWHM). The radiation intensity in the beam center was measured with a power meter installed behind the 2.6 mm centrally positioned diaphragm. The intensity measured in the beam center was P=4.9 mW/cm^2. The set of four calibrated neutral filters (NS10 and NS13) was used to reduce the laser power to the level close to that of dimole radiation. The transmittances of the filters measured with spectrophotometer SF-26 were 1.1; 0.85; 2.0 and 2.4%. Thus, the total transmittance of attenuator T was $T= 4.5 \cdot 10^{-8}$.

The polarization of He-Ne radiation was oriented at 45^0 with respect to spectrograph slit. It was made to equalize the losses introduced by spectrograph prisms for linearly polarized laser radiation and non polarized dimole one.

In both cases the measurements were carried out with 100 μm slit width, which was much over the normal one. The effective slit height was governed by that of CCD pixel and it was as high as H=11:0.4 = 27.5μm, where the coefficient 0.4 was equal to the spectrograph magnification. Thus the slit effective area was as large as $S = 2.75 \cdot 10^{-5}$ cm^2. The CCD array acquisition time τ of 4 s was the same for both cases.

In this experiment the slit width W of 100 μm was the maximal. Being observed from the center of M_3 mirror this slit had angular dimension of $\varphi = \frac{W}{f} = 2 \cdot 10^{-4}$. Thus, as it follows from ray optics, all photons emitted from the cell and propagating within the angle of φ to the optical axis can enter the spectrograph. As soon as this angle is very small, one can neglect the effect of vignetting due to cell output window. Indeed, even the beams passing along the longest way in the cell (that originally propagating from the output cell window to mirror M_1 and back) had a linear dimension $2L_d\varphi$=0.48 mm in horizontal plane. That value is negligibly small as compared to the cell diameter. The effective angular dimension in vertical of the spectrograph slit was even less. Thus, one can guess that a fraction of dimole radiation emitted at the spherical angle $\Omega = \frac{S}{f^2}$ entered a spectrograph slit.

It was mentioned above that the unfocused He-Ne laser radiation was used in the measurements. The incomplete filling of spectrograph collimator with light took place under given slit width. So, the losses of light due to spectrograph aperture were negligible. In operation with dimole radiation the latter was focused at slit.

Let us estimate the effective dimension D_M of dimole light spot at the mirror M_3. Let us suppose that the light beam of diameter D_d having the divergence of φ in horizontal enters the spectrograph slit. Then passing the distance of L the light beam will increase in diameter by φ $L = 2 \cdot 10^{-4} \cdot 700$ =0.14 cm. This value is negligible compared to D_d=4.5 cm, so $D_M \approx D_d$. Therefore, the angular dimension of dimole radiation beam focused at slit with mirror M_3 is D_M:f = 45:500 that does not exceed the relative aperture of spectrograph. Therefore, the losses of dimole radiation due to spectrograph aperture were negligible too.

Fig.II.2.2 demonstrates the signals in the same relative units from pixels of CCD array obtained under recording of both dimole radiation of 1Torr of oxygen with 50% of SDO and attenuated He-Ne laser radiation.

Summation of signals over all pixels of CCD array gives U_d=5770 for dimole radiation and $U_{He\text{-}Ne}$=2400 for He-Ne laser one. It is not difficult to write the expression for the number of photons passing through the effective area of spectrograph slit for acquisition time τ. For He-Ne laser one has

$$Q_{He\text{-}Ne} = \frac{TPS\tau}{h\nu}, \qquad \text{(II.2.1)}$$

where $h\nu = 3.14 \cdot 10^{-19}$ J is an energy of quantum with 633 nm wavelength. Substituting all values to (II.2.1) one can receive $Q_{He\text{-}Ne} = 7.7 \cdot 10^4$ photons. Thus, the absolute sensitivity of detecting system is $q = \frac{Q_{He-Ne}}{U_{He-Ne}}$ =32 photons/unit signal of CCD array.

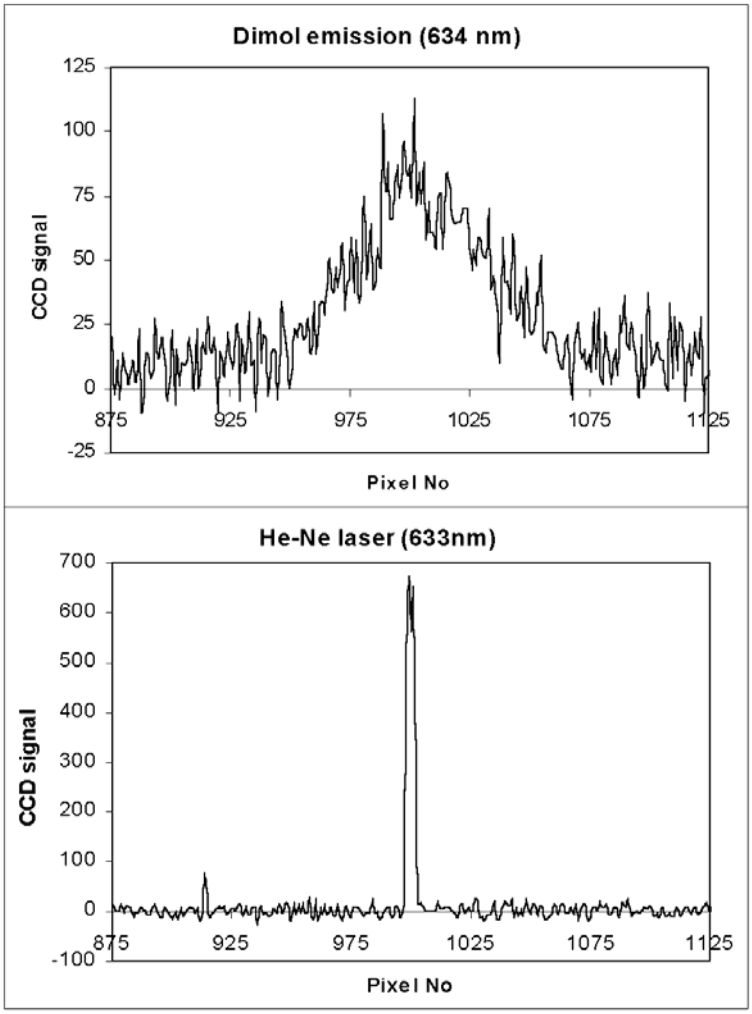

Fig. II.2.2. CCD array response to dimole radiation (upper) and He-Ne laser radiation (lower)

Dimole radiation with 634 nm wavelength is a result of the process

$$O_2(^1\Delta) + O_2(^1\Delta) \rightarrow O_2(X, v=0) + O_2(X, v=0) + h\nu(634\ \text{nm}), \qquad \text{(II.2.2)}$$

occurring with the rate constant k_d. It is not difficult to show that for acquisition time τ number of photons Q_d of dimole radiation entering the effective area of spectrograph slit can be written as

$$Q_d = \frac{KR_{2-3}k_d N^2 \tau V_d S}{4\pi f^2}, \qquad \text{(II.2.3)}$$

where $N=[O_2(^1\Delta)]$ is concentration of SDO in cell. As soon as the wavelengths of dimole radiation practically coincides with that of He-Ne laser one can not take into account the dependence of CCD array sensitivity on wavelength of detected radiation. Then,

$$\frac{Q_d}{Q_{He-Ne}} = \frac{U_d}{U_{He-Ne}}. \qquad \text{(II.2.4)}$$

It follows from (II.2.1) and (II.2.3) that:

$$\frac{U_d}{U_{He-Ne}} = \frac{KR_{2-3}k_d N^2 \tau V_d S}{4\pi f^2} \frac{h\nu}{TPS\tau} = \frac{KR_{2-3}k_d N^2 V_d h\nu}{4\pi F^2 TP}, \quad \text{(II.2.5)}$$

Therefore,

$$k_d = \frac{U_d}{U_{He-Ne}} \frac{4\pi f^2 TP}{KR_{2-3}N^2 V_d h\nu} = \frac{U_d}{U_{He-Ne}N^2} 8.89\cdot 10^9. \quad \text{(II.2.6)}$$

$$k_d = \frac{U_d}{U_{He-Ne}N^2} 8.89\cdot 10^9$$

Thus, substituting into (II.2.6) the values of parameters and assuming $N=1.65\cdot 10^{16}$ cm^{-3} (corresponds to 50% of SDO yield at 1 Torr of oxygen) one receives $k_d=7.85\cdot 10^{-23}$ cm^3/s. The value obtained is in agreement with literature (Bowell et al, 1983) within the accuracy of 50%. Note that the error of 10% in determination of SDO yield (that is rather high accuracy) results in an error of 20% for k_d. Thus, keeping in mind that other parameters are determined with some error too, one can consider the result obtained is satisfactory. This result is a good conformation that procedure used is valid.

This procedure was used for processing experimental data obtained for various SDO pressures. The results of data processing are presented in **Table II.2.1**.

Table II.2.1.

O_2 Pressure, Torr	SDO signal intensity, Arb.units	SDO yield, %	SDO concentration N, 10^{16} cm^{-3}	U_d	k_d, 10^{-23} cm^3/s
1.0	36	50	1.65	5767	7.85
1.5	43	40	1.97	8973	8.56
2.0	53	37	2.43	13330	8.36
0.5	27	75	1.24	3188	7.68
1.0	41	57	1.88	6633	6.95
1.5	51	47	2.34	9831	6.65
1.8	56	43	2.57	11760	6.60
1.2	44	51	2.02	6757	6.13

Absolute calibration of b→X radiation detectors using the chemically produced singlet delta oxygen.
(*Subtasks 1B.2 and 1B.4*)

The sparger type chemical singlet delta oxygen generator (SDOG) used previously to feed pulsed chemical oxygen-iodine laser was used for absolute calibration of detectors of dimole (λ=634 nm) and b→X (762 nm) radiation detectors. This SDOG was tested previously to determine the dependence of value of SDO yield on SDOG operation conditions. The spectra in visible of chemically produced SDO were obtained by using a prism spectrograph equipped with CCD array (**Fig. II.2.1**). The spectra of luminescence of chemically produced SDO were compared with that of pure oxygen excited with axial self-sustained electric discharge. The electric discharge took place in

the same cell, so in both cases the geometry of luminescence observation was absolutely the same. **Fig. II.2.3** demonstrates the typical spectra obtained under 4 s of storage time. The electric discharge operated at repetition rate 2.5 Hz, so the exposition time in this case was much shorter than storage time and was determined by the afterglow duration.

The chosen storage time was enough to record both bands of dimole emission corresponding to v = 0 → v = 0 (λ = 634 nm) and v = 0 → v = 1 (λ = 703 nm) transition and emission corresponding to b→X transition (λ = 762 nm) as well.

Unlike chemically produced oxygen the spectrum of discharge excited oxygen contains the lines corresponding to transition of oxygen atoms but it is free of bands of dimole emission. At the same time the intensity of b→X transition is much higher than that of chemically produced oxygen. This fact, in particular, is a result of water vapor presence in latter case. Water molecule is an efficient quencher of b-state of oxygen. The spectra of chemically produced SDO were recorded at different pressures of chemical SDOG operating with and without low temperature water vapor trap.

The comparison of intensities of b→X and dimole emission were performed via summation of signals of CCD elements over dimole and b→X bands taking into account the dependence of sensitivity of CCD on wavelength. The latter dependence was measured using the convenient method with the black body as a reference source. The values S_{634} and S_{762} of relative intensities of dimole and b→X radiation respectively, are presented in the **Table II.2.2**.

Dimole emission is a result of a process $O_2(a^1\Delta) + O_2(a^1\Delta) = 2\ O_2(X^3\Sigma) + h\nu$ (λ = 634 nm), which rate constant is $K_{dimole}=5.5\cdot10^{-23}$ cm^3 s^{-1} (Bowell et al, 1983). Knowledge of SDO concentration makes it possible to evaluate the intensity I_{634} of dimole radiation and, thus, calibrate CCD array.

$I_{634} = K_{dimole}\ [O_2(a^1\Delta)]\cdot[O_2(a^1\Delta)]$ photons / s cm^{-3}, where $[O_2(a^1\Delta)]$ is the O_2 $(a^1\Delta)$ concentration in cm^{-3}. Then, this calibration can be used to evaluate the absolute intensity of b→X emission:

$$I_{762} = (S_{762} \cdot I_{634}) / S_{634}. \qquad \text{(II.2.7)}$$

On the other hand, as soon as the radiation at the wavelength λ = 762 nm is a result of a spontaneous radiative decay of O_2 $(b^1\Sigma)$: $O_2(b^1\Sigma) \rightarrow O_2(X^3\Sigma) + h\nu$ (λ = 762 nm), $A_{b\rightarrow X} = 0.077$ s^{-1}, where $A_{b\rightarrow X}$ is the Einstein coefficient, the intensity I_{762} can be written as follows:

$$I_{762} = [O_2\ (b^1\Sigma)]\ A_{b\rightarrow X}. \qquad \text{(II.2.8)}$$

Combining (II.2.7) and (II.2.8) one can evaluate the stationary concentration of O_2 $(b^1\Sigma)$: $[O_2(b^1\Sigma)] = (S_{762}\ I_{634})/S_{634}\ A_{b\rightarrow X}$. The stationary concentration of O_2 $(b^1\Sigma)$ is formed in processes (II.2.9) and (II.2.10):

$$O_2(a^1\Delta) + O_2(a^1\Delta) = O_2(X^3\Sigma) + O_2(b^1\Sigma),\ K_{pooling} = 2.7\cdot10^{-17}\ \text{cm}^3\ \text{s}^{-1}, \qquad \text{(II.2.9)}$$

$$O_2(b^1\Sigma) + H_2O = O_2(a^1\Delta) + H_2O,\ K_{H2O} = 6.7\cdot10^{-12}\ \text{cm}^3\ \text{s}^{-1}, \qquad \text{(II.2.10)}$$

As it follows from (II.2.9) and (II.2.10) the value of stationary concentration of O_2 $(b^1\Sigma)$ is described by the expression:

$$[O_2(b^1\Sigma)] = ([O_2(a^1\Delta)]\cdot[O_2(a^1\Delta)]\ K_{pooling})/[H_2O]\ K_{H2O} \qquad \text{(II.2.11)}$$

Table II.2.2 presents experimental data obtained for chemically produced SDO and results of processing.

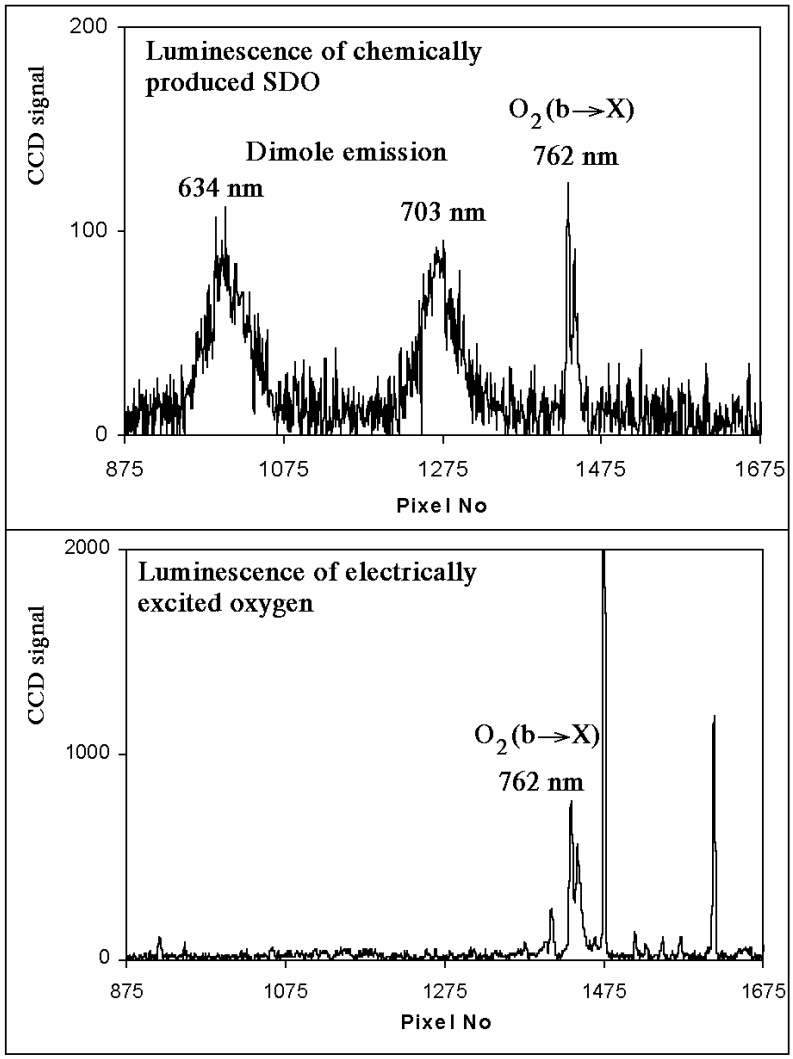

Fig. II.2.3. Luminescence spectra of chemically produced SDO (upper) and pure oxygen excited by axial self-sustained electric discharge.

Table II.2.2

S_{634},	S_{762},	P_{Cl2}, Torr	Y_{SDO}, %	$[O_2 (a^1\Delta)]$ cm^{-3}	I_{634}, ph/s cm^{-3}	I_{762}, ph/s cm^{-3}	$[O_2\ b^1\Sigma)]$, cm^{-3}	$[H_2O]$, cm^{-3}
No low temperature trap								
5776	3978	1.0	50	$1.60\cdot10^{16}$	$1.41\cdot10^{10}$	$9.71\cdot10^{9}$	$1.26\cdot10^{11}$	$8.18\cdot10^{15}$
8973	6099	1.5	40	$1.91\cdot10^{16}$	$2.03\cdot10^{10}$	$1.37\cdot10^{10}$	$1.77\cdot10^{11}$	$8.30\cdot10^{15}$
13330	7734	2.0	37	$2.36\cdot10^{16}$	$3.05\cdot10^{10}$	$1.77\cdot10^{10}$	$2.30\cdot10^{11}$	$9.72\cdot10^{15}$
Low temperature trap								
3188	5808	0.6	62.5	$1.20\cdot10^{16}$	$7.92\cdot10^{9}$	$1.44\cdot10^{10}$	$1.87\cdot10^{11}$	$1.51\cdot10^{15}$
6633	10779	1.0	57	$1.82\cdot10^{16}$	$1.83\cdot10^{10}$	$2.97\cdot10^{10}$	$3.85\cdot10^{12}$	$3.47\cdot10^{15}$
6757	13176	1.2	47	$1.82\cdot10^{16}$	$1.83\cdot10^{10}$	$3.56\cdot10^{10}$	$4.62\cdot10^{12}$	$2.89\cdot10^{15}$
9831	12444	1.5	41	$1.96\cdot10^{16}$	$2.10\cdot10^{10}$	$2.66\cdot10^{10}$	$3.46\cdot10^{12}$	$4.46\cdot10^{15}$
11760	14001	1.8	43	$2.49\cdot10^{16}$	$3.41\cdot10^{10}$	$4.06\cdot10^{10}$	$5.27\cdot10^{12}$	$4.74\cdot10^{15}$

The evaluation of water vapor concentration is an additional test of applicability of our approach. The water concentration can be evaluated from (II.2.11), and the values obtained for different experimental conditions are presented in **Table II.2.2**.

The values obtained for experiments performed without low temperature trap are in agreement with literature data for water pressure for working solution at - 20^0 C (temperature of SDOG). The water vapor trap was filled with alcohol chilled down to - 70^0 C but, because of low trap efficiency, the water pressure was over equilibrium value for this temperature.

The absolute calibration of detector of dimole and b→X radiation made using He-Ne laser (see above) can be used to evaluate the concentration of b-state too. Application of this approach to measure concentration of b-state under the experimental condition corresponding to the first row of **Table II.2.2** gives the value $[O_2 (b^1\Sigma)] = 0.75\cdot10^{11}$ cm^{-3}.

The spectra of luminescence of oxygen excited by axial self sustained electric discharge were obtained for different values of electrical energy stored in capacity bank and different oxygen pressure. The volume of the discharge zone was 1.8 l. The capacitance of capacitor bank was 20 nF. The value of stored energy was changed via variation of capacitor voltage. **Table II.2.3**. presents the experimental data and results of data processing.

Table II.2.3.

P_{Cl2}, Torr	Voltage, kV	Discharge Energy, J	S_{762}	$[O_2 (b^1\Sigma)]$, cm^{-3}
1.5	12	1.44	25200	$3.20\cdot10^{13}$
3.0	12	1.44	20475	$2.60\cdot10^{13}$
3.0	15	2.25	29934	$3.80\cdot10^{13}$
5.0	15	2.25	22770	$2.89\cdot10^{13}$

The results presented demonstrate the dependence of concentration of oxygen b-state produced in electric discharge on oxygen pressure and discharge energy.

The values of b-state concentration were evaluated via comparison with spectrum of chemically produced SDO assuming that duration of discharge afterglow is as long as 10 ms, i.e. real acquisition time is only 100 ms. Only one experiment with chemically produced SDO (the first row) was chosen as a reference to evaluate b-state concentration. In the case of zero error measurement the result must be the same for each experiment chosen as a reference. Let us estimate the error using all chemical SDO data as a reference points to evaluate the concentration of b-state for experimental conditions of the first row of **Table II.2.3**. The results obtained are: $3.20\cdot10^{13}$; $2.93\cdot10^{13}$; $3.00\cdot10^{13}$; $3.25\cdot10^{13}$; $3.60\cdot10^{13}$; $3.54\cdot10^{13}$; $2.80\cdot10^{13}$; $3.79\cdot10^{13}$ cm^{-3}. The average value is $3.26\cdot10^{13}$ cm^{-3} and average deviation is $0.29\cdot10^{13}$ cm^{-3}, which corresponds to an error of 8.6%.

Thus one can conclude the approaches used to calibrate detectors of dimole and b→X radiation have satisfactory accuracy and can be used to compare experiment with the results of numerical modeling.

Application of intracavity laser spectroscopy for absolute measurement of SDO concentration (*Subtasks 1B.2, 1B.4 and 3.1*)

Correct measurement of SDO concentration is a key problem in a program of designing an electrically driven SDO generator. Among a lot of different approaches used to measure SDO concentration, the method based on the measurement of radiation intensity on the $a^1\Delta_g \rightarrow X^3\Sigma_g$ transition with an absolutely calibrated detector is most convenient (McDermott, 1978). But in this case the absolute calibration of detector depends significantly on the geometry of calibration and,

being a very difficult task, it can be a source of error. Besides, this method is not free of influence of background illumination (for example, investigating electric discharge in gas) which can hinder the separation of very week signal of 1.27 μm emission (radiative lifetime of $O_2(a^1\Delta_g)$ state in a gas phase is 4000 s (Miller, 2001)). These effects may be responsible for appreciable scatter in literature of data on yield of SDO produced in electric discharge.

The absorption spectroscopy is free of demerits mentioned above. The direct measurement of SDO concentration can be made via measurement of absorption on the transition $a^1\Delta_g \rightarrow b^1\Sigma_g^+$ in the vicinity of 1.91 μm wavelength. This transition was observed for the first time by J.F. Noxon in the emission spectrum of electric discharge in the oxygen-helium mixture (Noxon, 1961). Being electric quadrupole transition with very low transition probability (0.0025 s^{-1} (Noxon, 1961), 0.0017 s^{-1} (Krupenie, 1972)) it needs application of very sensitive absorption method to be detected.

The intracavity laser spectroscopy (ICLS) is one of such methods (Pakhomycheva, 1970; Baev, 1999). The applicability of Co:MgF_2 laser based ICLS to detect SDO due to measurement of absorption on the $a^1\Delta_g \rightarrow b^1\Sigma_g^+$ transition was experimentally demonstrated in (Pazyuk, 2001). For this purpose lines of the *Q* – branch of the vibrational 0-0 band of the $a^1\Delta_g \rightarrow b^1\Sigma_g^+$ transition of molecular oxygen were used. The sensitivity of apparatus used made it possible to detect the SDO concentration as low as $5\cdot10^{14}$ см$^{-3}$.

To determine the species concentration by absorption spectroscopy (including ICLS too) one needs to know the exact value of absorption cross section. When the values of transition probabilities are known, the transition cross sections for separate lines of the *Q* – branch can be calculated, but, so far, the known data on transition probability of this transition are too poor and based on the only experimental results (Noxon, 1961). The obtained value of 0.0025 s^- has an accuracy of up to a factor 2. The another value of 0.0017 s^{-1} (Krupenie, 1972) is a result of reprocessing the data obtained by J.F.Noxon. Therefore, the experimental determination of a value of absorption cross section for lines of the *Q* – branch of the vibrational 0-0 band of the $a^1\Delta_g \rightarrow b^1\Sigma_g^+$ transition of molecular oxygen and comparison with numerical calculation was a primary task.

To solve this task the absorption spectra of SDO were recorded using a broadband Co:MgF_2-laser which cavity was filled with chemically produced oxygen with well known yield of SDO.

Experimental and data processing

The experimental setup (**Fig. II.2.4**) described in detail elsewhere (Pazyuk, 2001) was modified to work in assembly with a chemical SDO generator based on the gas – liquid reaction of molecular chlorine with base solution of hydrogen peroxide. A Co:MgF_2 crystal was longitudinally pumped by Nd:YAG laser operating in a free running mode at 1.34 μm. The pump radiation was focused with a lens L_1 into crystal center. The pulse duration of Co:MgF_2 laser was 80-110 μs depending on that of pumping pulse. The cavity of Co:MgF_2 laser was formed with a plane totally reflecting mirror M_1 and spherical (R=1000 mm) output one M_2. Cavity length was L_c=660 mm. The dispersion prism made of CaF_2 installed in a laser cavity made it possible to change the generation spectrum. When working with SDO, the center of spectrum of generation having width of 4 nm was tuned to the 1.91 μm wavelength. To reduce the influence of interference effects on the generation spectrum, the 5^0 edge mirror substrates and a Brewster-angled Co:MgF_2 crystal were used.

A Co:MgF_2 crystal was mounted inside the vacuum-tight metal chamber, mirror M_1 being a window of the latter. The output mirror M_2 was attached to an outlying PMMA flange. Flange was attached to the chamber by a quartz tube with an inner diameter 26 mm. Oxygen flow produced in the chemical SDOG passed along the tube and then pumped out by mechanical pump. The flow velocity in the tube was 29 m / s. Due to both, low probability of SDO quenching on the tube wall and high flow velocity, SDO losses during passing from chemical generator to outlet were minimal. Under experimental conditions used the thickness of absorption was L_a=300 mm.

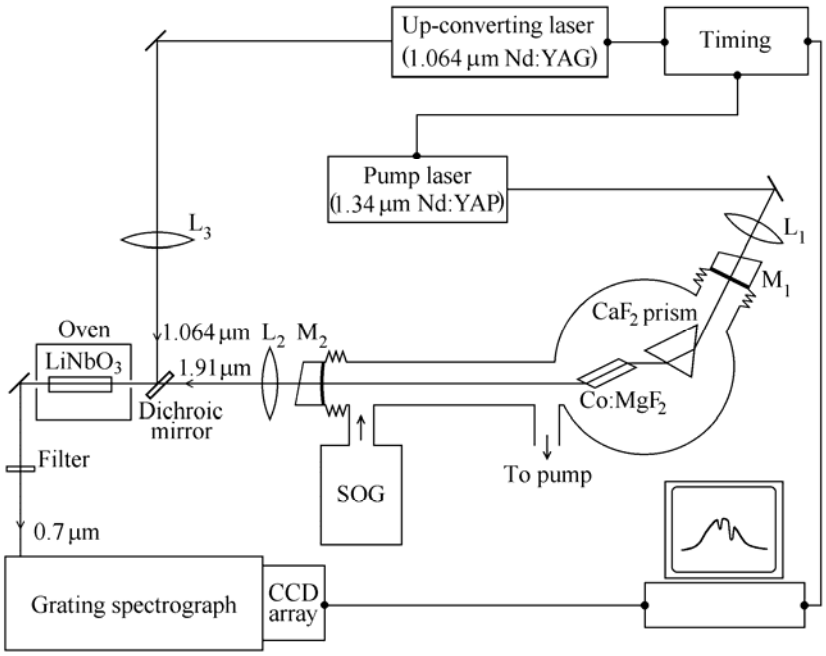

Fig.II.2.4. Schematic diagram of experimental setup.

The output spectrum of the Co:MgF_2-laser was detected with a diffraction spectrograph (with a spectral resolution of 0.018 cm^{-1}) couplet to an optical multichannel analyzer based on the CCD array and PC.

The broadband IR radiation from Co:MgF_2-laser was firstly up-converted to visible spectral range by mixing it with monochromatic radiation from Nd:YAG-laser (λ=1.064 μm, the linewidth is 0.017 cm^{-1}, the pulse duration is 5 μs, and the pulse energy is 1 mJ) in a nonlinear lithium niobate crystal, which was heated in oven to about 450^0 C to achieve the 90^0 phase matching. Dichroic mirror and lenses L_2 and L_3 were used for combining and focusing two laser beams inside the nonlinear crystal. The emission at the sum frequency was incident on the entrance slit of spectrograph. The random noises in the laser output spectrum were reduced by averaging the spectrum over 100 pulses.

The base of ICLS is as follows. The sample under investigation with the line absorption spectrum (gas mixture containing absorbing molecules, for example) is placed into the cavity of a broadband laser which output spectrum covers that of sample absorption. If the width of absorption lines is low compared to the homogeneous width of a gain profile of a laser active medium, the laser works like a multypass optical cell, which effective length is equal to the distance which light travels in the sample for time interval equal to pulse duration.

In other words, when ICLS method is used to detect absorption spectrum, the dip at absorption line frequency ω develops in the spectrum of a broadband laser for its generation time t_g. This dip is described by modified Beer-Lambert low (Baev,1999):

$$I(\omega,t_g)/I_0(t_g)=\exp(-k(\omega)ct_gL_a/L_c), \qquad \text{(II.2.12)}$$

where $I(\omega,t_g)$ is the generation intensity at absorption line frequency at instant of time t_g; $I_0(t_g)$ is the generation intensity in vicinity of absorption line frequency at instant of time t_g; c is the speed of light; $k(\omega)$ is the absorption coefficient; L_a/L_c is the coefficient of filling of the cavity with absorbing species. Thus, measuring the value of ratio $I(\omega,t_g)/I_0(t_g)$, one can evaluate the line absorption coefficient. By definition $k(\omega)=\sigma(\omega)N$, where $\sigma(\omega)$ is the absorption cross section, N is

the concentration of absorbing molecules. Then, it is not difficult to evaluate the concentration when the value of cross section is known.

To apply the expression (II.2.12) to evaluate the concentration of interest, one needs to record the spectral distribution of output radiation of broadband laser at specific moment of time. The optical shutter is usually used to cut out a necessary time interval from laser pulse and, thus, to record the spectral distribution corresponding to this time interval.

A pulse duration of the Nd:YAG-laser used to convert IR radiation to visible was short compared to that of Co:MgF_2-laser. The synchronization unit provided the variable time delay between the Nd:YAG-laser pulse and the leading edge of the pulse from a Co:MgF_2-laser. Thus, one could detect the emission spectrum at any specific moment of time without using any additional equipment.

An instrumental line width of detecting apparatus was wider than Doppler width of oxygen absorption line which is 0.0113 cm^{-1} at room temperature. It resulted in deformation of the real profile of absorption line and made it impossible to use expression (II.2.12) directly to process experimentally obtained spectra. Therefore, the numerical modeling of absorption spectra accounting instrumental function was used to evaluate the quantitative information. The instrumental function was approximated by diffraction profile of 0.03 cm^{-1} width. The best agreement of experiment and numerical modeling was obtained by variation of absorption coefficients. Then, the value of absorption coefficient corresponding to the best agreement was assigned to experimentally obtained spectrum.

Verification of processing procedure.

The validity of the processing procedure used was verified by preliminary experiments on measurement of absorption spectra of air in vicinity of 2.003 μm wavelength. The well known absorption lines of water and carbon dioxide fall into this spectral region. **Fig**. **II.2.5** presents an example of such a spectrum recorded with a cavity filled by air (L_a=L_c) at air pressure of 1.9 Torr and pulse duration of 80 μs. The absorption lines belong to CO_2 and H_2O molecules. The lower spectrum is a result of numerical modeling of transmission of air layer of 24 km length (the distance which light travels for 80 μs) at the same pressure. The HITRAN (Rothman, 1998) database was used in numerical modeling. The smooth spectrum envelope was assumed in numerical modeling. As one can see from **Fig. II.2.5** the theory and experiment are in a good agreement. We believe this agreement is a satisfactory cause for application of the processing procedure described above.

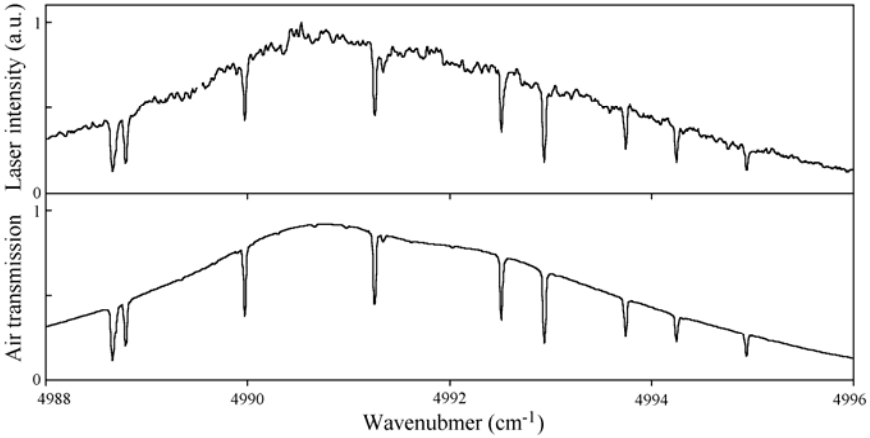

Fig. II.2.5. Spectral distribution of a Co:MgF_2 laser radiation recorded with a filled by air cavity at air pressure 1.9 Torr and pulse duration 80 μs (upper) and result of numerical modeling based on HITRAN database and accounting the laser spectrum envelope of transmission of a 24 km length of air at 1.9 Torr of pressure.

The measurement of cross-section of SDO absorption lines.

The series of experiments were performed to measure the cross-section of lines of the *Q* – branch of the vibrational 0-0 band of the $a^1\Delta_g \rightarrow b^1\Sigma_g^+$ transition of molecular oxygen. The absorption spectra of effluent of chemical SDO generator producing the SDO with known yield were recorded with ICSL method. This sparger chemical SDO generator based on gas-liquid reaction of molecular chlorine with base solution of hydrogen peroxide was earlier used in a work on investigation of a pulsed chemical oxygen iodine laser (Vagin, 1995). The generator design made it possible to work in both modes with and without low temperature water vapor trap. Within the framework of that activity the detailed measurements of SDO yield under different generator operation conditions were performed. The results of that work made it possible to know the partial SDO pressure correctly.

In present experiments the partial pressure of SDO was varied within 0.14 – 0.65 Torr. **Fig**. **II.2.6** (left column) demonstrates some of spectra obtained. Each of presented spectra is a result of division of experimentally obtained one by its smooth spectrum envelope, i.e. normalized to unit.

The spectra presented were obtained at SDO partial pressure in a cavity 0.42, 0.26, and 0.14 Torr. The lower spectrum was recorded with a flow free of SDO (chemical SDO generator was fed with air instead of chlorine). The total pressure of oxygen-buffer gas mixture was 2.2 – 2.3 Torr. At this pressure the spectral lines were Doppler broadened. The pulse duration of Co:MgF_2-laser was as long as 90 μs.

Identification of SDO lines was made using the results obtained by E.Fink and co-workers (Fink, 1986). Seven lines of SDO fall within the spectral range of **Fig**. **II.2.6**. Also the spectrum contains lines of water, some of which overlap the *Q*(2) and *Q*(8) lines of SDO. Thus, the latter lines can not be used for measurement, but the other five lines (labeled by circle in **Fig**. **II.2.6**.) are not overlapped and, thus, can be used.

The absorption coefficient at the center of line with number J for the Q branch under consideration of the 0-0 band of the $a^1\Delta_g \rightarrow b^1\Sigma_g^+$ oxygen transition is described by expression:

$$k_J = \frac{\lambda^2}{8\pi} A_{b\to a} S_J q_{00} \left(\frac{N_a}{g_a}\frac{B_a}{k_B T}\exp[-\frac{B_a}{k_B T}J(J+1)] - \frac{N_b}{g_b}\frac{B_b}{k_B T}\exp[-\frac{B_b}{k_B T}J(J+1)] \right) G(\lambda),$$ where λ is the wavelength; $A_{b\to a}$ is the probability of spontaneous transition from $O_2(b^1\Sigma_g^+)$ to $O_2(a^1\Delta_g)$; $S_J = \frac{2(2J+1)(J+2)(J-1)}{(2J-1)(2J+3)}$ (Fink, 1986); q_{00}=0,977 is the Franck-Condon factor; N_a, N_b are populations of proper levels; g_a=2, g_b=1 are the degeneracy factors; B_a=1,391262 см$^{-1}$, B_b=1,4178402 см$^{-1}$ are the rotational constants (Fink, 1986); k_B is the Boltzmann constant; T is the gas temperature in Kelvins; $G(\lambda)$ is the line profile function, which value at the center of Doppler broadened line is $G(\lambda) = \frac{1}{\Delta\nu_D}\sqrt{\frac{4}{\pi}\ln 2}$, $\Delta\nu_D = \frac{\nu}{c}\sqrt{\frac{8k_B T \ln 2}{M}}$ is the Doppler width of absorption line, where M is the molecule mass.

When the population N_b of the level $b^1\Sigma_g^+$ is low (that is valid for chemically produced SDO), then

$$k_J = \frac{\lambda^2}{8\pi} A_{b\to a} S_J q_{00} \frac{N_a}{g_a}\frac{B_a}{k_B T}\exp[-\frac{B_a}{k_B T}J(J+1)]G(\lambda) = \sigma_J N_a. \qquad \text{(II.2.13)}$$

It follows from (II.2.13) for absorption cross section at the line center

$$\sigma_J = \frac{\lambda^2}{8\pi} A_{b\to a} S_J q_{00} \frac{1}{g_a}\frac{B_a}{k_B T}\exp[-\frac{B_a}{k_B T}J(J+1)]G(\lambda).$$

As the value of absorption cross section depends on the temperature, one needs to know the gas temperature to perform correct measurement.

As it follows from (II.3.13), $\ln\frac{k_J}{S_J} = -\frac{B_a}{k_B T} J(J+1) + \text{const}$. It means that the plot of function $\ln\frac{k_J}{S_J}$ versus $J(J+1)$ is the straight line which slope is determined by the gas temperature.

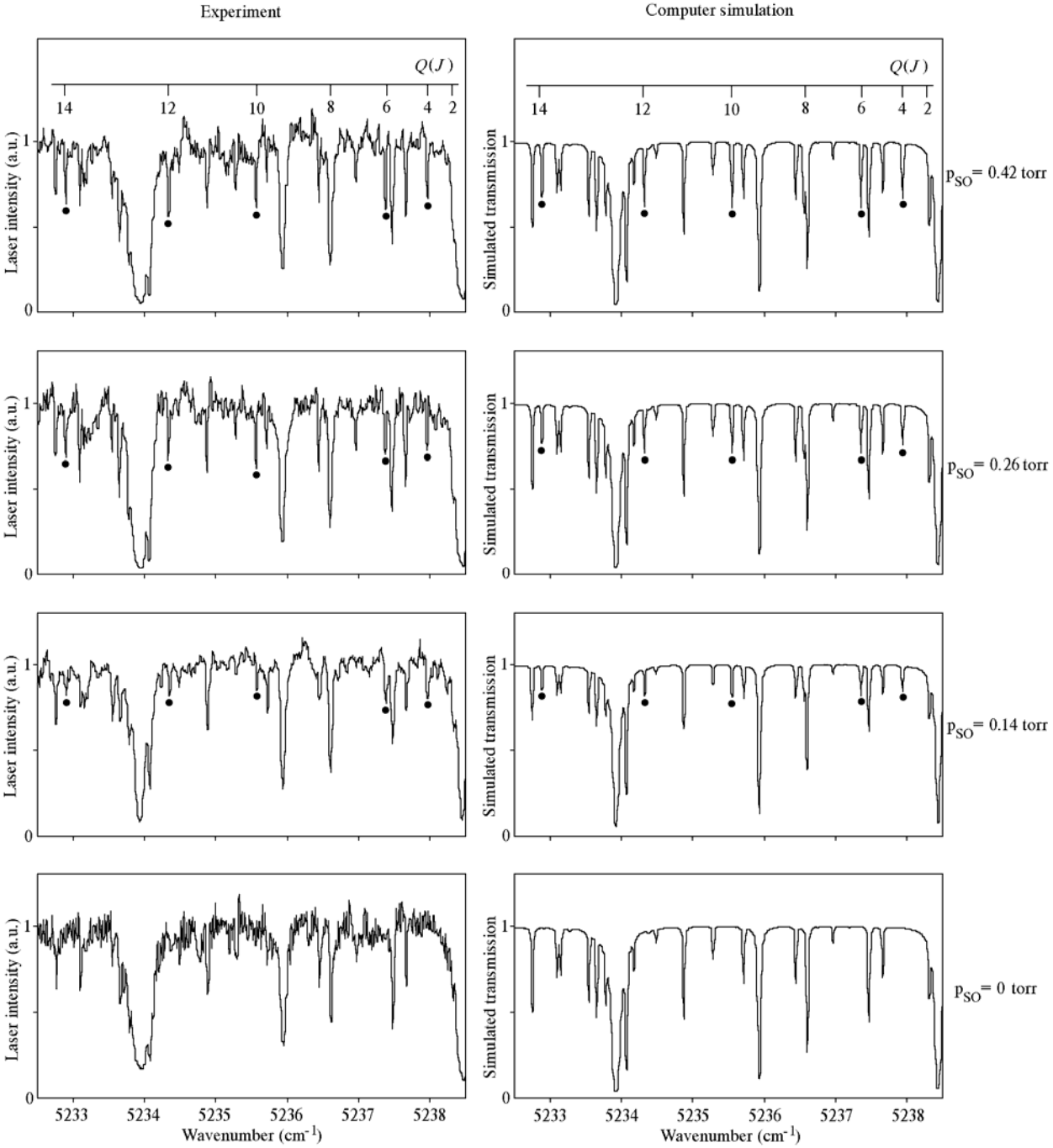

Fig. II.2.6. Absorption spectra of effluent of chemical SDO generator (lines applicable for measurements are labeled by circle) recorded under various partial pressures P_{SO} of SDO (left – experiment, right – numerical modeling)

It was noted above that all five absorption lines could be used in measurements at ones. Application of this procedure to the values of absorption coefficients obtained using ICLS method

for five absorption lines of SDO yielded the value of gas temperature in a laser cavity equaled to 310±25K. This value of temperature was used to calculate absorption cross sections for SDO lines. The transition probability in this calculation was presumed to be $A_{b\to a}$=0.0017 s^{-1}. The results obtained are presented in the **Table II.2.4**. The comparison of experimentally obtained spectra with that of modeling shows that the theoretical data presented in the **Table II.2.4** describe experimental results with an error which is not over 25 %.

Table II.2.4

J	ω, cm^{-1}	σ_J, 10^{-23} cm^2
2	5238.317	3.89
4	5237.944	7.84
6	5237.359	10.2
8	5236.561	11.1
10	5235.550	10.7
12	5234.325	9.46
14	5232.885	7.72

The water lines presenting in the spectra were taken into account under numerical modeling too.

As soon as the Co:MgF_2-laser output emission traveled 70 cm in free air from output mirror to up-conversion crystal, the numerical model included the absorption by atmospheric water vapor too.

The absorption spectra of effluent of chemical SDO oxygen generator obtained taking into account all conditions mentioned above, are presented in right column of **Fig. II.2.6**. The partial pressure of water vapor were varied in modeling within 0.1 - 0.2 Torr. One can see the good qualitative agreement between the modeled and experimentally obtained spectra. With respect to SDO lines, the quantitative agreement is observed too. Thus, analysis shows that the procedure described makes it possible to measure the SDO partial pressure with an accuracy of not worse than 25 %.

Measurement of concentration of SDO produced in a microwave discharge

The method developed was applied to measure the concentration of SDO generated in a microwave discharge in oxygen. In this case the quartz tube connecting the outlying flange with the metal chamber had inner diameter 16 mm, and chemical SDO generator was substituted by a 9 mm i.d. quartz tube feeding the cavity with oxygen at 1.9 Torr of pressure. The microwave discharge (discharge frequency is 2375 MHz, discharge power is about 100 W) was initiated in this tube to produce SDO molecules. The pulse duration of Co:MgF_2 – laser was 220 μs. The experimental setup is described in detail elsewhere (Pazyuk, 2001).

The left column in **Fig. II.2.7**. demonstrates the experimental absorption spectra obtained under experimental conditions described above. Besides the SDO absorption lines, the spectra include the absorption water lines too. The latter are labeled by square.

To remove oxygen atoms produced in the discharge zone, the ring of HgO was placed into the tube downstream of the microwave cavity. As a result the absorption of SDO increased (see lower spectrum in left column). It can be an evidence of a negative role of oxygen atoms in SDO production.

The spectrum modeling performed showed that the best agreement between experiment and modeling was observed when SDO partial pressures 0.07 and 0.11 Torr (see **Fig. II.2.7**, right column) and water vapor pressure 0.001 Torr were used in numerical modeling. These SDO partial pressures correspond to yields values 3.7% and 5.8% respectively.

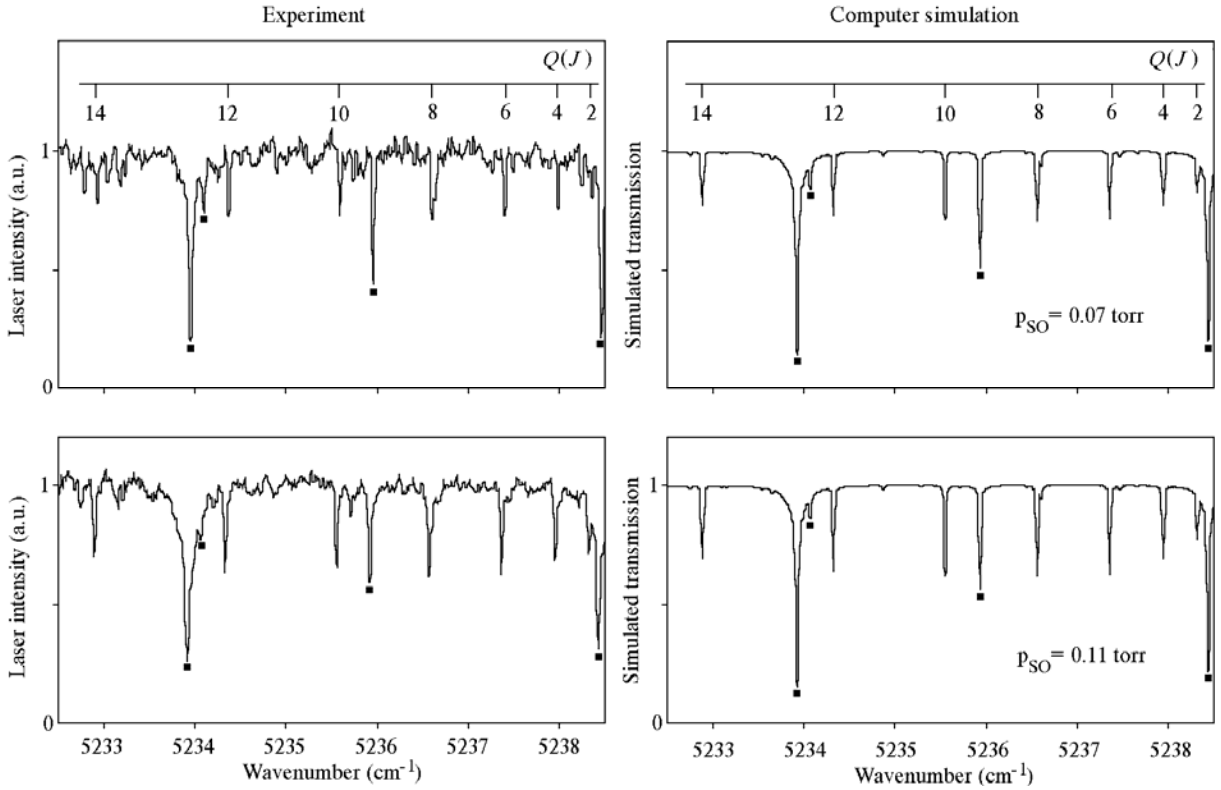

Fig. II.2.7. The experimental absorption spectra of water vapor (the water lines are labeled by square) and SDO recorded at operating microwave discharge (left) and spectra models (right). The spectra were obtained without (upper) and with (lower) HgO ring.

Thus, performed work on measuring the value of cross section of SDO absorption makes it possible to use ICLS method to measure the absolute concentration of SDO produced in electric discharge.

In accordance with the working plan the different types of electric discharge must be investigated as possible electrical sources of SDO. In our case they are microwave (MW) and capacitive radio frequency (RF) discharges. The first one is based on the discharge in oxygen containing mixture flowing through the 12 mm of outer diameter quartz tube installed in the quarter-wave cavity. The cavity is fed by the microwave generator having the 100 W of output power at 2.45 GHz.

The second one is a discharge initiated by RF generator, having up to 80 W of output power, between two outer ring electrodes.

Yields of SDO determined as the ratio of SDO concentration to the total oxygen concentration are shown in **Fig.II.2.8 and Fig.II.2.9**. These values were measured for pure oxygen gas. Admixture of He to oxygen resulted in increased SDO yield, while admixture of Ar decreased yield by 20 – 25 % as compared to pure oxygen at the same partial pressure. The maximum SDO yield of 19 % was measured for the $He:O_2$=2:1 mixture at total mixture pressure of 3.2 Torr and the pump capacity of 2 l/s. This yield is over the laser threshold at room temperature.

The behavior of dependences of SDO yield on partial oxygen pressure and pump capacity can be qualitatively explained by mutual influence of proportional to specific input energy process of SDO production and SDO relaxation due to atomic oxygen.

Measurements of SDO concentration produced in a RF discharge were performed too. SDO was generated in a 40.68 MHz capacity-coupled plasma by passing oxygen through the same 11 mm

quartz tube and coupling 80 W of RF power. SDO yield was less compared to that of the MW discharge.

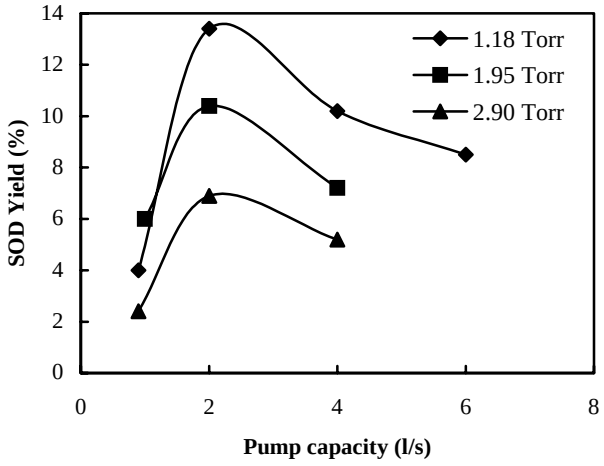

Fig.II.2.8. SDO yield versus pump capacity as function of total oxygen pressure for pure oxygen

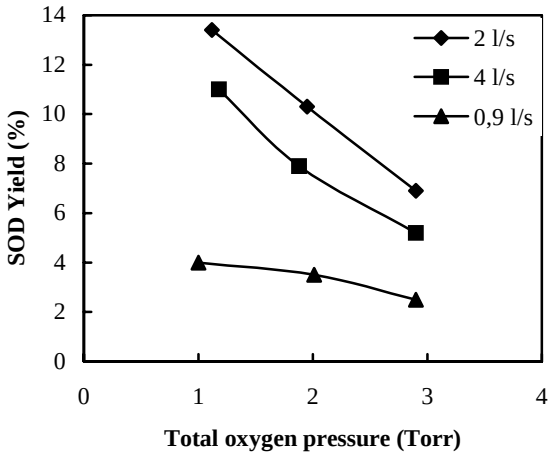

Fig.II.2.9. SDO yield versus pump capacity as function of total oxygen pressure for pure oxygen

Parametric study of SDO production in electrical generators driven by MW discharge by titration with iodide.
(Subtask 3.3)

Experimental facility and procedure

In principle, the methods required are well known but sometimes they need apparatus not available in our conditions. Therefore, such methods need to be modified for application of available instruments. For example, the SDO concentration can be successfully measured by detection of its luminescence at 1.27μm wavelength. However, relatively low intensity of the luminescence of SDO generated in electric discharge needs application of very sensitive IR photo detectors, in particular ones cooled by liquid nitrogen. Besides, the existence of oxygen atoms in effluent of discharge results in the broadband recombination emission due to the reaction with nitrogen oxide. This emission exerts influence on detection of the SDO emission in spite of application of interference filter. To overcome this obstacle, in our experiments small amount of iodine atoms is admixed to the

mixture under investigation. A probability of spontaneous emission of iodine atom at wavelength 1.315 μm more than five orders of magnitude exceeds that of 1.27 μm SDO emission. Thus, small amount of iodine atoms being admixed to the mixture containing SDO can work as a probe to get information about SDO yield. Such approach makes it possible to easily get qualitative information about SDO behavior. To get quantitative information, one has to make absolute calibration of detecting system. It can be made by using a chemical SDO generator (SOG). Output parameters of such a generator are well known as it widely used to feed chemical oxygen-iodine laser.

Thus, aforesaid dictates the design of the experimental set-up. The diagram of the experimental facility is shown in **Fig.II.2.10**. The quarts tube of 22 mm outer diameter (investigation section) is connected at its one side with the unit providing the mixing of discharge effluent with chemically produced SDO and additions under investigation. Another side of the tube is connected with the exhaust tube.

The investigation section is pumped out by a pump with pump capacity of 20 l/s. The electrically driven SDO generator consists of a quarter-wave cavity fed by 150±45W maximum output power of 2.375GHz medical physiotherapy device. The quarts tube of 12 mm outer diameter passing through the cavity is fed by pure oxygen or oxygen containing mixture. The downstream tube of the same diameter going out of the MW cavity has internal HgO coating acting as an oxygen atoms scavenger. A convenient sparger chemical SOG used earlier to drive the chemical oxygen-iodine laser is used for absolute calibration. To eliminate the water vapor from the chemical SOG, the low temperature trap (LTT) operating at the temperature down to -70 C is used.

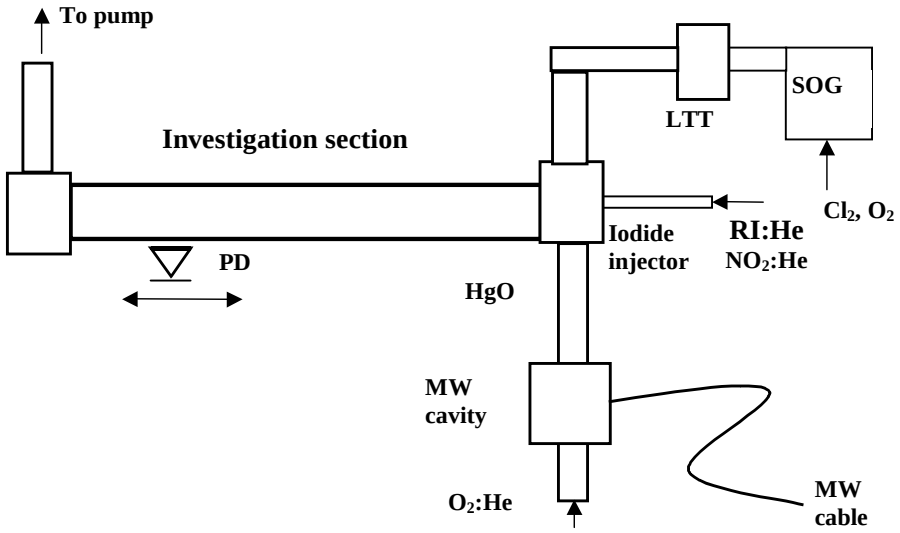

Fig.II.2.10. Schematic diagram of the experimental set-up

To maintain constant flow rate of all gas flows during experiments all gases are delivered from soft polyethylene bags being permanently under atmospheric pressure. Emission from investigation section is detected with germanium detector operating at the room temperature. To select the emission of interest, the detector is equipped with IR filter and removable interference filters having maximum transmittance at the 1.27 μm or 1.315 μm. The experimental facility is equipped with pressure gauge and flow meters. The design of experimental set-up makes it possible to easily substitute an electrical SDO generator by another one to compare their performances.

Measurement of absolute SDO yield

In the experiment on absolute calibration of the method the mixture composition in the investigation section is governed by the flow from the chemical SOG (0.9 Torr of unexcited O_2 and

0.39 Torr of O_2 produced in the chemical reaction of Cl_2 with BHP), the flow from MW source (0.78 Torr of O_2 : He = 1 : 2 mixture), and the flow from iodide injector (0.15 Torr of CH_3I : He = 1 :329). The total gas pressure in the investigation section is 2.2 Torr. As it was shown in our preliminary experiments, the SDO yield from chemical SOG operating under such pressure and pump capacity is as high as ~ 12 %. Such a low SDO yield is a result of both respectively high pressure and low pump capacity. It means that the SDO concentration at the inlet of the investigation section is $1.5 \cdot 10^{15}$ cm^{-3}. The total concentration of oxygen is a sum of concentration of all flows and, thus, it is $4.96 \cdot 10^{16}$ cm^{-3} (0.9 + 0.39 + 0.26 Torr). Thus, the effective SDO yield Y_{chem} (the ratio of SDO concentration to total oxygen one) governing the intensity of iodine luminescence is only Y_{chem} = 3.0%.

The equilibrium condition in the case of operation of chemical generator is written as $\frac{I^*}{I_{ground}} = K_{eq} \cdot \frac{Y_{chem}}{1-Y_{chem}}$, where K_{eq} is an equilibrium constant for the energy exchange reaction: $O_2(^1\Delta_g) + I(^2P_{3/2}) \leftrightarrow O_2(^3\Sigma_g) + I(^2P_{1/2})$, I* and I_{ground} are the concentrations of excited [$I(^2P_{1/2})$] and unexcited [$I(^2P_{3/2})$] iodine atoms, respectively. Iodine atoms are produced due to reaction of oxygen atoms formed in the discharge with iodide molecules. It is proposed that the concentration of oxygen atoms significantly exceeds that of iodide. Thus the concentration of iodine atoms is governed by the flow rate of iodide, which is maintained constant at all experiments. In fact, as soon as the MW discharge also operates in the experiment with the chemical generator, the Y_{chem} contains the fraction governed by SDO produced in the MW discharge. Below, this fraction is supposed to be negligible.

Note, that the intensity of iodine luminescence Φ_{chem} is proportional to the concentration of excited iodine atoms i.e. $\Phi_{chem} = \beta I^*$, where coefficient β is governed by detecting system. Taking into account that the total concentration of iodine atoms I_{total} is determined by given flow of RI : He mixture one has

$$\frac{\Phi_{chem}}{I_{total} - \Phi_{chem}} = K_{eq} \cdot \frac{Y_{chem}}{1-Y_{chem}} = \alpha_{chem} \qquad \text{(II.2.14)}$$

Under conditions of the experiment described one has Y_{chem} = 0.03; K_{eq} = 2.86 and, it follows that α_{chem} = 0.09.

When the chlorine flow in the chemical SOG is substituted by oxygen, i.e. the singlet oxygen is only generated by MW discharge, we have the new value of iodine luminescence intensity $\Phi_{discharge}$. In this case the equilibrium equation can be written as

$$\frac{\Phi_{discharge}}{I_{total} - \Phi_{discharge}} = K_{eq} \cdot \frac{Y_{discharge}}{1-Y_{discharge}} = \alpha_{discharge} \qquad \text{(II.2.15)}$$

Combining equations (1) and (2) and keeping in mind that I_{total} is the same for both runs, one can write for $\alpha_{discharge}$

$$\alpha_{dischage} = \frac{\frac{\Phi_{dischage}}{\Phi_{chem}}}{\frac{1+\alpha_{chem}}{\alpha_{chem}} - \frac{\Phi_{dischage}}{\Phi_{chem}}} \qquad \text{(II.2.16)}$$

It follows from results of experiment that $\frac{\Phi_{dischage}}{\Phi_{chem}}$ = 0.37. Thus, substituting this value into (II.2.16) one can evaluate $\alpha_{discharge}$ = 0.0315. Thus, following formula (II.2.15) one can evaluate the value of the yield of electrically generated SDO, $Y_{dischage}$ = 0.011 (It means that the fraction of electrically produced SDO in Y_{chem} is 25 %). This value corresponds to the ratio of SDO concentration ($0.55 \cdot 10^{15}$ cm^{-3}) to total oxygen concentration in the inlet of investigation section. The yield of SDO generated in MW discharge is defined as the ratio of SDO concentration to fraction of oxygen flowing from the MW cavity. Thus, one can find that the MW discharge operating with the O_2 : He = 1 : 2 mixture at gas pressure 3.8 Torr produces SDO with a yield of about 6.6 %. As it was mentioned above, the procedure of absolute calibration of probe method is correct if the fraction of electrically produced SDO is negligible. But in our case it is quite notable. Thus the value of 6.6 % cannot be considered as very accurate. But the accuracy can be improved via proper choosing of experimental conditions. This will be done in future experiments.

The flow rate of O_2 : He = 1 : 2 mixture through the MW cavity is determined by the product of mixture partial pressure by pump capacity. The pump capacity at the total pressure of 2.2 Torr (partial pressure of O_2 : He = 1 : 2 mixture is only 0.78 Torr) is about 16 l/s that corresponds to 0.22 mmole/s of oxygen flow rate. Assuming the power produced by the MW generator (100W) is deposited into oxygen completely one can find that the specific input energy is ε = 454 kJ/mole. Note, this value is rather high and it may be far from optimal one. For example, as it was shown in experiments with traveling microwave discharge (TMW) (Kolobyanin, 2005), the optimal specific energy is not higher than 150 kJ/mole. The reduction of MW power down to 30 W does not result in any decrease of intensity of 1.315 μm emission, and, hence, in the SDO yield. The dynamic of SDO concentration decrease along the investigation section remains the same.

The results of parametric study of generation of SDO in the MW discharge demonstrates strong dependence of iodine atoms luminescence on both mixture pressure in the MW cavity and MW power (**Fig.II.2.11**).

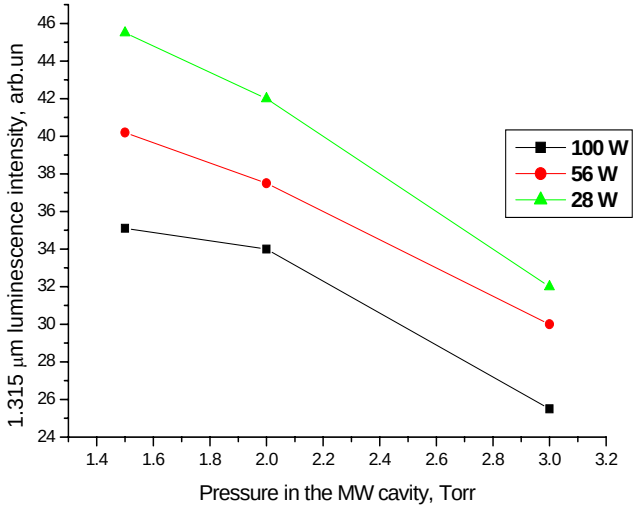

Fig.II.2.11. Influence of operation pressure and MW power on intensity of probe iodine luminescence

Analyzing the results of **Fig.II.2.11** one can approximate that the level of signal intensity at operation pressure 3.8 Torr and MW power of 100 W is as high as ~20 arb. un. The maximal value of signal in **Fig.II.2.11** is 2.2 times higher. As soon as the ratio of I^*/I_{total} is proportional to the ratio $O_2(^1\Delta_g)/O_{2\ total}$ at low SDO yield, one can evaluate the yield of SDO at operation pressure 1.5 Torr and MW power of 28 W as high as 14.5 %. This value obtained in the experiment is in agreement

with result of measuring SDO yield by using the method of intracavity laser spectroscopy (ICLS) (Frolov et al, 2005).

Study of three-body reaction.

To study the influence of three-body reaction

$$O_2(^1\Delta_g) + O + O_2 \leftrightarrow 2O_2 + O, \qquad \text{(II.2.17)}$$

having rate constant of about $1\cdot10^{-32}$ cm^6 s^{-1} (Rakhimova, 2005), the experimental procedure was modified. The variation of iodine luminescence intensity was observed along the investigation section in experiments with different content of components of three-body reaction. Thus, in the first experiment the mixture composition is governed by the flow from the chemical SOG (1.2 Torr of oxygen with SDO), the flow from MW discharge (0.93 Torr of O_2 : He = 1 : 2 mixture), and by small amount (0.12 Torr) of CH_3I : He = 1 :329 mixture. Under these conditions the pressure in the chemical SOG was 2.25 Torr. Operating under such pressure the chemical SOG produces SDO with yield Y_{chem} = 12% that corresponds to SDO concentration $[O_2(^1\Delta_g)] = 4.61\cdot10^{15}$ cm^{-3}. Such concentration corresponds to the yield Y = 9.5% at the inlet of investigation section (total oxygen concentration in the investigation section is $4.83\cdot10^{16}$ cm^{-3}). Iodide CH_3I dissociated by oxygen atoms produces the iodine atoms, which being in equilibrium with oxygen molecules, emit at the wavelength λ =1.315 μm. The luminescence intensity drops with the distance from the mixing point (**Fig.II.2.12**).

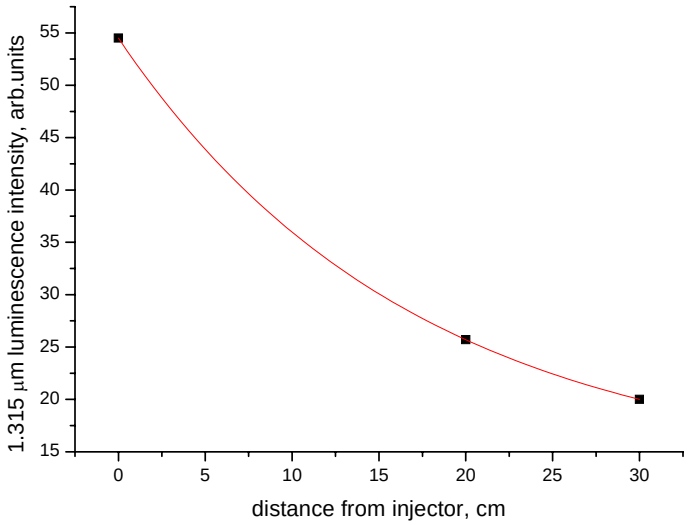

Fig.II.2.12. Variation of iodine luminescence intensity along the investigation section.

Knowing the singlet oxygen yield Y_0 at the inlet of the investigation section and using the equilibrium condition one can obtain the value of the yield Y_L at other observation point

$$Y_L = \frac{\alpha_L}{K_{eq} + \alpha_L}, \text{ where } \alpha_L = \frac{\Phi_L}{\Phi_0\left(\dfrac{1+\dfrac{K_{eq}Y_0}{1-Y_0}}{\dfrac{K_{eq}Y_0}{1-Y_0}}\right) - \Phi_L}, \qquad \text{(II.2.18)}$$

where Φ_0, Φ_L are the luminescence intensities at the inlet of investigation section and at the distance L respectively. Being applied, this procedure gives for the SDO concentration and yield:

Y_0 = 9.5% ($[O_2(^1\Delta_g)]$ = $4.61\cdot10^{15}$ cm^{-3}); Y_{20} = 4.3% ($[O_2(^1\Delta_g)]$ = $2.09\cdot10^{15}$ cm^{-3}) and Y_{30} = 3.1% ($[O_2(^1\Delta_g)]$ = $1.5\cdot10^{15}$ cm^{-3}). Subscripts denote the distance from the inlet to observation point.

To study the influence of reaction (II.2.17) on SDO relaxation, the mixture proportions were varied due to substitution of part of chlorine by unexcited oxygen. In this case the mixture composition in the investigation section was as follows: the flow from chemical SOG (0.9 Torr of unexcited O_2 and 0.39 Torr of O_2 produced in the chemical reaction of Cl_2 with BHP), the flow from MW source (0.78 Torr of O_2 : He = 1 : 2 mixture), and the flow from iodide injector (0.15 Torr of CH_3I : He = 1 : 329). As it was shown in the previous section, the SDO yield in the point near injection, i.e. L=0, was Y_0 = 3.0%. Processing the obtained results in a manner described above one can get the values of SDO yield and concentration for different positions in the investigation section. Thus, one can get: Y_0 = 3.0 % ($[O_2(^1\Delta_g)]$ = $1.5\cdot10^{15}$ cm^{-3}); Y_{10} = 1.9 % ($[O_2(^1\Delta_g)]$ = $0.95\cdot10^{15}$ cm^{-3}); Y_{20} = 1.4 % ($[O_2(^1\Delta_g)]$ = $0.7\cdot10^{15}$ cm^{-3}); Y_{30} = 1.0 % ($[O_2(^1\Delta_g)]$ = $0.5\cdot10^{15}$ cm^{-3}). Plotting the dependences of singlet oxygen concentration on the distance one has **Fig.II.2.13** and **Fig.II.2.14** obtained for different concentrations of unexcited oxygen (The value of concentration is indicated in the picture). Note, the concentration of atomic oxygen in both experiments remains constant, because the conditions in MW cavity are the same. In spite of not too significant variation in the concentration of unexcited oxygen one can note that both dependences can be approximated by first order exponential decay $y = y_0 + A*\exp(-x/t_1)$. The fitting parameters are also indicated in the figures. Variation of SDO concentration due to reaction (II.2.17) can be written as $[O_2(^1\Delta_g)] = [O_2(^1\Delta_g)]_0*\exp(-x/\tau)$, where $\tau = 1/K_4[O][O_2]$. One can see that the increased concentration of unexcited oxygen results in the reduced value of τ. Comparing fitting parameters for conditions of **Fig.II.2.13** and **Fig.II.2.14** one can find that they are in a qualitative agreement with the proposal on relaxation of singlet oxygen in reaction (II.2.17).

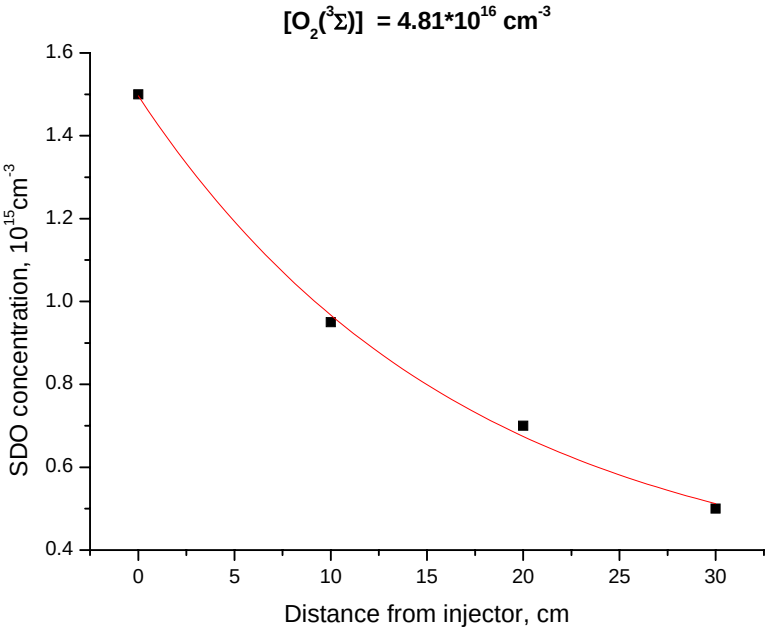

Fig.II.2.13. Dependence of SDO concentration on distance from injector of RI for $[O_2(^3\Sigma)]$ = $4.8\cdot10^{16}$ cm^{-3}

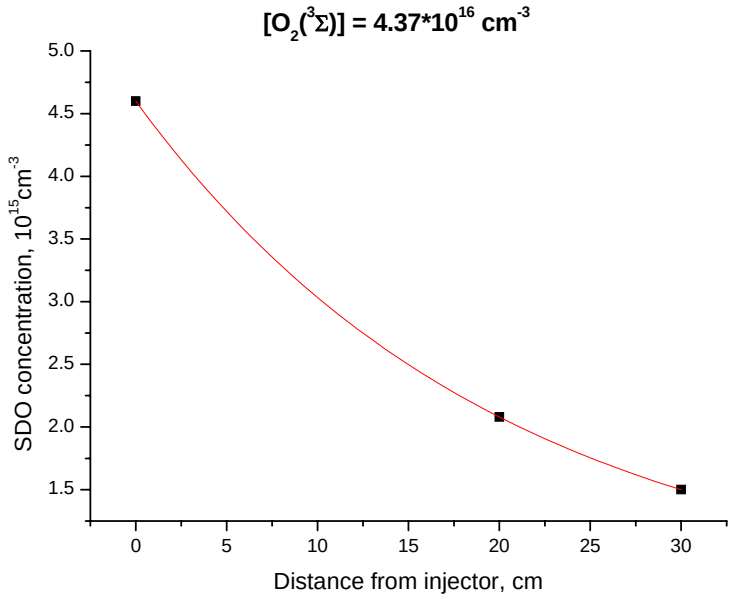

Fig.II.2.14. Dependence of SDO concentration vs distance from injector of RI for $[O_2(^3\Sigma)] = 4.37 \cdot 10^{16}$ cm^{-3}

The experiment is held at pumping capacity 16 l/s. It corresponds to 50 m/s of gas flow velocity in the investigation section (section diameter is 20 mm). Substituting the experimental data into exponential equation one can evaluate the value of characteristic time τ of singlet oxygen concentration drop. For experimental conditions of **Fig.II.2.13** and **Fig.II.2.14** one has $\tau = 5 \cdot 10^{-3}$ s and $\tau = 4.7 \cdot 10^{-3}$ s, respectively. As it is shown below, the oxygen atoms concentration for 4 Torr of total pressure of mixture O_2 : He = 1 : 2 in the MW cavity is about $8.5 \cdot 10^{14}$ cm^{-3} at maximal MW generator output power. Thus, assuming the SDO concentration drop is a result of three-body reaction (II.2.17) only one can find the value of rate constant K_4 of this reaction. For experimental conditions of **Fig.II.2.13** and **Fig.II.2.14** one has $K_4 = 5.1 \cdot 10^{-30}$ cm^6 s^{-1} and $= 5.8 \cdot 10^{-30}$ cm^6 s^{-1}. The obtained value of K_4 differs significantly from that of $(2 \pm 1) \cdot 10^{-32}$ cm^6 s^{-1} reported in (Rakhimova, 2005). The well-known processes inherent to COIL kinetics cannot explain such a fast quenching of SDO. One can suppose that the role of investigation section wall can be more essential in our case because of film deposited on the surface as a result of iodide application. It may be, because iodine atoms produced from iodide are deposited on the wall and, thus, iodine atoms concentration decreases along the investigation section resulting in the responsible decrease of the iodide luminescence. If so, the method of iodide probe to get information on singlet oxygen is not free of demerits. In general, one can conclude the more detail experiments are necessary to explain observed SDO behavior. At the same time, it seems that the comparative study of SDO generation via observation of probe luminescence at the point close to injector is valid.

Measurement of oxygen atom concentration

It is known that SDO is a very stable molecule and it has low efficiency of quenching in collisions with molecules of inherent to COIL. Therefore, chemically produced SDO can be easily transported to the place of utilization. Another situation takes place in the case of electrically produced SDO. It can be supposed that the species produced in the process of SDO generation in plasma are the effective SDO quenchers. One of species generated in the oxygen plasma is atomic oxygen. To measure the concentration of atomic oxygen produced in electric discharge one can use the method of titration with nitrogen dioxide NO_2 (Kaufman, 1961). Being added to the mixture containing oxygen atoms, NO_2 scavenges them in reaction NO2 + O = NO + O_2.

At this time the white emission due to recombination NO + O = NO_2 + hν increases and then drops and disappears when amount of NO_2 is equal to O atoms concentration. This method was used to study the dependence of oxygen dissociation on experimental conditions to select a most acceptable mode. **Fig.II.2.15** demonstrates dependence of concentration in investigation section of oxygen atoms generated in the MW cavity on pressure of O_2 : He = 1 : 2 mixture for different levels of MW power. As one could expect, the oxygen atoms concentration [O] increases with MW power. But increase of [O] with pressure does not seem obvious. The dissociation efficiency, i.e. the ratio of oxygen atoms concentration to that of molecular oxygen, within the variation of experimental parameters increases too. One should pay attention that the dissociation efficiency is more sensitive to MW power at increased pressure of oxygen mixture (**Fig.II.2.16**)

The similar dependences have place for pure oxygen but in this case the dissociation efficiency is about a half of that for oxygen – helium mixture.

It is well known the atomic oxygen reacts with molecular iodine producing iodine atoms in the chain of reactions $O + I_2 = IO + I$ and $IO + O = I + O_2$.

This mechanism is used as an iodine atoms source in the electrically driven oxygen iodine laser. Similar reactions take place for CH_3I (Gilles, 1996): $CH_3I + O = IO + CH_3$ and $IO + O = I + O_2$.

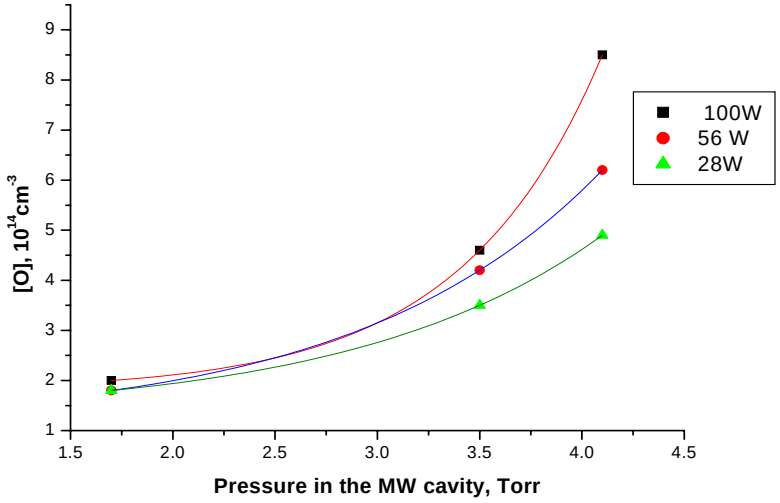

Fig.II.2.15. Dependence of [O] on pressure for mixture O_2 : He = 1 : 2

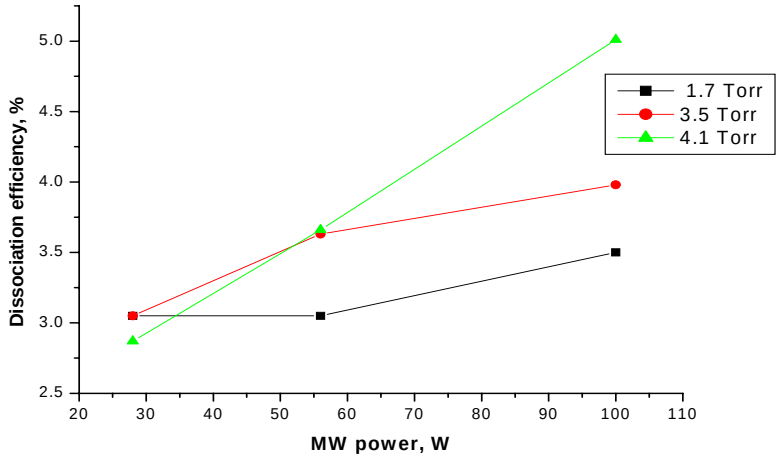

Fig.II.2.16. Dependence of dissociation efficiency on MW power for mixture O_2 : He = 1 : 2

But unlike NO_2 each molecule of CH_3I scavenges two oxygen atoms. One can suppose this reaction can be used to measure oxygen atoms concentration too. To check this idea the mixture CH_3I : He = 1 : 329 is admixed to the effluent of MW generator up to concentration resulting in elimination of white emission. Emission disappeared when 0.5 Torr of CH_3I : He = 1 : 329 was admixed to the 1 Torr of effluent of MW generator operating at the output power 100W. The total pressure in the investigation section was 1.5 Torr. Processing one can get: [O] ~ $1 \cdot 10^{14}$ cm^{-3}. Note, NO_2 titration under the same MW power and under total pressure of 2.4 Torr gives the value [O] = $1.5 \cdot 10^{14}$ cm^{-3}. Keeping in mind that [O] increases with pressure, one can see the satisfactory agreement.

One could expect that other iodides CF_3I and HI can be used for this purpose too. But application of CF_3I results in a value of approximately twice as much under the same experimental condition. As to HI, its amount necessary to suppress white emission is greater by seven fold as compared with CH_3I. Another distinction of HI from CF_3I and CH_3I is a sharp decrease of iodine luminescence. All these facts are the evidence of more intricate chemical kinetics. More detailed experiments are necessary to study it.

It is known that oxides of some metals (for example, HgO, AgO etc.) have rather high surface probability for oxygen atoms scavenging. Therefore the coating of transport tube inside wall with HgO is often used to eliminate oxygen atoms from gas flow. In our case the fused silica tube of 10 mm i.d. with HgO coating is placed just downstream of MW generator. HgO coating was performed by passing the effluent of RF discharge in oxygen through this tube. Before RF discharge oxygen passed over Hg metal drop and, thus, took Hg vapor. After coating process the tube got brown color. It is of interest, how effective the HgO coating as O atoms scavenger is. The experiments on measuring O atoms concentration by using NO_2 in a procedure described above show that is our case this efficiency is rather low.

Table II.2.5 presents results of O atoms concentration measuring in investigation section made for different operation pressure and MW power for both HgO coating (**Table II.2.5a**) and without it (**Table II.2.5b**). One can see small difference confirming influence of HgO coating but no significant reduction in O atoms concentration was obtained.

Table II.2.5a.

HgO coating	$P_{O2:He}$, Torr	P_{total}, Torr	$P_{NO2:He}$, Torr	[O], cm^{-3}	Diss., %	MW power, W	P_{cavity}, Torr
	1.08	2.1	1.02	4.59E+14	3.98E-02	100	3.5
	1.08	2.01	0.93	4.19E+14	3.63E-02	56	3.5
	1.08	1.86	0.78	3.51E+14	3.05E-02	28	3.5
	0.54	0.99	0.45	2.03E+14	3.52E-02	100	1.7
	0.54	0.93	0.39	1.76E+14	3.05E-02	56	1.7
	0.54	0.93	0.39	1.76E+14	3.05E-02	28	1.7
	1.59	3.48	1.89	8.51E+14	5.01E-02	100	4.1
	1.59	2.97	1.38	6.21E+14	3.66E-02	56	4.1
	1.59	2.67	1.08	4.86E+14	2.87E-02	28	4.1

TableII.2.5b.

No HgO coating	$P_{O2:He}$, Torr	P_{total}, Torr	$P_{NO2:He}$, Torr	[O], cm^{-3}	Diss., %	MW power, W	P_{cavity}, Torr
	0.63	1.2	0.57	2.57E+14	3.82E-02	100	1,77
	0.63	1.23	0.6	2.70E+14	4.02E-02	56	1.77
	0.63	1.21	0.585	2.63E+14	3.92E-02	28	1.77
	1.59	3.51	1.92	8.64E+14	5.09E-02	100	4.1
	1.59	3.09	1.5	6.75E+14	3.98E-02	56	4.1
	1.59	2.64	1.05	4.73E+14	2.79E-02	28	4.1
	1.05	2.13	1.08	4.86E+14	4.34E-02	100	2.9
	1.05	2.07	1.02	4.59E+14	4.10E-02	56	2.9
	1.05	1.98	0.93	4.19E+14	3.74E-02	28	2.9

Conclusions

He-Ne laser (λ = 633 nm) was used for absolute calibration of a system monitoring the dimole radiation (λ = 634 nm) of SDO. The presence of this radiation in a luminescence of effluents of SDO generator is an evidence of a high concentration of SDO in a flow. The chemical SDO generator was used as a source of oxygen flow with well known SDO yield.

The processing of experimental results showed the absolute sensitivity of detecting system is 32 photons/unity of CCD signal. Application of the value of sensitivity to experiments with chemical SDO generator made it possible to evaluate the rate constant for the process responsible for dimole emission. The value obtained $k_d=7.85\cdot10^{-23}$ cm^3/s is in agreement with literature (Bowell, 1983) with the accuracy of 50%.

Another approach, i.e. application of a chemical SDO generator as a reference source for absolute calibration of dimole (λ=634 nm) and $b\rightarrow X$ (λ=762 nm) radiation detectors, was applied for detector calibration too.

The spectra of luminescence of oxygen excited by axial self sustained electric discharge were obtained for different values of electrical energy stored in capacity bank and different oxygen pressure. The values of b-state concentration were evaluated via comparison with spectrum of chemically produced SDO on the assumption that duration of discharge afterglow is as long as 10 ms. The results obtained is $(3.26 \pm 0.29)\ 10^{13}$ cm^{-3}, which error is 8.6%.

The intracavity laser spectroscopy (ICLS) was used as SDO concentration measuring method. This method has a very high sensitivity and makes it possible to monitor the absorption corresponding to the $O_2(^1\Delta)\rightarrow O_2(^1\Sigma)$ (λ = 1.91 μm) transition. The series of experiments were performed to measure the cross-section of lines of the *Q* – branch of the vibrational 0-0 band of the $a^1\Delta_g \rightarrow b^1\Sigma_g^+$ transition of molecular oxygen. The absorption spectra of effluent of chemical SDO generator producing the SDO with known yield were recorded with ICSL method.

The experimentally obtained spectra are in agreement with the accuracy of about 25 % with that of modeling. The method developed was applied to measure the concentration of SDO produced in the microwave discharge. The SDO pressures values of 0.07 and 0.11 Torr were detected.

The method of titration with iodide was developed and used for parametric study of SDO generator based on the MW discharge. This method seems to be very attractive because of its very high sensitivity. It makes it possible to detect the presence of SDO molecules not using very

sensitive and, hence, not always available instrument. The results obtained are in a good agreement with that obtained by using intracavity laser spectroscopy.

The method of titration with nitrogen dioxide was successfully used to investigate the generation of oxygen atoms in oxygen plasma.

References for Part II.2.

Baev V.M., Latz T., Toschek P.E. (1999). *Appl.Phys.B.*, **B 69**, 171.

Bowell P., Rich N.H. (1983). *Chem. Phys. Lett*, **99**, 99.

Carroll D., et al. (2005a). *IEEE Journal of Quantum Electronics*, **41**, 213.

Carroll D. L., et al. (2005b). *IEEE Journal of Quantum Electronics*, **41**, 1309.

Carroll D.L., et al. (2005c). *Appl. Phys. Letters*, **86**, 111104-1.

Fink E.H,.Kruse H, Ramsay D.A.,.Vervloet M. (1986). *Can. J. Phys.*, **64**, 242.

Frolov M.P., et al. (2005). *Proc.SPIE*, **5777,** 70.

Gilles M.K., et al. (1996). *J Phys. Chem*. **100**, 14005.

Kaufman F. (1961). *Prog. React. Kinet*. **1**, 1.

Kolobyanin Yu.V., et al. (2005). *AIAA Paper 2005-4920***,** 36th AIAA Plasmadynamics and Laser Conference, 6-9 June 2005, Toronto, Canada.

Krupenie P.H. (1972). *J. Phys. Chem. Ref. Data*, **1**, 423.

McDermott W.E,.Pchelkin N.R. (1978). *Rev.Sci.Instrum.*, **49**, 794.

Miller H.C., McCord J.E., Choy J., Hager G.D. (2001). *JQSRT.*, **69**, 305.

Noxon J.F. (1961). *Can. J. Phys.*, **39**, 1110.

Pakhomycheva L.A., Sviridenkov E.A, Suchkov A.F., Titova L.V., Churilov S.S. (1970). *JETP Lett.*, **12**, 43.

Pazyuk V.S, Podmar'kov Yu.P., Raspopov N.A., Frolov M.P. (2001). *Quantum Electronics.* **31**, 363.

Rakhimova T.V., et al. (2005). *AIAA Paper 2005-4918***,** 36th AIAA Plasmadynamics and Laser Conference, 6-9 June 2005, Toronto, Canada.

Rothman L.S., Rinsland C.P., et al. (1998). "The HITRAN molecular spectroscopic database and HAWKS (HITRAN Atmospheric Workststion): 1996 Edition", *J. Quant .Spectrosc. Radiat. Transfer* **60**, 665.

Solomon W. (2002). ElectriCOIL meeting, University of Illinois Urbana Champain, 25 October 2002

Vagin N.P., Pazyuk V.S., and Yuryshev N.N. (1995). *Quantum Eelectronics*. **25**, 746.

Part II.3. NON-SELF-SUSTAINED DISCHARGE: SINGLET DELTA OXYGEN PRODUCTION

(Subtasks 1B.1, 1B.2, 1B.4, 2B.1, 2B.2, 2B.3, 2B.4, 3.1, 3.2, 3,3 and 3.4)

Introduction

Great success has been obtained in the research and development of a chemical oxygen-iodine laser (COIL) (McDermott, 1978; Lambertson, 2001; Hallada, 2000). The active medium of a COIL is atomic iodine emitting photons when changing its electronic state: $I^*(^2P_{1/2}) \rightarrow I(^2P_{3/2}) + h\nu$. Atomic iodine in the excited state $I^*(^2P_{1/2})$ is produced by energy transfer from the singlet delta oxygen (SDO) $O_2(a^1\Delta_g)$ molecule:

$$O_2(a^1\Delta_g) + I(^2P_{3/2}) \rightarrow O_2(^3\Sigma) + I^*(^2P_{1/2}).$$

But application of the COIL is limited because the SDO is produced in a chemical generator using toxic and dangerous chemicals. One of the alternative procedure for SDO production is SDO generation in an electric discharge. The procedure has been known since the 50's (see, for instance, review (Wayne, 1969)) and was applied in (Zalessky, 1974) (with a negative result) for the development of an electric discharge oxygen-iodine laser (OIL) long before the development of COIL. One of the possible reasons for the negative result is the fact that for achieving a positive gain in any OIL the SDO yield,

$$Y = [O_2(a^1\Delta_g)] / ([O_2(a^1\Delta_g)] + [O_2(^3\Sigma)]),$$

where $[O_2(a^1\Delta_g)]$ and $[O_2(^3\Sigma)]$ are concentrations of SDO and oxygen in a ground state, has to exceed its threshold value Y_{th}=15% at T=300 K (Yuryshev, 1996). A 21% yield under a MW discharge and 32% yield under an RF discharge excitation were quite recently demonstrated (Itami, 1999; Fujii, 2000; Schmiedberger, 2000). Moreover, iodine threshold lasing was claimed in (Schmiedberger, 2000) to be observed when mixing SDO with iodine, which looked more probably like iodine luminescence, because there was no notable spectral line narrowing. In March 2005 the first DOIL was launched in the USA with output power of ~0.2 W, output efficiency < 0.1% and extremely low small-signal gain less than 10^{-4} cm^{-1}, low-pressure RF discharge with subsequent supersonic expansion being applied (Carroll, 2005c). Despite the obvious success, the development of high-power DOIL with such characteristics of active medium is under question. Therefore, the search of efficient electric discharge SDO generators based on different sorts of electric discharges and adequate for DOIL development is needed.

The efficiency of excitation of oxygen from the ground state into the singlet state $O_2(a^1\Delta_g)$ versus a reduced electric field strength *E/N* was demonstrated in (Hill, 2001; King, 2001; Napartovich, 2001) to have a maximum at *E/N*~10 Townsend = 10^{-16} V cm^2. Only non-self-sustained discharge can exist at such an electric field that is too low for self-sustained discharge maintenance. An SDO yield of~16% was reported in (Hill, 2001), where the non-self-sustained discharge using ionization by high-voltage pulses was applied for the excitation of oxygen. The non-self-sustained combined discharge in which RF discharge was applied to low-temperature plasma formed by an AC discharge was studied in (King, 2001). It was pointed out in (Napartovich, 2001; Ionin, 2001a; Ionin, 2001b; Ionin, 2002) that the electron-beam-sustained discharge (EBSD) characterized by *E/N*~10 Townsend can be used as a non-self-sustained discharge for SDO production. The EBSD at such an electric field was successfully applied for the excitation of molecular CO_2-, CO,- and N_2O-lasers (see (Basov, 1990), for instance).

The EBSD in pure oxygen was experimentally studied in (Londer, 1981). The specific input energy (SIE) did not exceed ~90 J l^{-1} atm^{-1} at the pump volume of ~60 cm^3. It was suggested in (Fournier, 1980) to apply the high-pressure (1.2 atm) EBSD for the SDO production and the development of an electric discharge OIL. However, the SIE per partial oxygen pressure was not higher than ~150 J l^{-1} $atm[O_2]^{-1}$ for the gas mixture O_2:Ne=4:96 at the pump volume of ~150 cm^3. It

should be noted that the SIE which is formally needed for the excitation of all the molecular oxygen from the ground state $[O_2(^3\Sigma)]$ into the SDO state (excitation energy 0.98 eV) is 94 kJ mole$[O_2]^{-1}$ or 4.2 kJ l^{-1} atm$[O_2]^{-1}$. It means, that for the experimental conditions of (Londer, 1981; Fournier., 1980) only 2-3% of oxygen molecules comes into the $a^1\Delta_g$ state at best (~100%) pump efficiency.

Therefore, up to now, it was not possible to achieve in the EBSD an SIE into oxygen giving any opportunity to obtain a high SDO yield. The possibility of obtaining a high SIE higher than that previously observed in oxygen mixtures at gas pressure 10-100 Torr and pump volume adequate to a modern high-power OIL technology is demonstrated in this Report. The study of SDO production in gas with CO admixture excited by EBSD was carried out. Photodetectors for measurement of SDO concentration were calibrated by using chemical SDO generator. Absolute values of SDO concentration and yield producing in EBSD were measured by the photodetectors. The experimental results on measuring SDO concentration and yield in the EBSD afterglow were obtained and compared with theoretical calculations. Another non-self-sustained discharge system with external ionization by repeating high-voltage pulses was developed. To detect SDO produced in the non-self sustained slab discharge initiated by high voltage pulses, the Co:MgF_2 laser based intracavity laser spectroscopy was used.

Study of EBSD in oxygen containing mixtures.
(*Subtasks 1B.1; 1B.2*)

Pulsed EBSD facility was used for the study of electric discharge in oxygen gas mixtures. The electric conductivity of gas in a non-selfsustained EBSD is created by an external source of ionization. In the experiments a pulsed electron beam with electron energy of ~150 keV, current density up to ~10 mA cm^{-2} at pulse length of ~100 μs was applied to the gas for its ionization. Volumetric gas discharge was ignited in EBSD chamber with active volume $V_0=Sd\approx18$ l, where S is the area of the anode with the length of 1.2 m and d=93±1 mm is the gap between the electrodes.

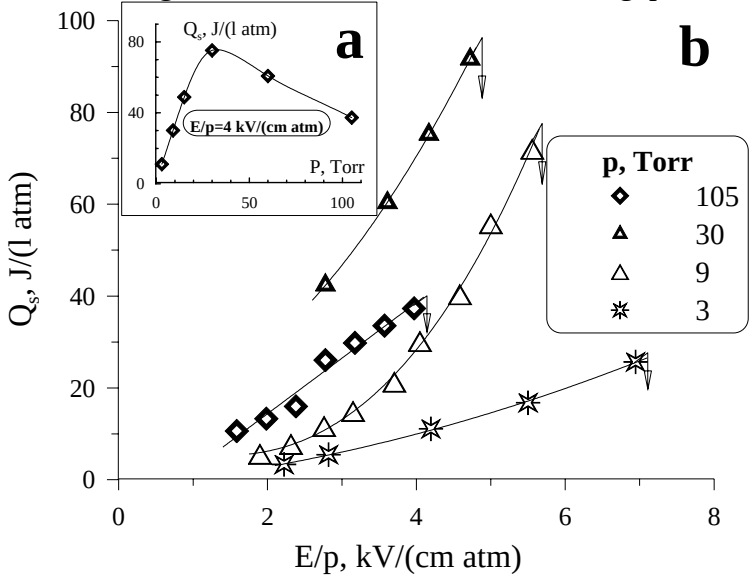

Fig. II.3.1. Energetic characteristics of the EBSD in pure oxygen. **a** - dependence of the SIE Q_s on gas pressure at the same parameter E/p=4 kV cm^{-1} atm^{-1}, **b** - dependence of the SIE Q_s on the initial reduced electric field strength E/p at different gas pressure.

High voltage was applied to the anode from the capacity bank with the total capacitance of $C_t\approx370$ μF. The energy Q_t loaded into the EBSD was determined by measuring the initial voltage U_0

and final voltage U_1 between the discharge electrodes: $Q_t = C_t (U_0^2 - U_1^2)/2$. A low resistance (~1.7 mΩ) shunt was used for measuring the time behavior of EBSD current pulse. The time behavior of the current pulse was detected by oscilloscope.

The features of pulsed EBSD in oxygen gas mixtures were studied in the experiments. Energetic characteristics of the EBSD in pure oxygen are presented in **Fig.II.3.1**. **Fig.II.3.1b** demonstrates the dependence of the SIE $Q_s = Q_t (V_0\, p)^{-1}$ on the initial reduced electric field strength $E/p = U_0 (d\, p)^{-1}$ at different gas pressure from 3 up to 105 Torr. The maximum value of the SIE for pure oxygen does not exceed 100 J l^{-1} atm^{-1} and is limited by an electric breakdown of the electric discharge gap (vertical arrows on the **Fig.II.3.1** and other figures). The dependence of the SIE Q_s on gas pressure at the same parameter E/p=4 kV cm^{-1} atm^{-1} (E/N≈15 Townsend) is in **Fig.II.3.1a**. This dependence has a maximum at gas pressure ~30 Torr. For comparing maximum values of specific input energy measured for different oxygen mixtures, most of the experiments were carried out at the same gas pressure p=30 Torr.

Dissolution of oxygen by heavy argon gives the opportunity to enhance a conductivity of the EBSD at the same value of E/p parameter and, respectively, to increase a SIE, the main fraction of which goes into the excitation of internal degrees of freedom of molecular component.

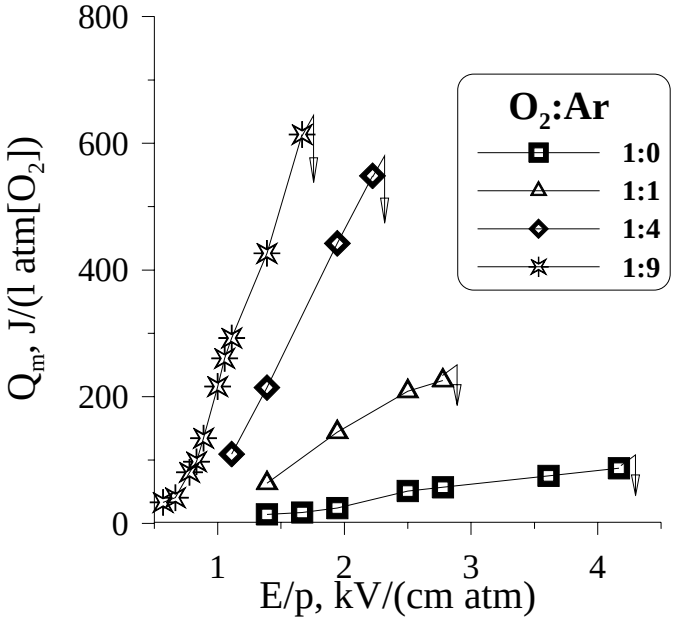

Fig.II.3.2. Dependences of the SIE Q_m per oxygen partial pressure p_m on E/p parameter at different gas ratio of O_2:Ar.

One can see in **Fig.II.3.2** the dependences of the SIE $Q_m = Q_s (p / p_m)$ per molecular component partial pressure p_m (in the given case the molecular component is oxygen) on E/p parameter. When increasing argon concentration in gas mixture O_2:Ar, the maximum value of the SIE increases from ~80 up to ~600 J l^{-1} atm$[O_2]^{-1}$ (gas mixture O_2:Ar=1:9). At the same time, the maximum reduced electric field strength $(E/p)_{max}$, at higher values of which electric breakdown of the EBSD gap takes place, decreases from ~4.3 kV cm^{-1} atm^{-1} (for gas mixture O_2:Ar=1:0) down to ~1.5 kV cm^{-1} atm^{-1} (O_2:Ar=1:9) because of electric discharge instability in argon containing gas mixture. Time behavior of EBSD current pulse in argon containing gas mixture is presented in **Fig.II.3.3**. The instability of electric discharge is clearly seen as some oscillations during the pulse. The physical mechanism of the instability, which results in such EBSD current pulse oscillations in gas mixtures of oxygen with argon, was discussed in (Aleksandrov, 1992). This mechanism is due to the fact that an electron drift velocity for such mixtures can decrease with the electric field rise within some range. One can see a flat part of the curve corresponding to the E/N parameter between

~2.5 and 6 Townsend (0.25-0.6 10^{-16} V cm^2) in **Fig.II.3.4**, which presents the calculated dependence of the electron drift velocity V_e on the *E/N* parameter for the gas mixture O_2:Ar=1:1 (curve 1). In attaching gas, such a dependence of V_e on *E/N* can result in formation of moving layers in plasma and current oscillations. But, if a small amount (~5%) of carbon monoxide CO is added to such a mixture, the electron drift velocity transforms into the monotonically rising function of the electric field strength (curve 2).

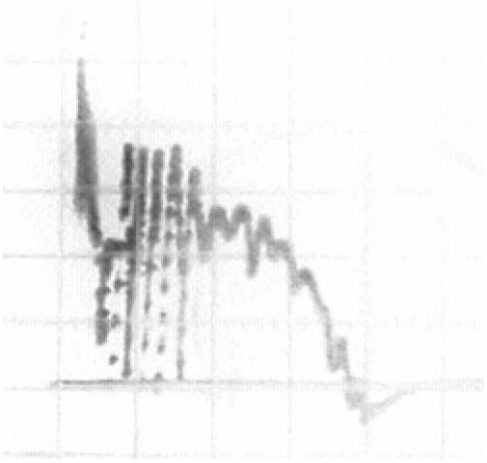

Fig. II.3.3. Time behavior of EBSD current pulse in argon containing gas mixture

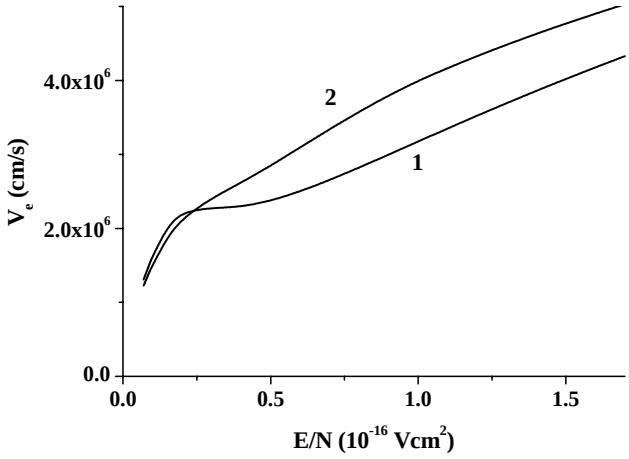

Fig. II.3.4. The electron drift velocity V_e versus the *E/N* parameter for the gas mixtures:
O_2:Ar = 1:1 (1) and
O_2:Ar: CO = 1:1:0.1 (2).

In the experiment, the addition of CO (or H_2) into the gas mixture O_2:Ar resulted in the strong decrease of EBSD current oscillations (**Fig**.**II.3.5**). Moreover, the addition of CO or H_2 into the gas mixture CO:Ar enabled us to enhance the maximum electric field strength $(E/p)_{max}$ in the EBSD and, accordingly, to significantly increase the value of the SIE Q_m per molecular component (**Figs**. **II.3.6** and **II.3.7**). It should be pointed out that the same effect was observed in (Ionin, 1988, 1991; Zhivukhin, 1989), where an addition of CO to nitrous oxide N_2O resulted in considerable enhancement of the SIE in the EBSD and the development of an efficient N_2O laser. In both cases, the major function of carbon monoxide is the decrease of the negative ions O^- amount in a discharge due to the reaction

$$O^- + CO \rightarrow CO_2 + e,$$

which results in the enhancement of a concentration of free electrons, an EBSD current, and an SIE. The same reaction takes place as hydrogen or deuterium is added into an oxygen mixture:

$$O^- + H_2 \,(\text{or } D_2) \rightarrow H_2O(\text{or } D_2O) + e.$$

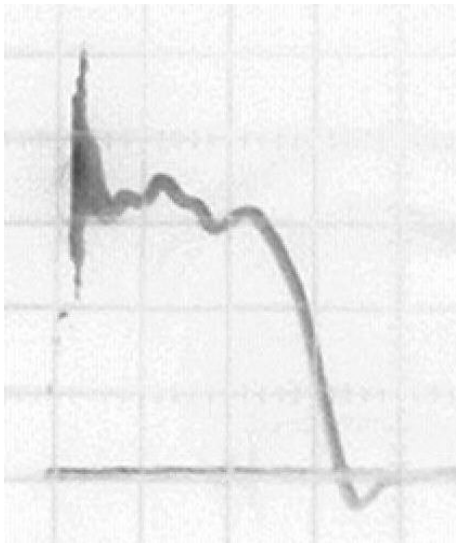

Fig. II.3.5. The pulsed EBSD current time behavior for the gas mixture O_2:Ar:CO = 1:1:0.1. Time scale is 20 μs/div.

The influence of carbon monoxide on EBSD characteristics was studied at its addition to pure oxygen. **Fig**. **II.3.6** presents the dependence of the SIE Q_m on the electric field strength E/p for pure oxygen and the gas mixture O_2:CO=1:0.1. The addition of 10% carbon monoxide results in almost a threefold enhancement of the maximum electric field strength $(E/p)_{max}$ up to ~12 kV cm^{-1} atm^{-1}, the maximum SIE Q_m coming up to ~2200 J l^{-1} atm^{--1}.

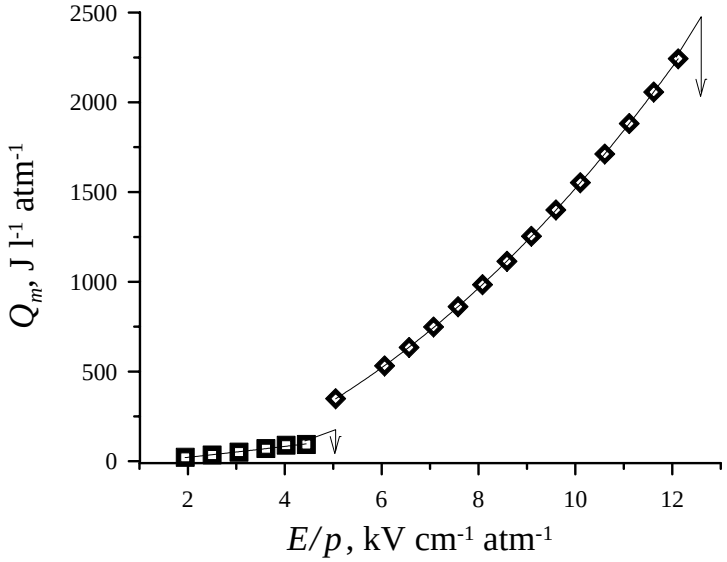

Fig. II.3.6. The dependence of the specific input energy Q_m on the E/p parameter for pure oxygen (□) and the gas mixture O_2:CO = 1:0.1 (◇) at the gas pressure 30 Torr.

The addition of 5% carbon monoxide to the gas mixture O_2:Ar=1:1 at the same total pressure of the mixture 30 Torr results in the $(E/p)_{max}$ parameter rising up to ~10 kV cm^{-1} atm^{-1} (**Fig**. **II.3.7**) for the gas mixture O_2:Ar:CO=1:1:0.1 and the SIE Q_m per molecular components of the mixture (O_2 and CO) coming up to ~6500 J l^{-1} atm^{-1} or ~150 kJ mole^{-1} in other units. When using helium instead of argon (O_2:He:CO=1:1:0.1) or 2.5% hydrogen instead of ~5% CO (O_2:Ar:H_2=1:1:0.05), the $(E/p)_{max}$ parameter for these mixtures appears to be less than that for the gas mixture O_2:Ar:CO=1:1:0.1. Nevertheless, the maximum value of Q_m comes up to ~2000 J l^{-1} atm^{-1}. A high conductivity of the gas mixture resulted in the fact that the voltage remaining on the capacity bank after the EBSD pulse was far less than its initial value $U_1 << U_0$. Therefore, the dependencies in **Figs.II.3.6** and **II.3.7** for the gas mixture O_2:CO=1:0.1 have the form of the square function $Q_m \sim (E/p)^2$, the value of the reduced electric field strength $\langle E/p \rangle$ averaged over the EBSD pulse duration being $\langle E/p \rangle \approx 0.5 E/p$.

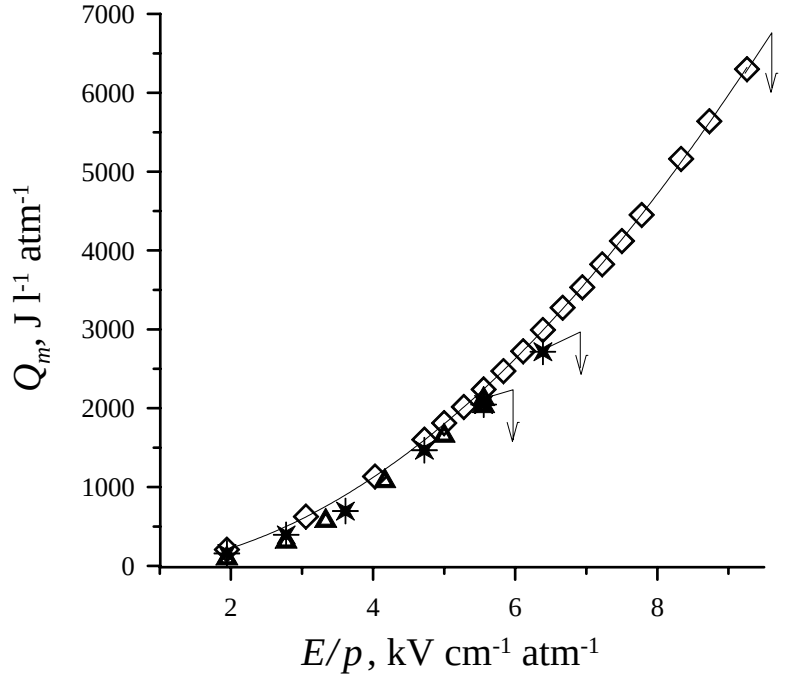

Fig. II.3.7. The specific input energy Q_m per molecular component O_2 and CO (or H_2) partial pressure as a function of the E/p parameter for the gas mixtures O_2:Ar:CO = 1:1:0.1 (◆); O_2:He:CO = 1:1:0.1 (△) and O_2:Ar:H_2 = 1:1:0.05 (✶) at the gas pressure 30 Torr.

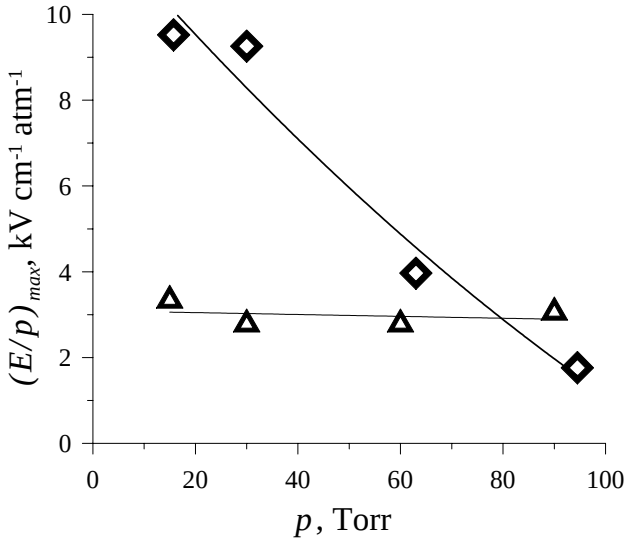

Fig. II.3.8. The maximum $(E/p)_{max}$ parameter versus a total gas pressure for two gas mixtures O_2:Ar = 1:1 (△) and O_2:Ar:CO = 1:1:0.1 (◆).

The increase of argon concentration in the gas mixture O_2:Ar:CO=1:1:0.1; 1:4:0.1 and 1:10:0.1 at the same ratio of the molecular components (O_2 and CO) results in a considerable (more than five times) decrease in the $(E/p)_{max}$ parameter. The dependence of the maximum $(E/p)_{max}$ parameter on the gas pressure for two gas mixtures O_2:Ar=1:1 and O_2:Ar:CO=1:1:0.1 is presented in **Fig. II.3.8**. For the two-component gas mixture O_2:Ar, the value of $(E/p)_{max}$ changes just a little around ~3 kV cm^{-1} atm^{-1} with a gas pressure. For the three-component mixture O_2:Ar:CO, the value $(E/p)_{max}$ drops nearly linearly with a gas pressure increase. At the gas pressure 15 Torr, the addition of carbon monoxide to the gas mixture O_2:Ar results in a rise in the $(E/p)_{max}$ parameter nearly three times up to ~9.5 kV cm^{-1} atm^{-1}. But at the gas pressure ~90 Torr, the carbon monoxide addition results even in $(E/p)_{max}$ drop comparing to the mixture O_2:Ar=1:1. Therefore, the gas mixture O_2:Ar:CO=1:1:0.1 at the total pressure 15-30 Torr ought to be used for achievement maximum values of SIE.

Theoretical estimation of the SDO yield in EBSD

(*Subtask 1B.1*)

To simulate processes discussed above, a kinetic model was employed. A system of dynamic equations was solved in time for a number of species including electrons, positive and negative ions, and chemical components: O_2; O; O_3; $O_2(v)$; $O_2(0.98)$; $O_2(1.63)$; $O_2(4.5)$; $O(^3P)$; $O(^1D)$; O^+; O_2^+; O_4^+; O^-; O_2^-; O_3^-. Figures in brackets denote energy of a correspondent molecular/atomic state in *eV*, $O_2(v)$ denotes vibrationally excited molecules. Rate coefficients for the processes with electrons involved were calculated by solving the steady state electron Boltzmann equation in two-term approximation. Expecting a noticeable SDO concentration, the following processes, in which molecules $O_2(^1\Delta_g)$ are involved, were included. These are: de-excitation by electrons; electron attachment; electron-impact induced transitions to higher electronic levels and into dissociation and ionization. Taking into account that electronic terms for ground and singlet states have similar shapes, the cross sections for upward transitions from $O_2(^1\Delta_g)$ were found from cross sections for respective transitions from the ground state by shifting the electron energy to 0.98 eV.

This model was extended to describe SDO production in an EBSD in mixtures of O_2 with Ar and molecular gases CO, H_2, and D_2. Namely, the following processes were included additionally: the electron impact excitation of vibrational levels of molecular additives; the electron detachment from O^- in collisions with CO, H_2, and D_2 molecules; the ionization and electronic states excitation of additional components; and the recombination with new appearing ion types. Some of these processes are listed in **Table II.3.1**.

Table II.3.1. Kinetic processes with molecular CO, H_2 и D_2.

	Reaction	K_f, cm^3/s	K_r, (cm^3/s)	Reference
1	$CO + e \leftrightarrow CO(V) + e$, V = 1, 10	calculation[1)]	calculation	Ehrhardt, 1968; Aleksandrov, 1986
2	$H_2 + e \leftrightarrow H_2(V) + e$, V = 1, 2	calculation	calculation	Gal'tsev, 1979
3	$D_2 + e \leftrightarrow D_2(V) + e$, V = 1, 2	calculation	calculation	Buckman & Phelps, 1985
4	$O^- + CO \rightarrow CO_2 + e$	$4.4\cdot10^{-10}$		Mc Ewan & Phillips, 1975
5	$O^- + H_2 \rightarrow H_2O + e$	$6.0\cdot10^{-10}$		Mc Ewan & Phillips, 1975
6	$O^- + D_2 \rightarrow D_2O + e$	$6.0\cdot10^{-10}$		our estimate

[1)] *The constants were calculated from Boltzman equation.*

The results of the numerical simulations demonstrated that the exact value of vibrational temperature of molecular additives plays an important role in kinetics, in particular in case of CO molecules. Ignoring the vibration-vibration (VV) energy exchange results in a strong growth of vibrational temperature with the increasing energy input. Then the second-kind collisions with excited molecules come essentially into the game, and energy flow into molecular vibrations saturates.

Actually, VV-exchange due to an anharmonicity of molecular vibrations leads to the redistribution of energy from lower to higher levels and the restriction of vibrational temperature of lower levels by a value determined from equilibration of VV-exchange and electron-impact excitation rates (Gordiets & Zhdanok, 1989). Therefore, the discharge model was extended to describe vibrational kinetics in an analytical approximation. In this approach, the vibrational temperature of the lower level T_v was calculated following a procedure described, for example, in

(Gordiets & Zhdanok, 1989). The specific vibrational distribution function at lower levels has the form

$$f(v) = f_0 \exp\left[-\frac{vE_1}{T_v} + \frac{\Delta E \cdot v(v-1)}{T}\right],$$

where E_1 is the energy of the first vibrational level, and ΔE is the anharmonism energy. This function describes the actual vibrational distribution function at $v < v^* = \frac{E_1}{2\Delta E}\frac{T}{T_v} + \frac{1}{2}$; v^* is the so-called Treanor number. Distribution ***f(v)*** was made equal to the function $f_V = c\,(V+1)^{-1}$ at the level $v=v^*$. The factor c can be expressed in the form $c = (W/\nu)^{0.5}$, W is the rate of vibrational level excitation, and ν is the effective VV-exchange rate, which was defined in (Dem'yanov., 1984). This analytical approximation accounts for the dependence of vibrational temperature at lower levels on pump power and gas temperature.

This method was employed when considering mixtures with CO or H_2 additives. For D_2 as an additive, VV-exchange is two orders of magnitude slower than for CO and H_2 (Dem'yanov, 1984). It begins to play a role long after the excitation pulse termination. In this situation, VV-exchange can be ignored in modeling.

The cross sections for electron impact excitation of H_2 and D_2 vibrations were taken from papers (Gal'tsev, 1979; Buckman & Phelps, 1985), respectively. The cross-sections for the electron impact vibrational excitation of CO molecules were taken from (Ehrhardt, 1968) and multiplied by a factor of 1.3 following recommendations in the paper (Aleksandrov, 1986).

The excitation of molecular vibrations in additives may result in a falling SDO excitation efficiency. **Figs II.3.9 - II.3.12** show the discharge power fraction, which electrons spend on excitation of SDO molecules, as a function of *E/N* in gas mixtures of O_2:Ar with CO, H_2, and D_2 as additives for the gas temperature 300 K. **Fig**. **II.3.9** shows the results of calculations for the mixture O_2:Ar = 1:1. Curve 1 is an energy fraction in processes of direct electron-impact excitation of SDO, curve 2 is an effective energy fraction spent in discharge on formation of SDO including cascade excitation through the levels $O_2(b^1\Sigma_g$; $A^3\Sigma^+_u$; $C^3\Delta_u$; $B^3\Sigma^-_u)$ and atoms $O(^1D)$. The effective fraction was computed by the formula

$$\eta_{SDO}^{eff} = \eta_{SDO} + \sum_i P_i \frac{\Delta u_{SDO}}{\Delta u_i}\eta_i \ ,$$

where η_{SDO} is the energy fraction of direct electron excitation; η_i is the energy fraction spent in the *i*-th process; P_i is probability of SDO formation from the electronic state produced in the *i*-th process; Δu_{SDO} is the energy of the $a^1\Delta_g$ state relative to the ground state; and Δu_i is the electron energy spent in the *i*-th process.

For the mixture O_2:Ar=1:1 the maximum of the effective energy fraction spent on the formation of SDO is ~56% at $E/N = 0.69\text{x}10^{-16}$ V cm^2. **Fig**. **II.3.10** demonstrates that the addition of 5% CO to this mixture results in some redistribution of the electron energy balance between the excitation of the SDO and vibrations of CO. The maximum effective energy fraction going into the SDO is about 18% at $E/N = 2.2\text{x}10^{-16}$ V cm^2. The reduced electric field *E/N*, for which the effective excitation of the SDO is maximum, strongly increased with CO addition. This is explained by a rather big value of cross-sections for the excitation of CO molecule vibrations. The addition of 2.5% H_2 or D_2 does not result in such a strong change in the electron energy balance in the discharge (**Fig**. **II.3.11** and **Fig**. **II.3.12**), since molecular vibrations of H_2 and D_2 are excited to a lesser degree than for CO molecules. The maximum effective energy fraction going into the SDO formation is

43 % at $E/N = 0.85 \times 10^{-16}$ V cm^2 for the mixture O_2:Ar:H_2 = 0.95:1:0.05 and 49 % at $E/N = 0.76 \times 10^{-16}$ V cm^2 for the mixture O_2:Ar:D_2 = 0.95:1:0.05.

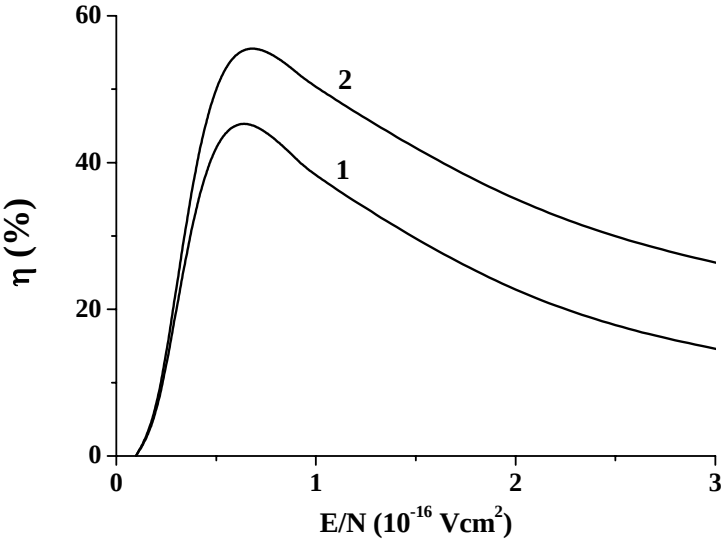

Fig. II.3.9. Theoretical electron energy portion η used for SDO formation in the gas mixture O_2:Ar=1:1.
1) - direct electron-impact excitation;
2) - plus cascade excitation.

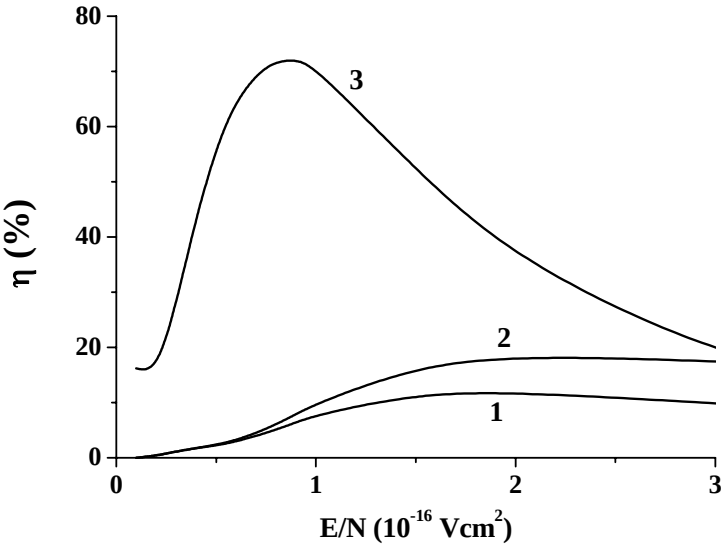

Fig. II.3.10. Theoretical electron energy portions η used for SDO formation and CO vibration excitation in the gas mixture O_2:Ar:CO= 0.9:1:0.1.
1) - direct electron-impact excitation of SDO;
2) - plus cascade excitation;
3) - excitation of vibrational levels of CO molecules.

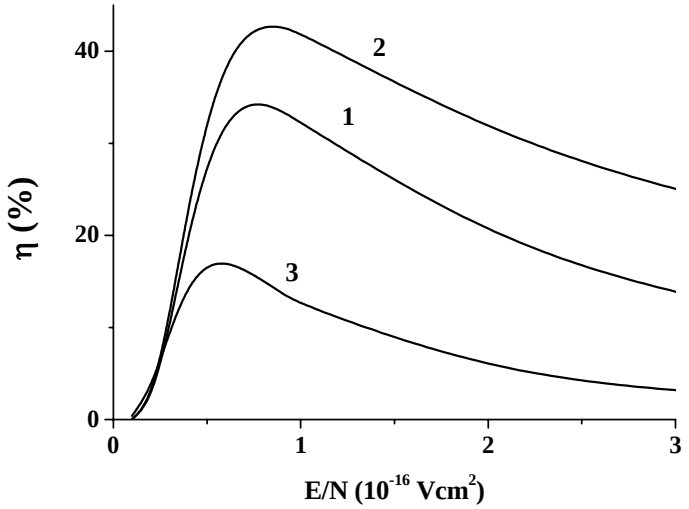

Fig. II.3.11. Theoretical electron energy portions η used for SDO formation and H_2 vibration excitation in the gas mixture O_2:Ar:H_2= 0.95:1:0.05.
1) - direct electron-impact excitation of SDO;
2) - plus cascade excitation;
3) - excitation of vibrational levels of H_2 molecules.

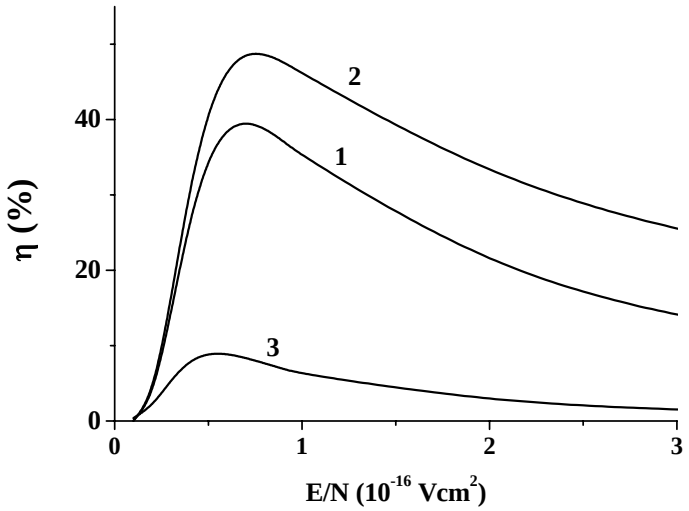

Fig. II.3.12. Theoretical electron energy portions η used for SDO formation and H_2 vibration excitation in the gas mixture O_2:Ar:D_2= 0.95:1:0.05.
1) - direct electron-impact excitation of SDO;
2) - plus cascade excitation;
3) - excitation of vibrational levels of D_2 molecules.

The dependence of the SDO yield on the discharge energy input shown in **Fig**. **II.3.13** was calculated for different gas mixtures at the gas pressure 30 Torr and temperature 300 K. It was supposed that an e-beam current was constant within the time interval 100 μs. The reduced electric field strength was taken equal to that which provides the maximum efficiency of the SDO formation for each gas mixture.

In the numerical simulations, the magnitude of the energy input in the discharge was varied by changing the e-beam current. The SDO concentration plotted in **Fig**. **II.3.13** was calculated at the moment 200 μs after the discharge started and 100 μs after its termination. Analyzing input energy as a function of the e-beam current, the dominance of recombination processes in the plasma electron density decay was found. This evidences that electron detachment processes are rather fast in the gas mixture containing oxygen and the molecular additives listed above.

The markers in **Fig**. **II.3.13** correspond to the experimentally achieved maximum energy input Q_s for different gas mixtures. The horizontal dashed line in **Fig**. **II.3.13** is the threshold SDO yield (15% at T=300 K) necessary for inversion formation in iodine atoms when exchanging energy with SDO molecules (Yuryshev, 1996). The numerically computed SDO yield is shown in **Fig**.**II.3.13** by curves 1 – 4 as a function of the Q_s. The growth of the SDO concentration with the specific energy

input is a linear function at low depositions, while the curve slopes are governed by the maximum effective energy fraction going to the SDO formation.

For the gas mixture O_2:Ar = 1:1, the maximum SIE Q_s realized experimentally in conditions of a stable e-beam sustained discharge was about 100 J l^{-1} atm^{-1}. The SDO yield at such SIE is remarkably lower than the threshold one.

The addition of H_2 to the gas mixture leads to a small reduction of the effective energy fraction for SDO production, while the experimental maximum SIE Q_s grows significantly approaching a value of 1.3 kJ l^{-1} atm^{-1}. At this SIE, the SDO yield is close to the threshold value Y_{th}. With the CO addition, the discharge stability became much higher. As a result, the SIE Q_s ≈3.3 kJ l^{-1} atm^{-1} was achieved. At this SIE the predicted SDO yield is about 20%, which is above the threshold value.

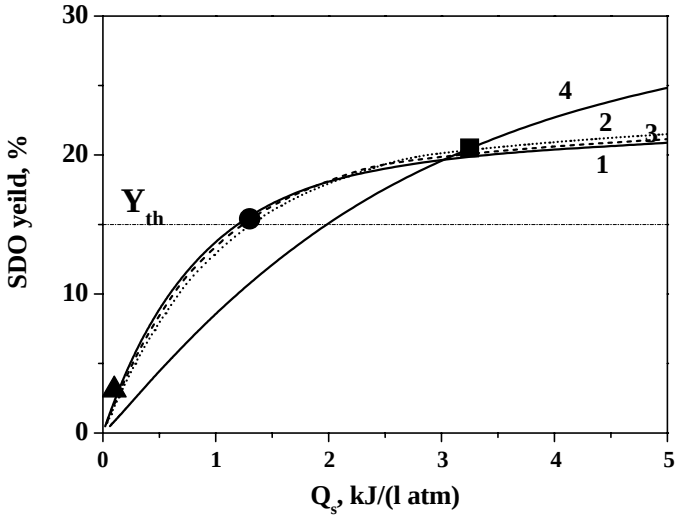

Fig. II.3.13. The SDO yield dependence on the Q_s.
1) - for the mixture O_2:Ar = 1:1;
2) - for the mixture O_2:Ar:H_2= 0.95:1:0.05;
3) - for O_2:Ar:D_2= 0.95:1:0.05;
4) - for O_2:Ar:CO= 0.9:1:0.1.
Experimentally achieved Q_s is shown by markers for the mixtures:
▲ - O_2:Ar = 1:1;
■ - O_2:Ar:CO= 1:1:0.1;
● - O_2:Ar:H_2= 1:1:0.05.
Dashed line shows the threshold yield Y_{th} at T = 300 K.

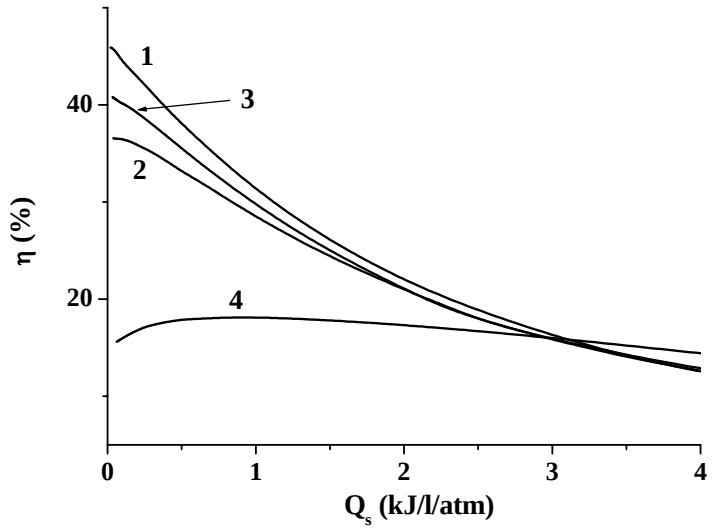

Fig. II.3.14. Calculated energy efficiency of SDO production as a function of the SIE Q_s for mixtures:
1) - O_2:Ar = 1:1;
2) - O_2:Ar:H_2= 0.95:1:0.05;
3) - O_2:Ar:D_2= 0.95:1:0.05; and
4) - O_2:Ar:CO= 0.9:1:0.1.

Fig. **II.3.14** shows an energy efficiency of SDO production predicted as a function of the SIE for different gas mixtures. The energy efficiency of SDO production was defined as a ratio of the energy saved in the $a^1\Delta_g$ state to the energy deposited into the discharge. At a low energy deposition, the efficiency of SDO production is maximal for the mixture O_2:Ar = 1:1 (curve 1). With the addition of H_2 and D_2, it decreases a little (see curves 2 and 3). The addition of CO results in a remarkable reduction of the efficiency of SDO production (curve 4). With SIE growth, the efficiency of SDO production falls for the gas mixtures O_2:Ar and for the mixtures with H_2 and D_2 additives (curves 1-3). In a CO-containing mixture, the efficiency of SDO production grows initially and then decreases a little bit. At an SIE higher than 3 kJ l^{-1} atm^{-1}, the efficiency of SDO production for the CO containing mixture is higher than for other mixtures under examination.

The reason for the different behavior is a higher value of the *E/N* parameter for the CO-containing mixture. The numerical simulations of the experimental conditions for the CO-containing mixtures predict a maximum of the efficiency of SDO production of nearly 20% (see **Fig**.**II.3.14**).

The energy efficiency of SDO production is an important characteristic of an SDO generator for its application in laser development since it is a factor controlling the laser efficiency. In contrast to a self-sustained discharge, the EBSD allows for variation in the reduced electric field strength and the energy input, respectively, within a wide range. In the self-sustained discharge, the energy is deposited at a high *E/N* value where the ionization is balanced by recombination/attachment processes; hence, O_2 is dissociated significantly. Under such conditions, a high SDO yield can be achieved with a low efficiency of SDO production, only. It is confirmed by the experiments in (Fujii, 2000), where an SDO yield of 32% is achieved at the energy efficiency of SDO production about 2%.

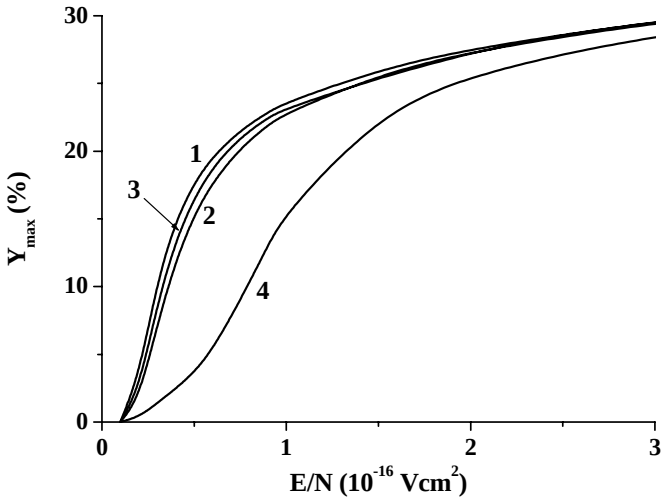

Fig. II.3.15. Maximum SDO yield as a function of the *E/N* parameter for mixtures:
1) - O_2:Ar = 1:1;
2) - O_2:Ar:H_2= 0.95:1:0.05;
3) - O_2:Ar:D_2= 0.95:1:0.05; and
4) - O_2:Ar:CO= 0.9:1:0.1.

Fig. **II.3.13** shows that the SDO yield saturates with the SIE growth. In calculations, the SIE growth was supposed to be due to the electron concentration increase. The saturation of the SDO yield is explained by the dominating electron impact processes with electron concentration growth. The SDO excitation and de-excitation rates by electron impact depend on the reduced electric field strength. Excited states in this situation play a minor role. Under such conditions, the maximum of the SDO yield Y_{max} can be evaluated solving the electron Boltzmann equation with a proper account of statistical weights of respective levels. **Fig**. **II.3.15** shows the calculated Y_{max} for different gas mixtures as a function of the *E/N* parameter. For the gas mixture with CO additive, the Y_{max} value is 25% at $E/N = 2.2\text{x}10^{-16}$ V cm^2 (curve 4), while for other mixtures it achieves 21% at *E/N* =

0.8×10^{-16} V cm^2 (curves 1-3). These values agree with the results obtained with the full kinetic model implication (compare with **Fig**. **II.3.13**). Note that Y_{max} was evaluated earlier in (Fournier, 1981), and its value was limited by the magnitude of 13%. It is hard to indicate a reason for such discrepancy because there is no detailed description of the calculation procedure in (Fournier, 1981). We guess that it is explained by an incomplete account of electron-induced processes in (Fournier, 1981).

EBSD spectroscopy and detection of $O_2(b^1\Sigma_g)$ and $O_2(a^1\Delta_g)$ states (*Subtask 1B.4*)

There are many methods of detecting SDO concentration (see, for instance, ("Singlet Oxygen", 1979; "Singlet O_2 , v.1", 1985; Wayne, 1969), the measurement of 1.27 μm luminescence of transition $O_2(a^1\Delta_g) \rightarrow O_2(X^3\Sigma^-_g)$ being most popular. However, to calculate the SDO concentration it should be used the Einstein coefficient for above transition which is known with an accuracy of factor two (Miller, 2001). The second point is that a measuring apparatus including an IR-detector, a monochromator or an optical filter is usually calibrated by 1.27 μm radiation emitted by a flat source of blackbody radiation instead of a volumetric IR source. The attention to this problem was driven in (Duo, 2001). We suggest to calibrate an apparatus detecting 1.27 μm radiation emitted by an electric discharge by measuring an intensity of 1.27 μm radiation emitted by SDO of known concentration which is produced in a chemical generator and radiates out of the volume of the same geometry as the geometry of the electric discharge. The optical schemes of the measurements should be the same. In this case the procedure of the calibration does not need any information about the Einstein coefficient for the $O_2(a^1\Delta_g) \rightarrow O_2(^3\Sigma_g^-)$ transition. This volumetric method can be also used for calibration, when determining concentration of $O_2(b^1\Sigma_g^+)$ in an electric discharge. In this case the concentration of the $O_2(b^1\Sigma_g^+)$ going out of the chemical generator can be determined, when comparing the intensity of its radiation ($\lambda \approx 762$ nm) with one of dimole radiation ($O_2(a^1\Delta_g) + O_2(a^1\Delta_g) \rightarrow O_2(X^3\Sigma^-_g) + O_2(X^3\Sigma^-_g)$) at the wavelength $\lambda \approx 634$ nm. Such a calibration method was successfully applied by us for estimation of $O_2(b^1\Sigma_g^+)$ concentration in pulsed longitudinal self-sustained discharge in pure oxygen (p=2.8 Torr, U=15 kV; C=10 nF, Q_{disch}=2 J, V=0.8 l). The $O_2(b^1\Sigma_g^+)$ concentration came up to ~10^{14}cm^{-3}.

As it follows from theory, the $O_2(b^1\Sigma_g^+)$ state plays an important role in SDO formation in electric discharge. Thus, the ~762 nm luminescence can be used as a source of information about the SDO also (King, 2001). The tentative measurements of the EBSD visible radiation spectra were carried out with a prism spectrometer supplied with a CCD array. Experimentally obtained data with spectral resolution ~2 nm for gas mixture O_2:CO (p=30 Torr) are presented in **Fig**. **II.3.16**. One can clearly see P- and R- branch of $O_2(b^1\Sigma_g^+) \rightarrow O_2(X^3\Sigma^-_g)$ transition (~760 nm) and atomic oxygen luminescence (~778 nm), and also a spectral line ~589 nm. The same line was identified in (Torchin, 1983) as that of gold oxide luminescence. The measurement with higher spectral resolution demonstrated that the ~589 nm line is an atomic doublet associated with sodium atom luminescence (589.0 and 589.6 nm) (**Fig**. **II.3.16**) which can be related to the trace of impurities in the EBSD chamber formerly applied for the research of a CO_2 laser using NaCl and KCl optics. Actually, we did observe the doublet of potassium (766.5 and 769.9 nm) arisen at SIE higher than ~1000 J l^{-1}atm^{-1} (**Fig**. **II.3.17**). This doublet overlaps partially with a long wavelength wing of luminescence of $O_2(b^1\Sigma_g^+) \rightarrow O_2(X^3\Sigma^-_g)$ transition and can be mistaken for the $O_2(b^1\Sigma_g^+)$ luminescence. However, one can still observe the short wavelength wing of luminescence of

$O_2(b^1\Sigma_g^+) \rightarrow O_2(X^3\Sigma^-_g)$ transition in the EBSD spectra (**Fig**. **II.3.17**) and atomic oxygen luminescence (λ≈778 nm).

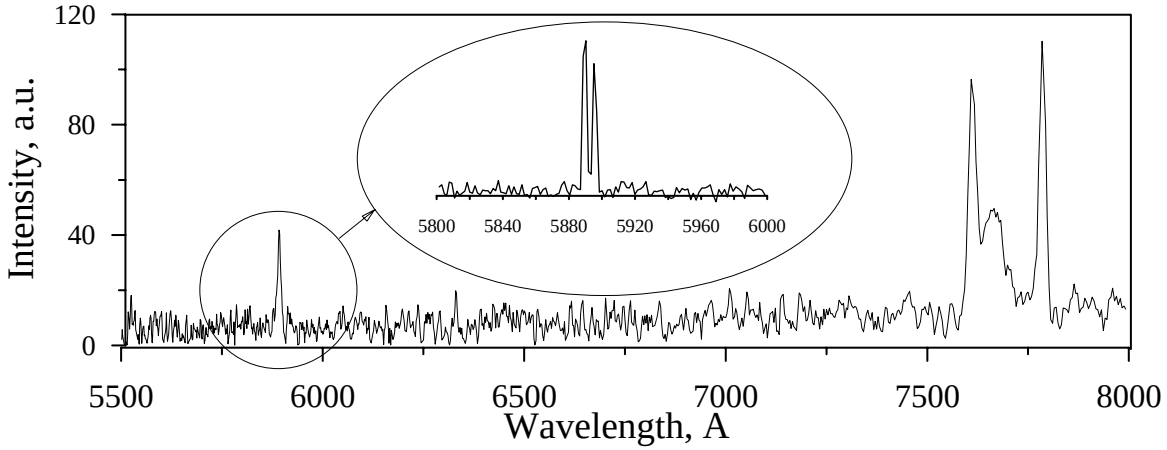

Fig. II.3.16. Visible spectrum of EBSD and its afterglow. Gas mixture O_2:CO = 1:0.1. p=30 Torr. SIE ~1000 J l^{-1} atm^{-1}

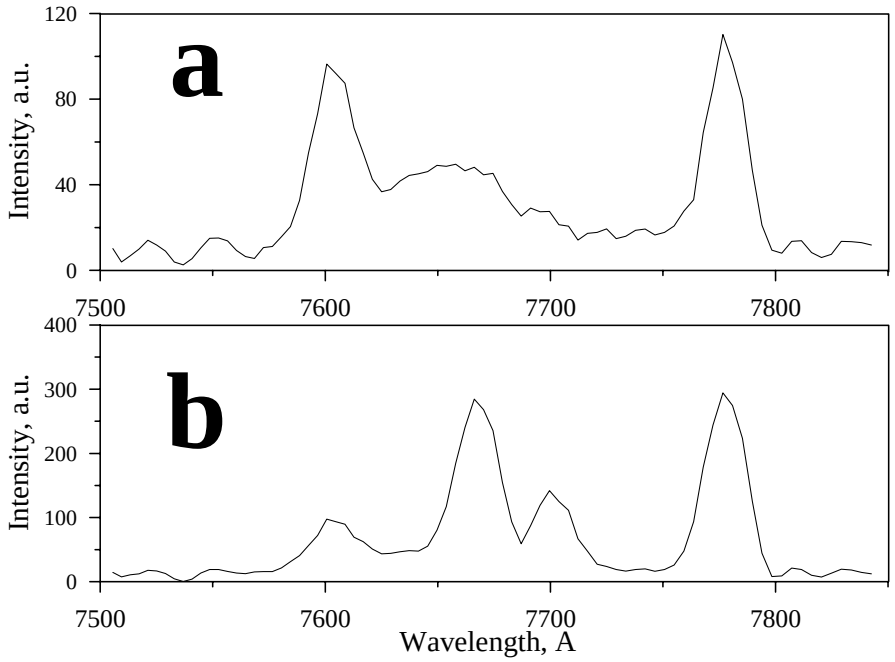

Fig. II.3.17. Visible spectrum of EBSD and its afterglow near 760 nm. Gas mixtureO_2:CO = 1:0.1. p=30 Torr. SIE ~ 1000 (a) and 2300 (b) J l^{-1} atm^{-1}

To detect optical signal corresponding to the spectral range of SDO luminescence (λ≈1.27 μm) a monochromator was used with spectral resolution being of 6 nm in the experiments. The SDO luminescence was observed with a room temperature Ge-photodiode. Typical time behavior of the optical signal at the wavelength of 1.27 μm is in **Fig**. **II.3.18**. To analyze the spectral and temporal characteristics of SDO luminescence the measurements of amplitude of time behavior at the same time point from EBSD beginning at different wavelengths were carried out. Spectral distribution of the luminescence at the 2-nd ms and 6-th ms from EBSD beginning are presented in **Fig**. **II.3.19**. The spectral line width was about 20 nm in both cases.

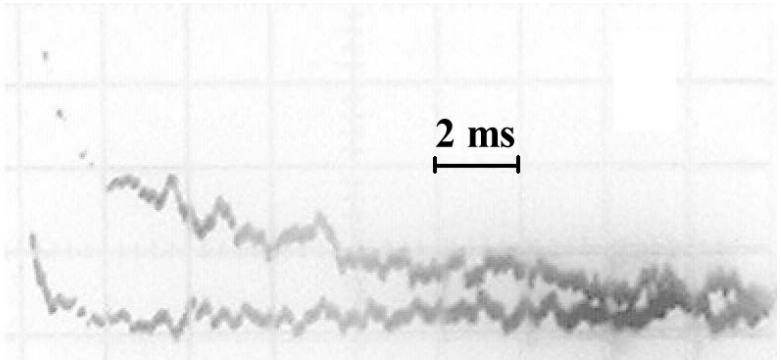

Fig. II.3.18. Typical time behavior of the SDO luminescence at the wavelength of 1.27 μm
O_2:He:CO = 1:2:0.01, p=90 Torr

Fig. **II.3.20** demonstrates dependencies of luminescence signal amplitude on SIE for two gas mixture with different CO contents: O_2:CO =1:0.01 and 1:0.1. It is clearly seen that using gas mixture with low CO concentration resulted in increasing of SDO luminescence signal. Other experiments shown that replacement of argon in gas mixture O_2:Ar:CO =1:1:0.01 to helium (O_2:He:CO =1:1:0.01) resulted in growth of the signal twice. Moreover, for argon containing gas mixture high intensity luminescence was observed with duration being of 1-2 ms identified as luminescence of argon metastable states at the wavelength of λ=1.2702 μm. So one of the most important experimental condition for effective SDO production is gas mixture contents. The experiments on calibration of the optical measurement scheme and SDO concentration measurement can be seen below.

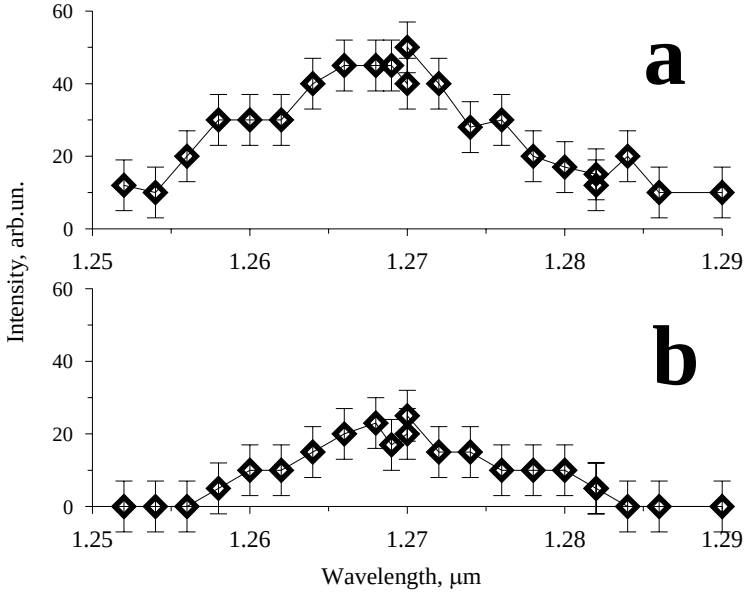

Fig. II.3.19. Spectral characteristic of SDO luminescence at the 2 ms (**a**) and 6 ms (**b**) from EBSD beginning
O_2:CO =1:0.01, p=60 Torr,
SIE=400 J l^{-1} atm^{-1}

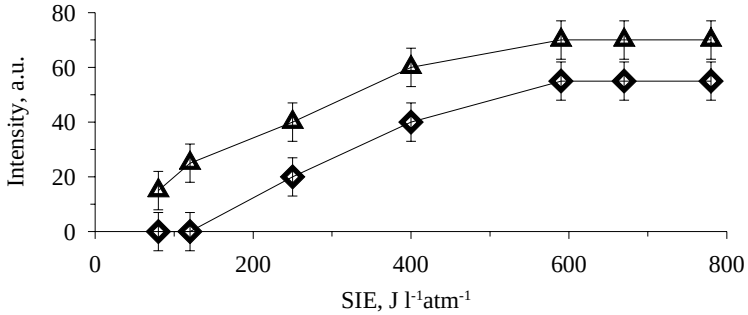

Fig.II.3.20. Dependencies of SDO luminescence signal amplitude on SIE at p=60 Torr.
△ O_2:CO =1:0.01
◇ O_2:CO =1:0.1

Experimental measurement of temperature of EBSD in oxygen containing mixture. (*Subtask 2B.1*)

Electric discharge excites electronic, vibrational and rotational levels of molecules in gas mixture. Distribution of molecules over rotational levels is described usually by Boltzmann distribution with rotational temperature equal to translational one because the rotational relaxation rate is very fast. So gas temperature can be calculated by using spectral distribution of luminescence within rotational structure range of some electron-vibration transitions.

Spectrum of oxygen luminescence on $O_2(b^1\Sigma_g^+)\rightarrow O_2(^3\Sigma_g^-)$ transition was synthesized for different rotational temperatures with spectral smoothing corresponding to experimental spectral resolution $\lambda/\Delta\lambda$ about 330. The results are presented in **Fig.II.3.21**. With temperature growth, maximums of luminescence intensity in R- and P- branches move away from the central wavelength of the transition (762 nm). For instance, wavelength of maximum intensity in R-branch λ_R decreased from 761.0 nm down to 759.7 nm and that of P-branch λ_P increased from 762.8 to 764.6 nm with temperature growing from 100 up to 1000 K. So, gas temperature can be evaluated from experimental measuring λ_R and λ_P wavelengths.

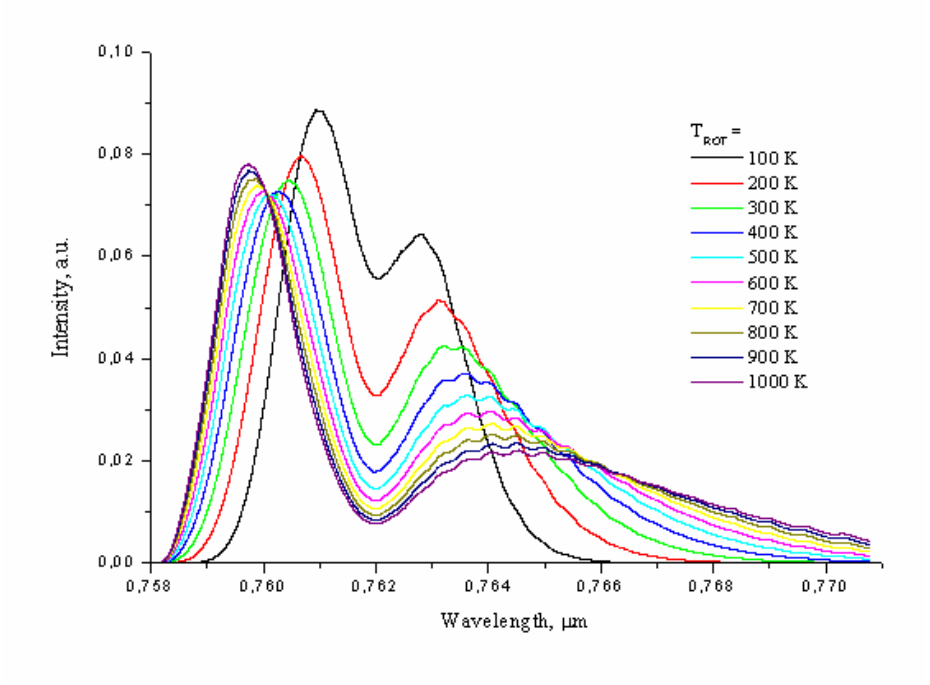

Fig. II.3.21. Spectral distribution of oxygen luminescence on $O_2(b^1\Sigma_g^+)\rightarrow O_2(^3\Sigma_g^-)$ transition calculated for various rotational temperature with spectral resolution being about 330.

Another way to find the temperature is based on the calculation of ratio of experimentally measured maximum intensity of R- and P-branches (I_R/I_P). Theoretically predicted dependence of the ratio I_R/I_P on temperature is presented in **Fig. II.3.22**.

Experiments were carried out on pulsed cryogenically cooled EBSD installation. Spectral distribution of luminescence within visible spectral range was measured by using spectrograph and CCD array. Spectral resolution $\lambda/\Delta\lambda$ was about 330 (unresolved rotational structure). Description of the measurement procedure was presented above in detail. To increase experimental accuracy averaging of several signals obtained for several pulses at the same experimental conditions was used.

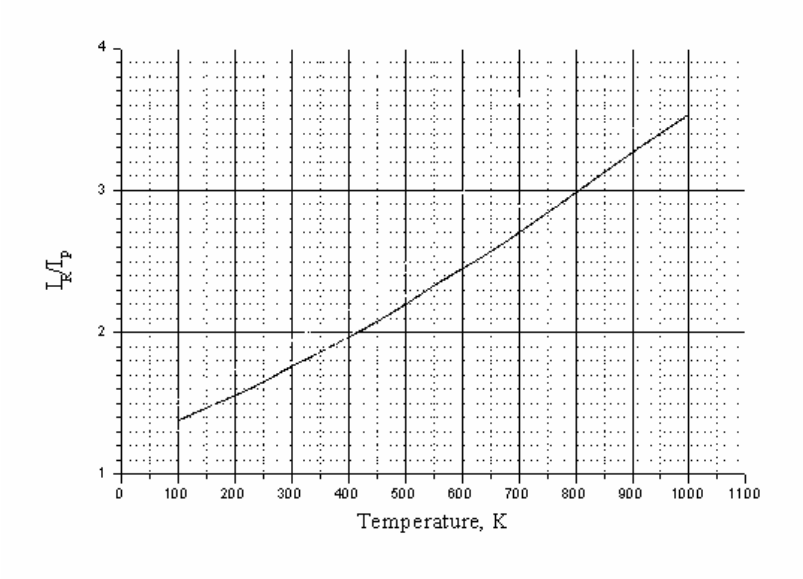

Fig. II.3.22. Dependence of ratio of maximum intensities of luminescence in R- and P- branches on temperature.

Typical spectra of oxygen luminescence ($O_2(b^1\Sigma_g^+)\rightarrow O_2(^3\Sigma_g^-)$ transition and atomic oxygen line at wavelength 778 nm) registered for various experimental conditions are presented in **Fig.II.3.23** and **Fig. II.3.24**. There is variation in wavelengths λ_R, λ_P and in intensities ratio I_R/I_P for variable specific input energy Q_{in} and initial gas temperature T_0. Gas temperatures calculated by using intensities ratio I_R/I_P for spectrum shown in **Fig. II.3.23** and **Fig. II.3.24** were ~550 K and ~260 K, respectively. Dependences of gas temperature calculated by using both wavelengths λ_R, λ_P and intensities ratio I_R/I_P methods on specific input energy Q_{in} are shown in **Fig. II.3.25**. It should be noted, the calculated wavelength values λ_R, λ_P strongly depend on temperature (about 0.0015 nm/K). Actually, the maximum, particularly for P-branch, is rather broad with modulations resulting from averaging of separate lines. Therefore, the temperature found from measured λ_P is rather sensitive to experimental uncertainties. Specifically, temperature of ~700 K found at initial gas temperature 150 K and specific input energy Q_{in}=250 J/l Amagat (**Figs. II.3.24, II.3.25**) is much higher than expected at such value of the input energy. One may conclude that the method of temperature calculation from intensities ratio I_R/I_P is more correct than that from the wavelengths λ_P for the experimental conditions. However, it should be tested in other experiments.

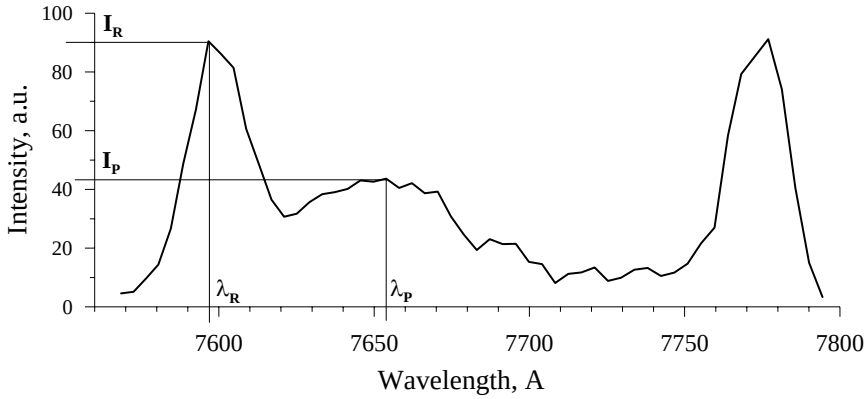

Fig. II.3.23. Spectral characteristic of oxygen gas mixture luminescence excited by EBSD.
O_2:CO=1:0.1;
30 Torr; Q_{in}=980 J/l atm;
T_0=300 K

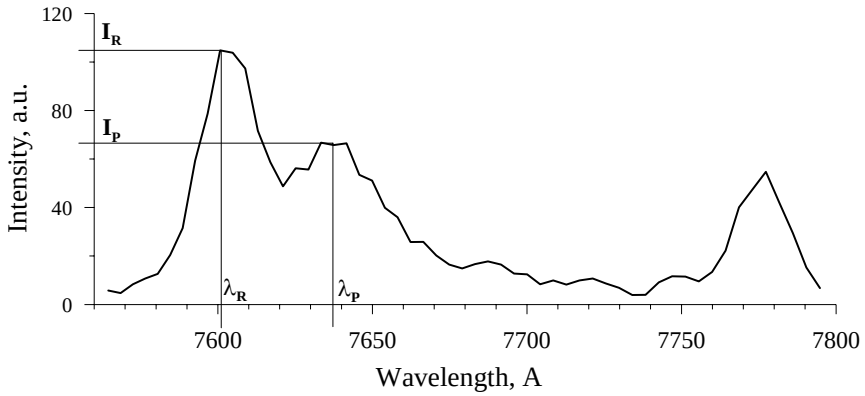

Fig. II.3.24. Spectral characteristic of oxygen gas mixture luminescence excited by EBSD.
O_2:CO=1:0.1;
0.04 Amagat (equivalent to 30 Torr at 300 K);
Q_{in}=250 J/l Amagat;
T_0=150 K

Gas temperature found from the intensities ratio I_R/I_P increased from 260 K up to 420 K with specific input energy growing from 250 to 1200 J/l Amagat at initial gas temperature T_0=150 K (**Fig. II.3.25**). The temperature determined from the shift of R-branch maximum is not so strongly subject to experimental uncertainties, because of narrower peak and it is less disturbed by the K line appearing at high energy loading. Therefore, the data obtained from maximum position of R-branch of the spectrum should be taken into account, in particular at high Q_{in} values.

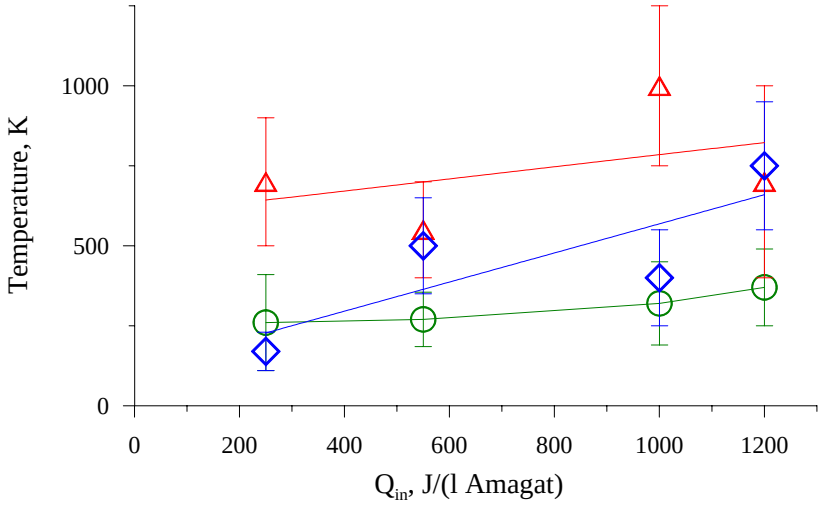

Fig. II.3.25. Dependence of gas mixture temperature on specific input energy Q_{in}.
O_2:CO=1:0.1; 0.04 Amagat (equivalent to 30 Torr at 300 K);
T_0=150 K
△ - temperature from measuring wavelength λ_P
◇ - temperature from measuring wavelength λ_R
○ - temperature from intensities ratio I_R/I_P

Gas pressure in oxygen gas mixture CO:O_2=1:50 excited in EBSD at initial gas density N = 0.08 Amagat and gas temperature T_0 = 170 K was measured with magnetic induction detector. The time behavior of gas pressure and temperature in EBSD pumped gas mixture is presented in **Fig. II.3.26**. The rise time of gas pressure inside EBSD chamber was 6 ± 1 ms. The increase of gas pressure and temperature was equal ΔP = 1.1 kPa and $\Delta T = T_0 \Delta P/P_0 \approx 40$ K at Q_{in}=800 J/l Amagat. When taking into account the relationship between volume of gas pumped in EBSD and total volume of the EBSD chamber being of 0.11 the increase of gas temperature in EBSD volume was about 350 K.

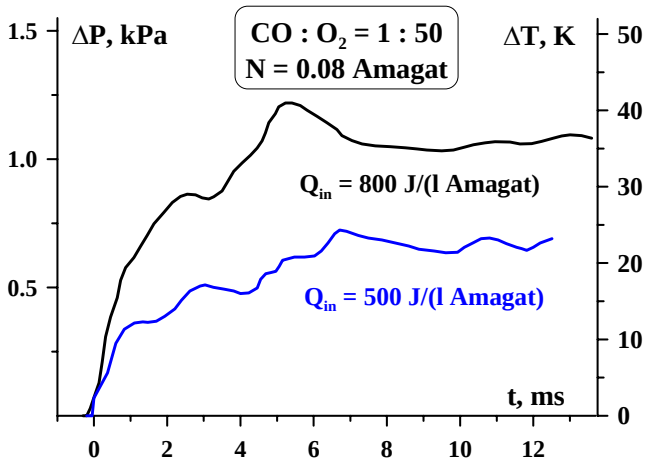

Fig. II.3.26. Time behavior of gas pressure (left scale) and gas temperature (right scale) in EBSD pumped gas mixture $CO:O_2$=1:50.
N = 0.08 Amagat,
T_0 = 170 K,
Q_{in} =500 and 800 J/l.Amagat.

Analysis of gas heating processes in e-beam sustained discharge and extension of the model for variable gas temperature.
(*Subtask 2B.1*)

Energy fractions spent in discharge on excitation of molecular rotations and dissipated in elastic collisions transform into gas heating for collision times. At some conditions, the ion component of electric current may be an important heat source (Londer, 1984). In parallel with $O_2(a^1\Delta_g)$ excitation, in the discharge a number of other levels are excited including vibrational and higher electronic levels, and some molecules are dissociated. Further evolution of the energy accumulated in the internal degrees of freedom is accompanied by release of some fraction into the translational motion. Rate constants for many processes depend strongly on gas temperature (Kondrat'ev and Nikitin, 1974). Therefore, our earlier developed model for description of non-self-sustained discharge in mixtures of oxygen with CO, H_2 и D_2 (Ionin, 2003) was modified. An equation for gas temperature was added:

$$Nc\frac{dT}{dt} = Q_e + Q_V + W\eta_T, \qquad \text{(II.3.21)}$$

where $N = \sum_M N_M$ is gas density, c is thermal capacity, Q_e gas heating rate in processes of energy from electronic states, Q_V gas heating rate in vibrational relaxation processes, η_T is the fraction of gas discharge power dissipated in elastic collisions and in processes of excitation of rotational levels of molecules, W is the discharge power density. Our estimations showed that gas heating by ion current in conditions of the experiments (Ionin, 2003) could be neglected. In experimental facility the external space in the vacuum vessel is much larger than the region occupied by electric current. As a result, at times longer than typical acoustic time for sound wave traversing across the discharge width $\tau = l/V_s$ (l is the discharge width; V_s the sound wave velocity) gas pressure is nearly constant, and equal to the initial one. At shorter times, an approximation of constant gas density is applicable. For experimental conditions in (Ionin, 2003) τ = 200 μs. The thermal capacity in such conditions varies in time. To describe this effect the following interpolation dependences of gas density and thermal capacity on time were used:

$$N = N_0\exp(-t/\tau) + \frac{N_0T_0}{T}(1-\exp(-t/\tau)), \qquad \text{(II.3.22)}$$

$$c = c_V \exp(-t/\tau) + c_P(1-\exp(-t/\tau)). \qquad \text{(II.3.23)}$$

Here N_0 and T_0 are initial gas density and temperature, c_V и c_P are gas capacities at constant volume and pressure, respectively. Such interpolation procedure was employed by us earlier while modeling pulsed self-sustained discharge in nitrogen (Akishev, 1982).

Typically, the charge stored in the capacity does not decay to the moment of electron-beam pulse termination. The remaining voltage is applied across the discharge gap, and the electric current continues to flow until the plasma decays completely. Meantime, the gas-dynamic expansion of gas persists (the acoustic time is 200 μs in comparison with e-beam current pulse duration 100 μs), and gas heating continues due to relaxation of energy stored in internal degrees of freedom and further excitation by the current in the decaying plasma. However, because the instantaneous current diminishes with plasma decay for characteristic times on the order of hundreds of microseconds the electric field almost stops to diminish. As a result the parameter E/N, that controls the electron mean energy, grows due to gas rarefaction. At approaching E/N value the critical magnitude providing plasma maintenance, a second peak in the discharge current appears seen in **Fig. II.3.27**. In a whole the discharge evolution proceeds as follows. Within the time interval of 100 μs, ionization by fast electrons produces plasma with high conductivity, and electric current appears in the discharge gap as a result of capacity discharging. After the e-beam terminates the electric current falls quickly, and capacity voltage is almost frozen. As long as gas expands, and its density diminishes, the reduced electric field strength E/N rises, what results at some moment in formation of self-sustained discharge with ionization produced by remaining electrons heated by electric field.

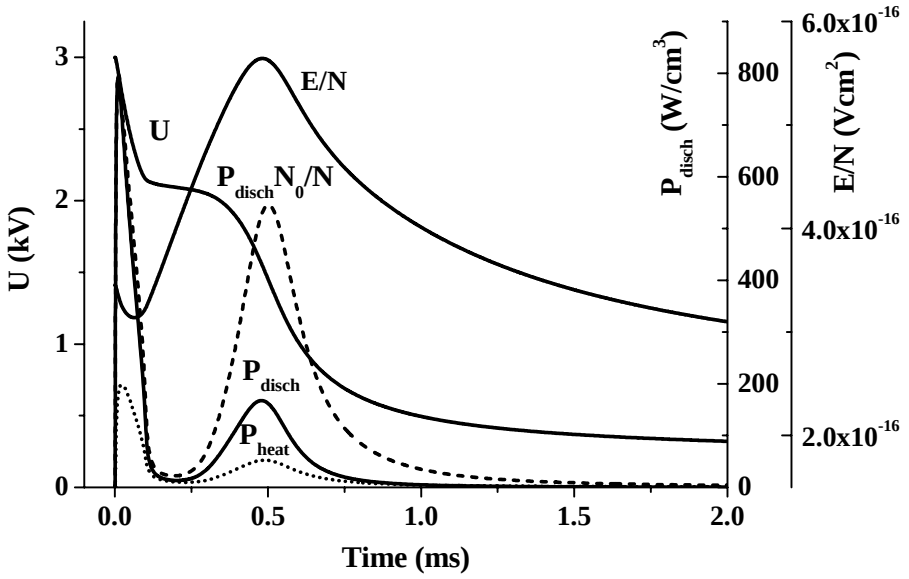

Fig. II.3.27. Time history of discharge characteristics. P = 30 Torr, $CO:O_2$=1:9, C = 370 μF, U_0 = 3 kV.

Gas discharge power density reduced to the current value of gas density is shown in **Fig. II.3.27** by dashed line. It turns out to be rather high, and most probably such a high value of the power dissipated in gas leads to development of discharge constriction. **Fig. II.3.28** demonstrates how the gas temperature and density evolve in time. Behavior of a number of species in plasma is shown in **Fig. II.3.29**.

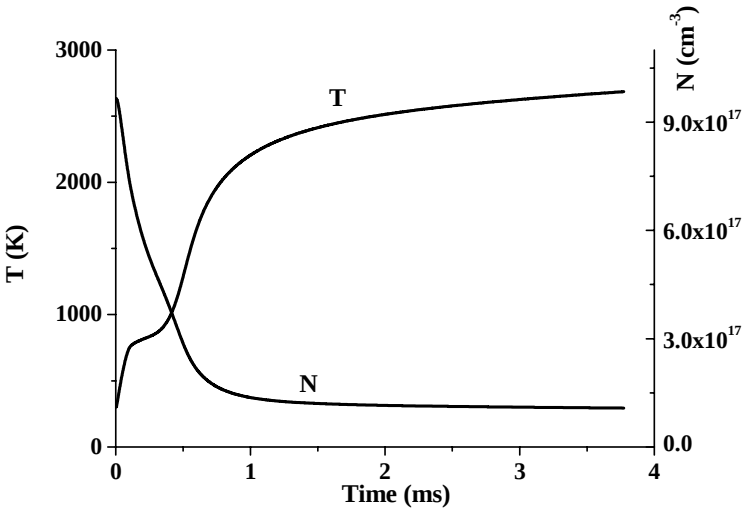

Fig. II.3.28. Gas temperature and density vs time.
P = 30 Torr, CO:O_2=1:9,
C = 370 μF, U_0 = 3 kV.

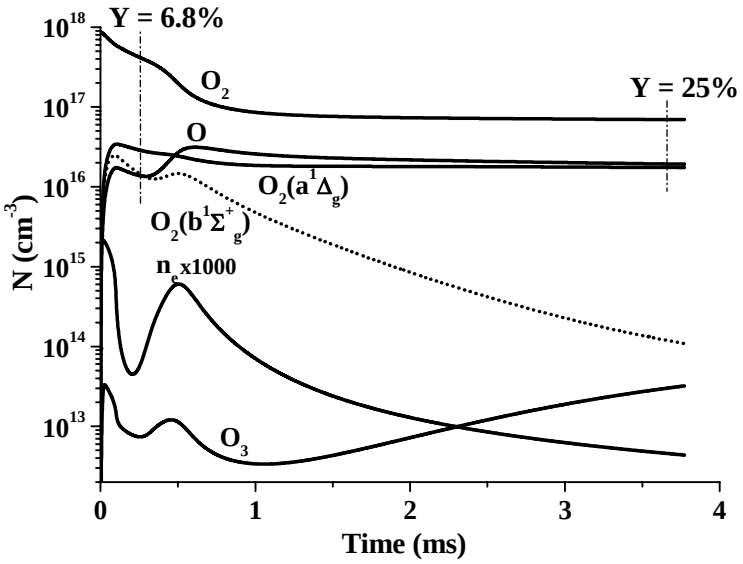

Fig. II.3.29. Time history of relevant species in the discharge.
P = 30 Torr, CO:O_2=1:9,
C=370 μF, U_0 = 3 kV.

Vertical dash-dot lines mark the moments, corresponding to the end of e-beam sustained discharge and to the end of simulated interval (about 3.75 ms). Singlet oxygen yields $Y = \dfrac{O_2(a^1\Delta_g)}{O_2 + O_2(a^1\Delta_g)}$ at these moments are 6.8% and 25%, respectively. It should be noted however, that an assumption of gas discharge uniformity persistence during all the time is very questionable.

Concluding, the extension of the kinetic model for time-dependent gas temperature and density demonstrates importance of such modification of theory. Strong indications are found that gas heating and gas-dynamic expansion may completely change evolution of gas discharge in after-glow phase.

Parametric study of effects influencing upon SDO production.
(*Subtasks 2B.2 and 2B.4*)

First results on singlet delta oxygen (SDO) production in pulsed e-beam sustained discharge (EBSD) were presented above, where the SDO luminescence signal at the wavelengths around λ= 1.27 μm was detected by using a diffraction monochromator with a grating of 300 grooves/mm and a room-temperature photodetector. The same optical scheme was used to study an influence of different parameters (E/N, specific input energy (SIE), and gas mixture content) on the intensity of SDO luminescence signal. The spectral resolution determined by the slit width of the monochromator was ~10 nm. However, a new germanium photodetector with a shorter response time (~10 μs) was used to detect a luminescence signal in the course of the EBSD. This photodetector (#2) was cooled by thermo-electrical Peltier effect. Its aperture was 3 mm in diameter.

A temporal behavior of the luminescence for the 1.27 μm wavelength range (b) and of the EBSD current (a) are presented in **Fig. II.3.30**. The EBSD current pulse duration was increased up to ~300 μs (**Fig. II.3.30**) to guarantee the luminescence signal rise time is not due to the detector response time. In the course of the EBSD pulse the intensity of the luminescence signal increases and falls down after the EBSD pulse end. The similar time behavior was observed within the wide range of experimental conditions. For instance, one can see the luminescence signal at shorter EBSD pulse duration (~50 μs) in **Fig. II.3.31a**. A tail of the luminescence signal after the first peak was observed only for the wavelength range of 1.27±~0.01 μm and was caused by the SDO luminescence. Luminescence signals out of this spectral range did not have any tail but did have the first strong peak correlating with the EBSD current. **Fig. II.3.31b** demonstrates such a luminescence signal at the wavelength 1.30 μm which does have a first peak and does not have any tail.

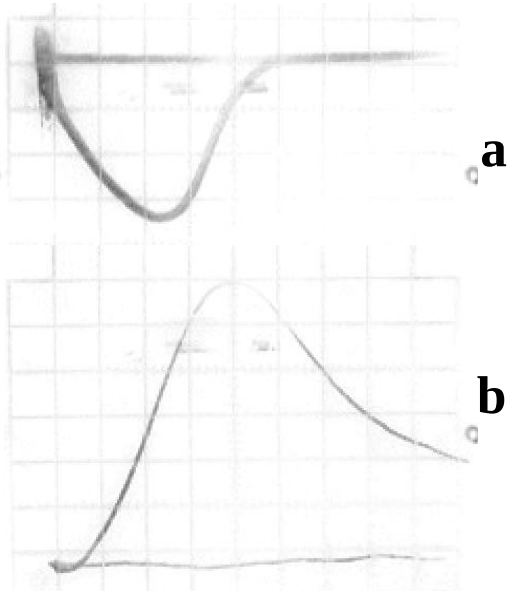

Fig. II.3.30. Temporal behavior of EBSD current (**a**) and luminescence (**b**) for the 1.27 μm wavelength range.
$CO:O_2$:He=1:20:20;
60 Torr;
50 μs/div.

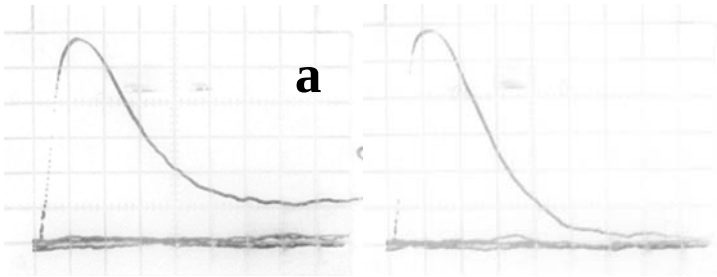

Fig. II.3.31. Temporal behavior of luminescence at wavelength of 1.27 μm (**a**) and 1.30 μm (**b**)
$CO:O_2$=1:20;
30 Torr;
50 μs/div.

A spectral distribution of the luminescence signal measured for its maximum intensity within the spectral range 1.20 - 1.33 μm is presented in **Fig. II.3.32** (diamonds). Experimental error was determined by deviation of the luminescence intensity for various EBSD pulses. One can see that

the spectrum of the first peak of the luminescence signal, which overlaps with the EBSD current, has a strong continuum with at least one strong spectral line near 1.32 μm. The spectral distribution of this peak was measured with higher resolution (~600 c (**Fig. II.3.32**, triangles). The peak observed in the spectrum can be identified as a luminescence of atomic oxygen at the wavelength 1.3164 μm.

The spectral distribution of the luminescence tail was measured 300 μs after the EBSD beginning (**Fig. II.3.32**, squares). Maximal intensity of the signal tail was observed at 1.27 μm, full spectral width at half maximum being ~20 nm which is in good agreement with theoretical estimation of SDO luminescence spectrum related to the rotational structure of the $O_2(a^1\Delta_g)\rightarrow O_2(X^3\Sigma_g^-)$ transition of oxygen molecule.

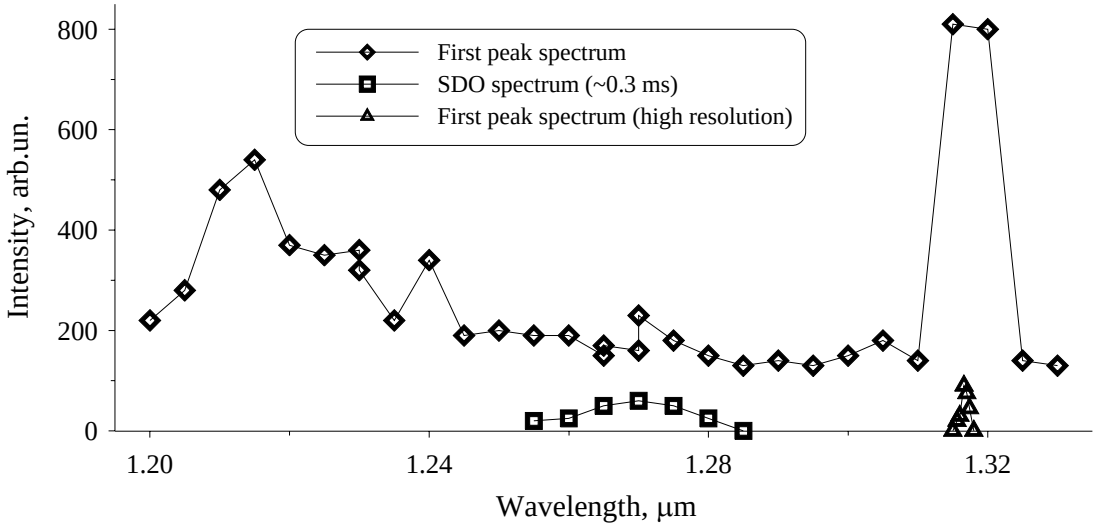

Fig. II.3.32. Spectral distribution of the first peak and tail (SDO) luminescence. $CO:O_2$=1:100; 30 Torr; 950 J/(l·atm)

The influence of the E/N parameter on the intensity of the SDO luminescence at the wavelength 1.27 μm was studied for various experimental conditions (**Fig. II.3.33** and **II.3.34**). The E/N parameter was changed by changing capacity C_{dis} of the electrical capacity bank feeding EBSD. The lower voltage applied to the discharge gap, i.e. the lower E/N we need, the higher capacity we have to use for loading the same energy into the EBSD. For instance, the E/N parameter changed from 6.9 down to 1.4 kV/(cm·atm) in the course of the EBSD, capacity C_{dis} being of 55 μF, and from 3.6 down to 2.3 kV/(cm·atm), C_{dis} being of 330 μF, at the same specific input energy SIE of 950 J/(l·atm(O_2+CO)) (upper pair of pictures in **Fig. II.3.34**).

The initial E/N parameter is as about twice lower in the second case as in the first one. Moreover, for the second case E/N parameter decreases by only 30% by the end of EBSD pulse. The voltage temporal behavior for the second case is much closer to rectangular form than for the first case, in which E/N decreases as much as four times during the EBSD. Although, there is a big difference between experimental conditions (E/N parameter value and its temporal behavior) for every pairs of the oscillogramms presented in **Fig.II.3.33** and **II.3.34**, the SDO luminescence temporal behaviors are very similar to each other. The E/N parameter seems to be not very crucial one for the SDO production for the experimental conditions corresponding to E/N changes from ~2 up to ~11 kV/(cm·atm).

420 J/(l·atm)	420 J/(l·atm)

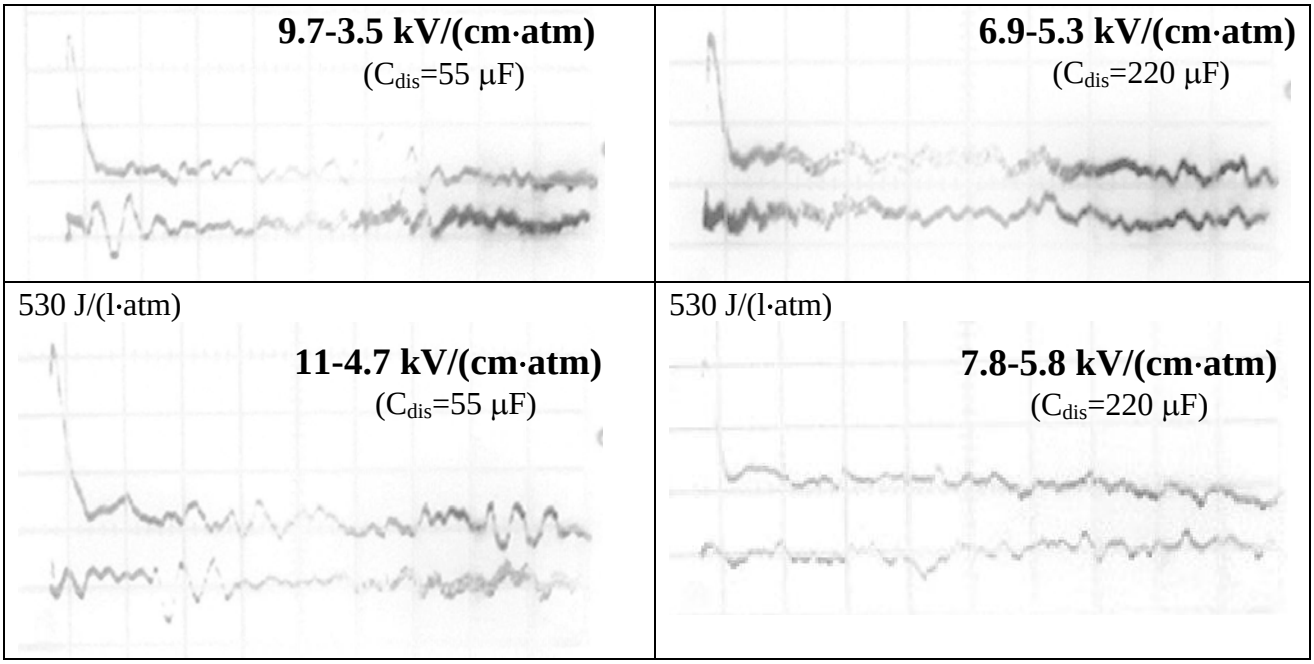

Fig. II.3.33. Temporal behavior of SDO luminescence. E/N parameter changing during EBSD, specific input energy and capacity C_{dis} are shown at every picture. $CO:O_2$=1:100; 30 Torr; 500 μs/div.

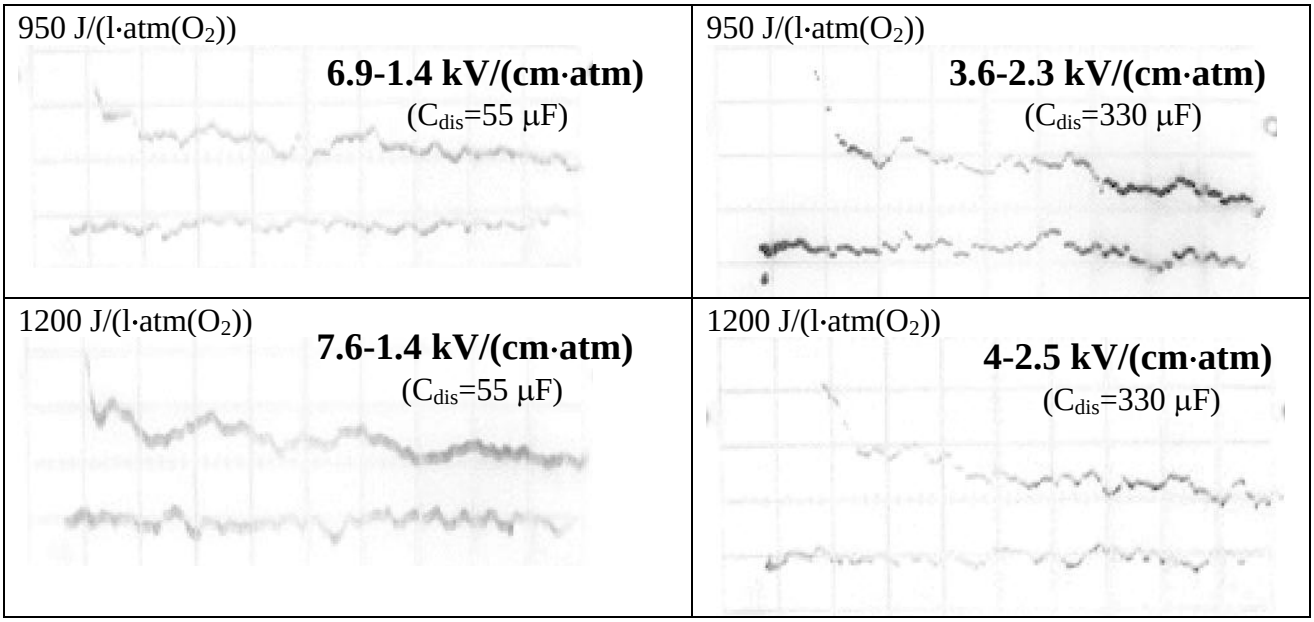

Fig. II.3.34. Temporal behavior of SDO luminescence. E/N parameter changing during EBSD, specific input energy calculated for partial pressure of molecular gases and capacity C_{dis} are shown at every picture. $CO:O_2$:He=1:19:20; 60 Torr; 500 μs/div

Figs. II.3.35, II.3.36 and **II.3.37** demonstrate the SDO luminescence signals at wavelength of 1.27 μm for different gas mixtures and for various SIE. One can see from the figures that the higher SIE, the higher SDO signal is. The experimental results obtained for oxygen mixtures with different carbon monoxide contents are presented in **Fig. II.3.35** (at total gas pressure 60 Torr) and **Fig. II.3.36** (at total gas pressure 30 Torr). It should be noted, the SDO luminescence at 60 Torr (**Fig. II.3.35**) was obtained by room-temperature photodetector #1. Excitation of the EBSD in

oxygen mixture with lower CO concentration resulted in enhancement of SDO luminescence intensity, which seems to be related to the increase of fraction of energy going into the excitation of oxygen.

A comparison of experimental results, obtained with noble gas free and helium (argon) mixtures $CO:O_2$ = 1:19 and $CO:O_2$:He(Ar) = 1:19:20 (**Fig. II.3.37**) at the same partial pressures of molecular gases (30 Torr) demonstrates that helium gives an opportunity to increase the SDO luminescence about twice at high (more than 600 J/(l·atm(O_2+CO)) input energy especially. Such an effect can be related to the enhancement of influence of diffusion and heat conductivity at helium mixture and spatial gradients smoothing. Dilution molecular gases by argon resulted in decreasing of SDO luminescence especially at low (less than 1 kJ/(l·atm(O_2+CO)) input energy. Therefore, the experiments demonstrated that the choice of gas mixture is an important factor influencing on the enhancement of SIE and SDO concentration.

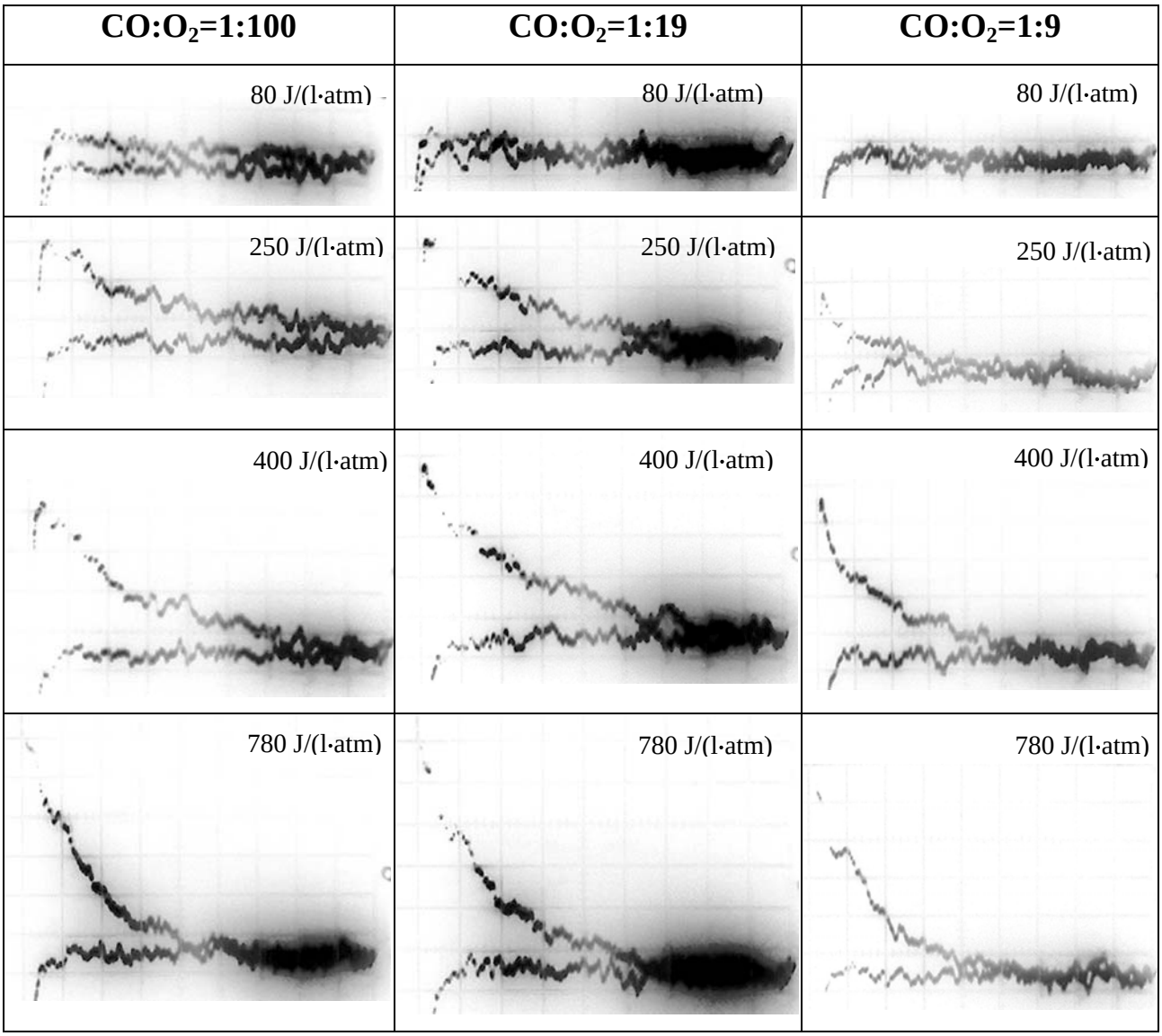

Fig. II.3.35. Time behavior of the SDO luminescence intensity at the wavelength of 1.27 μm for various gas mixtures at different SIE (shown in every picture), 60 Torr; 2 ms/div.

$CO:O_2$=1:100	$CO:O_2$=1:19	$CO:O_2$=1:9

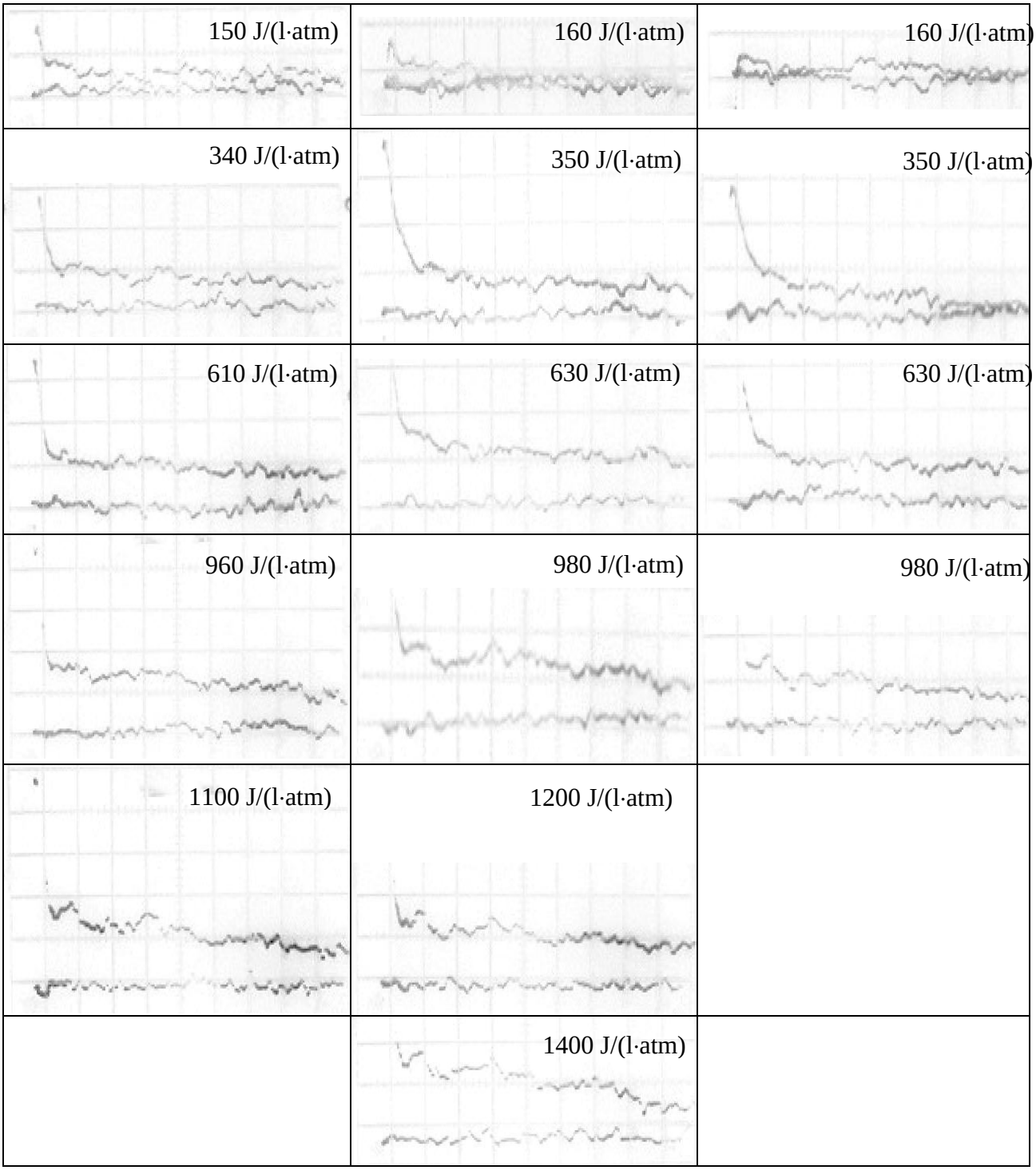

Fig. II.3.36. Time behavior of the SDO luminescence intensity at the wavelength of 1.27 μm for various gas mixtures at different SIE (shown in every pictures). 30 Torr; 500 μs/div.

$CO:O_2$=1:19	**$CO:O_2$:He=1:19:20**	**$CO:O_2$:Ar=1:19:20**

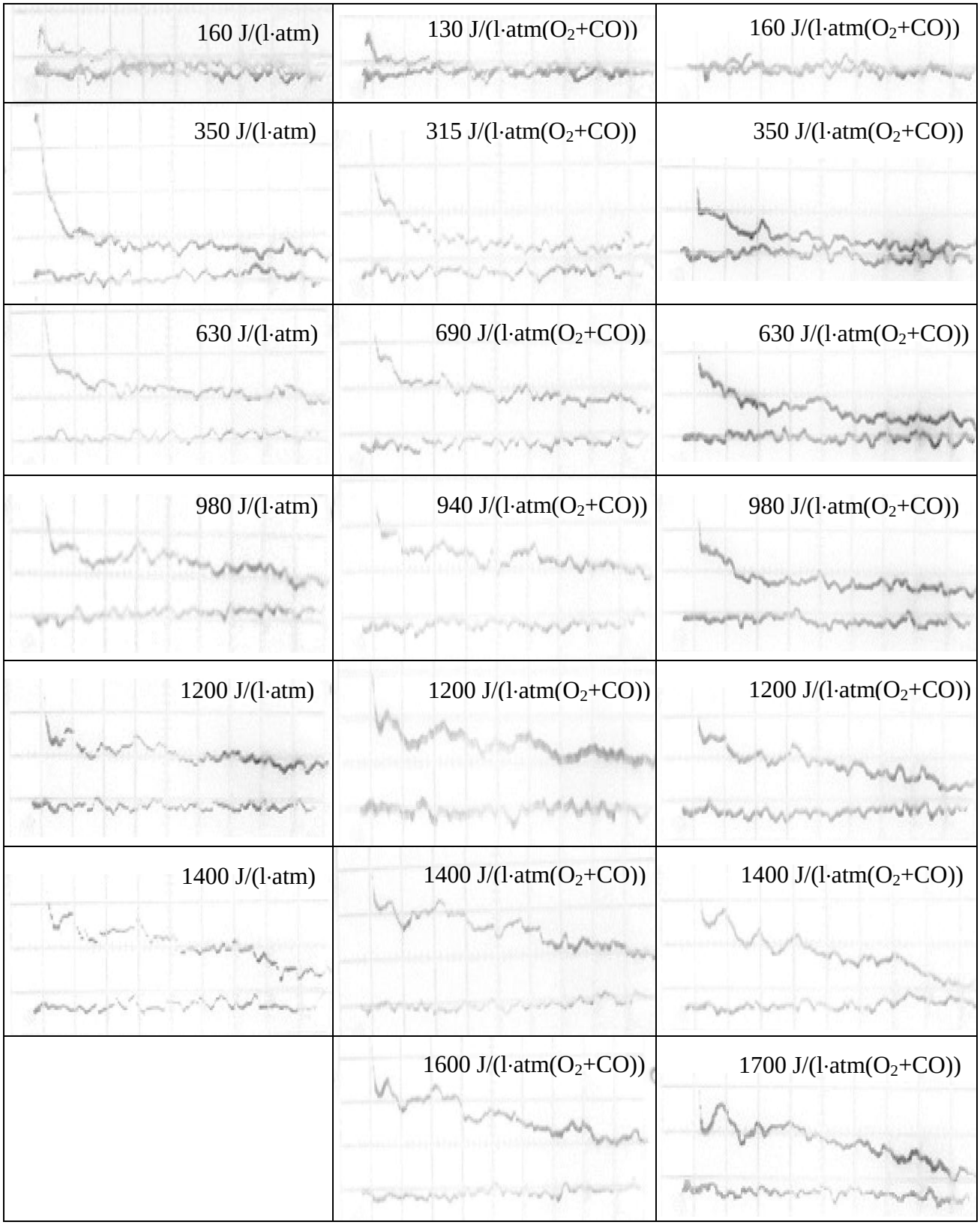

Fig. II.3.37. Time behavior of SDO luminescence intensity at 1.27 μm wavelength for various gas mixtures at different SIE calculated for partial pressure of molecular gases (shown in every pictures). Partial pressure of molecular gases ($CO+O_2$) was 30 Torr; partial pressure of noble gas (He or Ar) was 30 Torr. 500 μs/div.

SDO concentration was measured by the photodetectors calibrated by using a chemical generator of SDO. Optical scheme of the photodetector calibration procedure is presented in **Fig.II.3.38**. The chemical generator produced SDO of known concentration. Luminescence radiation of the SDO went through the monochromator and was measured by the photodetector. The same optical scheme of the measurement was employed with the EBSD facility producing the SDO and substituted for the chemical generator. Comparison of the measured electrical signals enabled us to determine the SDO concentration produced by the EBSD.

Experimental SDO yield Y_{SDO} was calculated for each time moment as $Y_{SDO}=n_{SDO}/n_{O2}$, where n_{SDO} and n_{O2} are concentrations of SDO and unexcited molecular oxygen, respectively. SDO concentration was measured by the procedure described above. Unexcited molecular oxygen concentration was evaluated from theoretical simulations for the experimental conditions including gas expansion from the diagnostic area. To find theory-independent experimental SDO yield, the measurements of gas temperature variations in time is necessary. The way to do this is an extraction of gas translation temperature for the mixture $CO:O_2$ by determining CO rotational temperature from measured CO small signal gain on several vibration-rotation transitions.

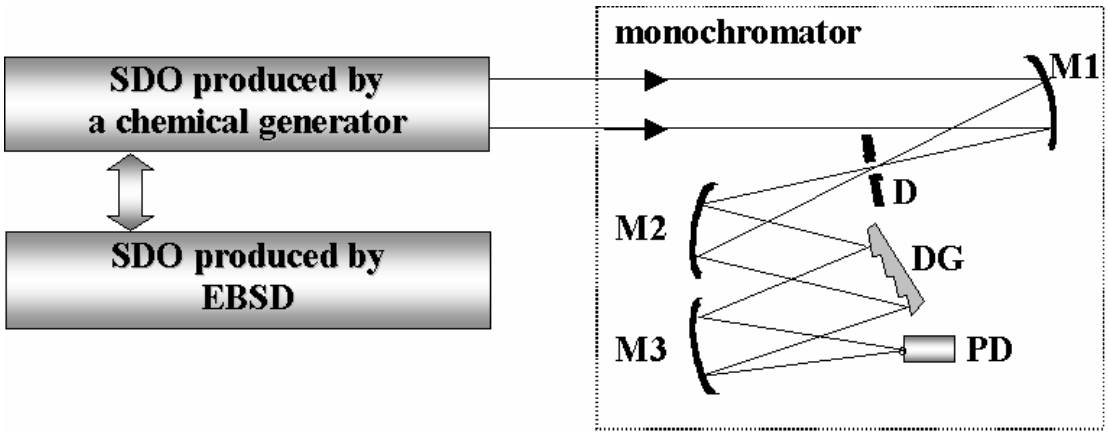

Fig. II.3.38. Optical scheme of photodetector calibration procedure. M1, M2, M3 – concave mirrors, D – diaphragm, DG – diffraction grating, PD – photodetector.

One of the most important parameters to design a powerful DOIL is a pressure of excited oxygen. Experimental study of EBSD in oxygen mixture at different gas pressure was carried out on the same (see above) EBSD facility. In the experiments gas pressure was varied from 15 to 60 Torr. To compare the experimental results obtained at different gas pressure the SDO concentration measured at 2-nd millisecond n_{SDO} was reduced to initial gas pressure n_{O2}^{start}. It should be pointed out that the reduced SDO concentration is not SDO yield because of gas temperature growth due to discharge heating was not taking into account. Dependencies of the reduced SDO concentration n_{SDO}/n_{O2}^{start} on specific input energy are presented in **Fig. II.3.39**. There was no great difference in the concentration measured at different gas pressure at low SIE (lower than 400 J/(l atm)). Further SIE increasing resulted in slow growing of the reduced concentration at low gas pressure (15 and 30 Torr) and saturation and even dropping of the concentration at high gas pressure (45, 60 Torr). It should be noted that the higher pressure is the higher SDO quenching rate, i.e. SDO luminescence signal pulse duration decreased with gas pressure increasing in the experiments.

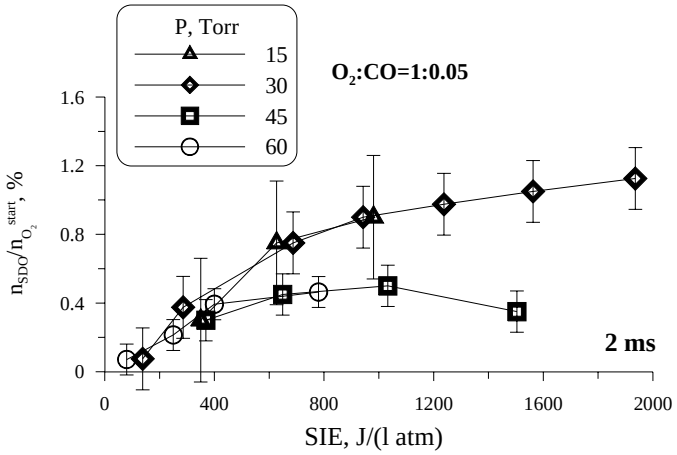

Fig. II.3.39. Dependences of the reduced SDO concentration n_{SDO}/n_{O2}^{start} on specific input energy (SIE). Gas mixture O_2:CO=1:0.05.

Gas mixture pressure increased by addition of helium to O_2:CO=1:0.05 gas mixture at partial pressure of 30 Torr. Dependence of SDO concentration on total gas pressure is presented in **Fig. II.3.40**. In the experiments total gas pressure increased from 30 Torr up to 210 Torr with E/N parameter decreasing from 11 down to 2 kV/(cm atm), respectively. The SDO concentration observed in the experiments was the same within the wide ranges of the parameters except one point obtained at gas pressure 210 Torr. This point is situated a little lower than other ones. In the experiments the characteristic time of pulsed SDO luminescence τ was measured. The time τ was determined as time interval from initial time moment being 2 ms (from EBSD beginning) to time (2 ms+τ) when the intensity of SDO luminescence decreased by the factor of e (~2.7). At variable gas pressure SIE growth resulted in the time τ decreasing (see **Fig. II.3.41**). It should be pointed out that the same behavior of SDO luminescence pulse duration at SIE increasing was observed for various experimental conditions (see, for instance, **Fig. II.3.35**).

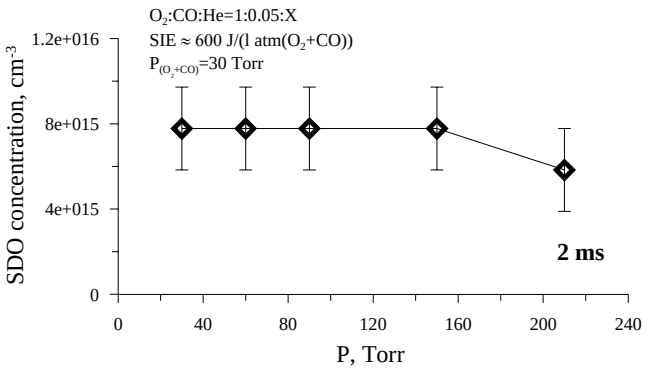

Fig. II.3.40. Dependence of SDO concentration on total gas pressure.

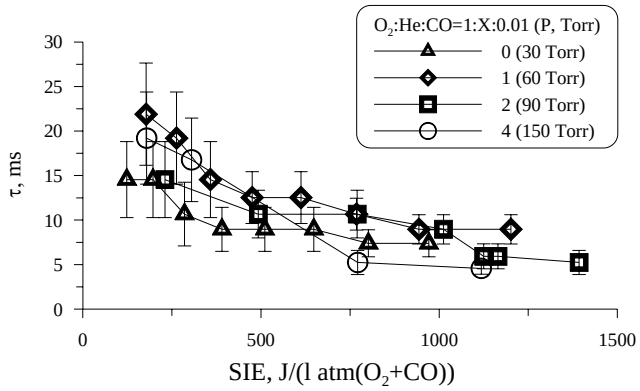

Fig. II.3.41. Dependences of characteristic time τ on SIE at different gas pressures.

In some papers (see, for instance, Vasil'eva, 1989; Blyabin, 1989; Fujii, 2003) it was noted that nitrogen addition to oxygen excited by self-sustained electric discharge resulted in SDO yield growth. The growth was explained by energy transfer from excited electronic states and vibration levels of nitrogen to oxygen. Experimental study of influence of nitrogen additions on SDO production in EBSD was carried out. Dependences of SDO concentration on nitrogen concentration in oxygen gas mixture at different SIE are presented in **Fig. II.3.42**. Nitrogen concentration increase resulted in SDO concentration decreasing that can be explained by growing of energy going to nitrogen excitation.

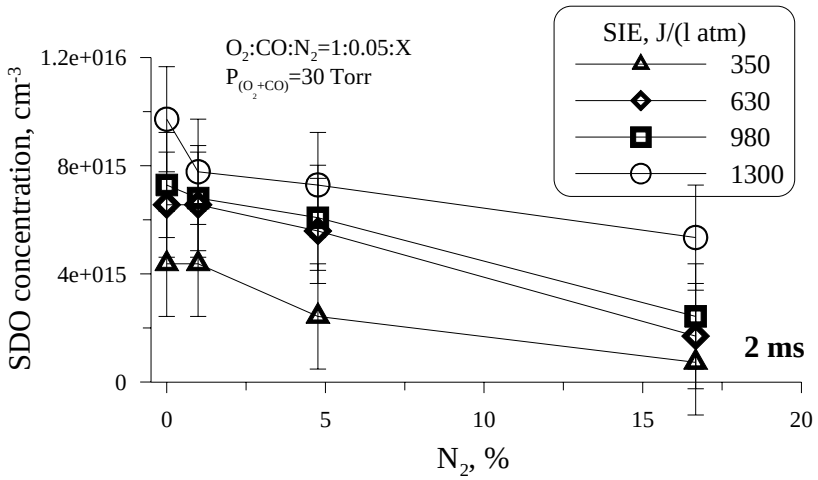

Fig. II.3.42. Dependences of SDO concentration on nitrogen percentage at different SIE

In other experiments binary gas mixture O_2:N_2 was used (**Fig. II.3.43**). Oxygen partial pressure was constant and equal to 9 Torr. Total gas mixture pressure changed from 18 to 45 Torr by N_2 addition. Growth of nitrogen concentration resulted in SDO concentration decreasing at SIE being constant. Perhaps, in the experiment the most part of input energy goes to vibrational excitation of nitrogen.

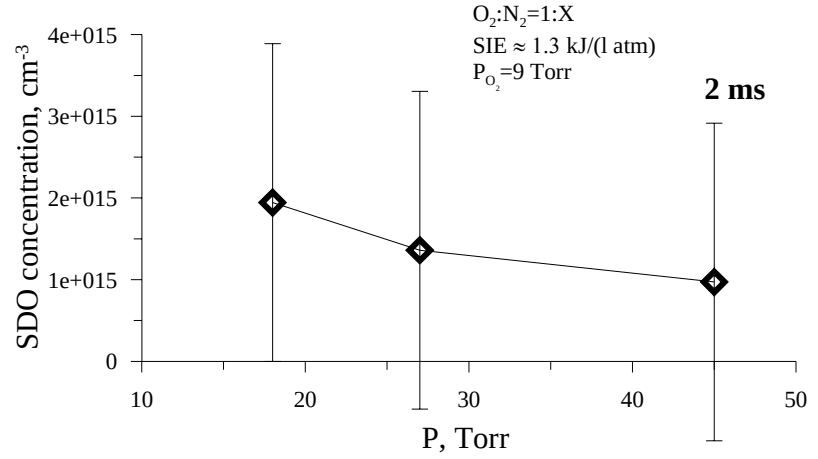

Fig. II.3.43. Dependence of SDO concentration on total gas pressure of binary gas mixture O_2:N_2. Partial pressure of O_2 was of 9 Torr.

Some gaseous admixtures (CO_2 and N_2O) were tested to exhibit enhancement of SDO production in EBSD (**Fig.II.3.44**). However, the gaseous admixtures resulted in SDO concentration decreasing. Therefore these gases are not perspective for enhancement of SDO production in EBSD.

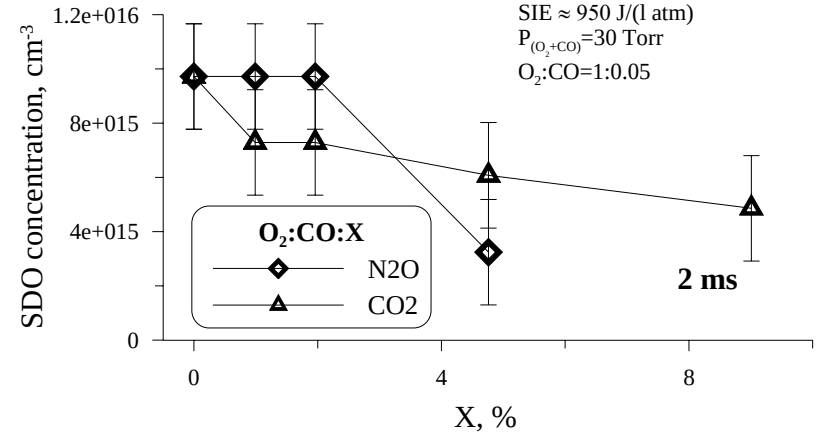

Fig. II.3.44. Dependences of SDO concentration on gaseous admixture concentration.

Comparison with experimental data on SDO yield.

(*Subtask 2B.3*)

Earlier developed kinetic model described above was applied to modeling experiments with SDO production in the EBSD. The model includes solving dynamic balance equations for populations of electronic and vibrational excited states, radical, electron and positive/negative ion number densities. Rate constants for electron-initiated processes were calculated by solving electron Boltzmann equation for the electron energy distribution function (EEDF). Quasi-steady Boltzmann equation was solved in two-term approximation, and the EEDF was a symmetric part of a whole electron energy distribution. Elastic and inelastic electron-molecule collisions including excited molecules and electron-electron collisions were taken into account. In parallel, thermal balance and electric circuit equations were solved. An effect of gas expansion after heat release was described using an interpolation between constant-density and constant-pressure regimes. Transition between these regimes occurs on times of acoustic wave propagation across the discharge width. Time history of electron-beam current was taken from experimental measurements. Amplitude of the e-beam current was not measured regularly and was fit to achieve an experimentally measured voltage remaining on the capacity after the discharge current termination. This approach provides equality of calculated and measured input energy.

In mixtures with O_2:CO diluted by rare gases He or Ar, excitation of electronic levels of He and Ar by fast electrons and plasma electrons, as well, was taken into account. Besides, quenching of these He and Ar levels by molecular oxygen was included into the model (Zhiglinskii, 1994). Charge transfer processes from ions of rare gases to oxygen were taken into account, too (Virin, 1979). The electron scattering cross sections set was modified, as well: cross section for electron impact induced transition $O_2(a^1\Delta_g)\rightarrow O_2(b^1\Sigma^+_g)$ was increased 12 times according to data in only experimental evaluation for this process (Hall and Trajmar, 1975).

A comparison between calculated and measured temporal behavior of SDO concentration and yield produced in the EBSD for different ratios O_2:CO in gas mixture is presented in **Fig.II.3.45**. The experimental errors in **Figs.II.3.45- II.3.48** are determined by photodetector noise. It should be pointed out that the experimentally observed SDO signal was detected ~0.3-1.5 ms later than the EBSD pump pulse (see **Figs.II.3.45- II.3.48**). This is related to the fact that a strong luminescence not belonging to the SDO was observed during the above interval depending on experimental conditions and photodetector response time (see details above). A probable reason for oscillations seen in graphs is gas dynamic effect. There was no great difference in measured SDO concentration and yield for gas mixture with low CO contents (1-5%). For gas mixture with ratio O_2:CO=1:0.1 the SDO concentration produced in EBSD was a little lower and SDO deactivation was faster than for gas mixtures with low CO contents. It should be pointed out that experimental SDO deactivation rate was higher than calculated one for all cases presented below.

For various gas mixtures SDO concentration and yield grow with specific input energy (SIE) increase. Comparison of the experimental and theoretically calculated results obtained for gas mixture O_2:CO = 1:0.05 at different SIE values is presented in **Fig.II.3.46**. The SDO yield increased from ~1.7% up to ~3.2% in the experiments and from ~3.7% up to 5.7% in the calculations with SIE growing from 600 to 1300 J/(l atm). A comparison of the experiment and theory with noble gas adding (partial pressure oxygen and carbon monoxide (O_2+CO) was constant and equal to 30 Torr) is presented in **Fig.II.3.47**. In the figures the SIE is reduced to partial pressure of molecular gases (O_2+CO). Dilution of O_2:CO gas mixture by helium (O_2:He:CO=1:1:0.05) resulted in a little SDO yield increasing. An addition of argon instead of helium resulted in approximately the same SDO yield value as without noble gas addition and in growing rate of SDO deactivation. So helium addition looks more beneficial than argon at the same SIE from the standpoint of higher SDO yield.

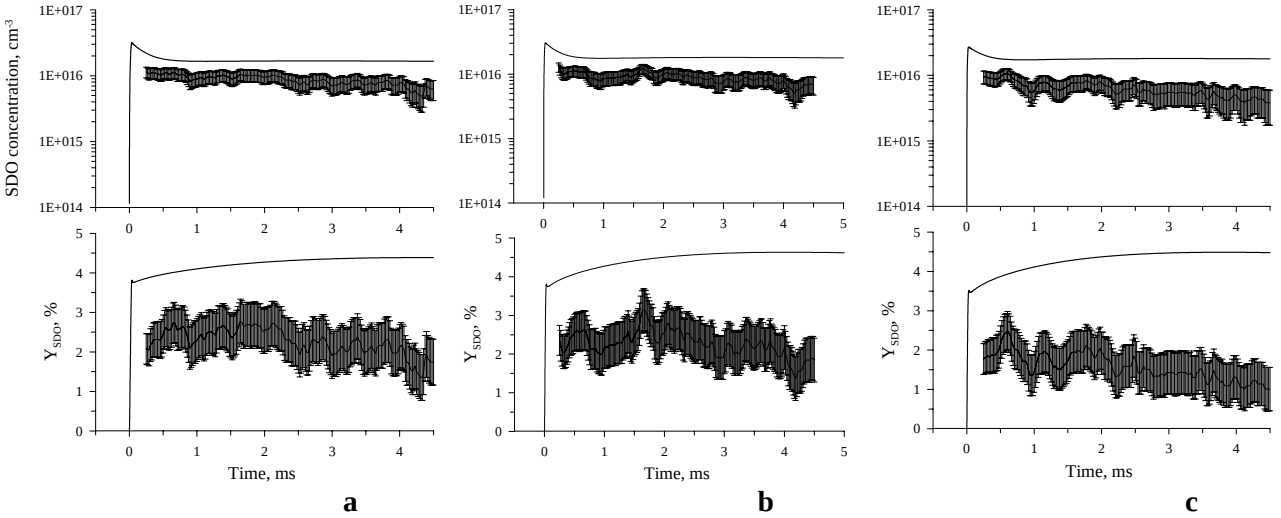

Fig.II.3.45. Temporal behavior of SDO concentration and yield Y_{SDO} produced in the EBSD (calculation and measurement) for different ratios O_2:CO: **a** - 1:0.01, **b** – 1:0.05, and **c** – 1:0.1. P= 30 Torr. SIE ~1 kJ/(l atm).

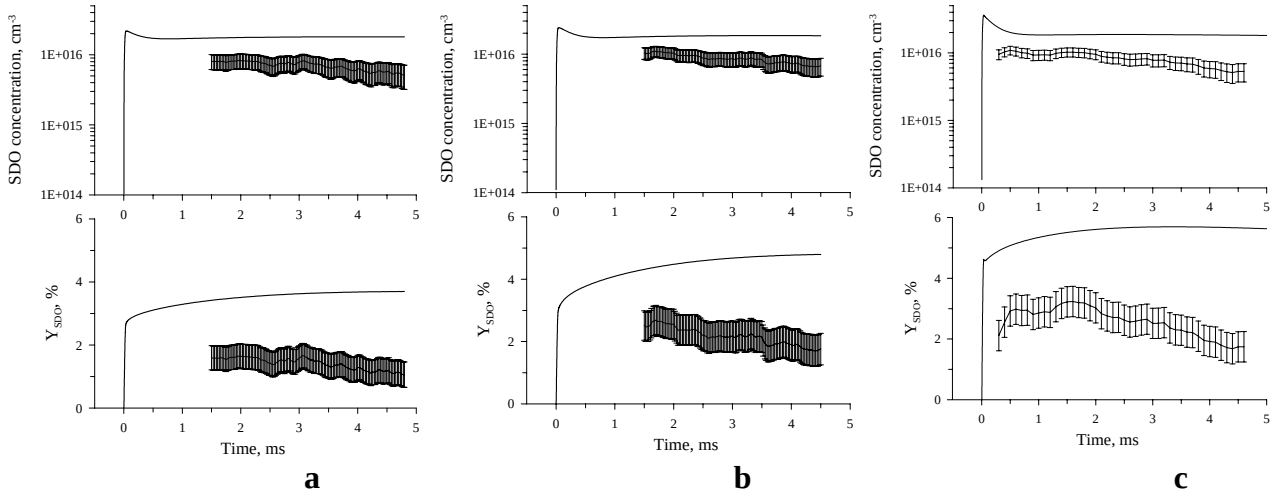

Fig.II.3.46. Temporal behavior of SDO concentration and yield Y_{SDO} produced in the EBSD (calculation and measurement) for different SIE values: **a**–600, **b**–950, and **c**–1300 J/(l atm). O_2:CO=1:0.05. P=30 Torr.

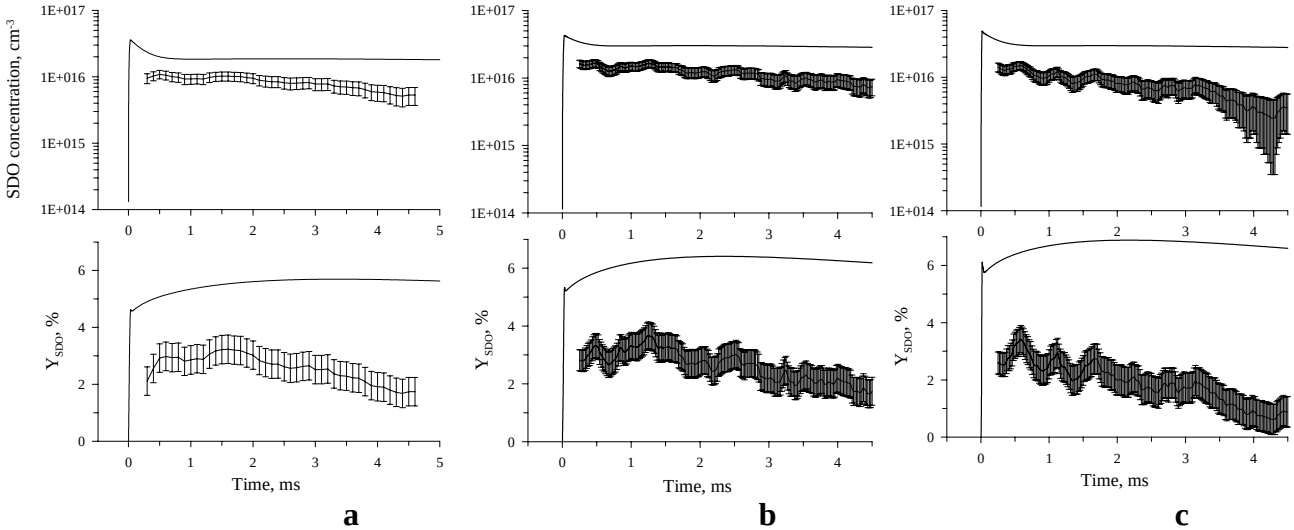

Fig.II.3.47. Temporal behavior of SDO concentration and yield Y_{SDO} produced in the EBSD (calculation and measurement) for different gas mixtures. **a** - O_2:CO=1:0.05, **b** – O_2:He:CO=1:1:0.05, and **c** – O_2:Ar:CO=1:1:0.05 at partial (O_2+CO) pressure 30 Torr. P=60 Torr. SIE ~1.3 kJ/(l atm(O_2+CO))

Temporal behaviors of SDO concentration and yield produced in the EBSD (calculation and measurement) for different helium contents are presented in **Fig. II.3.48**. In the experiments partial pressure of molecular gases (O_2+CO) was 30 Torr. SIE relative to the partial pressure of the molecular gases was constant. In the experiments SDO concentration was almost independent of helium content. However, the SDO yield diminishes with helium content. This is explained by reduced gas heating for helium-rich mixtures and not so strong gas rarefaction. So, experimental SDO yield decreased with helium contents increasing. It should be noted that the theoretically predicted maximum of SDO yield is practically independent of He content moving to shorter times with He content increase.

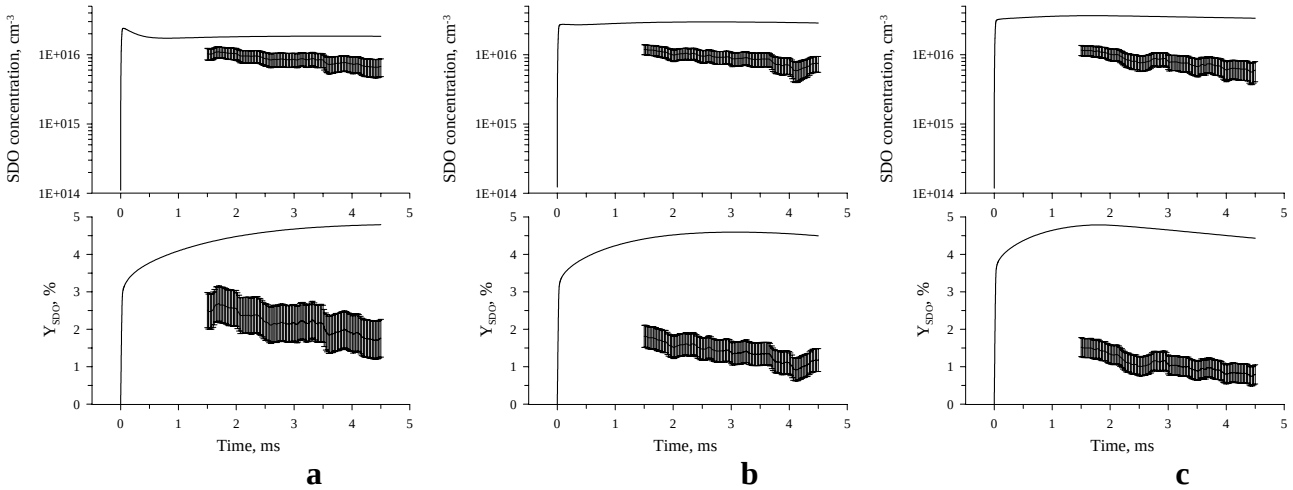

Fig.II.3.48. Temporal behavior of SDO concentration and yield Y_{SDO} produced in EBSD (calculation and measurement) for different gas mixture: **a** - O_2:CO=1:0.05 (30 Torr), **b** – O_2:He:CO=1:2:0.05 (90 Torr), and **c** – O_2:He:CO=1:6:0.05 (210 Torr) at partial (O_2+CO) pressure 30 Torr. SIE ~1 kJ/(l atm(O_2+CO)).

The maximum SIE is as twice higher for argon mixtures as for helium ones (see above). Just because of this reason the further SDO concentration measurements were made for oxygen gas mixture O_2:Ar:CO=1:1:0.05 at total gas pressure 30 Torr, E/N=3.5–7 kV/(cm atm) and SIE up to ~3.0 kJ/(l atm(O_2+CO)). **Fig.II.3.49** demonstrates the experimental and theoretical dependencies of the SDO concentration upon SIE. One can see that the theoretical prediction is 2.5 times higher than the experimental data. The theoretical and experimental dependencies of the SDO yield and efficiency on the SIE are presented in **Fig.II.3.50** and **Fig.II.3.51**, respectively. The experimental SDO yield obtained with taking into account theoretically calculated gas temperature rise (**Fig.II.3.52**) and gas mixture rarefaction because of gas expansion comes up to ~7%, whereas the theoretical one riches 17.5%. It should be pointed out that the experimental value of the SDO yield is obtained without taking into consideration the concentrations of atomic oxygen, molecular oxygen in $O_2(b^1\Sigma_g^+)$ state, ozone and other species formed in the EBSD (**Fig.II.3.50**). We believe that the experimental value of the SDO yield presented in this report is the lower limit of the real SDO yield, i.e. the real SDO yield is to be higher. The concentration of atomic oxygen in the ground state is fast growing with the SIE rise coming to the value close to one for the SDO at the SIE of ~6.0 kJ/(l atm(O_2+CO))as follows from the theoretical calculations (**Fig.II.3.50**). The tremendous rise of the atomic oxygen concentration results in the decrease of the SDO production efficiency which is ~20% at low SIE of 0.5 kJ/(l atm(O_2+CO)), and drops down to ~6% at ~3.0 kJ/(l atm(O_2+CO)), and to 2% at higher SIE of ~6.0 kJ/(l atm(O_2+CO)), whereas the efficiency of atomic oxygen production is monotonously coming up (**Fig.II.3.51**).

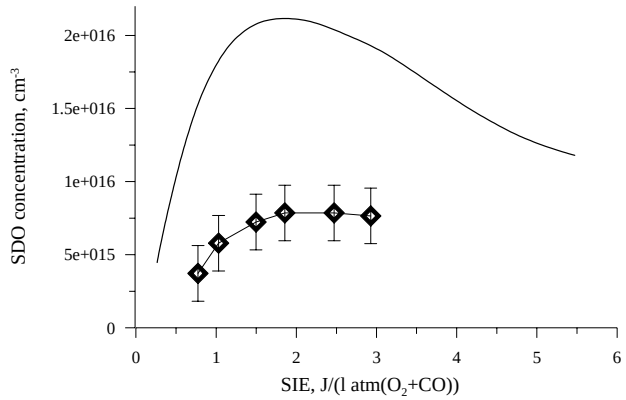

Fig.II.3.49. Dependence of SDO concentration on SIE. Experimental points and theoretical curve. O_2:Ar:CO=1:1:0.05, 30 Torr

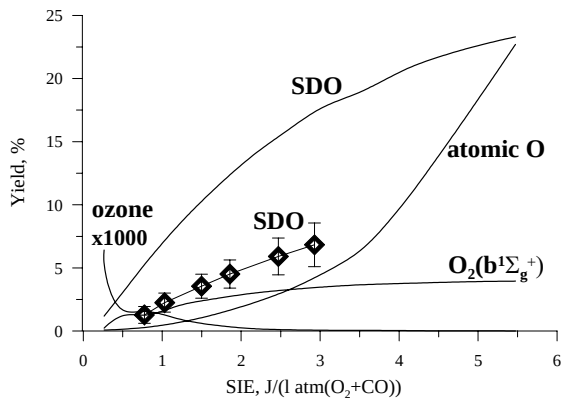

Fig.II.3.50. Dependence of different species produced in electric discharge on SIE. O_2:Ar:CO=1:1:0.05, 30 Torr

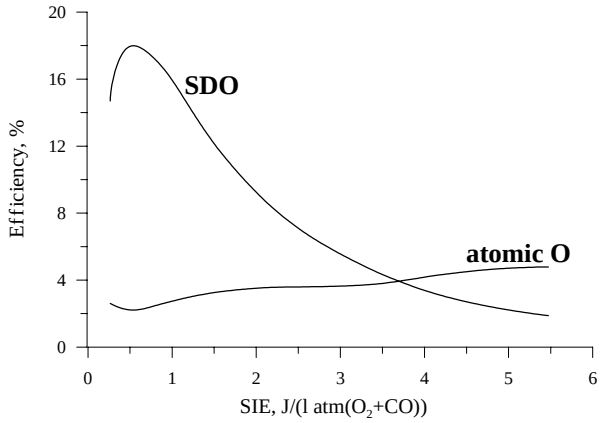

Fig.II.3.51. Dependences of predicted production efficiency of SDO and atomic O on SIE. O_2:Ar:CO=1:1:0.05, 30 Torr

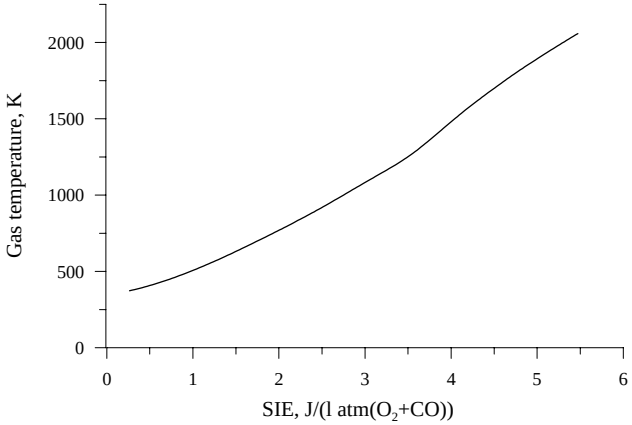

Fig.II.3.52. Dependence of predicted gas temperature on SIE. O_2:Ar:CO=1:1:0.05, 30 Torr

Recently, the work of Rakhimov's group was published (Vasilijeva, 2004) where a careful study was made about efficiency of $O_2(a^1\Delta_g)$ production in EBSD at low values of SIE when gas heating effects can be neglected. **Fig. II.3.53** demonstrates dependence of $O_2(a^1\Delta_g)$ concentration on the SIE in pure oxygen experimentally measured for two values of E/N parameter: ○ - E/N = 10.7 Td, ▲ – 20.3 Td. The reduced electric field strength was supported constant in the experiments. In the same figure results of theoretical simulations are plotted made by us (solid lines) and by the authors (Vasilijeva, 2004) (dashed lines). It is seen that near maximum SDO production efficiency both theories agree each with other and with the experiment. At higher E/N our model predicts higher SDO yield than the Rakhimov's model, and experimental data lie in between two theoretical curves. Concerning data on SDO production in Ar diluted mixture shown in Fig. **II.3.54,** our model (solid lines) gives notably higher (several times) values of $O_2(a^1\Delta_g)$ yield than observed experimentally. Authors of (Vasilijeva, 2004) noted that similar discrepancy took place when comparing predictions of their model with their experiments, but did not provide such a comparison.

Authors (Vasilijeva, 2004) explain this discrepancy by discharge instability. It is stated that as a result of this discharge instability plasma regions are formed with essentially different values of E/N. It is expected that E/N values in each region are far from optimum value for SDO production. Therefore, the $O_2(a^1\Delta_g)$ yield is notably lower in comparison with uniform discharge.

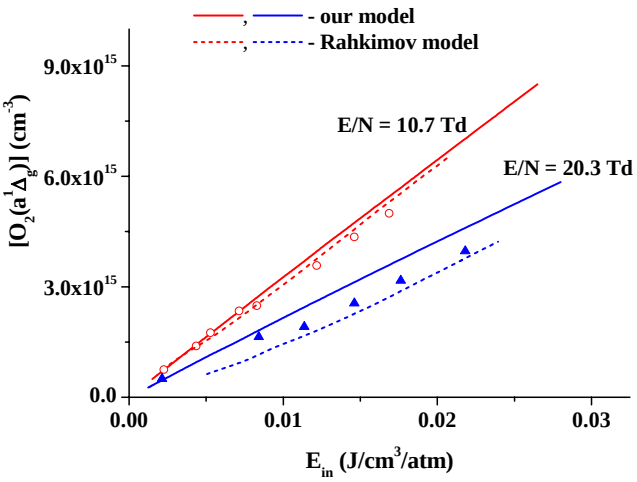

Рис.II.3.53. Dependence of $O_2(a^1\Delta_g)$ concentration on the SIE in pure oxygen. Markers - experiment (Vasilijeva, 2004). P = 100 Torr, lines – theory.

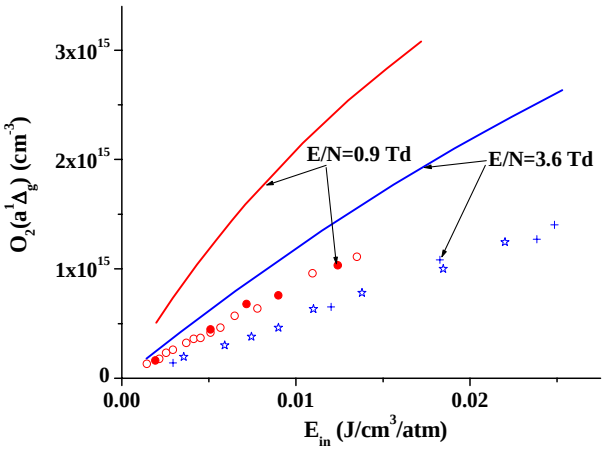

Рис.II.3.54. Dependence of $O_2(a^1\Delta_g)$ concentration on the SIE. Markers - experiment (Vasilijeva, 2004). P = 100 Torr, lines – our theory. P = 100 Torr, O_2:Ar=1:99.

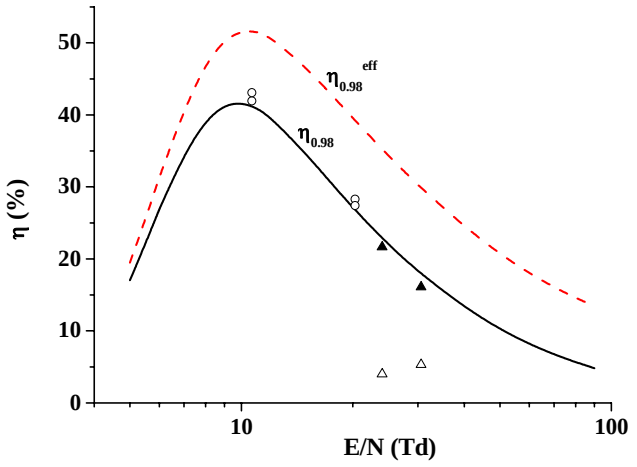

Рис.II.3.55. Dependence of $O_2(a^1\Delta_g)$ production efficiency on E/N in pure O_2. Solid line is for direct excitation, dashed line is for additionally incorporated cascade processes. ○ – experiment (Vasilijeva, 2004); Δ – our experiment; ▲ – our modeling for conditions of our experiment.

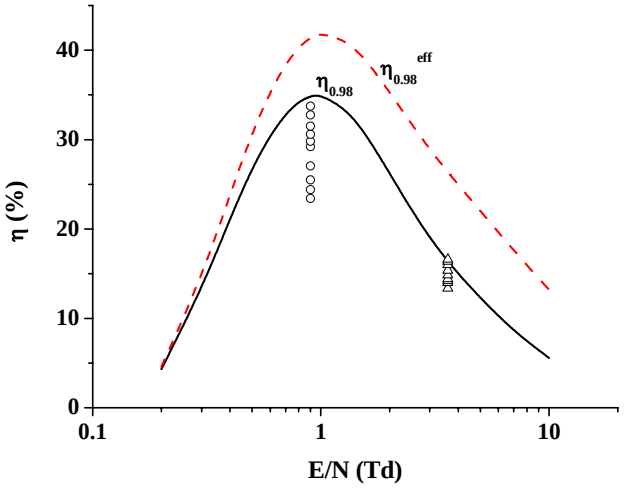

Рис.II.3.56. Dependence of $O_2(a^1\Delta_g)$ production efficiency on E/N. Solid and dashed lines show results of Boltzmann equation analysis. ○, Δ – full kinetic model. O_2:Ar=1:99.

It is of interest to evaluate $O_2(a^1\Delta_g)$ production efficiency. Such an analysis was made in (Ionin, 2003) for conditions of non-self-sustained discharge. This analysis is reduced to electron energy balance calculated from solving electron Boltzmann equation for electron energy distribution function. An effective energy fraction spent to excitation of $O_2(a^1\Delta_g)$ including cascade processes over higher electronic levels. **Fig. II.3.55** shows direct excitation efficiency (solid line) and the effective energy fraction spent for production of $O_2(a^1\Delta_g)$ (dashed line) as functions of E/N. Open circles show experimentally measured (Vasilijeva, 2004) efficiency found from data in **Fig. II.3.53.** Two circles at a fixed E/N value correspond to minimum (upper) and maximum (lower) SIE, respectively. Our theoretical predictions shown by lines practically coincide with theoretical data

from (Vasilijeva, 2004). For comparison with published data (Vasilijeva, 2004) we performed special experiments for pure oxygen. In our experiments E/N varies in time due to capacity discharging. Discharge current and E/N were theoretically evaluated using our full kinetic model. For comparison purposes, E/N was taken equal to theoretically calculated E/N at the moment of peak discharge current. **Fig. II.3.55** shows results of measurements (open triangles) and numerical simulations for conditions of the experiments with the full kinetic model (filled triangles). Different values of E/N parameter were realized at different capacity voltages. It is seen from **Fig. II.3.55** that measured in (Vasilijeva, 2004) and calculated theoretically $O_2(a^1\Delta_g)$ production efficiency are close to that of direct SDO excitation. Our measurements gave notably lower efficiency (open triangles). One of reasons of this effect could be discharge instability. Besides, variation of fast electrons energy in time and space can produce additional non-uniformity of plasma.

Fig. II.3.56 compares $O_2(a^1\Delta_g)$ production efficiency for the mixture O_2:Ar=1:99 calculated from Boltzmann equation (solid and dashed lines) and from the full kinetic model (markers). Starting from about direct excitation efficiency at fixed E/N the real efficiency lowers with the SIE growth according to **Fig. II.3.54**.

One of important parameters of electric discharge SDO generator is the duration of exciting pulse discharge. **Figs. II.3.57** and **II.3.58** show results of theoretical calculations of $O_2(a^1\Delta_g)$ yield and its efficiency as functions of discharge pulse duration at a fixed value of the SIE for two values of 25 and 100 J/l/atm. Maximum value of SIE was taken from (Ionin, 2003). In contrast to our experimental conditions, in these numerical simulations the discharge voltage was kept constant. Its magnitude was taken to that providing maximum of $O_2(a^1\Delta_g)$ production rate at the initial moment. The e-beam current was taken of a rectangular shape with variable duration τ_{beam}. Amplitude of e-beam current was fit to achieve the prescribed value of SIE. Our kinetic model predicts that for described conditions $O_2(a^1\Delta_g)$ yield and efficiency weakly depend on discharge pulse duration in the range 5 μs – 50 ms.

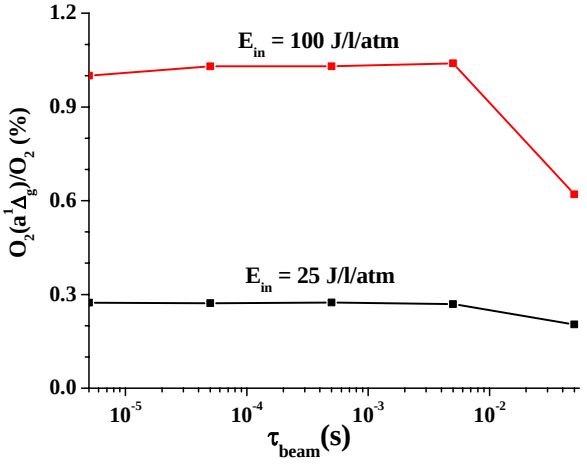

Рис.II.3.57. $O_2(a^1\Delta_g)$ yield vs discharge pulse duration at fixed SIE in pure oxygen.

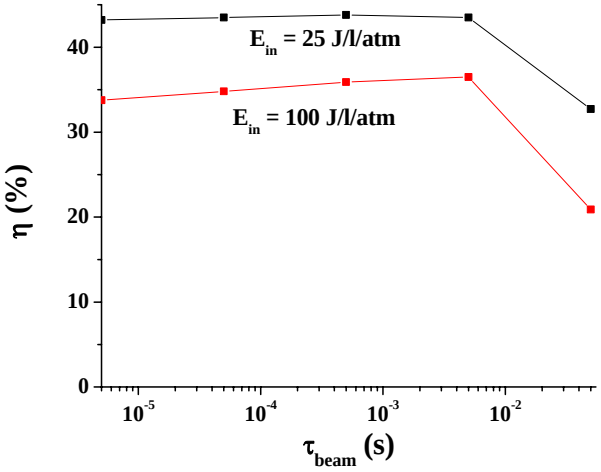

Рис.II.3.58. $O_2(a^1\Delta_g)$ production efficiency vs discharge pulse duration at fixed SIE in pure oxygen.

Small signal gain measurements on different carbon monoxide ro-vibrational transitions for oxygen gas mixtures with carbon monoxide additives.
(*Subtasks 3.1*)

It was mentioned above that the measured SDO density is lower than theoretically predicted one, and decay rate experimentally observed is somewhat faster than that of in the theory. One of the possible reasons for such discrepancies may be connected with difference between calculated and real gas temperature after EBSD excitation. Indeed, there is a serious problem to measure gas temperature under pulse EBSD. In order to resolve similar problem of gas temperature measurement inside CO laser active medium we developed in Part I.1 the approach of gas temperature reconstruction on the basis of experimental data on small signal gain (SSG) time behavior for several CO laser spectral lines. Taking into account the fact that the gas mixture, which is used for SDO production under EBSD, contains CO molecules as an additive we plan to apply the developed approach for gas temperature measurement in oxygen-rich gas mixtures. For such mixtures the SSG time behavior should be measured with high accuracy on different CO vibration-rotational transitions. As a first step of this study the SSG temporal characteristics were measured for different vibrational bands.

The SSG measurement was performed for the oxygen-rich gas mixture $CO:O_2$=1:20 excited by EBSD Q_{in}=190 J/(l·Amagat) at the initial temperature T=110 K (**Fig.II.3.59a**). The cryogenically cooled frequency selective DC discharge CW CO laser was used in the experiments as a probe laser. The schematic and technique of these experiments were described elsewhere in Part I.1. This experiment demonstrated that the SSG time behavior for high ro-vibrational transitions was quite different in comparison with SSG time behavior on the same transitions for the nitrogen gas mixture: $CO:N_2$=1:20 (**Fig.II.3.59b**).

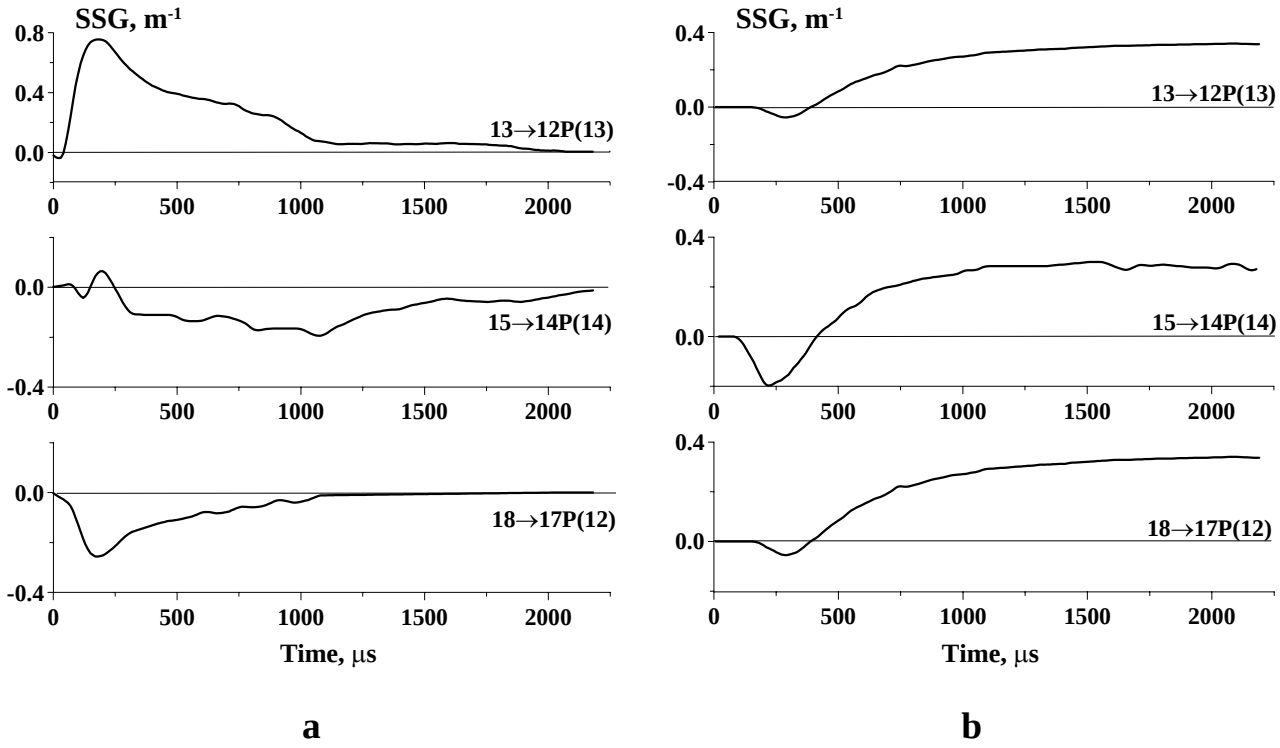

Fig.II.3.59. SSG time behavior for gas mixtures $CO:O_2$=1:20 (**a**) and $CO:N_2$=1:20 (**b**).
Gas density N=0.04 Amagat, T=110 K, Q_{in}=190 J/(l·Amagat).

It should be noted that the maximum value SSG in vibrational band 13→12 for the oxygen-rich gas mixture ~ 0.75 m^{-1} was twice higher than that of for nitrogen gas mixture ~ 0.35 m^{-1}. The SSG achieved its maximum value in the oxygen-rich gas mixture at the time moment being of ~200 μs that was approximately an order of magnitude shorter than corresponding value (~2000 μs) in nitrogen gas mixture. For higher ro-vibrational transitions (V>15) the SSG value in oxygen-rich mixture was transformed from positive (amplification) into the negative one (absorption). Besides that one can see that the lifetime of amplification/absorption in the oxygen-rich gas mixture decreases when vibrational number V increases. Taking into account that ro-vibrational transitions of CO molecule belonging to vibrational band 24→23 overlap with the 1→0 vibrational band transition of oxygen molecule, one can assume that CO molecules excited up to high vibrational levels could be involved into the vibrational energy exchange with O_2 molecules. As a result of such quasi-resonant VV-exchange between CO and O_2 molecules at V>15 the population of CO molecules at lower levels V<15 rises dramatically. This is the reason why maximum SSG for 13→12 transition was twice higher in the oxygen-rich gas mixture than that of in the nitrogen gas mixture.

Earlier in (Basov, 2002) the like SSG increase was observed for CO transitions at V=34÷36 as a result of asymmetric VV-exchange between CO and N_2 molecules. The analysis of these experimental results allowed us to choose vibrational bands with high amplification (positive SSG) and high absorption (negative SSG) in order to apply the approach of gas temperature reconstruction in oxygen-rich gas mixtures.

Measurement of gas temperature time behavior in oxygen gas mixtures with carbon monoxide additives using SSG data.

(*Subtasks 3.2*)

It was shown above that in order to measure SDO density the real gas temperature after EBSD excitation should be measured. The method of multiline laser probing was developed for the similar problem of gas temperature measurement inside CO laser active medium in Part I.1. This approach consists in gas temperature reconstruction from experimental data on small signal gain (SSG) measurement for several CO laser spectral lines due to the fact that the gas temperature is equal to the rotational temperature of gas molecules. Taking into account that gas mixture, which is used for SDO production under EBSD, contains CO molecules as an additive stabilizing EBSD in oxygen, we applied the developed approach for gas temperature measurement in oxygen-rich gas mixtures. The SSG (positive or negative) time behavior was measured with high accuracy for different CO ro-vibrational transitions. The cryogenically cooled frequency selective DC discharge CW CO laser was used in these experiments as a probe laser. The schematic and technique of these experiments were described earlier in Part I.1.

For gas mixtures CO:O_2 and CO:He we selected ten spectral lines from vibrational band 10→9 P(7÷16). Our analysis showed that for only one of selected lines 10→9 P(9) the SSG value can be disturbed by absorption on adjacent spectral line 13→12 R(13) because of small difference between centers of these lines $\Delta\nu \approx 0.01\ cm^{-1}$. Nevertheless, the result of gas temperature reconstruction practically did not depend on taking into consideration the SSG measurement on 10→9 P(9) spectral line. The SSG measurement was performed for the oxygen-rich gas mixture CO:O_2=1:19 (gas density 0.06 Amagat) excited by EBSD Q_{in}=130 J/(l·Amagat) and for the helium gas mixture CO:He=1:4 (gas density 0.12 Amagat) Q_{in}=100 J/(l·Amagat) at the initial gas temperature T=100 K (**Fig.II.3.60a**).

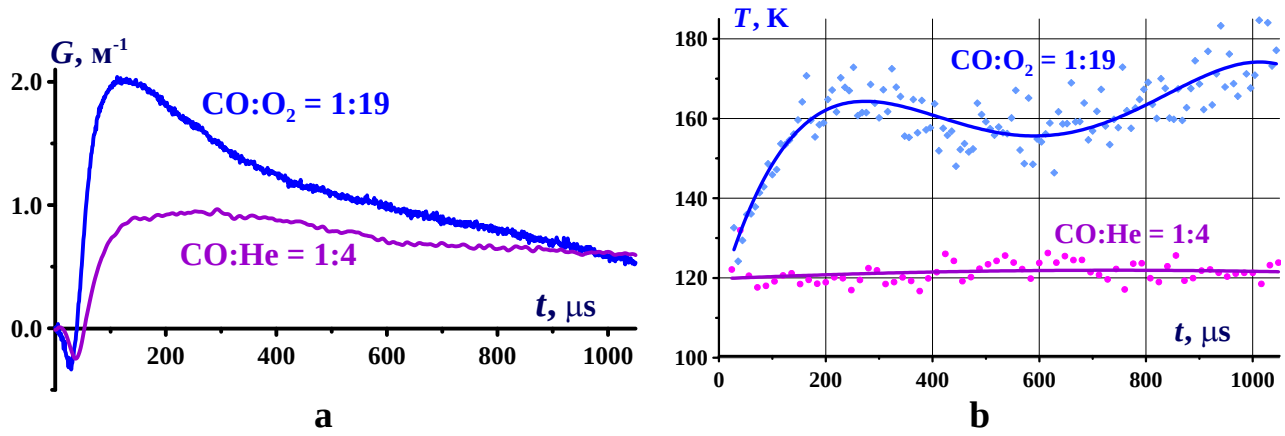

Fig.II.3.60. (**a**) - SSG time behavior $G(t)$ for ro-vibrational transition 10→9 P(10) in gas mixture $CO:O_2$=1:19 (0.06 Amagat) at the specific input energy Q_{in}=130 J/(l Amagat) and in gas mixture CO:He=1:4 (0.12 Amagat) at Q_{in}=100 J/(l·Amagat). The initial gas temperature T=100 K. (**b**) – Reconstructed time behavior of gas temperature in active medium excited by EBSD.

EBSD pulse duration was about 40 μs. For each spectral line the value of SSG $\alpha^{Exp}(t)$ was measured several (9÷12) times in order to evaluate standard deviation $\sigma^{Exp}(t)$. Gas temperature $T(t)$ and vibrational populations $\mathbf{N}(t)$ were reconstructed through minimization of residual function

$$F(T,\mathbf{N}) = \sum_{V,J}\left(\frac{\alpha^{Theory}_{V,J}(T,N_V,N_{V+1}) - \alpha^{Exp}_{V,J}(t)}{\sigma^{Exp}_{V,J}(t)}\right)^2,$$

where $\mathbf{N}$ is a matrix of populations of lower N_V and upper N_{V+1} vibrational levels, α^{Theory} – theoretically calculated SSG, $\alpha^{Exp}(t)$ – value of measured SSG for time moment t, $\sigma^{Exp}(t)$ - standard deviation of experimental data. The reconstructed time behavior of gas temperature is presented in **Fig.II.3.60b** for oxygen and helium gas mixtures. In order to evaluate an error of such reconstruction we calculated a set of temperatures (25 values) for random SSG values $\alpha_{V,J}$ having the normal distribution with mean $\alpha^{Exp}_{V,J}$ and standard deviation $\sigma^{Exp}_{V,J}$. The mean values of temperature are presented in **Fig.II.3.60b**. The standard error of mean values was ~7 K for the helium mixture and ~9 K for the oxygen mixture. During the first ~200 μs after EBSD excitation the gas temperature in oxygen mixture grew from local value 117±3 K to 160±10 K. In the helium gas mixture the temperature grew from 107±4 K to 122±7 K. Our analysis showed that the fraction of EBSD energy going into gas heating was 35±10% for the oxygen mixture and 14±4% for the helium mixture.

Only absorption (negative SSG) of CW probe CO laser radiation was observed at room gas temperature (**Fig.II.3.61a**). For the gas mixture $CO:O_2$=1:19 the SSG time behavior on ten ro-vibrational transitions: 9→8 P(9, 11, 15); 10→9 P(10, 11, 13, 15); 11→10 P(10, 12, 16) was measured. At the experiment the following systematic error was detected: an absolute value of absorption $\alpha^{Exp}(t>200\mu s)$ slowly fell down from pulse to pulse (the maximum reduction being ~0.006 m^{-1} per pulse was observed for t=400μs). This effect is apparently connected with some quenching of vibrational excitation of CO molecules through energy exchange with CO_2 molecules and more rapid VT relaxation of CO_2, which is produced under EBSD in oxygen rich $CO:O_2$ mixture due to oxidation ($2CO+O_2 \rightarrow 2CO_2$). In order to remove this systematic error we found that the correction function $f(t)$ was the same for all selected transitions and reduced all measured values of SSG to the first EBSD pulse. Gas temperature time history reconstructed by using these experimental data is presented in (**Fig.II.3.61b**). The gas temperature grew during 0.15 ms from

initial value ~300 K to (415±30) K being in a good accordance with calculated gas temperature 420 K. The fraction of specific input energy going into gas heating during pulsed EBSD (Joule heating) was ~35% .

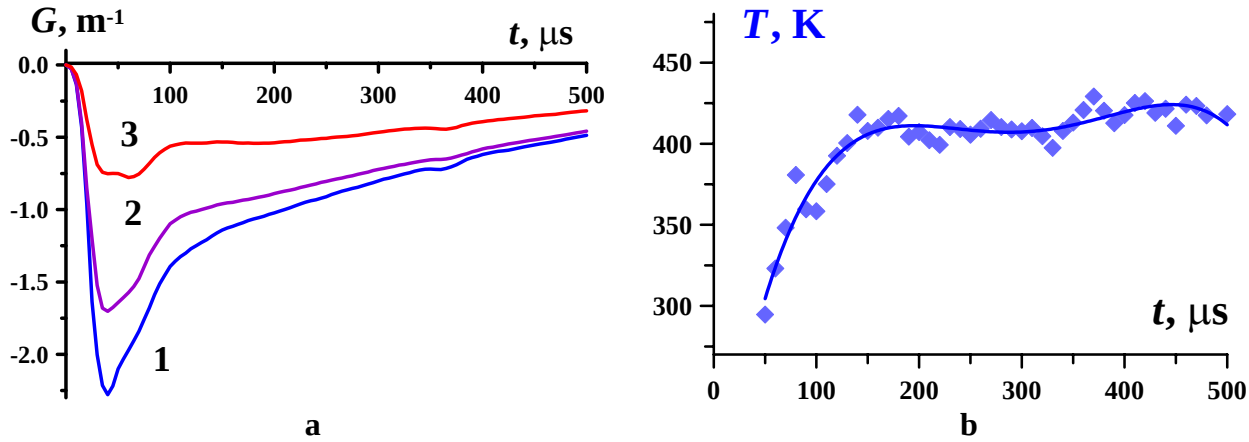

Fig.II.3.61. (**a**) - Absorption (negative SSG) time behavior $G(t)$ on three ro-vibrational transitions belonging one vibrational band 9→8 in gas mixture $CO:O_2$=1:19, gas pressure 0.04 atm, specific input energy Q_{in}=350 J/(l·atm), initial gas temperature 293 K. (**b**) - Reconstructed time behavior of gas temperature in active medium excited by EBSD.

Thus, the method of gas temperature reconstruction was developed and applied for the oxygen gas mixture $CO:O_2$=1:19 that was used to obtain SDO under pulsed EBSD. In this gas mixture at the initial gas temperature from 100 K to 300 K the Joule gas heating was 35±10% of EBSD input energy.

Numerical simulations of gas temperature time behavior with improved theoretical model for oxygen gas mixtures with carbon monoxide additives.
(*Subtasks 3.3*)

Careful examination of vibrational kinetics in the oxygen mixture $CO:O_2:Ar$=1:19:20 used for SDO production at the initial gas temperature 300 K at pressure 30 Torr allows us to describe more correctly heating rate of gas in the discharge taking into account kinetics of vibrational distribution functions (VDFs) of CO and O_2. Effect produced by more correct description of vibrational kinetics is illustrated in **Fig.II.3.62**. Curve 1 depicts gas temperature time behavior calculated by the previous version of our kinetic model, curve 2 is the prediction of the latest version for parameters listed above and initial voltage 1.3 kV. It is seen that correction of the model led to remarkably slower heating of the gas.

It is instructive to show calculated heating rates by two models. It is seen from **Fig.II.3.63** that the previous model strongly overestimates gas heating rate at short times.

The slower gas heating predicted by the corrected model is the consequence of the more accurate description of vibrational relaxation. Single- and multi-quantum VT relaxation processes are dominant in the post discharge phase, as it is seen in the **Fig.II.3.64**. For the experimental parameters the rate of gas heating in VV exchange processes is approximately one order of magnitude less than the heating rate in multi-quantum V-T relaxation.

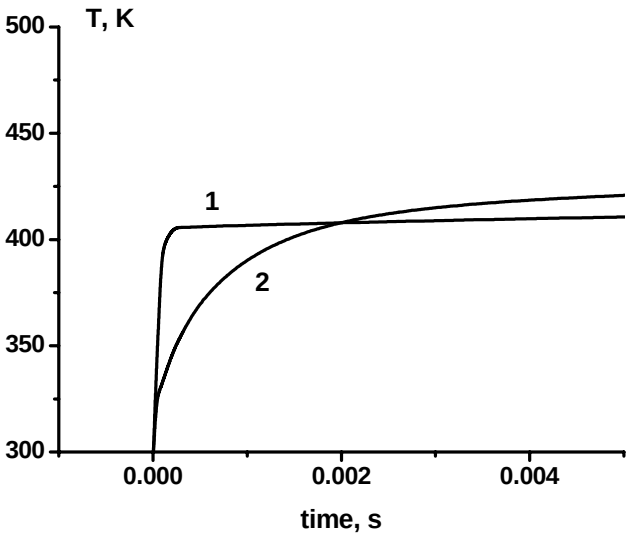

Fig.II.3.62. Simulated gas temperature time behavior. 1 is the result of the previous version; 2 is the result of corrected model.

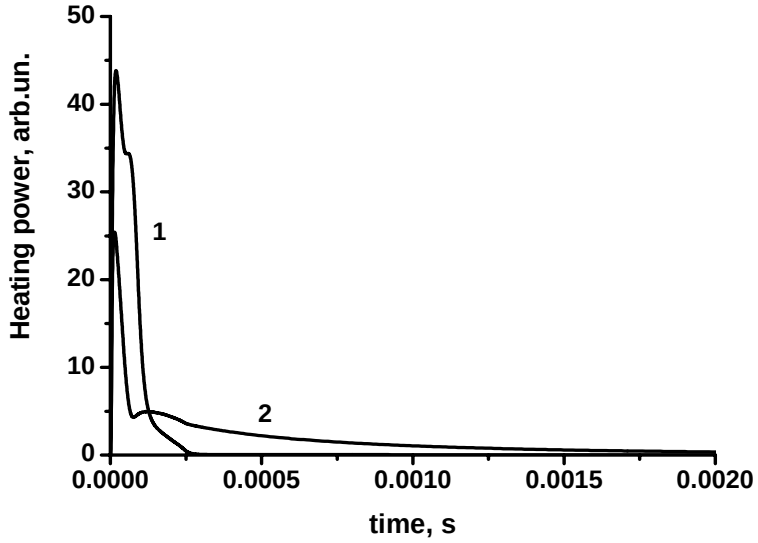

Fig.II.3.63. The gas heating power calculated with different theoretical models; curve 1 corresponds to the previous model; curve 2 corresponds to the updated model

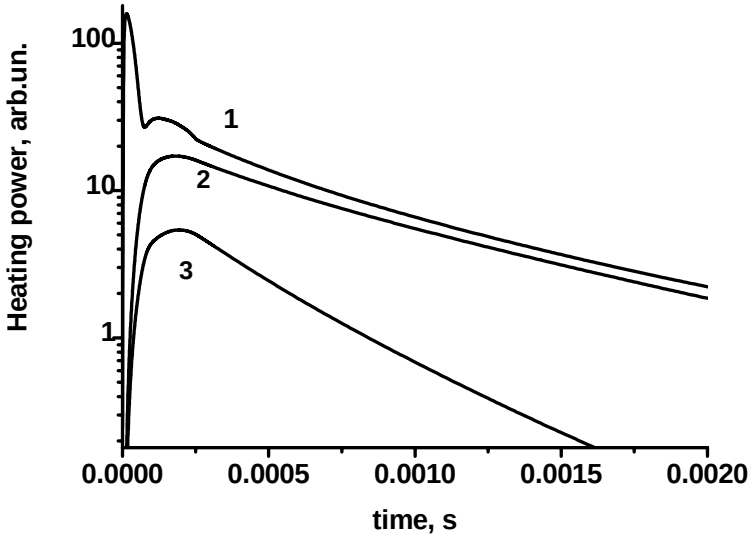

Fig.II.3.64. Role of the vibrational relaxation processes in the gas heating. The curve 1 describes the overall heating rate; curves 2 and 3 describe the gas heating in the processes of single-quantum VT relaxation and multi-quantum VT relaxation (O_2(v) on O atoms), respectively.

The updated kinetic model was also applied for calculations of gas temperature dynamics in the oxygen mixture $CO:O_2$=1:19 for conditions realized in experimental conditions. The following parameters of gas mixture and electric discharge were taken for calculations: the initial temperature 293 K, pressure 0.04 atm, discharge voltage 3 kV. The specific energy input (Q_{in}) realized in these calculations was 350 J/l Amagat. Calculated gas temperature dynamics is compared with the experimental data presented in **Fig.II.3.65**. The observed agreement between theory and experiment can be considered as quite satisfactory one.

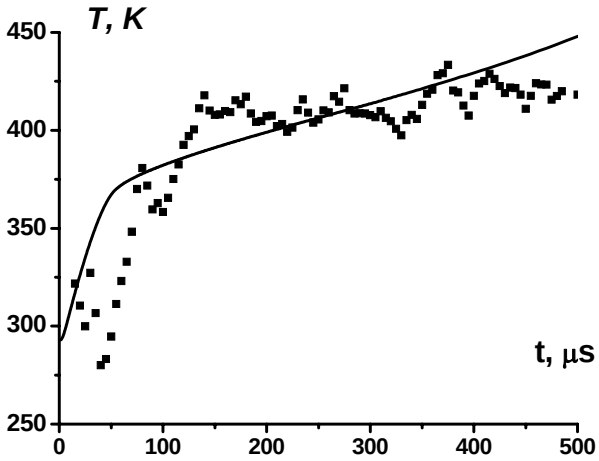

Fig.II.3.65. The gas temperature dynamics calculated (solid curve) and experimentally determined (filled squares) by virtue of the mathematical treatment of absorption coefficient measured for three ro-vibrational transitions.
The initial temperature is 293 K, pressure 0.04 atm, discharge voltage 3 kV, Q_{in}=350 J/l Amagat.

Inclusion the ion current effect into the theoretical model of an electric discharge in oxygen. (*Subtasks 3.1*)

The total electric current in the discharge comprises electron and ion components. The ion current completely goes to gas heating while the discharge power fraction spent for excitation of $O_2(a^1\Delta_g)$ diminishes. At a fixed energy input, the discharge efficiency and amount of $O_2(a^1\Delta_g)$ produced are lower. The purpose of this report is the theoretical study of ion current effects influencing on characteristics of the SDO generator.

The negative ion concentration in discharge in electro-negative gases can remarkably exceed the electron concentration. The discharge current density is a sum of electron, positive and negative ion current densities:

$$J_{disch} = J_e + J_{in} + J_{ip} = e\mu_e En_e + e\sum_k \mu_n^k En_k^n + e\sum_l \mu_p^l En_l^p .$$

Here e is electron charge, μ_e electron mobility, E the electron field strength, n_e electron concentration, μ^k_n the mobility of the positive ions of sort κ, n^n_k the concentration of κ-th negative ions, μ^l_p the mobility of l-th positive ions, n^p_l concentration of l-th positive ions. Our model includes three sorts of negative ions O^-, O_2^- и O_3^- and six sorts of positive ions O_2^+, O_4^+, O^+, CO^+, Ar^+ and Ar_2^+. Specific values of positive and negative ion mobilities were taken from (McDaniel and Mason, 1973). Some of them are reproduced in **Table II.3.2.**

Table II.3.2. The experimental values of ion mobilities in oxygen (McDaniel and Mason, 1973) at pressure one bar and temperature 300 K.

Ion	O^-	O_2^-	O_3^-	O_2^+	O_4^+
μ, cm^2/Vs	3.2	2.16	2.55	2.24	2.16

The electron mobility has been calculated from numerical solution of electron Boltzmann equation. At *E/N*=10 Td= 10^{-16} Vcm^2 it is 1300 cm^2/Vs for the pure oxygen, and 1600 cm^2/Vs for the mixture $CO:O_2:Ar$ = 1:19:20. For higher *E/N* values the mobility is a little lower. Comparing electron and ion mobilities, a conclusion can be drawn that the ion current is comparable with the electron current when the ion concentration is more than 100 times higher than that of electrons.

In the code, calculations of the ion current were added. It was assumed that the power dissipated by ions goes immediately to gas heating. Besides, we include the energy dependence of the three-body attachment rate to oxygen molecules from (Alexandrov, 1988).

This modified code was employed to simulate experimental data from (Vasilijeva, 2004), where the SDO yield was studied in detail for the e-beam sustained discharge at extremely low energy deposition when the gas heating effects can be neglected. **Fig.II.3.66** shows dependence of $O_2(a^1\Delta_g)$ concentration on the specific energy input at two values of *E/N* parameter. Markers show experimental data ● - 10.7 Td, ▲ – 20.3 Td (notice that *E/N* value was kept constant during the discharge); results of our simulations are shown by dash-dot lines for the model neglecting ion-current effects and by solid lines when these effects were included; dashed lines show results of numerical simulations from (Vasilijeva, 2004). Let's note that the ion current effects were included in the model of (Vasilijeva, 2004), too. Inclusion of ion current effects into our model improves an agreement with the experiments. Our model and the model of (Vasilijeva, 2004) give nearly the same results and agree satisfactorily with the experiments.

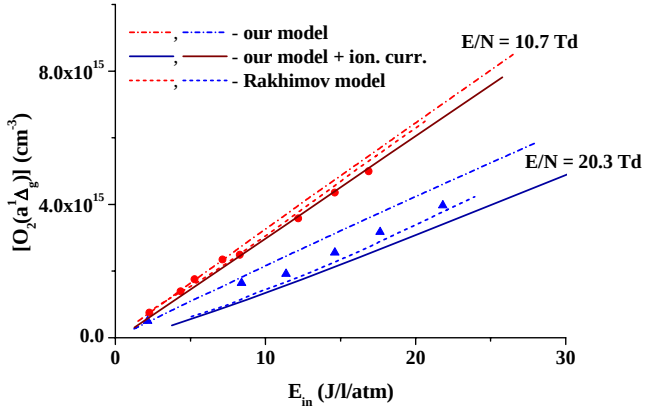

Fig.II.3.66. Dependence of $O_2(a^1\Delta_g)$ concentration on the specific energy input. Markers show experimental data (Vasilijeva, 2004), P=100 Torr, pure O_2.

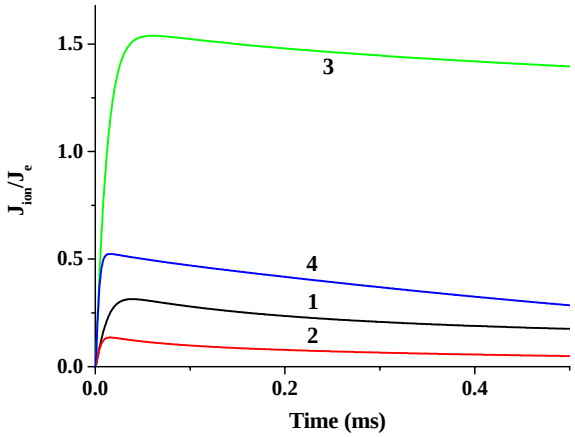

Fig.II.3.67. Evolution of ion current reduced to the electron current at different *E/N* and specific energy inputs.
E/N = 10.7 Td (1, 2) and 20.3 Td (3,4);
E_{in} = 2.3 J/l atm (1), 16.8 J/l atm (2),
2.2 J/l atm (3) and 20 J/l atm (4).

Fig.II.3.67 demonstrates our calculated time dependence of the ion current reduced to the electron current for conditions of the experiment (Vasilijeva, 2004) for two values of the specific energy input and two values of *E/N* parameter. Increase of *E/N* leads to a higher rate of dissociative

attachment to oxygen molecules, which is a dominant mechanism for electron loss in the discharge, and the fraction of the ion current grows, too. At higher specific energy input, $O_2(a^1\Delta_g)$ concentration is greater, and this results in more intense negative ion destruction and decay of the ion current.

Fig.II.3.68 shows calculated evolution of negative ion and electron concentrations for conditions of work (Vasilijeva, 2004). It is seen that at low specific energy inputs characteristic for this work the ion concentration is remarkably higher than that of electrons. At comparatively high oxygen pressure the dominant negative ion is O_3^-, while the dominant positive ion is O_4^+.

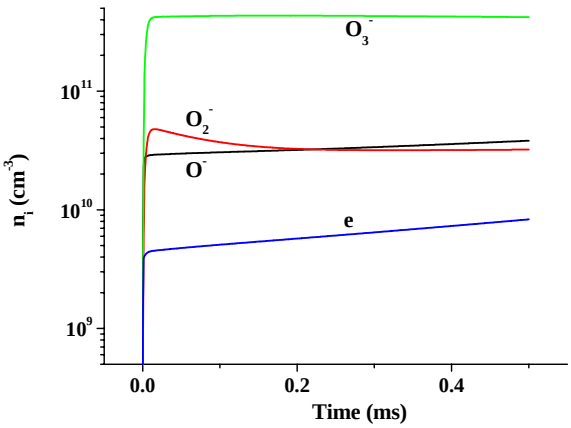

Fig.II.3.68. Evolution of electron and negative ion currents.
Pure oxygen, P=100 Torr, *E/N*=20.3 Td;
E_{in}= 20 J/l atm.

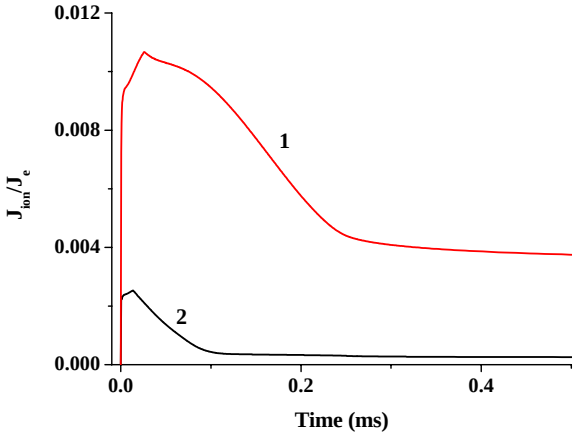

Fig.II.3.69. Evolution of the ratio of negative ion current to electron current.
P=30 Torr, CO:O_2:Ar = 1:19:20, c=330 μF,
E_{in} = 1.5 kJ/l atm (1) and 0.27 kJ/l atm (2) .

For conditions of our experiment, the specific energy input is typically much higher. It is expected that $O_2(a^1\Delta_g)$ concentration be higher, electron detachment faster and ion current relatively lower. Besides, in our mixture there exists an additional mechanism of negative ion O^- destruction in collisions with CO molecules. **Fig.II.3.69** demonstrates the predicted evolution of the ratio of negative ion current to electron current in conditions of our experiments.

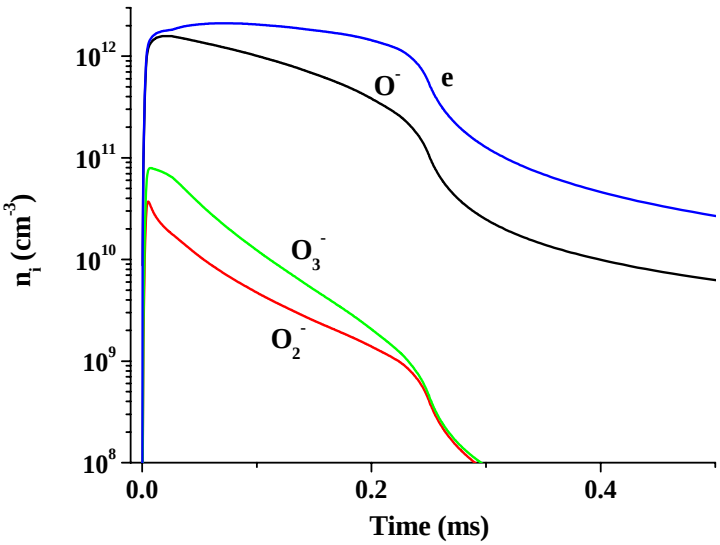

Fig.II.3.70. Evolution of electron and negative ion currents.
P=30 Torr, CO:O_2:Ar = 1:19:20,
c=330 μF, E_{in} = 1.5 kJ/l atm.

The fraction of ion current is not higher than 1%. Such a small level of ion current cannot influence on $O_2(a^1\Delta_g)$ yield and efficiency of its production in the discharge. Therefore, in contrast

to conditions of (Vasilijeva, 2004) ion current effects can be neglected. In our experiments, the energy input was varied by the capacity charging voltage. Therefore, higher energy inputs were realized at higher electric field strengths. From the other side, the rate of the dissociative attachment grows with *E/N* parameter resulting in greater ion current fraction at higher energy input (compare curves 1 and 2 in **Fig.II.3.69**). Evolution of specific sorts of negative ions in comparison with electron concentration is shown in **Fig.II.3.70** for conditions of a high energy input.

Extension of theoretical model for SDO generation by incorporating vibrational kinetics of O_2(X) and CO molecules. Collection of available rate coefficients and development of a relevant subroutine.

(*Subtasks 3.2*)

The existing theoretical model was strongly modified in respect of accurate description of vibrational kinetics in CO-O_2 mixtures. The newly developed subroutine allows one to solve a system of kinetic equations for populations of molecular vibrational levels. This subroutine was combined with earlier existing subroutine describing plasma chemical reactions, and both systems were solved self-consistently. Motivation for inclusion modeling vibrationally excited O_2 molecules is the following. The dissociative attachment cross section is higher for higher vibrational levels (O'Malley, 1967; Akhmanov, 1983), and this fact could be important for the electron number balance. Our plasma chemistry model includes additionally dissociative attachment processes for 5 vibrational levels of O_2 molecules. The relevant cross sections were taken from (O'Malley, 1967). Let's note that they agree with cross sections proposed in the later work (Akhmanov, 1983).

To describe vibrational kinetics we need to define a set of rate coefficients for VV (vibrational energy exchange between the same molecules), VV' (vibrational energy exchange between different molecules), and VT relaxation. VV exchange rates between CO molecules were collected by us earlier (Billing, 2003).

The VV rates for O_2 molecules were computed recently in (Coletti and Billing, 2002) in framework of semi-classical trajectory calculations. Our analysis of these data revealed that these rate coefficients could be analytically approximated with a good accuracy by expressions of the SSH theory (Capitelli, 2000):

$$K_{v+1,v}^{u,u+1} = K_{1,0}^{0,1} \cdot \frac{v+1}{1-(v+1)\cdot\delta} \cdot \frac{u+1}{1-(u+1)\cdot\delta} \cdot \exp(-\delta_{VV} \cdot |v-u|) .$$

Here δ is the anharmonicity of an O_2 molecule, δ_{VV} is the so-called "VV exchange radius". This statement is illustrated in **Fig.II.3.71** showing numerically computed points and analytical curves for two values of gas temperature: T=300 and 500 K.

Information about VV' exchange rates for CO-O_2 molecules is scarce and contradictory (Wang and Gu, 1998). In such a situation, analytical approximations of the modified SSH theory, presented in particular in (Cacciatore, 2004), were used. Implementation of these expressions for the molecules CO and N_2 provided a good agreement with experiments including data on different isotopic forms and with data of semi-classical trajectory simulations (Cacciatore, 2004). Taking into account the similarity in a type of intermolecular long-range interaction between CO-O_2 and CO-N_2 pairs, the function characterizing the role of energy defect in collisions was taken in the same form. **Fig.II.3.72** shows dependence of rate constant for the process $CO(v)+O_2 \rightarrow CO(v-1)+O_2(1)$ on vibrational number of colliding CO molecule calculated by us at gas temperature 300 K. Near the resonance (equality of exchanged vibrational energy quanta, took place for v=2---25) the rate constants are about 10^4 times higher than for the process $K(1,0 \rightarrow 0,1)$.

VT relaxation rate constants in collisions $O_2(v)+O_2 \rightarrow O_2(v-1)+O_2$ were calculated in (Coletti

and Billing, 2002), too. The results are shown in **Fig.II.3.73** by solid squares. The full set of the rate constants was found using an analytical approximation of these results:

$$k_{v+1,v}^{VT} = k_{1,0}^{VT} \cdot \frac{v+1}{(1-\delta\cdot(v+1))} \cdot \exp\{v\cdot\delta_{VT}\}.$$

Here δ is the relative anharmonocity, δ_{VT}, $k_{1,0}^{VT}$ are parameters of the approximation. Analytical approximation is compared with numerical results from (Coletti and Billing, 2002) in **Fig.II.3.73**.

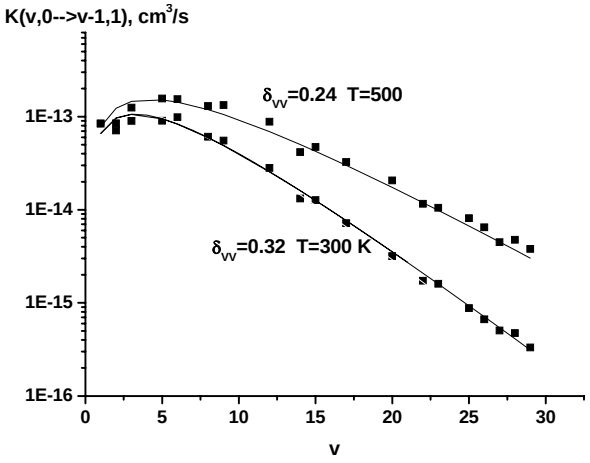

Fig.II.3.71. VV exchange rate constants $O_2(v)+O_2\rightarrow O_2(v-1)+O_2(1)$ as functions of vibrational number at gas temperatures 300 and 500 K. Curves are approximation, black squares are results of calculations (Coletti & Billing, 2002).

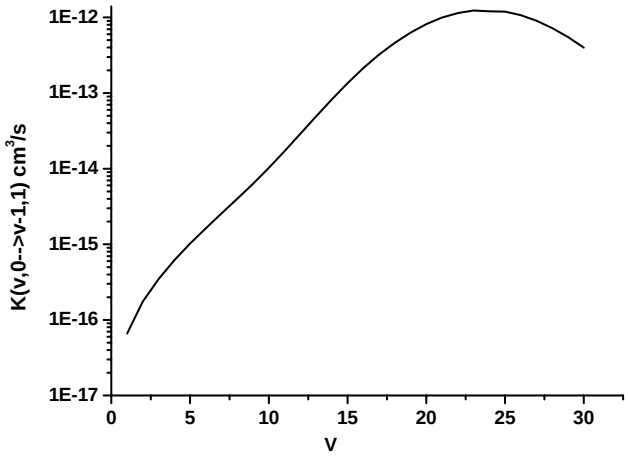

Fig.II.3.72. VV' exchange rate constants for $CO(v)+O_2\rightarrow CO(v-1)+O_2$ process as functions of v at gas temperature T=300 K.

VT relaxation rate constants for the first vibrational level of oxygen in collisions with atoms $O_2(1)+O\rightarrow O_2+O$ were calculated using the expression: $k_{1,0}[O_2-O] = 4.5\cdot10^{-15}\cdot T$ as recommended in (Capitelli, 2000). Generally, in collisions $O_2(v)+O$ some role can play chemical interactions. Then, the single-quantum relaxation, which is typically much faster, can become of the same order as the multi-quantum relaxation. Such processes are not well studied experimentally and theoretically, as well. It was stated in (Webster and Bair, 1972) that the VT multi-quantum relaxation rates in processes $O_2(v)+O\rightarrow O_2(v-\Delta v)+O$ weakly depend on both, v and Δv values. Therefore, we set all these constants equal to $k_{1,0}$ independent of v and Δv. Single-quantum relaxation in collisions with O atoms is set traditionally to be a linear function of the vibrational number: $k_{v+1,v}^{VT}[O_2-O] = k_{1,0}[O_2-O](3v-2)$. VT relaxation rate constants of CO vibrations in collisions with O atoms in the process $CO(1)+O\rightarrow CO+O$ was described by an expression from (Capitelli, 2000): $k_{1,0}[CO-O] = 5.3\cdot10^{-13}\cdot T^{0.5}\cdot\exp\left\{-\frac{1600}{T}\right\}$. The rate constants for an arbitrary vibrational number were calculated by an expression:

$$k_{v+1,v}^{VT}[CO-O] = k_{1,0}^{VT}[CO-O]\cdot\frac{v+1}{(1-\delta\cdot(v+1))}\cdot\exp\{v\cdot\delta_{VT}\}.$$

The parameter δ_{VT} was calculated using the SSH theory with interaction potential parameter L=0.25 (Capitelli, 2000).

Results provided by the modified model for vibrational kinetics are illustrated in **Fig.II.3.74** for conditions of the e-beam sustained discharge studied above. The gas mixture is $CO:O_2:Ar=1:19:20$ at the initial gas temperature 300 K and pressure 30 Torr. The vibrational distribution functions (VDF) for CO and O_2 molecules are presented at the moments 103 μs, 1070 μs and 10.7 ms. Despite the small percentage of CO in the mixture, the vibrational energy stored in CO molecules is of the same order as vibrational energy of O_2 molecules. **Fig.II.3.74** demonstrates that there is a big difference between vibrational temperatures for low levels in CO and O_2.

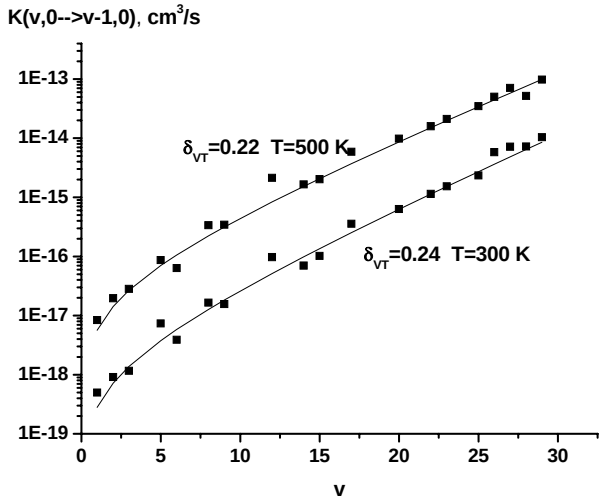

Fig.II.3.73. VT relaxation rate constants for the process $O_2(v)+O_2 \rightarrow O_2(v-1)+O_2$ in dependence on v. Black squares are results of numerical calculations (Coletti C. & Billing G. D., 2002).

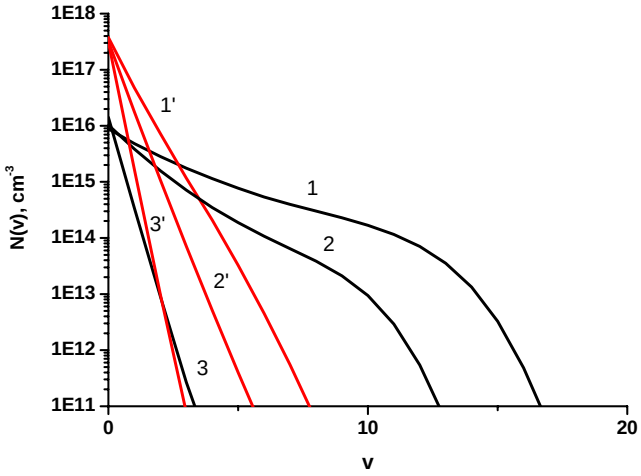

Fig.II.3.74. The VDFs for CO (1, 2, 3) and O_2 (1', 2', 3') molecules at the moments 103 μs, 1070 μs and 10.7 ms. Gas mixture $CO:O_2:Ar=1:19:20$, T_0=300 K, p=30 Torr, the initial voltage 1.3 kV.

Effect produced by extension of the model by inclusion detailed vibrational kinetics description is illustrated by dependence of the singlet oxygen production on the specific energy input calculated by two different models shown in **Fig.II.3.75**. Besides, both theoretical curves are compared with the experimental data. It is seen that more accurate calculations result in approaching the experimental data more closely.

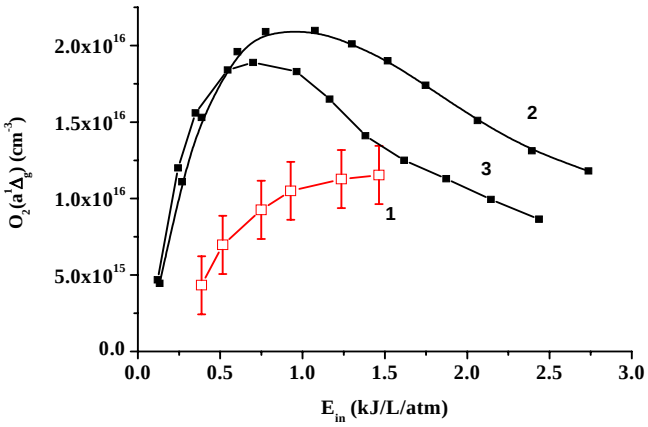

Fig.II.3.75. The singlet oxygen concentration produced by the e-beam sustained discharge.
1 – experimental data; 2-prediction by the old

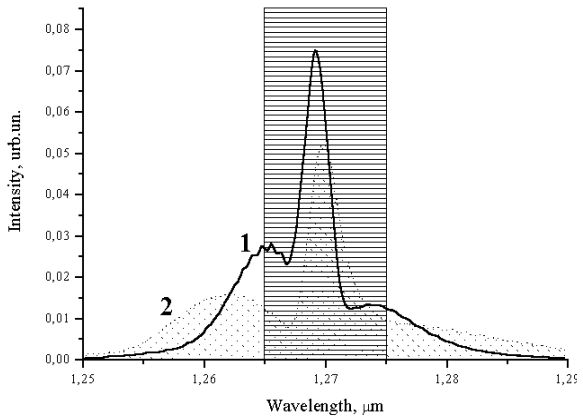

Fig.II.3.76. Spectral distribution of singlet oxygen luminescence at gas temperatures 300 K (**1**) and 1000 K (**2**). Dashed rectangular

model; 3-prediction by the new model. corresponds to spectral resolution of monochromator (10 nm).

The experimental data presented in **Fig.II.3.74** were taken from **Fig.II.3.49** with some changing. The calibration procedure carried out above did not take into account the difference of gas temperature in chemical and electric discharge SDO generators. However, the difference is very important to measure SDO concentration and yield correctly. **Fig.II.3.76** demonstrates the calculated spectral distribution of SDO luminescence at the same SDO concentrations at gas temperature 300 K (**1**) and 1000 K (**2**). With spectral resolution of monochromator of 10 nm (dashed rectangular in **Fig.II.3.76**), photodetector observes just a part of SDO luminescence placed in corresponding spectral region. Temperature increase results in spectrum SDO luminescence changing. In that case the observed part of the luminescence changed, respectively. With gas temperature taking into account, experimental values of SDO concentration and yield presented in **Fig.II.3.49, 50** increased. In the experiments maximal SDO yield achieved 10.5%.

Development of new type of an electric SDO generator based on the non-self sustained slab discharge initiated by high-voltage pulses. Incorporation this generator into the ICLS facility. (*Subtasks 3.1*)

Currently the great efforts in investigation of electrically generated singlet delta oxygen (SDO) resulted in achievement of SDO yield exceeding the room temperature threshold level. Observation of positive gain (Carroll, 2005a) and oscillation of oxygen iodine laser with electrical generator of SDO (Carroll, 2005c) validated the feasibility of electrically driven oxygen iodine laser. Thus, the problem of efficiency and usability of electrical SDO generator becomes of great importance now. This fact makes scientists investigate different types of electrical discharges looking for the best of them as a source of SDO.

The energy efficiency of nonequilibrium plasmachemical process depends on which set of channels it flows, i.e., on the mechanism of the process. On the other hand, the mechanism is defined, mainly, by the parameters of gas discharge. The reduced electric field strength E/N (E is the electrical field strength and N is the density of neutral plasma gas particles) is one of major parameters. This parameter determines mean energy of electrons in plasma and, accordingly, the energy balance of different degrees of freedom of the atomic and the molecular components in plasma. In its turn, E/N depends on the type of a discharge and the kind of plasma gas. For self-sustained discharges, its magnitude is determined by a balance of formation and losses of charged particles in plasma and cannot be changed by external effect (Raizer, 1991). This circumstance introduces considerable problems in optimization of plasmachemical processes.

It is known that the value of the reduced electric field strength for plasmachemical process of SDO formation must be ~ 10^{-16}V cm^2. The parameter E/N for self-sustained discharges of miscellaneous types, as a rule, is noticeably higher, because the electrical field in plasma should provide the ionization frequency necessary for compensation of inevitable losses of charged particles.

The discharge system on the basis of a non-self-sustained discharge with controlled parameters of electronic component of plasma for optimization of selective plasmachemical processes was developed (**Fig.II.3.77)**.

Similar discharge systems were previously used as efficient sources for pumping gas lasers (Kitaeva, 1968; Hoag, 1973; Railly, 1972; Basov, 1979; Kuznetsov, 2000;) that allow one to create the nonequilibrium plasma in large volumes with a high uniformity.

It is known the efficiency of the oxygen iodine laser depends on the active medium temperature. The decrease of the temperature results in the increase of the laser efficiency. As soon

as the electric discharge in gas results in gas heating one needs to reduce temperature. A slab structure of discharge system seems to be very attractive providing a very high gas cooling by convection.

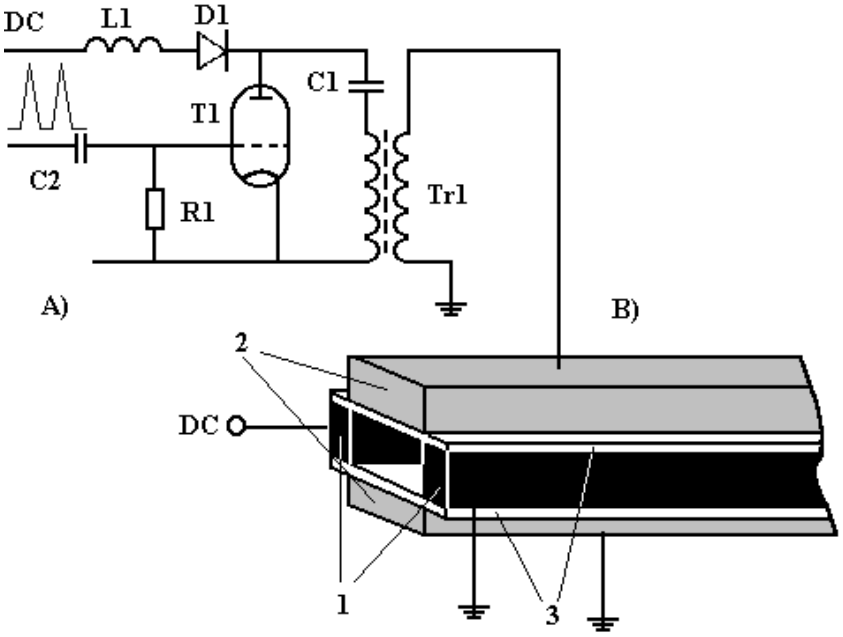

Fig.II.3.77. The diagrams of the power supply circuit **A)** and the discharge chamber **B)**.
1 - copper electrodes;
2 - aluminium electrodes;
3 - ceramic plates.

The diagrams of discharge system and its power supply are shown in **Fig.II.3.77**. A DC voltage of up to 1500V is applied to copper electrodes (1) and provides a current of up to 500 mA. A pulsed voltage is applied to aluminium electrodes (2). The working medium is bounded by two Al_2O_3 ceramic plates (3). The hollow electrodes (2) and electrodes (1) have a common water-cooled loop. The external ionization was served by repeating high-voltage pulses. A generator with a capacitive (C_1 =1…3 μF) storage is used. The capacitor is switched with a thyratron (T) (TGI-100/8) controlled by a driving generator. The repetition rate f ≤ 40 kHz is limited by the thyratron deionization time. The pulse voltage is stepped up by a transformer (Tr) to $U_p \cong 10$ kV. The pulse duration and rise time are ~ 1 μs and ~ 50 ns, respectively. The average power of the pulse circuit may vary due to changes in both f and U_p; in condition of this work it is limited by $W_p \le 30$ W. The length of the discharge chamber along the copper electrodes (1) was 95 mm, with the gap between electrodes of 20 mm. The minimum size (the slab height) was 2 mm. Most of experiments were performed with discharges in O_2 and in a mixture O_2-rare gas. The gas pressure may be varied from 1 to 100 Torr, and a gas flow rate at normal condition may be varied from 0.5…2 $l \cdot s^{-1}$. The average power of the DC circuit was about 100 - 150 W.

To detect SDO produced in the non-self sustained slab discharge initiated by high voltage pulses, the Co:MgF_2 laser based intracavity laser spectroscopy (ICLS) (Pazyuk, 2001) was used. For this purpose the spectral lines of the Q – branch of the vibration 0-0 band of the $a^1\Delta_g \rightarrow b^1\Sigma_g^+$ transition of molecular oxygen were used. The detailed description of the method and its possibility to be applied for measuring SDO concentration in the framework of the Project 2415 was discussed above in detail. A diagram of the experimental setup is shown in **Fig.II.3.78**. The experimental setup (Pazyuk, 2001) was modified to work in assembly with a non-self sustained slab discharge in oxygen initiated with high voltage pulses. Gas flow produced by the slab discharge passed through a 11 mm i.d. quartz tube and then along an intracavity quartz tube (an inner diameter of 16 mm) contained within the cavity of the Co:MgF_2 laser. The laser cavity was formed with a plane totally reflecting mirror HR and a spherical (R=1000 mm) output coupler OC. A total cavity length L_c was

L_c=660 mm. A length L_a of the intracavity absorption cell was L_a=400 mm. The CaF_2 prism installed in a laser cavity made it possible to tune the generation spectrum to the 1.91 μm wavelength.

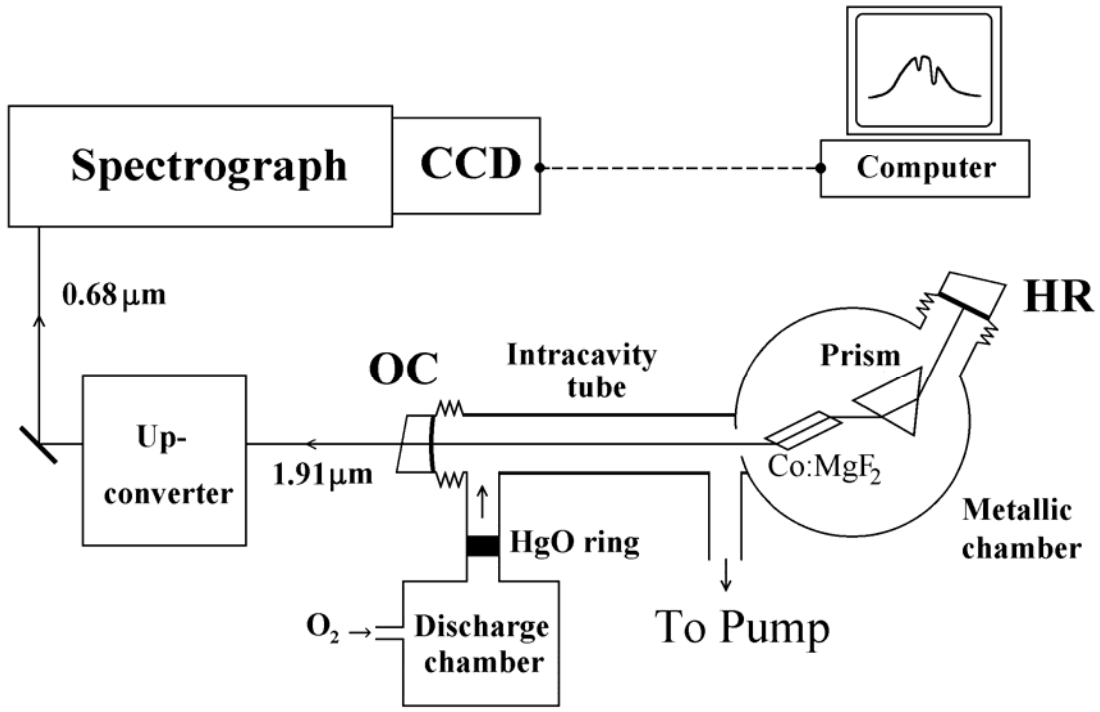

Fig.II.3.78. The diagram of experimental ICLS set-up for measuring the SDO concentration

A typical linear flow velocity in the intracavity tube was 10 m/s at pump capacity of 2 l/s (pump capacity could be varied from 0 to 14 l/s). Due to low probability of SDO quenching on the tube wall and high flow velocity, SDO losses during passing from discharge chamber to tube outlet were minimal. To remove oxygen atoms produced in the discharge zone, the HgO ring was placed into the tube downstream of the discharge chamber.

The broadband IR radiation from Co:MgF_2 laser was firstly up-converted to visible spectral range by mixing it with monochromatic radiation from Nd:YAG laser (λ=1.064 μm, the linewidth is 0.017 cm^{-1}, the pulse duration is 5 μs, and the pulse energy is 1 mJ) in a nonlinear crystal. The Nd:YAG-laser pulse duration was short compared to that of Co:MgF_2 laser (the pulse duration of Co:MgF_2 laser was 130 μs). The synchronization unit provided the variable time delay between the Nd:YAG laser pulse and the leading edge of the pulse from a Co:MgF_2 laser. Thus, one could detect the emission spectrum at any given moment of time without using any additional equipment. The output spectrum was detected with a high resolution grating spectrograph (a spectral resolution of 0.018 cm^{-1}) coupled to an optical multichannel analyzer based on the CCD array and PC. The random noises in the laser output spectrum were reduced by averaging the spectrum over 100 pulses.

The sensitivity of apparatus used made it possible to detect the SDO concentration as low as $5 \cdot 10^{14}$ $см^{-3}$. Analysis shows that the procedure described makes it possible to measure the SDO concentration with an accuracy of not worse than 20 %. **Fig.II.3.79** demonstrates the general view of experimental facility.

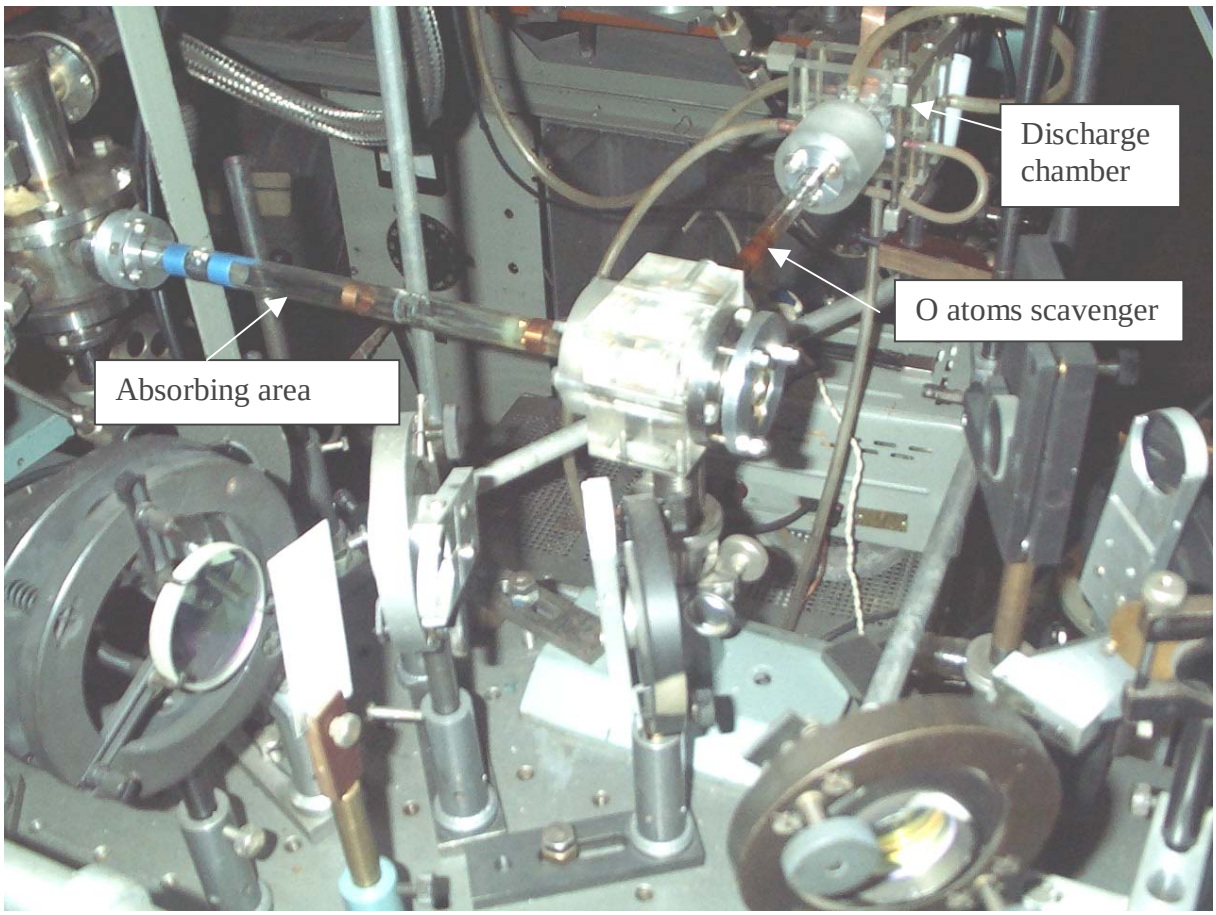

Fig.II.3.79. The experimental facility general view.

Study of electrical parameters of non-self sustained slab discharge initiated by high-voltage pulses under different experimental conditions.

(*Subtasks 3.2*)

The electric characteristics of the non-self-sustained slab discharge initiated by high-voltage pulses were measured for DC voltage circuit. The voltage of the DC source U_{dc} and the voltage U_e across the DC electrodes were experimentally measured. To stabilize these voltages in time during the application of preionizing pulses, a capacitor C=0.1μF and resistor R_s=1 kOhm were put between the DC power source and electrodes (see **Fig.II.3.80**) As the distance Z between the electrodes changes, the discharge length changes only due to the change of positive column length (Raizer, 1992). Therefore, by measuring the voltage across the electrodes $U_e(Z)$, we separated the voltage drop across the positive column U_{pc} from that of near-electrode zones.

Fig.II.3.80 demonstrates experimentally measured time behavior of the voltage U_e (curve 1) and discharge current *J (*curve 2) for the gas mixture O_2:He=1:8 at gas pressure p=50 Torr. (The preionizing pulse voltage U_p=10kV; preionizing pulse repetition rate f_P=36kHz; the moment of 27.7μs corresponds to the beginning of next preionizing pulse, Z=20 mm). One can see that the RC circuit well stabilizes the voltage across DC electrodes, and the non-self-sustained discharge current J is dropping down on the time interval corresponding to the preionizing pulse repetition rate, i.e. the non-self-sustained discharge current J has a deep modulation on the larger time scale.

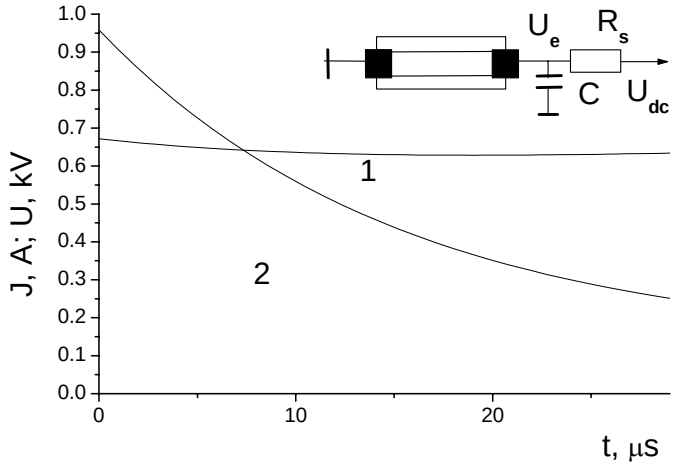

Fig.II.3.80. Time behavior of voltage $\mathbf{U_e}$ across the DC electrodes(1) and current **J** (2) for non-self-sustained slab discharge.

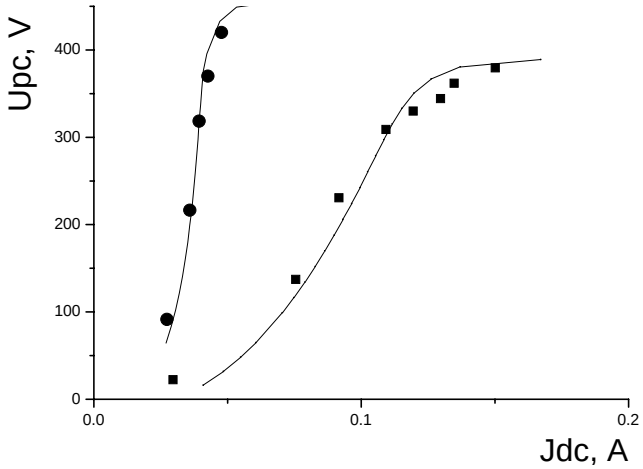

Fig.II.3.81. The CVCs of positive column for preionization power of 10W (the left curve) and of 30W (the right curve) for the gas mixture O_2:He=1:8 at gas pressure p=50 Torr, f_P=36kHz. Dots and solid curves correspond to the experiment and calculation, respectively.

The dots in **Fig.II.3.81** show the time-average current-voltage characteristics of the positive column (the dependence of U_{pc} on J_{dc}) for two different preionization powers W_p (W_p=10W for the left curve , and W_p=30W for the right curve). A change in W_p was attained by changing U_p at fixed preonizing pulse repetition rate. The largest average measured J_{dc} values (the extreme right dots) correspond to the maximum energy deposition into the homogeneous discharge. Instabilities arising at large energy deposition were observed visually and had a character of contracted narrow channels. As is seen, the maximum energy deposition significantly depends on the preionization power.

To interpret the experimental data and understand the basic tendencies in the discharge properties upon variations of the macroscopic parameters, we attempted to simulate the discharge. **Fig.II.3.81** shows a comparison of the experimental and calculated time-averaged current-voltage characteristics (CVCs) of the positive column. As is seen, the measured and calculated CVCs of the positive column agree well.

Both the experiment and calculation show that, as the current increases (in the CVCs saturation region), the discharge becomes less stable. The character of instability development is illustrated in **Fig.II.3.82**. **Fig.II.3.82a** shows an example of the CVC of the positive discharge column for the gas mixture O_2:He=1:8 at gas pressure p=50 Torr, and f_P=18kHz. **Fig.II.3.82b** shows the calculated dynamics of the current and the gas temperature increase during multiple preionization pulses. In this case, the voltage across the positive column corresponds the to point 1

in **Fig.II.3.82a** and is equal to 615V. After ~30 pulses are generated, both the averaged current and the gas temperature reach stationary values I_{st}=140mA and T=350K. If the voltage across the positive column increases even by 1% (up to 620V), then a catastrophic increase in the averaged current is observed already after 20 preionisation pulses (**Fig.II.3.82c**). These dependencies are close to dependencies obtained in (Azarov, 2003) for gas mixture $CO_2 : N_2 : He = 1 : 1 : 8$. From our point of view this similarity was determined by the large quantity of He in mixtures. The calculations and measurements performed helped to reveal that the instability limit significantly depends on preionization conditions.

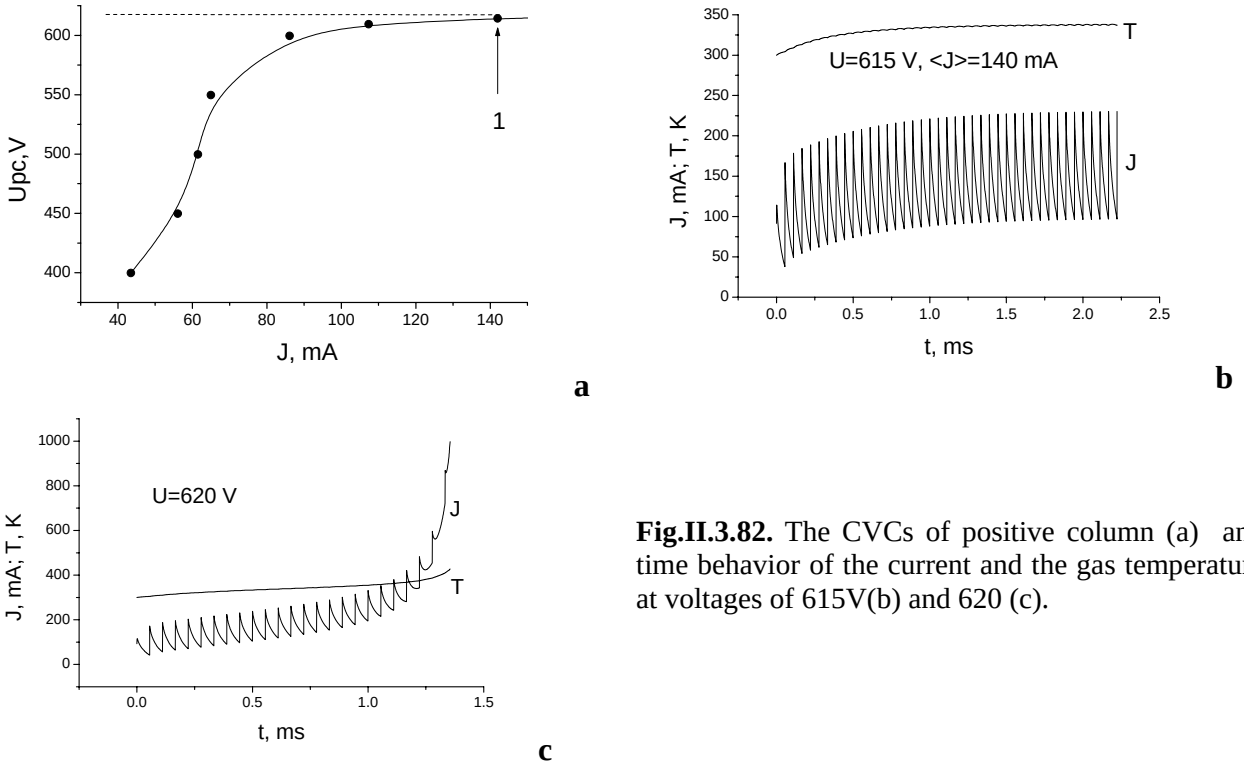

Fig.II.3.82. The CVCs of positive column (a) and time behavior of the current and the gas temperature at voltages of 615V(b) and 620 (c).

Parametric study of SDO production in a generator based on the non-self sustained slab discharge initiated by high-voltage pulses by ICLS method for SDO measuring

(*Subtask 3.4.)*

An analysis of physical processes in cathode layer of non-selfsustained discharge ignited in oxygen containing gas mixtures was performed. The following equation system was solved for cathode layer (in 1D approximation):

$$\left.\begin{aligned} \frac{\partial j_e}{\partial x} = -\frac{\partial j_i}{\partial x} = e \cdot S + \alpha \cdot j_e \\ \frac{\partial E}{\partial x} = 4\pi \cdot e \cdot (n_e - n_i) \end{aligned}\right\}$$

Here n_e and n_i are electron and ion densities, e is electron charge, α is the first ionized Townsend coefficient (Braun, 1961) $j_e = e \cdot n_e \mathrm{v}_e^d$ and $j_i = e \cdot n_i \mathrm{v}_i^d$ are densities of electron and ion currents, *E(x)* is the strength of the local electric field, *S* is preionization power.

Boundary conditions were as follows.

1) on cathode:

$$n_e(0)\cdot \mathrm{v}_e^d(0) = j_e(0) = \gamma\cdot n_i(0)\mathrm{v}_i^d(0) = \gamma\cdot j_i(0),$$

where γ is the second ionized Townsend coefficient(Braun, 1961);

2) on the plasma edge:

$$j_e(l_c) = j_0,$$

where j_0 is the discharge current density, l_c is the cathode layer length. We supposed that the drift velocities of electrons and ions are proportional to the strength of the local electric field

$$\mathrm{v}_e^d(x) = \mu_e E(x);\ \mathrm{v}_i^d(x) = \mu_i E(x).$$

Volt-ampere characteristics of the cathode layer (i.e. dependences of $j_0 = F(U_c, S)$, where U_c is cathode drop) of this discharge were calculated. The results of these calculations are represented in the **Fig.II.3.83** and **Fig.II.3.84**. Volt-ampere characteristics of the cathode layer of the selfsustained discharge correspond to limiting case under S→0 , i.e. $U_c = \lim_{S\to 0} F(j_0, S)$.

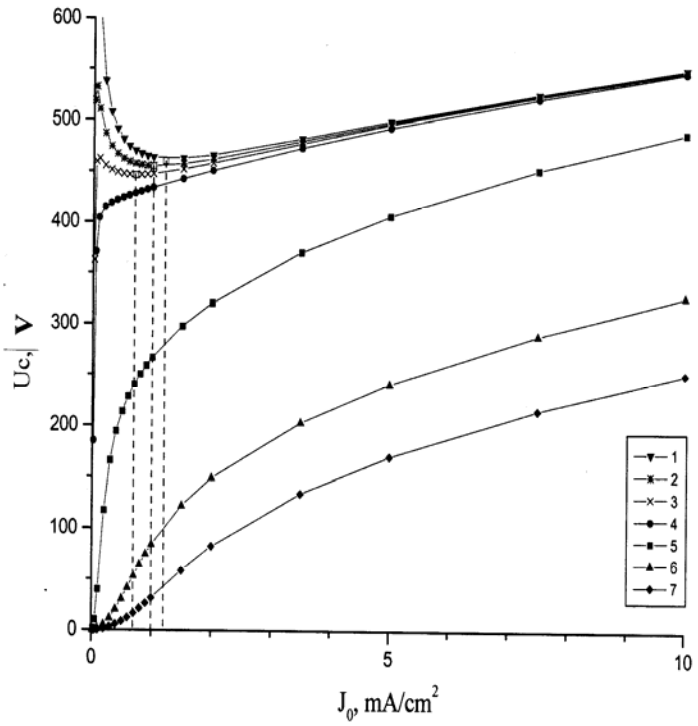

Fig.II.3.83. Volt-ampere characteristics of cathode layer for nonselfsustained discharge in $\mathbf{O_2}$ under pressure *p*=5 Torr and temperature T=330K.

1 - selfsustained discharge U_c=460 V, j_n=1,2 mA/cm^2,

2 - nonselfsustained discharge under $S=5\cdot10^{13}$ ion pairs /s·cm^3 , U_c=455V, j_n=1 mA/cm^2 .

3 - nonselfsustained discharge under $S=1\cdot10^{14}$ ion pairs /s·cm^3, U_c=446B, j_n=0,7 мА/см^2.

4 - nonselfsustained discharge under $S=2\cdot10^{14}$ ion pairs /s·cm^3.

5 - nonselfsustained discharge under $S=5\cdot10^{15}$ ion pairs /s·cm^3.

6 - nonselfsustained discharge under $S=5\cdot10^{16}$ ion pairs /s·cm^3.

7 - nonselfsustained discharge under $S=1.2\cdot10^{17}$ ion pairs /s·cm^3.

These measurements show that the behavior of the cathode layer of non-selfsustained discharge differs from one of selfsustained discharge. It is customary to assume that the discharge with ionized amplification in cathode layer is non-selfsustained only in positive column. The cathode layer of non-selfsustained discharge and the cathode layer of selfsustained discharge are almost the same.(Velichov, 1987), i.e. volt-ampere characteristics of the cathode layer of the non-selfsustained discharge have U-shape form, and the values of normal cathode drop and normal discharge current density are equal to those for selfsustained discharge. Our results show that the outer preionization modifies the behavior of the cathode layer. Cathode drop and normal discharge current density were decreased with increasing of the preionization power *S*. For example, U_c=460 V, j_n=23 mA/cm^2 for selfsustained discharge in $\mathbf{O_2}$ under pressure p=20 Torr and temperature T=330K, whereas for non-selfsustained discharge under S=10^{16} ion pairs /s·cm^3 U_c = 442V, j_n= 9 mA/см^2. Furthermore if S>10^{16} ion pairs /s·cm^3 under p=20 Torr and if S>1.5·10^{14} ion pairs /s·cm^3 under p=5 Torr, volt - ampere characteristics of the cathode layer are a monotone increasing functions. In this case there are no grounds to use concept of normal cathode drop and normal discharge current density.

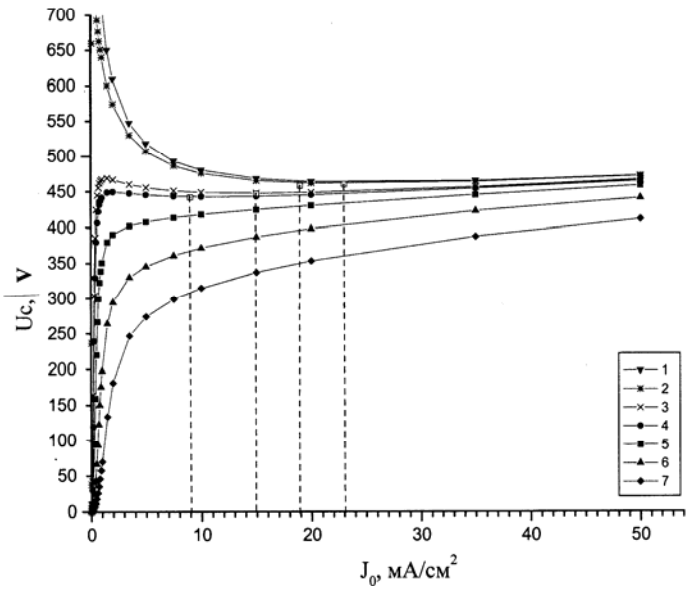

Fig.II.3.84. Volt-ampere characteristics of cathode layer for non-selfsustained discharge in $\mathbf{O_2}$ under pressure p=20 Torr and temperature T=330 K.

1 - selfsustained discharge U_c=460 V, j_n=23 mA/cm^2.
2 - nonselfsustained discharge under S=5·10^{15} ion pairs /s·cm^3 , U_c = 458V, j_n= 19 mA/cm^2 .
3 - nonselfsustained discharge under S=8·10^{15} ion pairs /s·cm^3, U_c = 447V, j_n= 15 mA/см^2.
4 - nonselfsustained discharge under S=10^{16} ion pairs /s·cm^3, U_c = 442V, j_n= 9 mA/см^2.
5 - nonselfsustained discharge under S=2·10^{16} ion pairs /s·cm^3.
6 - nonselfsustained discharge under S=5·10^{16} ion pairs /s·cm^3.
7 - nonselfsustained discharge under S=1.2·10^{17} ion pairs /s·cm^3.

The electric characteristics of the cathode layer of the non-selfsustained slab discharge in $\mathbf{O_2}$ were measured. A DC-voltage up to 1500V was applied to copper electrodes and provided a current up to 500 mA. A pulse voltage was applied to aluminum electrodes. The working medium was

bounded by two Al_2O_3 ceramic plates and copper electrodes. The length of the discharge chamber along the copper electrodes was 190 mm, and the interelectrode distance was 20 mm. The minimum size (the slab height) was 2 mm. Copper plate 190x3x2 mm^3 can be inserted inside discharge chamber parallel to copper electrodes. This plate can separate discharge volume into two chambers. In this case the copper plate was as anode for first chamber and as cathode for second chamber. As a result we obtain two discharge zones. The conditions of preionization and the discharge current for these zones are the same. The interelectrode distances can be different. This provides a way to calculate volt-ampere characteristics of the cathode layer $U_c(j_0)$:

$$U_c(j_0) = \frac{l}{(2l - l_1 - l_2)} \cdot \left(U_2(j_0) - \frac{l_1 + l_2}{l} \cdot U_1(j_0) \right) ,$$

where l, l_1, l_2 are interelectrode distances, $U_1(j_0)$ and $U_2(j_0)$ are volt-ampere characteristics of discharges with and without the copper plate.

The **Fig.II.3.85** shows examples of volt-ampere characteristics of cathode layer for non-selfsustained discharge in $\mathbf{O_2}$ under pressure p=20 Torr , temperature T=330 K and preionization electric power W_p=30W. In this figure one can see calculated volt-ampere characteristic of cathode layer for nonselfsustained discharge in $\mathbf{O_2}$ under $S=1.2\cdot10^{17}$ ion pairs /s·cm^3 and volt-ampere characteristics of cathode layer for Thomson's discharge under $S=1.2\cdot10^{17}$ ion pairs /s·cm^3. The experimental volt-ampere characteristic (dependence 1) is a monotone increasing function. This function distinguishes from Thomson's dependence. This is due to the effective ionized amplification in cathode layer of nonselfsustained discharge. Our theory takes into account both ionized amplification and influence of outer preionization. As is seen, the measured and calculated dependences agree well.

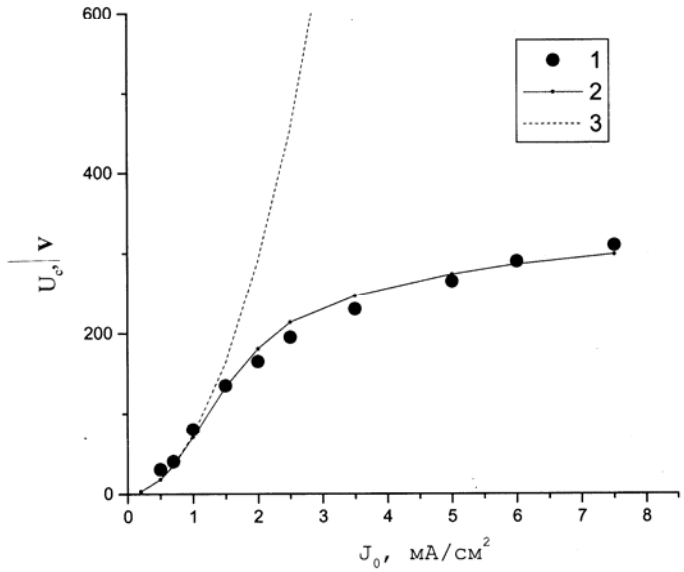

Fig.II.3.85. Volt-ampere characteristics of cathode layer for nonselfsustained discharge in $\mathbf{O_2}$ under pressure p=20 Torr and temperature T=330 K.

1 - Experimental dependence.

2 - Calculated dependence under $S=1.2\cdot10^{17}$ ion pairs /s·cm^3.

3 - Volt-ampere characteristics of cathode layer for Thomson's discharge, $S=1.2\cdot10^{17}$ ion pairs /s·cm^3.

The same picture we observed for non-selfsustained discharges in others gases: CO_2, air, mixtures CO_2:N_2, O_2:He. It is necessary to point out that discharge was to some extent more stable if volt-ampere characteristic of a cathode layer was a monotone increasing function. Singlet delta oxygen (SDO) production was detected (~$0.5 \cdot 10^{16}$cm^{-3}) under discharge in $\mathbf{O_2}$ (p=5 Torr) under specific input power ~ 0.4 eV / molec only for cases when volt-ampere characteristic of a cathode layer was a monotone increasing function. Addition of He to gas mixture made a discharge more stable. The development of an instability occurred at higher specific power. For mixture O_2:He=1:4 under pressure 20 Torr and specific input power ~ 0.7 eV / molec the measured concentration of SDO was about $1.5 \cdot 10^{16}$cm^{-3}. In order to increase specific input power it was necessary to increase preionization power W_p. Unfortunately under $W_p \geq 50$ W induction noises give no way to measure SDO by intracavity laser spectroscopy method.

Conclusions

The experimental study of energetic characteristics of the EBSD in oxygen gas mixtures demonstrated that the addition of CO or H_2 to the pure oxygen and gas mixture O_2:Ar enhances considerably the stability of the EBSD in the oxygen mixture and results in a high value of the SIE, more than an order of magnitude higher than that of EBSD without molecular additives. The maximum SIE per molecular component has come up to ~6500 J/(l atm) for the gas mixture O_2:Ar:CO=1:1:0.1 at the total pressure 30 Torr and pump volume ~18 liter. It should be pointed out that, in the experiments, the considerable improvement of the EBSD stability in a large volume of excitation is obtained only by the choice of the gas mixture. The well-known technical procedures leading to the increase in EBSD stability (sectioning electrodes, smaller pump volume, etc.) can strongly improve the stability of the EBSD and, accordingly, increase the SIE. The measurement of concentrations of $O_2(a^1\Delta_g)$ state was carried out with a new calibration scheme using a comparison of the intensity of $O_2(a^1\Delta_g)$ and $O_2(b^1\Sigma_g^+)$ radiation emitted both from an EBSD and a chemical generator.

It has been theoretically demonstrated that for the conditions obtained in the experiment one might expect to get singlet delta oxygen yield of 20% exceeding its threshold value needed for an oxygen-iodine laser operation at room temperature. It should be noted that the given results were obtained for a pulsed EBSD without gas cooling, which is necessary (Napartovich, 2001) for an oxygen-iodine laser with an electric SDO generator. The principal importance of the obtained data is the experimental demonstration of obtaining such a SIE in an electric discharge, that enables us to get a higher SDO yield than the threshold Y_{th} needed for the oxygen-iodine laser operation if one uses a cooling system. A comparison between predicted and measured $O_2(a^1\Delta_g)$ number density and its time variation demonstrated that the measured SDO density is about 2 times lower than predicted one, and decay rate experimentally observed is somewhat faster than one in the theory. The reasons for such discrepancies are not known at the moment. Further studies are necessary to clear this point. One of the possible reasons for the discrepancies could be the discharge non-uniformities resulting in location dependence of the specific energy input. For the mixtures with a low CO concentration the small-signal gain (SSG) was measured where the specific energy input can be determined from. Measurements of the SSG for several vibration-rotation transitions allow us to track time variations of gas temperature. The method of gas temperature reconstruction was developed and applied for the oxygen gas mixture CO:O_2=1:19 that was used to obtain SDO under pulsed EBSD. In this gas mixture at the initial gas temperature from 100 K to 300 K the Joule gas heating was 35±10% of EBSD input energy. Calculated gas temperature dynamics was compared with the experimental data. The observed agreement between theory and experiment can be considered as quite satisfactory one. With gas temperature taking into account, experimental

maximal SDO yield in pulsed EBSD achieved 10.5%. The experiments on SDO production in slab non-self-sustained discharge with gas flow were carried out. SDO concentration was measured by the method of intracavity laser spectroscopy based on Co:MgF_2 laser.

SDO production was detected (~0.5 $\cdot 10^{16} cm^{-3}$) in slab non-self sustained discharge with external ionization by repeated high-voltage pulses discharge ignited in $\mathbf{O_2}$ (p=5 Torr) under specific input power ~ 0.4 eV / molec only for cases when volt-ampere characteristic of a cathode layer was a monotone increasing function. For gas mixture O_2:He=1:4 under pressure 20 Torr and specific input power ~ 0.7 eV / molec the maximal measured concentration of SDO was about 1.5 $\cdot 10^{16} cm^{-3}$ with SDO yield being of ~7%.

References for Part II.3.

Ahmanov S.L., Klopovskiy K.S., Osipov A.P. (1983). *VINITI*, Moscow, №5472-83, (in Russian).

Akishev Yu.S., Dem'yanov A.V.et al. (1982). *Teplofizjka Vysokikh Temperatur*, **20**, 818.

Aleksandrov N.L., Kochetov I.V., Mazalov D.A. et al (1992) *Fizika Plazmi*, **18**, 1468 (in Russian).

Aleksandrov N.L., Kochetov I.V., Napartovich A.P. (1986) *Khimiya Visokith Energiy*, **20**, 291 (in Russian).

Alexandrov N.L. (1988). *Sov. Physics - Uspekhi*, **31**, 101.

Azarov A.V., Mit'ko S.V., Ochkin V.N., Savinov S.Yu. (2003). *Quantum Electronics*, **33**(5) 419.

Baev V.M., Latz T., Toschek P.E. (1999). *Appl. Phys. B.*, **B 69**, 171.

Basov N., Ionin A., Suchkov A. (1990). *Proc. SPIE*, **1225**, 389.

Basov N.G., Babaev I.K., et al. (1979). *Quantum Electronics*, **6**, 772.

Basov N.G., Ionin A.A., et al. (2002). *Quantum Electronics*, **32**(5), 404.

Billing G.D., Coletti C., et al. (2003). *J. Phys. B.: At. Mol. Opt. Phys.*, **36**, 1175.

Blyabin A.A., Vasil'eva A.N., Kovalev A.S., Lopaev D.V. (1989). *Plazma Phys*., **15**, 1012.

Bogdanov E.A., Kudryvtsev A.A., Tsendin L.D., et al. (2003). *Technical Physics*, **48**, 1151.

Braun S. (1961). "Elementary process in gas discharge plasma". M. Gosatomizdat (in Russian).

Buckman S.J., Phelps A.V. (1985). *J. Chem. Phys.*, **82,** 4999.

Cacciatore M., Kurnosov A., et al. (2004). *J.Phys. B: At. Mol. Opt. Phys*., **37**, 3379.

Capitelli M., Ferreira C. et al. (2000). "Plasma Kinetics in Atmospheric Gases", Springer.

Carroll D., et al. (2005a). *IEEE Journal of Quantum Electronics*, **41**, 213.

Carroll D. L., et al. (2005b). *IEEE Journal of Quantum Electronics*, **41**, 1309.

Carroll D.L., et al. (2005c). *Appl. Phys. Letters*, **86**, 111104-1.

Coletti C., Billing G.D. (2002). *Chem. Phys. Letters*, **356**, 14.

Dem'yanov A.V., Kochetov I.V., Napartovich A.P., Starostin A.N. (1984). *Teplofizika Visokith Temperatur*, **22**, 216 (in Russian).

Duo L., Cui T., Wang Z., Chen W., Yang B., Sang F. (2001). *J. Phys. Chem. A*, **105**, 281.

Ehrhardt H. et al. (1968). *Phys.Rev*., **173**, 222.

Fournier G., Bonnet J., Pigashe D. (1980). *Journal de Physique*, Colloque C9, **41**, 449.

Fournier G., Bonnet J., David D., Pigache D. (1981). "Proceedings of the XV International Conference on Phenomena in Ionized Gases. Part II." Minsk, 837.

Frolov M.P., et al. (2005). *Proc.SPIE*, **5777,** 70.

Fujii H., Itami S., Schmiedberger J. et al (2000) *Proc. SPIE,* **4065**, 818.

Fujii H., Kihara Y., Schmiedberger J. et al. (2003). Preprint AIAA 2003-4028

Gal'tsev V.E., Dem'yanov A.V., Kochetov I.V., Pevgov V.G., Sharkov V.F. (1979). Preprint of the Institute of Atomic Energy IAE -3156. Moscow. (in Russian).

Gilles M.K., et al. (1996). *J Phys. Chem*. **100**, 14005.

Gordiets B., Zhdanok S. (1989) "Analytical description vibrational kinetics of anharmonic oscillators". In book "Nonequilibrium vibrational kinetics" Edited by M. Capitelli. Springer Verlag, Berlin, Heidelberg, New York, London, Paris, Tokyo.

Hall R.I., Trajmar S.J., (1975). *J. Phys. B: Atom. Molec. Phys*., **8**, L293.

Hallada M., Seiffert S., Walter R., Vetrovec J. (2000). *Laser Focus World*, **5**, 205.

Hill A. (2001) "Proc. Int. Conf. LASERS' 2000." Ed. by V. Corcoran and T. Corcoran, STS Press, McLean, VA, 249.

Hoag E., Pease H., Staal J., Zar J. (1973). *Quantum Electronics*, **QE-9**, 652.

Ionin A., Suchkov A., Frolov K. (1988). *Sov. J.Quantum Electronics*, **18**, 1228.

Ionin A.A., Kelner M.S., Lobanov A.N. et al. (1991). *Journal de Physique*, IVColl.C7, **1**, 729.

Ionin A. (2001a). "Int. COIL R&D Workshop." Prague, Czech Rep., 28-29 May 2001, CD-ROM.

Ionin A., Napartovich A., Yuryshev N. (2001b). "Int. Workshop on High Energy Lasers Including Novel Pumping Schemes driven by Chemical Reactions or Explosives." French-German Res. Inst. Saint-Louis, France, Nov 13-14, 2001, CD-ROM.

Ionin A., Napartovich A, Yuryshev N. (2002). "Photonics West Conf LASE 2002." San Jose, CA, USA, Jan 2002, *Proc. SPIE,* **4631,** p.284; Int. Symp. High Power Laser Ablation, Taos, NM, USA, Apr 2002, *Proc.SPIE* **4760**, p.506.

Ionin A.A., Klimachev Yu.M. et al. (2003). *J. Phys. D: Appl. Phys.*, **36**, 982.

Itami S., Nakamura Y., Shinagawa K., Okamura M., Fujii H. et al. (1999). Proc. SPIE, **3889**, 503.

Ivanov V, Klopovsky K., Rakhimov A. et al. (1999). *IEEE Transactions on plasma science*, **27**, 1279.

Kaufman F. (1961). *Prog. React. Kinet.* **1**, 1.

King D., Carroll D., Laystrom J., Verdeyen J., Sexauer M. and Solomon W. (2001). *Proc. Int. Conf. LASERS'2000*, Ed. by V. Corcoran and T. Corcoran, STS Press, McLean ,VA, 265.

Kitaeva V.F., Osipov Yu.I. (1968). *J. Tech. Phys.*, **38**(2), 384.

Kolobyanin Yu.V., et al. (2005). *AIAA Paper 2005-4920***,** 36th AIAA Plasmadynamics and Laser Conference, 6-9 June 2005, Toronto, Canada.

Kondrat'ev V.N. and Nikitin E.E. (1974). *"Kinetics and Mechanisms of gas phase reactions"*, Moscow, "Nauka", (in Russian).

Kuznetsov A.A., Novgorodov M.Z., Ochkin V.N., et al. (2000). *Quantum Electronics*, **30**, 399.

Lambertson S. (2001). *Proc. SPIE* ,**4184**, 1.

Londer Ya., Menakhin L., Ul'yanov K. (1981). *Teplofizika Visokith Temperatur*, **4**, 720 (in Russian)

Londer Ya.I., Menakhin L.P., Ul'yanov K.N. (1984). *Teplofizjka Vysokikh Temperatur*, **19**, 720, (in Russian).

McDaniel E.W., Mason E.A. (1973). "The mobility and diffusion of ions in gases", "J.Wiley an Sons".

McDermott W.E., Pchelkin N.R. et al. (1978). *Appl. Phys. Lett*., **32**, 469.

Mc Ewan M.J., Phillips L.F. (1975). “Chemistry of the Atmosphere”, Chemistry Department, University of Canterbery Christchurch. New Zealand. Edward Arnold.

Miller H.C., McCord J.E, Choy J., Hager G.D. (2001). *J.Quantitative Spectroscopy and Radiative Transfer*, **69**, 305.

Napartovich A., Deryugin A., Kochetov I. (2001). *J. Phys. D: Appl. Phys.*, **34**, 1827.

O’Malley T.F. (1967). *Phys. Rev*., **155**, 59.

Pazyuk V.S., Podmar'kov Yu.P., Raspopov N.A, Frolov M.P. (2001). *Quantum Electron*., **31**, 363.

Railly J.P. (1972). *J. Appl. Phys.*, **43**, 3411.

Raizer Yu.P., (1991). "Gas Discharge Physics", Springer-Verlag, Berlin.

Raizer Yu.P., (1992). "Physics of gas discharge", Nauka, Moscow.

Rakhimova T.V., et al. (2005). *AIAA Paper 2005-4918***,** 36th AIAA Plasmadynamics and Laser Conference, 6-9 June 2005, Toronto, Canada.

Rybkin V.V., Smirnov S.A., Ivanov A.N. (2005). Proceeding of the IV International Symposium on Theoretical and Applied Plasma Chemistry, Ivanovo, Russia, Published by Ivanovo State University of Chemistry and Technology, **1**, 247 (in Russian).

Schmiedberger J., Hirahara S., Fujii H. et al. (2000). *Proc. SPIE*, **4184,** 32.

“Singlet Oxygen” ed. by H.H.Wasserman and R.W.Murray. (1979). Academic Press, N.Y.

“Singlet O_2 , v.1 Physical-Chemical Aspects”, ed. by A.A.Frimer (1985). CRC Press, Inc., Boca Raton, Florida .

Torchin L., Jegou R., Brunet H. (1983). *J.Chem.Phys*., **79**, 2100.

Vagin N.P., Ionin A.A., et al. (2003). *Plasma Physics Reports*, **29**, 211.

Vasil’eva A.N., Grishina I.A., Klopovskii K.S. et al. (1989). *Plazma Phys.*, **15**, 190.

Vasilijeva A.N., Klopvskiy K.S., Kovalev A.S. et al. (2004). *J.Phys.D: Appl.Phys.* **37,** 2455.

Velichov E.P. (1987). "Gas Discharge Physics". M. Nauka (in Russian).

Virin L.I., Dzhagatspanyan R.V., Karachevtsev G.V., Potapov V.K., Tal’roze V.L. (1979). "Ion-molecular reactions in gas", Nauka, Moscow.

Wang B., Gu Y. (1998). *J. Phys. Chem. A*., **102**, 9367.

Wayne R.P., (1969). “Singlet Molecular Oxygen” in “Advances in Photochemistry”, **7**, 311.

Webster H., Bair E. J. (1972). *J. of Chemical Physics*, **56**, 6104.

Yuryshev N.N. (1996). *Quantum Electronics*, **26** (7), 567.

Yuryshev N.N. (2003). *Plasma Physics Reports*, **29**, 211-219.

Yuryshev N.N., et al. (2004). *Proc. SPIE*, **5448,** 790.

Zalessky V. (1974). *J.Experimental and Theoretical Physics*, **67**, 30 (in Russian).

Zhiglinskii A.G. ed. (1994). "Handbook of constant of elementary processes with atoms, ions, electrons and photons", St.-Petersburg State University, St.-Petersburg.

Zhivukhin I., Ionin A., Kel’ner M., Sinitsyn D et al. (1989). *Sov. J.Quantum Electronics*, **19**, 1036.

Part II.4. SINGLET DELTA OXYGEN PRODUCTION IN A VORTEX DISCHARGE (Samara)

(Subtasks 1B.1, 1B.2 and 2B.4)

Introduction

A study of physical mechanisms, governing the production of singlet delta oxygen (SDO) in a vortex stabilized DC glow discharge was performed.

In the experiments with discharge in a vortex gas flow of oxygen or oxygen containing mixtures performed earlier within the frame of the ISTC project #1826, the dependencies of SDO concentration upon discharge current and discharge current-voltage characteristics were obtained. In particular, it was found that with discharge current SDO concentration first increased and then, after a minor jump, decreased. Current-voltage characteristics had a corresponding jump too.

Within the frame of the current Project the studies of discharge were continued (*Task 1B.1*) in order to determine the physical origin of the said jump. In particular, high resolution spectra were obtained of the pink glow, identical in color with the dimole $O_2(^1\Delta)$-$O_2(^1\Delta)$ emission if viewed by the naked eye or with low resolution, that aroused in the central part of the discharge after the jump. The dependence of SO concentration upon the time of interaction of the gas with the discharge was determined (*Task 1B.2*). The rates of SO quenching in the afterglow in the near vicinity of the discharge region were determined for different flow velocities.

According to the work plan of the 2-nd year of the project (*Subtask 2B.4*) the experiments were performed to study the effect of additives that may be quenchers of SDO molecules, and the effect of decrease of mean electron energy on the concentration of SDO produced in discharge. Decrease of mean electron energy in the DC vortex-flow discharge was achieved using double discharge technique, when the first discharge upstream acted as the source of preionization for the second discharge downstream.

The 3-d year of the project (Part II.4) was not financed by the decision of the project manager due to the diminished budget partially cut by the Partner.

Study of the vortex-flow discharge in oxygen-containing gas mixtures (*Subtask 1B.1*)

A series of current-voltage characteristics were obtained for various oxygen pressures and flow rates (**Fig.II.4.1**). It has been found that the said voltage (**Fig.II.4.1a**) and $O_2(a^1\Delta)$ concentration (**Fig.II.4.1b**) jumps occurred for the power load into the discharge positive column of ~ 30 kJ/mol. At the moment of the jump, homogeneous diffuse pink glow appeared on the axis of the discharge, identical by color to $O_2(a^1\Delta)$-$O_2(a^1\Delta)$ dimole emission if viewed by the naked eye. Diameter of this pink glow region was approximately 1/3 of diameter of the tube, i.e. about 1 cm, and its length was nearly equal to interelectrode distance.

The emission greatly resemble $O_2(a^1\Delta)$-$O_2(a^1\Delta)$ dimole emission as visually also in low resolution spectra. As known maximum of the $O_2(a^1\Delta)$ dimole emission lies at 635 nm. The emission had maximum at 635 nm in low resolution spectra too. Note that appearances of the dimole glow like that usually indicate high SDO concentration.

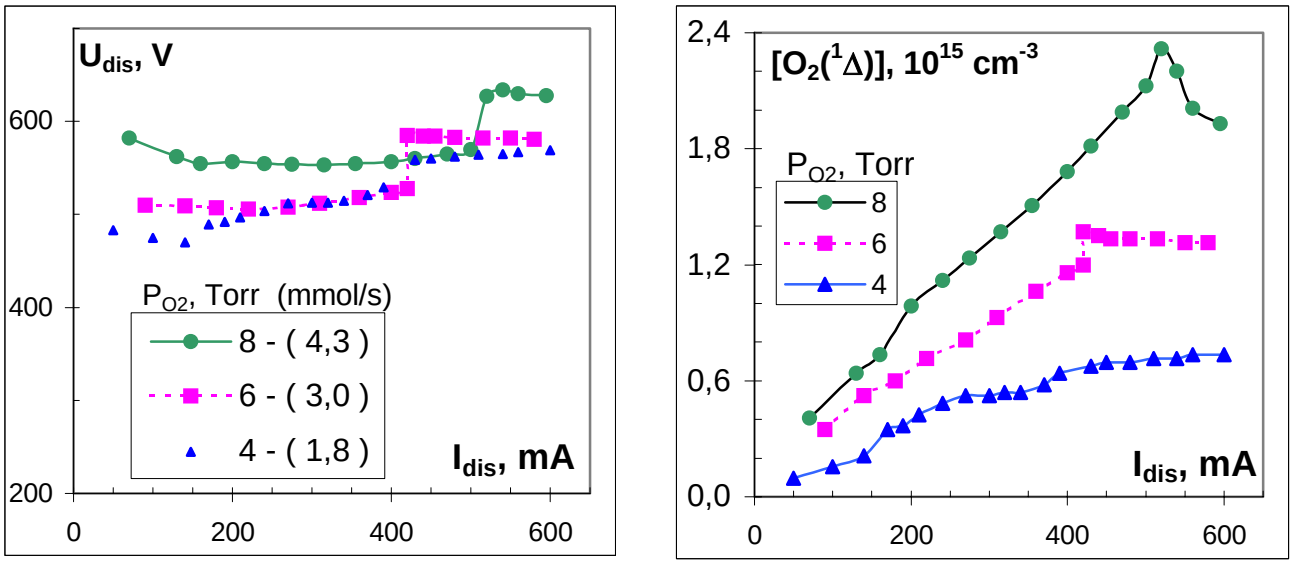

a) b)

Fig.II.4.1. Discharge voltage (a) and $O_2(a^1\Delta)$ concentration (b) depending on discharge current with appropriate jumps.

Spectral measurements of the emission from the central region of discharge plasma were performed. The measurements had shown that observed pink glow, is emitted by oxygen atoms. The most intensive are two groups of atomic oxygen lines – 616 and 645 nm (**Fig.II.4.2**), i.e. near the dimole emission band. At the moment of voltage jump intensity of atomic oxygen lines increased an order of magnitude, whereas current increased only 10%.

The recorded spectra with 0.1 nm resolution had shown that observed pink glow, which intensity increased by an order of magnitude at the moment of the jump, is emitted by oxygen atoms.

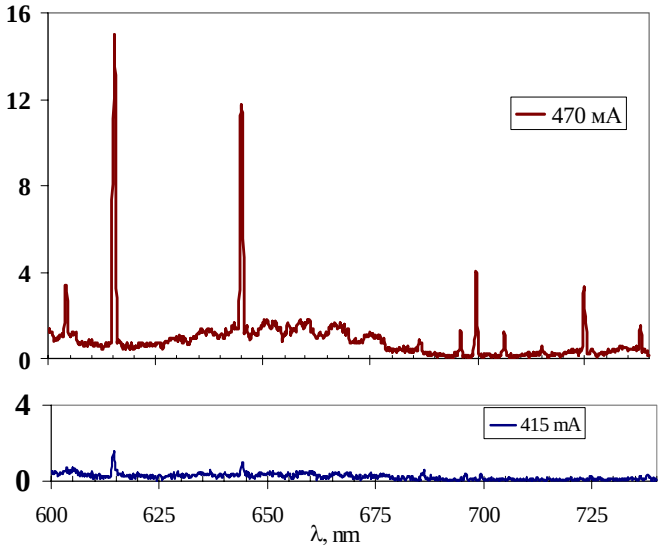

Fig.II.4.2. Spectra of the discharge central region for two discharge conditions.

The cause of swift appearance of pink glow is the change of discharge shape. At the moment of jump contraction of the positive column takes place, and current channel becomes smaller. Under these conditions electron concentration in the central region of the plasma and oxygen atoms excitation rate increase by an order of magnitude.

Measurements of singlet oxygen number density varying gas velocity and interelectrode distance in discharge.
(*Subtask 1B.2*)

The aim of the first series of experiments was to study the kind and amount of influence of the duration of flowing gas exposure to the discharge upon $O_2(a^1\Delta)$ number density. In particular, the experiments checked the prediction of the previously developed numerical model, that in the conditions of our experiments, the duration of gas interaction with the discharge (usually 1-3 ms in our experiments) might be insufficient for $O_2(a^1\Delta)$ number density to reach stationary value. Note that the change of residence time of gas in the discharge region at a constant current corresponds with the change of specific power load.

The second series of the experiments was aimed to determine the amount of quenching of $O_2(a^1\Delta)$ in the downstream afterglow in the near vicinity of the discharge region.

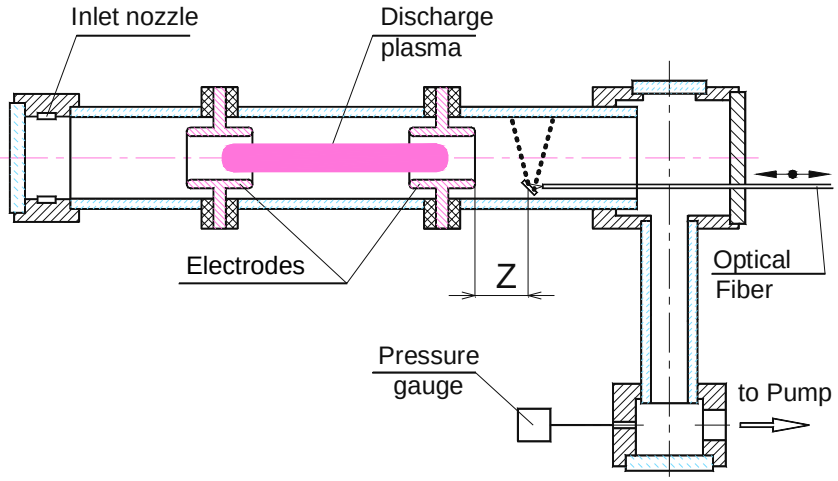

Fig. II.4.3. Experimental setup.

DC glow discharge in the gas flow was sustained in a quartz tube 3 cm in diameter (**Fig.II.4.3**). Water cooled copper electrodes with inner working surfaces of 1.8 cm diameter and 5 cm length were used. Interelectrode distance was 7 and 4.5 cm. Oxygen pressure in the diagnostic arm was 6 and 10 Torr with corresponding flow rate up to 3.3 and 5 mmol/s. Under these conditions mean mass flow velocity amounted up to 30 m/s with the gas transport time across the discharge region down to ~1.5 ms. $O_2(a^1\Delta)$ number density was measured in the downstream afterglow measuring emission intensity at 1.27 μm (**Fig.II.4.3**).

With the help of an optical fiber optical emission at the right angle to the flow direction in the near vicinity to the anode was collected. Optical emission was sampled near the anode of the discharge chamber (1 cm downstream was the nearest) to eliminate possible quenching of SDO along the flow in the first series of experiments. In the second series the optical fiber was moved along the flow to observe change in SDO concentration due to quenching.

The first series.

The obtained results had shown two distinctly different regions of $O_2(a^1\Delta)$ number density dependence on current for all flow rates. The results of the measurements for interelectrode distance of 7 cm at 6 torr pressure are shown in the **Fig.II.4.4 a, b**.

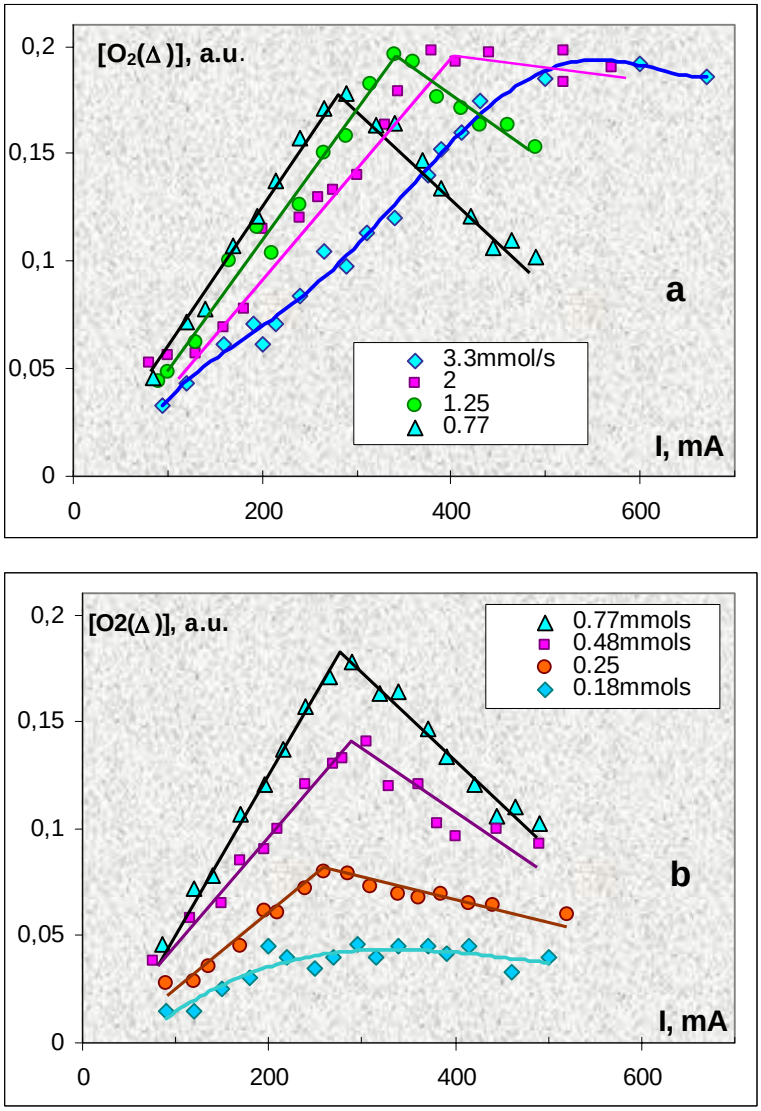

Fig.II.4.4. Dependence of $O_2(a^1\Delta)$ number density on discharge current for different flow rates. **a)** - high flow rates (0.77-3.3 mmols/s), **b)** - low flow rates (0.18-0.77 mmols/s).

Starting from small currents, $O_2(a^1\Delta)$ number density increased in essence linear with the current. Then, after certain current magnitude, the number density decreased, also essentially linear. Gas flow rate affected those current dependencies differently at high and low flow rates. At high flow rates (more than 0.77 mmol/s at 6 torr, **Fig.II.4.4 a**) in the region of the $O_2(a^1\Delta)$ number density growth, the $O_2(a^1\Delta)$ number density is higher for lower flow rates at the same values of discharge current. At low flow rates (less than 0.77 mmol/s, **Fig.II.4.4 b**) – vice versa. Also, at low flow rates the maximum value of $O_2(a^1\Delta)$ number density became smaller with the decrease of the flow rate (see **Fig.II.4.4 a, b)** and was observed at smaller current. Analogous dependencies were obtained at 10 torr pressure.

For the discharge with interelectrode distance of 4.5 cm the obtained dependencies were of the same nature as in the previous case. However, $O_2(a^1\Delta)$ number density maximum was shifted to higher currents. Nevertheless, the highest concentrations observed did not exceed those obtained for 7 cm interelectrode distance.

Therefore, in accordance with prediction of our numerical model, the duration of interaction of discharge with gas flow affects $O_2(a^1\Delta)$ number density, although in a more complicated manner

then in computations. In the conditions of our experiment, $O_2(a^1\Delta)$ number density increased when gas and discharge interacted up to 10 ms. Further increase of the gas exposure to the discharge had lead to the decrease of $O_2(a^1\Delta)$ number density.

The second series.

The results of the second series of experiments are presented in the **Fig.II.4.5**. Interelectrode distance was 7 cm. The specified value of discharge current corresponded to contracted state of the discharge when the $O_2(a^1\Delta)$ number density was near its highest value. The decrease of $O_2(a^1\Delta)$ concentration along the flow was observed, indicating the presence of quenching. The results obtained permitted us to estimate the effective loss frequency ν_{ef} of $O_2(a^1\Delta)$ molecules in the downstream afterglow region:

$$\frac{1}{N_{O2(\Delta)}}\frac{\partial N_{O2(\Delta)}}{\partial t} = -k_{ef} N_x = -\nu_{ef},$$

where k_{ef} is effective rate constant of the second order process of quenching by unknown particles X with concentration N_x.

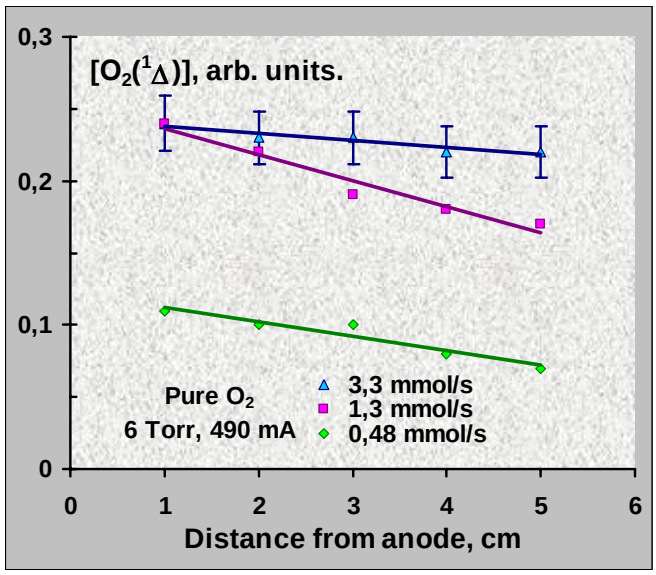

Fig.II.4.5. $O_2(a^1\Delta)$ signal along the flow.

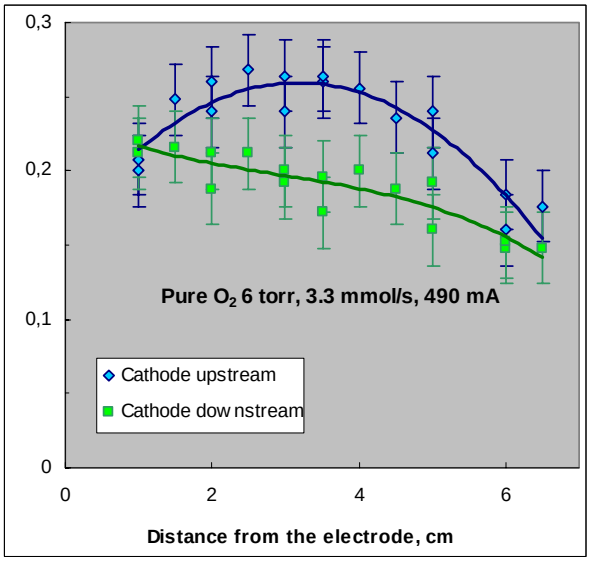

Fig.II.4.6. $O_2(a^1\Delta)$ signal along the flow with dependence to electrode position along the flow.

At 6 torr pressure and flow rate of 3.3 mmol/s ν_{ef} ≈75 s^{-1}. For the data on RF discharge from (Klopovskii et al, 1992) at 10 torr pressure we obtained ν_{ef} ≈60 s^{-1} that is close to our estimated value. The observed quenching rate is 3-4 times smaller than the model predicts for the conditions of the discharge. Therefore, powerful quenchers existed in the discharge are absent in the afterglow.

The change of the electrodes polarity relatively to the flow direction affected $O_2(a^1\Delta)$ number density. As it is seen from the **Fig.II.4.6**, $O_2(a^1\Delta)$ concentration is higher, when the cathode is placed upstream. The data in the **Fig.II.4.6** corresponded to interelectrode distance 45 mm and 490 mA discharge current and differed from the data presented in Fig.**II.4.5** because for smaller interelectrode distance no contraction was observed at 490 mA.

Experimental study of the effect of varying of mean electron energy in discharge and removing quenchers in the downstream afterglow on the SDO yield. Measurement of SDO

concentration using discharge with different mean electron energies varying it using different mixtures and using the combination of two discharges.
(Subtask 2B.4)

1. Information about possible influence of $O_2(^1\Delta)$ quenchers was obtained in the experiments with discharge when SDO concentrations were measured in two cases: first for the "clean" chamber and second – "dirty", when uncontrolled products of methyl iodide decomposition were deposited on the walls of the discharge chamber and the diagnostic arm. The experiments were conducted in mixtures of oxygen with argon using the setup represented in **Fig. III.11.** Those products were prepared beforehand, admixing methyl iodide in the oxygen-argon mixture immediately downstream of the discharge during 20-30 minutes. (see Part III of the Report).

It was found that contamination by products of CH_3I decomposition, with other conditions equal, had led to a substantial, up to two times, increase of SDO contrary to the “clean” state of the discharge setup. This effect revealed itself over a long period of time, at least during several hours of discharge operation. It disappeared only after the inner surfaces of the discharge chamber and the diagnostic arm were washed by water.

As it was found in our previous experiments (Mikheyev, 2000), small additions of hydrogen containing organic substances into the downstream afterglow of a discharge in oxygen or oxygen-containing mixtures led to 2-3 times increase of SDO concentration in the discharge products. However, in these experiments “memory” effect was not noticed, presumably due to the short time of operation with additives.

The emission spectra of SDO recorded in the “clean” and “dirty” discharge system are represented in the **Fig. II.4.7**. As it is seen, there are no visible distortions of the spectra by additional lines. Note that the amplitudes of the spectra obtained from the contaminated setup is almost twice higher other conditions being equal.

The physical mechanism of such an effect of CH_3I decomposition products on SDO concentration is presumably due to heterogeneous processes on the walls of the discharge chamber, diagnostic arm and, may be, on the surface of the electrodes. The hypothesis may be proposed that residual quantities of additives on the walls increase the rate of heterogeneous removal of SDO quenchers. For example, it is known that the rate of heterogeneous recombination of the oxygen atoms strongly depends on surface conditions. The O atoms and SDO, as is known, are present in discharge products in about the same amounts. O atoms in the ground state do not quench SDO molecules substantially, but O atoms in some excited states, like $O(^1S)$, quench SDO very efficiently (Shepelenko and Fomin, 2002).

Another hypothesis – residual amounts of additives on the walls decrease the rate of heterogeneous quenching of SDO itself. The possibility that some particles that are the products of CH_3I decomposition, desorbing from the walls substantially affect SDO concentration cannot be discarded too.

At present insufficient data is available to explain the found effect. Nevertheless, the understanding of its mechanism should be quite useful for discharge SDO generator development. To gain this understanding and to determine the potential of the described effect further studies are needed.

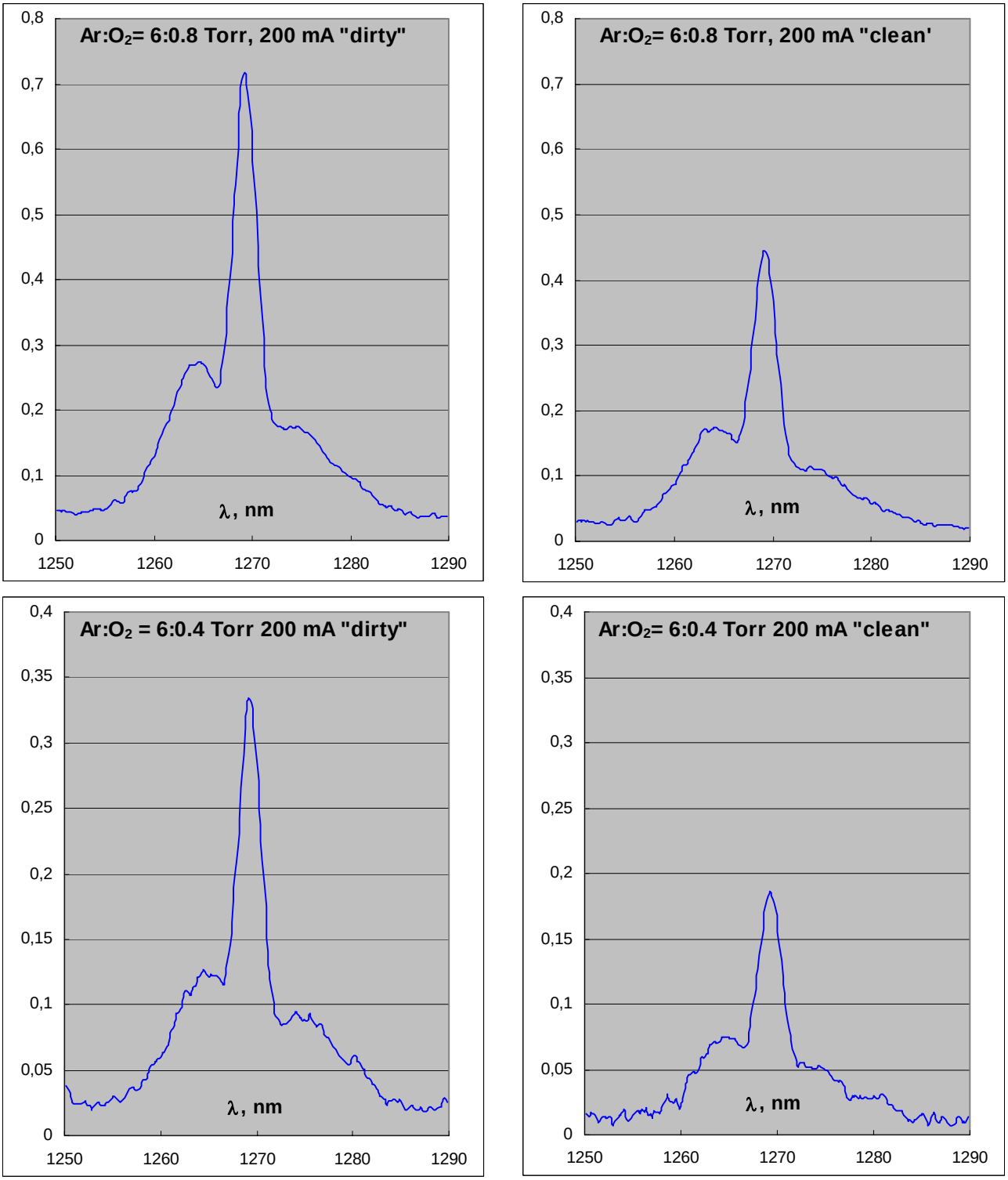

Fig. II.4.7. Emission spectra of $O_2(a^1\Delta)$ in the "clean " and "dirty" discharge systems for two $Ar:O_2$ mixtures.

2. Influence of the mean electron energy on the SDO yield in the discharge plasma was studied with the help of the combination of two DC discharges in the vortex flow, when the first discharge upstream was used as the external source of preionization for the second. In these

experimental conditions the second discharge was not totally non self sustained due to this external preionization, nevertheless it provided the decrease of the E/N parameter of plasma and, consequently, the decrease of mean electron energy.

The experiments were performed to measure concentration of SDO produced in the double discharge in the gas flow. To produce double discharge, the discharge chamber was modified and the additional power supply was manufactured. The design of the discharge chamber with the diagnostic arm is shown schematically in **Fig. II.4.8**. The chamber includes two discharge devices placed in series around the gas flow.

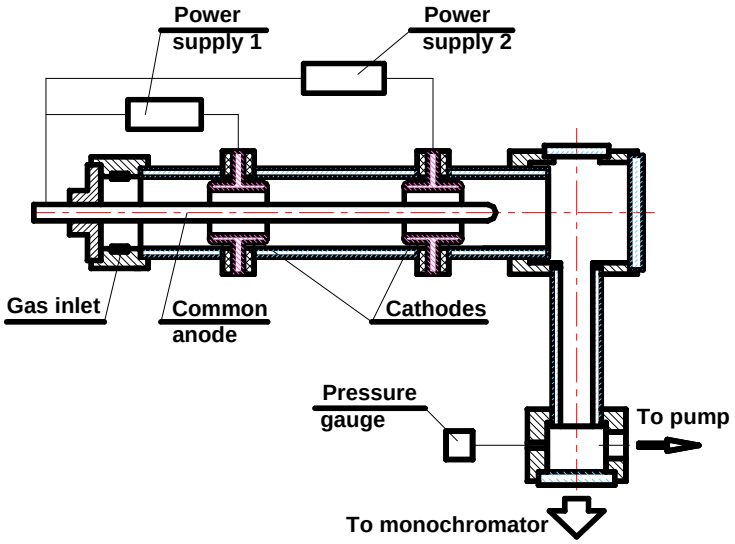

Fig. II.4.8. Schematic diagram of the discharge chamber and the diagnostic arm for the experiments with double discharge

The experiments were performed with coaxial configuration of electrodes. The inner anode was a water cooled copper cylinder 10 mm in diameter, common for both discharges and the outer electrodes – water cooled copper cathodes 29 mm of inner diameter. The distance between the outer electrodes was 50 or 25 mm.

Plasma produced by the first discharge is transported by the gas flow and does not have time to fully recombine before it enters the region of the second discharge. Therefore, the second discharge operates in non self sustained regime and its external ionization is provided by inflow of plasma and, possibly, by the UV ionization from the first discharge.

Oxygen pressure varied in experiments from 6 to 12 torr, and also oxygen-argon mixture O_2:Ar = 2:10 torr was used. SDO concentration was determined like in previous experiments measuring emission intensity at 1.27 μm.

The experiments has shown substantial decrease of the discharge voltage of the second discharge when the first discharge was in operation. It is seen in **Fig. II.4.9**, where current-voltage characteristics of the second downstream discharge are plotted for pure oxygen at 10 torr pressure. Therefore, the influence of the first discharge on the second one led to substantial decrease of the mean electric field in plasma. E/N parameter and mean electron energy, substantial decrease compared to the situation when the first discharge was absent. For example, in oxygen at 10 torr pressure in the self sustained mode of discharge with the first discharge absent E/N was ~$25 \cdot 10^{-17}$ V·cm^2. In the non self sustained mode the mean E/N value decreased down to ~$16 \cdot 10^{-17}$ V·cm^2.

Note that such a decrease in E/N is not due to the heating of the gas. It is easily seen from **Fig. II.4.9.** We can see, as the increase in current of the first discharge from 100 to 500 mA and, therefore, different prior heating of the gas does not lead to substantial changes in the voltage of the

second discharge. Consequently, changes in E/N are insignificant. Mean E/N in the plasma was estimated using the experimental date in two different ways. First – using the measured values of discharge voltage and the values for cathode and anode falls from literature. Second – using the measured values of discharge voltage at different pressures – 6, 8 and 10 torr and assuming that there is no dependence of mean E/N on pressure. The results of these estimations coincide within the accuracy of the used values of anode and cathode falls.

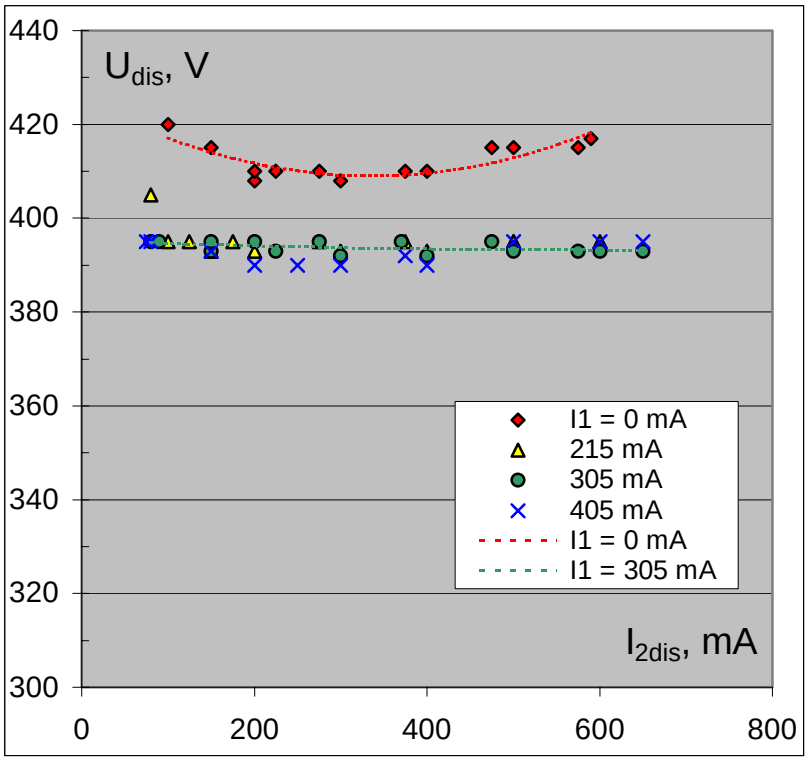

Fig. II.4.9. Current-voltage characteristics of the second discharge with different discharge currents of the first discharge. Distance between the 1-st and the 2-nd discharges 2.5 cm. Oxygen at 10 torr pressure.

SDO concentration in the presence of two discharges differed from the case, when the first discharge was absent. The measured SDO concentrations are plotted in **Fig. II.4.10** with dependence on current of the second discharge. At low currents of the second (non self sustained) discharge SDO concentration was higher than that in the absence of the first discharge. Evidently, it should be so, because the gas flow entering the second discharge contains SDO produced by the first discharge. However, considering all the data and comparing three cases: two discharges operate, only the first operate and only the second operate we have found that double discharge produce concentration of SDO smaller then the sum of concentrations produced by the first and the second discharges separately. Considering the data obtained at different pressures one can conclude that increment of SDO due to switching on the first discharge in addition to the operating second discharge is much lower then the concentration produced by the first discharge separately.

SDO concentration increased in essence linear with the second discharge current for both double discharge and separate modes of operation. However, the slope of this dependence decreased as the current of the first discharge increased. In other words, with the first discharge in operation the increment in SDO was smaller for the same increment of the second discharge power. As the result, for high values of the second discharge current the achieved SDO concentration was even lower then in the absence of the first discharge.

Therefore, non additive behavior of power load delivered into two discharges on SDO production was observed. Power loaded in one discharge produces SDO more efficiently, then the same power loaded into two discharges. The observed effect cannot be explained by the decrease of SDO concentration along the flow from the first to the second discharge. This statement is supported by the results of our previous experiments (*Subtask 1B.2*, (Shepelenko, 2002)). The results had also shown that no increase in efficiency of SDO production was observed due to the decrease of E/N parameter and, consequently, mean electron energy in plasma.

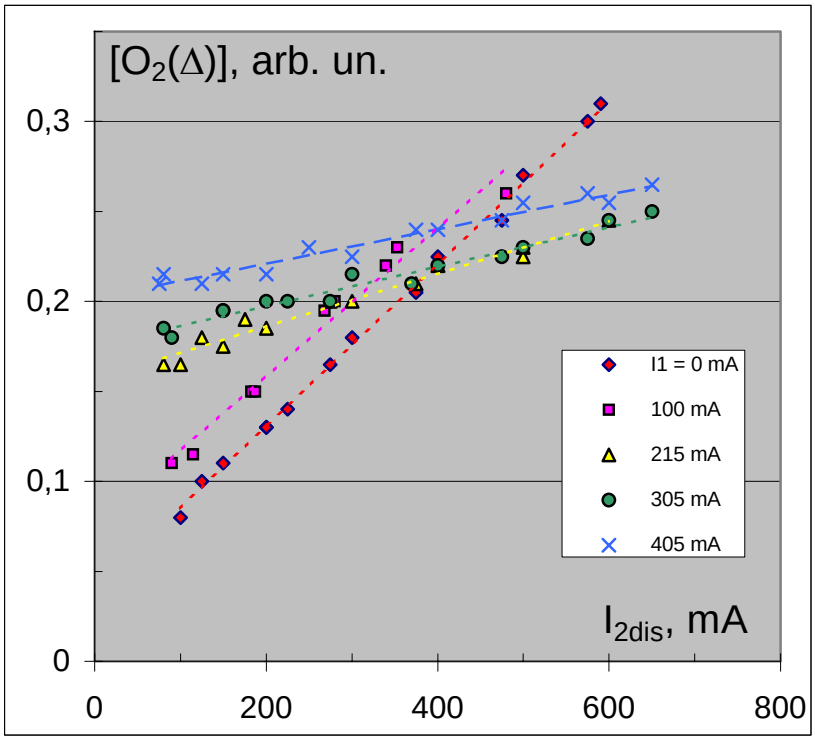

Fig. II.4.10. Plots of $O_2(^1\Delta)$ concentration on discharge current of the second discharge with different currents of the first discharge.
Distance between the 1-st and the 2-nd discharges 2.5 cm. Oxygen at 10 torr pressure.

In the experiments with the mixture O_2:Ar, as it is seen from **Fig. II.4.11**, similar, however, less pronounced effect of the first discharge on the SDO concentration was observed. We point out that in this case relative SDO concentration $[O_2(\Delta)]/[O_2(X)]$ is twice or more higher then in pure oxygen.

Therefore the decrease of the E/N parameter in plasma and, therefore decrease in the mean electron energy achieved using the discharge with external preionization did not lead to more efficient SDO production.

Only the most important trends of SDO production in the double discharge, found in the experiments, are described here. Further studies are needed to explain their physical mechanisms and to obtain comprehensive and more precise data, in particular, absolute values of E/N and SDO concentrations in plasma.

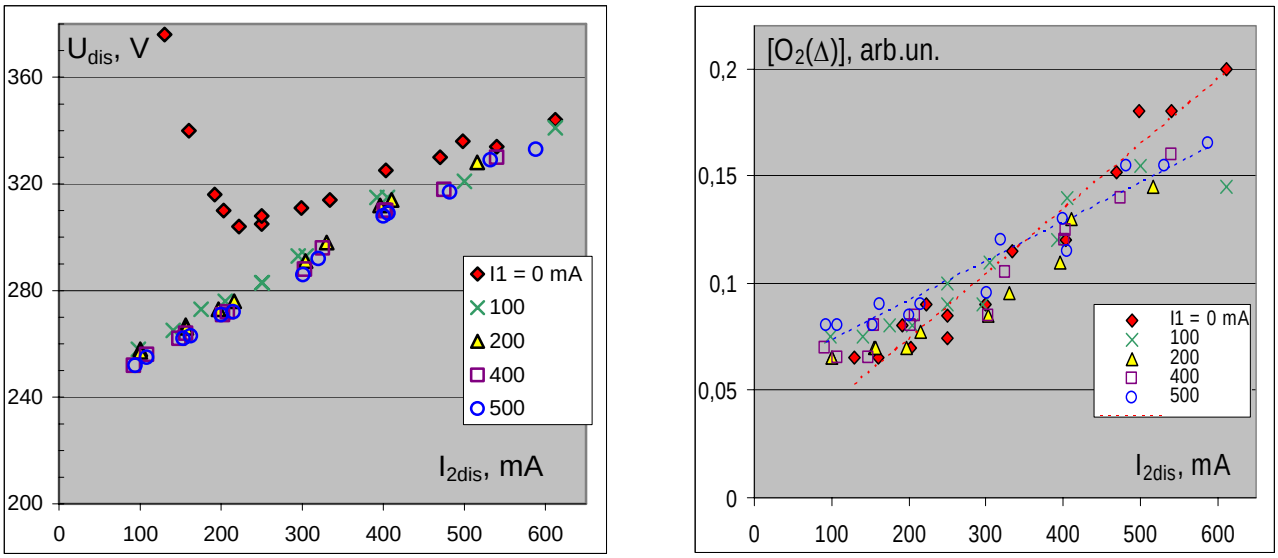

a **b**

Fig. II.4.11. Current-voltage characteristics of the second discharge (a) and plots of $O_2(^1\Delta)$ concentration on discharge current of the second discharge (b) with different currents of the first discharge. Distance between the 1-st and the 2-nd discharges 2.5 cm. O_2:Ar mixture at 2:12 torr.

Conclusions

Spectral measurements of the emission from the central region of discharge plasma were performed that appeared at the moment of the jump of the discharge characteristics. This pink glow was identical in color with the dimole $O_2(^1\Delta)$-$O_2(^1\Delta)$ emission if viewed by the naked eye. Appearance of the dimole glow like that usually indicate high SDO concentration. At low resolution its maximum coincides with the SDO dimole peak. The recorded spectra with 0.1 nm resolution had shown that observed pink glow, which intensity increased by an order of magnitude at the moment of the jump, is emitted by oxygen atoms.

The experiments studying the kind and amount of influence of the duration of flowing gas exposure to discharge upon $O_2(a^1\Delta)$ number density were performed. Previously developed numerical model predicted that the duration of gas interaction with discharge might be insufficient for SDO number density to reach stationary maximum. The experiments had shown that duration of gas exposure to discharge significantly affects SDO number density, although in a more complicated manner, then in computations. In the conditions of our experiment, SDO number density increased when gas and discharge interacted up to ~10 ms. Further increase of gas exposure to discharge had lead to decrease of $O_2(a^1\Delta)$ number density.

SDO number density distributions along the flow were determined in the afterglow region in the near vicinity to the discharge region. A decrease in concentration was observed indicating quenching. The SDO quenching rates in the afterglow in the near vicinity of the discharge region were determined for different flow velocities. The observed quenching rates are 3-4 times lower than that predicted by the numerical model in the discharge. It may be concluded that strong quenchers present in a discharge are absent in the afterglow.

The information about the possible influence of SDO quenchers on the SDO concentration from the discharge was obtained in the experiments with Ar:O_2 mixtures when uncontrolled products of methyl iodide decomposition were present on the walls of the discharge chamber and the diagnostic arm. It was found that presence of the products of CH_3I decomposition lead to

considerable increase – up to 2 times compared to a "clean" discharge system, in the SDO concentration other conditions being equal. This effect remained stable during a lengthy time interval, at least several hours, of the discharge operation. Evidently, the residual quantities of the contaminants on the walls either increase quenching rate of the SDO quenchers, or decrease heterogeneous quenching of SDO molecules.

The effect of an external influence on the discharge, leading to decrease in the mean energy of the electrons in the plasma and on the SDO production was studied. The decrease in the mean energy was achieved using a double-discharge configuration, where the first upstream discharge was the source of external preionization for the second downstream discharge. The performed measurements has shown considerable decrease in the E/N parameter of the second downstream discharge when the first upstream discharge had operated. Considerable changes in SDO production in the second discharge were found when the current of the first discharge varied. The effect of non-additivity of power loaded in both discharges on SDO generation was observed. Power loaded in one discharge generated SDO more efficiently than the same power distributed between two discharges. The increase in efficiency of SDO production due to lower E/N values and correspondingly lower mean electron values was not observed.

References for Part II.4.

Klopovskii K.S., Kovalev A.S., Lopaev D.V., et al. (1992). *Sov. J. Plasma Phys*., **18**, 834.

Mikheyev P.A, Shepelenko A.A, Kupryayev N.V and Voronov A.I. (2000). "Singlet Oxygen Production in Vortex-Flow DC Glow Discharge". *Proc. SPIE*, **3931**, 81.

Shepelenko A.A, Mikheyev P.A, Kupryayev N.V, Voronov A.I. (2002). "Singlet delta oxygen concentration in the afterglow of a dc glow discharge in oxygen". Proc. 3-d Int. Symposium "Theoretical and applied plasma chemistry", Ples, Russia, 2002, Vol.1, pp. 138-141. (in Russian).

Shepelenko A.A, Fomin E.V. (2002). "Mechanisms of production and decay of $O_2(^1\Delta)$ molecules in oxygen plasma of a DC discharge". Proc. 3-d Int. Symposium "Theoretical and applied plasma chemistry", Ples, Russia, 2002, Vol.1, pp. 199-202. (in Russian).

Shepelenko AA, Mikheyev PA, Voronov AI, Kupryayev NV. (2005*). Proc. IV-d Int. Symposium on Theoretical and Applied Plasma Chemistry"*, Ivanovo, Russia, 2005, Vol.**1**, pp. 159-162. (in Russian).

Shepelenko AA, Mikheyev PA, Voronov AI, Kupryayev NV. "Double discharge in oxygen and singlet oxygen concentrations produced there". *Izvestia of the Samara scientific center of RAS, V. **7**(1) P. 65-70.* (in Russian)

Part II.5. SINGLET DELTA OXYGEN PRODUCTION IN RF SLAB DISCHARGE (*Subtasks 3.1, 3.2, 3.3 and 3.4*)

Introduction

Observation of positive gain (Carroll, 2005a) and lasing (Carroll, 2005b) in OIL with electrical generator of SDO validates the feasibility of electrically driven OIL. Thus, the problem of the development of efficient and usable electrical SDO generator becomes of great importance now. This fact makes scientists investigate different types of electrical discharges looking for the best of them as a source of SDO. In (Carroll, 2005b), where lasing in RF discharge OIL was demonstrated, gas mixture was cooled through supersonic expansion. Gas pressure in a resonator region of the laser was 1.55 Torr, and output power achieved 0.22 W (Carroll, 2005b). The very possibility of getting lasing in (Carroll, 2005b) depended on the active medium temperature. As soon as an electric discharge in gas results in gas heating, one needs to reduce gas temperature.

A slab structure of discharge system seems to be very attractive providing a very high gas cooling by gas diffusion and convection. To extract heat released in discharge and to decrease gas temperature in an electric discharge, a slab geometry widely applied to excitation of RF discharge CO_2 and CO lasers can be used. Moreover, in this geometry gas mixture can be cryogenically cooled without supersonic gas flow (Jianguo Xin, 1999). In that case gas pressure in OIL resonator region can achieve tens Torr, and output power of the potential electrically excited OIL can be considerably increased. It should be noted that electrodes material can influence on plasma-kinetic processes in a slab discharge, because the inter-electrode gap is usually very small ~2-3 mm. To estimate a potential of SDO production in a slab discharge, an experimental research of the discharge in oxygen gas mixtures is needed. The easiest way we follow in this paper is to study RF slab discharge in oxygen and SDO production by using a facility analogous to one used for a slab RF discharge CO_2 or CO laser.

The results of the experiments on studying SDO production in slab RF discharge ignited in oxygen gas mixtures are presented in the Report.

Study of slab RF discharge in oxygen mixtures. *(Subtask 3.1)*

Oxygen-iodine laser (OIL) operates on transitions of atomic iodine exciting by energy exchange with singlet delta oxygen (SDO). In chemical OIL SDO is produced by using dangerous and toxic substances. Electric discharge can be used as alternative method for SDO production. To achieve a positive gain in OIL the SDO yield $Y=[O_2(a^1\Delta_g)]/([O_2(a^1\Delta_g)]+[O_2(^3\Sigma_g^-)])$ where $[O_2(a^1\Delta_g)]$ and $[O_2(^3\Sigma_g^-)]$ are concentrations of SDO and oxygen in a ground state, has to exceed its threshold value Y_{th}. The value depends strongly on temperature T: $Y_{th} = [1+1.5\exp(402/T)]^{-1}$. In (Carrol, 2005b), where lasing in RF discharge OIL being demonstrated, gas mixture was cooled by supersonic extension. Gas pressure in laser resonator region was 1.55 Torr, and output power achieved 0.22 W. To decrease gas temperature in RF discharge a slab geometry of electrode system can be used. In such a discharge gas mixture can be cryogenically cooled (see, for instance, Part I.2 of the Report) without supersonic gas flow. Also, in this case gas pressure in OIL resonator region can achieve tens Torr, and output power of the laser can be increased considerably. From other standpoint perhaps in slab RF discharge some SDO quenchers can be removed by choosing the electrodes material, for instance, mercury oxide.

To study slab RF discharge in oxygen-containing mixtures, the RF generator described in (Part I.2 of the Report) was used. The generator with base frequency of 81.36 MHz can operate in continuous and pulse-width modulated mode. The modulation shape period T_{mod} can be varied from

40 μs up to 10 ms (modulation frequency 25 kHz - 100 Hz) (**Fig.II.5.1**). Each pulse consists of discharge initiation pre-pulse with duration of t_{PP} and pulse of main RF power with duration of t_P. Time t_{PP} can be varied from 0% (without pre-pulse mode) up to 10% of T_{mod} and, independently, t_P can be tuned in the range from 10% up to 100% of T_{mod} . The pre-pulse amplitude always corresponds to maximum power P_{RF}^{max} = 500 W. Amplitude of main RF power pulse can be changed from 25% to 100% of P_{RF}^{max}.

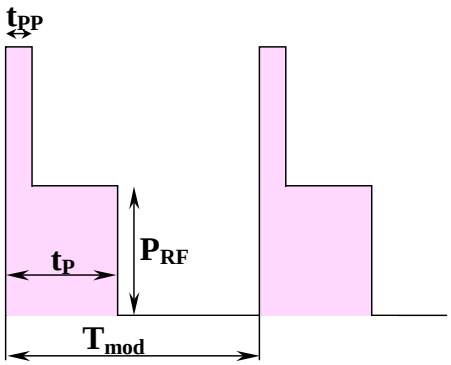

Fig.II.5.1. Pulse-width modulation shape of RF power.

An installation with slab discharge geometry was designed and manufactured for the experiments. The main view of the installation is presented in **Fig.II.5.2a**. Two water-cooled aluminum electrodes were placed inside the discharge chamber with total inner volume about 1.5 liter. RF discharge area of 285 x 30 mm^2 was determined by the electrodes size. The discharge gap was 3 mm. The installation was designed to have a possibility to change flexibly electrodes material by inserting thin plates made of different substances in the discharge area. RF discharge luminescence is supposed to be observed in longitudinal direction through the output glass window (**Fig.II.5.2b**).

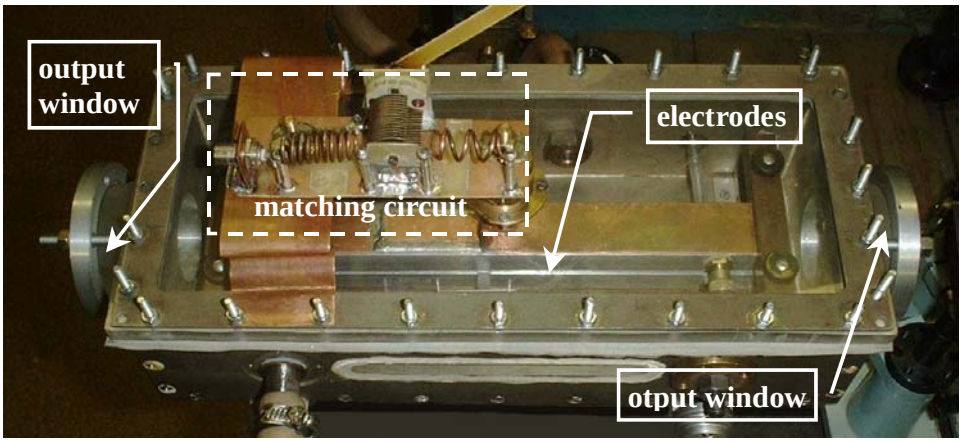

a

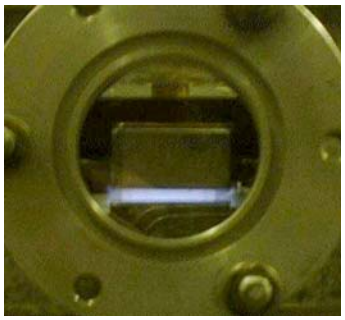

b

Fig.II.5.2. Installation with slab RF discharge geometry.
Main view (a) and front view with discharge glow in oxygen (b).

T-like matching circuit consisted of two variable inductance coils and tunable capacitor (see **Fig.II.5.3**) was used to load effectively RF power in the discharge plasma. The inductance of coils was varied stepwise by using a set of coils. The capacitance was tuned continuously to get the best matching between output impedance of the RF power supply (50 Ohm) and total impedance of the discharge system. The level of reflected RF power was controlled by oscilloscope connected to RF generator. Input power was measured by thermocouples placed at inlet and outlet of electrodes cooling water.

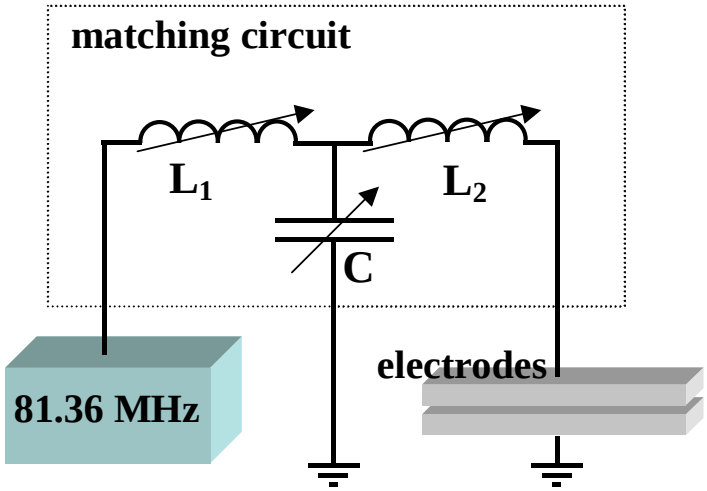

Fig.II.5.3. Matching circuit of RF power supply and discharge system.

The discharge in pure helium was stable up to gas pressure about 300 Torr. In oxygen contained gas mixture stable RF discharge was observed up to gas pressures 30 Torr (pure O_2), 45 Torr (O_2:He=1:1) and 60 Torr (O_2:He=1:3). In the experiments specific input energy can be varied in wide range. For instance, in pure oxygen at gas pressure 15 Torr specific input energy (calculated for single RF power pulse) was about 3.2 kJ/(l atm) at modulation frequency of 100 Hz, with pulse duration being of 3 ms at maximal RF power of 500 W. The typical picture of discharge glow in pure oxygen at gas pressure 15 Torr is presented in **Fig.II.5.2b**.

Development of SDO luminescence detection scheme with reduced noise using multi-pulse summing and averaging technique for RF slab discharge in oxygen.

(Subtask 3.2)

There are two problems connected with the experiments on slab RF discharge in oxygen gas mixtures for SDO production: a) very week SDO luminescence signal is expected because of respectively small RF discharge facility active volume (~20 cm^3); b) it is necessary to separate correctly the SDO luminescence spectrum and radiation from other species which could be produced in the RF discharge plasma. To solve these problems, special SDO luminescence detection scheme was developed. The scheme is based on diffraction monochromator and multi-pulse summing and averaging technique aiming to increase significantly signal-to-noise ratio.

Experiments on study of SDO production in slab RF discharge were carried out. Optical scheme of the experiments is presented in **Fig.II.5.4**. The SDO luminescence signal at the wavelengths around λ= 1.27 μm was detected by using a diffraction monochromator with a grating of 300 grooves/mm.

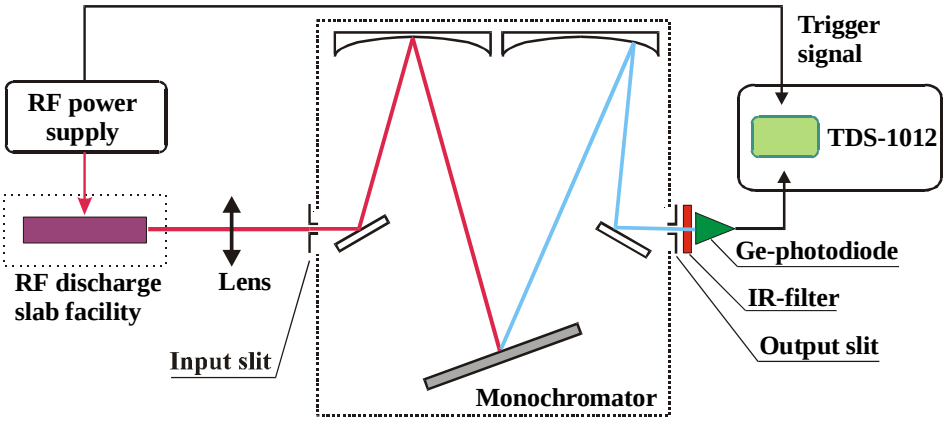

Fig.II.5.4. Optical scheme of SDO luminescence detection in slab RF discharge.

In the experiments spectral resolution of the monochromator determined by the output slit width was about 8 nm. After the monochromator, RF discharge glow and afterglow was directed to a room temperature Ge-photodetector equipped with hand-made high-gain differential electronic amplifier (rise time of ~1 ms). Output signal from the amplifier together with trigger signal from RF power supply were connected to digital oscilloscope "Tektronix TDS-1012". Significant photodetector noise was observed when using single sequence registration mode of the oscilloscope (**Fig.II.5.5a**). To increase signal-to-noise ratio, average signal function of the oscilloscope was used with the number of averaged sequences 4, 16 or 64 (**Fig.II.5.5b-d**). All the following experiments were carried out using registration technique with averaging of 64 sequences.

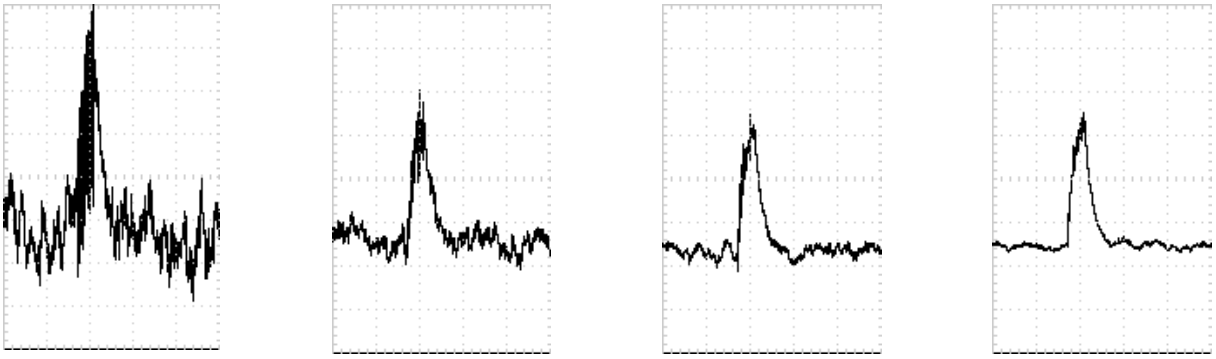

Fig. II.5.5. Typical SDO luminescence signals. **a** - single sequence mode, **b-d** - multi-sequence averaging mode. A number of averaged sequences: 4 (b), 16 (c), and 64 (d). Time scale 2.5 ms/div.

Typical time behavior of the optical signal at the wavelength of 1.27 μm obtained in pulse-width modulated RF power discharge mode is presented in **Fig.II.5.6**. High intensity luminescence was observed during the discharge within wide spectral range. Similar luminescence was observed in Part II.3 of the Report during pulsed electron-beam sustained discharge in oxygen containing gas mixtures. As was demonstrated in Part II.3 of the Report the luminescence was caused not only by SDO. Because of the strong luminescence during RF discharge the experiments were carried out only in pulse-width modulated mode with minimal modulation frequency of RF power supply (100 Hz).

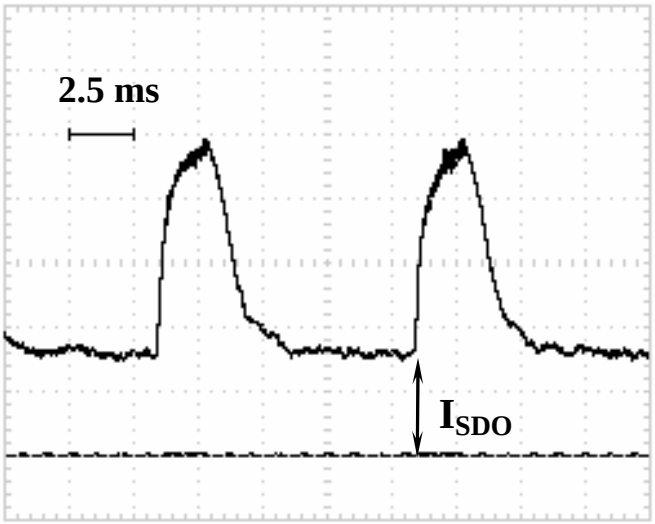

Fig.II.5.6. Oscillogram of RF discharge glow and afterglow at wavelength 1.27 μm.

Period of modulation T_{mod} = 10 ms,
RF pump pulse duration t_P = 2 ms.

Relatively low intensity of luminescence was observed between RF discharge pulses in afterglow. Spectral distribution of the intensity measured before the beginning of a discharge pulse (I_{SDO} in **Fig.II.5.6**) is presented in **Fig.II.5.7.** In the figure the spectral distribution of SDO luminescence calculated at gas temperature of 300 K is presented also. An agreement between measured and calculated curves is the evidence that the observed luminescence was caused by SDO. It should be pointed out that the experiments were carried out without any gas flow. Several minutes after RF discharge being switched on, a decrease of SDO luminescence intensity was observed. It might be connected with production of long-living species in RF discharge such as ozone, atomic O, etc. The existence of the species in the discharge area resulted in changing electric characteristics of the slab RF discharge. The following experiments plan to be carried out for a period of time less than about one minute.

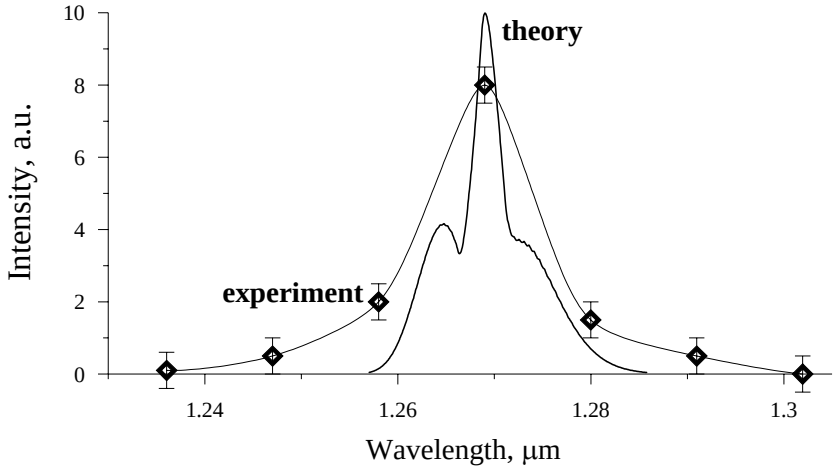

Fig.II.5.7. Spectral distributions of the experimentally observed (experiment) and theoretically calculated (theory) luminescence of SDO.
O_2:He=1:1, 30 Torr,
1800 J/(l·atmO_2).

Parametric study of influence of experimental conditions on SDO luminescence intensity in RF discharge oxygen-containing plasma afterglow.

(Subtask 3.3)

Experiments on parametric study of SDO production in slab RF discharge was carried out In the experiments to increase luminescence signal detected by a room temperature Ge-photodetector the slit width of monochromator was increased, with spectral resolution being ~15 nm. To increase signal-to-noise ratio, average signal function of digital oscilloscope "Tektronix TDS-1012" was used with averaging of 64 sequences. In the experiments the influence of electrodes material, specific input energy (SIE), gas pressure, and gas mixture content on SDO production in slab RF discharge was studied.

Preliminary experiments described above showed that using RF discharge electrodes made of aluminum we can reliable observe the SDO luminescence signals in the afterglow of pulse-periodic RF discharge excited oxygen containing gas plasma. It should be noted that electrodes material can influence on plasma-kinetic processes in a slab RF discharge, because usually the inter-electrode gap is respectively small (~2-3 mm). It is well known that copper is a strong SDO quencher. Indeed, when thin Cu-plates were attached to the initial aluminum electrodes to form "new" discharge gap with electrodes made of Cu, the SDO luminescence was not observed at all. Only weak SDO luminescence signals were observed with coating of the Cu-plates by Hg, with attaching thin Ag-plates to the initial Al-electrodes or with covering of the initial Al-electrodes by Teflon foil. It should be noted that mercury and silver were oxidized very rapidly in oxygen containing gas mixtures excited in RF discharge. Oxides HgO and AgO are efficient quenchers of atomic O, which could result in SDO luminescence growth, but quite the opposite effect was observed in our experiments. It should be noted that optical reflectivity of the electrodes' surface coated by oxidized Hg or Ag was reduced considerably (with respect to initial Al-electrodes), especially for silver electrodes visually becoming black. Teflon surface optical reflectivity was not high also. For this reason, if a photodetector detected SDO luminescence not only directly from the discharge region but also reflected from the electrodes' surface, the luminescence fraction of the latter could be very low because of low optical reflectivity of oxidized material. So, to estimate unambiguously the influence of the electrode material on SDO production, the further experiments with another experimental scheme (with gas flow, for example) should be carried out. In our experiments the best results corresponding to the maximal observed value of SDO luminescence intensity were obtained using tantalum (Ta) or aluminum (Al) electrodes. The experiments described below were carried out with aluminum electrodes.

The study of influence of gas mixture contents on the SDO luminescence corresponding to SDO concentration was carried out. **Fig.II.5.8** demonstrates the dependencies of the SDO luminescence intensity on specific input energy (SIE) loaded during one RF pulse for different gas mixtures. The SIE was reduced to oxygen partial pressure being of 15 Torr in the experiments. Dilution of pure oxygen by helium resulted in growth of the SDO concentration about 1.5 times at different SIE. Argon gave an opportunity to increase the SDO luminescence a little bit at low SIE. There was no difference between pure oxygen and gas mixture with heavy xenon. So, helium gas mixture looks more attractive than another ones to produce SDO in a slab RF discharge. The influence of helium content in binary (O_2:He) gas mixture on SDO luminescence intensity is presented in **Fig.II.5.9**. Maximal intensity of the luminescence was observed at different SIE with helium concentration 30-70% of total gas pressure.

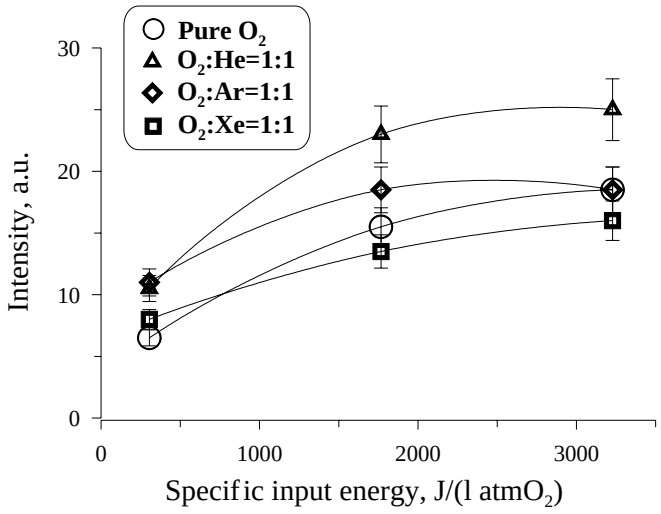

Fig.II.5.8. Dependencies of SDO luminescence intensity on SIE for different gas mixtures at oxygen partial pressure of 15 Torr.

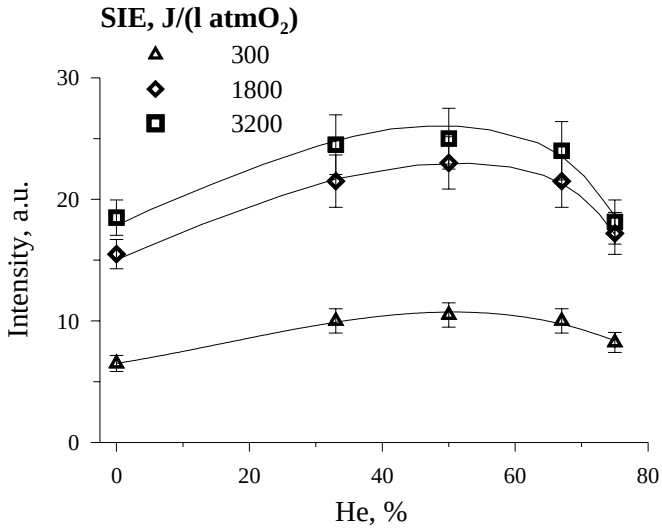

Fig.II.5.9. Dependencies of SDO luminescence intensity on He concentration in gas mixtures O_2:He for different SIE at partial oxygen pressure 15 Torr.

One of the most important parameters to design a high-power DOIL is SDO partial pressure. The experimental study of RF discharge in oxygen mixtures at different gas pressure was carried out. To compare the experimental results obtained at different gas pressures, the measured intensity of SDO luminescence was reduced to gas pressure. Dependencies of the reduced intensity on averaged input power are presented in **Figs**.**II.5.10 & II.5.11** . In the experiments pure oxygen pressure was varied from 7.5 to 30 Torr. For gas mixture O_2: He=1:1 gas pressure was between 15 and 45 Torr. For both cases the decrease of gas pressure resulted in reduced intensity growth, which means that the lower gas pressure, the higher SDO yield. The SDO yield roughly estimated by calibration method described in Part II.3 of the Report was about 10±5%.

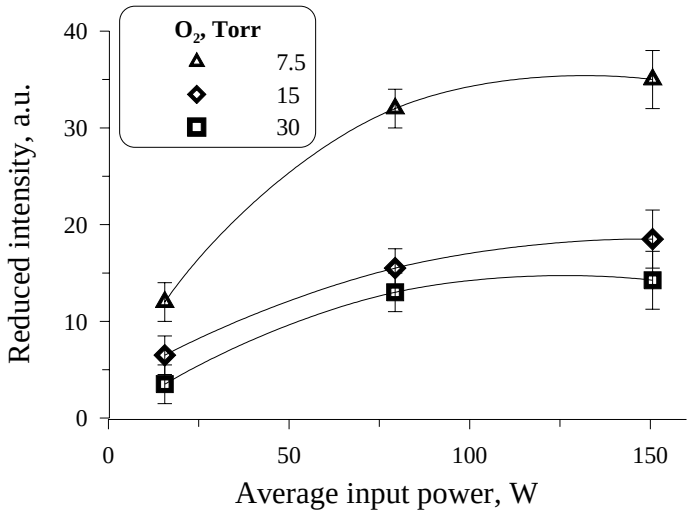

Fig.II.5.10. Dependencies of reduced SDO luminescence intensity on averaged input power for different oxygen pressure

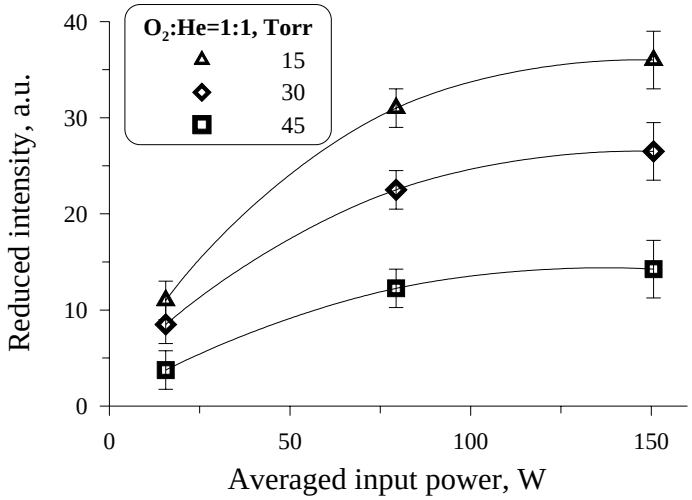

Fig.II.5.11. Dependencies of reduced SDO luminescence intensity on averaged input power for different gas pressure. O_2: He = 1:1

Application of theoretical model to interpretation of experimental data on SDO in slab RF discharge and estimation of perspectives to realize discharge pumped OIL.
(Subtask 3.4)

The detailed experimental studies on the SDO production in the slab RF discharge by measuring the SDO luminescence intensity in the afterglow were described above. The experimental measurements were concentrated on finding parametric dependences of the SDO yield. We implemented our detailed kinetic model to analyze the parametric dependences of the SDO yield in conditions approximately corresponding to the experimental conditions but replacing the RF discharge in pulse-periodic mode with each pulse being time modulated by the glow discharge with the same average power density.

The electric current and respective reduced electric field strength were calculated self-consistently in an assumption that the discharge vessel is connected to the simplest electric circuit consisted of the power supply and ballast resistor. Our experience gained from our previous modeling of electric discharges of different types indicates that such an approximation possesses quite a reasonable accuracy in predictions. In the experiments the average characteristics were measured, which correspond to the diffusion-controlled plasma state. We did not introduce diffusion processes, because they proceed on rather long times and actually disturb the established

concentrations of neutral and charged species in a small degree (the balance attachment/detachment-ionization is achieved quickly). Additionally, gas temperature in the experimental conditions is non-uniform in space and was not measured. In our modeling we have neglected the temperature profile effects and set it equal to 300 K independently of the discharge power and gas pressure. Estimations indicate that the temperature rise in experimental conditions is not too important.

In the detailed kinetic model, dynamics of the glow discharge was numerically simulated. **Fig. II.5.12** illustrates calculated evolution of the SDO, atomic oxygen, O, and $O_2(b^1\Sigma^+_g)$ concentrations in the discharge in He:O_2=1:1 mixture at pressure 30 Torr with the established power density 5.6 W/cm^3. It is seen clearly that within a few milliseconds concentrations of O and $O_2(b^1\Sigma^+_g)$ are practically established. The SDO concentration continues to grow but much slower after 20 ms. Therefore, in further parametric studies we present the results of calculations of the SDO concentration at the moment 30 ms.

Using the described approach, a series of numerical simulations was performed for the conditions of the experimental measurements. Assuming the gas density is constant, the following relationship can be derived between concentrations of the SDO, $[O_2(a^1\Delta_g)]$, and the yield defined as the ratio of the current SDO concentration to the whole molecular oxygen concentration: $[O_2(a^1\Delta_g)]/[O_2]_0=Y/[1+2\alpha(1-Y)]$. Here $[O_2]_0$ is initial oxygen concentration, $\alpha=[O]/[O_2]$. In the experiments, the luminescence intensity was measured, which is proportional to the SDO concentration. For the laser action, the yield plays more important role. Therefore, the most part of our results here are presented for the yield. **Fig. II.5.13** shows the difference between these two characteristics of the SDO production.

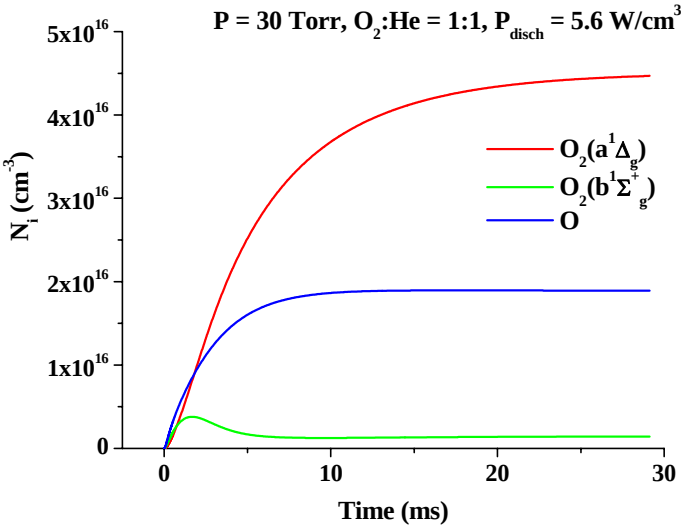

Fig.II.5.12. Calculated time evolution of metastable and atomic species produced in the glow discharge.

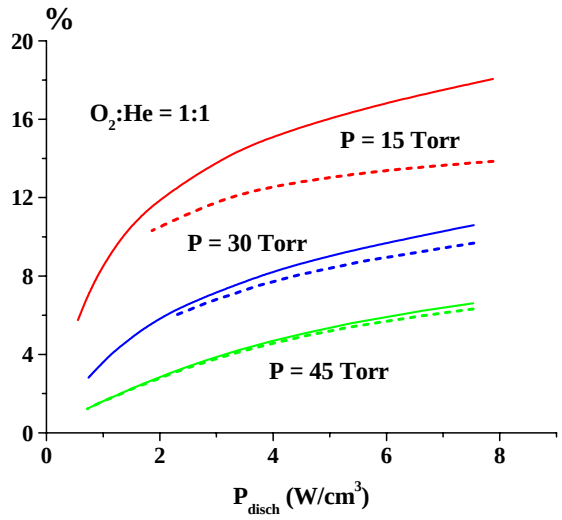

Fig.II.5.13. The SDO yield (solid lines) and SDO concentration reduced to the initial oxygen concentration (dotted lines) vs. the established discharge power density.

It is seen that at lower pressure the difference between the SDO concentration and the yield is notable, but at higher pressures measurements of the SDO emission can serve as a good indicator for the yield.

Influence of gas pressure on the yield dependence on the discharge power density is demonstrated in **Fig. II.5.14** for the case of pure oxygen. At lower pressure the yield grows with the discharge power remarkably faster at low powers and saturates with growth of the discharge power. In **Fig. II.5.15** the yield is compared for pure oxygen and the mixture He:O_2=1:1 for the same

pressure. Helium as a diluent does not consume the electric power resulting in higher yield production. Taking into account better stability of the He-based discharge, the dilution of oxygen by He certainly plays a positive role. Comparing results of numerical simulations with the experimental data, it is seen a good qualitative agreement between predicted and observed parametric dependences on gas pressure, composition and discharge power density.

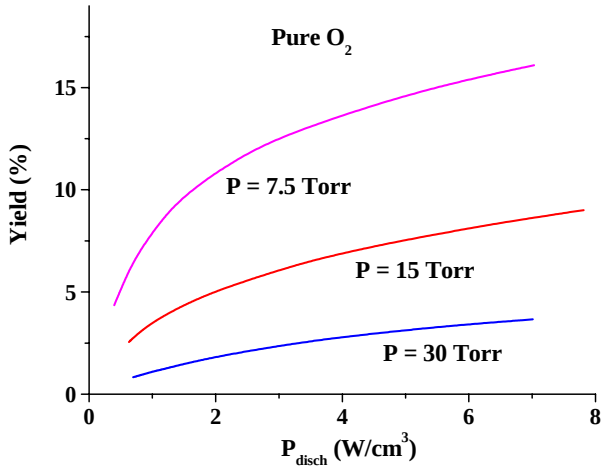

Fig.II.5.14. Calculated SDO yield vs. discharge power density for pure oxygen at different pressures.

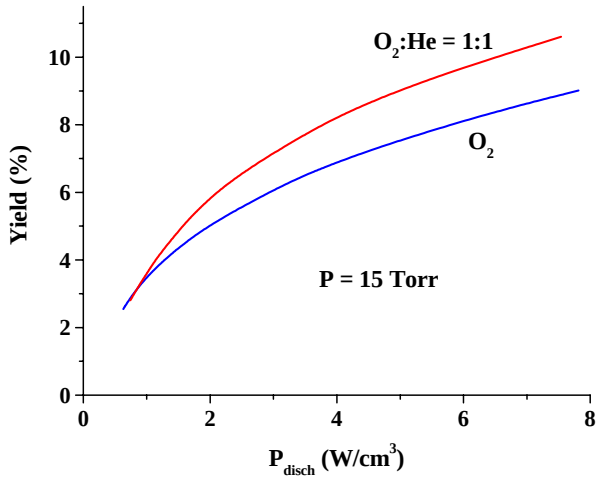

Fig.II.5.15. Comparison of dependences of calculated yield on the discharge power for pure oxygen and helium diluted oxygen mixtures at pressure 15 Torr.

Conclusions

The experiments on study of SDO production in self-sustained slab repetitively pulsed RF discharge were carried out. SDO luminescence was observed for the discharge afterglow. SDO yield was about 10±5%. It was demonstrated that the choice of electrodes' material is very important. Incorporation of the RF discharge in a gas flow system can result in discharge characteristics changing because of elimination of influence of long-living species produced in the discharge on electric gas characteristics. To estimate a potential of electric discharge OIL development with SDO production in a slab RF discharge, an experimental research of the discharge with gas flow is needed. The preliminary experiments SDO production in a slab RF discharge with gas flow and with SDO detecting by intracavity laser spectroscopy method are described in Part II.3.8 of the Report.

Concluding, a fairly well qualitative agreement takes place between numerically simulated parametric dependences of the SDO yield and results of measurements of the SDO luminescence intensity.

References for Part II.5.

Carroll D., et al. (2005a). *IEEE Journal of Quantum Electronics*, **41**, 213.

Carroll D.L., et al. (2005b). *Appl. Phys. Letters*, **86**, 111104-1.

Jianguo Xin, Wang Zhang, Wentao Jiao (1999). *Applied Physics Letters*, **75**, 1369

Part II.6. THE WAYS OF R&D OF DOIL (*Subtask 3.3*)

Introduction

Extensive experimental and theoretical studies of singlet delta oxygen $O_2(^1\Delta_g)$ production in low-temperature plasma of electric discharge, which have been done in the last years (see, for instance, reviews (Napartovich, 2001; Ionin, 2002)), indicated the real possibility of obtaining SDO yield exceeding the value (15% at room temperature) providing positive gain for oxygen-iodine gas mixture. Positive gain ~$2\text{-}5\cdot10^{-5}$cm^{-1} was for the first time achieved in (Carroll, 2004a,b) by cooling oxygen mixture excited in RF discharge (threshold SDO yield is 1% at gas temperature T=100 K). Quite recently, in a series of papers (Carroll, 2005a,b,c) it was reported about realization of a laser on the atomic iodine transition $I(^2P_{1/2})\text{->}I(^2P_{3/2})$ with the wavelength 1.315 μm excited by an energy transfer from $O_2(a^1\Delta_g)$ produced in electric discharge generator. These achievements make it reasonable to apply our theoretical model for evaluation of possibility to realize the DOIL. Generally, conditions adopted in the theory should be a result of compromise between required ideal conditions and that, which can be realized experimentally. As a first step, we can verify our model by simulations of successful experiments. Then, further evaluations can be made for feasibility of the DOIL development with available at Lebedev Institute experimental technique.

Theoretical evaluation of electric discharge oxygen-iodine laser feasibility.

The key condition for laser operation is a sufficiently high singlet delta oxygen (SDO) yield, $Y = O_2(a^1\Delta_g)/(O_2 + O_2(a^1\Delta_g))$ not less than 15% at room temperature. In a course of experimental work, some data were gained about the SDO yield. It is reasonable to compare predictions of our model with these experimental data.

In (Carroll, 2005a,b,c) the required $O_2(a^1\Delta_g)$ concentration was achieved with the help of a longitudinal RF discharge. Though parameters of this discharge such as spatial sizes and plasma density gradients are not well characterized, it is of interest to simulate this discharge implementing our detailed zero-dimensional model. Experimental data (Fig. 7 from (Carroll, 2005b)) indicate that an increment of gas temperature in gas discharge is not so large, and can be neglected. Strictly speaking, the length of the discharge in (Carroll, 2005a,b,c) varies with total discharge power and geometry of electrodes, in particular, with the distances from the earthed units. We supposed that the discharge occupies the tube of 4.9 cm diameter on the length 25 cm. Gas temperature was fixed at the value 300 K. Gas mixture pressure was taken equal to 10 Torr. The gas flow velocity was found from the reported flow rates of components (16 mmol/s for He, 3 mmol/s for O_2, 0.15 mmol/s for NO). In addition to earlier developed kinetic model, new processes were included describing reactions of NO. These processes are: electron impact excitation of vibrational and electronic levels of NO, ionization, dissociative attachment and electron-ion recombination for NO^+, the respective ion-molecule reactions, charge transfer, and the energy transfer from electronic levels of NO to electronic levels of O_2. Earlier a combination of this extension of our model with an old version of O_2 kinetics was implemented by us (unpublished) to simulate experimental data from (Itami, 1999). **Fig.II.6.1** shows the reduced electric field, E/N, and discharge power density, W as a function of transportation time with the gas flow. The discharge power density $\langle W_{disch} \rangle$ averaged over the length is equal to 0.8 W/cm^3 for specified conditions. For comparison, calculations were performed for the same mixture but without NO.

It is worth noting that appearance of NO leads to faster establishment of E/N (for about 100 μs in comparison with about 1 ms in the absence of NO). This effect is explained by a process of negative ion O^- destruction in the reaction:

$$O^- + NO \rightarrow NO_2 + e,$$

having the rate coefficient $1.6 \cdot 10^{-10}$ cm^3/s (Mc Ewan and Phillips, 1975).

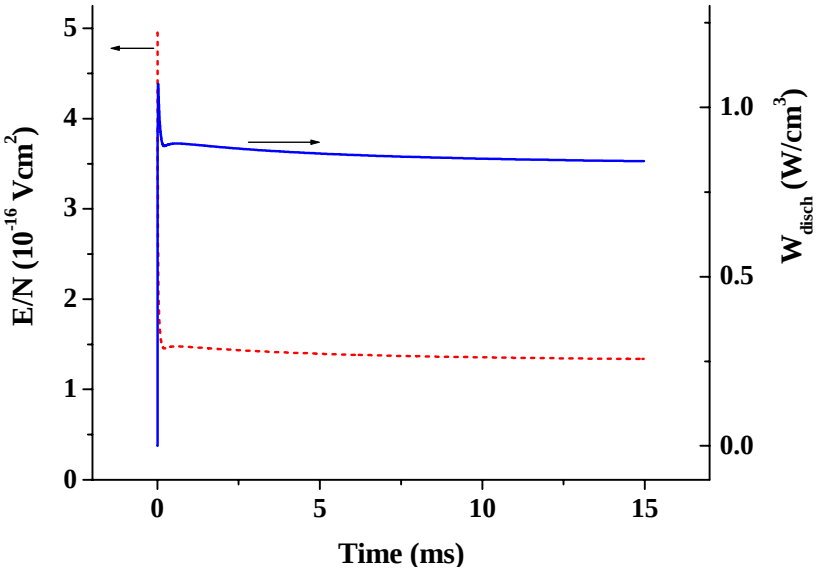

Fig.II.6.1. Reduced electric field, E/N, and discharge power density, W, as a function of transportation time.
P = 10 Torr, T = 300 K,
$He:O_2:NO = 16:3:0.15$.
$\langle W_{disch} \rangle = 0.8$ W/cm^3.

In the absence of NO molecules the similar role is played by the process of electron detachment in collisions with $O_2(a^1\Delta_g)$ molecules generated in the discharge for the observed time. As noted in (Carroll, 2005a), the lower ionization potential of NO in comparison with that of O_2 causes diminishing of the operating value of E/N by about 10%. In **Fig.II.6.2** the SDO yield measured in (Carroll, 2005c) is compared with theoretical predictions for mixtures with (curve 1) and without NO (curve 2). At an average power density less than 1 W/cm^3 Y is about 10% higher in the mixture with NO than without NO. This is explained by reduction of E/N and respective increase of SDO production efficiency.

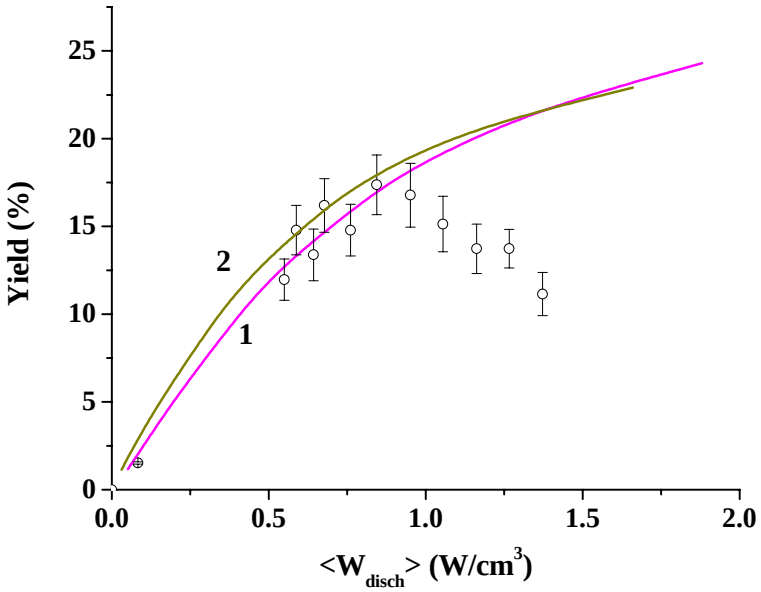

Fig.II.6.2. SDO yield as a function of the average discharge power density.
P = 10 Torr,
T = 300 K,
1 - $He:O_2 = 16:3$,
2 - $He:O_2:NO = 16:3:0.15$.
Markers are for data from (Carroll, 2005c).

Let's note that experimentally observed effect of the SDO yield growth is about 30%. Generally, our model predicts the SDO yield which is in a good agreement with the experiments (Carroll, 2005c) for powers up to 0.85 W/cm^3. At higher power densities falling down of the experimental data can be explained by loss of discharge stability, as it was noted in (Carroll, 2005b). Our model is inapplicable to non-uniform discharge description. Besides, in this case the RF power absorbed in plasma can become lower due to reflection of the power supplied by RF generator. Calculations of atomic oxygen concentration in the discharge revealed that appearance of NO in the mixture causes a strong reduction of O production rate. **Fig.II.6.3** presents atomic oxygen concentration reduced to the current molecular oxygen concentration as a function of the average discharge power. Triangles are the data from (Carroll, 2005a), curves are results of numerical simulations for the mixture without (1) and with (2) NO. Taking into account that in the experiments of (Carroll, 2005a) data shown were measured for NO free mixture, our predictions for O concentrations are twice higher than the observed ones. Reasons for such discrepancy are not clear at the moment.

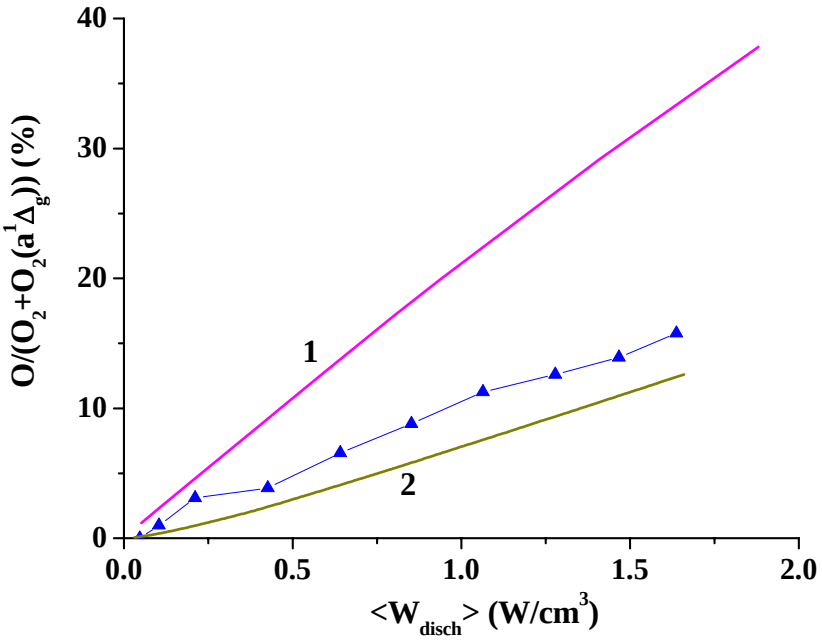

Fig.II.6.3. Oxygen atom concentration reduced to the current molecular oxygen concentration as a function of the average discharge power.
P = 10 Torr,
T = 300 K,
1 - He:O_2 = 16:3,
2 - He:O_2:NO = 16:3:0.15.
Markers are for data from (Carroll, 2005a).

Concluding, a good agreement for not too high discharge power densities between our predictions and experimental measurements of the SDO yield can be considered as a clear indication that with further gas cooling and injection of iodine into the flow the laser can operate on I($^2P_{1/2}$)->I($^2P_{3/2}$) transition.

Designing and manufacturing of an experimental facility based on the most promising SDO electrical generator for obtaining the laser effect

The SDO yields demonstrated in the experiments and observed trends in dependences of this parameter on experimental conditions make it possible to expect the yield value close to room temperature threshold level to be obtained. The laser effect under such yield was observed in experiments on measuring the SDO yield by threshold method (Yuryshev, 2004). The approach of instantaneous volume generation of iodine atoms in active medium containing SDO was applied in this method. It is obvious the electric discharge cannot be used for iodine atoms generation because

of great heat release and, hence, active medium heating. But pulse photolysis seems to be appropriate for this purpose. Thus the experimental facility (**Fig.II.6.4)** for obtaining the laser effect differs from that in **Fig.II.2.1** by presence of Xe - flash lamp placed in parallel with investigation section. The assemblage is surrounded with reflecting aluminum film. The emitting length of the lamp is 25 cm. The discharge in the lamp is fed from a capacitor battery with stored energy of up to 1 kJ.

The mirror holders are installed at the both sides of investigation section to provide feedback. The facility is equipped with fast response photo detector and oscilloscope to measure the laser parameters. To reduce the temperature of laser section and, thus, the temperature of active medium the assemblage laser section-flash lamp can be placed into the heat insulated box filled with dry ice.

If necessary, the chemical SDO generator can be attached to the laser facility to calibrate the experimental conditions.

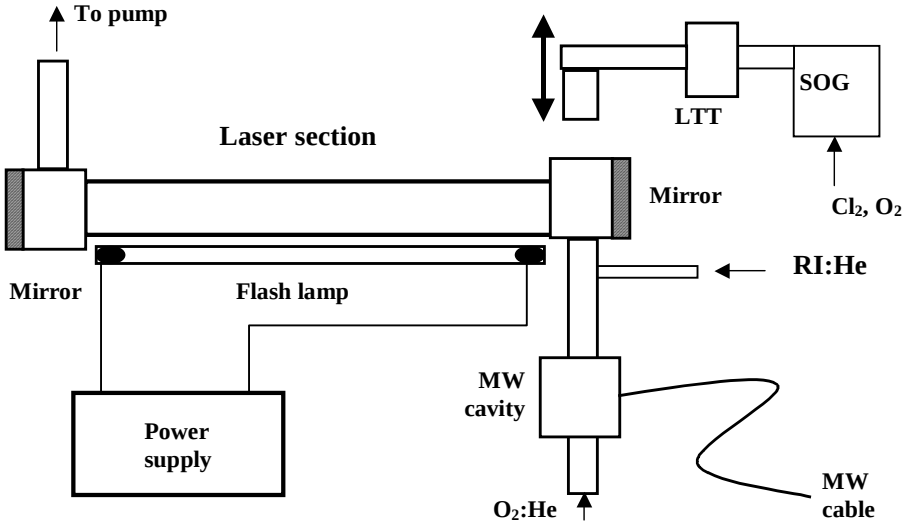

Fig.II.6.4. Schematic diagram of laser facility

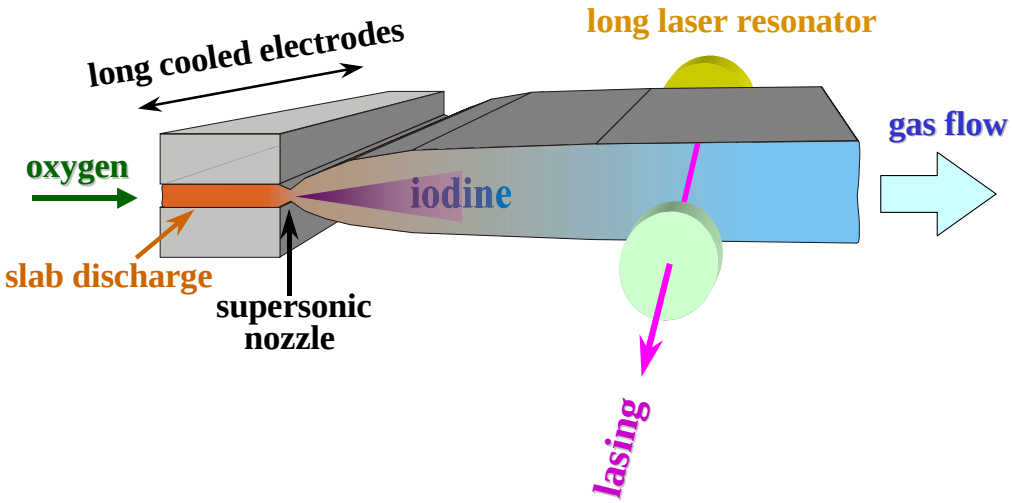

Fig.II.6.5. Design of DOIL with long discharge excitation with transverse gas flow direction.

Another approach can be proposed to design the DOIL. For instance, the slab RF discharge facility with electrodes length being ~0.3 m was described above. Coupling of similar RF discharge system with transverse supersonic cavity and iodine injection allows us to design DOIL with resonator length of about 0.3 m (**Fig.II.6.5**).

For the DOIL design with critical cross section being about 3x300 mm^2 the pumping flow rate ~1000 liter/s will be needed to support supersonic flow of helium containing gas mixture (a vacuum pump providing flow rate 3000 liter/s is available in our Lab). The slab RF discharge system can provide also diffusive and convective gas pre-cooling in discharge region (before supersonic flow) by using cooled electrode system. Thus, with Mach number of supersonic gas flow being about 3, gas temperature in a laser resonator region can be ~100 K (or even lower). Threshold SDO yield at this temperature is about 1% and the real SDO yield in RF discharge is much higher (as described above). Thus the DOIL design with the value of threshold SDO yield and with long laser resonator can provide a powerful DOIL lasing.

Conclusions

Our theoretical model was extended to include nitrogen oxides chemistry and applied to numerical simulations of experimental data from (Carroll, 2005a,b,c). It was found that a reasonable agreement is observed between the theory and the experiments at not too high discharge power density. Discrepancy taken place at higher discharge power densities can be ascribed to appearance of discharge non-uniformities associated with instabilities. The agreement with the experimental data proves that the theory is workable and can be exploited for evaluations of laser operation feasibility at specified experimental conditions.

The SDO yield demonstrated in the experiments with different types of electrical SDO generators and observed trends in dependences of this parameter on experimental conditions make it possible to expect the yield being enough for laser effect demonstration. The approach of instantaneous volume generation of iodine atoms by flash photolysis of iodides in active medium containing SDO can be used for this purpose.

The slab RF discharge facility with electrodes length being ~0.3 m can be used as alternative approach to design the DOIL. Coupling of similar RF discharge system with transverse supersonic cavity and iodine injection allows us to design DOIL with resonator length of about 0.3 m.

References for Part II.6.

Carroll D.L., Verdeyen J.T., King D.M. et al. (2004a). *Appl. Phys. Lett.*, **85**, 1320

Carroll D.L., Verdeyen J.T., King D.M. et al. (2004b). *XV Int.Symp. Gas Flow and Chemical Lasers & High Power Laser Conf.*, Prague, Czech Republic, 30 Aug – 3 Sept 2004, Book of abstracts, paper S12-4, p.76

Carroll D., et al. (2005a). *IEEE Journal of Quantum Electronics*, **41**, 213.

Carroll D. L., et al. (2005b). *IEEE Journal of Quantum Electronics*, **41**, 1309.

Carroll D.L., et al. (2005c). *Appl. Phys. Letters*, **86**, 111104-1.

Ionin A., Napartovich A., Yuryshev N. (2002). *Proc. SPIE*, **4760**, 506

Itami S., et al. (1999). *Proc. SPIE*, **3889**, 503.

Mc Ewan M.J. & Phillips L.F. (1975). "Chemistry of the atmosphere", Chemistry Department, University of Canterbery Christchurch, New Zealand.

Yuryshev N.N., et al. (2004). *Proc. SPIE*, **5448,** 790.

Part II.7 TECHNICAL WORK DURING YEAR III (Quarter 9) (*Tasks a, b, c, d, e, f, g*)

Repairing the hot cathode of the e-beam gun inside e-beam sustained discharge facility.
(Task a)

Extensive experiments with e-beam sustained discharge facility necessitate to exchange periodically working elements of e-beam gun hot cathode because its component being made of thin tungsten filaments have limited lifetime. The old filaments were removed and substituted for new ones, the cathode was reinstalled in the facility.

Cleaning the inner surfaces of the laser chamber and e-beam chamber of the facility.
(Task b)

During the experiments, tungsten vapors from hot cathode and small amount of vacuum oil from gas pump system were coating slightly the high voltage insulators inside the e-beam gun and need to be removed. The cleaning procedure was performed for organic-glass e-beam gun insulator, for ceramic insulators of main discharge anode (outside the laser chamber) and for all other internal surfaces of the e-beam gun. Also, internal surfaces of the laser chamber were cleaned from the products of the chemical reactions that could appear during the experiments.

Full disassembling of probe CO laser and cleaning quartz and metallic parts of its gas duct.
(Task c)

Low pressure CW CO laser used in the experiments as a probe laser has gas duct for slow flowing of the active gas medium. CW DC discharge in the CO containing gas mixtures leads to appearing carbon coating of inner walls of working quartz tube. CW CO laser was completely disassembled and all of its components were washed and cleaned from carbon and other chemicals. After the cleaning procedure the laser was fully assembled back and now it is ready to further experiments.

Modification of RF CO laser resonator system.
(Task d)

For more convenient operation with slab RF discharge CO laser facility, its laser resonator system was modified. Now the resonator system have four invar rods for better thermal stability and each of four tuning screws (used for mirrors alignment) has reduction gear for precise positioning of the mirrors.

Calibration of measuring electronic equipment.
(Task e)

Some electronic equipment used in the experiments (calorimeters, laser power meters, IR and visible detectors, spectral devices and electronic oscilloscopes) were tested and calibrated if necessary for increasing the reliability of the experimental data of further research on the Project.

Repairing the central heating system in lab rooms.
(Task f)

According to the internal LPI plan, the central heating system in some lab rooms was repaired to support more comfortable conditions for working staff.

Preparing publications.

(Task g)

Two publication were prepared using the results obtained during the second year of work on the Project and sent to editorial offices:

- Vetoshkin S.V., Ionin A.A., Klimachev Yu.M., Kozlov A.Yu., Kotkov A.A., Kurnosov A.K., Napartovich A.P., Rulev O.A., Seleznev L.V., Sinitsyn D.V., Shnyrev S.L. "Small signal gain time behavior in active medium of pulsed electron beam sustained discharge CO laser: theory and experiment". Preprint LPI #27. Moscow, 2004 (in Russian).
- Ionin A.A., Sinitsyn D.V., Terekhov Yu.V., Kochetov I.V., Napartovich A.P., Starostin S.A. "Influence of vibrational excitation of CO molecules on RF discharge characteristics". Plasma Physics Reports, **31**(9), 786-794 (2005).

Six presentations were prepared for attending the Scientific Session - 2005 of Moscow Engineering-Physics Institute:

- Klimachev Yu.M. "Vibrational exchange of highly excited CO molecules and its influence on physical processes in active medium of pulsed EBSD CO laser";
- Kozlov A.Yu., Vetoshkin S.V., Ionin A.A., Klimachev Yu.M., Kotkov A.A., Kurnosov A.K., Napartovich A.P., Seleznev L.V., Sinitsyn D.V. "Multi-frequency laser sounding of an active medium of pulsed e-beam sustained discharge CO laser";
- Konev Yu.B., Kochetov I.V., Kurnosov A.K., Lobarev Yu.V. "Investigation of different models of kinetic processes in CO laser active medium";
- Rulev O.A., Vagin N.P., Ionin A.A., Klimachev Yu.M., Kotkov A.A., Kochetov I.V., Napartovich A.P., Seleznev L.V., Sinitsyn D.V., Yuryshev N.N. "Singlet delta oxygen in low temperature plasma of non-self-sustained discharge";
- Ionin A.A., Kochetov I.V., Napartovich A.P., Sinitsyn D.V., Terekhov Yu.V. "Compact cryogenically cooled slab CO laser with RF excitation";
- Vetoshkin S.V., Ionin A.A., Klimachev Yu.M., Kozlov A.Yu., Kotkov A.A., Seleznev L.V., Sinitsyn D.V. "E-beam sustained discharge CO laser operating on gas mixture with high (~95%) oxygen content".

PART III. IODINE ATOMS PRODUCTION IN A VORTEX ELECTRIC DISCHARGE (**Samara**)
(Task 1C and 2C)
(Subtasks 1C.1, 1C.2, 1C.3, 1C.4, 2C.1, 2C.2, 2C.3 and 2C.4)

Introduction

Earlier experiments of the authors of this project had shown that a DC glow discharge in a vortex gas flow could be successfully implemented to obtain atomic iodine concentration ~$3.6\cdot10^{15}$ cm^{-3} at carrier gas pressure up to 15-20 Torr. The achieved quantities are high enough to use them in an oxygen-iodine laser; however, it is desirable to achieve higher pressures and atomic iodine concentrations. Further increase of pressure was limited by discharge instability.

Within the framework of the current project the experiments of atomic iodine discharge generation were continued. To further improve discharge stability at higher carrier gas pressure and provide uniform fill of the discharge chamber with plasma the discharge system has been modified. The necessary laboratory equipment to produce hydrogen iodide and nitrogen dioxide has been developed for the provision of these experiments. The measurement of the atomic iodine concentration has been conducted measuring I_2, produced via recombination, using I_2 absorption in the visible region.

During the work on the project (*Subtasks 1C.1, 1C.3*) the modified discharge chamber was designed and manufactured to produce basic components of the active medium of oxygen-iodine laser (singlet oxygen $O_2(a^1\Delta)$ and iodine atoms) by means of the DC glow discharge in vortex gas flow.

Designed and tested were: the apparatus for NO_2 production needed for the experiments (*Subtask 1C.2*), and the apparatus for HI production (*Subtask 1C.4*).

The apparatus for measurements of iodine atoms concentration measuring I_2 molecules concentration produced as the result of recombination of I atoms (*Subtask 1C.3*) was designed and manufactured. The analysis of the measurement technique was performed based on numerical modeling and experimental data from literature (*Subtask 1C.4*)

According to the work plan (*Subtasks 2C.1, 2C.2, 2C.3* and *2C.4*) experiments were conducted studying kinetics of iodine atoms production in discharge, using CH_3I and HI as the precursors, parametric dependencies of the concentrations of I atoms were determined. Measurements of concentrations of excited iodine atoms in the $I(^2P_{3/2})$ state were performed.

The 3-d year of the project (part III) was not financed by the decision of the project manager due to the diminished budget partially cut by the Partner.

Development of discharge chamber design for atomic iodine production with the help of DC glow discharge at high pressures and application of the discharge electrode configuration found for achieving stable DC discharge at higher pressure of Ar or other gases. (*Subtask 1C.1.*)

In the previous experiments within bounds of ISTC Project #1826 with the help of vortex-flow DC glow discharge atomic iodine concentration up to ~ $3.6\cdot10^{15}cm^{-3}$ were obtained for carrier gas pressure 15-20 Torr (Mikheyev, 2001 & 2002). Further increase of pressure was restricted by discharge instability. The said parameters are sufficient to use atomic iodine in the oxygen-iodine laser active medium. However, to achieve higher carrier gas pressure and atomic iodine concentration is desirable to improve conditions of iodine gas jet injection and mixing with singlet oxygen flow.

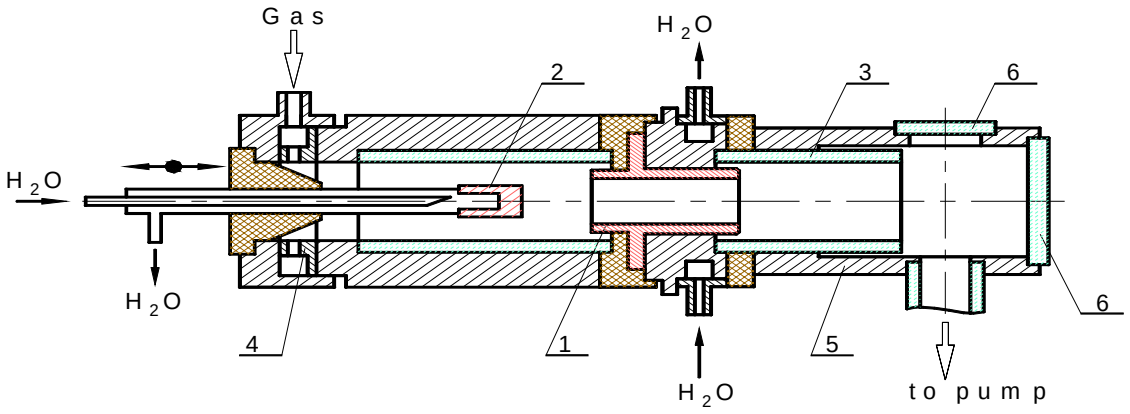

Fig.III.1. Schematic of design of the improved discharge chamber. 1, 2 – water-cooled electrodes; 3 – quartz tube; 4 – input nozzle block; 5 – casing; 6 – observation windows.

An improved version of discharge chamber was designed to perform experiments on further studies of atomic iodine production in discharge with the aim to achieve higher carrier gas pressures and iodine concentrations. It is expected that with the help of the designed chamber the conditions to sustain DC discharge at higher pressures of Ar or other gases will be found. The improved design is shown schematically in **Fig.III.1.** It permits to change interelectrode space and use electrode configurations found in previous experiments or test other configurations.

The electrode system initial design consists of two water-cooled electrodes: first placed upstream has cylindrical shape with working end and side surfaces; second placed downstream is a hollow cylinder with working inner surface. Interelectrode space could be varied, in particular it could be made small up to several millimeters. It is also possible to place one cylinder inside the other. Changeable input nozzle block permits to form the flow with variable vortex parameters. Bearing in mind the results of previous experiments it is expected that the designed electrode system will permit to sustain the discharge at higher gas pressure and current.

Design and development of the equipment for NO_2 production, necessary to measure atomic iodine number density, using thermal decomposition of $Pb(NO_3)_2$.
(Subtask 1C.2.)

Nitrogen dioxide NO_2 is necessary to measure atomic iodine concentration, if the tunable semiconductor laser is not available from Partner. In the presence of NO_2 rapid recombination of iodine atoms takes place. Number density of iodine molecules I_2 will be measured using absorption in the visible region at ~500 nm.

An apparatus to produce NO_2 is as shown in the **Fig.III.2**. Round-bottom flask 1 filled with the mixture of quartz sand and $Pb(NO_3)_2$ was connected by the tube filled with $CaCl_2$ 2 with NO_2 receiver 3, immersed in the refrigerator 4. The receiver was open to atmosphere via additional tube with $CaCl_2$. Flask 1 was heated by the laboratory heater 5.

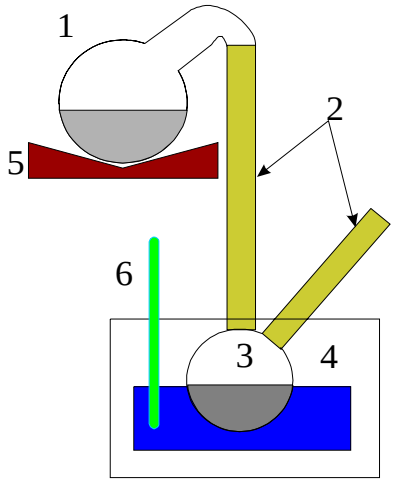

Fig.III.2. Apparatus for NO_2 production.

With the help of the heater the flask was heated up to ~320 °C. The refrigerator with the receiver was chilled by alcohol-water mixture, cooled by liquid nitrogen down to -10 °C. The temperature of the alcohol-water mixture was monitored by thermometer 6.

$Pb(NO_3)_2$ decomposes at a temperature higher then 300 ^oC emanating nitrogen dioxide that was collected in the receiver as a liquid. Liquid NO_2 was then transferred into a stainless steel gas bottle with a valve. The bottle was cooled down to ~0 °C before the transfer. At room temperature gaseous NO_2 is at equilibrium with liquid at ~1.5 atm pressure. The apparatus produced about 3 cm^3 (100 mmol) of liquid NO_2 after 8 hours of work.

Manufacturing and assembling an improved discharge chamber for atomic iodine production. (*Subtask 1C.3.*)

The modified discharge chamber was manufactured, to conduct experiments on atomic iodine production out of iodine containing molecules in Ar carrier gas, with the help of DC glow discharge. The aim is to achieve atomic iodine number density sufficient to operate oxygen-iodine laser at higher, than in previous experiments, Ar pressure.

Design of the discharge chamber and technical documents were developed in the *Subtask 1B.1*. New parts and assemblies have been manufactured, the chamber has been assembled, vacuum checked and first experiments with discharge conducted.

Fig.III.3. Photograph of the central relocatable water-cooled electrode.

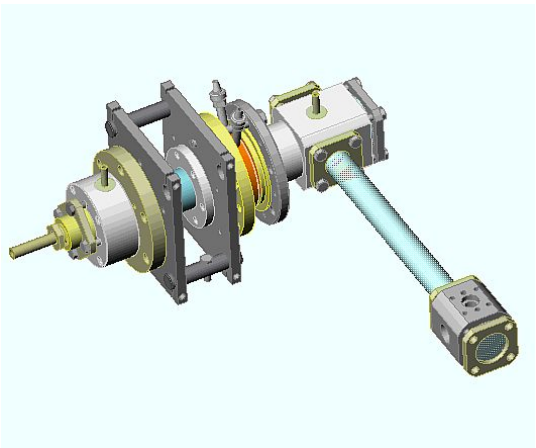

Fig.III.4. Overall view of the designed discharge chamber with the diagnostic arm.

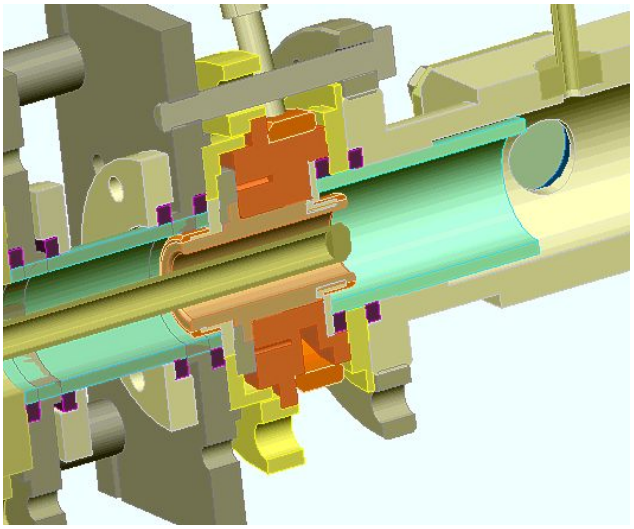

Fig.III.5. Coaxial electrode configuration.

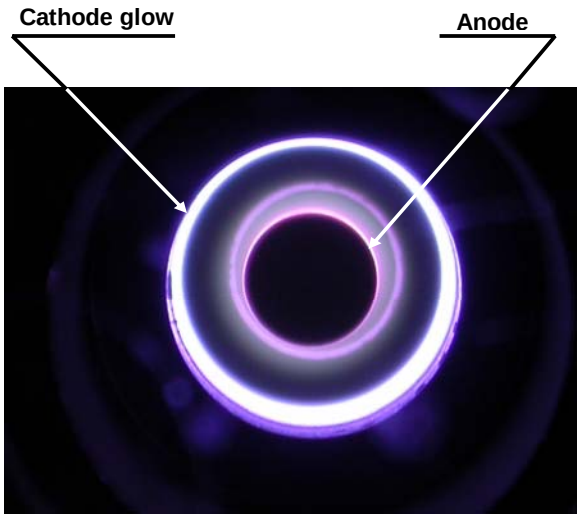

Fig.III.6. Photograph of discharge in Ar:O_2= 20:3.5 Torr mixture. Distance between electrodes 4 mm, discharge current ~600 mA.

Design of the discharge chamber permits to change interelectrode spacing, use electrode configuration found in previous experiments, or try new electrodes. The initial electrode system consists of two water cooled electrodes: 10 mm outer diameter cylinder with side and end working surfaces (**Fig.III.3**), placed upstream; 19 mm inner diameter hollow cylinder with inner working surface placed downstream.

Overall view of the discharge chamber with the diagnostic arm is represented in the **Fig.III.4**. Interelectrode distance may be in the range from 0 to 50 mm. Also, coaxial configuration is possible, when one electrode is placed inside the other, as it is seen in the **Figs.III.5** and **III.6**.

Test experiments have shown adequacy of the design. Stable glow discharge was sustained up to 45 Torr pressure at 800 mA current (**Fig.III.6**).

Equipping and developing of apparatus to determine I_2 concentration, measuring absorption. in the visible region.
(*Subtask 1C.3.*)

The apparatus had been developed to determine number density of iodine atoms measuring number density of iodine molecules. NO_2 is to be mixed with the carrier gas containing I atoms. Molecules I_2 is to be produced via quick recombination of I in the presence of NO_2. I_2 number density will be determined measuring absorption of light at ~500 nm.

An apparatus containing visible light source and photomultiplier with their power supplies and monochromator has been assembled. Diagnostic cell of up to 30 cm length placed downstream of the discharge will be used in experiments. Upstream of the cell an assembly to mix NO_2 with carrier gas containing iodine atoms is placed. The necessary additional assemblies and parts had been designed and manufactured. The software was developed to collect and process data.

Development of an equipment for HI production based on analysis of the known methods.

(*Subtask 1C.4.*)

The analysis of known methods of laboratory HI production revealed that in our conditions the reaction of the red phosphorus with iodine in water is the most convenient:

$$2P + 5I_2 + 8H_2O = 2H_3PO_4 + 10HI.$$

Water vapor is removed from the gaseous products by cooling them down to -30 °C. Then, at -50 °C, HI is liquefied. This method was tested in experiment. The setup depicted in the **Fig.III.7** had been assembled for HI production.

A dropping funnel 1 was placed on the neck of a Vurz flask 2. The outlet of the Vurz flask 2 was connected by polyethylene tubes 3, filled with glass wool, with a cooler 4a placed in a vessel 5a and with a cooler 4b, placed in a vessel 5b.The vessel 5a was filled by water-alcohol mixture and the vessel 5b – by n-octane. 130 grams of grounded iodine mixed with 13 ml of water were placed on the bottom of the Vurz flask. A suspension of 6.5 grams of red phosphorus thoroughly grounded with 13 ml of water was placed in the dropping funnel. The commercial grade red phosphorus was at first refined by 24 hours boiling in 7% solution of NaOH and 24 hours boiling in water. Then, the sediment was cleansed in water till neutral reaction and dried in vacuum.

The suspension of red phosphorus in water was poured from the dropping funnel 1 into the Vurz flask 2. The first drop of red phosphorus initiated vigorous reaction. The rest of suspension was slowly poured in drops. When HI discharge became slow the flask was heated a little. Gaseous HI flowed through the cooler 4a and was purified from water vapor, and then it was liquefied and stored as a liquid in the cooler 4b.

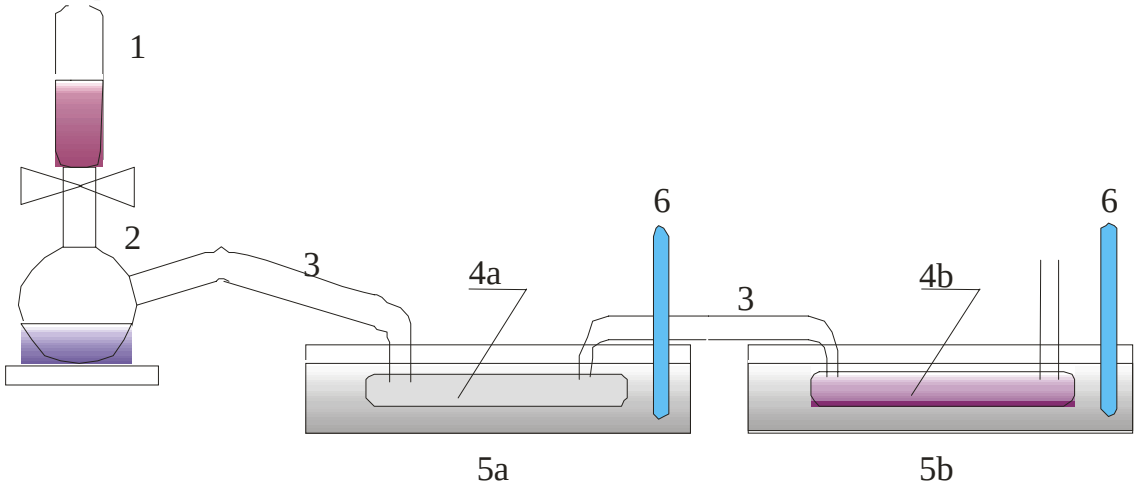

Fig.III.7. Experimental setup for HI production. 1 – dropping funnel; 2 – Vurz flask; 3 – polyethylene tubes; 4 – a) – Libich cooler, b) – ball cooler; 5 – a) ,b) vessels for cooling liquids; 6 – thermometers.

To freeze water out of the gaseous products in the cooler 4a, the vessel 5a was filled by water-alcohol mixture cooled by liquid nitrogen down to -30 °C. To liquefy gaseous HI in the cooler 4b, the, the vessel 5b was filled by n-oktane cooled by liquid nitrogen down to -50 °C. The temperature of the cooling liquids was monitored by the thermometers 6. The experiments with the described setup had shown that for the mentioned quantities of reagents about 30 ml of liquefied HI was produced during two hours of operation.

Development of the method of atomic iodine number density measurement.
(*Subtask 1C.4.*)

Atomic iodine number density produced with the help of glow discharge is to be measured determining molecular iodine number density obtained through quick recombination of iodine atoms in the presence of nitrogen dioxide. For those measurements to be correct one has to be sure that almost all iodine atoms had recombine during transportation to diagnostic region. To determine the necessary conditions, sufficient for full recombination of iodine atoms (NO_2 pressure and corresponding transportation time), an analysis was performed based on numerical simulation of kinetics of recombination and experimental data from literature.

Modeling was performed for the conditions of the discharge downstream afterglow. The following reactions listed in the **Table III.1** were taken into account.

Table III.1

	Reaction	Rate constant	Reference
1	$I + NO_2 + Ar \rightarrow INO_2 + Ar$	$k_1 = 5.6\cdot10^{-32}$ см$^6\cdot$с$^{-1}$ (†) $k_1 = 1.38\cdot10^{-31}$ см$^6\cdot$с$^{-1}$	Our estimate (Van den Berg et al, 1975)
2	$I + INO_2 \rightarrow NO_2 + I_2$	$k_2 = 8.3\cdot10^{-11}$ см$^3\cdot$с$^{-1}$	(Van den Berg et al, 1975)
3	$2INO_2 \rightarrow 2NO_2 + I_2$	$k_3 = 2.9\cdot10^{-11}\cdot\exp(-2600/T)$ см$^3\cdot$с$^{-1}$	(J.Phys.Chem., 2000)
4	$INO_2 + Ar \rightarrow I + NO_2 + Ar$	$k_4 = 5.3\cdot10^{-18}$ см$^3\cdot$с$^{-1}$ (†)	Our estimate
5	$I + I + Ar \rightarrow I_2 + Ar$	$k_5 = 3.26\cdot10^{-33}$ см$^6\cdot$с$^{-1}$ (450 °K)	(Ip et. al, 1972)
6	$I + I + I_2 \rightarrow 2I_2$	$k_6 = 4.54\cdot10^{-31}$ см$^6\cdot$с$^{-1}$ (450 °K)	(Bunker et al, 1958)

(†) *Rate constants k_1 and k_4 were estimated from analysis of experimental data (Van den Berg et al, 1975).*

To test if the model was sound, simulations were performed for the conditions of (Van den Berg et al, 1975). In this paper measured temporal behavior of $[I_2]$ number density due to iodine atoms recombination is represented (figures 1 and 2 from (Van den Berg et al, 1975)). Modeling, using those six listed reactions, had shown that rate constants k_1 and k_4 determined in (Van den Berg et al, 1975) are not in good agreement with rate of increase and absolute values of $[I_2]$ represented in (Van den Berg et al, 1975). Our estimates of k_1 and k_4 give excellent fit with experiment corresponded to fig.1 of (Van den Berg et al, 1975) (pressure of buffer He – 7.57 atm). For the other experiment (fig.2 in (Van den Berg et al, 1975)) the agreement is not so good, but the discrepancy is less than 10%.

In our previous experimental studies of atomic iodine production in discharge using methyl iodide as precursor, we had achieved the best results using Ar as a carrier gas. There is no data in the literature about iodine recombination in Ar in the presence of nitrogen oxides. Therefore, for our modeling we assumed that rate constants of the reactions of interest are equal for He and Ar.

The results of modeling are represented in the **Fig.III.8** for temperature 450 °K, Ar pressure 30 torr, and the following initial number densities: $[I] = 10^{15}$ cm^{-3}, $[NO_2] = 1.2\cdot10^{16}$ cm^{-3} (0.5 torr NO_2 at 450 K). It follows from **Fig.III.8** that all iodine atoms recombine after ~6 ms at the specified conditions. With twofold increase of $[NO_2]$ number density the time of full recombination decreases down to ~4 ms.

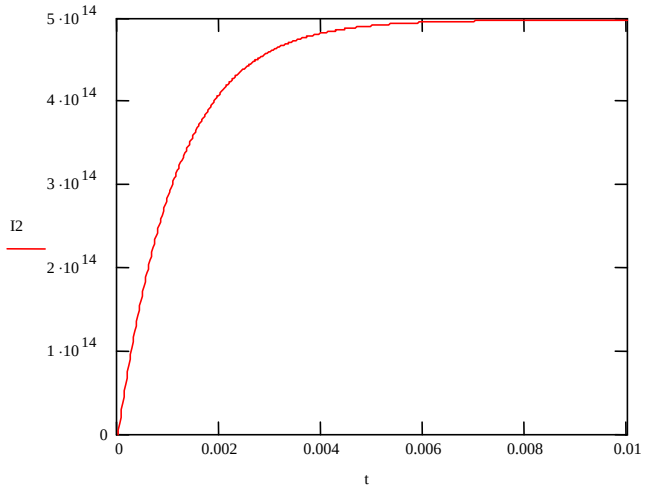

Fig.III.8. Temporal behavior (t in seconds) of I_2 concentration (cm^{-3}) in conditions of I recombination (NO_2 pressure ~0.5 Torr at 450K).

The value of k_1 used in our modeling is ~2.5 times lower than in (Van den Berg et al, 1975). If k_1 from (Van den Berg et al, 1975) is used the time of full recombination at the conditions of our experiment becomes ~2 times smaller. The influence of k_4 at our conditions becomes noticeable only if we increase its value 3 orders of magnitude. Therefore, our analysis has shown that at the conditions of our experiments one should measure molecular iodine number density after iodine atoms interact with NO_2 at 0.5 torr pressure no less than 4 – 6 ms or no less then 2 – 4 ms at 1 torr of NO_2.

Measurements of atomic iodine number density measuring number density of iodine molecules. Measurements of I_2 molecules number density using absorption in the visible range of spectrum.
(Subtask 2C.1)

A sketch of the discharge chamber with the diagnostic arm used in experiments is represented in **Fig. III.9a**, and its overall view – in **Fig.III.9b**. The design provided vortex gas motion through coaxial water cooled copper electrodes. The external electrode was used as a cathode with inner working surface 18 mm in diameter. The internal cylinder with outer working surface 10 mm in diameter was used as the anode. Experiments were performed with the cathodes of 5 and 10 cm in length.

A mixture of a carrier gas and an iodine precursor was injected into the discharge chamber through the nozzles providing vortex flow motion. Then, vortex gas flow passed through the discharge region and into the diagnostic arm.

CH_3I and HI were used as iodine precursors, and Ar or Ar with small addition of He – as carrier gas. We found in our previous experiments (Mikheyev et al, 2002) that higher atomic iodine concentration could be obtained in Ar plasma than in He, N_2, O_2 or air.

Concentrations of iodine atoms obtained in discharge were determined measuring concentrations of iodine molecules, produced as a result of recombination of I atoms on their way to the diagnostic arm.

Concentration of I_2 was measured in the diagnostic arm of 24 cm length using light absorption at 495.5 nm. An incandescent lamp was used as the light source. Spectral region of ±0.3 nm was cut out with the help of a monochromator. I_2 absorption cross section is known to be $2\times10^{-18}cm^2$ (Okabe, 1978). In the chosen spectral region no absorption by CH_3I, HI and NO_2 was detected for typical concentrations of these molecules in experiments.

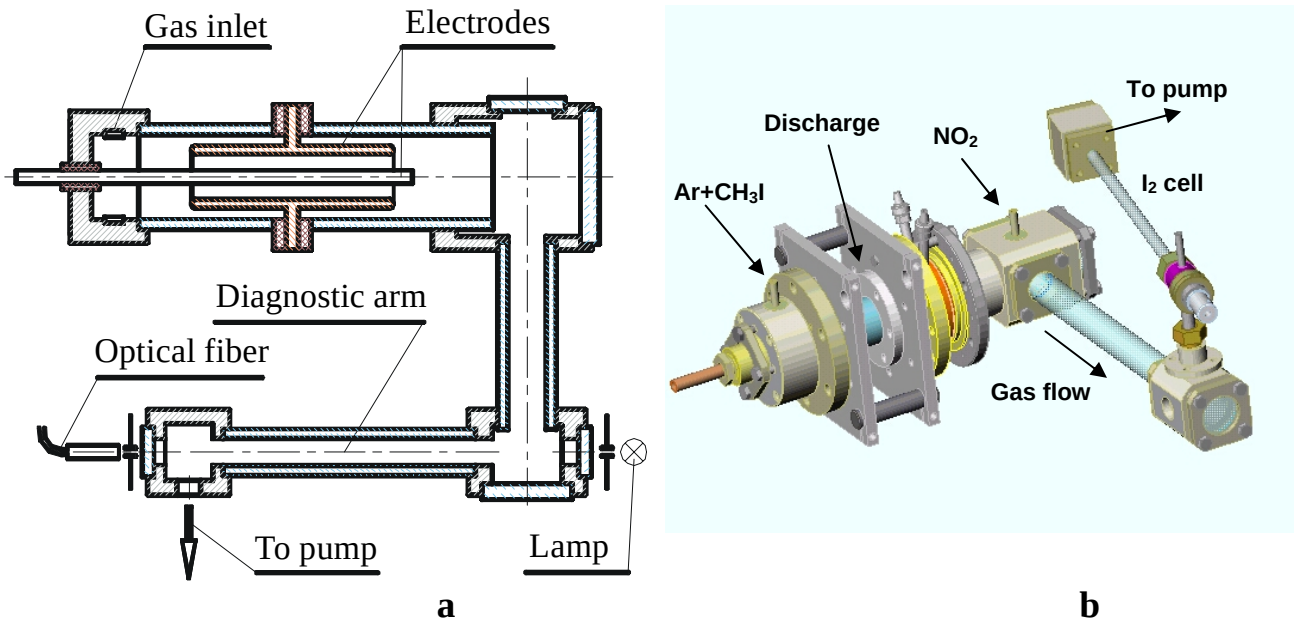

Fig.III.9. Setup (a) and overall view (b) of the discharge chamber with the diagnostic arm for I_2 concentration measurements.

To ensure full recombination of iodine small quantities of NO_2 were admixed downstream of the discharge region and before the diagnostic arm. In our experimental conditions iodine atoms interacted with NO_2 during 20-30 ms. Numerical modeling, using the results from (Van den Berg, 1976), shows that at 30 Torr Ar pressure, 350 °K temperature and initial iodine atoms concentration of $10^{16}cm^{-3}$ 70% of iodine atoms recombine due to volumetric processes in 20-30 ms. In the same conditions, but in the presence of $3\times10^{15}cm^{-3}$ of NO_2 molecules virtually all iodine atoms recombine in 20 ms.

During experiments it was found, that after 20-30 minutes of discharge operation with iodine precursor, presence or absence of NO_2 did not affect the results of measurements. Presumably, this is due to accumulation of iodine on the walls of the discharge chamber and the gas ducts that speeds up iodine recombination during transportation to the diagnostic arm.

Gas flow rates were measured by the flow meters. To measure CH_3I flow rate, with vapor pressure about 400 Torr at room temperature, the flow meter was calibrated using a vessel with known volume. To measure HI flow rate with vapor pressure about 10 atm at room temperature, the flow meter was calibrated with SF_6.

Experiments with the mixture of Ar:CH_3I showed that with longer discharge region along the flow, discharge remained stable at higher current. In our experiments cathode length determined the length of the discharge region. Stable discharge could be sustained up to 750 mA with 10 cm cathode – nearly twice as much against 430 mA with 5 cm cathode, all other factors being equal. Discharge voltage amounted to 250-270 V.

The highest pressure of the carrier gas Ar amounted to 30 Torr. Maximum CH_3I pressure for the discharge to remain stable in all cases did not exceed ~0.5 Torr. Maximum flow rate of iodine precursor could be increased, the discharge remaining stable, with increase of flow velocity. At 30 Torr pressure with increase of Ar flow rate from 4.5 to 12.5 mmol/s it was possible to increase CH_3I flow rate from 0.09 to 0.2 mmol/s.

Atomic iodine concentrations obtained in experiments with CH_3I recalculated from measured molecular iodine concentrations are represented in **Fig.III.10** with dependence on discharge current. As **Fig.III.10** suggests, there is, in essence, a linear dependence of [I] on discharge current. For the largest [I] concentrations obtained in these experiments – $1.2\cdot10^{16}$ cm^{-3}, the amount of iodine atoms

was about 80% of iodine contained in CH_3I for the precursor flow rate 0.2 mmol/s. And for CH_3I flow rate of 0.15 mmol/s this value amounted to almost 100%.

Stable discharge operation could be obtained during 20-30 minutes and was limited by contamination of electrodes by some kind of a black coating. Anode was contaminated to a considerably lesser extent. After cleaning of the electrodes stable discharge operation continued.

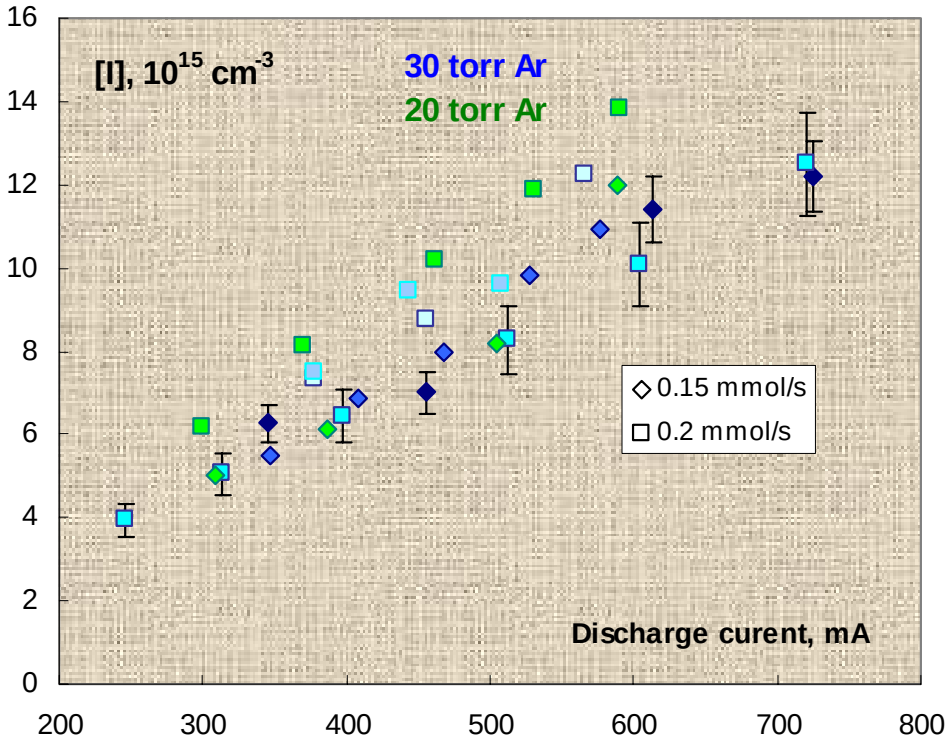

Fig.III.10. Plot of iodine atoms concentration [I] on discharge current for CH_3I flow rates of 0.15 and 0.2 mmol/s at carrier gas pressures 20 and 30 torr.

Study of iodine atoms production, using HI as precursor. Measurement of iodine number density produced when HI was added in the discharge region.
(Subtask 2C.2)

There may be disadvantages when CH_3I is used as the precursor. In the process of dissociation various carbon-containing radicals like CH_3 appear in the medium. Their influence on oxygen-iodine active medium is unknown and may be adverse. Besides, those radicals may contaminate the surfaces of electrodes. Therefore, HI molecule arise considerable interest, because of different and more simple nature of possible contaminants, with effect on the active medium that should be different and, presumably, weaker.

Experiments with HI were performed with the same experimental setup (**Fig. III.9**) using 10 cm cathode. Stable discharge in a mixture of carrier gas and HI was obtained up to the maximum pressure of 30 Torr. The largest concentrations of iodine atoms were obtained at 20 Torr of Ar pressure and 8.5 mmol/s Ar flow rate with small admixture of He (1 Torr, 0.43 mmol/s). Maximum HI flow rate amounted to 0.18 mmol/s, corresponding to the pressure of 0.4 Torr.

Dependence of concentration of the iodine atoms [I] on discharge current is represented in **Fig.III.11**. As seen in this figure, there was no increase in [I] when discharge current exceeded 450 mA. Complete dissociation of HI was observed. Discharge voltage in the range of discharge current 450-650 mA amounted to 270 V.

When HI was used instead of CH_3I different type of contamination of the electrodes was observed. Copper electrodes became covered by a light colored coating that degraded discharge stability after 20-25 minutes of operation.

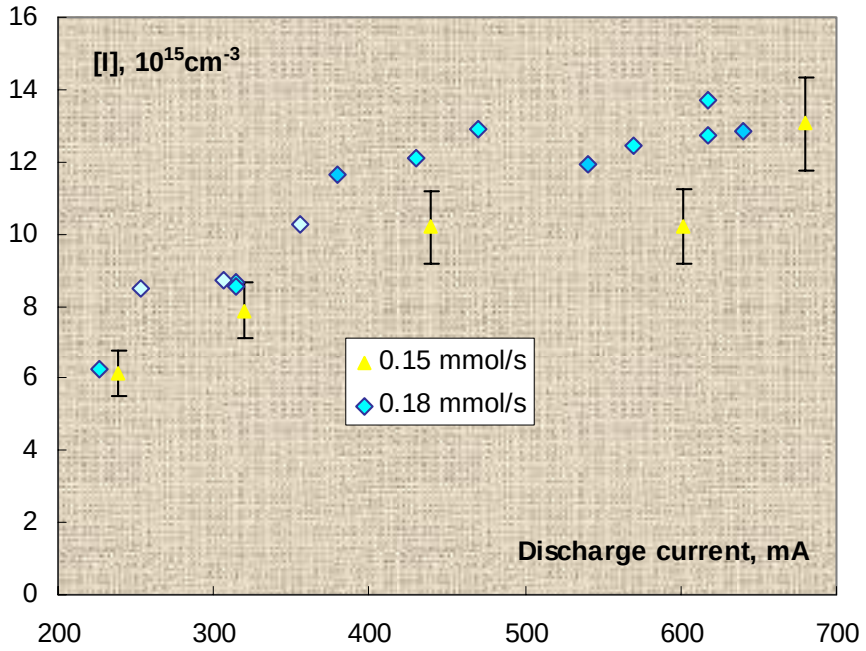

Fig.III.11 Plot of iodine atoms concentration [I] on discharge current for HI flow rates of 0.15 and 0.18 mmol/s at a pressure of carrier gas Ar:He 20:1 torr.

Discussion of the experiments on Subtasks 2C.1 and 2C.2.

The dependencies of the iodine atoms concentration on discharge current turned out to be different for CH_3I and HI precursors. When CH_3I was used, [I] increased linear with discharge current within the current range where discharge remained stable. Sometimes, discharge stability degraded when complete dissociation of the precursor was not yet achieved. With HI, complete dissociation occurred at smaller discharge current, and saturation of the dependence of [I] on current was observed when discharge was still stable.

Possible explanation is that the rate constant of the interaction of electrons with HI is larger compared to that with CH_3I. Measured rate constants of dissociative attachment for low energy electrons in (Schramm et al, 1999; Klar et al, 2001) support this assumption. For the electrons with energy 1 eV those constants are of order of $10^{-8}cm^3\ c^{-1}$ and the rate constant for HI is 2-3 times larger then for CH_3I.

The peculiarity of the discharge system used in experiments is that due to rather small interelectrode gap a substantial part of the power loaded in the discharge is released in the cathode fall region. At a pressure higher then 10 Torr, this region is very small – of the order of a tenth of millimeter. It is generally accepted and shown in experiment (Ivanchenko et al, 1982), that almost all power released there sink as heat into the cooled cathode wall. Due to the physical properties of that region – strong electric fields, relatively low electron concentration and, especially, extremely small dimension – it cannot make a substantial contribution to dissociation of the molecules of iodine precursor.

Cathode fall in pure Ar with copper cathode amounts to 130 V. The reasonable assumption for our conditions is that it should be somewhat higher, to compensate for additional loss of electrons

due to attachment to electronegative halogen containing species. However, as no such data is available, we use the cathode fall value of 130 V for estimations. As the total observed discharge voltage amounted to 260-280 V, no less then half of the of the power loaded in the discharge was released in the cathode fall region and was not used to dissociate the precursor molecules. Therefore, from all the power loaded into the flowing gas – that is, total power minus power released in the cathode fall region – the fraction expended on dissociation exceeds 40% for CH_3I and 80% for HI. In (Quillen et al, 2003), where I_2 was dissociated by an RF discharge only 5% of discharge power was expended on dissociation.

Mean values of E/N in our case are not representative, because positive column with constant electric field along the current appeared to be absent due to rather small, less then 1 cm interelectrode gap. Therefore, it may be assumed that electric field strength changes from almost zero near the cathode fall region up to higher values near anode. So, electric field strength in the substantial part of the discharge gap is low and, consequently, mean electron energy is low there. In our opinion, mainly due to this circumstance, dissociation of iodine precursors is efficient, if the main mechanism is dissociative attachment. The lower is the electron energy – the higher is the cross section of dissociative attachment.

Estimations of gas temperature, performed using the results of (Mikheyev et al, 2002), showed that in the conditions of experiment gas temperature after discharge should not exceed 350-370 °K.

Measurements of excited iodine atoms concentration in the discharge products. Determination of exited atoms concentration measuring absolute intensity of iodine emission at 1.315 μm, calibrating the apparatus against black body radiation.
(*Subtask 2C.3)*

Experiments were performed to determine concentration of excited iodine atoms in $I(^2P_{3/2})$ state, produced in the downstream afterglow of a DC glow discharge in the mixtures of argon and oxygen with admixture of gaseous iodides.

A drawing of the experimental setup is represented in **Fig.III.12.** Gas mixture was injected through two nozzles tangentially to the discharge tube wall forming a vortex that stabilized glow discharge. Water cooled copper cylinder 12 mm in diameter along the axis of the discharge chamber acted as a cathode. Water cooled anode was the hollow copper cylinder 12 mm in inner diameter placed near the nozzles. Interelectrode distance amounted to 3 cm.

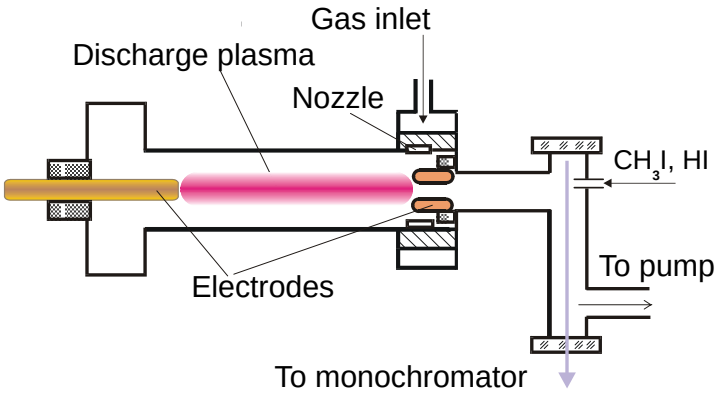

Fig.III.12. Experimental setup for measurements of excited iodine atoms concentration.

Methyl iodide (CH_3I) and hydrogen iodide (HI) were used as iodine precursors that were admixed in the afterglow region. Argon pressure was in the range from 3 to 10 Torr, oxygen pressure – from 0.3 to 2.7 Torr, iodides pressure – from 0.06 to 0.36 Torr. The concentrations of

excited iodine atoms ([I*]) were determined measuring intensity of 1.315 μm iodine line. Absolute calibration of the measured light intensity was performed with the help of a black body radiation.

The results of measurements for the mixture $Ar:O_2$ = 6:0.4 Torr (2.8:0.2 mmol/s), discharge current 230 mA and voltage 400 V are represented in **Fig.III.13**. With discharge current [I*] concentration reached saturation at about 150 mA. When HI was used as iodine precursor the measured concentrations [I*] turned out to be half as much as they were with CH_3I.

Fig.III.14 shows the results of measurements of 1.315 μm iodine line intensity along the flow in the diagnostic arm. Line intensity downstream decreased linearly about 5 times along 15 cm (time of flight is roughly 3 ms) similarly for both iodides. The highest concentration of excited iodine averaged along the diagnostic region amounted to ~10^{13}cm^{-3}. The concentration of iodine atoms in ground state assumed to be constant along the flow and roughly estimated to amount to ~10^{14}cm^{-3}, taking into account ~450 °K gas temperature. Maximal relative concentration of the excited iodine atoms, taking into account their distribution along the flow amounted to more then 6% near the discharge.

Numerical modeling of the dependence of the excited iodine concentration on time had shown that known quenching reactions could not explain such a steep decrease of concentration along the flow observed in the experiments. Loss of excited atoms due to diffusion to the wall also could not explain the observed rate of signal decrease.

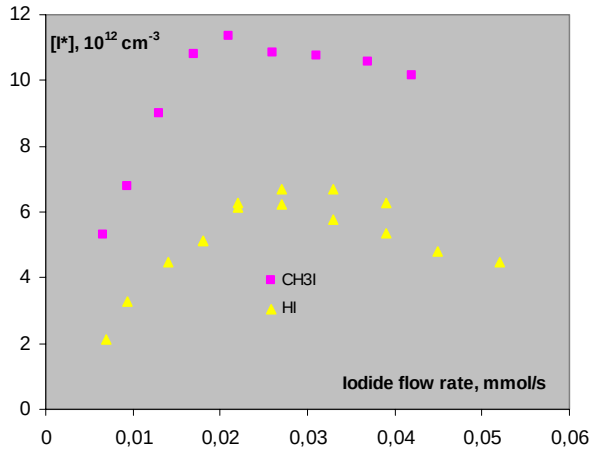

Fig.III.13. Typical dependence of excited iodine atoms concentration on the iodide precursor flow rate averaged along the diagnostic region. $Ar:O_2$ = 6:0.42 torr (2.8:0.2 mmol/s), 230 mA, 400 V discharge current and voltage.

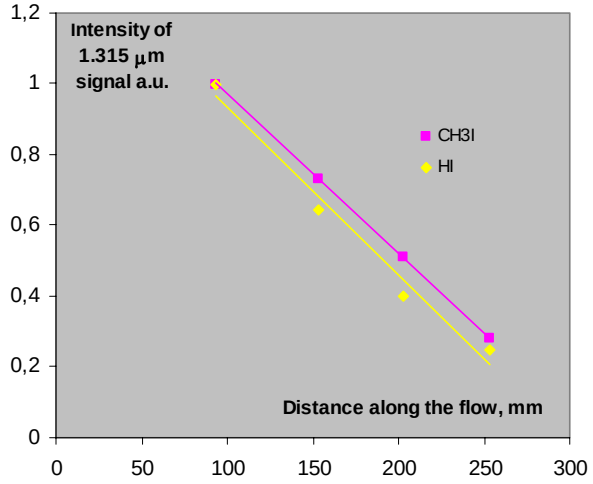

Fig.III.14. Decrease of iodine 1.315 μm line intensity along the flow. Iodides' flow rate 0.2 mmol/s. Other conditions as in fig.2C.3.2. Zero point corresponds to the rear end of the diagnostic zone.

Study of iodine atoms production decomposing iodides by discharge products. The measurements of iodine atoms concentration produced in the downstream afterglow by chemically active particles that exist in glow discharge in oxygen and oxygen mixtures.

(Subtask 2C.4)

The experiments were performed like in the *task 2C.3* using the same experimental setup. Interelectrode distance amounted to 6 cm. Pressure of the Ar:O_2 mixtures was varied in the range from 3 to 10 Torr. Methyl iodide CH_3I was used as an iodine precursor and was admixed in the afterglow adjacent to discharge.

In all cases the signal 1.315 μm reached saturation with current at about 150 mA, then even slight decrease of the signal was observed. Maximal concentration of the excited iodine atoms increased with oxygen flow rate up to 0.15-0.2 Torr and remained, in essence, constant with further increase of oxygen flow. At a fixed flow rate and pressure of argon-oxygen mixture the dependence of [I*] concentration on iodide flow rate also exhibited maximum. With flow rate and pressure of argon-oxygen mixture this maximum moved to higher flow rates of methyl iodide.

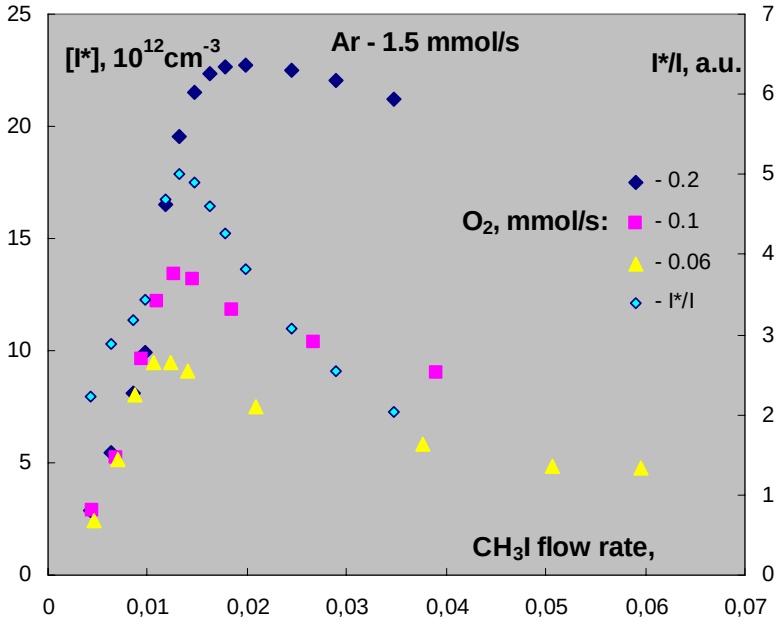

Fig.III.15. Plot of [I*] absolute concentration on CH_3I flow rate for different O_2 flow rates (left axis). Plot of relative concentration I*/I on CH_3I flow rate for O_2 flow rate 0.2 mmol/s (right axis).Ar pressure 3 torr (1.5 mmol/s), discharge current 200 mA.

The results of the measurements are represented in the **Fig.III.15** for those Ar:O_2 mixtures, where the largest absolute and relative concentrations of excited iodine atoms were observed. The highest absolute concentration amounted to ~2×10^{13} cm^{-3}. The highest relative concentration of excited iodine atoms I*/I near discharge (accounting for their distribution along the flow) was estimated to be about 10%.

Conclusions

As the result of work on the Part III of the project an efficient DC discharge iodine generator capable to produce iodine atoms with concentration of more than $1 \cdot 10^{16}$ cm^{-3} at 30 Torr Ar carrier pressure was developed. Iodine atoms were obtained in a glow discharge with coaxial electrodes and vortex gas flow stabilization using CH_3I and HI as iodine precursors. The degree of dissociation amounted to 80-100%. From all the power loaded into the flowing gas the fraction expended on dissociation exceeds 40% for CH_3I and 80% for HI. The flow rate of the iodine precursors amounted to 0.2 mmol/s.

It was found that HI dissociated more efficiently in comparison with CH_3I, most likely due to higher rate coefficient of dissociative attachment. However, experiments with $O_2(a^1\Delta)$ generated in a DC discharge has shown possible adverse effect of HI or the products of its decomposition in the discharge plasma on the oxygen-iodine active medium.

References for Part III

Bunker D.L., Davidson N. (1958). *J. Am. Chem .Soc.*, **80**, 5085.

Ip J.K.K., Burns G. (1972). *J. Chem. Phys*. **56**, 3155.

Ivanchenko A.I., Shepelenko A.A. (1982). *High Temp.,* **4**, 636.

J. Phys. Chem. (2000). Ref. Data. **29**, 167.

Klar D., Ruf M.-W., Fabrikant I.I., Hotop H. (2001). *J. Phys .B: At. Mol. Opt. Phys.* **34,** 3855.

Mikheyev P.A. et al. (2001). "Atomic Iodine Production in Vortex-Flow Glow Discharge". *CD Proceedings of COIL R&D Workshop*, Prague, 28-29 May 2001.

Mikheyev P.A., Shepelenko A.A., Voronov A.I., Kupryaev N.V. (2002). *Quantum Electron*., **32,** 1.

Okabe H. (1978). *Photochemistry of small molecules* (John Wiley & Sons, Inc.)

Quillen B., Schall W. (2003). Iodine dissociation with an RF discharge. *COIL R&D Workshop (Stuttgart, Germany, October 2003),* CD-ROM.

Schramm A., Fabrikant I.I., Weber J.M., Leber I., Ruf M.-W., Hotop H. (1999) *J.Phys.B: At. Mol. Opt. Phys.* **32,** 2153.

Van den Berg H., Troe J., 1975, *J. Chem. Phys.*, **64**, 736.

LIST OF PUBLISHED PAPERS AND REPORTS WITH ABSTRACTS

"**Gain dynamics on fundamental ro-vibrational transitions of pulsed CO laser**"
S.V.Vetoshkin, A.A.Ionin, Yu.M.Klimachev, A.A.Kotkov, L.V.Seleznev, D.V.Sinitsyn
Proc. of Scientific Session of Moscow Engineering Physics Institute, **4**, 23 (2003) (in Russian)

Preliminary results on the experimental study of gain dynamics at the fundamental band rotational-vibrational transitions in the active medium of pulsed electron beam sustained discharge CO laser amplifier were presented. The gain dynamics was studied for the transitions in vibrational bands V→V-1 from 6→5 up to 18→17.

"**Small signal gain time behavior on high vibrational transitions of CO molecule**"
S.V.Vetoshkin, A.A.Ionin, Yu.M.Klimachev, A.Yu.Kozlov, A.A.Kotkov, O.A.Rulev, D.V.Sinitsyn, A.K.Kurnosov, A.P.Napartovich, S.L.Shnyrev
Proc. of 7th International Scientific Conference on Vibrational Kinetics, p.179-189 (2003) (in Russian)

Small-signal gain time behavior for a pulsed e-beam sustained discharge CO laser amplifier operating on fundamental band vibrational transitions V→V-1 from 6→5 (λ~5.0 μm) up to 32→31 (λ~7.5 μm) was studied both experimentally and theoretically at various parameters of active medium. Master oscillator - laser amplifier setup was used in the experiments. Cryogenically cooled DC discharge frequency selective CW CO laser was used as a master oscillator, and pulsed cryogenically cooled e-beam sustained discharge CO laser with active medium length of 1.2 m was used as laser amplifier. The complete kinetic model of a CO laser was employed for theoretical description of the small-signal gain time behavior. The theoretical results were compared with the experimental data.

"**Characteristics of RF discharge in helium and carbon monoxide mixtures**"
A.A.Ionin, I.V.Kochetov, A.P.Napartovich, D.V.Sinitsyn, Yu.V.Terekhov
Proc. of Scientific Session of Moscow Engineering Physics Institute, **4**, 25 (2003) (in Russian)

The properties of RF discharge in He:CO gas mixtures containing from 5% up to 20% CO were studied experimentally and theoretically. Volt-power characteristics of the RF discharge at gas mixture total pressure 60 and 100 Torr were measured using discharge setup of special design. The experimental data were compared with calculated results.

"**Slab RF discharge modeling for gas mixtures typical for carbon monoxide lasers**"
A.A.Ionin, I.V.Kochetov, A.P.Napartovich, D.V.Sinitsyn, S.A.Starostin, Yu.V.Terekhov
Preprint FIAN #34, pp.1-20 (2002) (in Russian)

The experimental discharge facility of special design was developed for studying slab RF discharge properties in gas mixtures containing carbon monoxide molecules. Voltage-power characteristics of the RF discharge were measured experimentally for gas mixtures with different content of CO in the gas pressure range of 10 ÷ 100 Torr. Experimental dependencies of RMS voltage applied to the electrodes on specific power loaded into the RF discharge were modeled theoretically using 1D model. The experimental data were compared with the results of numerical calculations.

"**Non-selfsustained electric discharge in oxygen gas mixtures:**

singlet delta oxygen production"

A.A.Ionin, Yu.M.Klimachev, A.A.Kotkov, I.V.Kochetov,
A.P.Napartovich, L.V.Seleznev, D.V.Sinitsyn, G.D.Hager

Preprint FIAN #27, pp.1-20 (2003) (in Russian)

The opportunity of obtaining a high specific input energy in a non-selfsustained e-beam sustained discharge ignited in oxygen mixtures O_2:Ar:CO (or H_2) at the total gas pressures of 10-100 Torr has been experimentally demonstrated. The specific input energy has exceeded ~6 kJ l^{-1} atm^{-1} (150 kJ $mole^{-1}$) as a small amount of carbon monoxide is added into a gas mixture of oxygen and argon. It has been theoretically demonstrated that one might expect to obtain the singlet delta oxygen yield of 25% exceeding its threshold value needed for an oxygen-iodine laser operation at room temperature, when igniting a non-selfsustained discharge in gas mixtures with molecular additives CO, H_2 or D_2. The efficiency of the singlet delta oxygen production in non-selfsustained discharge can be as high as 40%

"**Non-self-sustained electric discharge in oxygen gas mixtures: singlet delta oxygen production**"

A.A.Ionin, Yu.M.Klimachev, A.A.Kotkov, I.V.Kochetov,
A.P.Napartovich, L.V.Seleznev, D.V.Sinitsyn, G.D.Hager

J.Phys.D: Appl.Phys., **36**, 982-989 (2003)

The opportunity of obtaining a high specific input energy in a non-selfsustained e-beam sustained discharge ignited in oxygen mixtures O_2:Ar:CO (or H_2) at the total gas pressures of 10-100 Torr has been experimentally demonstrated. The specific input energy has exceeded ~6 kJ l^{-1} atm^{-1} (150 kJ $mole^{-1}$) as a small amount of carbon monoxide is added into a gas mixture of oxygen and argon. It has been theoretically demonstrated that one might expect to obtain the singlet delta oxygen yield of 25% exceeding its threshold value needed for an oxygen-iodine laser operation at room temperature, when igniting a non-selfsustained discharge in gas mixtures with molecular additives CO, H_2 or D_2. The efficiency of the singlet delta oxygen production in non-selfsustained discharge can be as high as 40%

"**Electron-beam sustained discharge in oxygen gas mixtures: electric properties, spectroscopy and $O_2(a^1\Delta_g)$ yield**"

M.P.Frolov, G.D.Hager, A.A.Ionin, Yu.M.Klimachev, A.A.Kotkov, I.V.Kochetov,
A.P.Napartovich, Yu.P.Podmar'kov, L.V.Seleznev, D.V.Sinitsyn, N.P.Vagin, N.N.Yuryshev

Preprint AIAA 2003-4031 (2003)

Electric properties and spectroscopy of an e-beam sustained discharge in oxygen and oxygen gas mixtures at gas pressure up to 100 Torr was experimentally studied in large excitation volume (~18 liter). The discharge in pure oxygen and its mixtures with noble gases was shown to be very unstable and characterized by low input energy. When adding small amount of carbon monoxide or hydrogen, the electric stability of the discharge increases, specific input energy per molecular component being higher more than order of magnitude and coming up to 6500 J/(*l* atm). Theoretical calculations demonstrated that for the experimental conditions the $O_2(a^1\Delta_g)$ yield may reach ~20% exceeding its threshold value needed for oxygen-iodine laser operation at room temperature. The results of tentative experiments on spectroscopy of the $O_2(a^1\Delta_g)$ and $O_2(b^1\Sigma_g^+)$ states in the EBSD are presented.

“Supersonic RF discharge CO laser: Fundamental Band Electrical Efficiencies >20% and Observation of Overtone Band Lasing from a Short Gain Length Cavity“

J.E.McCord, G.D.Hager, S.Dass, A.A.Ionin

Preprint AIAA 2003-3475 (2003)

Radio-frequency (RF) excitation of carbon monoxide (CO) in a supersonic cavity with only a 10 cm gain length has yielded an observed fundamental band (ΔV=1) output power of 2.1 kW utilizing a one-pass resonator, with an electrical efficiency of 21%. More importantly, this work generated 50 W of overtone lasing at 2.7 micron. This was the first time lasing on CO overtone bands (ΔV=2) had been demonstrated with a RF –pumped supersonic system. This work also characterized the fundamental band and overtone band multi-line lasing transitions.

“**Method of obtaining singlet delta oxygen in non-self-sustained electric discharge plasma**“

A.A. Ionin , Yu.M. Klimachev , A.A. Kotkov , I.V. Kochetov , A.P. Napartovich ,
L.V. Seleznev , D.V. Sinitsyn, G.D. Hager

Russian Federation Patent #2206495, obtained 20 June 2003, priority 10 April 2002
(application #2002109190) (in Russian).

The invention could be applied for physics and technique of oxygen-iodine lasers. In order to produce singlet delta oxygen in non-self-sustained discharge in oxygen gas mixtures at pressure 10-100 Tor the molecular gases CO, H_2, D_2 with concentration 1-20% were added into gas mixtures.

“RF discharge physics in slab carbon monoxide lasers“

A.A.Ionin, I.V.Kochetov, A.P.Napartovich, D.V.Sinitsyn, Yu.V.Terekhov

Proc.CLEO/PR-2003, **2**, 663 (2003)

RF discharge properties in gas mixtures containing CO molecules were studied experimentally and modeled theoretically for different gas mixture compositions and initial pressures. It was shown a good agreement between experimental results and theoretically calculated data

“Theoretical model of a high-frequency-discharge-pumped CO laser”

I.V. Kochetov, A.P. Napartovich, S.A. Starostin

Quantum Electronics, **33** (10), 856 (2003)

The theoretical model of a high-frequency-discharge-pumped CO laser is described. The model consists of a block for calculating the spatial characteristics of a capacitive high-frequency discharge along the interelectrode distance and the distribution of the translational temperature of the gas. Another block contains the equations of the vibrational kinetics and the condition for stationary lasing in the resonator. The model was used to calculate the energy and spectral parameters of the CO laser in the stationary regime for different temperatures of the walls and two different spatial intensity distributions. The results are compared with the experimental data reported in the literature.

"RF discharge model: influence of CO molecules vibrational excitation on the discharge properties "

A.A.Ionin, I.V.Kochetov, A.P.Napartovich, D.V.Sinitsyn, S.A.Starostin, Yu.V.Terekhov

Preprint FIAN (LPI) №38, p.1-24 (2003)

1D theoretical model of RF discharge in gas mixtures containing carbon monoxide molecules was developed taking into account the influence of CO molecules vibrational excitation degree on discharge structure and its characteristics. Experimentally measured data on voltage-power characteristics of RF discharge in gas mixtures of different CO content were presented for gas pressure range 10-100 Torr. Obtained dependencies were simulated numerically using the model developed. The comparative analysis showed a satisfactory agreement between measured and calculated data on voltage-power characteristics for gas pressure ~100 Torr optimal to slab CO laser operation. The influence of vibrationally excited CO molecules on RF discharge space structure and electrical characteristics was studied theoretically.

"Theoretical model of pulsed EBSD CO laser"

Y.M.Klimachev, A.K.Kurnosov, A.P.Napartovich, S.L.Shnyrev

Proc. of Scientific Session of Moscow Engineering Physics Institute, **4**, 25 (2004) (in Russian)

Energy exchange processes between molecules and atoms in active medium of pulsed electron-beam sustained discharge (EBSD) CO laser were studied. Theoretical spatial uniform model was corrected with new rate constant of multiquantum VV exchange and VT relaxation taking into account. New kinetic processes were included.

"Dynamic of small signal gain on high ro-vibrational transitions of pulsed CO laser"

S. Vetoshkin, A. Ionin, Yu. Klimachev, A. Kotkov, O. Rulev, L. Seleznev, D. Sinitsyn

Proc. of Scientific Session of Moscow Engineering Physics Institute, **4**, 27 (2004) (in Russian)

For effective pulsed CO lasing on high ro-vibrational transitions in fundamental (V→V-1) and first-overtone (V→V-2) bands the study of small signal gain dynamic is necessary. Especially it is important for first-overtone CO laser. The time behavior of small-signal gain on high ro-vibrational transitions from 17→16 (λ~5.9 μm) to 32→31 (λ~7.5 μm) was measured with probe low-pressure single-line CW CO laser. In the experiments the conditions of supersonic CO laser (temperature, pressure and contents of gas mixture) were modeled. The obtained data allow us to optimize laser resonator position in supersonic cavity with efficiency of the supersonic laser increasing.

"Influence of admixture concentration on gas heating in CO laser"

Konev Yu.B., Kochetov I.V., A.K.Kurnosov, Lobarev Yu.V.

Proc. of Scientific Session of Moscow Engineering Physics Institute, **4**, 29 (2004) (in Russian)

Systematic calculations of electron energy balance were carried out with some admixture CO_2, H_2O and CH_4 in CO. It was shown that within the reduced admixture concentration range X_{ad}=0.001÷0.003 gas heating due to admixture vibration relaxation was in order more than in pure CO. When the value X_{ad} being lower 0.0005 (it corresponds to <0.1% concentration), the direct CO heating and gas heating due to admixture vibration relaxation are equivalent to each other.

"Theoretical studies on kinetics of singlet oxygen in nonthermal plasma"

M.P. Frolov, A.A. Ionin, A.A. Kotkov, I.V. Kochetov, A.P. Napartovich, Yu.P. Podmarkov, L.V. Seleznev, D.V. Sinitsyn, N.P. Vagin, N.N. Yuryshev

Proc. SPIE, **5448**, 294-306 (2004)

An idea to replace singlet delta oxygen (SDO) generator working with wet chemistry by electric discharge generator has got much attention last years. Different kinds of discharge were examined for this purpose, but without a great success. The existing theoretical models are not validated by well-characterized experimental data. To describe complicated kinetics in gas discharge with oxygen one needs to know in detail processes involving numerous electronic excited oxygen molecules and atoms. To gain new knowledge about these processes experimental studies were made on electric discharge properties in gas mixture flow with independent control of inlet SDO concentration. The theoretical model extended to include minor additives like oxygen atoms, water molecules, ozone was developed. Comparison with careful experimental measurements of electric characteristics along with gas composition allows us to verify the model and make theoretical predictions more reliable. Results of numerical simulations using this model for an electron-beam sustained discharge are reported and compared with the experimental data.

"Electric properties, spectroscopy, and singlet delta oxygen yield of electron-beam sustained discharge in oxygen gas mixtures"

M.P.Frolov, G.D.Hager, A.A.Ionin, Y.M.Klimachev, I.V.Kochetov, A.A.Kotkov, J.McIver, A.P.Napartovich, Y.P.Podmar'kov, L.V.Seleznev, D.V.Sinitsyn, N.P.Vagin, N.N.Yuryshev

Proc. SPIE, **5334**, 111-121 (2004)

Electric properties and spectroscopy of an e-beam sustained discharge in oxygen and oxygen gas mixtures at gas pressure up to 100 Torr was experimentally studied in large excitation volume (~18 liter). The discharge in pure oxygen and its mixtures with noble gases was shown to be very unstable and characterized by low input energy. When adding small amount of carbon monoxide or hydrogen, the electric stability of the discharge increases, specific input energy per molecular component being higher more than order of magnitude and coming up to 6.5 kJ/(*l* atm). Theoretical calculations demonstrated that for the experimental conditions the singlet delta oxygen $O_2(a^1\Delta_g)$ yield may reach ~20% exceeding its threshold value needed for oxygen-iodine laser operation at room temperature. The results of tentative experiments on spectroscopy of the $O_2(a^1\Delta_g)$ and $O_2(b^1\Sigma_g^+)$ states in the EBSD are presented.

"Electron-beam sustained discharge in oxygen gas mixtures: singlet delta oxygen production for oxygen-iodine laser"

M.P.Frolov, G.D.Hager, A.A.Ionin, Y.M.Klimachev, I.V.Kochetov, A.A.Kotkov, J.K.McIver, A.P.Napartovich, Y.P.Podmar'kov, L.V.Seleznev, D.V.Sinitsyn, N.P.Vagin, N.N.Yuryshev

Proc. SPIE, **5448**, 307-321 (2004)

Electric properties and spectroscopy of an e-beam sustained discharge (EBSD) in oxygen and oxygen gas mixtures at gas pressure up to 100 Torr were experimentally studied. The pulsed discharge in pure oxygen and its mixtures with noble gases was shown to be very unstable and characterized by low input energy. When adding small amount of carbon monoxide or hydrogen, the electric stability of the discharge increases, specific input energy (SIE) per molecular component being more than order of magnitude higher and coming up to 6.5 kJ/(*l* atm) for gas mixture O_2:Ar:CO = 1:1:0.1. The results of experiments on spectroscopy of the singlet delta oxygen $O_2(a^1\Delta_g)$(SDO) and $O_2(b^1\Sigma_g^+)$ states in the EBSD are presented. The calibration of the optical scheme for measuring the SDO absolute concentration and yield using the detection of luminescence of the SDO going from a chemical SDO generator was done. The preliminary measurement of the

SDO yield demonstrated that it was ~3% for the SIE of ~1 kJ/(*l* atm), which is close to the results of theoretical calculations for such a SIE. Theoretical calculations demonstrated that for the SIE of 6.5 kJ/(*l* atm) the SDO yield may reach ~20% exceeding its threshold value needed for oxygen-iodine laser operation at room temperature, although a part of the energy loaded into the EBSD goes into the vibrational energy of the molecular admixture, (which was experimentally demonstrated by launching a CO laser operating on an oxygen-rich mixture O_2:Ar:CO = 1:1:0.1 and measuring its small-signal gain).

"The methods of singlet oxygen detection for DOIL program"

N.N.Yuryshev, A.A.Ionin, M.P.Frolov, Y.M.Klimachev, I.V.Kochetov, A.A.Kotkov, A.P.Napartovich, Y.P.Podmar'kov, L.V.Seleznev, D.V.Sinitsyn, N.P.Vagin

Proc. SPIE, **5448**, 790-804 (2004)

The problem of development of a singlet delta oxygen $O_2(^1\Delta_g)$ (SDO) generators alternative to chemical one needs application of the accurate methods of measuring the SDO concentration. A chemical SDO generator providing efficient operation of a chemical oxygen-iodine laser (COIL) is proposed to be used as a reference source for absolute calibration of the system measuring the SDO concentration. The principle of the COIL operation results in the threshold and output COIL parameters make it possible to evaluate the SDO yield with a satisfactory accuracy. A convenient sparger chemical SDO generator was applied as a reference source for absolute calibration of detectors of dimole (λ=634nm) and b→X (λ=762 nm) radiations. The values of b-state concentration formed in a longitudinal electric discharge were evaluated. The intracavity laser spectroscopy (ICLS) was absolutely calibrated for measuring the SDO concentration. ICLS method has a very high sensitivity and makes it possible to monitor the absorption corresponding to the $O_2(^1\Delta_g)\rightarrow O_2(^1\Sigma_g^+)$ (λ = 1.91 μm) transition. The cross-sections of lines of the *Q* - branch of the vibrational 0-0 band of the $a^1\Delta_g \rightarrow b^1\Sigma_g^+$ transition of molecular oxygen were measured. The method developed was applied to measure the concentration of singlet oxygen produced in the microwave discharge. He - Ne laser (λ = 633 nm) was used for absolute calibration of a system monitoring the dimole radiation. The rate constant of the process responsible for dimole emission was measured. The value obtained $k_d=7.34\cdot10^{-23}$ cm^3/s is in agreement with literature

"Supersonic RF discharge CO laser operating in fundamental (Δ=1) and overtone (Δ=2) spectral bands"

J.E.McCord, R.F.Tate, S.Dass, G.D.Hager, A.A.Ionin, L.V. Seleznev, W.L.Bohn, H.von Buelow, J.K.McIver

Proc. SPIE, **5448**, 379-383 (2004)

Radio frequency (RF)-excitation of carbon monoxide (CO) in a supersonic cavity with only a 10 cm gain length has yielded an observed fundamental band (Δv=1) multi-line lasing output power of 2.1 kW utilizing a one-pass resonator, with an electrical efficiency of 21%. More importantly, this work generated 50 W of overtone multi-line lasing around 2.7 micron. This was the first time lasing on CO overtone bands (Δv=2) had been demonstrated with a RF-pumped supersonic system.

"Singlet Delta Oxygen Production in E-Beam Sustained Discharge:

Theory and Experiment"

A.Ionin, M.Frolov, G.Hager, Yu.Klimachev, I.Kochetov, A.Kotkov, A.Napartovich, Yu.Podmar'kov, L.Seleznev, D.Sinitsyn, N.Vagin, N.Yuryshev

Book of Abstracts of XV Int. Symp. on Gas Flow and Chem. Lasers & High Power Lasers Conf, p.75 (2004)

Singlet delta oxygen (SDO) production in a pulsed e-beam sustained discharge (EBSD) ignited in molecular oxygen with carbon monoxide stabilizing this discharge is theoretically and experimentally studied. Temporal behavior of SDO concentration and yield in the EBSD afterglow is analyzed. Experimentally measured SDO yield for oxygen mixture O_2:Ar:CO=1:1:0.05 at total gas pressure 30 Torr comes up to 7% at specific input energy (SIE) of ~3.0 kJ/(l atm(O_2+CO)), whereas its theoretical value riches ~17.5%. The efficiency of SDO production is theoretically analyzed as a function of the SIE.

"Measurements of the thermodynamic parameters for CO laser gas mixtures excited by pulsed electron-beam sustained discharge"

L.Seleznev, A.Ionin, Yu.Klimachev, I.Kochetov, A.Kotkov, A.Kozlov, A.Kurnosov, A.Napartovich, D.Sinitsyn, S.Vetoshkin

Book of Abstracts of XV Int. Symp. on Gas Flow and Chem. Lasers & High Power Lasers Conf, p.126 (2004)

Time behavior of gas temperature in CO containing gas mixture excited in pulsed electron-beam sustained discharge (EBSD) was experimentally studied under different experimental conditions. To study time behavior of gas temperature, the fact that the gas temperature is equivalent to the rotational temperature of gas molecules was used. Rotational distribution of the excited states of CO molecule was reconstructed from measured small-signal gain dynamics on different ro-vibrational transitions. The time behavior of small-signal gain was obtained with probe low-pressure CW CO laser for ten ro-vibrational spectral lines. Gas mixtures CO:He=1:4 and CO:N_2=1:9 typical for a CO laser were used. It was demonstrated that gas temperature grew from 110 K (initial temperature) up to ~150 K for the first hundred microsecond after EBSD beginning and was staying at this value for a long time (more than 1 ms) for both gas mixtures. EBSD pulse duration was ~30μs. The method of reconstruction of gas temperature time history was also applied for oxygen gas mixture CO:O_2=1:20 at gas pressure 0.04 atm, which was used for obtaining singlet delta oxygen in EBSD. The method can be used for diagnostic of non-equilibrium gas mixtures containing CO molecule.

"Time behavior of small-signal gain on high vibrational transitions for pulsed CO laser amplifier with gas mixtures CO:He, CO:N_2, and CO:O_2"

Y. Klimachev, A. Ionin, A. Kotkov, D. Sinitsyn, L. Seleznev, S. Vetoshkin A. Kozlov, O. Rulev

Book of Abstracts of XV Int. Symp. on Gas Flow and Chem. Lasers & High Power Lasers Conf, p.133 (2004)

Small-signal gain time behavior for cryogenic pulsed e-beam sustained discharge CO laser amplifier on high (V>15) fundamental band vibrational transitions was studied experimentally for different CO containing gas mixtures including ones typical for CO lasers and amplifiers (CO:He and CO:N_2), and CO:O_2 used for singlet delta oxygen production.

"$O_2(a^1\Delta_g)$ concentration measuring by intracavity laser spectroscopy

of $b^1\Sigma_g^+ - a^1\Delta_g$ transition"

M.Frolov, A.Ionin, I. Kochetov, A. Napartovich, Y. Podmar'kov, N.P.Vagin, N.N.Yuryshev

Book of Abstracts of XV Int. Symp. on Gas Flow and Chem. Lasers & High Power Lasers Conf, p.159 (2004)

Absorption spectra of chemically produced singlet oxygen $O_2(a^1\Delta_g)$ in the vicinity of 1.91 μm wavelength were recorded by intracavity laser spectroscopy technique. The line strengths for Q-branch transitions of the (0,0) band of the $b^1\Sigma_g^+ - a^1\Delta_g$ system were measured. Measurements of the $O_2(a^1\Delta_g)$ yield for an electric discharge are presented.

"Pulsed electron-beam sustained discharge in oxygen gas mixtures: electric characteristics, spectroscopy and singlet delta oxygen yield"

N.P. Vagin, A.A. Ionin, Yu.M. Klimachev, A.A. Kotkov, I.V. Kochetov, A.P. Napartovich, Yu.P. Podmar'kov, L.V. Seleznev, D.V. Sinitsyn, M.P. Frolov, G.D. Hager, N.N. Yuryshev

Quantum Electronics, **34** (9), 865-870 (2004)

Electric properties and spectroscopy of an e-beam sustained discharge (EBSD) in oxygen and oxygen gas mixtures at gas pressure up to 100 Torr was experimentally studied in large excitation volume (~18 liter). The discharge in pure oxygen and its mixtures with noble gases was shown to be very unstable and characterized by low input energy. When adding small amount (~1-10%) of carbon monoxide or hydrogen, the electric stability of the discharge increases, specific input energy (SIE) per molecular component being higher more than order of magnitude and coming up to 6.5 kJ/(*l* atm). A part of the energy loaded into the EBSD goes into the vibrational energy of the molecular admixture which was experimentally demonstrated by launching a CO laser operating on an oxygen-rich mixture O_2:Ar:CO = 1:1:0.1. The results of experiments on spectroscopy of the singlet delta oxygen $O_2(a^1\Delta_g)$ (SDO) and $O_2(b^1\Sigma_g^+)$ states in the EBSD are presented. The calibration of the optical scheme for measuring the SDO absolute concentration and yield using the detection of luminescence of the SDO going from a chemical SDO generator was done. The preliminary measurement of the SDO yield demonstrates that it is ~3% for the SIE of ~1 kJ/(*l* atm), which is close to the results of theoretical calculations for such a SIE. Theoretical calculations demonstrate that for the SIE of 6.5 kJ/(*l* atm) the SDO yield may reach ~20% exceeding its threshold value needed for oxygen-iodine laser operation at room temperature.

"Theoretical study of the energy efficiency of CO laser on fundamental or overtone transitions as a function of the laser spectrum width"

A. K. Kurnosov, A. P. Napartovich, S. L. Shnyrev

Quantum Electronics, **34**, #10, 1027-1032 (2004)

The theoretical model taking into account the multi-quantum VV-exchange processes is developed and applied for modeling of CO laser operating on CO:N_2 mixture. The energy characteristics are studied versus a number of ro-vibrational transitions in the spectral band of selective laser cavity. The characteristics of laser on the fundamental band or overtone transitions are analyzed separately. In this work the particular emphasis was given on the prognoses of energy efficiency for narrow band (incorporating one, three or five transitions) lasing versus the central ro-vibration transition disposition and the laser cavity quality. It is shown, that the usage of the single quantum approximation for description of VV exchange leads to sizeable error in modeling of CO laser with narrow band (1-5 transitions) selective resonator. The low of rising of laser efficiency as functions of spectral width of resonator (from 1 up to 35 transitions) is studied for the cases when the central fundamental/overtone transitions are 23→22 or 24→22. It's found, that for the resonator spectral band, enabling lasing on 5 neighbor transitions, the output energy exceeds one halve from the value, reachable for maximum width of the band.

"Production of iodine atoms dissociating CH_3I and HI in the DC glow discharge

in the flow of argon"

P.A. Mikheyev, A.A Shepelenko, A.I. Voronov, N.V. Kupryayev

J. Phys. D: Appl. Phys., **37**, 3202-3206 (2004)

Production of iodine atoms by means of glow discharge in gas flow with intention to use them in chemical oxygen-iodine laser was studied. DC glow discharge was sustained between coaxial electrodes in the vortex flow of argon, used as the carrier gas, with addition of iodine-containing molecular precursors CH_3I and HI. In the experiments high atomic iodine concentration more than 10^{16} cm^{-3} was achieved at a pressure of the Ar carrier up to 30 Torr. The dissociation degree of the precursor molecules was 80 – 100% for CH_3I and 100% for HI. Losses of iodine atoms in volumetric processes and due to diffusion to the walls of the transporting duct from the discharge region to the active medium were estimated. For the existing designs of iodine injectors of oxygen-iodine lasers loss of iodine atoms during transportation can be made small.

"Vibrational energy exchanges between N_2 and strongly excited co molecules: their role in vibrational kinetics"

M. Cacciatore, A. Kurnosov, A. Napartovich, S. Shnyrev

Journal of Physics B: At., Mol., Opt. Phys., **37,** 3379-3398 (2004)

The rate constants for multiquantum vibration-to-vibration V-V' energy exchanges in CO(v)-N_2(w) collisions, with CO in highly excited vibrational levels v and N_2 is in the first few low-lying vibrational levels w, were obtained from ab initio semiclassical calculations. A large temperature interval was explored, T=100-500K, while the vibrational quantum numbers v and w are in the range v=(30-44) and w=(0-2). Specific features of the vibrational kinetics of CO:Ar/He:N_2 gas mixtures for a wide range of the nitrogen content are explored in detail by using a recently developed kinetic modeling. In particular, it was found that the vibrational energy exchanges between N_2 and strongly excited CO molecules exert the essential influence on the vibrational population evolution and on the associated small signal gain and spectral characteristics of CO laser in both fundamental and overtone bands.

"Measurement of the O_2 ($b^1\Sigma_g^+ \rightarrow a^1\Delta_g$) transition probability by the method of intracavity laser spectroscopy"

Vagin N.P., Ionin A.A., Kochetov I.V., Napartovich A.P.,
Podmar'kov Yu.P., Frolov M.P., Yuryshev N.N.,

Quantum Electronics, **35** (4), 378 (2005).

The method of intracavity laser spectroscopy using a Co:MgF_2 laser is applied to record the absorption spectra from the first excited $a^1\Delta_g$ state of gaseous molecular oxygen at the $a^1\Delta_g \rightarrow b^1\Sigma_g^+$ transition at 1.91 μm. The gas flow from a chemical singlet oxygen generator with a known concentration of singlet oxygen O_2 ($a^1\Delta_g$) was supplied to the cavity of the Co:MgF_2 laser. The absorption line intensities are measured for five spectral lines of the Q-branch of the 0—0 vibrational band for the $a^1\Delta_g \rightarrow b^1\Sigma_g^+$ transition. The O_2 ($b^1\Sigma_g^+ \rightarrow a^1\Delta_g$) transition probability calculated from these data was $(1.20 \pm 0.25) \times 10^{-3}$ s^{-1}.

"Effect of the Vibrational Excitation of CO Molecules on the Parameters of an RF Discharge"

Ionin A.A., Sinitsyn D.V., Terekhov Yu.V., Kochetov I.V., Napartovich A.P., Starostin A.N.
Plasma Physics Reports, **31 (**9), 786 (2005)

A one-dimensional model of an RF discharge in CO-containing gas mixtures is developed. The model takes into account the effect of the degree of vibrational excitation of CO molecules on the structure of the discharge and on its parameters. Experimental data are presented from measurements of the voltage–power characteristics of RF discharges in gas mixtures with different CO contents in the pressure range of 10–100 torr. The model developed is used to calculate the dependence of the root-mean-square discharge voltage on the specific power deposition in an RF discharge under our experimental conditions. The experimental data are compared to the results of numerical simulations. For working gas pressures of about 100 torr, which are typical of the operation of slab CO lasers, the calculated voltage–power characteristics of an RF discharge agree satisfactorily with those obtained experimentally. The theoretical model predicts that the vibrational excitation of CO molecules leads to a redistribution of the RF field in the discharge gap and to an increase in the laser efficiency.

"Multiline laser probing for active media CO:He, CO:N_2 and CO:O_2 in wide-aperture pulsed amplifier"

Vetoshkin S.V., Ionin A.A., Klimachev Yu.M., Kozlov A.Yu., Kotkov A.A., Rulev O.A., Seleznev L.V., Sinitsyn D.V.

Preprint of P.N.Lebedev Physics Institute, **#13**, 1-55, Moscow, Russia, 2005 (in Russian).

Multiline laser probing was applied for diagnostics of active medium of wide-aperture carbon monoxide laser amplifier. Time behavior of small-signal gain in active medium of pulsed electron-beam sustained discharge CO laser amplifier was studied with especially designed probe CO laser in wide range of ro-vibrational spectral lines (from V=5 up to V=31). The results were analyzed in order to reconstruct temporal behavior of gas temperature and vibrational populations in CO contained gas mixtures: CO:He, CO:N_2 and oxygen rich mixture CO:O_2 .

"Highly excited CO molecules vibrational exchange and its influence on the physical processes in active medium of pulsed EBSD CO laser"

Klimachev Yu.M.

Proc. of Scientific Session of Moscow Engineering Physics Institute, **4**, 24 (2005) (in Russian)

Dynamics of small signal gain on high fundamental and overtone vibrational-rotational transitions of CO molecule was studied at different experimental conditions for pulsed electron beam sustained discharge CO laser active medium. Restoration time of inversion population after its short pulsed perturbation was measured in the laser by means of double Q-switching technique. Experimental results were compared with theoretical calculations.

"Electron-beam sustained discharge CO laser operating on gas mixtures with high (~95%) content of oxygen"

Vetoshkin S.V., Ionin A.A., Klimachev Yu.M., Kozlov A.Yu., Kotkov A.A., Seleznev L.V., Sinitsyn D.V.

Proc. of Scientific Session of Moscow Engineering Physics Institute, **4**, 26 (2005) (in Russian)

Pulsed electron beam sustained discharge CO laser was realized on active gas mixture with high (~95%) content of oxygen. Small signal gain in laser gas mixture CO:O_2 appeared to be twice higher than that for typical CO laser gas mixture CO:N_2.

"Singlet delta oxygen in low-temperature plasma of non-selfsustained discharge"

Rulev O.A., Vagin N.P., Ionin A.A., Klimachev Yu.M., Kotkov A.A., Kochetov I.V., Napartovich A.P., Seleznev L.V., Sinitsyn D.V., Yuryshev N.N.

Proc. of Scientific Session of Moscow Engineering Physics Institute, **4**, 28 (2005) (in Russian)

An influence of gas mixture content and pressure on singlet delta oxygen yield in pulsed electron beam sustained discharge was studied experimentally. Maximal obtained yield was estimated as about 7% for gas mixture $CO:O_2:Ar$ at total pressure of 30 Torr.

"Multiline laser probing of active medium of pulsed EBSD CO laser"

Kozlov A.Yu., Vetoshkin S.V., Ionin A.A., Klimachev Yu.M., Kotkov A.A., Kurnosov A.K., Napartovich A.P., Seleznev L.V., Sinitsyn D.V.

Proc. of Scientific Session of Moscow Engineering Physics Institute, **4**, 30 (2005) (in Russian)

Gas temperature temporal behavior and vibrational levels population dynamics in active medium of pulsed electron beam sustained discharge CO laser were measured using multi-frequency laser probing technique. It was concluded that the fraction of pumping discharge energy going into direct gas heating was equaled to ~15% for nitrogen containing mixture and ~10% for helium containing one.

"Compact cryogenically cooled slab CO laser with RF excitation"

Ionin A.A., Kochetov I.V., Napartovich A.P., Sinitsyn D.V., Terekhov Yu.V.

Proc. of Scientific Session of Moscow Engineering Physics Institute, **4**, 63 (2005) (in Russian)

Results of preliminary experiments on study compact cryogenically cooled slab CO laser with RF excitation were reported. Output laser characteristics obtained in fundamental band lasing mode were as follows: average power ~5W, efficiency ~2.5%. Possibilities of improving the laser characteristics and realizing overtone band lasing were discussed.

$O_2(a^1\Delta_g)$ concentration measuring by intracavity laser spectroscopy of $b^1\Sigma_g^+ \rightarrow a^1\Delta_g$ transition

Frolov M.P., Ionin A.A., Kochetov I.V., Napartovich A.P., Podmar'kov Yu.P., Vagin N.P., Yuryshev N.N.

Proceedings SPIE, **5777**, 70 (2005).

Absorption spectra of chemically produced singlet oxygen $O_2(a^1\Delta_g)$ in the vicinity of 1.91 μm wavelength were recorded by intracavity laser spectroscopy technique. The line strengths for Q-branch transitions of the (0,0) band of the $b^1\Sigma_g^+ - a^1\Delta_g$ system were measured. Measurements of the $O_2(a^1\Delta_g)$ yield for an electric discharge are presented.

"Measurements of the thermodynamic parameters for CO laser gas mixtures excited by pulsed electron-beam sustained discharge"

Seleznev L., Ionin A., Klimachev Yu., Kochetov I., Kotkov A., Kozlov A., Kurnosov A., Napartovich A., Sinitsyn D., Vetoshkin S.

Proceedings SPIE, **5777**, 418 (2005).

Time behavior of gas temperature in CO containing gas mixture excited in pulsed electron-beam sustained discharge (EBSD) was experimentally studied under different experimental conditions. To study time behavior of gas temperature, the fact that the gas temperature is equivalent to the rotational temperature of gas molecules was used. Rotational distribution of the excited states of CO molecule was reconstructed from measured small-signal gain dynamics on different ro-vibrational transitions. The time behavior of small-signal gain was obtained with probe low-pressure CW CO laser for ten ro-vibrational spectral lines. Gas mixtures $CO:He=1:4$ and $CO:N_2=1:9$ typical for a CO laser were used. It was demonstrated that gas temperature grew from 110 K (initial temperature) up to ~150 K for the first hundred microsecond after EBSD beginning and was staying

at this value for a long time (more than 1 ms) for both gas mixtures. EBSD pulse duration was ~30μs. The method of reconstruction of gas temperature time history was also applied for oxygen gas mixture $CO:O_2$=1:20 at gas pressure 0.04 atm, which was used for obtaining singlet delta oxygen in EBSD. The method can be used for diagnostic of non-equilibrium gas mixtures containing CO molecule.

"Time behavior of small-signal gain on high vibrational transitions for pulsed CO laser amplifier with gas mixtures CO:He, $CO:N_2$, and $CO:O_2$"

Klimachev Yu., Ionin A., Kotkov A., Sinitsyn D., Seleznev L.,
Vetoshkin S., Kozlov A., Rulev O.
Proceedings SPIE, **5777**, 414 (2005).

Small-signal gain time behavior for cryogenic pulsed e-beam sustained discharge CO laser amplifier on high (V>15) fundamental band vibrational transitions was studied experimentally for different CO containing gas mixtures including ones typical for CO lasers and amplifiers (CO:He and $CO:N_2$), and $CO:O_2$ used for singlet delta oxygen production.

"Singlet Delta Oxygen Production in E-Beam Sustained Discharge: Theory and Experiment"

Ionin A., Frolov M., Hager G., Klimachev Yu., Kochetov I., Kotkov A., Napartovich A.,
Podmar'kov Yu., Seleznev L., Sinitsyn D., Vagin N., Yuryshev N.
Proceedings SPIE, **5777**, 207 (2005).

Singlet delta oxygen (SDO) production in a pulsed e-beam sustained discharge (EBSD) ignited in molecular oxygen with carbon monoxide stabilizing this discharge is theoretically and experimentally studied. Temporal behavior of SDO concentration and yield in the EBSD afterglow is analyzed. Experimentally measured SDO yield for oxygen mixture O_2:Ar:CO=1:1:0.05 at total gas pressure 30 Torr comes up to 7% at specific input energy (SIE) of ~3.0 kJ/(l atm(O_2+CO)), whereas its theoretical value riches ~17.5%. The efficiency of SDO production is theoretically analyzed as a function of the SIE.

"CO laser: advances in theory and experiment"

Napartovich A., Kurnosov A., Shnyrev S., Ionin A., Klimachev Yu.,
Kotkov A., Seleznev L., Sinitsyn D.,
Proceedings SPIE, **5777**, 408 (2005).

Last years, CO laser physics has been advanced by researches of CO overtone laser operated on high vibrational levels. An extension of kinetic model to multi-quantum vibration-vibration exchange and development of fully self-consistent model of CO laser are described. The theoretical model developed is verified by comparison with experimental data on overtone CO laser characteristics and laser gain dynamics. Current status of experimental achievements in CO laser characteristics in both fundamental and overtone bands are reported.

"Singlet delta oxygen production in slab discharges ignited in oxygen gas mixtures"

Ionin A.A., Frolov M.P., Ochkin V.N., Kotkov A.A., Kochetov I.V., Napartovich A.P.,
Podmar'kov Yu.P., Rulev O.A., Savinov S.Yu., Seleznev L.V., Sinitsyn D.V.,
Terekhov Yu.V., Vagin N.P., Yuryshev N.N.
AIAA Paper 2005-4917 (2005).

Singlet delta oxygen $O_2(a^1\Delta_g)$ production in slab discharges ignited in oxygen gas mixtures was experimentally studied. In slab self-sustained RF discharge experimental SDO yield was about 10%. It was demonstrated that the choice of electrodes' material is very important. Experiments on SDO production in slab non-self-sustained discharge with external ionization by repeated high-

voltage pulses were carried out. SDO concentration was measured by the method of intracavity laser spectroscopy. The measured concentration of SDO was about 10^{16} cm^{-3}, with SDO yield being of ~7%.

"Fundamental and overtone band lasing of RF discharge supersonic CO laser"

Seleznev L.V., Bohn W., von Buelow H., Dass S., Hager G.D., Ionin A.A., McIver J.K., McCord J.E., Tate R.F. .

ICONO/LAT 2005 Conference Program, p. 93 (2005).

RF discharge CO overtone lasing with output power of 50 W was demonstrated with supersonic cooling system. Output power of 2.1 kW with efficiency of 21% in fundamental band was obtained.

"Multiline laser diagnostics of active medium parameters in the wide-aperture CO laser amplifier"

Kotkov A.A., Ionin A.A., Klimachev Yu.M., Kozlov A.Yu., Seleznev L.V., Sinitsyn D.V., Vetoshkin S.V., Kochetov I.V., Kurnosov A.K., Napartovich A.P.

ICONO/LAT 2005 Conference Program, p. 152 (2005).Local value of specific input energy, temporal behavior of gas temperature and vibrational populations in active medium excited by pulsed electron beam sustained discharge in the wide aperture CO laser amplifier was studied both experimentally and theoretically.

"Powerful supersonic CO laser on fundamental and overtone transitions"

Bohn W., Von Bülow H., Dass S., Hager G.D., Ionin A.A., Klimachev Yu.M., Kotkov A.A., McIver J.K., McCord J.E., Seleznev L.V., Tate R.F.

Quantum Electronics, **35** (12), 1126 (2005) (in print).

Lasing characteristics of carbon monoxide laser with RF discharge pumping in subsonic flow and following supersonic cooling of active medium were studied. Within spectral range 4.9-5.7 μm corresponding fundamental band (V+1→V) transitions the laser output power achieved 2.1 kW, with laser efficiency being up to 21%. First-overtone lasing was observed on transitions 9→7, 10→8 and 11→9 (spectral range 2.6-2.7 μm), with output power being 50 W. Possibilities of supersonic overtone CO laser design improvement to obtain overtone lasing on highly excited vibrational transitions of CO molecule were discussed.

"Gain dynamics in active medium of pulsed electron beam sustained discharge CO laser: theory and experiment"

Vetoshkin S.V., Ionin A.A., Klimachev Yu.M., Kozlov A.Yu., Kotkov A.A., Kurnosov A.K., Napartovich A.P., Rulev O.A., Seleznev L.V., Sinitsyn D.V., Shnyrev S.L.

Quantum Electronics, **35** (12),1107(2005) (in print).

Small-signal gain (SSG) time behavior was studied both experimentally and theoretically in active medium of pulsed e-beam sustained discharge CO laser for a wide range of vibrational transitions at various parameters of active medium and at different locations of probe laser beam in electric discharge region. Experimental data were compared with results of theoretical simulation carried out on the basis of spatially homogeneous kinetic model taking into account the processes of multiquantum VV exchange. The sensitivity of SSG time behavior to variation of active medium parameters was analyzed. A good agreement between theoretical and experimental data on SSG time behavior was demonstrated when corrected value of local input energy was used for numerical simulation.

"Double discharge in oxygen flow and singlet oxygen concentration produced by it"

A.A. Shepelenko, P.A. Mikheyev, A.I. Voronov, N.V. Kupryaev

Izvestia of the Samara scientific center of RAS. **7** (1), 65-70 (2005) (in Russian)

A transverse-flow double dc discharge with coaxial electrodes was studied experimentally as the means to produce singlet oxygen (SO). The distinctive feature of the investigated double discharge is that the upstream discharge (the 1-st) significantly affects the downstream discharge (the 2-nd), so that the second discharge becomes non-self-sustained. Current-voltage characteristics and SO concentrations have been measured at a pressure range of oxygen 6-12 Torr. It has been shown that the first discharge affects the second so, that the electric field strength in the plasma *E* and, consequently, the reduced electric field *E/N* decreases. At the pressure of oxygen 10 Torr *E/N* decreased from $\sim 31 \cdot 10^{-17}$ V·cm^2 down to $\sim 25 \cdot 10^{-17}$ V·cm^2. Electric power, loaded into the gas (without the power in the electrode regions) by one discharge, produced SO more efficiently than the sum of the powers loaded in series by two discharges.

"Supersonic overtone CO laser: research and development"

W.Bohn, H.von Bülow, S.Dass, G.D.Hager, A.A.Ionin, Yu.M.Klimachev, A.A.Kotkov, J.E.McCord, J.K.McIver, L.V.Seleznev, D.V.Sinitsyn, R.F.Tate

Proc. SPIE (2006) (in print)

Characteristics of cw CO laser with supersonic gas flow are discussed. Radio frequency discharge CO overtone (V+2→V) lasing with output power 50 W was demonstrated with supersonic cooling system. The overtone lasing was observed on 9→7, 10→8 and 11→9 vibrational transitions within spectral range 2.6 - 2.7 μm wavelength. The laser active medium length was 10 cm. The small signal gain on the overtone transitions was estimated to be 0.1 m^{-1}. Fundamental band (V+1→V) lasing was observed within 4.9 – 5.7 μm spectral range. In fundamental band output power 2.1 kW with efficiency 21% was obtained, with typical small signal gain being about 1 m^{-1}. Modeling experiments on electron-beam sustained discharge facility were carried out at experimental conditions (gas pressure, temperature) corresponding to those of supersonic gas flow. Possibilities of supersonic overtone CO laser design improvement to obtain overtone lasing on highly excited vibrational transitions of CO molecule corresponding to the spectral range ~3 – 4 micron are discussed.

"Electric generators of singlet delta oxygen for oxygen-iodine laser"

A.A.Ionin, A.P.Napartovich* and N.N.Yuryshev

Laser Physics, (2006), (in print).

Experimental and theoretical research of electric generators of singlet delta oxygen (SDO) for oxygen-iodine laser made at the Lebedev Physics Institute and TRINITI is discussed. Breakdown and volt-ampere characteristics of self-sustained electric discharge in SDO were studied both experimentally and theoretically indicating the fact that SDO and pure oxygen have quite different electric features. Electric properties and spectroscopy of an e-beam sustained discharge (EBSD) in oxygen and oxygen gas mixtures were experimentally studied. A comprehensive numerical model describing SDO kinetics in different kinds of discharge was developed. The pulsed EBSD in pure oxygen and its mixtures with noble gases was shown to be very unstable and characterized by low input energy. When adding small amount of carbon monoxide or hydrogen, the electric stability of the EBSD increases, specific input energy (SIE) per molecular component being more than order of magnitude higher and coming up to 6.5 kJ/(*l* atm(O_2+CO)) for gas mixture O_2:Ar:CO = 1:1:0.1. Theoretical calculations demonstrated that for the SIE of 6.5 kJ/(*l* atm) the SDO yield may reach ~20% exceeding its threshold value needed for oxygen-iodine laser operation at room temperature. The calibration of the optical scheme for measuring the SDO absolute concentration and yield using

the detection of luminescence of the SDO going from a chemical SDO generator was done. The measurement of the SDO yield demonstrated that it was ~10.5% for the SIE of ~3.0 kJ/(*l* atm(O_2+CO)), which is about 1.5 times less than the results of theoretical calculations for such an SIE. SDO production in RF slab discharges ignited in oxygen gas mixtures was experimentally studied, experimental SDO yield being about 10%. The choice of electrode material was demonstrated to be very important.

"Singlet oxygen in low-temperature plasma of e-beam sustained discharge"

Vagin N.P., Ionin A.A., Klimachev Y.M., Kotkov A.A., Kochetov I.V., Napartovich A.P., Podmar'kov Yu.P., Rulev O.A., Seleznev L.V. , Sinitsyn D.V., Frolov M.P., Yuryshev N.N.

Plasma Physics Report, (2006) (in print).

Singlet delta oxygen (SDO) production in a pulsed e-beam sustained discharge (EBSD) ignited in large volume (18 l) at total gas mixture pressure up to 210 Torr is theoretically and experimentally studied. Experimentally measured SDO yield was about 10.5%. It was shown experimentally that the value of reduced electric field beeng in the range 2-11 kV/(cm atm) not influenced significantly upon SDO yield. It was shown experimentally that an increase of a gas mixture pressure and specific input energy leaded to a decrease of SDO luminescence duration. The comparison of measured and calculated SDO concentration temporal behaviour was carried out.

LIST OF PRESENTATIONS AT CONFERENCES AND MEETINGS WITH ABSTRACTS

"**Gain dynamics on fundamental ro-vibrational transitions of pulsed CO laser**"
S.V.Vetoshkin, A.A.Ionin, Yu.M.Klimachev, A.A.Kotkov, L.V.Seleznev, D.V.Sinitsyn
Scientific Session of Moscow Engineering Physics Institute, 27-31 Jan 2003, Moscow, Russia

Preliminary results on the experimental study of gain dynamics at the fundamental band rotational-vibrational transitions in the active medium of pulsed electron beam sustained discharge CO laser amplifier were presented. The gain dynamics was studied for the transitions in vibrational bands $V \rightarrow V\text{-}1$ from $6 \rightarrow 5$ up to $18 \rightarrow 17$.

"**Small signal gain time behavior on high vibrational transitions of CO molecule**"
S.V.Vetoshkin, A.A.Ionin, Yu.M.Klimachev, A.Yu.Kozlov, A.A.Kotkov, O.A.Rulev, D.V.Sinitsyn, A.K.Kurnosov, A.P.Napartovich, S.L.Shnyrev
7th International Scientific Conference on Vibrational Kinetics, 7-13 Sept 2003, Moscow-Ples, Russia

Small-signal gain time behavior for a pulsed e-beam sustained discharge CO laser amplifier operating on fundamental band vibrational transitions $V \rightarrow V\text{-}1$ from $6 \rightarrow 5$ ($\lambda \sim 5.0$ μm) up to $32 \rightarrow 31$ ($\lambda \sim 7.5$ μm) was studied both experimentally and theoretically at various parameters of active medium. Master oscillator - laser amplifier setup was used in the experiments. Cryogenically cooled DC discharge frequency selective CW CO laser was used as a master oscillator, and pulsed cryogenically cooled e-beam sustained discharge CO laser with active medium length of 1.2 m was used as laser amplifier. The complete kinetic model of a CO laser was employed for theoretical description of the small-signal gain time behavior. The theoretical results were compared with the experimental data.

"RF discharge physics in slab carbon monoxide lasers"
A.A.Ionin, I.V.Kochetov, A.P.Napartovich, D.V.Sinitsyn, Yu.V.Terekhov
5th Pacific Rim Conference on Lasers and Electro-Optics, 15-19 Dec 2003, Taipei, Taiwan.

RF discharge properties in gas mixtures containing CO molecules were studied experimentally and modeled theoretically for different gas mixture compositions and initial pressures. It was shown a good agreement between experimental results and theoretically calculated data

"**Characteristics of RF discharge in helium and carbon monoxide mixtures**"
A.A.Ionin, I.V.Kochetov, A.P.Napartovich, D.V.Sinitsyn, Yu.V.Terekhov
Scientific Session of Moscow Engineering Physics Institute, 27-31 Jan 2003, Moscow, Russia

The properties of RF discharge in He:CO gas mixtures containing from 5% up to 20% CO were studied experimentally and theoretically. Volt-power characteristics of the RF discharge at gas mixture total pressure 60 and 100 Torr were measured using discharge setup of special design. The experimental data were compared with calculated results.

"**Small signal gain time behavior on high vibrational transitions of CO molecule**"

A.A.Ionin, Yu.M.Klimachev, A.A.Kotkov, L.V.Seleznev, D.V.Sinitsyn, S.V.Vetoshkin, A.K.Kurnosov, A.P.Napartovich, S.L.Shnyrev

XI Conference on Laser Optics, 30 June - 4 July 2003, St.Petersburg, Russia

Small-signal gain time behavior for a pulsed e-beam sustained discharge CO laser amplifier operating on fundamental band vibrational transitions V→V-1 from 6→5 (λ~5.0 μm) up to 32→31 (λ~7.5 μm) was studied both experimentally and theoretically at various parameters of active medium. Special attention was paid to the small-signal gain time behavior on high vibrational transitions (V>15). To make easier theoretical interpretation of the experimental results, the binary nitrogen free gas mixture CO:He=1:4 was used in our experiments. Total gas density and initial gas temperature was 0.12 Amagat and ~100 K, respectively. The complete kinetic model of a CO laser taking into account multi-quantum vibrational exchange was employed for theoretical description of the small-signal gain time behavior. The theoretical results were compared with the experimental data.

"**Electron-beam sustained discharge in oxygen gas mixtures: electric properties, spectroscopy and $O_2(a^1\Delta_g)$ yield**"

M.P.Frolov, G.D.Hager, A.A.Ionin, Yu.M.Klimachev, A.A.Kotkov, I.V.Kochetov, A.P.Napartovich, Yu.P.Podmar'kov, L.V.Seleznev, D.V.Sinitsyn, N.P.Vagin, N.N.Yuryshev

34th AIAA Plasmodynamics and Lasers Conference, 23-26 June 2003, Orlando, Florida, USA

Electric properties and spectroscopy of an e-beam sustained discharge in oxygen and oxygen gas mixtures at gas pressure up to 100 Torr was experimentally studied in large excitation volume (~18 liter). The discharge in pure oxygen and its mixtures with noble gases was shown to be very unstable and characterized by low input energy. When adding small amount of carbon monoxide or hydrogen, the electric stability of the discharge increases, specific input energy per molecular component being higher more than order of magnitude and coming up to 6500 J/(*l* atm). Theoretical calculations demonstrated that for the experimental conditions the $O_2(a^1\Delta_g)$ yield may reach ~20% exceeding its threshold value needed for oxygen-iodine laser operation at room temperature. The results of tentative experiments on spectroscopy of the $O_2(a^1\Delta_g)$ and $O_2(b^1\Sigma_g^+)$ states in the EBSD are presented.

"Supersonic RF discharge CO laser: Fundamental Band Electrical Efficiencies >20% and Observation of Overtone Band Lasing from a Short Gain Length Cavity"

J.E.McCord, G.D.Hager, S.Dass, A.A.Ionin

34th AIAA Plasmodynamics and Lasers Conference, 23-26 June 2003, Orlando, Florida, USA

Radio-frequency (RF) excitation of carbon monoxide (CO) in a supersonic cavity with only a 10 cm gain length has yielded an observed fundamental band (ΔV=1) output power of 2.1 kW utilizing a one-pass resonator, with an electrical efficiency of 21%. More importantly, this work generated 50 W of overtone lasing at 2.7 micron. This was the first time lasing on CO overtone bands (ΔV=2) had been demonstrated with a RF –pumped supersonic system. This work also characterized the fundamental band and overtone band multi-line lasing transitions.

"**Non-self-sustained electric discharge in oxygen gas mixtures:**

singlet delta oxygen production for an oxygen-iodine laser"

A.A.Ionin, Yu.M.Klimachev, A.A.Kotkov, I.V.Kochetov,
A.P.Napartovich, L.V.Seleznev, D.V.Sinitsyn, G.D.Hager

XI Conference on Laser Optics, 30 June - 4 July 2003, St.Petersburg, Russia

The possibility of obtaining a high specific input energy in an e-beam sustained discharge ignited in oxygen gas mixtures at the total gas pressures of 10-100 Torr has been experimentally demonstrated. It has been theoretically demonstrated that one might expect to obtain a singlet delta oxygen yield of 25%.

"**Application of vortex-flow DC glow discharge for atomic iodine production for oxygen-iodine laser**"

P.A.Mikheyev, A.A.Shepelenko

XI Conference on Laser Optics, 30 June - 4 July 2003, St.Petersburg, Russia

The possibility to produce atomic iodine decomposing methyl iodide with the help of the vortex-flow DC glow discharge for use in oxygen-iodine laser has been investigated experimentally. Number density of iodine atoms had been measured via absorption of single frequency tunable semiconductor laser radiation at 1.315 μm. Two cases were studied: 1 – the products of discharge in oxygen decomposed methyl iodide in the downstream afterglow; 2 – methyl iodide was decomposed in the discharge plasma. Atomic iodine concentrations enough to operate oxygen iodine laser were obtained. In the first case iodine atoms number density up to $1.3 \cdot 10^{15}$ cm^{-3} was achieved for oxygen pressure 24 Torr. A kinetic model showing good agreement with experiment had been developed. In the second, vortex flow discharge stabilization permitted to sustain glow discharge in highly negative gas mixture that contained halogen, using Ar as carrier gas at pressures up to 20 Torr. Iodine atoms number density of $3.6 \cdot 10^{15}$ cm^{-3} was achieved at 15 Torr pressure of Ar.

"Non-selfsustained electric discharge in oxygen gas mixtures: singlet delta oxygen production for an oxygen-iodine laser"

A.A.Ionin, Yu.M.Klimachev, A.A.Kotkov, I.V.Kochetov*, A.P.Napartovich*,
L.V.Seleznev, D.V.Sinitsyn, G.D.Hager**

VI Int. Conference "Atomic and Molecular Pulsed Lasers" AMPL-2003, 15-19 September, Tomsk, Russia

The possibility of obtaining a high specific input energy in an e-beam sustained discharge ignited in oxygen gas mixtures at the total gas pressures of 10-100 Torr has been experimentally demonstrated. The specific input energy has exceeded ~6 kJ l^{-1} atm^{-1} (150 kJ $mole^{-1}$) in multicomponent mixtures containing oxygen. It has been theoretically demonstrated that one might expect to obtain a singlet delta oxygen yield of 25% exceeding its threshold value needed for an oxygen-iodine laser operation at room temperature, when maintaining a non-selfsustained discharge in oxygen gas mixtures. The efficiency of singlet delta oxygen production can be as high as 40%.

"Theoretical model of pulsed EBSD CO laser"

Y.M.Klimachev, A.K.Kurnosov, A.P.Napartovich, S.L.Shnyrev

Scientific Session of Moscow Engineering Physics Institute, 26-30 Jan 2004, Moscow, Russia

Energy exchange processes between molecules and atoms in active medium of pulsed electron-beam sustained discharge (EBSD) CO laser were studied. Theoretical spatial uniform model was corrected with new rate constant of multiquantum VV exchange and VT relaxation taking into account. New kinetic processes were included.

"Dynamic of small signal gain on high ro-vibrational transitions of pulsed CO laser"

S. Vetoshkin, A. Ionin, Yu. Klimachev, A. Kotkov, O. Rulev, L. Seleznev, D. Sinitsyn

Scientific Session of Moscow Engineering Physics Institute, 26-30 Jan 2004, Moscow, Russia

For effective pulsed CO lasing on high ro-vibrational transitions in fundamental (V→V-1) and first-overtone (V→V-2) bands the study of small signal gain dynamic is necessary. Especially it is important for first-overtone CO laser. The time behavior of small-signal gain on high ro-vibrational transitions from 17→16 (λ~5.9 μm) to 32→31 (λ~7.5 μm) was measured with probe low-pressure single-line CW CO laser. In the experiments the conditions of supersonic CO laser (temperature, pressure and contents of gas mixture) were modeled. The obtained data allow us to optimize laser resonator position in supersonic cavity with efficiency of the supersonic laser increasing.

"Influence of admixture concentration on gas heating in CO laser"

Konev Yu.B., Kochetov I.V., A.K.Kurnosov, Lobarev Yu.V.

Scientific Session of Moscow Engineering Physics Institute, 26-30 Jan 2004, Moscow, Russia

Systematic calculations of electron energy balance were carried out with some admixture CO_2, H_2O and CH_4 in CO. It was shown that within the reduced admixture concentration range X_{ad}=0.001÷0.003 gas heating due to admixture vibration relaxation was in order more than in pure CO. When the value X_{ad} being lower 0.0005 (it corresponds to <0.1% concentration), the direct CO heating and gas heating due to admixture vibration relaxation are equivalent to each other.

"Theoretical studies on kinetics of singlet oxygen in nonthermal plasma"

M.P. Frolov, A.A. Ionin, A.A. Kotkov, I.V. Kochetov, A.P. Napartovich, Yu.P. Podmarkov, L.V. Seleznev, D.V. Sinitsyn, N.P. Vagin, N.N. Yuryshev

High-Power Laser Ablation V Conf., 25-30 April 2004, Taos, NM, USA.

An idea to replace singlet delta oxygen (SDO) generator working with wet chemistry by electric discharge generator has got much attention last years. Different kinds of discharge were examined for this purpose, but without a great success. The existing theoretical models are not validated by well-characterized experimental data. To describe complicated kinetics in gas discharge with oxygen one needs to know in detail processes involving numerous electronic excited oxygen molecules and atoms. To gain new knowledge about these processes experimental studies were made on electric discharge properties in gas mixture flow with independent control of inlet SDO concentration. The theoretical model extended to include minor additives like oxygen atoms, water molecules, ozone was developed. Comparison with careful experimental measurements of electric characteristics along with gas composition allows us to verify the model and make theoretical predictions more reliable. Results of numerical simulations using this model for an electron-beam sustained discharge are reported and compared with the experimental data.

"Electron-beam sustained discharge in oxygen gas mixtures: singlet delta oxygen production for oxygen-iodine laser"

M.P.Frolov, G.D.Hager, A.A.Ionin, Y.M.Klimachev, I.V.Kochetov, A.A.Kotkov, J.K.McIver, A.P.Napartovich, Y.P.Podmar'kov, L.V.Seleznev, D.V.Sinitsyn, N.P.Vagin, N.N.Yuryshev

High-Power Laser Ablation V Conf., 25-30 April 2004, Taos, NM, USA.

Electric properties and spectroscopy of an e-beam sustained discharge (EBSD) in oxygen and oxygen gas mixtures at gas pressure up to 100 Torr were experimentally studied. The pulsed discharge in pure oxygen and its mixtures with noble gases was shown to be very unstable and characterized by low input energy. When adding small amount of carbon monoxide or hydrogen, the electric stability of the discharge increases, specific input energy (SIE) per molecular component being more than order of magnitude higher and coming up to 6.5 kJ/(*l* atm) for gas mixture O_2:Ar:CO = 1:1:0.1. The results of experiments on spectroscopy of the singlet delta oxygen $O_2(a^1\Delta_g)$(SDO) and $O_2(b^1\Sigma_g^+)$ states in the EBSD are presented. The calibration of the optical

scheme for measuring the SDO absolute concentration and yield using the detection of luminescence of the SDO going from a chemical SDO generator was done. The preliminary measurement of the SDO yield demonstrated that it was ~3% for the SIE of ~1 kJ/(*l* atm), which is close to the results of theoretical calculations for such a SIE. Theoretical calculations demonstrated that for the SIE of 6.5 kJ/(*l* atm) the SDO yield may reach ~20% exceeding its threshold value needed for oxygen-iodine laser operation at room temperature, although a part of the energy loaded into the EBSD goes into the vibrational energy of the molecular admixture, (which was experimentally demonstrated by launching a CO laser operating on an oxygen-rich mixture O_2:Ar:CO = 1:1:0.1 and measuring its small-signal gain).

"The methods of singlet oxygen detection for DOIL program"

N.N.Yuryshev, A.A.Ionin, M.P.Frolov, Y.M.Klimachev, I.V.Kochetov, A.A.Kotkov, A.P.Napartovich, Y.P.Podmar'kov, L.V.Seleznev, D.V.Sinitsyn, N.P.Vagin

High-Power Laser Ablation V Conf., 25-30 April 2004, Taos, NM, USA.

The problem of development of a singlet delta oxygen $O_2(^1\Delta_g)$ (SDO) generators alternative to chemical one needs application of the accurate methods of measuring the SDO concentration. A chemical SDO generator providing efficient operation of a chemical oxygen-iodine laser (COIL) is proposed to be used as a reference source for absolute calibration of the system measuring the SDO concentration. The principle of the COIL operation results in the threshold and output COIL parameters make it possible to evaluate the SDO yield with a satisfactory accuracy. A convenient sparger chemical SDO generator was applied as a reference source for absolute calibration of detectors of dimole (λ=634nm) and b→X (λ=762 nm) radiations. The values of b-state concentration formed in a longitudinal electric discharge were evaluated. The intracavity laser spectroscopy (ICLS) was absolutely calibrated for measuring the SDO concentration. ICLS method has a very high sensitivity and makes it possible to monitor the absorption corresponding to the $O_2(^1\Delta_g)\rightarrow O_2(^1\Sigma_g^+)$ (λ = 1.91 μm) transition. The cross-sections of lines of the *Q* - branch of the vibrational 0-0 band of the $a^1\Delta_g \rightarrow b^1\Sigma_g^+$ transition of molecular oxygen were measured. The method developed was applied to measure the concentration of singlet oxygen produced in the microwave discharge. He - Ne laser (λ = 633 nm) was used for absolute calibration of a system monitoring the dimole radiation. The rate constant of the process responsible for dimole emission was measured. The value obtained $k_d=7.34\cdot10^{-23}$ cm^3/s is in agreement with literature

"Supersonic RF discharge CO laser operating in fundamental (Δ=1) and overtone (Δ=2) spectral bands"

J.E.McCord, R.F.Tate, S.Dass, G.D.Hager, A.A.Ionin, L.V. Seleznev, W.L.Bohn, H.von Buelow, J.K.McIver

High-Power Laser Ablation V Conf., 25-30 April 2004, Taos, NM, USA.

Radio frequency (RF)-excitation of carbon monoxide (CO) in a supersonic cavity with only a 10 cm gain length has yielded an observed fundamental band (Δv=1) multi-line lasing output power of 2.1 kW utilizing a one-pass resonator, with an electrical efficiency of 21%. More importantly, this work generated 50 W of overtone multi-line lasing around 2.7 micron. This was the first time lasing on CO overtone bands (Δv=2) had been demonstrated with a RF-pumped supersonic system.

"Singlet Delta Oxygen Production in E-Beam Sustained Discharge: Theory and Experiment"

A.Ionin, M.Frolov, G.Hager, Yu.Klimachev, I.Kochetov, A.Kotkov, A.Napartovich, Yu.Podmar'kov, L.Seleznev, D.Sinitsyn, N.Vagin, N.Yuryshev

XV International Symposium on Gas Flow and Chemical Lasers & High Power Lasers Conference,
30 Aug – 3 Sep 2004, Prague, Czech Republic.

Singlet delta oxygen (SDO) production in a pulsed e-beam sustained discharge (EBSD) ignited in molecular oxygen with carbon monoxide stabilizing this discharge is theoretically and experimentally studied. Temporal behavior of SDO concentration and yield in the EBSD afterglow is analyzed. Experimentally measured SDO yield for oxygen mixture O_2:Ar:CO=1:1:0.05 at total gas pressure 30 Torr comes up to 7% at specific input energy (SIE) of ~3.0 kJ/(l atm(O_2+CO)), whereas its theoretical value riches ~17.5%. The efficiency of SDO production is theoretically analyzed as a function of the SIE.

"Measurements of the thermodynamic parameters for CO laser gas mixtures excited by pulsed electron-beam sustained discharge"

L.Seleznev, A.Ionin, Yu.Klimachev, I.Kochetov, A.Kotkov,
A.Kozlov, A.Kurnosov, A.Napartovich, D.Sinitsyn, S.Vetoshkin

XV International Symposium on Gas Flow and Chemical Lasers & High Power Lasers Conference,
30 Aug – 3 Sep 2004, Prague, Czech Republic.

Time behavior of gas temperature in CO containing gas mixture excited in pulsed electron-beam sustained discharge (EBSD) was experimentally studied under different experimental conditions. To study time behavior of gas temperature, the fact that the gas temperature is equivalent to the rotational temperature of gas molecules was used. Rotational distribution of the excited states of CO molecule was reconstructed from measured small-signal gain dynamics on different ro-vibrational transitions. The time behavior of small-signal gain was obtained with probe low-pressure CW CO laser for ten ro-vibrational spectral lines. Gas mixtures CO:He=1:4 and CO:N_2=1:9 typical for a CO laser were used. It was demonstrated that gas temperature grew from 110 K (initial temperature) up to ~150 K for the first hundred microsecond after EBSD beginning and was staying at this value for a long time (more than 1 ms) for both gas mixtures. EBSD pulse duration was ~30μs. The method of reconstruction of gas temperature time history was also applied for oxygen gas mixture CO:O_2=1:20 at gas pressure 0.04 atm, which was used for obtaining singlet delta oxygen in EBSD. The method can be used for diagnostic of non-equilibrium gas mixtures containing CO molecule.

"Time behavior of small-signal gain on high vibrational transitions for pulsed CO laser amplifier with gas mixtures CO:He, CO:N_2, and CO:O_2"

Y. Klimachev, A. Ionin, A. Kotkov, D. Sinitsyn, L. Seleznev, S. Vetoshkin A. Kozlov, O. Rulev

XV International Symposium on Gas Flow and Chemical Lasers & High Power Lasers Conference,
30 Aug – 3 Sep 2004, Prague, Czech Republic.

Small-signal gain time behavior for cryogenic pulsed e-beam sustained discharge CO laser amplifier on high (V>15) fundamental band vibrational transitions was studied experimentally for different CO containing gas mixtures including ones typical for CO lasers and amplifiers (CO:He and CO:N_2), and CO:O_2 used for singlet delta oxygen production.

"$O_2(a^1\Delta_g)$ concentration measuring by intracavity laser spectroscopy of $b^1\Sigma_g^+ - a^1\Delta_g$ transition"

M.Frolov, A.Ionin, I. Kochetov, A. Napartovich, Y. Podmar'kov, N.P.Vagin, N.N.Yuryshev

XV International Symposium on Gas Flow and Chemical Lasers & High Power Lasers Conference,

30 Aug – 3 Sep 2004, Prague, Czech Republic.

Absorption spectra of chemically produced singlet oxygen $O_2(a^1\Delta_g)$ in the vicinity of 1.91 μm wavelength were recorded by intracavity laser spectroscopy technique. The line strengths for Q-branch transitions of the (0,0) band of the $b^1\Sigma_g^+ - a^1\Delta_g$ system were measured. Measurements of the $O_2(a^1\Delta_g)$ yield for an electric discharge are presented.

"Highly excited CO molecules vibrational exchange and its influence on the physical processes in active medium of pulsed EBSD CO laser"

Klimachev Yu.M.

Scientific Session of Moscow Engineering Physics Institute, 24-28 Jan 2005, Moscow, Russia

Dynamics of small signal gain on high fundamental and overtone vibrational-rotational transitions of CO molecule was studied at different experimental conditions for pulsed electron beam sustained discharge CO laser active medium. Restoration time of inversion population after its short pulsed perturbation was measured in the laser by means of double Q-switching technique. Experimental results were compared with theoretical calculations.

"Electron-beam sustained discharge CO laser operating on gas mixtures with high (~95%) content of oxygen"

Vetoshkin S.V., Ionin A.A., Klimachev Yu.M., Kozlov A.Yu., Kotkov A.A., Seleznev L.V., Sinitsyn D.V.

Scientific Session of Moscow Engineering Physics Institute, 24-28 Jan 2005, Moscow, Russia

Pulsed electron beam sustained discharge CO laser was realized on active gas mixture with high (~95%) content of oxygen. Small signal gain in laser gas mixture $CO:O_2$ appeared to be twice higher than that for typical CO laser gas mixture $CO:N_2$.

"Singlet delta oxygen in low-temperature plasma of non-selfsustained discharge"

Rulev O.A., Vagin N.P., Ionin A.A., Klimachev Yu.M., Kotkov A.A., Kochetov I.V., Napartovich A.P., Seleznev L.V., Sinitsyn D.V., Yuryshev N.N.

Scientific Session of Moscow Engineering Physics Institute, 24-28 Jan 2005, Moscow, Russia

An influence of gas mixture content and pressure on singlet delta oxygen yield in pulsed electron beam sustained discharge was studied experimentally. Maximal obtained yield was estimated as about 7% for gas mixture $CO:O_2$:Ar at total pressure of 30 Torr.

"Multiline laser probing of active medium of pulsed EBSD CO laser"

Kozlov A.Yu., Vetoshkin S.V., Ionin A.A., Klimachev Yu.M., Kotkov A.A., Kurnosov A.K., Napartovich A.P., Seleznev L.V., Sinitsyn D.V.

Scientific Session of Moscow Engineering Physics Institute, 24-28 Jan 2005, Moscow, Russia

Gas temperature temporal behavior and vibrational levels population dynamics in active medium of pulsed electron beam sustained discharge CO laser were measured using multi-frequency laser probing technique. It was concluded that the fraction of pumping discharge energy going into direct gas heating was equaled to ~15% for nitrogen containing mixture and ~10% for helium containing one.

"Compact cryogenically cooled slab CO laser with RF excitation"

Ionin A.A., Kochetov I.V., Napartovich A.P., Sinitsyn D.V., Terekhov Yu.V.

Scientific Session of Moscow Engineering Physics Institute, 24-28 Jan 2005, Moscow, Russia

Results of preliminary experiments on study compact cryogenically cooled slab CO laser with RF excitation were reported. Output laser characteristics obtained in fundamental band lasing mode

were as follows: average power ~5W, efficiency ~2.5%. Possibilities of improving the laser characteristics and realizing overtone band lasing were discussed.

"CO laser: advances in theory and experiment"

Napartovich A., Kurnosov A., Shnyrev S., Ionin A., Klimachev Yu.,
Kotkov A., Seleznev L., Sinitsyn D.,

XV International Symposium on Gas Flow and Chemical Lasers & High Power Lasers Conference,
30 Aug – 3 Sep 2004, Prague, Czech Republic.

Last years, CO laser physics has been advanced by researches of CO overtone laser operated on high vibrational levels. An extension of kinetic model to multi-quantum vibration-vibration exchange and development of fully self-consistent model of CO laser are described. The theoretical model developed is verified by comparison with experimental data on overtone CO laser characteristics and laser gain dynamics. Current status of experimental achievements in CO laser characteristics in both fundamental and overtone bands are reported.

"Singlet delta oxygen production in slab discharges ignited in oxygen gas mixtures"

Ionin A.A., Frolov M.P., Ochkin V.N., Kotkov A.A., Kochetov I.V., Napartovich A.P.,
Podmar'kov Yu.P., Rulev O.A., Savinov S.Yu., Seleznev L.V., Sinitsyn D.V.,
Terekhov Yu.V., Vagin N.P., Yuryshev N.N.

35th AIAA Plasmadynamics and Lasers Conf., 6-9 June 2005, Toronto, Canada

Singlet delta oxygen $O_2(a^1\Delta_g)$ production in slab discharges ignited in oxygen gas mixtures was experimentally studied. In slab self-sustained RF discharge experimental SDO yield was about 10%. It was demonstrated that the choice of electrodes' material is very important. Experiments on SDO production in slab non-self-sustained discharge with external ionization by repeated high-voltage pulses were carried out. SDO concentration was measured by the method of intracavity laser spectroscopy. The measured concentration of SDO was about 10^{16} cm^{-3}, with SDO yield being of ~7%.

"Fundamental and overtone band lasing of RF discharge supersonic CO laser"

Seleznev L.V., Bohn W., von Buelow H., Dass S., Hager G.D., Ionin A.A., McIver J.K.,
McCord J.E., Tate R.F. .

ICONO/LAT 2005 Conference, St. Petersburg, Russia.

RF discharge CO overtone lasing with output power of 50 W was demonstrated with supersonic cooling system. Output power of 2.1 kW with efficiency of 21% in fundamental band was obtained.

**"Multiline laser diagnostics of active medium parameters
in the wide-aperture CO laser amplifier"**

Kotkov A.A., Ionin A.A., Klimachev Yu.M., Kozlov A.Yu., Seleznev L.V.,
Sinitsyn D.V., Vetoshkin S.V., Kochetov I.V., Kurnosov A.K., Napartovich A.P.

ICONO/LAT 2005 Conference, St. Petersburg, Russia.

Local value of specific input energy, temporal behavior of gas temperature and vibrational populations in active medium excited by pulsed electron beam sustained discharge in the wide aperture CO laser amplifier was studied both experimentally and theoretically.

"Singlet delta oxygen production in slab discharge"

Ionin A.A., Frolov M.P., Ochkin V.N., Kotkov A.A., Kochetov I.V., Napartovich A.P., Podmar'kov Yu.P., Rulev O.A., Savinov S.Yu., Seleznev L.V., Sinitsyn D.V., Vagin N.P., Yuryshev N.N.

COIL R&D Workshop, Stuttgart, Germany, 5-6 Sept 2005, CD, (2005)

Singlet delta oxygen $O_2(a^1\Delta_g)$ production in slab discharges ignited in oxygen gas mixtures was experimentally studied. In slab self-sustained RF discharge experimental SDO yield was about 10%. It was demonstrated that the choice of electrodes' material is very important. Experiments on SDO production in slab non-self-sustained discharge with external ionization by repeated high-voltage pulses were carried out. SDO concentration was measured by the method of intracavity laser spectroscopy. The measured concentration of SDO was about 10^{16} cm^{-3}, with SDO yield being of ~7%.

"Preliminary study of singlet oxygen generator driven by MW discharge"

M.P.Frolov, A.A.Ionin, Y.M.Klimachev, I.V.Kochetov, A.A.Kotkov, A. P. Napartovich, Y.P.Podmar'kov, O.A.Rulev, L.V.Seleznev, D.V. Sinitsyn, N.P.Vagin, N.N.Yuryshev

COIL R&D Workshop, Stuttgart, Germany, 5-6 Sept 2005, CD, (2005)

The experimental results on influence of experimental parameters on the yield of singlet oxygen generated in the MW discharge were presented. The method of probe specimen was used to get information on SDO yield. Generation of atomic oxygen in oxygen plasma was investigated too by using the method of titration with nitrogen dioxide. The SDO yield of 14.5 % was detected at 1.5 Torr of operation pressure and at 28 W of input power.

"Supersonic overtone CO laser: research and development"

Bohn W., von Buelow H., Dass S., Hager G.D., Ionin A.A., McIver J.K., McCord J.E., Seleznev L.V., Tate R.F.

VII Int Conf Atomic and Molecular Pulsed Lasers, 12-16 Sept 2005, Tomsk, Russia

Characteristics of cw CO laser with supersonic gas flow are discussed. Radio frequency discharge CO overtone (V+2→V) lasing with output power 50 W was demonstrated with supersonic cooling system. The overtone lasing was observed on 9→7, 10→8 and 11→9 vibrational transitions within spectral range 2.6 - 2.7 μm wavelength. The laser active medium length was 10 cm. The small signal gain on the overtone transitions was estimated to be 0.1 m^{-1}. Fundamental band (V+1→V) lasing was observed within 4.9 – 5.7 μm spectral range. In fundamental band output power 2.1 kW with efficiency 21% was obtained, with typical small signal gain being about 1 m^{-1}. Modeling experiments on electron-beam sustained discharge facility were carried out at experimental conditions (gas pressure, temperature) corresponding to those of supersonic gas flow. Possibilities of supersonic overtone CO laser design improvement to obtain overtone lasing on highly excited vibrational transitions of CO molecule corresponding to the spectral range ~3 – 4 micron are discussed.

INFORMATION ON PATENTS AND COPY RIGHTS

"**Method of obtaining singlet delta oxygen in non-self-sustained electric discharge plasma**"

A.A. Ionin , Yu.M. Klimachev , A.A. Kotkov , I.V. Kochetov , A.P. Napartovich ,
L.V. Seleznev , D.V. Sinitsyn, G.D. Hager

Russian Federation Patent #2206495, obtained 20 June 2003, priority 10 April 2002
(application #2002109190) (in Russian).

The invention could be applied for physics and technique of oxygen-iodine lasers. In order to produce singlet delta oxygen in non-self-sustained discharge in oxygen gas mixtures at pressure 10-100 Tor the molecular gases CO, H_2, D_2 with concentration 1-20% were added into gas mixtures.